CORROSION FATIGUE OF REINFORCED CONCRETE

A Thesis Submitted to
The University of Glasgow

By

Moufaq Jassem Katwan
B.Sc. (Basrah 1977)

for

The Degree of Doctor of Philosophy
in
The Department of Civil Engineering

September 1988

CONTAINS PULLOUTS

"To my dear wife, Wafa..."

ACKNOWLEDGEMENTS

This work has been carried out in the Departments of Civil and Mechanical Engineering, University of Glasgow under the general direction of Professor A. Coull whose encouragement is deeply acknowledged.

Thanks are also due to Dr. D.R. Green of the Department of Civil Engineering and to Professor B. Scott of the Mechanical Engineering for support and provision of laboratory facilities.

I would like to express my deep sense of obligation to my supervisors:

Dr. P.D. Arthur for his generous advice and guidance particularly those pertaining to the structural side of the work, admirable interest, understanding and support throughout the research and;

Dr T. Hodgkiess for his matchless supervision on subjects pertaining to the corrosion side of this work, his intimate involvement, brilliant criticisms and constant encouragement.

I am also greatful to:

The staff of concrete laboratory, in particular Mr. A. Burnett, Mr I. Todd, Mr B. Thomson, Mr R. Hawthorn, Mr J. Thomson and the late Mr J. Dowall for their valuable assistance in all tedious work involved in this research.

Thanks are also reserved to:

Mr. J.T. Maguire and Mrs G.E.S. O'Dea, for their continuous support and encouragement.

Mr L.S. Kadem, a research student in the Department of Geology, for his assistance in conducting deposit identification tests.

Mr F. Lombos and Miss J. Anderson of L.A. Design and Print for efficient typing of the manuscript.

Sincere thanks are due to the Government of the

Republic of Iraq, Ministry of Housing and Construction for financial support without which this work would not have been possible.

Finally, I pay my heartfelt feeling of acknowledgement to my father, mother, brother Talal and mother in law for their continuous support and encouragement. My wife, son, Osama, and daughter, Zena for their priceless forbearance and peerless endurance throughout the period of this research.

September 1988

SUMMARY

This work is concerned with the corrosion fatigue characteristics of full-scale reinforced concrete beams partially submerged in 3.5% NaCl solution or in tapwater of low dissolved salt content. The test beams were subjected to constant amplitude fatigue loading in uni-directional or reverse bending at slow cycle rate of 0.17 Hz and various load levels. The test programme had two stages, Stage I, carried out at relatively high load levels, represented a study of the fatigue-failure phenomenon but also provided guides for the more detailed study undertaken in Stage II which was devoted to low load conditions under which the main steel deterioration process was corrosion. In the latter stage, attention was focussed on the monitoring of a number of electrochemical parameters including the corrosion rate. Late in the programme, electrochemical noise technique was also examined.

The phenomenon of concrete crack blocking, previously reported in seawater environment, was observed in both test environments in this work. This phenomenon was closely examined and the mechanisms of the formation of deposits and its effects were described. A hypothesis was proposed for the structural behaviour of reinforced concrete beams during cyclic loading in aqueous environment. Failure normally occurred by the fracture of one of the main tensile bars due to fatigue, often followed immediately by yield of the remaining bar and beams collapse. Fracture surfaces were examined under SEM.

Corrosion rate measurements involved formidable difficulties which had to be overcome to obtain accurate measurements. For instance, the current interruption technique for the estimation of the IR-drop was developed and established as the most appropriate method for concrete beams with complex reinforcement configuration. Extensive polarisation measurements indicated clear effect of the test condition on the technical variables involved in various measuring techniques (viz potentiodynamic and potentiostatic techniques). Based on these observations a criterion has been proposed to determine the appropriate

variables necessary for the accurate determination of the polarisation resistance R_p.

The work has demonstrated that the corrosion behaviour of reinforced concrete sustaining dynamic loading is extremely complex, and short term indications could not be used safely for long term predictions. Based on corrosion rate measurements and the actual corrosion pattern observed upon completion of the tests, a concept of a change in corrosion mechanism from a microcell process of relatively low corrosion rates to a macrocell process at much accelerated high rates is introduced. The prevailing mechanism depends on time of exposure, load level and reinforcement details. Results from long running fatigue tests in seawater from concurrent research were incorporated which also support this concept.

CONTENTS

CHAPTER 1

INTRODUCTION

1.1 The Problem and the Research.

1.2 Historical Background.

1.3 Significance of Fatigue Data.

1.4 General Considerations.

1.5 Objectives.

CHAPTER 1

INTRODUCTION

1.1 The Problem and the Research.

Concrete has been excellently described[1] as the "most noble material on earth" - a miracle material". In fact not only is its use limited solely by our imagination but also it can actually improve with time. Concrete is by far the most utilised artificial material made by mankind. The efficiency of use of this material has been greatly improved following the introduction of reinforced concrete during the second half of the nineteenth century, the scope of its application grew rapidly as its composite properties were appreciated.

Since the turn of this century,[2,3] reinforced concrete has been in use in great variety of constructions: from massive structures such as dams, bridges, storage tanks down to small component such as fencing posts and railway sleepers. It is also exposed to many types of environment. In most of these applications, reinforced concrete has been destined to withstand, during its service life, both structural and non-structural forces. However, despite the joint effect of these forces, all literature[3,4] on durability of concrete structures has generally indicated fascinating examples of success in the long history of concrete technology. Excellent service performance spanning a number of decades has already been achieved by many reinforced concrete structures under various environmental conditions.

However, there are several degradative[1,2,3,5] processes which have affected a minority of reinforced

concrete structures leading to loss of serviceability or in extreme cases to structural collapse. Amongst these, the most common cause of deterioration is corrosion of reinforcing steel. Over the past two decades there has been an increasing number of reports from many parts of the world of corrosion failure particularly associated with de-icing salts, marine environment, calcium chloride additives and contaminated aggregates and also sometimes involving carbonation phenomena.

Recent Development.

Concrete structures[6] have existed in corrosive media for almost as long as we have considered concrete as a building material. They are extensively used in marine environment for constructing harbour structures like jetties and wharves and for protective structures like embankments and sea walls. Perhaps the most striking development in this field has been the evolution of concrete platforms to produce hydrocarbons in the North Sea during the early 1970's. Since that time 20[6,7,8] other concrete platforms have been constructed in the North sea, the Baltic sea and offshore of Brazil and three more are under construction for delivery in 1987-1989. All indications seem to suggest that this trend is set to continue as the pressure of[6,9] the growing world population and the corresponding demand for resources is rapidly extending. Oceans make up 80 per cent of the surface of the earth and already 22 per cent of the world oil and gas comes from reservoirs under the sea. Seabed mining for mineral resources is a definite possibility in the near future.

Further, according to metha,[9] consideration is being given to the idea of locating cities, airports, nuclear power and waste disposal plants on offshore floating platforms.

Recent and Future Challenge.

The recent applications have, in fact, enhanced our

faith in the durability of portland cement concrete and strongly suggest that most future structures in aggressive environments can, indeed, be built from this material. New demands will most probably give birth to new breed of concrete structures not necessarily on offshore but also on land. For each novel application, however, their certainly exits some unknowns, uncertainties and in some cases risks, this is particularly evident when the non-structural forces assume more important role. While accepting the challenge, there is obviously increasing demand for additional knowledge on the behaviour of reinforced concrete under several types of unconventional forces to which it is subjected. Such knowledge is necessary not only to provide safe, efficient and economical design but to serve as a rational basis for the conception of improved and extended application for the future.

Fatigue.

Another area of important development has been that of fatigue.[10,11,12,13,14,15] The problem of fatigue failure in engineering materials and structures is by no means new.[16,17,18] The introduction of high strength materials, dramatic changes in operating conditions and the adoption of new design codes have prompted a need to establish the fatigue performance of reinforced concrete. When the concrete structures are exposed to hostile media, the risk of fatigue is tremendously increased as the design working stresses, although initially safe from the stand point of pure fatigue, may considerably change to less favourable situation due to the progressive loss of the tensile capacity of the steel in proportion to the loss of its cross-sectional area.

Of particular importance in this respect is the fact that the design regulations do not allow for the reduction in the ultimate tensile capacity due to corrosion as they pre-assume the structural immunity to corrosion, yet corrosion attack is always a possibility. This assumption is, most likely, linked to the present state of knowledge

which lacks a reliable predictive basis for the occurrence and extent of damage experienced due to corrosion.

Despite the fact that the effect of corrosive environment on fatigue characteristics of reinforced concrete has been of concern since the early twenties of this century.[19,20] Research in this area, however, has been intensified since the early 1970s, partly spurred on by recent construction activities in the North and Baltic seas. This research, in general, has illustrated the way in which the behaviour of reinforced concrete under cyclic loading can be critically affected by the prevailing environmental conditions and, probably more importantly, that the deterioration process is extremely complex. Nevertheless, the understanding of this phenomenon and the application of that understanding to real world design is far from complete leaving many areas of uncertainty and even conflicting views.

The Research.

The detrimental influence of sea water on the fatigue properties of reinforced concrete has been the main object of most studies[20] and very little has been done to study the effect of other aqueous environment. Accordingly the research work reported in this thesis is an attempt to provide some more fundamental information on the fatigue behaviour of a full scale reinforced concrete beam in less investigated corrosion-conductive media namely 3.5% sodium chloride solution and low total- dissolved-solids (T.D.S) tap water.

1.2 Historical Background.

The problem of fatigue has been recognised by engineers ever since failure occurred at design stresses considerably less than the ultimate tensile strength of the material concerned.[17]

Historically, interest was shown in fatigue of metal as early as 1829[16,17,18] when W.A. Albert in Germany subjected iron chains to repeated loading. He was then

followed by a number of investigators associated with railway companies who were motivated by then practical problems. Notable among them are Hodgkinson (1849) and Wohler (1852).

Poncelet,[17] in 1839, appears to have been the first to associate the word "Fatigue" with failure under repeated loads but the first relevant paper in which this word appeared in the title was read by Braithwaite before the Institute of Civil Engineers, London in 1854. Since then it has become well established in engineering terminology.

In the nineteenth century, the limited amount of research on the phenomenon of fatigue was carried out almost exclusively on iron and steel, the commonly used structural and constructional material of the time. Concrete fatigue investigations have lagged until the end of the last century when Considere and De Joly[17,18] began tests on mortar specimens under tension fatigue. The earliest fatigue investigation on concrete in compression was carried out by Van Ornum in 1907 whereas the first fatigue tests on flexural concrete specimens was reported by Feret in 1906. More extensive investigation on flexural fatigue of concrete were carried out at Purdue university (1922) and Illinois department of highways (1921). The aim was to provide information vital for the optimum design of airports runways and highways.

Although early studies did not lack strong incentives they were confronted by difficulties in obtaining financial support because of their fundamental character and the length of time between inception of the tests and economic returns.

Most of these tests, however, are of little value today but they provided the engineers in the early part of this century with information of vital importance.

The fatigue investigation of reinforced concrete[18] commenced almost concurrently with the research on properties of plain concrete in fatigue. Van ornum,[18] in 1907, was the first to extensively examine reinforced concrete beams, he tested 59 beams of two age groups and attempted to describe the mechanism of fatigue failure.

Since then considerable amount of research has been carried out. These activities are particularly intensified during the last two decades.

The first investigation[18] on the effect of corrosive environment on the fatigue characteristics of reinforced concrete was performed by Amose in 1924. It is interesting to note that these early tests were carried out at low cyclic frequency, a practice commonly regarded as more simulative to many real loading conditions which is increasingly adopted in recent investigations including the present one. However, unlike fatigue tests in air, research on fatigue of reinforced concrete in corrosive environment has been very limited, in fact no literature could be traced in the period between 1924 and 1974. In 1975 several investigations including the works of Browne[21] et al, Bannister[22] and Lacroix[23] were reported. In 1976[24] the concrete in the Ocean programme was set up in the U.K. as a result of a survey undertaken to identify research needs for marine and off shore concrete structure and particularly for concrete gravity platforms. This programme included a major experimental project on fatigue of reinforced concrete in sea water.

Essentially provoked by the same incentives, interest in this topic was also generated[8,25] in five other European countries as well as the United States and Japan. Since then systematic research activities were undertaken, and are still underway, the results of which constitute virtually all our knowledge of this phenomenon. As a result the term "corrosion fatigue of reinforced concrete" has become increasingly well known in the society of engineering.

1.3 Significance of Fatigue Research.

In practice there are many cases in which concrete structures can be subjected to low, moderate and high intensity of repeated proportional and non proportional type. These type[26] of loading require the structure to resist certain strains at critical sections several times. Only rarely are the structural elements subjected to

constant or monotonically increasing loads throughout their entire service history. Such cases may be schematically represented by the line marked static[17] in Figure 1.1. These conditions should, theoretically, result in infinite lives. The real loading condition is typified by the pattern marked fatigue in Figure 1.1.

Reinforced concrete structures such as bridge and offshore installations are distinctive examples for structures subjected to this type of loading in civil engineering areas. In Britain,[13] designs of highway bridges are assessed for lives of 120 years during which time up to 7×10^8 cycles of traffic induced stress may be applied. Offshore structures in the North sea[6,13,26] and Baltic sea will be subjected to more than 10^8 cycles of loading by the wave action during a 25 to 30 years service life. The magnitude of the numbers suggests that fatigue should be one of the major design considerations. Natural forces such as earthquakes and hurricanes may add additional risk of failure in fatigue under low cycles - high intensity conditions.

Until recently the fatigue problem has not been given much attention in national codes and regulations. For instance in Swedish regulations[11] for concrete structures of 1968, the only allowance for fatigue is the reduction of permissible stresses in reinforcement by 10-25% in certain type of structures. The lack of fatigue design criteria is probably related to the fact that codes reflect practical needs and practical experience and also suggests that risks due to fatigue effects were considered sufficiently small to be safely tolerated. There can, however, be other reason for the slight interest in fatigue of concrete structures. These are according to Westerberg:[11]

1. The vast majority of concrete structures are relatively heavy in which case the variable loads form a minor part of the total load i.e. high dead load to live load ratio.

2. Loads on structures are generally of rather steady

character.

3. Disastrous failures caused by fatigue have not occurred. Failures known to be caused by fatigue have been of rather innocent nature such as breaking of the corner of concrete pavement due to frequent wheel loads.

However, within the last decade, increasing attention has been focused on the fatigue[10,12,13] and corrosion fatigue behaviour of reinforced concrete structures. This interest was stimulated by some major developments in design practice and engineering materials and applications. More specifically, the motives include.[10,11 12,27,28]

1. Refinements in the method of structural analysis and design, the increase in working stresses and the increased use of more slender reinforced concrete elements as a result of more efficient use of the material.

2. Increased material strength makes it possible for more variable load to be carried by a structural element of a given dimensions.

3. Improved tensile strength of reinforcing bars not being accompanied by a similarly improved fatigue strength.

4. New recognition of the effect of repeated loads on the serviceability of a concrete member, such as the increase of crack widths and deflections, even if repeated loading does not cause fatigue failure.

5. The growing use of reinforced concrete structures such as bridge, chimneys, towers and the new breed of offshore structures which in service are predominantly subjected to loads of a repeated nature.

6. Increased awareness of the joint effect of the environmental loads and metal loss due to corrosion in reducing the margins of safety and accelerating fatigue phenomenon for the ever-increasing use of reinforced concrete in corrosive environment.

The effect of items 1,2 and 3 can be considerable, according to Moncrieff[29] who considered changes in British Codes. The moment capacity of a rectangular reinforced concrete section with a given dimensions and material strength is about twice as large when computed according to modern design regulation as according to older regulations, Figure 1.2. This is mainly due to progressive decline in materials (reinforcement and concrete) margins of safety, Figure 1.3a,b. Westerberg[11] indicated that when a general increase of about 50% in material strength is added, the same structural element with given dimensions will be able to carry three time more load to day than before the change in regulation. Since the weight of the element is unchanged, the whole increase can be taken by variable loads. If the variable load was half the total load, it could be 5/6 of the total load to day or five times the absolute variable load at that time, Figure 1.4.

On the other hand, the fatigue limit[11] of deformed bars can be as low as 200 N/mm^2 regardless of the yield strength. (In fact, some investigators[13,14] have indicated that fatigue limit can not be assumed unless verified experimentally). Thus when the yield strength exceeded 400 N/mm^2 the maximum strength level under service conditions might reach the fatigue limit if the minimum stresses are low, Figure 1.5.

The changes and improvements in design regulations, however, resulted primarily from improvements in the methods of analysis and in the understanding of the factors dictating the behaviour of structures under static or monotonically increasing loading,[29,30,31] they obviously lack the necessary information on long-term fatigue safety particularly for structures subjected to loading conditions with high live load to dead load ratio

and also to aggressive environment.

The construction of offshore reinforced concrete platforms in recent years involves some performance uncertainties evolved mainly from the severe environmental and loading conditions. Information on the corrosion fatigue behaviour under these conditions is of considerable importance. This is because, firstly, a high level of safety[8,32] is required for these structures which have rarely been applied before as the consequences of failure during operation are potentially catastrophic. Secondly, these structures should be free from deterioration and excessive maintenance[33] because there is little possibility of applying remedial measures after they have been built and put into service.

Research on corrosion fatigue behaviour of reinforced concrete has also been motivated by increasingly reported instance of structural distress due to corrosion in bridge and highway structures.[34]

Finally, it should be pointed out that research activities in this area are further encouraged by the improvement in monitoring techniques, including the electrochemical one, which allow quantitive information about features relevant to service conditions to be more accurately obtained.

1.4 General Considerations.

One of the major technical problems associated with investigations on fatigue of reinforced concrete in general and corrosion fatigue in particular is the interpretation of information from relatively short-term laboratory-based studies for use in predicting long-term performance. A problem has always existed in compromising between what happens on real construction sites whether it is on land or offshore and research that is performed in the laboratory. Generally, however, no satisfactory method existed of relating the results from simplified laboratory tests to the behaviour of structural members in actual use.

As a result, laboratory-deduced data in this field

were met, perhaps, rightfully, with a good deal of scepticism which was reflected in stringent design regulations and a high degree of conservatism.

Deleterious processes of the kind in which corrosion intervention assumes major contribution are substantially time-dependent, thus, development of realistic test data for these specific conditions requires unduly long test duration. Nevertheless, laboratory based investigations with very big acceleration factors in relation to service have, historically, been employed for the purpose of developing information from which design criteria are developed.

Under such circumstances, in order to obtain realistic information, the experimental variables should be carefully considered. These include, specimen details and size, test frequency, loading configuration, loading order and magnitude and environmental exposure.

Enormous differences exist among research workers as to the best combination of these variables and the problem is further complicated due to the fact that research on fatigue are often restricted by practical limitations and the lack of full understanding of the nature, order and magnitude of the environmental loadings actually imposed on real structures.

However, despite the lack of consensus, it is generally accepted that tests under conditions of low stress magnitude and low cyclic frequencies are a more accurate simulation of reality.

At this stage, it should be appreciated that there, still, are considerable unknowns in this complex subject. It may, thus, be rational to perform rather simple tests with the use of efficient monitoring techniques to obtain some fundamental understanding of the mechanism of the phenomenon of corrosion fatigue before undertaking more elaborate testing particularly in relation to loading spectrum and configuration.

The strategy of the present research places more emphasis on the serviceability aspects of cyclically loaded reinforced concrete beams in corrosive environments under conditions more relevant to service life. The

factors dictating the choice of the experimental variables are detailed in Chapter 5 of this thesis.

1.5 Objectives and Scope.

Objectives.

In this investigation, various aspects of the fatigue behaviour of full scale reinforced concrete beams in corrosive environments were studied. The aim was, in general, to develop a better fundamental understanding of the corrosion fatigue phenomenon with particular emphasis on low-stress low-frequency loading conditions in an attempt to provide a more realistic assessment of the possible interaction between stress and corrosion which prevails in real-life structures.

The research comprised two stages. In the first stage a number of high amplitude loading tests were performed as a basis for the second stage of appreciably less severe conditions in terms of stress level.

Electrochemical measuring techniques were extensively employed in the latter stage and the factors affecting its accuracy in predicting the corrosion rates for large scale reinforced concrete specimens and the interpretation of the electrochemical results were thoroughly investigated.

Scope.

A total of 28 reinforced concrete beams were fatigue tested under various combinations of load level, environment and period of exposure in sodium chloride solution and in water. In addition, 7 other static tests were carried out and served as a controlling tests.

The research work is reported in this thesis through 13 chapters:

Chapter 2 presents some basic information on the phenomenon of fatigue with a literature review of the available data on this subject drawn from fatigue investigations in air.

Chapter 3 considers the electrochemical aspects of

corrosion of reinforced concrete and the theoretical and practical basis of corrosion rate measurement.

Chapter 4 reviews the available information on the corrosion fatigue of reinforced concrete and presents the current national code recommendations.

Chapter 5 explains the strategy of the research programme and the factor dictating the choice of the experimental details and the instrumentations.

Chapters 6 to 11 present the experimental results in logical order starting from endurance and structural behaviour to the corrosion rate measurements. Each chapter includes a discussion section which discusses the direct implementation of each different set of results.

Chapter 12 presents the general discussion chapter which links the whole results presented previously through the result chapters.

The findings and the final recommendations are presented in Chapter 13 which also includes proposals for future work.

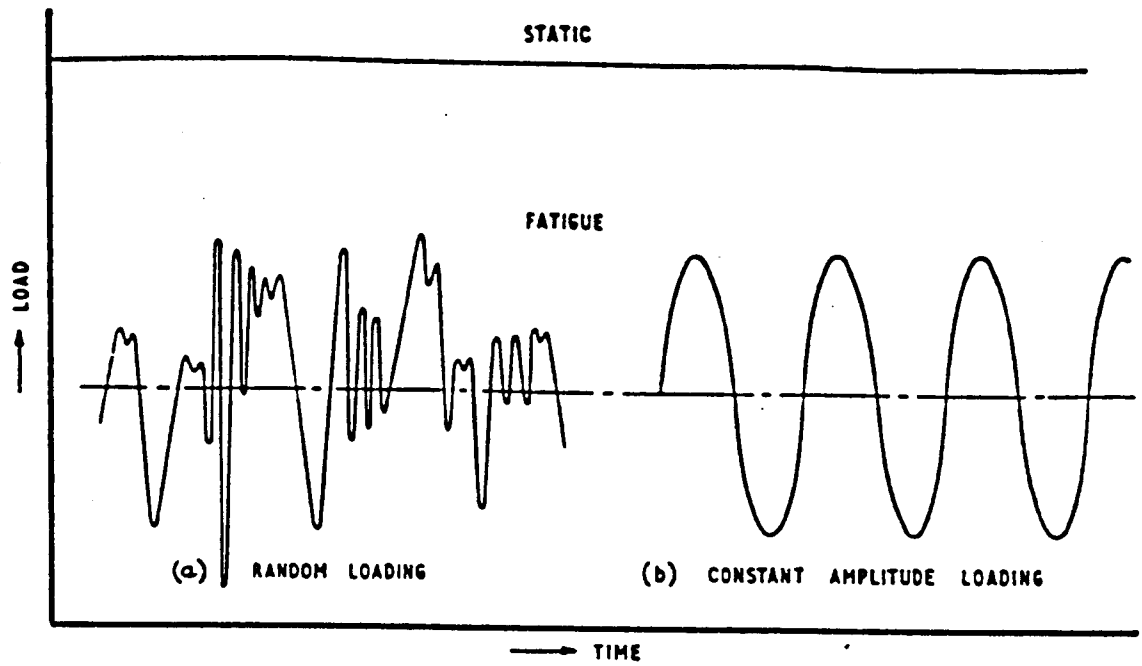

Figure (1-1): Static and fatigue loading conditions (Ref.17).

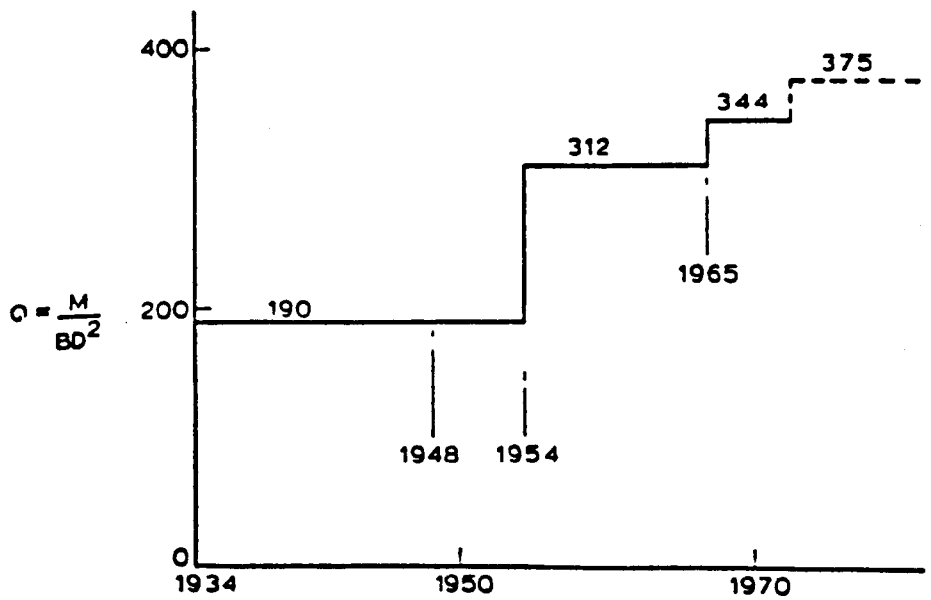

Figure (1-2): Increase in moment of resistance for a given cross section and material properties due to refind methods of design (Ref.29).

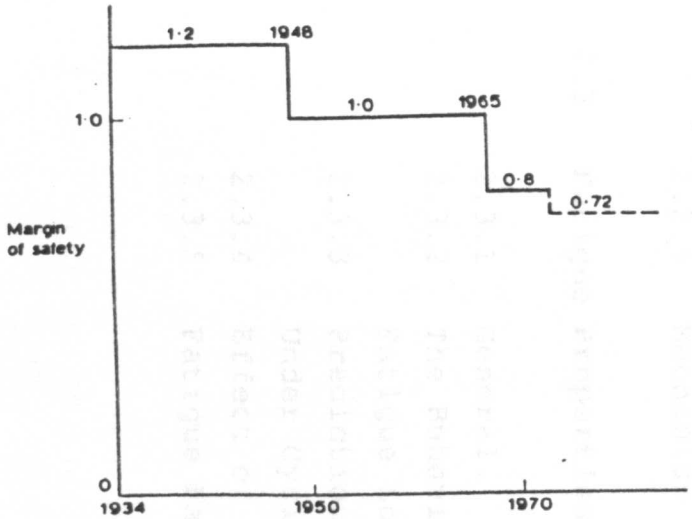

a) Reinforcement

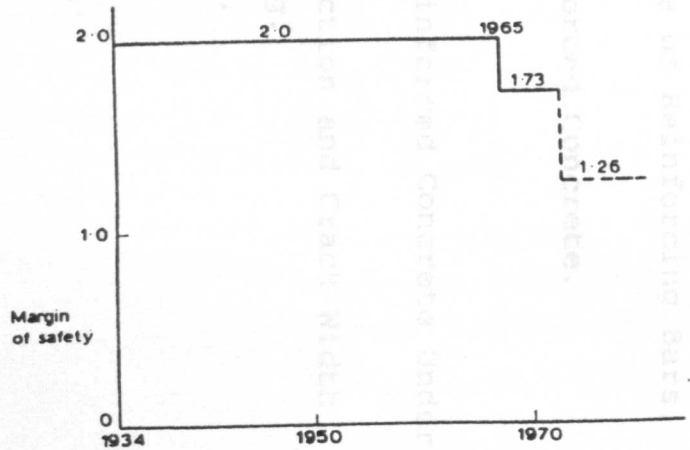

b) Concrete in bending

Figure (1-3): Decrease in margins of safety in British codes of practice (Ref.29).

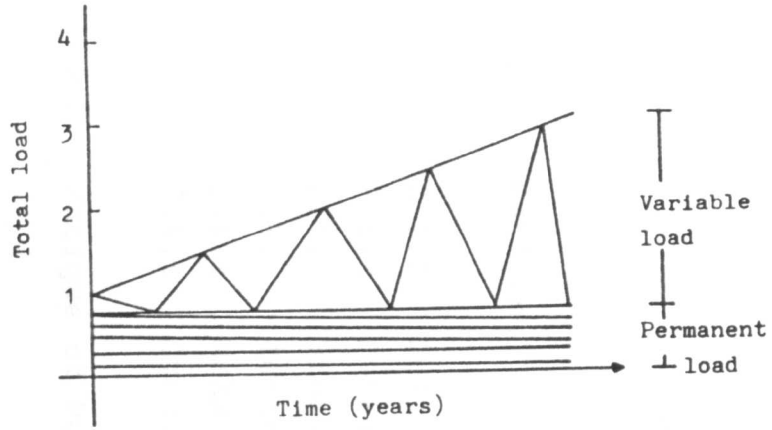

Figure (1-4): Increase in load carrying capacity due to refined methods of calculation and increase material strength (Ref.11).

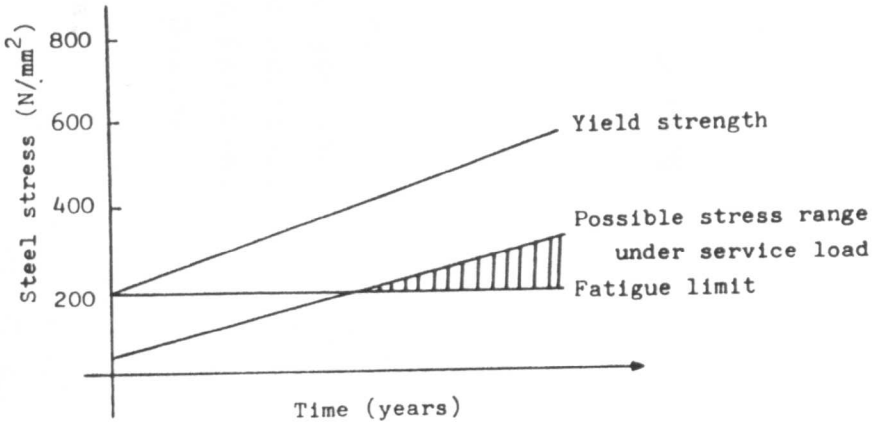

Figure (1-5): Increased risk of fatigue due to use of steel with higher yield strengths (Ref.11).

CHAPTER 2

FUNDAMENTALS OF FATIGUE

2.1 Fatigue.

2.1.1 Definition.
2.1.2 Fatique Nomenclature.
2.1.3 Presentation of Fatigue Data.
2.1.4 Testing Methods and Scatter.
2.1.5 Mehanism of Fatigue Failure.
2.1.6 Cumulative Fatigue Damage.

2.2 Fatigue of Reinforcing Bars.

2.2.1 General.
2.2.2 Fatigue Limit and S-N Curve.
2.2.3 Type of Test.
2.2.4 Factor Affecting Fatigue of Reinforcement.
2.2.5 Mechanism of Fatigue of Reinforcing Bars.

2.3 Fatigue Properties of Reinforced Concrete.

2.3.1 General.
2.3.2 The Behaviour of Reinforced Concrete Under Fatigue Loading.
2.3.3 Prediction of Deflection and Crack Width Under Cyclic Loading.
2.3.4 Effect of Frequency.
2.3.5 Fatigue Failure.

CHAPTER TWO

FUNDAMENTALS OF FATIGUE

2.1 Fatigue.

2.1.1 Definition.

Fatigue is a process[12,36] of progressive irreversible internal structural changes in a material subjected to repetitive stresses. These changes may be damaging and result in initiation and progressive growth of cracks and complete fracture if the stress repetitions are sufficiently large. Fatigue failure may be defined as the phenomenon that occurs after more than 100 repeated applications of variable stresses whose maximum values are less than the short term ultimate static strength, failure in less than 100 cycles of high level are referred to as low-cycle fatigue.

Corrosion fatigue is a generic term that is used to describe a special case of fatigue damage in which the fatigue process occurs in a corrosive environment. The deterioration process involves the joint effect of cyclic loads and environmental effects and can result in considerable reduction in fatigue strength in comparison with fatigue in an inert environment. The joint effect of these two factors is greater than the sum of their individual effects.

2.1.2 Fatigue Nomenclature.[17,16,37]

Stress cycle: The section of the stress-time function which is repeated periodically. When identical, i.e. the

case of constant-amplitude fatigue loading, the stress cycle may be defined by the stress components, the shape and the frequency i.e. the number of load repetitions per minute or second. Variable or random fatigue loading may be defined by blocks of stress or stress-time curves.

Constant amplitude fatigue loading: The fatigue loading in which the loads fluctuate between a prescribed constant minimum and maximum stress each cycle.

Variable or random fatigue loading: The fatigue loading in which the load fluctuate in a sequence of variable minimum and maximum stresses.

Fatigue life or endurance (N_F): The number of stress cycles at which fatigue failure occurs for a given loading condition.

Fatigue strength (S_N): The stress or the fraction of the static strength, the material can support repeatedly for a given number of cycles (N).

Fatigue limit (S_L): The stress level below which the fatigue life will be infinite.

Run out (N_r): The number of cycles at which test is discontinued.

Other nomenclature relating to the common characteristics of the stress or load cycles such as stress amplitude (S_a), stress range (S_r), maximum stress (S_{max}), minimum stress (S_{min}) and mean stress (S_m) are self-evident and are illustrated in Figure 2.1.

2.1.3 Presentation of Fatigue Data.

The main purpose of most fatigue tests is the experimental determination of the relation between endurance and the magnitude of the applied stress range for the specimens under consideration. However, a number of other significant factors are always involved and consideration of their effects is always necessary for correct interpretation of the test results.

Endurance results are, commonly, given in the form of table containing the various stress levels and observed fatigue lives as well as the run outs. It is recommended that all individual values be given in the tables. The use

of relative instead of absolute values of applied stresses is also recommended in tables, thus the ratio of the applied stresses S_a or the applied loads P_a to the ultimate or design static stresses S_u or loads P_u may be substituted for S_a or P_a as it facilitates comparison between specimens of different strength.

Graphical presentations in the form of curves and diagrams have frequently been used in conjunction with the tables so that the significance of the data could more clearly be understood. Many graphical methods have been proposed for various purposes, nevertheless, the most common ways of presentation have been in terms of an S/N diagram and more recently in terms of fracture mechanics concepts and serviceability behaviour.

S-N Curves:

The S-N or Wohler curves are usually plotted for a given constant minimum stress level S_{min} or a constant ratio between the minimum and maximum stresses (S_{max}/ S_{min}). In these curves the applied stress, either absolute or relative, is plotted along the ordinate and the number of cycles to failure (N) on the abscissa. In order to present conveniently both long and short endurance on the diagram, a logarithmic scale is commonly used for N. A linear stress scale is frequently used although logarithmic scales are sometimes used for these parameters. The reasons for not applying a linear plotting is the danger that the general tendency of the curve will lead the investigators to assume that a fatigue limit has been reached at a comparatively low value of N and also the difficulties in accommodating on the same diagram both small and large values of N. A common convention is to represent specimens unfailed at the completion of the test by an arrow extending beyond the test point.

The scatter[16,37] in fatigue results is often considerable. This inherent statistical nature of fatigue results can be accounted for, although not always practically possible, by applying probablistic procedures. For given loading conditions and numbers of cycles, the

probability of failure can be obtained by repeating the test several times. An example of the S-N curve for various probabilities of failure is shown in Figure 2-2. This type of curve is commonly referred to as S-N-P curve.

The influence[38] of the minimum stress level and the range of stress can be incorporated in a Goodman diagram (first introduced to concrete fatigue by Graf and Brenner in 1934)[18] or Smith diagram as shown in Figures 2.3 and 2.4 respectively.

These curves give the various stress combination for failure at a given number of cycles and can be combined with Wohler diagrams in one of the following ways:

$$\log_{10}N = x \frac{1 - \frac{S_{max}}{S_s}}{1 - \frac{S_{min}}{S_s}} \qquad \text{--- Goodman}$$

$$\log_{10}N = x \frac{1 - \frac{S_{max}}{S_s}}{1 - \frac{S_{min}}{S_s}} \qquad \text{--- Smith}$$

where x = a value for the gradient of the S-N curve
S_s = static strength

Fracture Mechanics and Serviceability.

Presentation of fatigue data in terms of fracture mechanics and serviceability behaviour including the change during fatigue loadings of strain, stress, deflection, crack growth rate etc. have been increasingly employed in recent investigations. This approach was absolutely necessary following the growing need for better understanding of the underlying principles which explain the macro and micro-structural changes responsible for

failure in fatigue and also due to the need for more realistic data pertaining to low stress-low cyclic frequency conditions in which case obtaining an S-N relationship is practically difficult as fatigue failure may not be attainable except after several millions of load applications. Information on the serviceability behaviour is particularly important in the field of plain and reinforced concrete where fatigue loading may not constitute an immediate hazard of failure but could cause loss of serviceability at early stages, which necessitate continuous monitoring of the operating conditions.

The rapid developments in the use and the interpretation of fatigue data are related to the development of the powers of observation, monitoring and analysis techniques in recent years.

2.1.4 Testing Methods and Scatter.

Testing Methods.

Fatigue tests are generally performed to provide specific information related to the performance of real structural components under given loading conditions expected to be encountered in actual service. In most cases, however, it is required that the test be designed in such a way that it does not only answer the specific questions that were put but will also allow generalisation of the results and contribute to the available body of knowledge. The development of fatigue testing from the simple to the present more complex testing has been associated with a number of basic problems and expanding design requirements, as outlined in Chapter 1, for which other mechanical tests, which are generally related to the static nature of the components, are unable to provide adequate information on the behaviour under repeated loads.

Fatigue tests can provide a better assessment of the fatigue behaviour at an accelerated rate, it also gives more confident prediction of the service life, probability of fatigue failure and information on the most prone

region in the system to fatigue so that more realistic precautionary measures can be undertaken before introduction of the element into service.

To obtain meaningful fatigue data, it is necessary to simulate as closely and as practically as possible the service loading experienced by components and structures. This implies the requirements of complicated sequences of stress amplitude (also called the spectrum of loading). Such tests are designated variable amplitude test and consists mainly of two categories:-
(1), cumulative damage test which composed of two or three stress levels only and, (2), the service simulating test which is a more elaborate pattern for simulation purposes. It should be appreciated, however, that realistic simulation for the time being is very difficult particularly in the field of reinforced concrete.

The more widely used amplitude sequence is the so-called constant amplitude test, in this test different specimens of the test series may be subjected to different stress amplitude but for each individual specimens the amplitude will be kept constant. This type of test may be classified into three categories.[16]

i. The routine test - where the applied stresses are chosen such that the specimens are expected to fail after a moderate number of cycles. The purpose of this test is to estimate the relation between load and life.

ii. Short life test - where the stress levels are situated above the yield stress and some of the specimens are expected to fail statically upon the application of the load. This test provides information on the fatigue behaviour under stresses leading to fatigue failure after small numbers of cycles.

iii. Long life test - where the stress levels are situated below or just above the fatigue limit and a proportion of the specimens do not fail after a pre-

assigned number of cycles. This test is conducted to determine the fatigue strength at a given number of cycles.

In the planning stage of a fatigue test programme, careful attention should be exercised in choosing the test variables which include:

1. Details of the test specimens.
2. Loading regime: broadly classified into bending, axial loading, torsion and combined stresses.
3. Cycle stress (or load, bending moment, torque) amplitude.
4. Cycles stress range.
5. The pattern of loading sequence.
6. Time of cycle i.e. frequency.
7. The test environment.

Nevertheless, expense and time are decisive factors in this kind of test and, hence, should be considered at an early stage. However, the relative importance of each factor mentioned above is directly related to the actual structural loading history and the type of information required.

Scatter.

Scatter in the experimental results is common in most physical test. However, the results of fatigue tests usually exhibit substantially larger scatter than static tests. This is mainly attributed to the fact that the behaviour of material under repeated load is dependent essentially on small-scale variables and thus the fatigue performance is sensitive to quite minor variations in the material structure, preparation and manufacturing process and the environmental conditions. As a result, larger number of specimens are required if the stress-endurance (S-N) relation ships are to be accurately established.

Different numbers of specimens have been proposed for the determination of this kind of relationship. Findley[39]

(quoted by Weibull[16]) suggested that at least ten specimens be tested for an S-N diagram but that a larger number would be desirable for more accurate conclusions. For this purpose he proposed 20 (preferably 50) specimens should be tested. However, it is common practice to test between fifteen and forty specimens with up to five or more at each stress level. It was stated that the limiting stresses of metal could be determined with a number of specimens which cannot be safely reduced below four even under the best circumstances. On the other hand, in the area of reinforced concrete where fatigue tests are exceptionally costly Taylor[12] proposed a maximum of five tests at any one stress level. Nevertheless, Weibull[16] indicated that although the number of specimens has a marked influence on the accuracy of the parameters computed for the observations, other factors may be of equal importance. In this respect the efficiency of a test series depends also on the choice of the stress level, the inherent scatter in the properties of the specimens used and the testing machine and (perhaps larger than commonly believed) the error in the applied nominal load. Therefore, a small number of specimens can to some extent be compensated by a more efficient design and control of the test conditions. Apparently, a similar conclusion has been drawn from investigations[40,41] on the fatigue properties of concrete which indicate the scatter in the number of cycles to failure can be fully explained from the scatter in the static strength.

Experimentally, the phenomenon of scatter can best be accounted for by applying probablistic procedures, also for a set of endurance results at a given stress level the median (the middle value) may be considered as a representative result for any particular stress level.

2.1.5 Mechanism of Fatigue Failure.

Fatigue deterioration involves the slow growth of cracks either pre-existing or initiated under the influence of the oscillating loads. Consequently the fatigue processes are often associated with points of

stress concentration in the structure.

Stress raisers[12] may be flaws inadvertently or inevitably present in the material structure. Stress concentration may occur at (1) Pre-existing flaws in metal (2) discontinuities in the geometry of the structure (3) sites of damage caused by the use of the structure (4) notches or corrosion pits.

The fatigue fracture of the structural material containing large flaws or crack is caused[42] by the growth of these defects during cyclic loading.

For unclad metals, two approaches have been successfully used to predict, model and describe the mechanism of fatigue. These are[43] (1) accumulation of cyclic strains for specimens with no flaws at the onset of fatigue loading (i.e. to predict crack initiation) (2) fracture mechanics concepts for predicting crack growth in specimens with initial flaws, notches and points of stress concentration.

The detailed mechanism of fatigue of unclad metal is considered beyond the scope of this study although it may be briefly referred to when considering the common aspects of fatigue failure in the following sections. However, for composite components such as reinforced or prestressed concrete structures where the various material elements involved may be susceptible to fatigue separately, the detailed mechanism of fatigue is far more complex and still incapable of physical modelling.

It is widely accepted[12,38] that in reinforced or prestressed concrete elements, fatigue in the concrete is normally less critical than fatigue in the reinforcing steel. However the fatigue mechanism of these elements is not solely dictated by the mechanism of the embedded reinforcing bars since the latter mechanism fails to take into account the complex interaction between concrete and the embedded reinforcement particularly:-

(1) Although the details and amount of reinforcement control, for a given loading condition, the pattern and the width of cracks in concrete these cracks constitute[11,13] effective stress raisers irrespective of

the state of the microstructure and geometry of the embedded reinforcement at these sites. In corrosive environment this effect is even more pronounced. As a result their is a very high statistical probability (almost 100%) of fatigue failure occurring by steel failure at locations of concrete cracks.

(2) As reinforcing bar lugs transmit[44] a large part of the bond stress to the concrete, only by testing concrete covered bars can forces be applied to the bar in the same way as these experienced by the steel in a reinforced concrete structure.

Similarly, the mechanism of fatigue of plain concrete can not be representative of the mechanism of the composite material. In other words, whichever constituent material properties (steel or concrete) controls the eventual fatigue failure of the composite structure, the resultant mechanism of fracture is unlikely to obey the individual mechanism of either of them.

For the vast majority of structure where the steel is the critical part from the standpoint of fatigue, observation of the detailed mechanism is, obviously, obscured by the concrete cover, consequently, important fracture mechanics parameters including the initiation and the rate of crack growth are usually immeasurable and can only be speculated on or extrapolated from the study of the fracture surfaces retrieved upon fatigue failure. Meanwhile, cracks on the concrete surface may, at the best of the cases, give a rough indication as to the expected state of cracking of the embedded reinforcement.

The mechanism of fatigue of bare steel reinforcement will be discussed in light of the available information in the following section (Section 2.2). However, it is generally accepted, regardless of the type of structure, that the fatigue process involves two stages: an initiation stage in which a small local point of failure develops to a sufficient size to form the start of a growing fatigue crack and a propagation stage during which the cracks grow to such extent that failure occurs.

Depending on the loading condition variable periods of time are required for the complete process.

2.1.6 Cumulative Fatigue Damage.

Concrete structures are often subjected to randomly varying loads, but the accumulation of fatigue damage due to random loading, is still unknown and no cumulative fatigue damage hypothesis for concrete has been proposed.[40] The design of concrete structures subjected to a spectrum of repeated loads is frequently based on the Miner hypothesis,[45] which establishes a relation between the amount of damage and the results of constant-amplitude tests on the assumption that the contribution to the fatigue damage of a single stress cycle ranging from a minimum stress S_{min} to maximum stress S_{max} has a magnitude of $1/N_i$ where N_i is the number of cycles which will cause fatigue failure in a constant amplitude test at the same level of stress. That is the Miner's hypothesis assumes that there is a linear accumulation of damage due to successive loading cycles. Accordingly the damage contribution 'M' due to a number (c) stress cycles is the sum of the damage contribution of the individual cycles and given by the formula

$$M = \sum_{i=1}^{c} \frac{1}{N_i}$$

Failure occurs when the total damage M becomes equal to unity. The application of Miner's hypothesis (sometimes called Palmgren-Miner hypothesis) to concrete was first examined by Hilsdorf and Kesler[46] in 1966 using two different load levels applied in different sequences. In their tests systematic deviation from this rule was observed and resulted in both unsafe and conservative prediction of the fatigue life. Further, this hypothesis was unable to account for certain effects of a multistage

loading history[40,46] such as the loading sequences effects and the rest period. It was found that a high load early in the loading history gives more damage (M>1) than a high load later in the loading sequence (M<1).

Very little research has been done on the validity of Miners hypothesis on the non-constant-amplitude loading (random) on concrete elements. The limited data available are conflicting although it is generally accepted that the variable amplitude tests are more damaging than would be expected from constant-amplitude tests.[38,40,41]

2.2 Fatigue of Reinforcing Bars.

2.2.1 General.

Fatigue of reinforcing bars has not been the dominating requirement in their application as a reinforcement in the concrete structures. The rib patterns are designed to give good pull-out strength and the acceptance of reinforcement deliveries is mainly based on the minimum characteristic strength. However, following increased concern about the problem of fatigue, the fatigue properties of reinforcing bars have been thoroughly researched and a considerable number of investigations have been reported. The current state-of-the-art is excellently reviewed in References 11,13,36.

In reviewing the available data, it is clear that separate researches have been largely[18] unco-ordinated and have concentrated on several different factors which can vary considerably between different types of reinforcement. The size and variety of the available data raises an obvious need for data manipulation and compilation systems. Some successful attempts towards this have been made and are still under development by the British Steel corporation.[47]

2.2.2 Fatigue Limit and S-N Curve.

The relationship between stress range and fatigue life (N) are often determined by a series of fatigue tests

on bars which were either embedded in concrete or unclad in air.

Most of the S-N curves show, Figure 2.5, a transition from steeper slope referred to as the finite life region which is characterised by the fatigue life at a given stress level and flatter slope in the vicinity[11,13,36] of one to ten million cycles and referred to as the long-life region characterised by the fatigue limit. It is noted that many of the S-N curves in the latter region are conjectural, there is, however, a clear indication of a fatigue limit which varies with stress ratio such that, for a given stress range, for higher stress ratio (S_{min}/S_{max}) the value of fatigue limit is reduced. Consequently the transition point (from steep to flat) extends to longer endurances. Snowdon[48] indicated that there may well exist a critical range of stress below which the fatigue life is very high (over 10^7 cycles). For hot rolled bar this range was about 190 N/mm^2. Other references stated that no fatigue failures have occurred for straight deformed bars at a stress range below 140 N/mm^2. Current thinking,[13,47,49] nevertheless, suggests that although the S-N curves may have very low slopes at endurances greater than 10^6 cycles, failure can occur at lives in excess of 10^8 cycles so that a fatigue limit can not be assumed unless verified experimentally.

2.2.3 Type of Test.

There are two types of fatigue testing frequently used to evaluate the fatigue properties of reinforcing steel:

Axial tests: which are usually carried out on unclad bars. This test permits the application of more a complex loading spectrum and can be conducted at relatively higher frequencies (3-10 Hz as recommended by RILEM-FIP-CEB).[13] It is, therefore, inexpensive in terms of machine occupancy and less time consuming, further, the applied loads can be calculated unambiguously. The major criticism to this type of testing is that it is not representative of the complex force transfer between concrete and

embedded reinforcement.

Bending tests on reinforced concrete beams: Fatigue tests in flexure are usually made on concrete beams having a single reinforcement bar, tests on beams with more complex reinforcement configuration are usually associated with the general behaviour of the composite material rather than the reinforcement alone. These kind of tests are commonly conducted at 3-5 Hz although use of 6.7 Hz cyclic frequency has been reported.

Bending tests usually exhibit wider band of scatter in both directions than in axial tests.

2.2.4 Factors Affecting Fatigue of Reinforcement.

The fatigue strength of reinforcing bars depends upon several factors including the chemical composition, microstructure inclusions and others. However, the variables related to the physical characteristics and the testing conditions are of greater importance, these include.

Embedment in Concrete.

There are contradictions in the literature as to whether a bar has the same fatigue strength when tested in air as when embedded in a concrete beam. Jhamb[85] et al observed that both finite and long life regions of the S-N curve for beams are higher than those for tests in air, Figure 2.6, with a reduction of 141 N/mm^2 in the fatigue limit. Increases in fatigue strength due to embedment in concrete of 10%[13] and 20%[14,50] have also been reported. The opposite conclusion, however, was reached in other investigations.[36]

The observed discrepancy in the test results may be attributed to the statistical balance between positive and negative effects of embedment on the probability of failure. Bending tests[36,13] would be expected to have longer endurances because highest stresses are restricted to the parts of the bar in the vicinities of cracks in the

concrete, this gives a purely statistical effect in that the likelihood of these locations coinciding with the worst defects in the bar is low. Meanwhile due to the transfer of forces between the concrete and the reinforcement the ribs act as stress raisers and so add to the probability of failure. In contrast, axial tests subjected the bar to uniform stress so that fracture can be initiated from the worst defects.

For design purposes, however, it has been suggested that the fatigue properties of reinforcement should be assessed from axial tests as the beneficial effect of embedment in concrete may vary in different structures.

Steel Stress Level.

Minimum stress level influences the fatigue strength to the extent approximately indicated by a modified Goodman diagram with a straight line envelope. The relationship between the mean and the range of stress has been assumed to be straight line or parabola, the effect of increasing the mean stress is to reduce the allowable stress range for a given number of cycles to failure. It has been found, however, that the stress range is the dominating parameter which controls the fatigue strength and thus it is more convenient to consider fatigue strength in relation to it.

Type of Steel and Manufacturing Process.

Jhamb[55] et al fatigue tested unclad American Grade 40 and 60 deformed steel bars and found that fatigue strength is insensitive to the grade of steel. Contrary to this conclusion, they observed that fatigue strength of as-rolled plain bars increased with an increase in grade of steel. Statistical analysis showed that the effect of stress concentration is higher for higher grade bars, thus, although the fatigue strength of the metal improved with an increase in grade this was offset by greater susceptibility to stress concentrations. Other investigators indicated that above 420 N/mm^2

characteristic yield strength there is very little improvement in fatigue strength.

On the other hand, cold working of reinforced bars, although it improves the tensile strength of deformed hot-rolled bars, was found to reduce the fatigue strength of the embedded bars. Hetherington[44] attributed this observation to three factors which act simultaneously to reduce the crack initiation phase:-

1. Cold working concentrates dislocations at the metal grain boundaries and, thus, increases the size and density of stress raisers.

2. The process imparts residual stresses which are generally tensile.

3. Twisting of the bars aligns diagonally those inclusions from the bar rolling process that are normally longitudinal and possess lower potential to act as stress raisers.

Bar Geometry.

Fatigue strength is considerably influenced by the severity of the surface deformation of the bars. Although they have good bond properties, deformed bars have fatigue strengths which are lower than those of plain bars because the deformation involves stress concentration at the base of the ribs or at points of intersection with other deformation, these serve as crack initiation site, typically in the range of 1.5 to 2.0[11,13,52] for normally shaped ribs, and thus reduces the crack initiation phase. Transerve ribs at right angles to the axis of the bar were found to have the most serious effect.[48] Fatigue strength is also influenced by the height and the root radius of the transverse ribs.

The orientation[11] of the longitudinal ribs of the bars could also have a significant effect. It was found that for ribs in the vertical plane, the fatigue strength can be as much as 40% lower than when placed in a

horizontal plane.

On the other hand, experiments[13,53] confirmed that reinforcement produced using worn rolls, has better fatigue strength, since new rolls give sharper base radii to the deformation and hence cause greater stress concentration factors.

The effects of the type of deformation are difficult to assess quantitively because other variables such as chemical composition, method of manufacturing etc. also influence the fatigue strength.

Bar Diameter.

It is commonly appreciated that fatigue strength decreases with an increase in bar diameter. This effect is relatively small for plain bars. Rotating bending on bars of diameter 12.5 to 38 mm showed a maximum reduction in fatigue life of 5%. For deformed bars this effect is more pronounced, Tilly reported[14] a reduction in 2 x 10^7 cycles fatigue strength of 30% for beams with 40 mm Torbar as compared with beams with 16 mm torbar, Figure 2.7.

The explanation[11,13,51] given for size effect is that it is partly due to the statistical size effect, as bigger section implies greater probability of containing large flaws, bars of smaller diameter can be more effectively worked, and partly due to increase of grain size with diameter which facilitates the grain boundary slip and hence earlier crack initiation.

Surface Condition.

Under this heading notches, decarburisation and corrosion may be considered.

Bannister[56] carried out fatigue tests on beams with notched-ductile steel (hot-rolled) at 2 Hz cyclic frequency and observed that previous damage has no effect at stress ranges below a limited value, the limited value was about two thirds of specified characteristic strength. Jhamb et al[55] pointed out that ordinary rust and mill scale did not influence the fatigue strength of bars.

Decarburisation[11] has the same effect as notches, the surface of lower carbons content is weaker than the rest of the material and thus fatigue cracks can be initiated at these positions at lower stresses. In one investigation[55] it was found that decarburisation can produce an average value of reduction factor of 1.41 in fatigue strength.

The interaction of corrosion and fatigue loading can have serious consequences, on the properties of reinforcing steel. This aspect, however, will be discussed in detail later in this thesis.

Welding.

The effect of welding is important in welded wire fabric, bar mats and in tack welding of stirrups. Welding may considerably reduce the fatigue performance as compared with weld-free bars.

There have been several investigations on the effect of welding. Burton[54] et al indicated the substantial effect of tack welding of stirrups on fatigue life compared to bars having tied stirrups, a reduction of 75% for both intermediate grade and high strength steel has been observed.

Snowdon[48] reported results of stepped fatigue tests on reinforced concrete beams which showed reduction in fatigue life of 25-60% when using stirrups lightly tack-welded to main bars and failure always occurred at welds.

Tilly[14] also observed that butt welded bars exhibited substantially weaker fatigue performance than continuous bars. It is generally recognised that the effect of welding dominates only when it causes greater stress concentrations than the bar deformation.[11] It is also affected by the statistical probability of weld points coinciding with concrete cracks. Consequently, welded joints can have better fatigue strength[13,50] when tested in concrete beams than in air although the strength is usually lower than for continuous bars.

2.2.5 Mechanism of Fatigue of Reinforcing Bars.

The process of fatigue can be divided into two stages, namely a stage of crack initiation and a stage of crack propagation. The delineation between these two stages, however, is not always clear in terms of specifying a crack size. It can often be quite arbitrary depending on the opinion of the investigator. Unfortunately few studies on the fatigue mechanism of reinforcing steel in general and those embedded in concrete in particular are known as compared to numerous experimental studies on the fatigue process of metal. The following summarises the current physical understanding of this phenomenon.

Crack Initiation.

Some models,[12] especially directed to pure and flaw-free metals, have described this stage as being associated with slip planes from the tension and compression halves of the stress cycles producing an irregular surface profile on the metal leading to the formation of microcracking. In this stage small points of failure develop to sufficient size to form the start of growing fatigue cracks. In commercial metals, cracks usually develop from initial flaws, including non-metallic inclusions, which causes stress raisers. These cracks begin at the surface when they have an observed length greater than 25μm. The growth of such embryo cracks will not continue if the cyclic stress level is not sufficiently large. Fractographic examination indicates that fatigue under axial loading tends to initiate at the worst surface flaw whereas the range of initiation sites in bending tests is restricted to the vicinity of cracks in concrete.

Fatigue tests[28] on concrete-clad 32 mm reinforcing Torbar have shown different expectancies of the initiation of a fatigue crack in the bars at the locations of concrete cracks. For high stress it was found that 8 out of 10 concrete cracks may be expected to produce fatigue

cracks in the bar, while at lower stress range the ratio decreased to only 5 out of 10.

Manfred et al[58] fatigue tested structural welded steel beams and noted that 80 per cent of the cracks had originated from porosity caused by entrapment of gas, these cavities were completely inside the weld.

Local corrosion damage (e.g. pitting) arising through the ingress of corrosive substances and oxygen to the steel reinforcement is also likely to create initiation sites[12,13,33] for fatigue cracks, thus, superseding other mechanical factors, e.g. rib intersections.

Propagation Stage.

In this stage the surface nucleated microcracks grow at an increasing rate until the cross sectional area of the component is so reduced that it can not support the applied load and structural failure eventually occurs. The propagation phase always shows an initial period of growth, as shown in Figure 2.8, continuing exponentially to fracture. Therefore for most of the life of the component the crack length is small. Phase I of the propagation is often considered an extension of the initial stage because of its microscopic nature. Crack growth in this stage often occurs by the progressive development and linking up of flaws along the slip band or grain boundaries at about 45 degrees to the tensile stress axis.[60] The second propagation stage of crack growth has a different surface characteristic of regular distinctive striations Figure 2.9. It is usual to assume in fatigue tests that there is one-to-one relationship between striations and number of fatigue cycles which allows an estimate to be made of the rate of growth although this can be inaccurate for high levels of mean stress.

In 1963[61] Paris developed a law that describes the growth of stage II fatigue cracks by relating the crack growth rates da/dN to the stress intensity factor range ΔK in the form:

$$\frac{da}{dN} = c(\Delta K)^m$$

where a = is the crack length, N = the number of stress cycles, c = a factor that depends on the average stress level, K = the stress concentration factor, m = the material factor.

On the assumption that the crack initiation phase occupies a small part of the fatigue life, it has been suggested that the slope of the logarithmic S-N curve must be the same as the exponent in the Paris low. However, researches indicate that there can be a substantial crack initiation phase being dependent on the stress range and environmental conditions. That is, as the applied stress range decreases the initiation time increases, whereas the effect of a corrosive environment is to reduce the initiation phase. Further, a longer propagation stage produces a higher statistical probability that several fatigue cracks will develop before any individual crack leads to rupture.

It is generally recognised that embedment in concrete brings further new complications due to the fact that concrete is in macro-scale a heterogeneous material. Little work using the fracture mechanics approach has been undertaken on reinforcing steel and the technique becomes even more difficult in practice to apply to concrete-coated steel bar.

Salah eldin et al[28] fatigue tested 5 samples cut from 32 mm Torbars with stress ratio R between 0.125 and 0.5 and found that fatigue cracks growth in Tor bar steel may be estimate by the following equations.

$$da/dN = 3.83 \times 10^{-29} (\Delta K)^{20.86} \quad \text{for } \Delta K < 9 \text{ MNm}^{-3/2}$$

$$da/dN = 3.16 \times 10^{-12} (\Delta K)^{3.14} \quad \text{for } \Delta K > 9 \text{ MNm}^{-3/2}$$

Rupture.

Rupture occurs when the fatigue crack grows to such a stage that the remaining cross-sectional area can no longer support the applied load. Examination[49] of the fracture surfaces reveals that straight fronted fractures are always associated with short lives and high ranges of stress, partially curved fractures with medium lives and stress ranges and circular fronted fractures with long lives and low ranges of stresses.

Salah Eldin et al[28] compared the tensile strength and the ductility of reinforcing bars of different size cracked by fatigue loading with identical unloaded bars. They found that the transition from elastic to plastic bulk behaviour appeared to be a little pronounced in the case of fatigue cracked bars but no change was observed in the value of 0.2% proof strength. On the other hand the tensile strength was reduced by an amount which was dependent on crack size. However, the most pronounced effect of fatigue damage was that observed on ductility. The ductility of bars containing fatigue cracks with a ratio of crack depth to bar diameter a/D = 0.05 was found to be equal to 70% of the ductility of the fresh un-loaded bar. The ductility was negligible at a/D = 0.3.

2.3 Fatigue Properties of Reinforced Concrete.

2.3.1 General.

The fatigue properties of reinforced concrete structures are directly related to the fatigue properties of their constituents; namely, steel and concrete.[11,62] Structural collapse will occur when the weakest one fails, thus, for under-reinforced members failure almost certainly occurs in bending due to failure in the reinforcing bars. In the case of over-reinforced members the stress conditions are more complicated and failure may occur in compression, shear or bond. It is generally recognised, however, that fatigue in concrete is normally less critical than in reinforcing steel.

Fatigue fracture of reinforced concrete is characterised[36,63] by considerably larger strain and a greater degree of microcracking as compared to fracture under static. A large number of studies have been carried out to determine the fatigue strength of reinforced concrete beams. Recently, however, more emphasis has been placed on the serviceability aspects i.e. the structural change before the point of failure. Mostly restricted to tests in air, the common features of these tests have been the observation of variable degrees of change sometimes considerable, in concrete and steel strains, deflection and crack width and the reduction in stiffness. These effects will be discussed in the following section.

2.3.2 The Behaviour of Reinforced Concrete Under Fatigue Loading.

Experimental investigations on the serviceability behaviour of reinforced concrete sustaining cyclic loading have generally indicated an increase in the total deformation, the precise nature,[64] however, of such increase is not known and the methods to predict these deformations accurately are not available.

Jagdish[65] reported an increase of 6-7% in the stress of the tension steel at crack locations in the maximum bending moment zone. In the same zone, the maximum bond stress between cracks dropped about the same percentage.

Hetherington[44] noted an increase in crack width of approx. 100% for beams containing cold-worked bar and 50% for beams with hot rolled bars after approx. 1 million cycles.

The same observations were also reported by Bishara[66] and Bennett.[67] Variable degrees of increase in deflection and crack width due to cyclic loading were reported by different authors.[14,56,68]

Lovegrove et al[69] observed an increase in the deflection, the curvature and the maximum crack width of rectangular reinforced concrete beams of different cross sections and steel area subjected to cyclic loading at a frequency of 1 Hz. The long term cyclic deflection and average curvature were higher than their initial values by

a maximum of 35%, 57% and 80% at 10^6, 10^7 and 10^8 load cycles respectively, the corresponding increase in max crack width were 47.5%, 56% and 60.3%. They also observed that the increase in the deflection is slightly higher at the maximum load than at the minimum load which indicates a slight decrease in the rigidity of the beam with a number of load repetitions.

Similarly, in step-loading tests at the Building Research Station, Snowdon[48] found that deflection and crack width increased by 20 to 25 percent in the early stages on tests. The effect was not cumulative under continuing fatigue loading and was proportional to the stress on the steel.

These observations, of increased deformation due to cyclic loading, are not particularly confined to reinforced concrete beams, Ass Jakobsen et al[70] investigated the behaviour of reinforced concrete columns subjected to fatigue loading and observed an increase of deflection after 1 million load cycles between 40-60% of the deflection in the first load cycles. More over Bertero et al[71] examined the behaviour of rectangular portal reinforced concrete frames with fixed-based columns subjected to repeated reversible overloads. They found considerable reduction in bond strength around the critical sections of the frame and that the rate of reduction was rapid for the first 10 cycles and then decreased as the number of cycles increased. After 100 cycles practically all bond resistance had disappeared. Reduction in stiffness was also noted.

In other investigations, fatigue loading was found to produce an increase in the strains of the concrete in the compression zone with a subsequent decrease in the secant modulus of elasticity.

Finally, it can be noted that, regardless of the type of the structural element, the total damage due to fatigue loading usually involves two stages: the initial stage which is characterized by a rapid deterioration process and the semi-stable stage where the rate of change is relatively small. The life proportion occupied[14] by each stage is dependent on the loading level and the testing

condition. In most reported results, however, the dramatic changes occur during the first 1/4 of the fatigue life.

2.3.3 Mechanism of Deformation of Reinforced Concrete Under Fatigue Loading.

Ruiz et al[25] suggested that the deformations observed in reinforced concrete elements subjected to repeated loading can be attributed to the interaction between destruction of bond and progressive cracking in the tension zone. The fact that tensile strains are always greater, two or three times, than those measured in the compression zone is a strong indication that these deformations are actually originated in the tension zone. Thus if the applied repeated load is sufficiently large to form cracks, cracks will form at points of stress concentration in the maximum bending moment zone. The stress distribution in a segment of a bar located between two tension cracks may be considered as shown in Figure 2.10a, stress in the bar is a maximum at the faces of the crack reducing to a minimum about half way between the cracks. The non-uniform distribution along the bar is caused by the gradual transfer of load from steel to concrete by bond, the bond stress, being proportional to the steel stresses, is a maximum at the face of the crack decreasing to zero near the centre of the segment. With the development of cracks during the consecutive cycles the bond transfer near the faces of the crack and along the crack width will be destroyed, as a result steel stresses at these regions will be increased as shown in Figure 2.10b. During the initial stage of loading, in particular, the deterioration of bond strength can be facilitated[65] by the residual stresses in the tension reinforcement upon un-loading which create bond stresses of opposite sign to those existing under load. This effect decreases with increased repetition of load. Further it is likely that secondary internal cracks develop between the principal cracks which produce a new local peak in steel stresses, Figure 2.10c.

The end result of the progressive deterioration of

bond is to produce high and gradually more uniform steel stresses between the cracks without necessarily being accompanied by changes at the principal cracks[25] or proportional increases in the deflection of the element[66].

As the incremental deformations with repeated loads appear to be caused by destruction of bond, it can be expected that these deformations will increase as the available bond strength decreases. It seems rational thus to envisage the importance of bar type in terms of deformation (with due concern to other effect of deformations stated earlier) as well as the severity of loading conditions since, for example, long regions of high constant moment will lead to more destruction of bond.

There are, however, other interactive deterioration processes taking place which add to the total observed deformation.

Cyclic loading may result in an increase in crack height particularly in the zone of high bending moment. This in turn eliminates[66] the possible existing contribution of concrete below the neutral axis to the tensile resistance of the section. Accordingly, it was observed that the increase in the ratio between the cyclic deflection at a given number of cycles and the initial (static) deflection is higher for beams in which the steel stress is low as the contribution of tension zone-concrete becomes substantial for beams carrying relatively less load.

In addition, cyclic loading was found to produce additional compressive strains in the compression zone of the beam similar to creep[62,68,72,73] under sustained load but greater in magnitude this means that, similar to static creep, cyclic creep of the concrete compression zone can produce an increase in the crack width and deflection as well as tensile stresses in the tension steel. This effect, however, is not always clear particularly in the case of high applied load and some investigators[25] have in fact expressed the opinion that creep effects have little influence on the incremental deformation particularly under conditions of short-term

application and indicated that the major damage due to fatigue loading is directly related to the behaviour of the tension zone.

On the other hand, the effect of reinforcement in the compression zone is to reduce the neutral axis depth and hence increase the height of the internal resisting couple which may result in a slightly lower tensile steel stress and consequently smaller crack width. Higher compression to tension steel results in smaller increase in crack height during cyclic loading.

2.3.4 Prediction of Deflection and Crack Width Under Cyclic Loading.

Analytical and empirical methods have been proposed to predict the increase in deflection and crack width of reinforced concrete beams under fatigue loading.

Based on fatigue tests of beams with sustained load at 1 Hz cyclic frequency, Spark et al[68] have indicated that long term deflection of reinforced concrete elements can be predicted with acceptable accuracy using available methods of creep analysis provided it is assumed that any fluctuating component of the loading acts as if it were a sustained load at the maximum level of the fluctuations. They also indicated that the assumption that only the sustained component of the load contributes to the creep of a beam leads to a considerable under-estimation of the true long-term deflections.

Lovegrove et al[69] proposed empirical expressions for prediction of cyclic deflection, curvature and crack width, these are:

$$\text{Deflection} \quad \Delta_n = 0.225\ \Delta_o \log n$$
$$\text{Curvature} \quad K_n = 0.225\ K_o \log n$$
$$\text{Crack width} \quad W_n = W_o\ (0.382-0.0227 \log n) \log n$$

where Δ_o, K_o, W_o are the initial values of deflection, curvature, crack width which may be calculated using one of the existing methods for deformations under short term application of load.

Comparison between the predicted values of deflection and the maximum crack widths using these equations and the experimentally measured values of other earlier investigations generally shows reasonable agreement.

Balagurn et al[72] adopted an apparently more promising approach which is based on the fatigue properties of the constituent materials. They proposed a step by step analytical method to predict the increase in deflection and crack width in which they introduced the concept of cyclic parameters such as the cyclic modules of elasticity (E_N), the cyclic modules of rupture (F_N), the cyclic creep and the corresponding applied cyclic moment ($M_{cr,N}$) and the cyclic moment of inertia $I_{cr,N}$. The effect of concrete creep was accounted for by the term E_N and $I_{cr,N}$ whereas the effect of the progressive reduction in the tensile contribution of concrete was included in the term $M_{cr,N}$.

The aforementioned methods, however, are of limited applicability as they are generally based on one set of data for particular testing conditions and may not be capable of describing other conditions with substantially different variables.

2.3.5 Effect of Cyclic Frequency.

The effect of test frequency on the fatigue strength is a matter of conflicting views and is, apparently, one of the less investigated subjects. In relative terms, however, this effect is more clearly defined for plain concrete than for reinforced concrete. For plain concrete, there is a substantial agreement that this effect is usually considered to have little influence on fatigue strength, at least up to 20 Hz.[11,76,77]

For fatigue tests on reinforced concrete, Tilly[13] suggested that cyclic frequencies are limited by the high range of deflection and the necessity to avoid local heating due to friction at cracks in the concrete. It has been pointed out (Section 2.2.3) that these tests are usually carried out at 3-5 Hz. Recent trends, nevertheless, place more emphasis on substantially lower

frequencies (0.1 - 0.2 Hz) particularly when information on the environment effects are required, for which the test frequency is of greater importance since for a given number of cycles the exposure of the reinforcement to the aggressive environment is longer for slower frequencies. This will be discussed later in Chapter 4.

Hockenhull[78] (quoted by Patterson)[59] reported a number of sources indicating a reduction in fatigue strength at lower frequencies, whereas research at Glasgow University[79] indicated that frequency in the range from 0.17 to 5 Hz has no noticeable effect on the endurance in air. The same conclusion was also reported by Hawkins[31] who observed that the behaviour and the fatigue life of a reinforced concrete beam loaded in air at 8 Hz were almost identical with those of the duplicate specimens loaded at 4 Hz.

On the other hand, Balagurn et al[72] did not show much consideration of the effect of frequency in their analytical approach to structural changes during fatigue loading. By relating frequency to time, they suggested the applicability of expressions based on fatigue tests at 10 Hz to a wider range of frequencies. Lovegrove[69] et al also ignored this effect in their empirical formula for the prediction of deflection and crack width under cyclic loading.

In the absence of investigations devoted specifically to the effect of frequency, particularly those relating this effect to the stress range, the general trend seems to favour the opinion which assumes little or no influence on fatigue strength.

This assumption permits the conduct of fatigue tests in air at conveniently higher frequencies.

2.3.6 Fatigue Failure.

The fatigue strength of reinforced concrete elements is a complicated subject which is influenced by many factors.

Variables[74,75,76,77] such as concrete strength, percentage of compression and tensile reinforcement, span/

depth ratio, aggregate size and shape, moisture condition, maximum value of repeated loading, the range of loading (stress), rate of loading and others may have significant effects on the final results.

The commonest form of failure is by tensile fracture of the reinforcement. Compression failure of the concrete is restricted to members with a large percentage of tension reinforcement.

However, other less predictable types of failure such as bond and shear failure may also occur under fatigue loading even though duplicate beams fail by other mechanism (e.g. tensile fracture) under static load.[11]

In the following the principal modes of fatigue failure are outlined.

Fatigue Fracture of the Longitudinal Tensile Reinforcement.

This type of failure usually occurs at the maximum bending moment zone either with or without diagonal tension cracking, Figure 2.11a,b and often associated with points of stress concentration in the bar. Beams critical[77] in longitudinal reinforcement seems to have a fatigue strength of 54-70% of static ultimate strength for 10^6 cycles.

Destruction of the Concrete-Compression Zone.

In this, the compression zone of the beam is destroyed by crushing, Figure 2.11c. Failure[74] occurs due to the development of tensile diagonal cracking to such extent that the concrete at the top end of the crack becomes too small to resist the applied load. Special case of this failure is the so-called "Diagonal Cracking Failure" in which the concrete failed by compression as soon as the diagonal cracks form, Figure 2.11d, i.e. the number of cycles to failure is the same as that for cracking. In this type of failure[80] the stress in the tensile reinforcement can be lower, equal to or higher than the yield stress. The process, however, does not

involve fracture of either the main bars or the shear stirrups.

For beams critical in compression, Le camus[81] (quoted by Nordby[18]) obtained a fatigue strength for 10^6 cycles of about 60% of the static ultimate strength. While Lambotte[82] (quoted by Westerberg[11]) found that over-reinforced beams failing due to fatigue of the compression zone could sustain 70% of their static ultimate load for 10^7 cycles.

Failure in Bond.

Bond failure implies that the adhesion between the reinforcement and the surrounding concrete is reduced over a certain length which results in progressive reduction in force transmission and relative slip between steel and concrete. Nordby[18] indicated that results on bond fatigue are extremely erratic and failures at as little as 50% of the flexural capacity are possible after several million cycles.

Verna et al[83] fatigue tested reinforced concrete beams with a single 19 mm bar at 7 Hz and stated that bond failure under fatigue loading is not predictable. Their results indicated that for 56,000 cycles the bond fatigue strength dropped to 55% of the static strength.

Barnoff[84] (quoted by Hawkins)[31] estimated bond fatigue strength for 10^6 cycles as 65% of the static strength. He concluded, however, that fatigue failure in bond is not likely to be critical in practice.

Hawkins[31] observed that bond failures were triggered by inclined cracks that caused splitting along the line of the longitudinal reinforcement and concluded that this type of failure is probably strongly dependent on shear effects. He also noted that bond failure is not significantly influenced by either the embedment length, the height of the deformation on the bar or the rate of loading (between 4-8 Hz). Hawkins investigation indicated that bond fatigue strengths, being partially dependent on bar diameter are likely at 10^6 cycles to be of the order of 40-60 percent of the static bond strength.

Failure in Shear.

Fatigue failure in shear starts with diagonal cracks in the shear span. Cracking then proceeds towards the region of the maximum moment as additional load cycles are applied,[74,75] and destruction of the compression zone normally occurs at the top of major diagonal crack Figure 2.11e accompanied by fracture of one or more stirrups. It was found, however, that stirrups fractures were not always associated with external warning of such fracture.

The probability of fatigue failure in shear increases as the ratio of the shear span to effective depth (a/d) increases, simultaneous fatigue failure with inclined cracking was reported[31] for a beam with a/d ratio of 6.36.

The fatigue strength in shear varies a great deal between different investigators.[31,74,75,85,86] Beams with adequate shear capacities for static loading were reported to have failed in shear under fatigue loading in the range of 21-65% of the theoretical static shear strength. Accordingly, Hawkins suggested that the checking of the stress range in longitudinal reinforcement bars may not be sufficient to ensure protection against fatigue failure even if member is designed to fail in flexural. He also indicated that for beams developing inclined cracks under service loads or unexpected overloads, the stress range in the stirrups should be limited to $\simeq$ 103 N/mm^2 regardless of their yield strength. Furthermore, the shear capacity of a beam containing compression reinforcement may be calculated using truss analogy and assuming zero contribution of the concrete to the shear capacity.

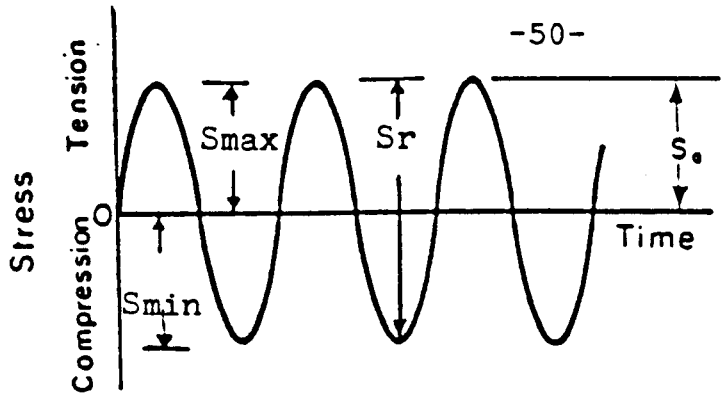

(a) Alternating stress

$S_m = 0$

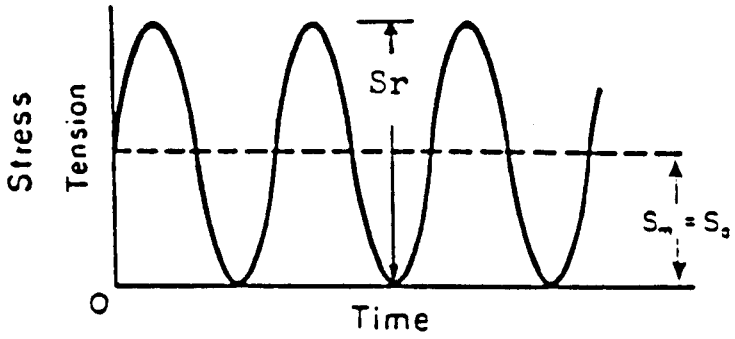

(b) Pulsating tension

Sr=S

Smin=0

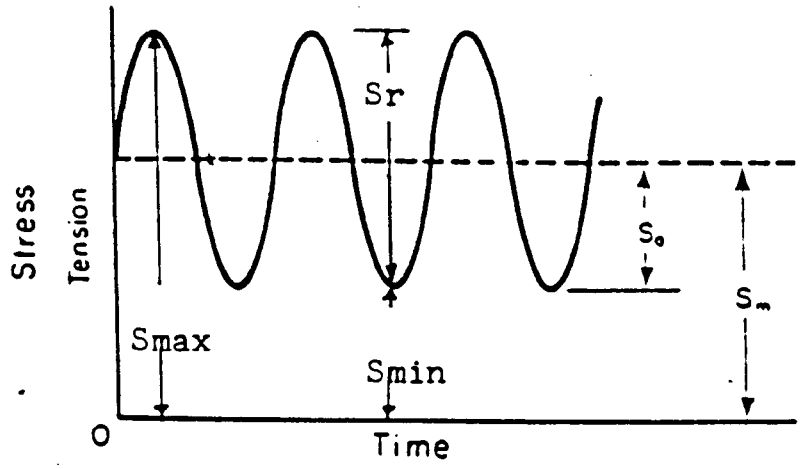

(c) Fluctuating tension

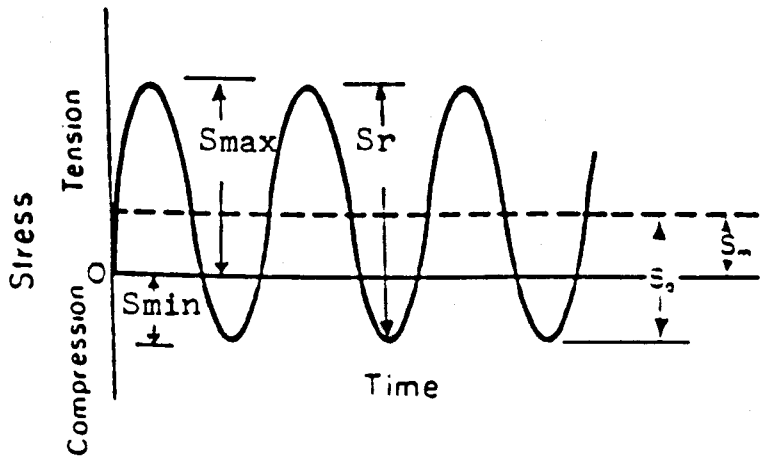

(d) Fluctuating

Figure (2-1): Types of fatigue stress cycles (Ref.5).

$S_m=(S_{max}+S_{min})/2$ $\quad S_r=2S_a=S_{max}-S_{min}$

$S_{min}=S_m-S_a$ $\quad R=\frac{S_{min}}{S_{max}}=\frac{S_m-S_a}{S_m+S_a}$

$S_{max}=S_m+S_a$

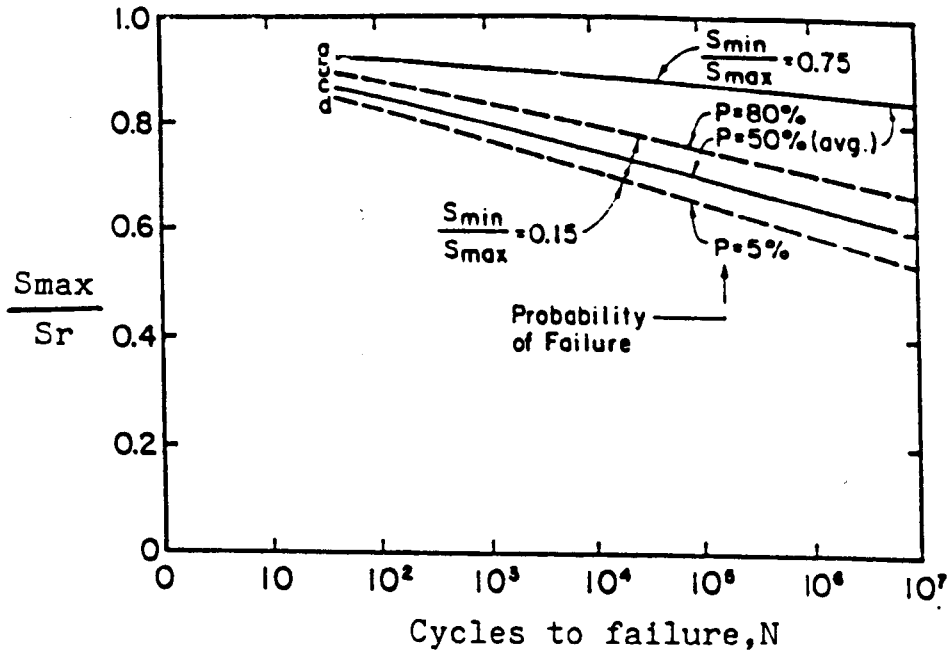

Figure (2-2): Probability of failure;fatigue of plain concrete beams (Ref.1).

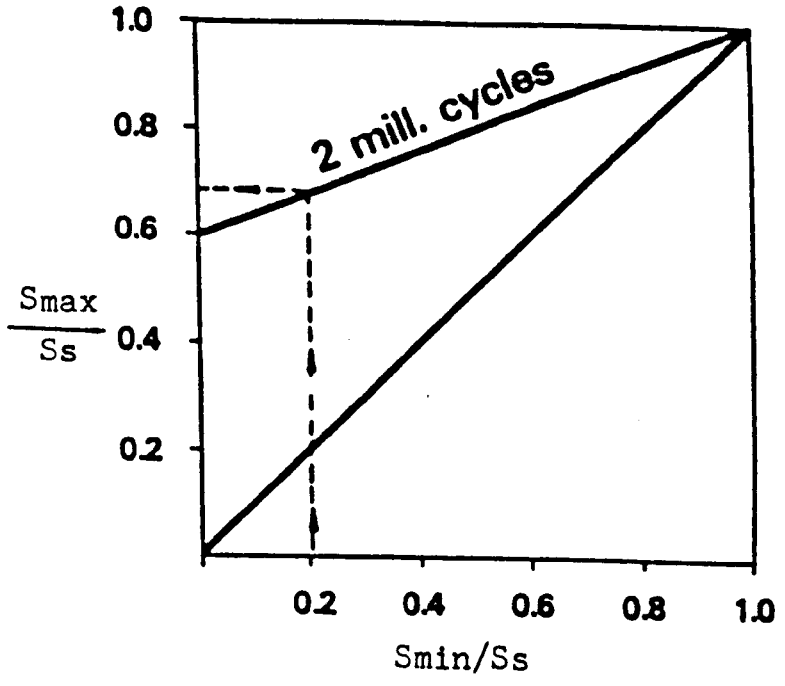

Figure (2-3): Goodman diagram for concrete (Ref.38).

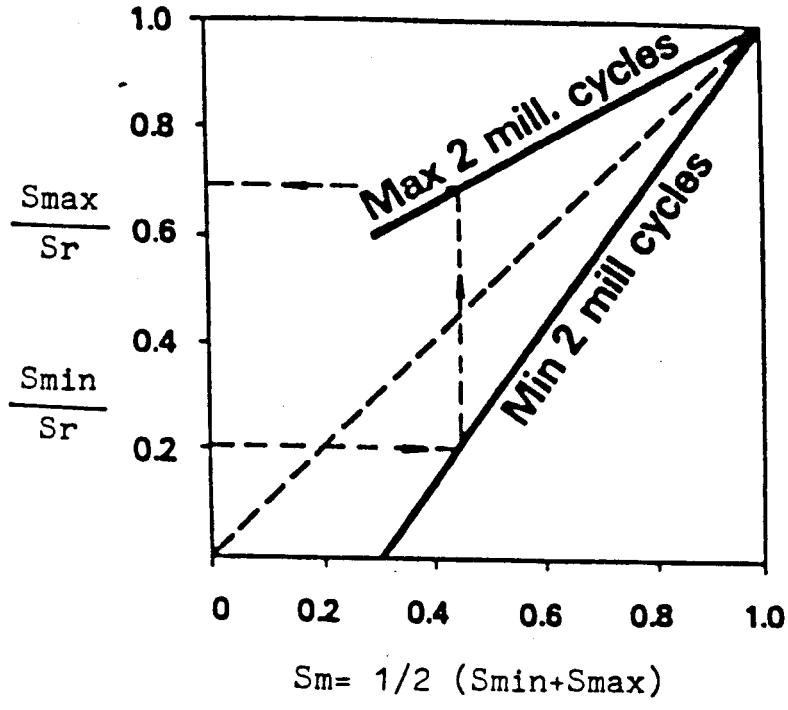

Figure (2-4): Smith diagram for concrete (Ref.38).

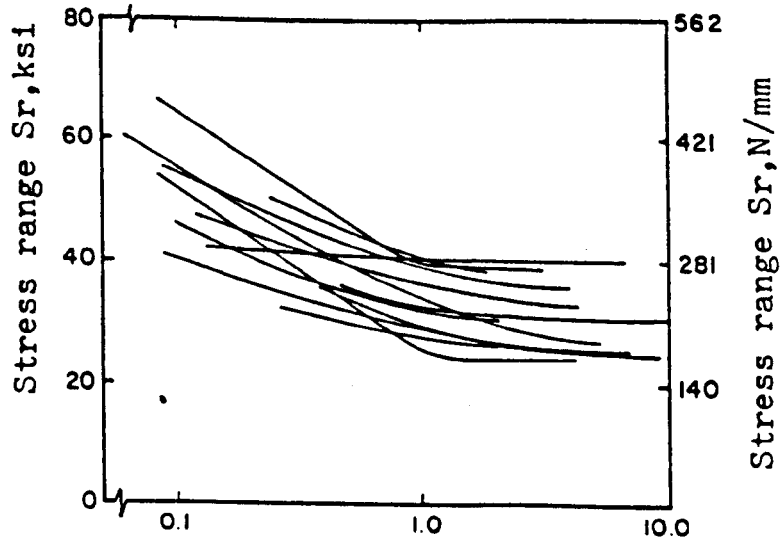

Figure (2-5): Stress range-fatigue life curves for reinforcing bars (Ref.36).

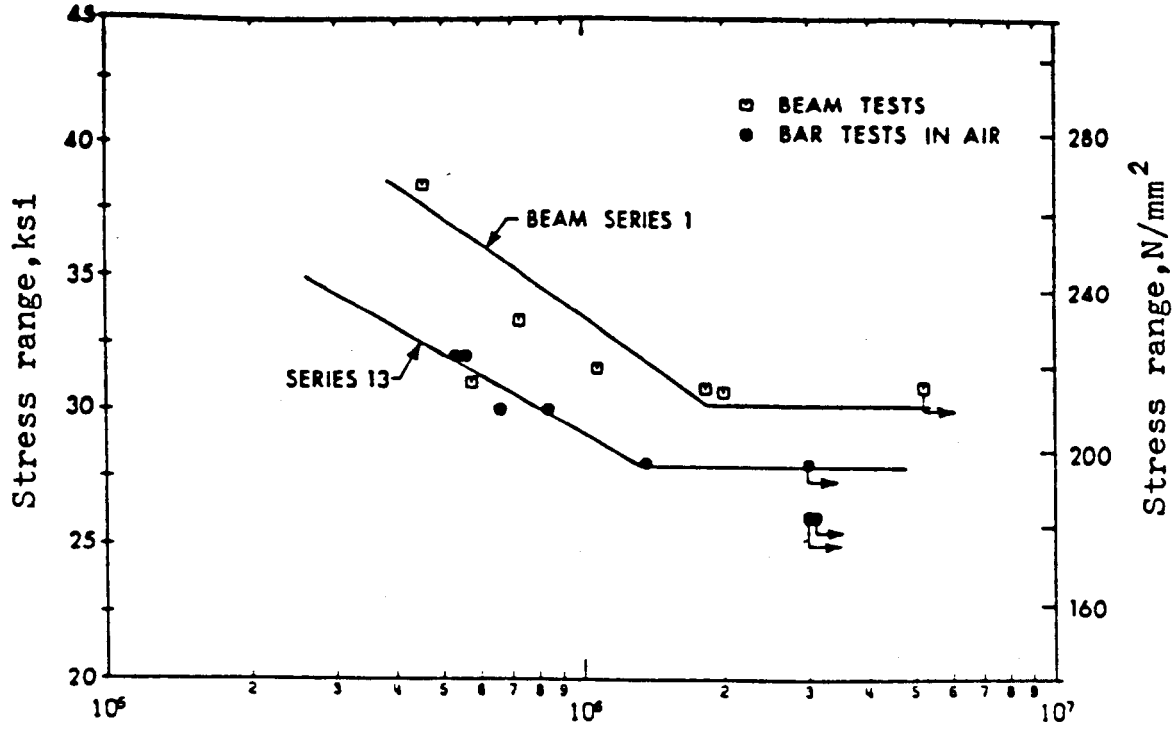

Figure (2-6): Comparison of S-N curves of 12mm diameter bars in beams and in air (Ref.85).

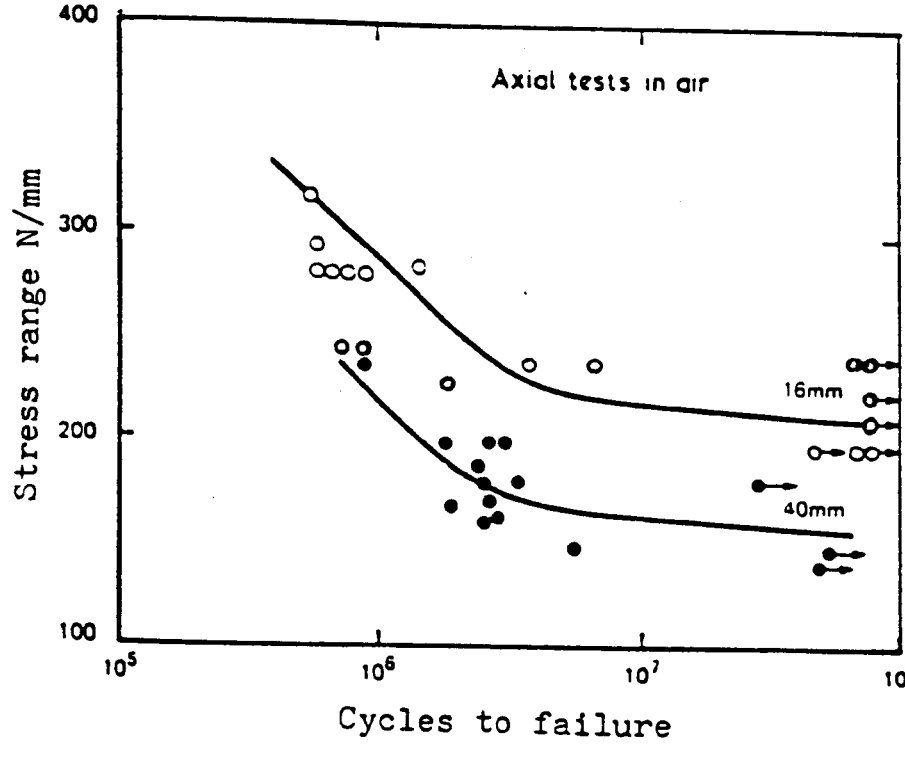

Figure (2-7): Effect of diameter for Torbar (Ref.14).

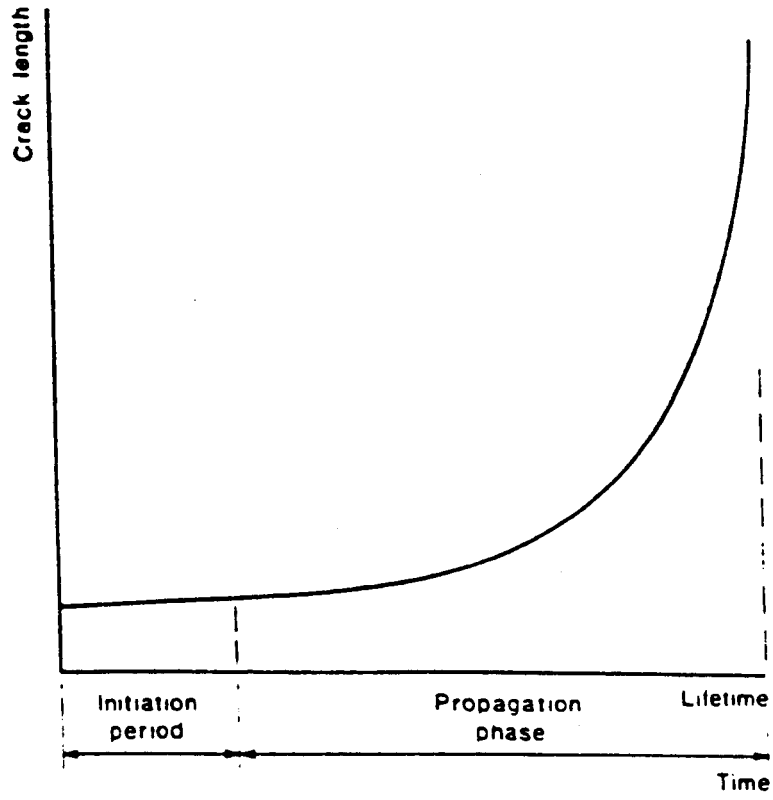

Figure (2-8): Crack length vs. lifetime of a section (Ref.12).

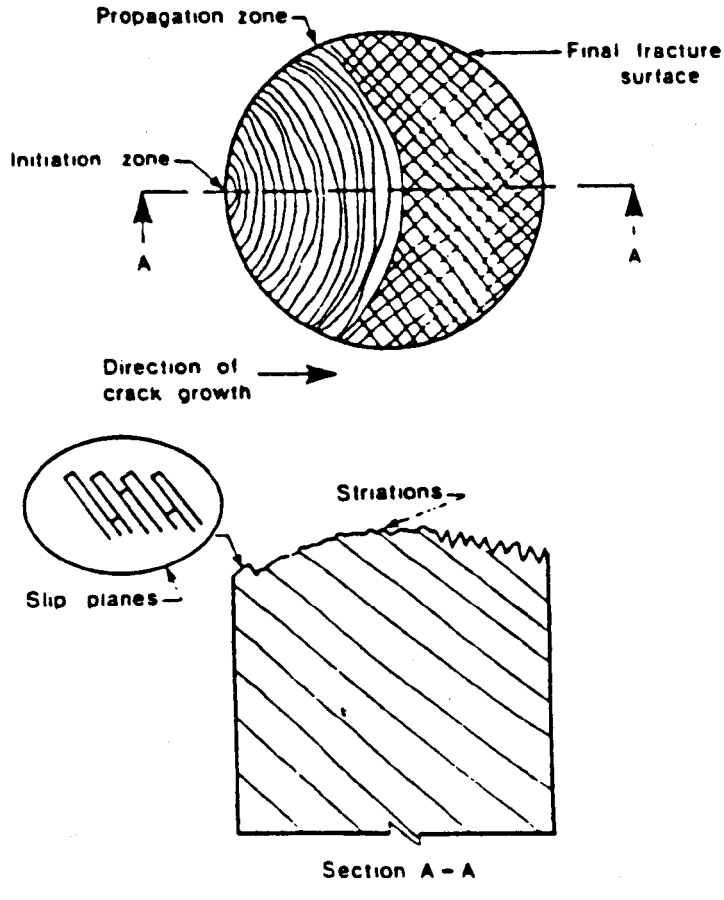

Figure (2-9): Fatigue failure surface in reinforcing bar (Ref.12).

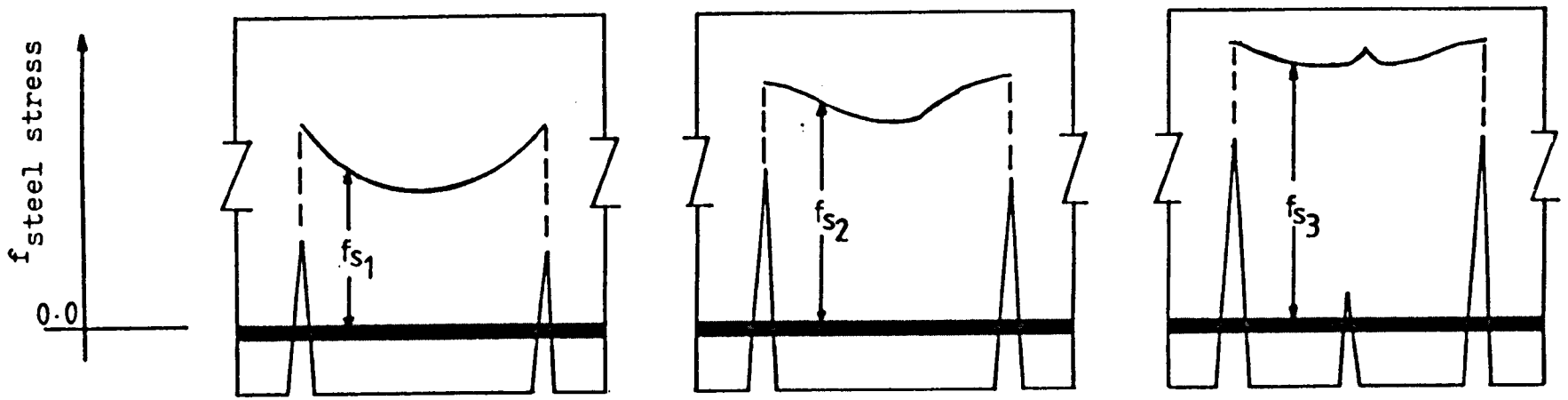

a) After initial loading

b) After some destruction of bond near the tension cracks

c) After the formation of secondary internal cracks

Figure (2-10): Steel stress and distribution in a segment of bar located between two tension cracks (Ref.25).

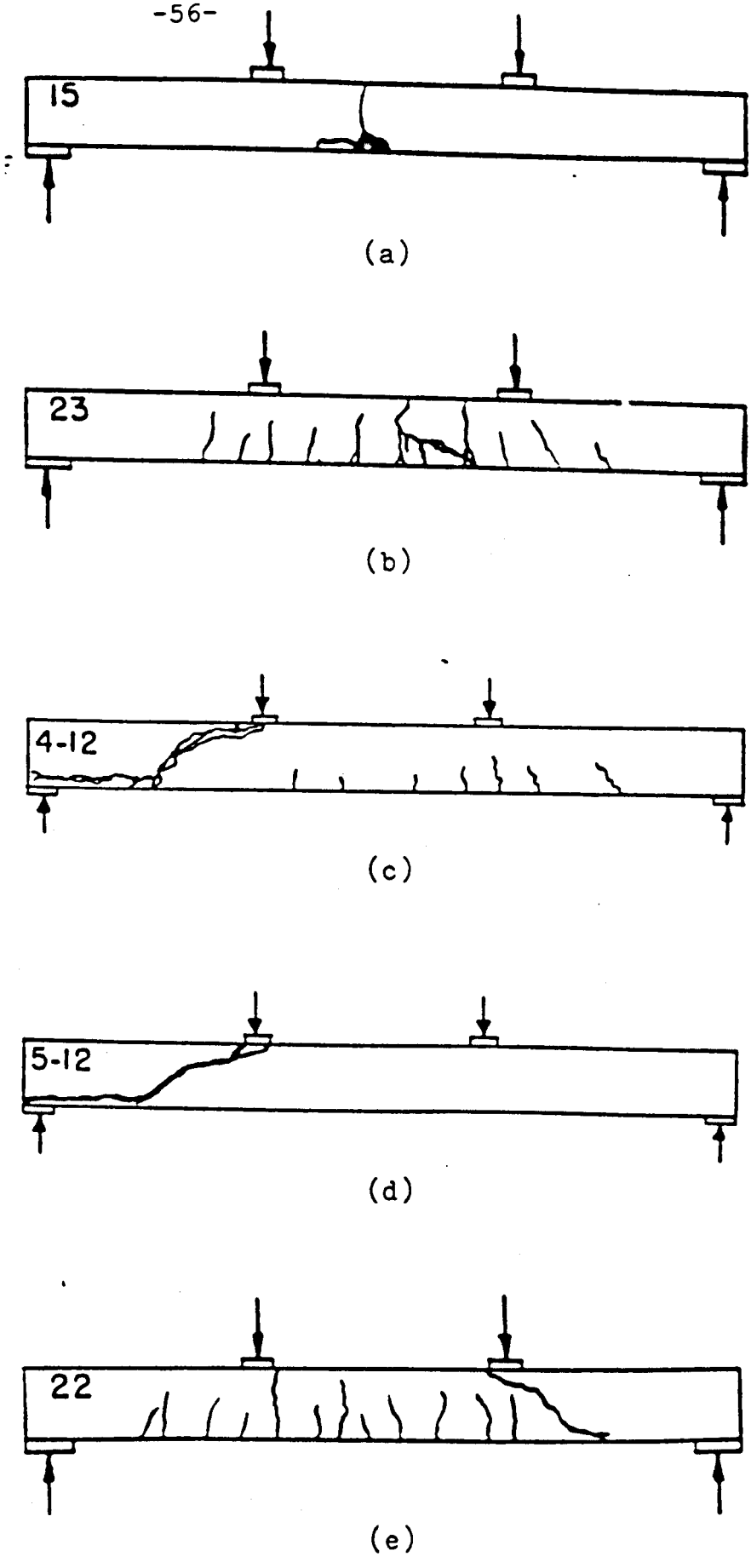

Fatigue fracture of tensile reinforcement (a,b)

Destruction of the concrete compression zone (c)

Diagonal cracking failure (d)

Shear failure (e)

Figure (2-11): Mode of failure in fatigue (Refs.74,75).

CHAPTER 3

CORROSION OF STEEL IN CONCRETE

3.1 Basic Corrosion and Oxidation.

- 3.1.1 Definition.
- 3.1.2 Types of Corrosion.
- 3.1.3 Mechanism of Aqueous Corrosion.
- 3.1.4 Corrosion Rates and Extents.
- 3.1.5 Equilibrium and Electrode Potentials
- 3.1.6 Electrode Polarization.
- 3.1.7 Potential-Current Diagrams.
- 3.1.8 Potential-pH Diagrams.
- 3.1.9 Passivation.

3.2 Corrosion Rate Measurement.

- 3.2.1 Absolute vs. Relative Data.
- 3.2.2 Corrosion Rate Measuring Techniques.
- 3.2.3 Linear Polarization Method.

3.3 Corrosion of Steel in Concrete.

- 3.3.1 The Corrosion Problem.
- 3.3.2 Loss of Protection.
- 3.3.3 Mechanism of Corrosion of Steel in Concrete.
- 3.3.4 Cracking and Corrosion.
- 3.3.5 Resistivity of Concrete and Corrosion of Steel Bars.
- 3.3.6 Design Against Corrosion.
- 3.3.7 Corrosion Rate Measurements of Steel in Concrete.
- 3.3.8 Method of Preventing Corrosion in Reinforced Concrete Structures.
- 3.3.9 Corrosion Inspection Techniques.

3.4 Electrical Resistivity of Concrete.

- 3.4.1 Concept of Resistivity.
- 3.4.2 Conduction Paths Through Concrete.
- 3.4.3 Mechanism of Conduction Through Concrete.
- 3.4.4 Electrical Resistivity Measurements.

CHAPTER 3

CORROSION OF STEEL IN CONCRETE

3.1 Basic Corrosion and Oxidation.

3.1.1 Definition.

Corrosion may be defined as the electrochemical reaction of a metal with a non-metal (or non-metals) in the surrounding environment in which the metal itself is a reactant and is oxidised (loss of electrons) to a higher valency state, whilst the other reactant, an electron acceptor, in solution is reduced (gain of electrons) to a lower valency state. This reaction results in the formation of compounds which are referred to as corrosion products and if allowed to proceed will result in the deterioration of the metallic construction or component.

Virtually all metals are basically unstable and have a tendency in most environments to revert to their more stable state and lower their free energies by combining with other elements. The corrosion characteristics of a metal component are not an intrinsic property and the rate and the nature of the corrosion will depend upon the environment to which it is exposed.

3.1.2 Types of Corrosion.

Corrosion may take a variety of forms that range from fairly uniform wastage resulting in general loss of thickness to highly localised attack resulting in pitting and perforation or in cracking and fracture. Components can also deteriorate in an aqueous environment by the

joint action of stress and corrosion.

General Corrosion.

General corrosion is perhaps the most common form of corrosion, it is characterised by progressive and uniform thinning of the metallic component over a large area of the surface.

Galvanic Corrosion.

This occurs when two different metals are in electrical contact and exposed to an aqueous electrolyte. Galvanic attack, sometimes called bimetallic corrosion, is characterised by accelerated dissolution of the more reactive metal and less corrosion of the more noble metal component than if they were placed unconnected in the same environment. This kind of corrosion is particularly sensitive to the relative area of the two metals. A high ratio of the cathode to the anode area will result in accelerated attack on the anodic component and vice versa.

Pitting Corrosion and Crevice Corrosion.

Pitting corrosion is, usually, extremely localised (Figure 3.1) and is often initiated at sites of localised damage to a protective oxide film in situations preventing its reformation. These pits are sometimes so close together as to merge into a general rough surface. Corrosion rate in the pit may be accelerated by the development of a macrocell in which the pit acts as a small anode and the external surface as a large cathode.

Crevice corrosion is another form of localised corrosion which occurs at points of geometrical discontinuity, holes, joints, bolts, rivets etc. Crevice corrosion occurs at these locations due to the build-up of a detrimental ion species, depletion of oxygen or change in pH value.

Intergranular Corrosion (Figure 3.2).

In this type of corrosion the grain boundaries in the metal are attacked preferentially to the interior of the grain. It is usually related to the segregation of specific elements or the formation of a compound in the boundary, in severe cases this kind of attack can cause the whole grain to fall out.

Stress Corrosion Cracking (SCC) (Figure 3.3).

This usually refers to failure of the compound in a certain environment after sustaining stresses, tensile in particular, for a period of time. Sometimes specific metalurgical requirements in terms of composition and structure are necessary for SCC. Cracks can initiate at pits after a slow corrosion attack then propagate to sufficient size to cause failure. It worth mentioning that SCC tends to occur in relatively passive materials and is generally accelerated in progressively more innocuous environment as the material's strength increased.

Erosion Corrosion.

Erosion corrosion occurs under turbulent conditions where the corrosion rate is facilitated by:

a. easy and rapid transport of species to and from the metal surface,
b. continuous removal of the corrosion products and breaking of the surface film by mechanical stress.

The process is sometimes accentuated by entrained particles in the flowing corrodent or slurry.

Cavitation Corrosion.

An alternative mechanism for damaging the surface film is cavitation, which can lead to localised mechanical damage or combined cavitation/corrosion attack in a

corrosive environment. The cavitation process usually takes place extremely rapidly and is caused by the collapse of low-pressure bubbles which produces a strong shock wave.

Corrosion Fatigue.

The process in which a metal fractures prematurely under conditions of simultaneous corrosion and repeated cyclic loading at lower stress levels or fewer cycles than would be required in the absence of the corrosive environment.

3.1.3 Mechanism of Aqueous Corrosion.

Corrosion that occurs in an aqueous solution is electrochemical in nature and is similar to that occurring in an electrochemical cell. The corrosion cell must consist of two types of electrode reactions: anodic reactions involving oxidation as the predominant reaction and the cathodic reactions in which reduction is the predominant reaction. The two half cell reactions constitute the overall reaction and are interdependent so that their rate and extent will be equal; in other words oxidation of one species can not occur with out the simultaneous reduction of the other.

For a simple corrosion cell such as, for example, a single isolated piece of steel in neutral or alkaline water, the half cell reactions are likely to be:

$$\text{Anode} \quad 2Fe \longrightarrow 2Fe^{2+}(aq) + 4e^{-} \qquad \ldots 3.1$$

$$\text{Cathode} \quad O_2 + H_2O + 4e^{-} \longrightarrow 4OH^{-} \qquad \ldots 3.2a$$

$$2H^{+} + 2e^{-} = H_2 \qquad \ldots 3.2b$$

The total anodic current I_a (Equation 1) must be

exactly balanced by the total cathodic current I_c (Equation 2).

i.e. $I_a = I_c$

Now if a metal is placed into a solution of its cations such as a system $Cu^{+2}(aq)/Cu$ then there is a tendency for an exchange process in order to attain the electrochemical equilibrium. This is achieved either by metal/dissolution $Cu \rightarrow Cu^{+2} + 2e$ or by metal deposition $Cu^{+2} + 2e \rightarrow Cu$, the prevailing process is dependent on the free energies of the metal ions in the solution and that of the metal which can also be related to the electrochemical electrode potential (E) of the metal and the equilibrium electrode potential (E_o). Thus

if $E > E_o$, an electrochemical reaction may occur only as an oxidation.

if $E < E_o$, an electrochemical reaction may occur only as a reduction.

In a corrosion cell with two different electrodes immersed in a solution and connected externally, the direction of the reaction will depend on the electrode potentials such that the electrode with more negative potential will act as an anode i.e. dissolution takes place which results in a change in the potential to a more positive value. Whereas the electrode with less negative potential will sustain cathodic reactions with the corresponding change in potential towards more negative value. The e.m.f. of the cell (E_{cell}) is the difference between the two values at which a corrosion current I_{corr} will flow.

3.1.4 Corrosion Rates and Extents.

Corrosion is quantified by specifying the corrosion rate under the environmental conditions prevailing. The current I is the rate of charge transfer and the rate of 1 Ampere = 1 Coulomb/sec. The charge of an electron is 1.602×10^{-19} C and 1 mol of an element contains 6.0235×10^{23} atoms (Avagadro's number). Thus the cathodic reduction or anodic oxidation of a mole of a metal M of a given valency z will require $z \times 6.0235 \times 10^{23} \times 1.602 \times 10^{-19} = z96500C$.

This statement is essentially Faraday's law and 1 Faraday = 96,500C, it follows that the rate of charge transfer of an electrochemical reaction is given by:

$$R = \frac{I}{zF} \text{ mole sec}^{-1} \qquad \ldots 3.3$$

or

$$R = \frac{IM}{zF} \text{ kg sec}^{-1} \qquad \ldots 3.4$$

where M is the molar mass (kg/mole). The rate per unit area is the current density i and:

$$i = I/A \quad \text{where A is the area} \qquad \ldots 3.5$$

In the case of general corrosion or localised corrosion of known anodic area, Equation 3.4 can be expressed in terms of rate per unit area:

$$R = \frac{iM}{zF} \text{ kg/m}^{-2} \cdot \text{sec}^{-1} \qquad \ldots 3.6$$

The extent of an electrochemical reaction can be expressed as a total charge Q in coulombs for a given period of time t:

$$Q = \int_0^t i(t) \qquad \ldots 3.7$$

since 1 mole of charge transfer requires zF coulombs then the total metal loss W equals:

$$w = \frac{Q}{zF} = \frac{1}{zF} \int_0^t I(t) \quad \text{mole} \qquad \ldots 3.8$$

or

$$w = \frac{M}{zF} \int_0^t I(t) \quad \text{kg} \qquad \ldots 3.9$$

The average penetration of corrosion attack δ can be estimated, assuming uniform depth of attack, from the total metal loss w by the expression:

$$\delta = \frac{w}{A \times D} \qquad \ldots 3.10$$

where D = density

3.1.5 Equilibrium and Electrode Potentials.

The term potential is widely used when considering corrosion reactions. The electrochemical potential E is a measure of the ease of electron charge transfer from or to the corroding electrode, it is a property of the metal/

environment interface not the metal itself, and thus changes with changes in environment. It is not possible to determine the absolute value of the potential and therefore the potential difference between the electrode surface and a suitable electrode such as the standard hydrogen electrode SHE, or standard calomel electrode SCE is taken as a measure of the actual potential and is usually quoted in volts relative to the electrode used.

The value of the potential existing in a freely corroding system, i.e. when no current flows externally to or from it, is known variously as the corrosion potential, rest potential or mixed potential and often given the symbol E_{corr}.

The potential difference across the electrode is dependent upon the thermodynamic driving force, ΔG, for the electrode reaction which in turn is dependent upon the activities (a) of the species taking part in the reaction and on the temperature.

The Nernst Equation[87] provides the basis for the thermodynamic approach to corrosion in an aqueous solution, and according to this equation the relationship between the equilibrium electrode potential E_o, and the activities of the reactants and products for any electrothermal equilibrium of the type:

$$aA + bB + ne^- \rightarrow cC + dD \qquad \ldots 3.11$$

is given by:

$$E_o = E_o^o - \frac{RT}{zF} \ln\left(\frac{a^c_C \times a^d_D}{a^a_A \times a^b_B}\right) \qquad \ldots 3.12a$$

where R is the gas constant (8.3143 $Jmol^{-1}K^{-1}$),
T the temperature in K,
F the Faraday's constant (96,500 coulomb per equivalent),

a represents the activity of the ion,
E_o^o is the "standard electrode potential" at 25°C (298.16 K).

Equation 3.12 becomes:

$$E_o = E_o^o - \frac{0.059}{z}\log\left(\frac{a^c_C \times a^d_D}{a^a_A \times a^b_B}\right) \qquad \ldots 3.12a$$

The standard electrode potential or Redox potential E^o_o is the potential of a metal electrode in an electrolyte containing its ions present at "unit activity" against a standard reference electrode. The standard electrode, to which an arbitrary value of equilibrium potential of zero at all temperatures is assigned, is the standard hydrogen electrode which is used to obtain the electrochemical series (EMF series) for a wide range of electrode reaction. This EMF series lists the elements according to their standard electrode potential with noble metals such as gold being positive and active metals such as zinc being negative, Table 3.1.

3.1.6 Electrode Polarization.

The equilibrium of a half-cell electrode in which the net transfer of charge or rate of reaction approximates z is characterized by its reversible potential. However, when a reversible electrode becomes a part of a system in which current is produced at an appreciable rate, the electrode potential becomes displaced from its equilibrium value as indicated in Figure 3.4 which shows a spontaneous change in equilibrium potential upon operation of a Daniell cell (an electrochemical cell which consist of Zn and Cu electrodes). This departure of an electrode from its potential is due to electrode polarization and is termed the overpotential. Polarization occurs as a result of charge transfer at or near an electrode being unable to keep up with charge transfer elsewhere in the cell

circuit. There are various types of polarization, Figure 3.5, these are:

Activation Polarization (ηA).

Charge transfer at a finite rate will involve an activation over potential which provides the activation energy required for the charged species to surmount the energy barrier that exists between the energy states of the reactant and product. The activation over potential varies exponentially with the rate of charge transfer (Figure 3.5a) as defined by the Tafel Equation:

$$\eta_{Aa} = ba \log 10\frac{i_a}{i_{corr}} \qquad \ldots 3.13a$$

$$\eta_{Ac} = bc \log 10\frac{i_a}{i_{corr}} \qquad \ldots 3.13b$$

where η_{Aa}, η_{Ac} the anodic and cathodic overpotential relative to E_{corr}

ba, bc the anodic and cathodic Tafel constants in mv/decade

i_{corr} the corrosion current at corrosion potential E_{corr}

i_a, i_c the anodic and cathodic current at some component potential displaced from E_{corr}

Concentration Polarization (η_c).

Concentration polarization (Figure 3.5b) occurs when the reaction rate or the applied external current is so large that the species being oxidized or reduced can not reach or be removed from the surface at a sufficiently rapid rate. The solution adjacent to the electrode surface becomes depleted of the reacting species or concentrated in products and the rate then is controlled

by the maximum rate at which the reacting species or products can diffuse to or from the surface. The electrode potential change caused by this process may be obtained by the equation:

$$\eta_c = \frac{RT}{zF} \ln \left(1 - \frac{i}{i_L}\right) = \frac{0.059}{z} \log\left(1 - \frac{i}{i_L}\right) \quad \text{at } 25^{\circ}C \qquad \ldots 3.14$$

where i_L is the limiting diffusion current.

From Equation 3.14 it is evident that the smaller i_L is the greater the magnitude of the overpotential due to transport. Experimentally, when the current i approaches $0.1i_L$, concentration polarization starts to become significant.

Resistance Polarization (ηR).

Resistance polarization Figure 3.5-c is the third term of the total over potential and is a function of the electrical resistance of the solution R_{sol} and the resistance produced by films or coatings formed on or applied to the surface R_f. Thus it is defined as:

$$\eta R = I(R_{sol} + R_f) \qquad \ldots 3.15$$

3.1.7 Potential-Current (E-I) Diagrams.

The graphical method of showing the dependency of the corrosion rate I_{corr} on the polarization of the electrodes of the corrosion cell was originated by U.R. Evans[87] and such plots are often called Evans diagrams. A corroding electrode is characterized by a corrosion potential E_{corr} which can be readily determined by means of an appropriate reference electrode, and by the corrosion rate I_{corr} which is not directly measurable and needs to be evaluated

indirectly. The experimental determination of E-I diagrams involves shifting the electrode potential cathodically and then anodically by means of an external source of e.m.f. and measuring the corresponding current flowing through a suitable counter electrode. I_{corr} is the intersection of the anodic and the cathodic curves projected on the current scale. This method is presented in detail in Chapter 10 of this thesis. Figure 3.6 represents the extrapolated extension of the anodic and cathodic curves and shows various types of corrosion control. Figures 3.6a to d illustrate how the reaction rate can be controlled by either the polarisation of one or both of the partial reactions, or by the resistivity of the electrolyte. Figures 3.6e and f illustrate how E_{corr} provides no information on the corrosion rate.

3.1.8 Potential - pH Diagrams.

Potential - pH diagrams which are also known as Pourbaix diagrams summarise the electrode potential/ solution pH dependence of all different equilibria between metal, metal cations and anions and solid oxides. These diagrams are constructed for specific concentrations of metal ions in solution from calculations based on the Nernst equation and solubility data and consist, generally, of zones of corrosion, immunity and passivation. Pourbaix diagrams can not be used to determine or predict quantitatively the rate of corrosion but they serve a useful purpose as a means of qualitative prediction of corrosion processes.

3.1.9 Passivation.

In some situations, the formation of sparingly soluble corrosion products results in a compact barrier isolating the metal from the environment, the conditions necessary for passivation to occur are.

1. The corrosion product must be thermodynamically stable in the environment.

2. The corrosion product must form on the surface of the metal as a coherent and adherent film.

3. The film must be mechanically stable so that during formation it is not disrupted by cracking, flaking and blistering.

3.2 Corrosion Rate Measurement.

Whilst the possibility of a corrosion reaction occurring can be predicted theoretically, the kinetics of the reaction i.e. the rate at which it proceeds is, by its nature, less predictable and can only be determined empirically.

Various monitoring techniques have been developed to assist in the assessment or prediction of the corrosion process in the plant or on a structure. The use of these techniques is a particularly common procedure in the study of corrosion of metals in an aqueous environment but they have not been widely used for other systems such as steel in concrete. The latter case will be discussed in the following section. In this section, however, special emphasis will be placed on the theoretical background, the application and the limitation of the widely used "Linear Polarisation Method" (L.P.M.) as it constitutes the main electrochemical measuring technique adopted in this study.

3.2.1 Absolute vs Relative Data.

Regardless of the measurement method, the accuracy and reliability of corrosion rate data are always open to question. Particularly in the absence of direct visual access to the corroding electrode in "hidden situations" and of other independent non-electrochemical measurements e.g. weight loss data. This, however, has little importance for practical application where the selection of material[90] is based on differences in the corrosion rate of some order of magnitude. Bandy[91] indicated that in most industrial processes only semi-quantitative measures

of corrosion rate is necessary and an error of 60% or so is entirely acceptable.

It seems, therefore, that of greater significance is detecting changes in the corrosion process and perhaps the relative magnitude of these changes. Recent developments in the field of monitoring techniques, nevertheless, are directed to widening their application and improving their accuracy.

3.2.2 Corrosion Rate Measuring Technique.

Measuring techniques can be divided into four broad groups which are:

i. Use of coupons of specific material.
ii. Analytical measurements.
iii. Electrical Resistance Method.
iv. Electrochemical Techniques.

i. Use of Coupons.

The method involves placing coupons of known weight, made of the material whose corrosion rate is to be measured, in the corrosive environment for a period of time, the coupons are then removed, cleaned of the corrosion product and re-weighed. The weight difference is calculated and converted into suitable units of penetration. The coupons may also be inspected for pits, stress corrosion cracking etc.

The method gives the average rather than the instantaneous corrosion rate over the exposure time. If the variations[92] in rate are desired, it is necessary to use several coupons and remove them at regular intervals. Using one sample intermittently removed for weight change measurement often affects the subsequent corrosion rate upon re-exposure to the environment.[93] The method is comparatively cheap and simple but generally requires considerable time to obtain data. This is particularly so when dealing with extremely low rates[91] in which case long exposure times or large sample sizes must be employed to

obtain reasonable accuracy.

ii. Analytical Measurements.

The method is based on the chemical analysis of the surrounding solution and the determination of the concentration of metal ion produced by the corroding metal. Other variables which can influence the corrosion process such as pH, oxygen concentration and temperature can also be monitored as a part of the overall monitoring process. This method also presents difficulties[88] particularly when the rate changes markedly with time or when corrosion products are insoluble.[93] Generally the method is not sufficiently sensitive and is only applicable to certain conditions also it is unlikely to be fully quantitative.

iii. Electrical Resistance Method.

The electrical resistance[92] method of measuring corrosion rate is based on the fact that the electrical resistance change of a metal is directly proportional to the change in its cross-sectional area. In this method the resistance of the probe, which consists of wire or a strip of the metal being monitored, is measured by a suitable bridge circuit and then converted into penetration units. Temperature compensation for resistance change is incorporated into the probe by a reference electrode protected from the environment. The method can in principle be used in any environment and is able to make continuous measurements. It has been widely[88] used in oil-refineries and multi-stage flash distillation plants. The main shortcoming[93] in the application of this method, however is that it is only quantitative if the corrosion process produces very uniform attack.

iv. Electrochemical Methods.

a. Extrapolation Method.

Sometimes called "full polarization method", it involves polarising the electrode whose corrosion rate is measured both cathodically and anodically for relatively high over-potentials and simultaneously determining the current. The extrapolation of the linear region of the separate anodic and cathodic plots to the corrosion potential should give a common value of the corrosion current which can be converted to corrosion rate using Faraday's law. Further, the slope of the linear region of the plots gives the values of the cathodic and anodic tafel constants b_c, b_a.

The measurements may be accomplished either potentio-dynamically with a suitable sweep rate, which is usually used for moderate to high corrosion rate systems or potentio-statically where the potential is applied in steps and the system allowed to come to equilibrium at each step before the current is measured. This technique is more convenient for systems corroding at low rate such as passivated steel in reinforced concrete.

The major limitations of this method are, firstly: the applied current is normally several times the corrosion current and thus the nature of the surface may change significantly, especially during anodic polarization with subsequent change in the corrosion rate, secondly: in certain systems the linear tafel behaviour may not be obtained because of the effects of resistance and concentration polarization[91].

b. Electrochemical Noise Measurement.

The method is based on the observed relationship between the standard deviation of the potential signals and the corrosion rate. The method has recently been examined for use in reinforced concrete structures and will be discussed further in Chapter 11.

c. linear Polarisation Method (L.P.M.)

This method, alternatively termed polarization resistance method, or Stern-Geary method, is widely used for the evaluation of the instantaneous corrosion rate in the laboratory and in the field.

For its importance, the method is presented in detail in the following sub-section.

3.2.3 Linear Polarization Method.

Background:

Wagner and Traud[94] showed theoretically in 1938 that the polarization curves for the corroding electrode obtained by plotting the applied current I against the potential change ΔE are linear for $\Delta E \to 0$. Later the occurrence of linear corrosion kinetics was well established and confirmed experimentally. Following this observation, several attempts have been made to relate the slope of E-I plot to the corrosion rate. Simmons[95] in a study on evaluation of inhibitors indicated that there may be a quantitative relationship between the $\Delta E/\Delta I$ slope and the weight loss tests. He also observed that the slope of the line, $\Delta E/\Delta I$, was higher for specimens having low corrosion rates than those having a high corrosion rate. Skold et al[96] found in their studies of steel and cast iron in natural waters that a linear relation existed between potential and applied cathodic and anodic current at low applied current density. A plot of a corrosion rate versus $\Delta E/\Delta I$ on a logarithmic scale gave a straight line with a negative slope. In 1957 stern and Geary[89] and Stern[97] discussed the shape of polarization curves and showed that a linear relationship is expected in the region where the polarized potential is close to the corrosion potential. For these conditions the following equation was derived:

$$\frac{\Delta E}{\Delta I} = \frac{b_a \, b_c}{2.3 \, I_{corr} \, (b_a + b_c)} \qquad \ldots 3.16$$

where $\Delta E/\Delta I$ is the slope of the E-I polarisation curve close to E_{corr} which was then called the polarisation resistance R_p.

b_a, b_c are the slopes of the logarithmic local cathodic and anodic curves

and I_{corr} is the corrosion current.

Thus:

$$I_{corr} = \frac{b_a\, b_c}{2.3\ (b_a + b_c)} \cdot \frac{1}{R_p} = \frac{B}{R_p} \qquad \ldots 3.17$$

$$\text{Where } B = \frac{b_a\, b_c}{2.3\ (b_a + b_c)}$$

Stern and Geary concluded that the polarisation resistances measured anodically or cathodically are identical and that the extent of the linear region depends on the Tafel slopes of the E-log I anodic and cathodic curves.

Later Stern[97] considered the case in which the corrosion rate is equal to the diffusional limiting current density for the cathodic reaction. For this case the corrosion current equals:

$$I_{corr} = \frac{b_a}{2.3\ R_p} \qquad \ldots 3.18$$

The derivation of Equations 3.17 and 3.18 was based on the assumption that the corrosion potential E_{corr} is remote from the reversible potentials of both partial reactions E_{o1} and E_{o2} i.e. the corrosion current I_{corr} is very large compared with the exchange currents i_{o1} or i_{o2}.

The use of polarisation resistance for measuring

corrosion rates has one particularly important advantage, that is, the potential range investigated is close to the corrosion potential. Thus the nature of the surface is not changed significantly because the currents measured during polarisation are relatively low.

Extensive literature has developed which discusses the potential sources of error in the technique and their influence on the accuracy of measurements. These include:

i. <u>The case where the corrosion potential is close to reversible potentials:</u>

Mansfeld and Oldham[98] show that the range of E_{corr} values for which Equations 3.17 and 3.18 are valid is:

$$Z_1(E_{corr} - E_{o1}) >> \frac{RT}{F} << Z_z(E_{o2} - E_{corr}) \qquad \ldots 3.19$$

Where Z_1, Z_2 are the number of electrons involved in reversible metal dissolution and the cathodic reduction process respectively.

E_{o1}, E_{o2} are the reversible potential of metal dissolution process and cathodic reduction respectively.

Equation 3.19 is satisfied for the majority of corroding systems.[99] However, the case where the corrosion potential is close to one of the partial reactions reversible potential under activation polarization has been analysed in detail by Mansfeld and Oldham.[98] They demonstrated that when E_{corr} lies close to the reversible potential of the metal i.e. $Z_1(E_{corr} - E_{o1}) << RT/F$ then following relationship applies

$$R_p^{-1} = i_{corr} \left\{ \frac{1}{b_{a1}} + \frac{1}{b_{c2}} + \frac{1}{(E_{corr} - E_{o1})} - \frac{Z_1 F}{2RT} \right\} \qquad \ldots 3.20$$

and when E_{corr} is close to the reversible potential of the

cathodic process i.e. $Z_z(E_{o2} - E_{corr}) << RT/F$ then:

$$R_p^{-1} = i_{corr} \left\{ \frac{1}{b_{a1}} + \frac{1}{b_{c2}} + \frac{1}{(E_{o1} - E_{corr})} - \frac{Z_2 F}{2RT} \right\} \quad \ldots 3.21$$

where i_{corr} in both equations is the corrosion current density. Clearly the use of Equations 3.20 and 3.21 is not easy as they require the knowledge of the reversible potentials as well as the activation of any species involved in the equilibrium and its change with time. Mansfeld and Oldham[98] suggested that where $E_{corr} - E_{rev} >$ 26 mv the errors produced are < 20% and even when the potentials are as close as 13 mv, the error is only a factor of 2. For these situations,[100] however, the use of Stern-Geary relationship results in over-estimation of the corrosion current.

ii. Non linearity of the E-I polarisation curve in the vicinity of E_{corr}:

Barnartt[101] indicated that the extent of the linear E/I region varies widely with the ratio of anodic and cathodic Tafel slopes, in some systems the linear relationship is obeyed within 5% over 60 mv or more whereas in others linearity is valid for 3 mv or less. He observed little difference in the anodic and cathodic ranges of linearity except in the case when E_{corr} is close to the reversible potential.

Oldham and Mansfeld[102] indicated that linearity in the vicinity of the corrosion potential is only expected when b_a and b_c are equal. Thus only exceptionally will polarisation curve of the corroding metal be linear at E_{corr}. Mansfeld[103] suggested that in some cases the linearity close to E_{corr} might merely reflect the domination of the polarisation response by the IR-drop across the solution. Oldham and Mansfeld,[102] however, indicated that whether or not the polarisation curve is linear at the corrosion potential, its gradient there may

be employed to determine the corrosion current.

iii. IR-Drop in the Solution.

The voltage drop across the electrolyte and or any existing surface film can constitute an appreciable part of the polarising voltage. Mansfeld[103] indicated that it is not the absolute value of the solution plus the film resistance (RΩ) but the ratio RΩ/Rp which determines the magnitude of the error occurring in the polarisation resistance. Failure to allow for IR-drop results in a calculated corrosion rate lower than the true value. Section 3.4 deals with this problem in more detail.

iv. Electrode Perturbation.

In some systems, such as passivated steel in concrete, the corrosion potential is irreversibly altered with the passage of time under polarisation, despite the small polarising potential or current. In this case, the real applied potential is lower than the initially applied amount and thus introduces error into the calculated corrosion rate. The case[104] may be presented as follows:

$$\Delta E_{real} = \Delta E_{applied} - (E_{corr_{final}} - E_{corr_{initial}}) \quad \ldots 3.22$$

and $$E_{corr_{final}} = E_{corr_{initial}} + \Delta E_{pert} \quad \ldots 3.23$$

Under such circumstances it is advantageous to perform a.c. measurements at frequencies sufficiently high to preclude this possibility as will be shown later.

v. Time-Dependent Tafel Slopes.

One of the major limitations of L.P.M. is that a fore knowledge of the values of the Tafel constants is necessary for accurate determination of the corrosion

rate. Their values need to be assumed or measured in a separate experiment. This fact makes the use of Stern-Geary method very difficult especially in cases where the corrosion rate is to be determined as a function of time as the constancy of Tafel slopes is at least suspect[105] particularly for systems in which a corrosion product layer is formed.

Stern et al[93] examined the error due to inaccuracies in the determination of Tafel slopes and concluded that the worst possible error, obtained when one of the values (b_a or b_c) is infinite, is 200%. A number of methods have been[91,106,107] proposed for manipulating polarisation data close to the corrosion potential which allow calculation of corrosion current without a knowledge of the proportionality constant B. These techniques are generally tedious[108] and their use probably confined to the laboratory environment. An alternative method[108] for the determination of B is based on the dependence of corrosion potential on pH and uses the relation

$$B = \frac{1}{2.3} \frac{dE_{corr}}{dpH} \qquad \ldots 3.24$$

B values can also be determined empirically from weight loss data in conjunction with Rp measurements.

Measurement of Polarisation Resistance.

The majority of polarisation resistance measurements both in the laboratory and on the plant are made using D.C. techniques. Recently, however, more attention has been paid to the use of an A.C. impedance technique which is particularly attractive for systems whose corrosion potential is likely to change during D.C. measurement. In both cases, the proportionality constant B should be obtained separately and the IR-drop should be allowed for. The latter may either be compensated for electronically or

determined experimentally by other available means. (Section 3.4).

i. D.C. Technique.

A typical experimental set up of the corrosion cell for polarisation measurements is shown in Figure 3.7. The circuit consists of a device known as a "potentiostat" which provides carefully controlled out-put voltage or current, a working electrode whose corrosion rate is being measured, a reference electrode and an inert counter electrode.

R_p is estimated by applying a step of appropriately small potential (potentiostatic) or intensity (galvanostatic) and measuring the other variables in the steady state. It may also be estimated by applying a ramp of voltage (potentiodynamic) or intensity (galvanodynamic) at a given sweep rate. R_p is then the slope of E-I plot. Gonzalez et al[90,104] examined the cell response for different kinds of D.C. measurement using the modified Randel circuit (Figure 3.8). They found:-

a) For Steps of Voltage or Intensity:-

For systems corroding at relatively high rate, the steady-state conditions are achieved relatively quickly after polarisation. Conversely, systems whose corrosion rates are low require a relatively long time to achieve the steady state. The correct R_p can be obtained when the transitory component of current or voltage response of the circuit becomes negligible. The attenuation rate has a time constant:

$$\tau_E \simeq C R_e \quad \text{potentiostatic measurement} \quad \ldots 3.25$$

$$\tau_I \simeq C R_p \quad \text{galvanostatic measurement} \quad \ldots 3.26$$

where R_e the electrolyte resistance

R_p the polarisation resistance

C the capacitance of the electrolyte double layer.

Therefore the use of galvanostatic polarisation in passivated systems with high R_p values involves much longer time constants (τ proportional to R_p) than the potentiostatic or potentiodynamic ones (τ proportional to R_e).

b) For Ramp of Voltage or Intensity.

The time constant is a function of sweep rate. It has been suggested that the sweep rate must be slower the higher the R_p. In practice, Gonzalez et al[90,104], suggested that the relation between R_p values and the sweep rate must be established initially and then the sweep rate must be chosen within the range where Rp achieves a constant value. Usually for potentiodynamic operation, the sweep rate must be such that the sweep time to apply $\Delta E = \pm$ 10mV is longer than 5-6 τ.

ii. A.C. Technique.

In this method the impedance of the system is considered over a range of frequencies of interest, normally 100 Hz to 1 mHz.[110,111] An alternating signal of small amplitude is used to minimise changes in the surface activity of the reacting species. When the sinusoidal voltage is applied[112] to a corroding system, a sinusoidal current with a given phase shift relative to the input signal is obtained. The value of the polarization impedance 'z' is another sinusoidal function which can be decomposed in a resistive term and a capacitive term with phase shift of 90°, thus:

$$z = R_e + \frac{R_{ct}}{1 + j\omega CR_{ct}} \qquad \ldots 3.27$$

where ω is the angular frequency ($=2\pi f$)
j the imaginary unit $\sqrt{-1}$

The response of a corrosion cell as a function of frequency is usually presented as a plot of the real vs. the imaginary part of the measured impedance, Figure 3.9, and it may be modelled by an equivalent electrical circuit (Randles) as shown in Figure 3.10. The technique is able to measure electrochemical parameters such as the double layer capacitance C_{dt}, charge transfer resistance R_f and Warburg diffusion w as each of these responds to the applied voltage or current within a specific frequency range.

The a.c. impedance method can be used in low conductivity systems and because it is essentially transient it can provide information with out the requirement that the system reach a steady state condition.[113]

Finally, the following conclusions can be drawn for the evaluation of polarization resistance measurements.

1. The method is applicable for systems where the redox partial reactions can be neglected

2. At the time of measurement, knowledge of the proportionality constant B and the IR-drop is necessary for accurate determination of corrosion rate.

3. Corroding metals in the active state in electrolytes of sufficient conductivity and in the absence of surface 'barriers' may be evaluated using D.C. technique. In the case of systems with high apparent capacitances, polarization impedances 'z' and not polarization resistances 'R_p' are required which need special methods and equipment for their determination.

3.3 Corrosion of Steel in Concrete.

3.3.1 The Corrosion Problems.

Reinforcing steel is usually very effectively protected from corrosion when embedded in portland cement concrete. Good quality concrete often provides excellent protection for steel due to both its physical and, perhaps more importantly, chemical protective capacity. The most significant feature of cement hydration is that the aqueous phase rapidly acquires a high pH value. pH values in the range 12.5-13.1 are frequently reported for portland cement concrete of the w/c ratios commonly used in practice.[114,115,116] The high alkaline environment results in the formation of a tightly adhering film which passivates the steel over a wide range of potentials.[2,117,118,119] In addition concrete can be proportioned[120] to have low permeability which minimizes the penetration of corrosion-inducing species and increases the electrical resistivity so impeding the flow of corrosion current. Concrete, however, due to its porous structure is a far from perfect physical barrier.[4,120] Observations have indicated that a detrimental amount of chloride ions are capable of penetrating into high quality concrete beyond what would be a practical limit for the thickness of a concrete cover. Dense concrete is also normally fairly permeable to oxygen. Consequently the corrosion protection mechanism hinges mainly on the maintenance at the steel-concrete interface of the alkaline condition developed during the hydration process.

Nevertheless, despite the high protective ability of concrete, corrosion of steel reinforcement is becoming the most common cause of deterioration of concrete structures. Salted bridge decks,[34,122] coastal and offshore structures,[123,124,125] sewers[126,127] and structures in aggressive soils are some examples where severe corrosion attack occurs. Many such structures undergo costly repairs while many others are torn down prematurely. Apart from the architectural problem,[128] where rust spots appear on the concrete surface destroying the aesthetics of the

structure, corrosion has two detrimental effects from the structural point of view.[117,129] It reduces the cross section of the steel reinforcement and thereby its load carrying capacity and because corrosion products occupy a substantially greater volume than the steel from which they have been produced, it can also cause cracking and spalling of the concrete cover. Thus is likely to occur well before the strength capacity of the structure has been significantly reduced.

3.3.2 Loss of Protection.

Regardless of the exposure conditions, steel in concrete will only corrode when it becomes depassivated. Erlin et al[130] pointed out that reduction of pH to < 11.5 destroys the passivity of the protective film. Depassivation can occur either of two major ways, by carbonation and by the attack of aggressive ions. the two factors, however, can act synegistically.

Carbonation.

Carbonation is the reaction between concrete and acidic gas (usually CO_2 but possibly also SO_2) in the atmosphere which results in conversion of $Ca(OH)_2$ to $CaCO_3$ and the subsequent reduction in pH to around 9[2,126,131] Accelerated carbonation of the concrete in CO_2 - rich atmosphere generates bicarbonate[132] in the pore solution and results in even lower pHs in the range 6-7.

Generally there is a widespread tendency to discount atmospheric carbonation as a serious cause of steel corrosion. This is because well-hydrated portland cement pastes contain up to 20% weight $Ca(OH)_2$ and therefore possess considerably CO_2 neutralization capacity. Provided that the depth of cover to reinforcement is adequate. Carbonation should not penetrate to an extent which endangers the passivity of steel during the design life of the structure.[2,131] In practice[133] carbonation rates average some 20 mm in 12 years with a maximum of 32 mm.

Carbonation, nevertheless, appears to be a potentially dangerous possibility in particular climatic conditions of high temperature - humidity regions such as those prevailing in the Arabian Gulf seaboard.[121,123,134]

It has been generally observed that the relationship between carbonation layer depth (d) and the exposure time (t) is approximately parabolic in the form:

$$d = A\sqrt{t} \qquad \ldots 3.28$$

The magnitude of the constant (A) depends[126] on several variables such as the permeability of the concrete, the relative humidity and the concentration of gas in the service environment. Carbonation is also sensitive to the proper curing of the external surfaces and the alkali content of the cement. Research has indicated[134] that the application of different types of coatings has improved considerably the concrete resistance to CO_2 diffusion.

When the carbonation front reaches the steel quite general corrosion will commence at a rate determined by the availability of oxygen and water.

Carbonation of concrete can be detected using the standard phenolphthalein spray method on the outer concrete surface and cross-sections. The carbonated area remains colourless in the spray test on account of the indicator's property of being colourless in neutral and acidic conditions but turning purple coloured under alkaline conditions above a pH of $\simeq$ 8 to 9.

Chloride Ion Attack.

It is well documented[2,135,136,137] that the intrusion of chloride ions in reinforced concrete can cause corrosion if oxygen and moisture are present. Chloride ions may be introduced into concrete in a variety of ways, such as during manufacturing as intentional or accidental intrusion or by penetration from an external source. In

concrete, chloride ions may be present in various forms such as:

- Free chloride ions in the pore solution.
- Chloride loosely bonded to hydrates of calcium silicate.
- Chloride strongly bonded to hydrates of calcium aluminates.

It is principally only the free chloride ions that influence the corrosion process. There is, however, a general lack of information about the level of chloride likely to remain un combined for a long period in the solution phase.

The concept of a critical chloride level or corrosion threshold for steel in concrete has been suggested by a number of investigators using a variety of experimental techniques. There is some evidence that the hydroxyl ion concentration of concrete has an influence on the critical chloride level and Hausman[16] has suggested a critical chloride/hydroxyl ion activity of R = 0.6. The Building Research Establishment[139] categories the chloride ion content of concrete in terms of corrosion risk as follows: < 0.4% low risk, 0.4 - 1% medium risk and > 1% high risk.

It is widely recognized that chloride has negligible influence on the pH of concrete. The enhancement of the C_3A content reduces the chloride content within the cement Figure 3.11 but the optimum level has not been established.[126,135,140,143] The chloro-complex with C_3A, however, becomes unstable when carbonation occurs which tends to liberate chloride ions. On the other hand, the diffusion kinetics of chloride ions in hardened concrete is a decisive factor in relation to corrosion risk. Investigations[140,141,142] have confirmed that diffusion is strongly influenced by cement type, Figure 3.12, and fineness, the ion exchange capacity of the system, and the curing of the concrete surface. The effect of the w/c ratio is only limited to a surface layer of the concrete and to short duration of chloride exposure (Figure 3.13).

The precise mechanism by which depassivation occurs

is still a subject of contention.[120,131,138] Either the chloride ions convert the insoluble iron-oxides to soluble ion-chlorides which diffuse away and destroy the passive film or ions are absorbed on the metal surface and promote the hydration and dissolution of metal ions.

3.3.3 Mechanism of Corrosion of Steel in Concrete.

The corrosion of steel in concrete is an electrochemical process in which the moist concrete forms the electrolyte. the possible electrochemical reactions taking place on embedded steel can be thermodynamically represented by a simplified Pourbouix diagram, Figure 3.14.

The primary anodic reactions of interest are:

$$3Fe + 4H_2O \longrightarrow Fe_3O_4 + 8H^+ + 8e^- \quad ...3.29$$

$$2Fe + 3H_2O \longrightarrow Fe_2O_3 + 6H^+ + 6e^- \quad ...3.30$$

$$Fe + 2H_2O \longrightarrow HFeO_2^- + 3H^+ + 2e^- \quad ...3.31$$

$$Fe \longrightarrow Fe^{++} + 2e^- \quad ...3.32$$

The possible cathodic reactions are:

$$2H_2O + O_2 + 4e^- \longrightarrow 4OH^- \quad ...3.33$$

$$2H^+ + 2e^- \longrightarrow H_2 \quad ...3.34$$

However, in alkaline environment such as that of concrete, oxygen reduction is recognized as the cathodic reaction in most cases of significant corrosion.

Wilkins et al,[118] Hansson[117] and Arup[144] described the sequence of events generally encountered in practice and defined four states of protection and corrosion. These

basically include passive state, pitting condition, general corrosion and active low potential corrosion.

In good quality concrete and in the absence of pH lowering agencies, Equations 3.29 and 3.30 are the primary anodic reactions the oxides Fe_3O_4 and Fe_2O_3 will form a very thin protective layer. A small passive current is required to maintain the protective film, but, the mechanisms involved in the cathodic reduction of oxygen on the passive surface of steel are not at all clear.[118,144] In this state, the corrosion rate is significantly low (0.1 - 1μm/year) and in the absence of chlorides the passive potential range is very wide, from +0.2 to -0.7 V(SCE) at pH 13. This range reduces to +0.1 to -0.2 V(SCE) in aerated concrete. The passive state in a chloride-bearing environment is normally characterised by a very negative potential in the range -0.8 to -1.1 V(SCE).[118]

Corrosion initiates when the passive film is destroyed either generally over the metal or locally in which case a corrosion cell is formed with an adjacent area of passive steel acting as a cathode where oxygen is reduced and the dissolution of iron takes place only at small areas. Thus, depassivation can lead to pits in the steel (Figure 3.15).

In order for corrosion to proceed, there must be a complete electrical circuit between anodic and cathodic areas of the steel. The reaction kinetics, thus, are controlled by the electrical resistance of the concrete.

Pitting is most likely to develop[144] in concrete with good conductivity, high alkalinity (non-carbonated) if a sufficient amount of chloride reaches an isolated area of the reinforcement. It is generally recognized that pit growth is accompanied by the development of solution conditions within the pit of locally elevated chloride ion concentration and depressed pH, a pH gradient[146] from approximately 2 to 12 is reported to have existed between local regions within the concrete. Under these conditions, the corrosion products formed are soluble near the anodic area and thus spalling of concrete is unlikely and also other evidence of corrosion by solid corrosion products on

outer surface of the concrete may not be seen. Arup[144] indicated that the process involves a drop of the average corrosion potential due to the polarization of the cathode and this probably is the strongest factor in preventing formation of new pits in the neighbourhood until much higher chloride concentrations are established elsewhere.

Factors which limit the diffusion of chloride ions or enhance the diffusion of hydroxyl ions in the vicinity of pits will tend to promote repassivation of the pits. Repassivation, however, depends on a complex interaction between the physical and chemical characteristics of the cement paste and is therefore a field of continuing research. Typically, steel undergoing pitting corrosion exhibits a potential between -0.2 to -0.5 V(SCE).

General corrosion is a result[144] of a general loss of passivity brought about by either carbonation or the presence of excessive amount of chloride and both cathodic and anodic reactions take place every-where on the surface. Thus metal dissolution takes place in neutral or alkaline environments which, where oxygen has access, produces solid rust and likely to cause spalling at early stage.

Carbonation-induced corrosion rates can be restricted in high resistivity/low water condition. Corrosion[2,144] due to chloride is more often found in concrete where water is abundant in which case the diffusion of oxygen through the pore solution is to be the rate-determining factor. The average potential lies typically between -0.45 to-0.6 V(SCE).

The state of active low potential corrosion occurs when the access of oxygen is very limited to support the cathodic reaction necessary to maintain the passive current density. The free corrosion potential is therefore very low, say -1.2 V(SCE), and consequently even if the steel is active (ie. is not covered by passive film) the actual corrosion rates are likely to be very low. Wilkins et al[118] indicated that in extreme cases, the steel embedded in concrete would be anodic to bare steel in fully immersed condition and would tend to cathodically protect it to the limit of the repassivation current.

3.3.4 Concrete Cracking and Corrosion.

The problem of concrete cracking-rebar corrosion interaction represents a classical case where separation of cause and effect is not easy.

There seems little disagreement that corrosion can, in circumstances of insoluble corrosion products, cause cracking in concrete. Cracking due to corrosion is a result of large amount of expansive insoluble corrosion products which exert tensile stresses greater than the tensile strength of concrete. The process depends on several factors including[146] (1) corrosion rate of the embedded steel, (2) diffusion rate of metal away from the steel-concrete interface, (3) solubility and specific volume of the corrosion products and, (4) chemistry of the pore solution.

Conversely, there are two different[126] theories about the effect of cracks on the corrosion of steel in concrete. Theory No. 1 states that cracks significantly reduce the service life of structures and accelerate the onset of corrosion by permitting access of aggressive species, moisture and oxygen to the reinforcement. This consideration is the most important single factor upon which the crack width limitations in the national codes have been based.

Theory No. 2 indicates that although cracks can be instrumental in accelerating the onset of corrosion, they do not play any direct role in increasing the cathodic area. Such corrosion is localised and confined to the reinforcing bars intersecting the concrete cracks and after a few years of service there is little difference between the amount of corrosion in cracked and uncracked concrete. Considerable experimental evidence[128,131,147,148,149] has been presented which support this theory in atmospheric conditions. Tuutti[147] indicated that the cracks in concrete cover do not change the basic corrosion mechanism but only influence the local flow and at a later stage the total flow reaches the same value as in homogeneous concrete.

However Beeby[145,149] pointed out that the corrosion process under water might lead to quite different conclusions from those drawn from atmospheric situations. Metha et al[131] proposed a cracking-corrosion interaction model for concrete exposed to marine environment as illustrated in Figure 3.16 which shows a clear relation through a continuing chain of reactions. More recently Wilkins et al[118] have substantiated this view, they observed that longitudinal static cracks or wide (>2 mm) transfer cracks did not show passive behaviour in totally submerged specimens.

The role of cracks in corrosion propagation and extent seems to be particularly critical in concrete structures exposed to fatigue loading in sea water. Considerable loss of bar cross section at sites of cracks in the concrete have been reported by several research workers.[59,150] In direct contrast with atmospheric corrosion, these studies suggest that the severity of attack was found to be dependent on crack widths and time of exposure.

3.3.5 Resistivity of Concrete and Corrosion of Steel Bars.

It is generally agreed that the resistance of concrete does not determine whether corrosion of reinforcing steel is occurring, thus passive steel does not sustain corrosion even though the resistivity is low. Once the steel is depassivated,[100,110,151] conditions which lead to low resistivity such as high pore water content and the presence of electrolyte salts usually favour active corrosion as they allow significant current flow in the concrete part of the electric cell. Conversely, high resistivity of the concrete becomes one of the important factors which controls the rate of corrosion.

Gonzalez et al[152] presented data showing that in the presence of factors stimulating corrosion, the current density is inversely proportional to the resistivity of the mortar.

Hope et al[151] found that the half cell potential dropped from about -0.45 V SCE to about one-third of this value as the resistivity of concrete increased from 6500 to 8500 Ω cm. Cornet et al[198] observed a decrease in resistance after the test beam reached the time to exhibit visible signs of corrosion. This was considered to be a result of the shortening of the electrical current path at and after this point.

Attempts to relate corrosion and resistance in quantitive terms have given as many different results as the number of the attempts themselves. It seems, however, that resistivity can give better predictions of the probability of corrosion than of its rate. Browne[153] investigated off shore concrete structures and stated that the resistance must fall below the range 5000 - 10000 Ω cm in order to support corrosion. Clear[154] found, however, that there were significant corrosion currents at resistivities in excess of 20,000 Ω cm whereas Temper et al[148] suggested a value of 60,000Ωcm to inhibit or prevent accelerated corrosion. Cavalier and Vassie[122] investigated corrosion damage in highway bridges and provided information which relates the probability of corrosion to concrete resistivity as follows:

Concrete Resistivity Ωcm	Corrosion
>12,000	Usually not Significant
5,000 - 12,000	Probable
<5,000	Almost Certain

The observed large differences in the results obtained by different investigators are not readily explainable in terms of different experimental conditions and measuring techniques and will be discussed further in Chapter 9.

3.3.6 Design Against Corrosion.

Theoretical models[147,155,156,157] for the process of initiation and propagation of corrosion including the introduction of a finite-element technique have been proposed by several researchers. In studying these it readily became clear that the process is very complex, and that none of these models can be predictive at present. Assessment of the safe life of the structure in relation to corrosion[149] is still lacking acceptable criteria defining the tolerable corrosion and the degree of environmental aggressiveness.

The present approach[145,158,159,160] considers the service life (t_s) of a concrete structure as the sum of a corrosion initiation stage (t_o) in which the steel is passive and the subsequent propagation stage (t_1) when corrosion damage is sustained, Figure 3.17. This may be expressed as follows:

$$t_s = t_o + t_1 \qquad \ldots 3.35$$

$$t_1 = Q_{max}/i_{corr} \qquad \ldots 3.36$$

where Q_{max} is the maximum tolerable corrosion per unit area.

i_{corr} is the average corrosion rate.

The design problems is to ensure that the service life (t_s) is greater than or equal to the design life (t_D) of the structure, ie.

$$t_D \leq t_o + t_1 \qquad \ldots 3.37$$

Browne[159] indicated that it is reasonable to base the design method on the assumption that the initiation time

should not exceed the design life, that is $t_D \leq t_o$. He also presented a design nomogram for life prediction in relation to chloride diffusion and cover thickness.

Except when concrete is made[158,159] from materials containing deleterious levels of chloride salt 't_o' is the time taken for carbonation to reach the outermost steel bars or for chloride to penetrate the concrete until a threshold concentration is reached at that level. Time for significant damage to occur is less predictable due to many parameters including the rate of oxygen diffusion, concrete quality, cover thickness and others. The values of 't_1' observed in practice,[161] however, appear to be significantly lower than those of 't_o'.

It should be pointed out that the prediction model assumes sound un-cracked concrete. In cracked concrete, however, the mechanism of deterioration may be substantially different as cracks provide short-circuit paths and hence reduce t_o.

Another increasingly important approach is that concerned with appraisal of existing structures and repair of damage due to corrosion as will be discussed later.

3.3.7 Corrosion Rate Measurements of Steel in Concrete.

Electrochemical measurements on steel embedded in concrete are essentially laboratory-based techniques. Field investigations are mainly restricted to corrosion potential measurements and their change with time. Wilkins et al,[118] however, indicated that the change in potentials is not, necessarily, an indication of corrosion activities since change to a more negative potential could be due to increased corrosion or a limiting cathodic reaction (Figure 3.18). Nevertheless it is usually accepted[110] that potentials more negative than certain critical values are an indication of active corrosion and this is the basis of an increasingly employed potential mapping technique for the assessment of corrosion risk in the field. Other electrochemical measurements are generally troublesome and, as yet, less applicable outside laboratories. In the

laboratory the correct determination of the corrosion rate is limited by one or more of the factors given earlier in subsection 3.2. However, in reinforced concrete the accuracy of the electrochemical measurement is particularly sensitive to the degree of accuracy in the allowance made for the very high resistivity of the concrete and for the very restricted diffusion process through concrete.[111] Electrochemical measurements on steel embedded in concrete can be made by two basic methods.

i. Anodic and Cathodic Polarization Curves.

These measurements investigate the active/passive behaviour of steel in concrete[117,118,162] and may be conducted potentiodynamically or potentiostatically at relatively high over potentials. The shape of the polarisation curve for passivated steel in concrete is shown in Figure 3.19. In the passive region the measured currents are low and the change in potential with current is quite steep ($\Delta E/\Delta I \simeq \alpha$). At very positive potential the slope of the curve is essentially zero, that is very large current for very small change in voltage, and oxygen evolution takes place and significant corrosion of the steel may be re-initiated. This portion of the curve is referred to as the transpassive region which initiates at transpassive potential (E_{TP}). Under actual field conditions such high potentials are not encountered unless large stray voltages are applied.

The cathode polarization curve approximates to Tafel behaviour when oxygen is plentiful but at much more negative potentials (not usually encountered in practice) hydrogen reaction becomes the predominating cathodic reaction.

The presence of chloride ions causes the passivity to break down at potentials at which the steel would remain passive in their absence resulting in possibly rapid localized or pitting corrosion. Figure 3.20 compares different anodic polarization curves for steel in different states.

ii. Linear Polarization method (L.P.M.).

A large number of researches[90,104,132,163] have indicated the reliability of this technique in assessing the corrosion rate of steel embedded in concrete. There are, however, some major technical difficulties in obtaining as well as interpreting these measurements. At small overpotentials usually $\pm$ -20 mV, the net current for steel that is not actively corroding is extremely small giving rise to measuring difficulties. Hansson,[117] suggested that the technique is appropriate for actively corroding steel but less so for passivated steel. The second difficulty is that a B value has not been determined accurately for steel in concrete.

Gonzalez et al[90] indicated that good agreement relative to gravimetric weight losses, is achieved with a constant B value of 26 mV for steel in the active state ($I_{corr} \geq 0.1 - 0.2\mu$ A/cm^2) and 52 for the passive state ($I_{corr} < 0.1\mu$ A/cm^2). The validity of these values has also been confirmed by other research workers.[163,206]

In another study, Gonzalez et al[104] showed that a sweep rate between 2.5 and 10 mV/min and a waiting time of 15 - 60 sec for $\pm$ 10 mV step give almost coincident values (Figure 3.21). For a fast sweep rate the R_p value may be underestimated and overestimated for very slow sweep rate (Figure 3.22). On the other hand a longer waiting time will increase the possible diffusion processes and this may transform the system into a different one. The recovery of potential upon the latter kind of measurement is dependent on the state of steel as shown in Figure 3.23, which indicated that, contrary to passive steel, active steel exhibits early recovery of potential. It should be appreciated, however, that most of the aforementioned limitations and recommended values were mainly drawn from investigations on small specimens with very simple steel arrangements. Galvanostatic and galvanodynamic measurements[104] are not recommended for reinforced concrete since they require considerably longer time to achieve the steady state condition necessary for

accurate determination of R_p. Finally A.C. impedance techniques are not widely used for corrosion rate measurements of steel embedded in concrete. More attention, however, has been paid recently to their application as it is though that they can be very useful tools particularly in high resistivity concrete.

3.3.8 Methods of Preventing Corrosion in Reinforced Concrete Structures.

A large number of reinforced concrete structures around the world are now deteriorated to varying extents. The size of the problem is horrific. For example[164] according to a report published in 1981, the estimated number of deficient bridges due to corrosion in the United States alone was well over 50,000 with an estimated cost of 11-17 billion Dollars to replace or rehabilitate these bridges. The size of the problem, naturally, stimulates action to improve the available techniques for corrosion prevention and to introduce other less expensive techniques for both existing and new structures. The following presents a summary of the techniques presently used.

i. Existing Structures.

These methods are used in structures sustaining tolerable damage which do not require complete replacement of the structure.

Cathodic Protection.

The method was first used in bridge decks and was pioneered in 1974 by Stratful.[165]

In this method an external current is applied to reduce the potential value below the open-circuit potential (E_{corr}) of the reinforcement. Two methods[120,164] are used to supply the external current. In one, the sacrificial anodic system, the protected metal is made the cathode by connecting it to a more active metal acting as

an anode (a metal with more negative corrosion potential). In the second, the impressed current system, an external direct current power source supplies the current. The latter is by far the most commonly used technique, mainly because of the poor conductivity of concrete and other practical problems evolving from the necessity to place the anode on the concrete surface. The criteria for the cathodic protection of steel in concrete are not clearly established and potential values ranging from -0.5 to -0.9 V SCE have been indicated.[164,166,167] It is generally recognized, however, that the most negative value must be limited to about -1.10 V SCE. This is believed necessary to avoid loss of bond between steel and concrete as a result of hydrogen evolution at the cathodic steel surface.

The cathodic protection has the advantage that the contaminated concrete does not have to be removed and is especially promising, therefore, for Cl^- damaged corrosion.

Electrochemical Removal of Chloride From Concrete[120,168]

This method tends basically to modify the environment surrounding the steel reinforcement to make it less corrosive and involves the application of a large D.C. potential between the steel and the external surface anode.

Placement of Overlays.

The method involves placement of overlays on the concrete surface to prevent further ingress of aggressive species. This can be accomplished by placing either an overlay of high density, low permeability concrete or latex modified concrete or an asphaltic membrane on the concrete surface. This technique,[168] however, is controversial because some field data exists which suggests that the applications of membranes or overlays to chloride contaminated concrete may exacerbate rather than reduce the level of corrosion. Other experimental data

together with field data suggests that the opposite is true. The successful application of this method seems to depend on the degree of corrosion damage already sustained by the structure and further research needs to be carried out to clarify this point.

Repair.

This approach is widely used for stopping and subsequently controlling corrosion in reinforced concrete structures. It is usually undertaken after careful consideration of cost factor and involves breaking open the corroding regions, clean back to bars, clean the bars and paint them and re-cover with (usually cementitious) mortar.

ii. New Structures.

- Application of coatings[120,168] on the reinforcement such as epoxy resin or metallic coatings (zinc, cadmium, nickle).

- Increase concrete cover to reinforcement, good construction practice and quality control.

- Decrease the permeability of concrete by polymer impregnation of the surface, placement of waterproof membranes and the internal sealing by the addition of wax bread. The latter method has been shown to greatly reduce the permeability and involves[169] the addition of wax breads on a solid volume basis by replacing approximately 7.8 percent of the volume of concrete occupied by fine aggregate. The wax is mixed with the other components of the concrete until it is well dispersed in the mix, the concrete is then placed and cured in a normal manner. After the characteristic strength is achieved, the concrete is heated which causes the wax to melt and flow into capillaries and pores. Five to nine hours of heating are required for a bridge deck if melting to a 76 mm depth is desired.

3.3.9 Corrosion Inspection Techniques.

Methods currently available[111,161,170,171] for detecting the corrosion of steel in concrete are broadly categorised into two types, non-electrochemical and electrochemical techniques.

i. Non-Electrochemical Techniques.

Visual Inspection.

Which often provides the first indications of the corrosion problem. The visual on-surface signs of corrosion may include hairline cracking, brown stains and spalling. Visual inspection also includes opening up the concrete to expose the reinforcement at a few representative locations.

Mechanical and Ultrasonic Tests.

Delamination can be detected by the hollow sound produced upon hitting the concrete surface with a hammer. Rebound or Schmidt hammer usually used for this purpose. Ultrasonic pulse velocity (Pundit) is also used to detect cracks and assess the quality of cover.

Core Sampling and Chemical Tests.

Core sampling is useful to assess the condition of the concrete and to determine the depth of carbonation by the application of phenolphthalein.

Chemical tests to determine the chloride content and in particular its variation with depth from the top surface gave valuable indications of the likelihood of corrosion risk.

ii. Electrochemical Techniques.

Electrical Resistivity.

The method provides information on the concrete composition and performance. Typical guide lines have been proposed to relate the resistivity measurements to the probability of corrosion these are discussed in Subsection 3.4.

Rate of Corrosion Probes.

Which provide cumulative rate of corrosion data from periodic measurement of the electrical resistance of a steel wire or hollow cylinder embedded in concrete.

Polarization Resistance Method.

This method is essentially a laboratory-based technique. Field applications are difficult[110] because the reinforcing steel is part of a grounded network and current measurements are troublesome. However, electrically isolated corrosion probes inserted in the concrete could be used.

Electrochemical Noise Measurement.

The technique has recently been introduced to the field of reinforced concrete. Some degree of success has already been reported[111] on the application of this technique in real concrete structures.

Potential Mapping.

The technique is well known and is widely advocated for the inspection of bridge decks.[122,172] Corrosion potential is measured using a reference electrode placed on the concrete surface which is connected via a high impedance voltmeter to the reinforcement, Figure 3.24. The

standard method for conducting these measurements is described in the American Standard[173] ANSI/ASTM C876-77. According to this standard the interpretation of half cell measurements with respect to SCE is:

E_{corr} volts (SCE)	Probability of corrosion
< - 0.140	> 90% corrosion not occurring
-0.140 to -0.290	Uncertain corrosion activity
> -0.290	> 90% corrosion occurring

Although this method can give good prediction of the corrosion state of the embedded reinforcement, there are three major drawbacks:[174]

1. The measurements are sensitive to the uniformity and degree of saturation.
2. The technique reflects, mainly, the potential of the steel nearest the surface.
3. Measurements can not be made when direct access to the surface is not possible.

Recently, Wood et al[174] described a new 3-D half cell measuring technique which is assumed to overcome most of the above mentioned drawbacks. The measuring device employ flexible extendable probes with a side contact, thus permits the monitoring of reinforcement potential at different depths through a hole in the concrete.

Sometimes, it is found that a better indication, than the actual level of potential measured, for identifying corroded regions of rebar or change in local environment, is the detection of local steep potential gradients during the potential survey.

3.4 Electrical Resistivity of Concrete.

The electrical resistivity of concrete has been the subject of many investigations. Attempts to relate

different physical and chemical changes in cement and concrete to its electrical properties have been made with some success in laboratory and field measurements.

Electrical resistivity measurements were made and interpreted to provide information on various aspects of concrete technology which can be categorised into the following main lines.

1. Determination of the physical and chemical changes during the setting and hardening processes of cement and concrete.[178,179,180,181,182]
2. Assessment of the variation of concrete quality in surface and in depth, salt contamination and the likely occurrance of corrosion of embedded steel.[122,183,184]
3. Electrical insulation strength of concrete.[185,186,187]
4. Determination of the moisture content.[188,189]

In this section, the basic concept of electrical conduction through concrete as well as the methods available for electrical resistivity measurements will be reviewed and discussed.

3.4.1 Concept of Resistivity.

The electrical resistivity of any material is defined as the resistance in ohms between opposite faces of a unit cube of that material. Thus if R is the resistance of a block of concrete having a length, L (m) and a cross-sectional area, A (m^2) the resistivity, is expressed by the formula:

$$\rho = \frac{R\,A}{L} \quad \Omega m \qquad \ldots 3.38$$

Resistivity, being a fundamental property of the material is independent of the volume, whereas resistance depends upon the shape and size of the specimen. The conduction of material is defined as the reciprocal of its

resistivity i.e.

$$\sigma = \frac{1}{\rho} \quad \text{siemens m-1} \qquad \ldots 3.39$$

3.4.2 Conduction Paths Through Concrete.

i. Physical Model.

Concrete may be considered as a composite of solid particles of aggregate of various sizes in a matrix of cement paste. The microstructure of cement paste is composed of three main components, the solid particles surrounded by ions atmosphere, solid particles in contact with each other and pore spaces mostly filled with water and containing dissolved compounds.

Whittington et al[177] studied the conduction properties of concrete and suggested that when a voltage is applied to such a hetergeneous medium, current can have three possible paths:

I through the aggregate and paste in series.
II through the aggregate particles in contact with each other.
III through the paste itself.

The conduction through the paste, however, that is Path III, was discussed earlier by Monfore[185] who suggested that the paste itself may also be considered as a composite of non-conductive particles in a matrix of conductive evaporable water.

Taylor et al[180] have also proposed the idea that the current can possibly be transmitted in the paste through:

a. the solution and conducting particles in series.
b. particles in contact with each other.
c. the solution.

the relative contributions of each of these paths is hydration dependent and although markedly changeable during the setting and hardening processes but remain constant for the rest of time should environmental factors remain constant.

The resistivity of typical aggregates used in concrete are several order of magnitude higher[177,185] than that of concrete. Consequently, a higher proportion of current will be conducted through the paste. Monfore[185] presented data showing that the resistivity of sandstone and limestone are considerably greater than the resistivity of the paste which implies that the resistivity of moist concrete must be considerably dependent upon the resistivity of the paste matrix.

The combined conduction model for the possibilities described above is shown in Figure 3.25.

ii. Electrical Equivalent Circuits.

Hammond and Robson[186,187] and Monfore[185] found that the capacitive reactance of hardened concrete is much greater than its resistance. In consequence, only the latter is contributing to the resistance, thus for practical purposes the D.C. model can also be assumed for A.C. and the electrical model may with sufficient accuracy be considered purely resistive with concrete constituents represented by a parallel combination of resistive elements, Figure 3.26a. This model, however, does not fully explain[180,181] the A.C. characteristics in the liquid state when the capacitative element has an influence upon the overall impedance of the paste and hence on concrete. This necessitates the inclusion of a capacitative element in parallel with the resistive element, Figure 3.26a.

3.4.3 Mechanisms of Conduction Through Concrete.

The preceding section describes the conduction paths through concrete and indicates the resistance and conduction characteristics of concrete are considerably

dependent on the paste matrix. The mechanism of conduction through concrete is commonly described, as suggested by Nikkannon,[185] as being essentially electrolytic in nature, Calleja[178,179] utilised electric resistivity measurements to study the setting process of the cement paste and observed an increase in resistance as the amount of water which combines with solids increases. A small constant drop in resistivity was observed in the early stages of setting which was attributed to an increase in ionic conduction produced by the hydrolysis of alkali compounds and aluminates. Subsequent tests by Robson et al,[186,187] Monfore,[185] Taylor et al[180] and Hansson[175] supported the view that conduction is by means of ions in the evaporable water. The most common ions in the cement pore solution are Na^{+}, K^{+}, Ca^{+2}, SO^{-4} and OH^{-}.

The volume of evaporable water in typical cement paste varies from about 60% at the time of mixing to about 20% when the portland cement is completely hydrated.

The concentration of ions and conductivity vary with time. Another conduction possibility is by means of electronic conduction through cement compounds.

The conduction process can, thus, be visualised as having two components.[177,178,179,181]

- Ionic conductivity of the solution which depends on ionic concentration, temperature and type of ions present.
- Electronic conduction through gel, gel-water and un-reacted cement particles which depends on cohesiveness and setting progresses.

Whittington et al,[177] indicated that the two above mentioned components are virtually inseparable as the paste itself is in a constant state of change. However, for hardened concrete, the current flows predominantly by the migration of ions in the pore solution. Electronic conduction is a contributory factor to a greater extent in the case of reinforced concrete where reinforcing bars provide an effective least resistance path.

Hansson et al[175] and McCarter et al[185] described the electric conduction through concrete as follows:

On the application of an electrical potential between two metal electrodes in contact with or embedded in the

concrete, current flows by migration of free ions in the pore water and discharge at the electrodes producing a conduction effect. Other charges which are bound to the particle surface displace in sympathy with the applied electric field and produce polarisation of different types i.e. separation between centres of positive and negative polarity. This will create an opposite electric field and causes a decrease in the current. On the electrode, however, one or more of the following electrochemical reactions take place.

$$2H_2O + 2e^- = H_2 + 2OH^- \quad ...3.40a$$

$$4OH^- = O_2 + 2H_2O + 4e^- \quad ...3.40b$$

$$3Fe + 4H_2O = Fe_3O_4 + 8H^+ + 8e^- \quad ...3.40c$$

$$2Fe + 3H_2O = Fe_2O_3 + 6H^+ + 6e^- \quad ...3.40d$$

The dissociation of water will be the dominant reaction when steel at the electrode is passive and these reactions result in the build up of polarised layer in the vicinity of the electrodes and produce an effective back emf. During the application of an alternating electric field, it is generally thought that the polarisation layers would not have time to develop or that their effects cancel out on reversal of the electric field which is obviously frequency dependent since certain polarisation mechanisms are only operative over a particular frequency band.[181]

3.4.4 Electrical Resistivity Measurement.

The characteristics of the cement and hence concrete vary to an enormous extent throughout the setting and hardening processes. Consequently the relative influence and importance of the electrochemical factors such as polarisation and capacitance change with time. Also, the electrical properties may not be constant throughout the concrete body[186] since:

1. Concrete itself is a heterogeneous material.
2. Stratification occurs during placing.
3. Subsequent drying out takes place preferentially from the exposed surface resulting in a moisture gradient from the centre to the exposed face of the concrete.

Moreover, a review of the published literature on the resistivity of cement and concrete indicates that a wide variety of measuring techniques have been utilised and that there is a little agreement on which is the most appropriate.

Accordingly, although general trends may be detected substantially different results have been obtained by different investigators. Hansson et al[175] have concluded that the required information is not generally obtainable from one technique, and therefore, the most appropriate technique for measuring resistivity depends largely on adequate foreknowledge of the predominant electrical field the system is exposed to, the degree of saturation, and the possibility of a metal contribution to the conduction ability in case of reinforced or metal containing concrete.

Methods of Measurement.

The methods of determining concrete resistivity can be put into three different main categories D.C., A.C. and current interruption techniques. The D.C. and A.C. techniques are basically conducted by applying the specific electric field between two electrodes across the concrete specimens and determining the current-potential relationship, the resistance being the slope of the curve. The electrodes may be made of[151,175] brass, mild steel and stainless steel. It has been the custom to embed the electrode in the concrete or cement specimens in order that the current only passes through the interior portion of the specimens, Figure 3.27a. This practice, however, was subjected to criticism primarily due to the fact that it did not take into account the surface resistance which

may be considerable in real structures because of the moisture gradient. This of course, is of little importance in the fully submerged condition, i.e. no moisture gradient. Another objection to the use of this method[186] is that it is a matter of conjecture which area should be used for calculating the volume resistivity, the area of the electrode or cross section area of the specimens. To ensure that the applied current traverses the whole of the specimen, external electrodes identical to the area and the shape of the specimens have been used, Figure 3.27b. Yet another problem arises as to how intimate contact between the electrode and the specimens can be ensured. In this respect the following conductive materials have been used:

1. Stiff paste[186] of colloidal graphite.
2. A gel made of 2% agar.[151]
3. A liquid cement paste of preferably 0.5 water/cement ratio.[179,191]

However, the superiority of using cement paste compared with other methods has been suggested by many authors.

i. <u>D.C. Measurement.</u>

D.C. measurements are accomplished by applying a constant electric field between the two electrodes and measuring the resultant current, Figure 3.27. The current is allowed to decay to a steady state value before measurements.[175,180,185] Hausmann[190] and Monfore[185] have shown that the D.C. resistivity can not be determined by single measurements of the applied potential and current because a certain potential is required to overcome the polarisation effects. Hansson et al[190] and Hammond et al[186] emphasised the necessity of ensuring that the applied voltage should be above the level of the polarisation drop.

Various methods and circuits are available for D.C. measurements, but the choice of a convenient method depends on the magnitude of resistance to be measured and

the electrical properties of the material. At early ages when the resistivity is comparatively low, low voltage must be employed in order to minimise the current and the consequent heat development in the sample. The effect of polarisation is very considerable if allowed to build up. Hammond et al[186] investigated the effect of polarisation at these ages and presented data showing the marked effect of the phenomenon and that the back emf may attain values of the same order as the impressed voltage. To minimise this effect they introduced a test meter supplying its own small D.C. voltage and included in the circuit a switch which reversed the current approximately twice per second. The setup, which included mercury electrodes, had also been used to measure high resistivity concrete, and this device provides information about both the surface and volume resistivity.

The effect of polarisation is commonly considered as a major problem in D.C. measurements, but very little information is available about its effects on the electrochemical equilibrium of the system. Hausmann,[190] has shown that the initial response of the cathodic electrode in D.C. measuring circuits is predominately a chemical reaction occurring at the surface opposes the impressed voltage with an electromotive force of almost equal magnitude. Therefore, if an investigator were to confine his measurement to the lower voltage range, concrete would show a behaviour as in portion I of Figure 3.28 until a limiting polarisation was attained. Therefore a sharp increase in the current would occur resulting in a linear E-I relationship as in Figure 3.28 portion II. The cell resistance being the slope of the linear portion of the curve and the intercept on the voltage axis the voltage drop due to the polarisation effect.

Monfore[185] has also discussed this effect and showed that the effective applied potential rather than the measured applied potential should determine the resistance. Thus:

$$I = \frac{E_{eff}}{R} = \frac{E_a - E_p}{R} \qquad \ldots 3.41$$

where

E_{eff} is the effective potential.
E_a is the applied potential.
E_p is the polarisation potential.

In order to evaluate R and E_p from measurements of I and E_a, it is necessary to make measurements using at least two different values of E_a. E_p can be assumed to be independent of E_a over a certain range of E_a values, and thus Equation 3.41 can be written as:

$$I_1 = \frac{E_{a1} - E_p}{R} \quad \ldots 3.42a$$

$$I_2 = \frac{E_{a2} - E_p}{R} \quad \ldots 3.42b$$

From Equations 3.42a and 3.42b:

$$E_p = \frac{E_{a1}I_2 - E_{a2}I_1}{I_2 - I_1} \quad \ldots 3.43$$

and

$$R = \frac{E_{a2} - E_{a1}}{I_2 - I_1} \quad \ldots 3.44$$

It can be noted that Equation 3.44 is the slope of the linear position of E-I curve.

ii. A.C. Measurement.

A.C. measurements can be conducted in essentially the same way as for D.C. method except that the direct voltage supply must be replaced by an oscillator of suitable range of frequency and voltage. The principal advantage of this method is that it negates the effect of polarisation phenomena. During A.C. measurements, it is generally though, as mentioned earlier, that the polarisation layers

would not have enough time to develop or that their effects would cancel out on reversal of the electric field[175,191] thus keeping unaltered the concentration of electrolyte.

Several authors have studied the A.C. characteristics of cement and concrete, and several electric circuits have been proposed or used for this purpose.

To explain the effect of polarisation on the electrolyte conduction during A.C. measurement, Jones and Christian[197] (quoted by Monfore[185]) presented data indicating that it has the effect of a large capacitance in series with the resistance of the electrolyte. However, for concrete and cement paste it is generally believed that the system may be considered as a complex network of resistance and capacitance which can be expressed as a parallel combination of resistance and capacitive elements as in Figure 3.26. The model may further be reduced to a single capacitance, C, connected in parallel with a resistance,[177,180,187] Figure 3.29.

The impedance of the concrete to an alternating current is given by:

$$\frac{1}{Z^2} = \frac{1}{X^2} + \frac{1}{R^2} \qquad \ldots 3.45$$

where z = Impedance, ohms

R = Resistance, ohms

$X = \frac{1}{2\pi fC}$ = Capacitative reactance, ohms

f = Frequency of alternating current, Hz

C = Capacitance, Farads

As explained by Hammond and Robson[187] the effect of reactance on the total impedance is governed by the relative magnitude of X and R, and the effect will be appreciable when X is of the same order as, or smaller than, R. The relative contribution of the capacitance and

resistance in the conduction of the current is indicated by the power factor, given by the expression:

$$\text{Power factor} = \frac{\text{Power Loss in Resistivity}}{\text{Total Power Passing Through}} \quad \ldots 3.46$$

which is related to the capacitance and frequency by the formula:

$$\cos\phi = \frac{1}{\sqrt{1 + (2\pi fC)^2}} \quad \ldots 3.47$$

ϕ being the phase angle.

When current of low frequency is applied to low capacitance system $(2\pi fC)^2 \dashrightarrow 0$, the Power Factor = 1. Calleja[175,186,92] has shown that under these circumstances the expression:

$$\frac{1}{Z} = \frac{1}{X} + \frac{1}{R} \quad \ldots 3.48$$

gives a sufficiently accurate approximation. In this case, however, the D.C. resistance approximates to the A.C. impedance which implies that the capacitative reactance, X, is much greater than the resistance and only the latter is contributing to the impedance. In other words current will only flow through the resistance.

From the above discussion it is apparent that the frequency of the applied current can be very effective unless counter balanced by the capacitance value. Calleja[192] investigated the effect of frequency on the electrical resistance of the cement paste over a range of 40 to 20,000 Hz. He indicated that as the frequency becomes higher, the measured resistance at a given time will be lower. Considerable scatter in the values was observed when working at lower frequencies therefore, a lower frequency limit of 100 Hz was suggested. Little difference between resistance values obtained with

frequencies ranging between 5 and 20 KHz.

Hammond and Robson[187] studied the frequency effect on both the resistance and the capacitance of concrete and neat cement, they concluded:

1. Capacitance is inversely proportional to frequency.

2. The frequency is much greater for neat cement than for concrete of the same age.

3. The resistance at 50 Hz does not differ appreciably from the D.C. resistance.

4. The capacitance reactance is appreciably greater than the resistance. As a result the impedance is almost determined by the resistance.

5. The resistance decreases with increasing frequency and this effect is much more apparent in specimens made with high-alumina cement than with portland cement.

Nevertheless, meaningful comparisons can only be made between experiments carried out at the same tests frequency.

The dependence of capacitance on age has also been investigated, and it was reported that for air-dried specimens, the capacitance decreases with time[187] in contrast to specimens kept under water where the capacitance value increases with time.[191] It is apparent, however, that capacitance effectiveness is a function of evaporable water and the original water cement ratio.

Several electrical circuits have been developed and utilised for A.C. resistance measurements over years of research and experimentation. The prevailing consideration that capacitance is in parallel with resistance in concrete or cement paste system has led to a wide spread use of an A.C. bridge circuit,[186,191,193] which is capable of measuring simultaneously the resistance and capacitance over a required range of frequency, (Figure 3.30). The reference arms of the bridge are equal. Consequently the

measured resistance and capacitance are equal to those of the corresponding variable resistor and capacitor at balance, the variable balancers being connected in parallel.

Other investigations[175,177,192,194] were conducted with a simpler circuit, Figure 3.27, where the capacitance values cannot be determined.

Hughes et al[191] proposed an electrolytic ohmeter, the electric circuit of which is shown in Figure 3.31. The ohmeter applies small levels of square-wave form, alternating current. The significant feature of the instrument is a constant-current generator. Thus the voltage developed during measurements across the specimens is directly proportional to its resistance R. The small alternating current is particularly beneficial for low-aged specimen measurements since it minimises the gas formation. When comparing results obtained by this method with those from conventional D.C. and A.C. measurements, they found good agreement, particularly with A.C. results.

iii. Current Interruption Technique.

This method seems to have first been discussed by Hausmann[190] in 1964 when he studied the anodic and cathodic behaviour of cement coated steel and bare steel and presented data showing that there is no change observed in potential of the bare steel after the interruption of current in contrast to coated steel where an immediate drop was detected. This indicates the effect of a resisting layer on the measured potential.

Later, Martin[195] adopted this method to determine the ohmic component of the measured potential of a pipe line under cathodic protection. He indicated that this method can not readily be used in stray current areas or on pipe lines with multiple protection system, galvanic earthing beds or polarisation cells.

Cherry et al[176] investigated the cathodic protection of steel embedded in porous concrete and used a current interruption potentiostat to carry out a potentiodynamic polarisation scan of the reinforcing steel. They indicated

that this technique enables the polarisation resistance to be determined within ±10%, they also obtained resistivity values that compare well with the values obtained by other investigators.[196]

The basis of this technique rests on the fact that when the potential of the working electrode is monitored during interruption of the cell current, then, at the instant the current is turned off, the ohmic component of the measured potential is immediately eliminated and then subsequently followed by a slower decay of the polarisation potential towards its original rest potential value, Figure 3.32.

The immediate change in potential represents the IR-drop in the polarisation circuit, and when subtracted from the measured potential of the electrode gives the corrected potential, therefore:

$$E_m = \Delta E = E_p + E_D \qquad \ldots 3.49$$

where E_m = Measured potential.
E_p = Polarisation potential.
E_D = Potential drop.

The magnitude of the electrolyte resistance thus equals:

$$R_e = E_D \times I \qquad \ldots 3.50$$

where I = current before interruption.

The ohmic resistance can be converted to resistivity if the concrete area which carries the current is determined or can be approximated.

iv. Field Resistivity Measurements.

In the field, the resistivity of concrete is estimated using 4-probe technique. In this technique four equally spaced electrodes are fixed in a holder and embedded in the top 25 mm of concrete. It is important to ensure that the electrodes are not too close to any

reinforcing bars as these could influence the readings. An A.C.[122] or D.C.[196] current is made to flow between the outer electrodes and the resulting difference in potential between the inner electrodes is measured. The concrete resistivity, thus, equals $2\pi ar$ where r is the difference between the potential of the electrodes and a is the spacing between the electrodes. The volume of concrete whose resistivity is measured is basically that between the inner electrodes having an assumed cross-section which is equal to the square of half the distance between the two outer electrodes and a penetration equal to a.

Table (3-1): **EMF series of metals or standard equilibrium potentials $E^{o}_{M^{n+}(aq)/M}$ of $M^{n+}(aq) + ne^- \rightleftharpoons M$ equilibria (SHE)**

Metal	*Equilibrium*	E^{o} (V)
Gold	$Au^{3+}(aq) + 3e^- \rightleftharpoons Au$	1.5
Silver	$Ag^{+}(aq) + e^- \rightleftharpoons Ag$	0.799
Mercury	$Hg_2^{2+}(aq) + 2e^- \rightleftharpoons 2Hg$	0.789
Copper	$Cu^{2+}(aq) + 2e^- \rightleftharpoons Cu$	0.337
(Hydrogen)	$H^{+}(aq) + e^- \rightleftharpoons \frac{1}{2}H_2$	0.000
Lead	$Pb^{2+}(aq) + 2e^- \rightleftharpoons Pb$	−0.126
Tin	$Sn^{2+}(aq) + 2e^- \rightleftharpoons Sn$	−0.136
Nickel	$Ni^{2+}(aq) + 2e^- \rightleftharpoons Ni$	−0.250
Cadmium	$Cd^{2+}(aq) + 2e^- \rightleftharpoons Cd$	−0.403
Iron	$Fe^{2+}(aq) + 2e^- \rightleftharpoons Fe$	−0.440
Chromium	$Cr^{3+}(aq) + 3e^- \rightleftharpoons Cr$	−0.74
Zinc	$Zn^{2+}(aq) + 2e^- \rightleftharpoons Zn$	−0.763
Titanium	$Ti^{2+}(aq) + 2e^- \rightleftharpoons Ti$	−1.63
Aluminium	$Al^{3+}(aq) + 3e^- \rightleftharpoons Al$	−1.66
Magnesium	$Mg^{2+}(aq) + 2e^- \rightleftharpoons Mg$	−2.37

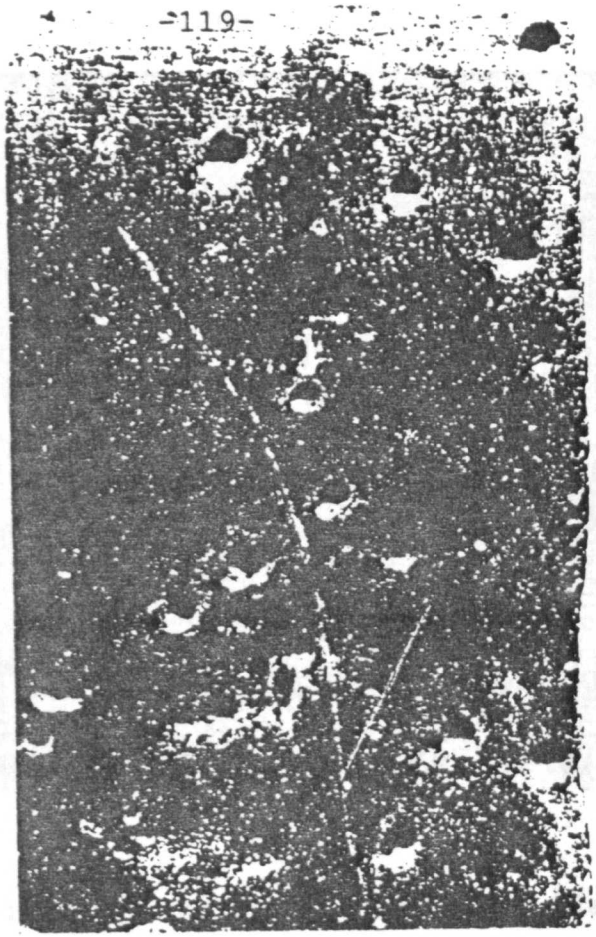

Figure (3-1): Pitting corrosion of steel plate (Ref.87)

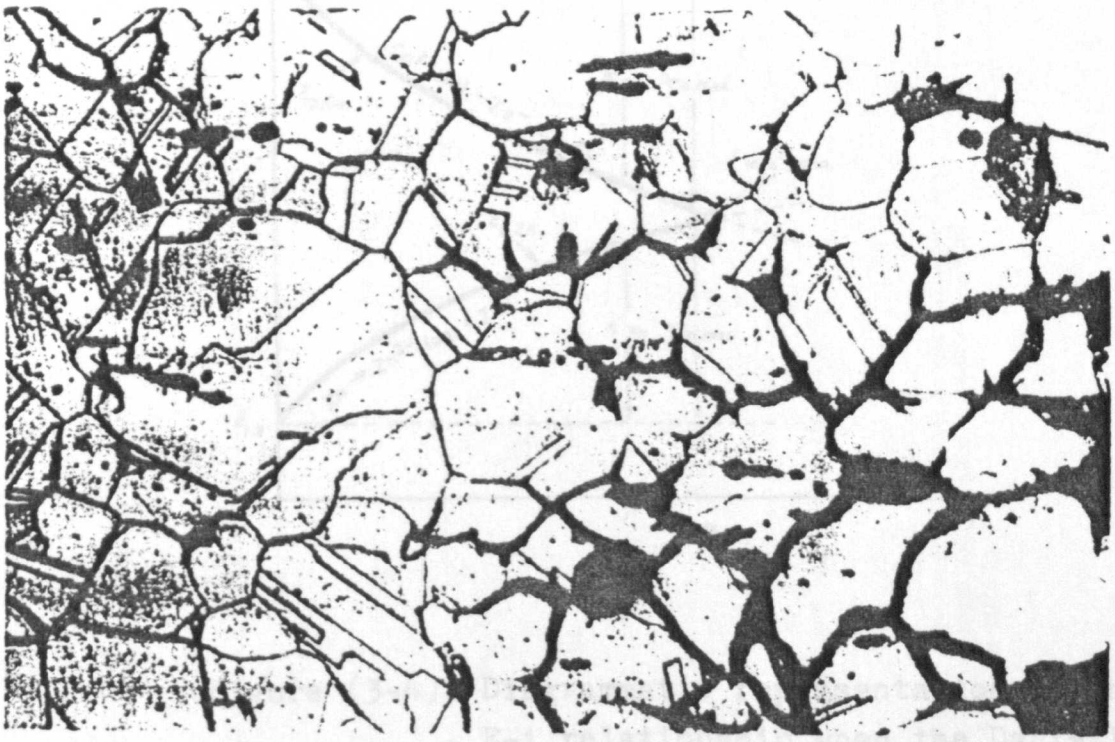

Figure (3-2): Intergranular corrosion (Ref.88)

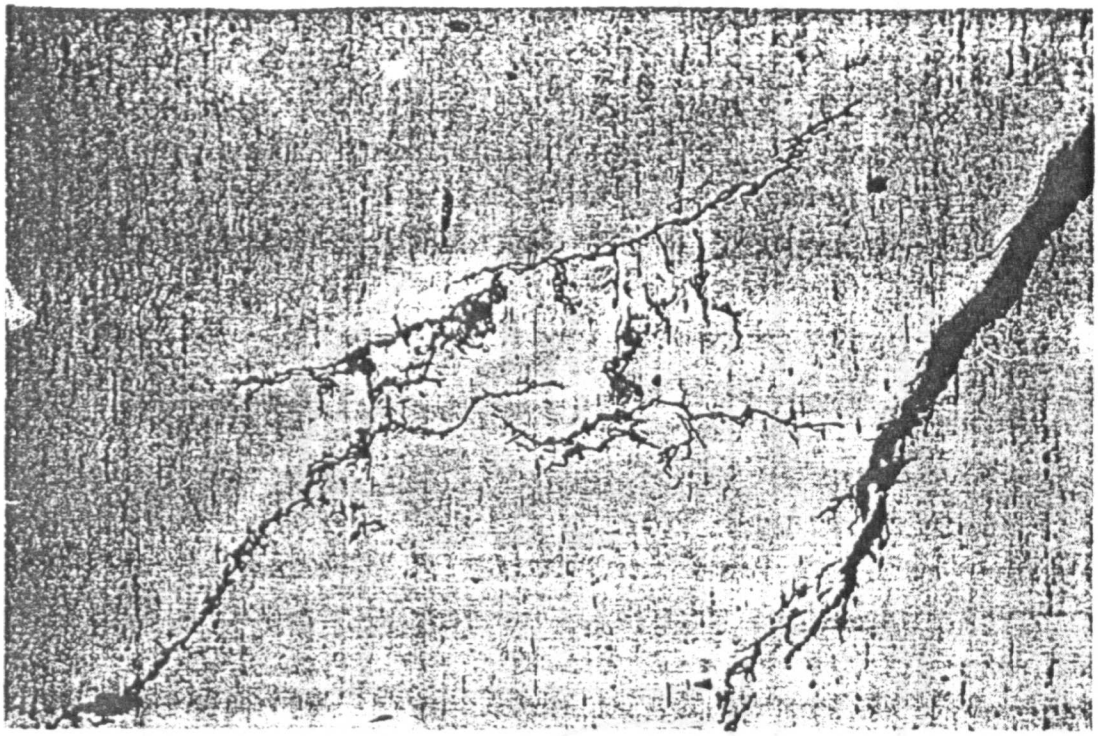

Figure (3-3): Stress corrosion cracking (Ref.88).

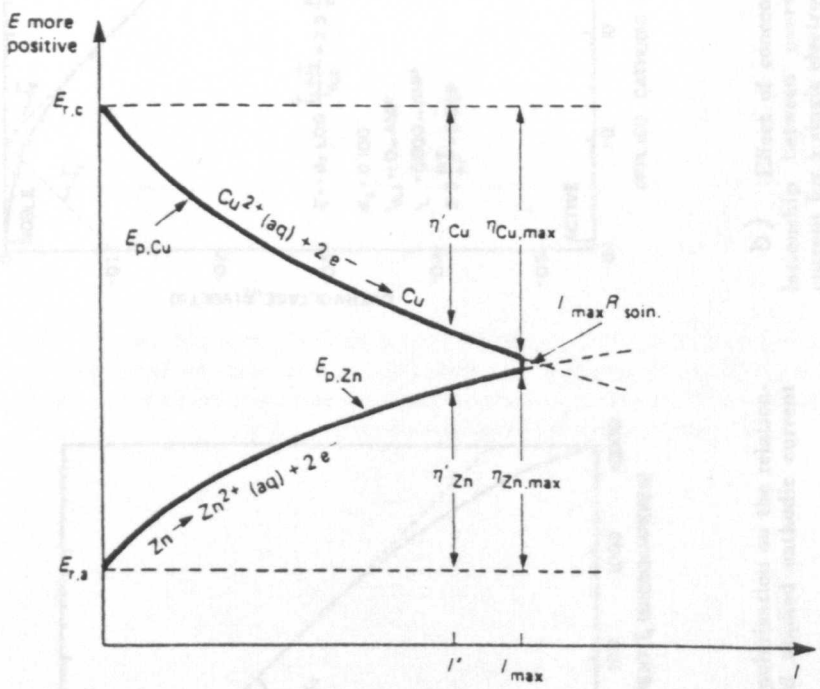

Figure (3-4): Diagrammatic representation of the E-i relationship when the Daniell cell operates spontaneously.

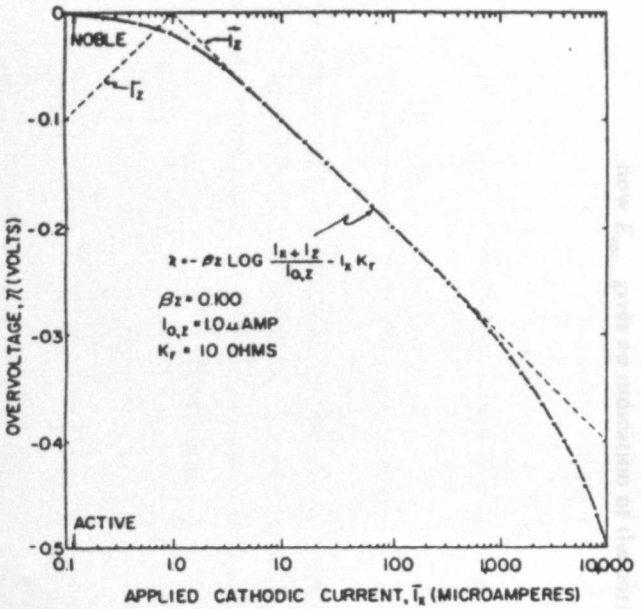

c) Effect of resistance polarization on the relationship between overvoltage and applied cathodic current for a single electrode system.

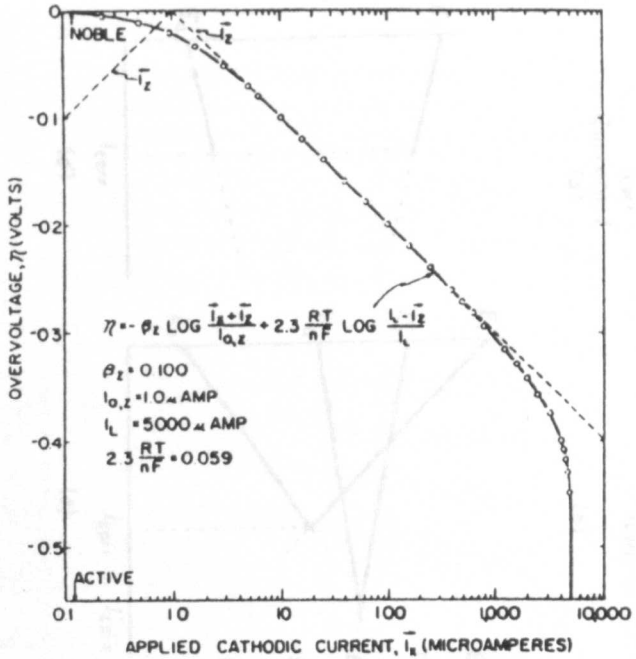

b) Effect of concentration polarization on the relationship between overvoltage and applied cathodic current for a single electrode system.

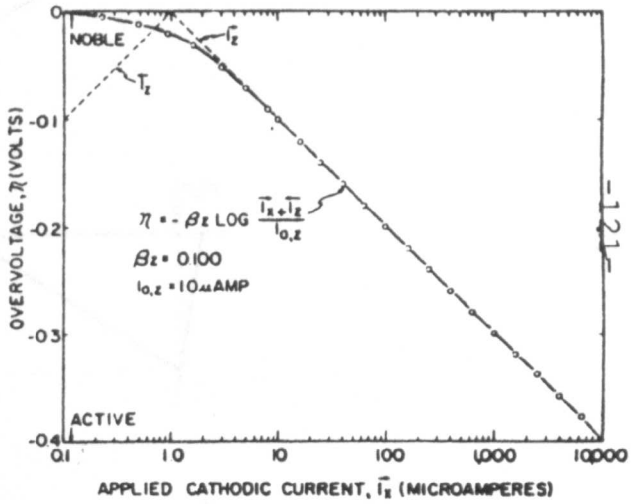

a) Relationship between overvoltage and applied cathodic current for a single electrode system.

Figure (3-5): Electrode polarization (Ref.89).

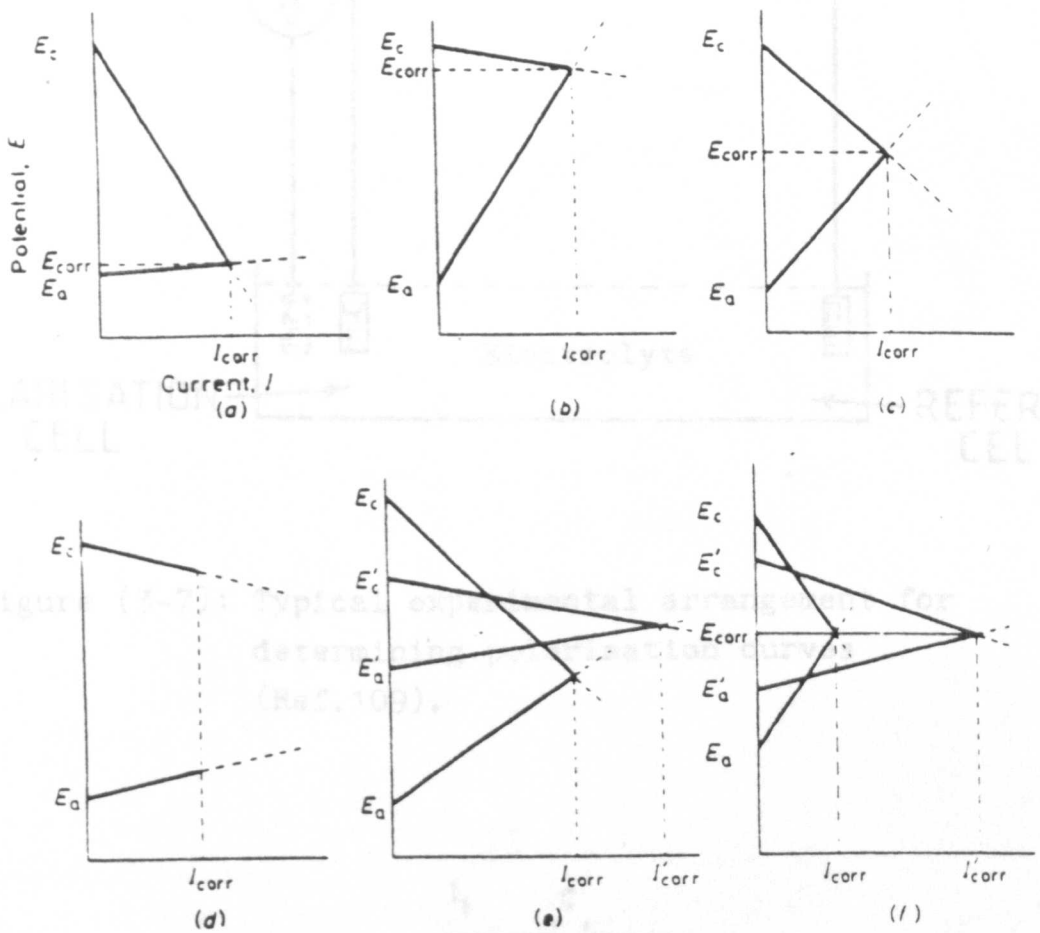

Figure (3-6): Evans diagrams illustrating (*a*) cathodic control, (*b*) anodic control, (*c*) mixed control, (*d*) resistance control, (*e*) how a reaction with a higher thermodynamic tendency ($E_{r.cell}$) may result in a smaller corrosion rate than one with a lower thermodynamic tendency and (*f*) how $E_{corr.}$ gives no indication of the corrosion rate

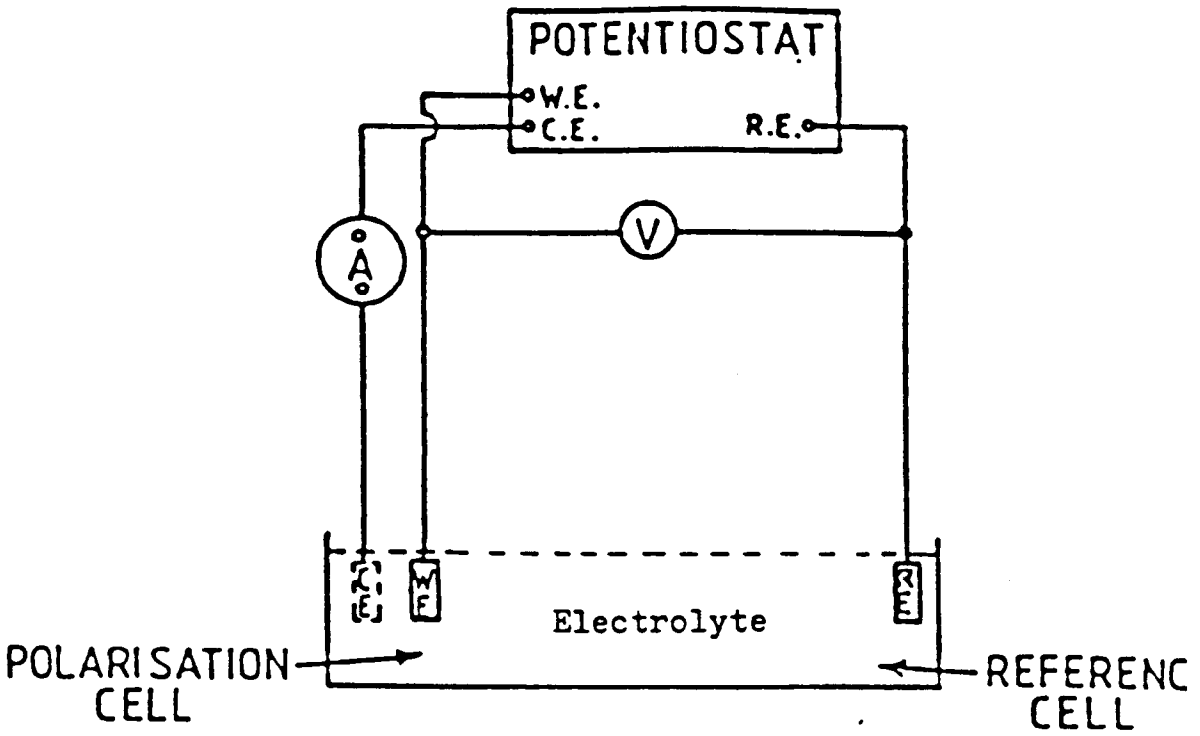

Figure (3-7): Typical experimental arrangement for determining polarisation curves (Ref.109).

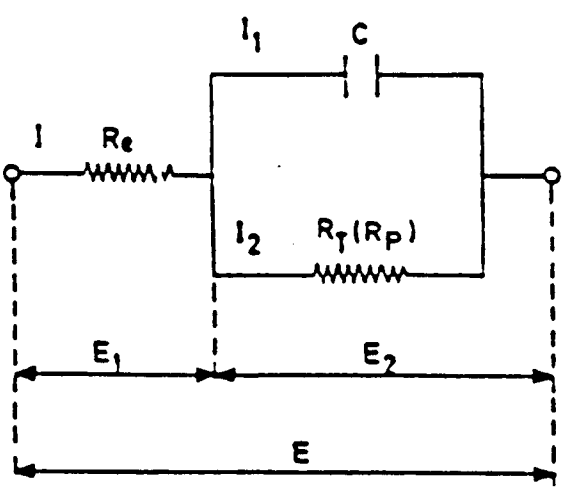

Figure (3-8): Equivalent circuit for metal–electrolyte interphase. R_e is the resistance of the electrolyte and the layers on the electrode. C is the capacitance of the double layer and R_T (R_p) is the Faradaic resistance or the Transference Resistance, linked to the corrosion reaction.

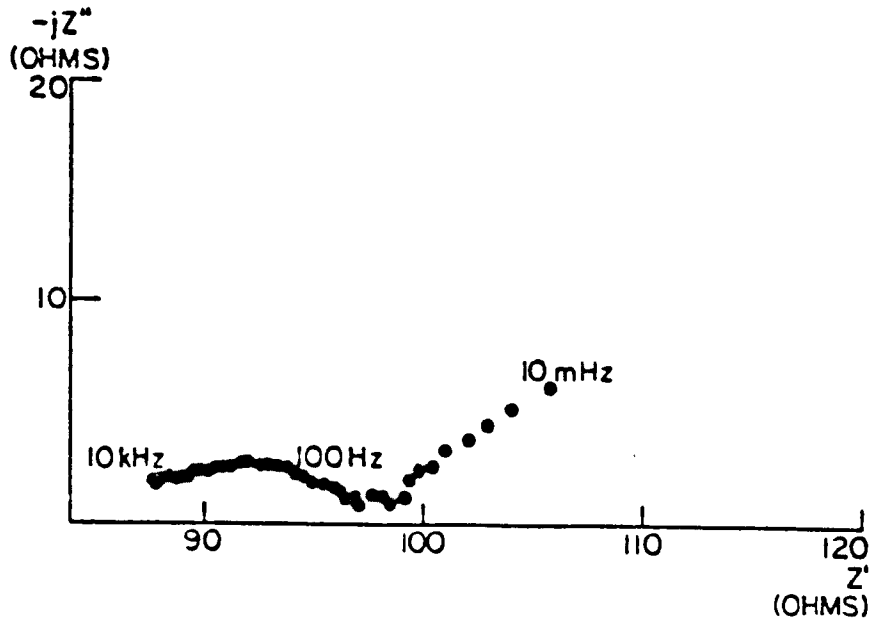

Figure (3-9): AC impedanc spectrum for concrete slab containing admixed $CaCl_2.2H_2O$ (Ref.110).

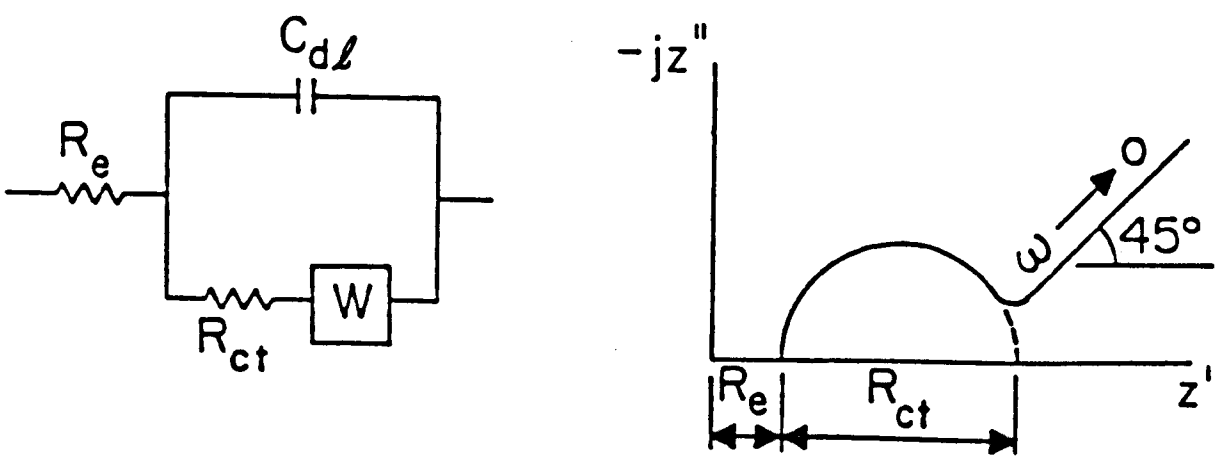

Figure (3-10): Equivalent circuit and impedance spectrum for a corroding system (Ref.110).

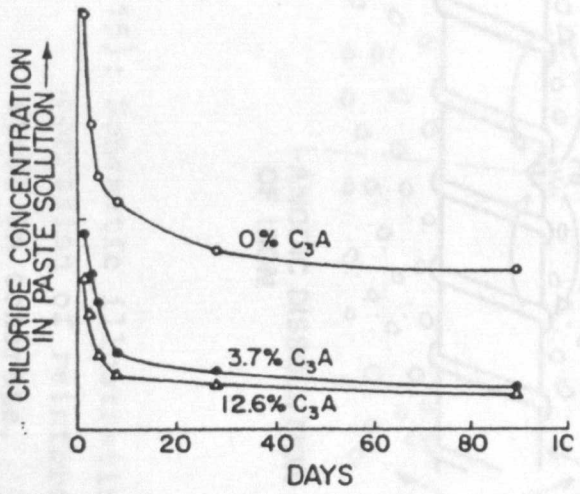

Figure (3-11): Chloride concentration in paste solution decreases with hydration age and with increasing C_3A content of cement (Ref.143).

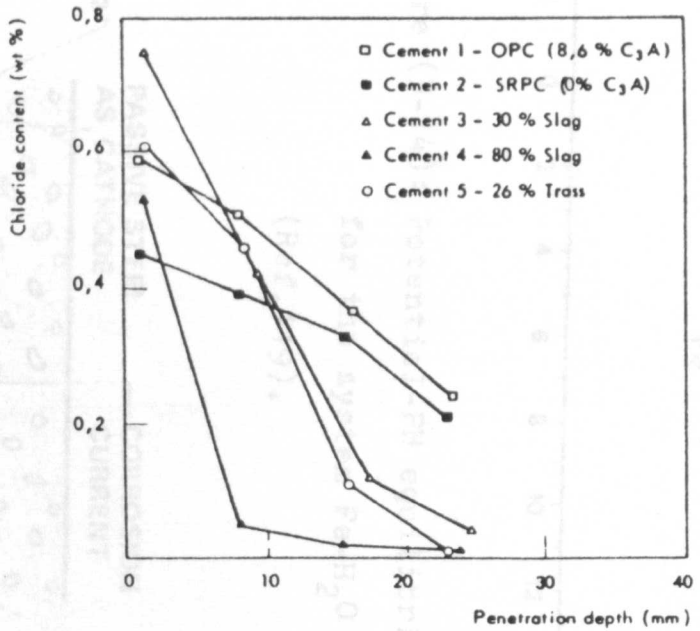

Figure (3-12): Effect of cement type on chloride penetration after six months of exposure (Ref.140).

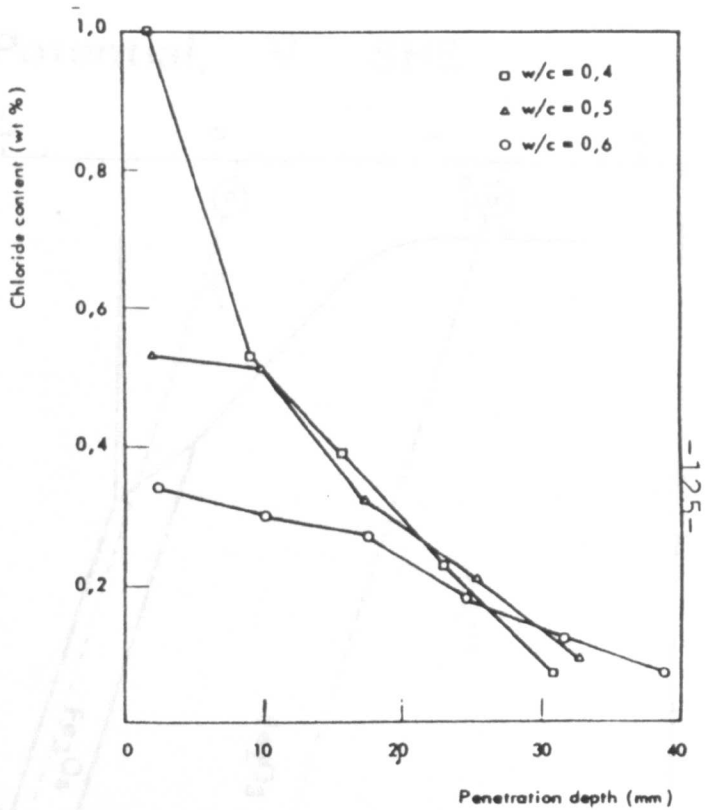

Figure (3-13): Effect of water-cement ratio on chloride penetration after two years of exposure (Ref.140).

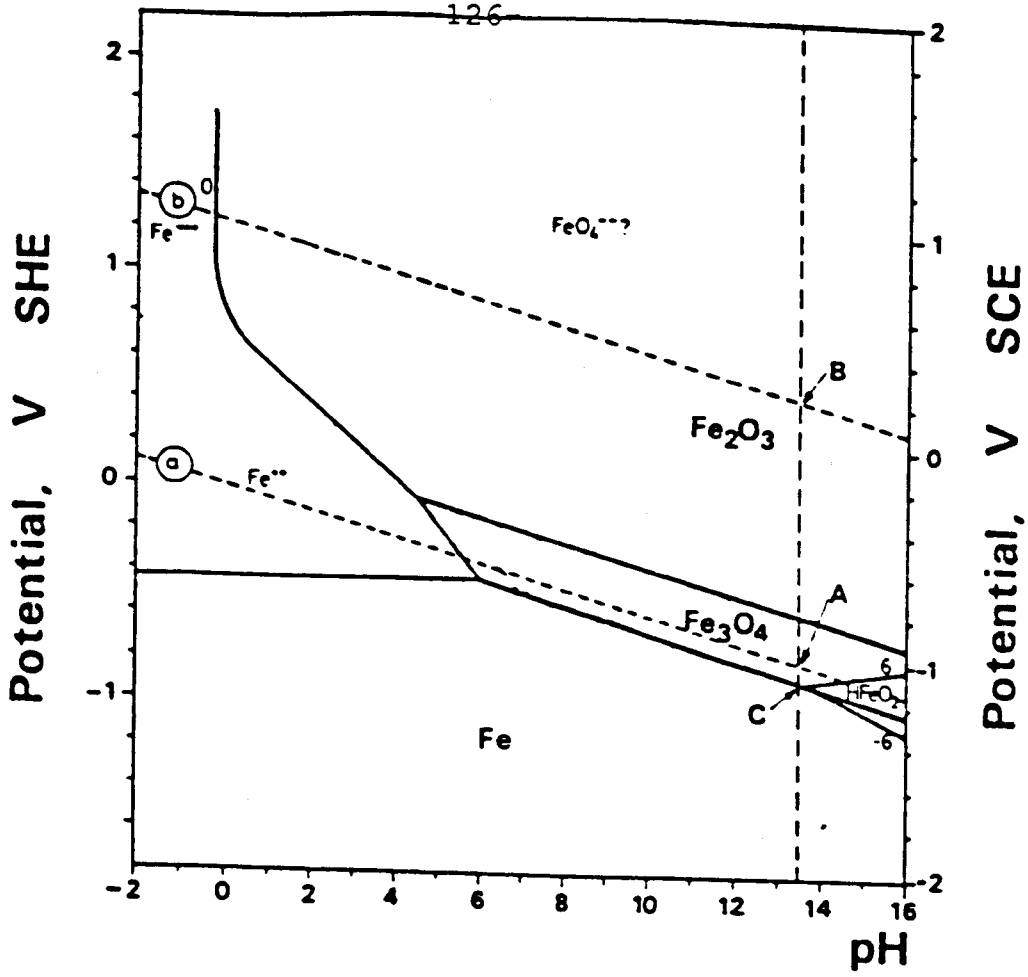

Figure (3-14): Potential-PH equilibrium diagram for the system Fe-H_2O at 25°C (Ref.119).

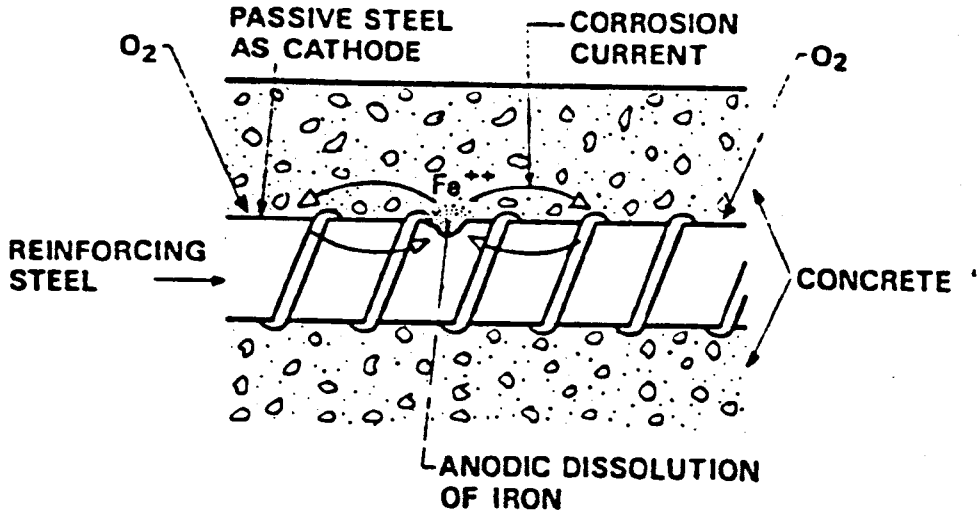

Figure (3-15): Schematic illustration of the corrosion of reinforcement steel in concrete.

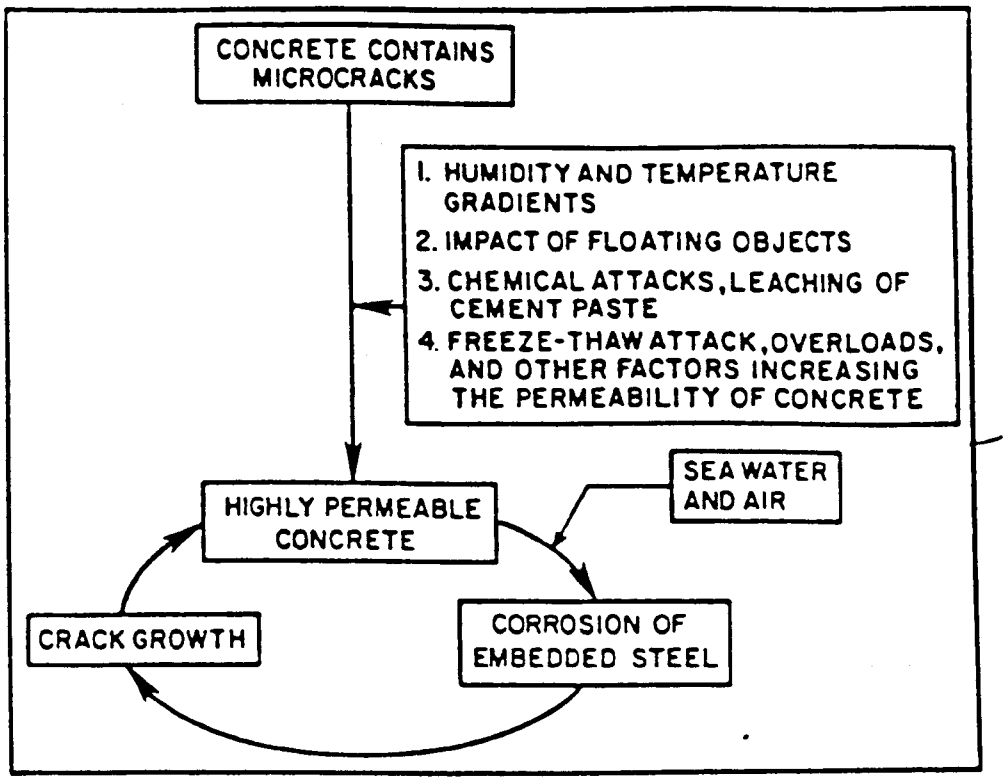

Figure (3-16): Schematic model of cracking-corrosion interaction (Ref.131).

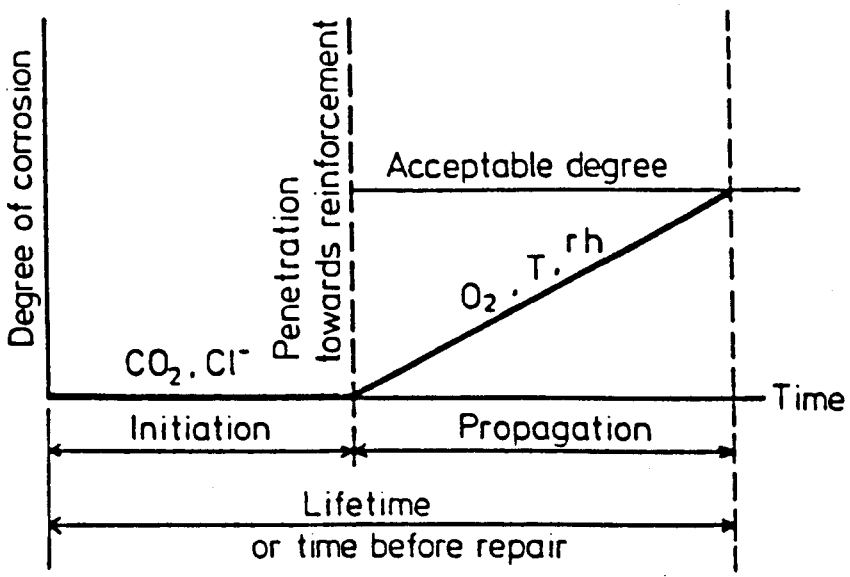

Figure (3-17): Schematic drawing of the corrosion process of steel in concrete (Ref.160).

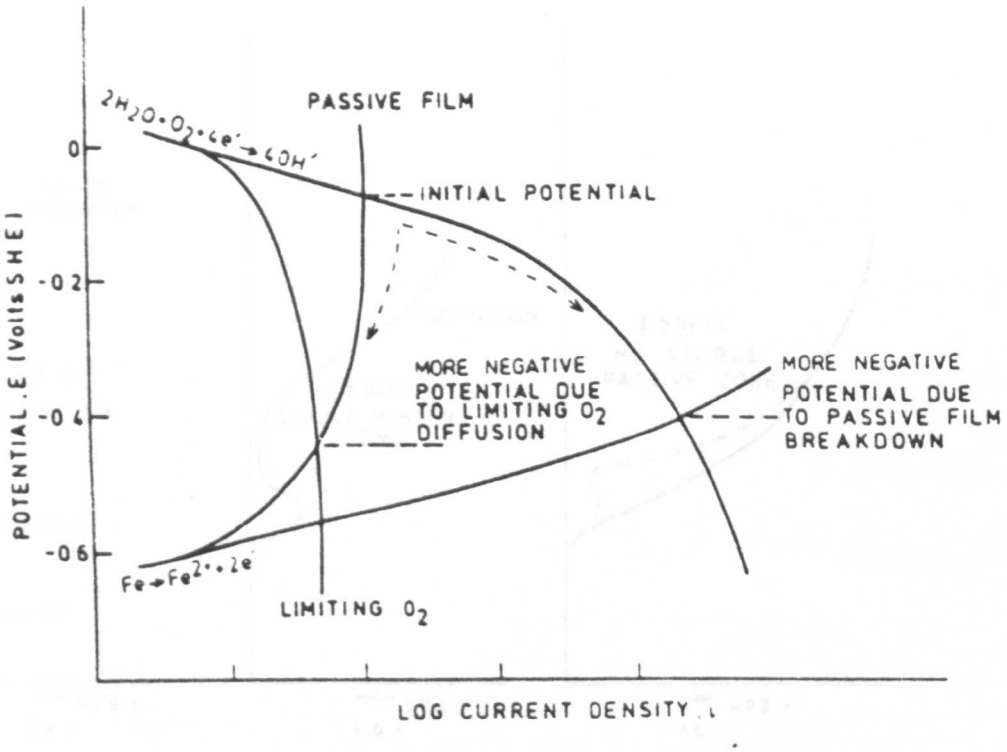

Figure (3-18): Movement of potential due to changes of anodic and cathodic polarisation (Ref.118).

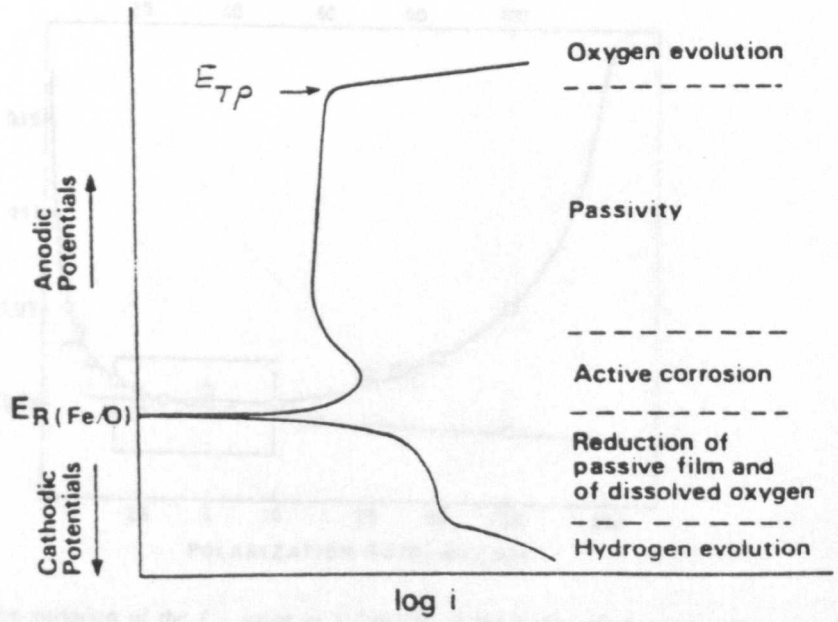

Figure (3-19): Schematic polarization curve for passivated steel in concrete.

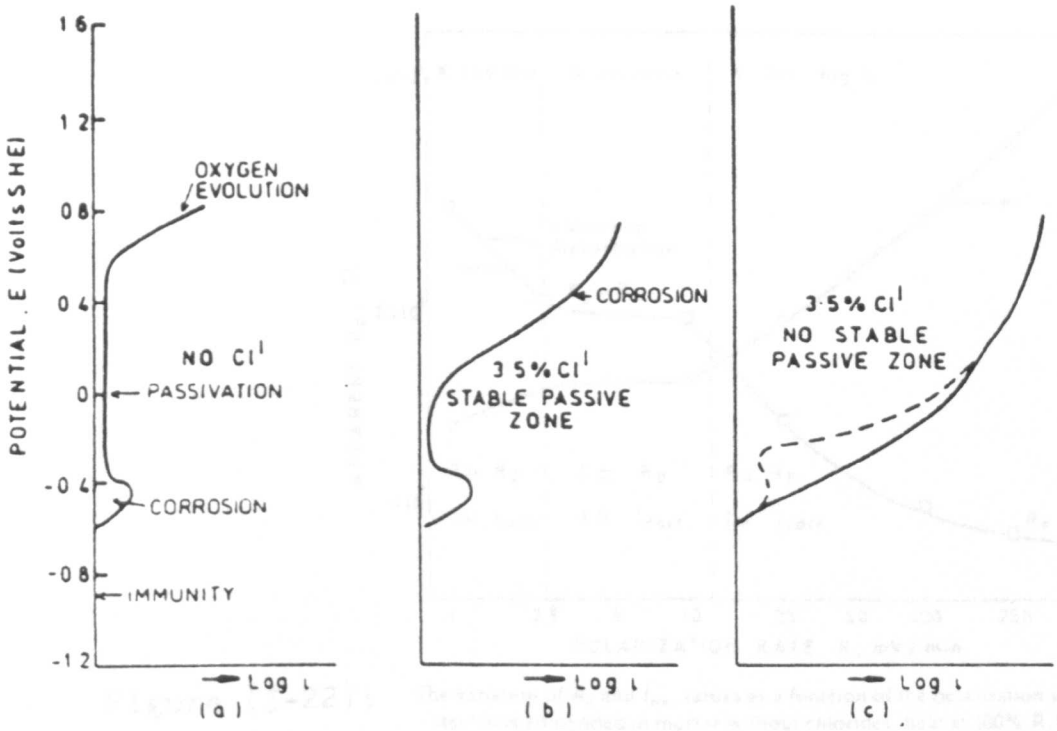

Figure (3-20): – Anodic polarisation curves for steel in concrete (schematic). (Ref.118).

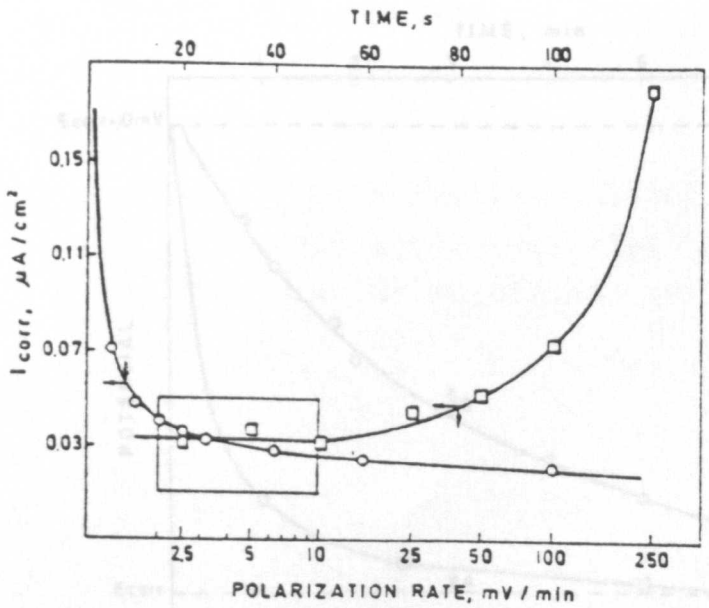

Figure (3-21): The variation of the I_{corr} value as a function of the polarization sweep rate (potentiodynamic test) for steel bars embedded in mortar without chlorides and held at 100% R.H. (Ref.104).

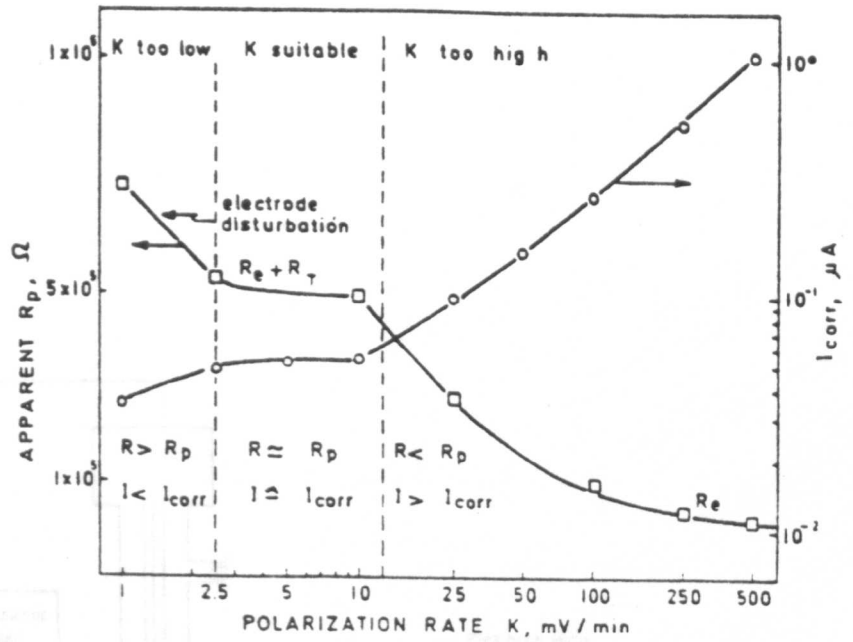

Figure (3-22): The variation of R_p and I_{corr} values as a function of the polarization sweep rate for steel bars embedded in mortar without chlorides, held at 100% R.H (Ref.104).

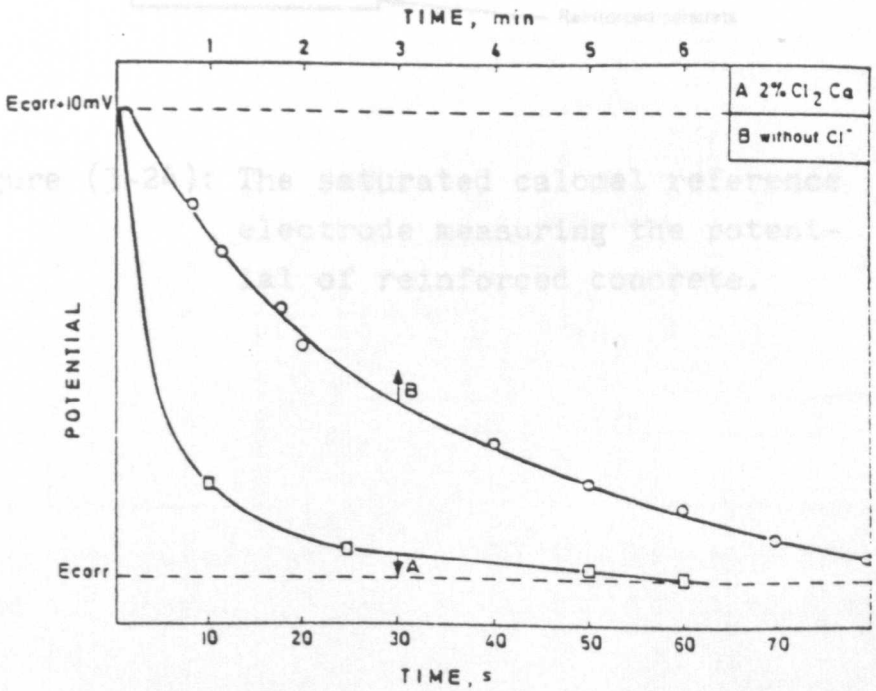

Figure (3-23): The recovery of the corrosion potential after application of a step of +10 mV during 1 min to steel bars embedded in mortar: (A) without chlorides, (B) with 2 wt% of $CaCl_2$. (Ref.104).

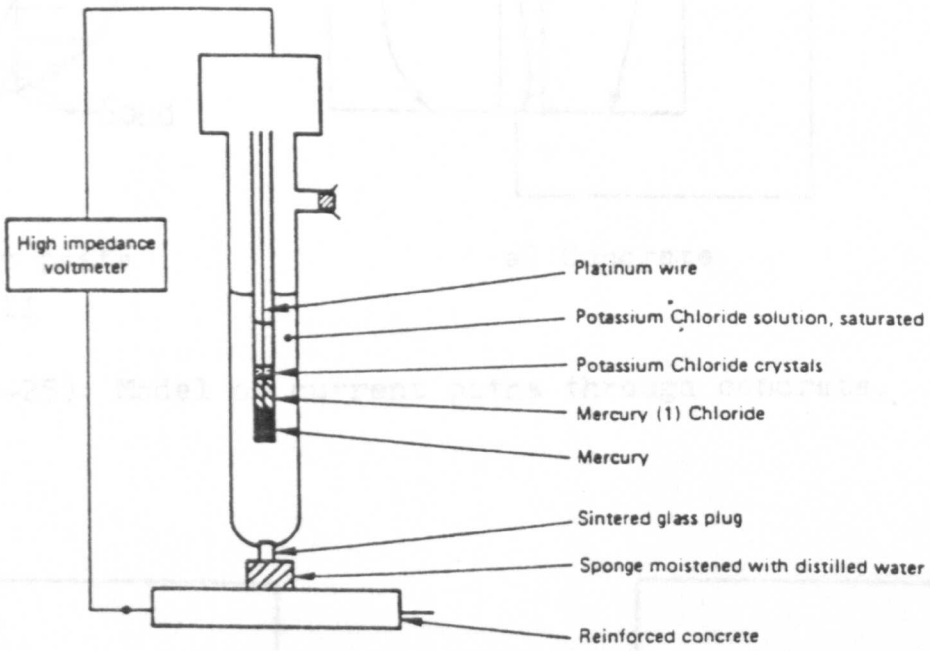

Figure (3-24): The saturated calomel reference electrode measuring the potential of reinforced concrete.

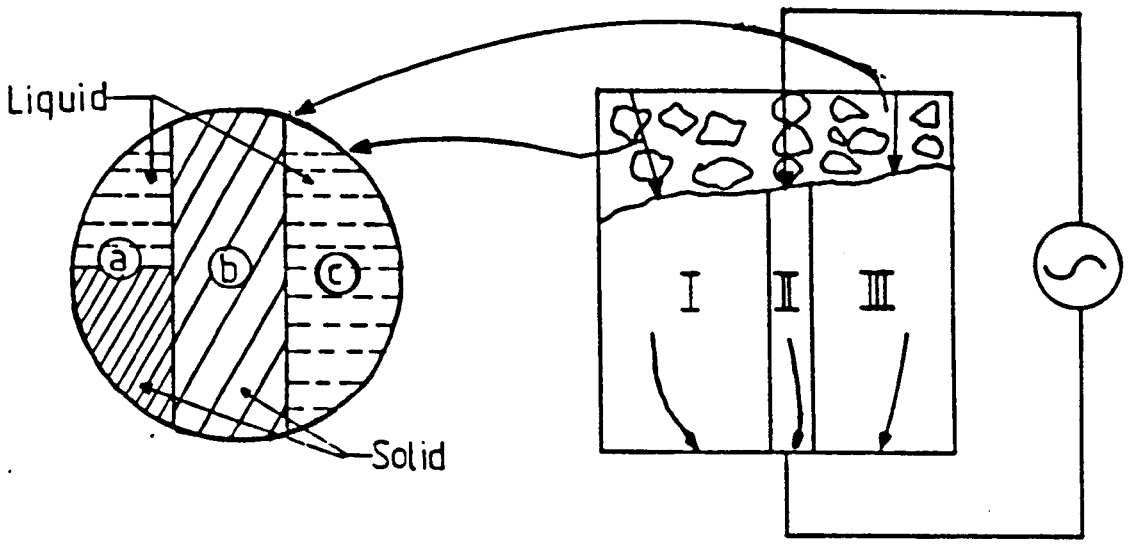

b) Cement paste path II

a) Concrete

Figure (3-25): Model of current paths through concrete.

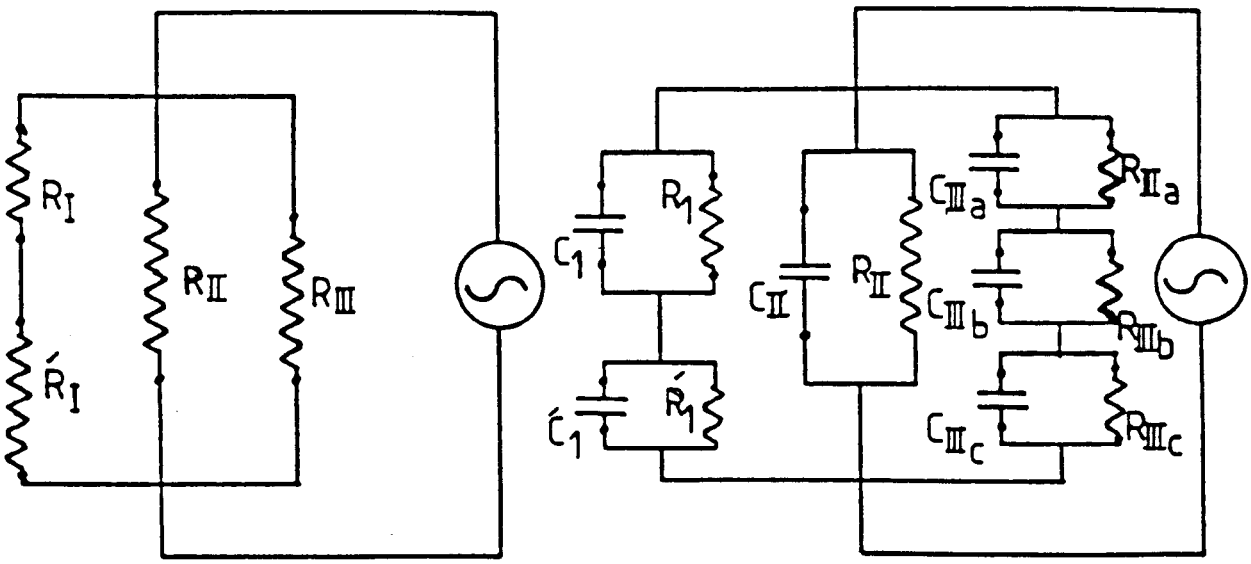

a) Hardened concrete D.C and A.C characteristic

b) Pre-hardened concrete A.C characteristic

Figure (3-26): Electrical analogy of current path model.

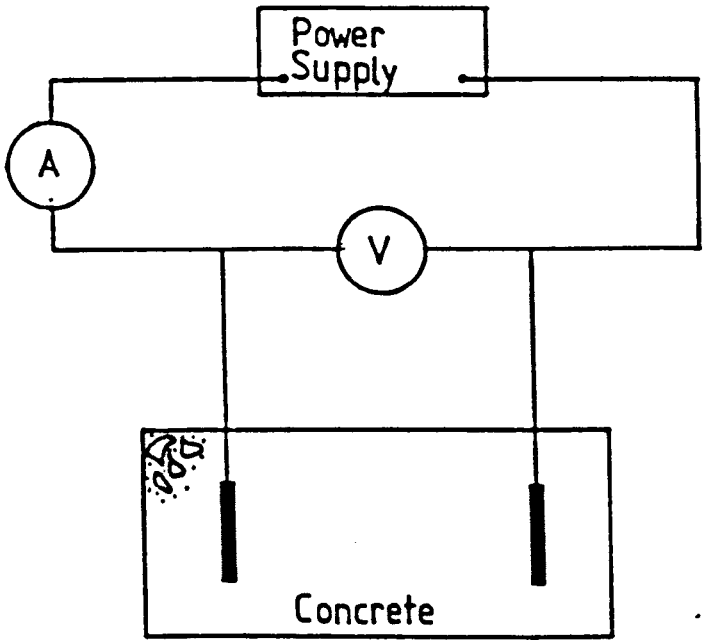

a) Embedded electrode

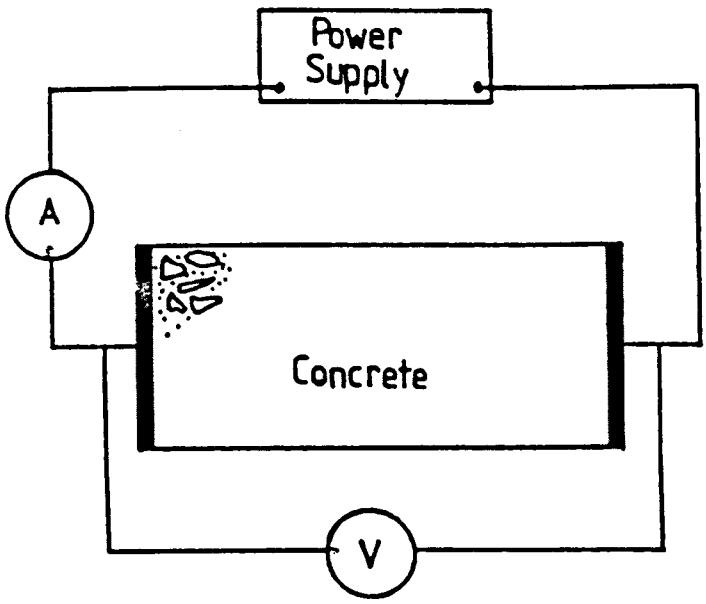

b) External plate electrode

Figure (3-27): Measurements of resistance.

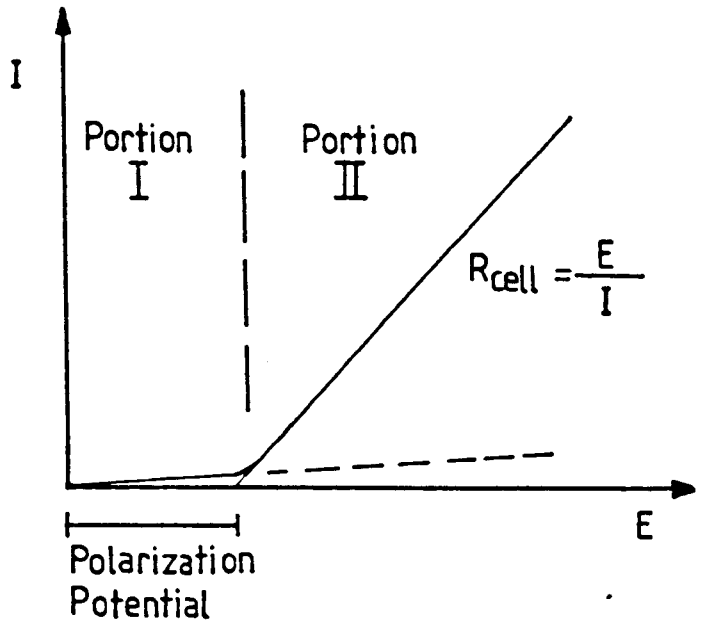

Figure (3-28): D.C measurements;polarization potential.

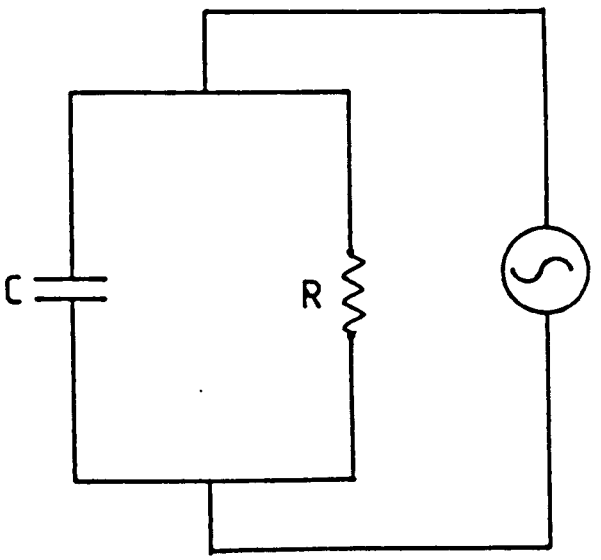

Figure (3-29): A.C conduction modle for concrete.

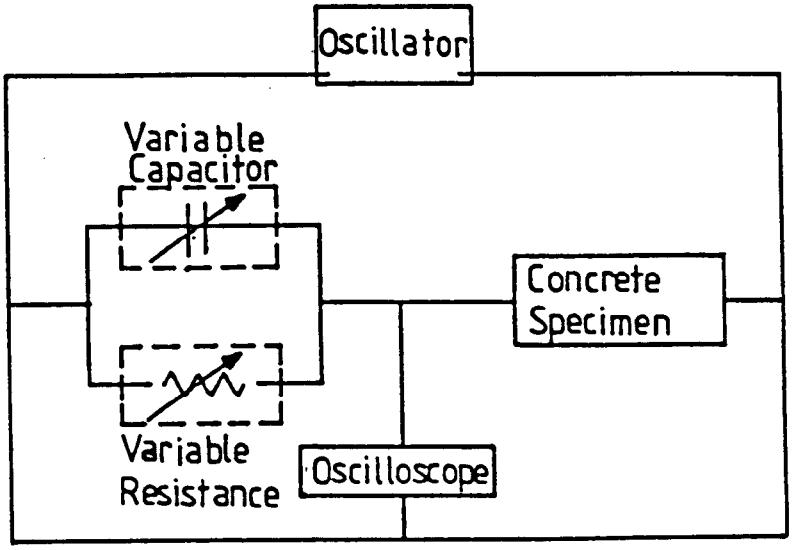

Figure (3-30): Typical A.C resistivity measurement circuit.

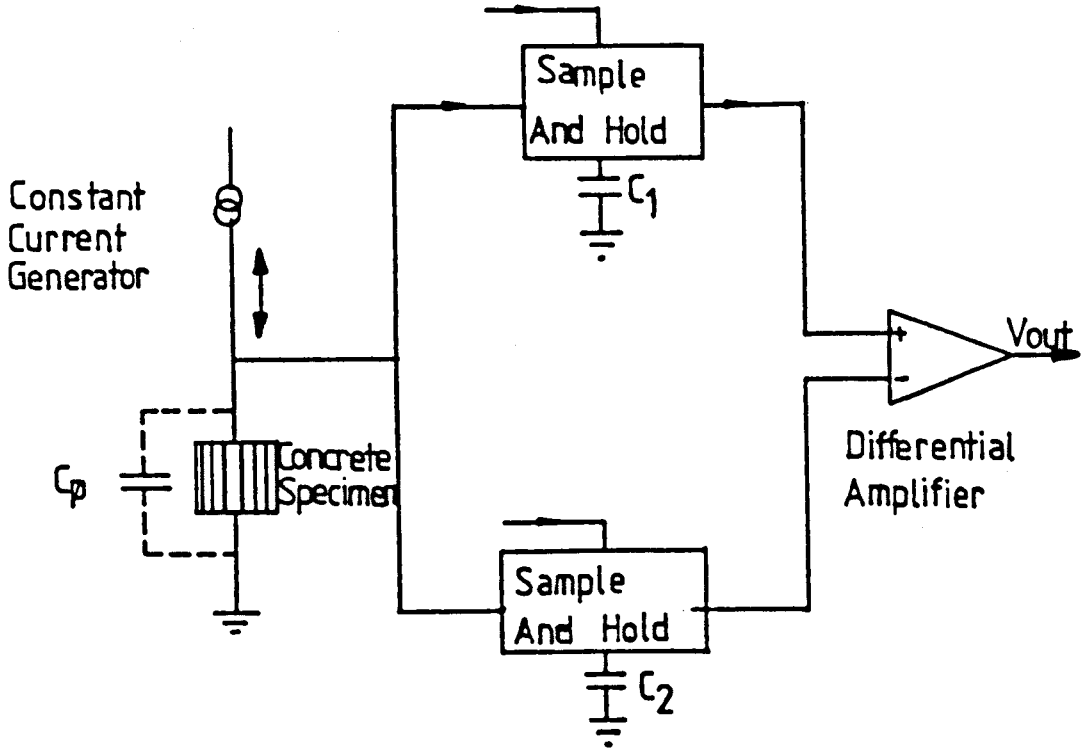

Figure (3-31): Electrolytic ohmeter circuit (Ref.191).

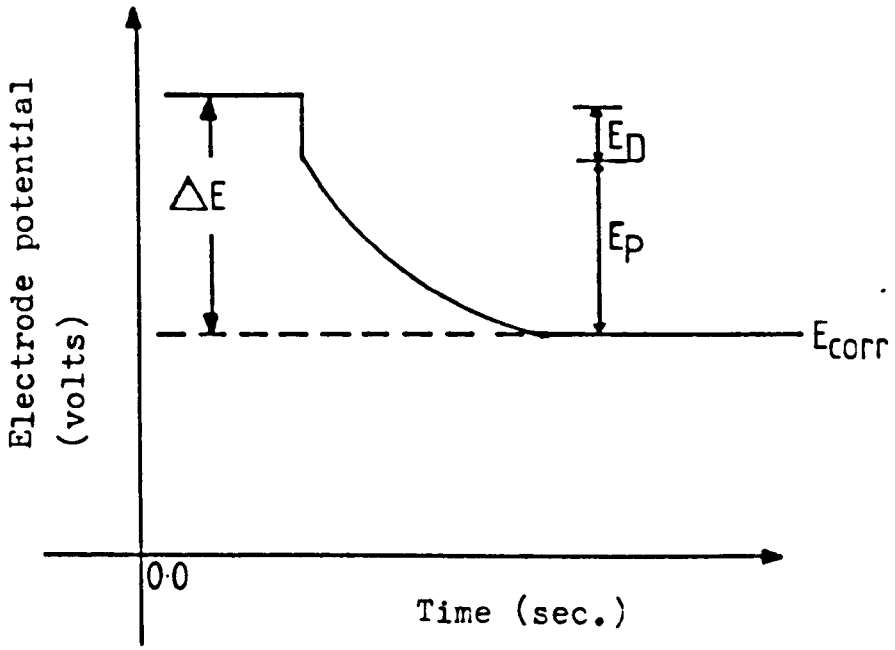

Figure (3-32): Current intrruption technique; electrode potential behaviour.

CHAPTER 4

CORROSION FATIGUE OF REINFORCED CONCRETE

4.1 State of the Art.

4.1.1 Development of Corrosion Fatigue Tests
4.1.2 Fatigue Properties of Reinforced Concrete in Corrosive Environments.

4.2 Crack Blocking.

4.2.1 Definition.
4.2.2 Literature Review.
4.2.3 Concluding Remarks.

4.3 National Codes Recommendations.

4.3.1 Mix Design, Cover and Crack Width Limitations.
4.3.2 S-N Curve for Steel Reinforcement.
4.3.3 S-N Curve for Concrete in Compression.
4.3.4 Transverse Shear Capacity.
4.3.5 Cumulative Fatigue Damage.

CHAPTER 4

CORROSION FATIGUE OF REINFORCED CONCRETE

4.1 State of the Art.

4.1.1 Development of Corrosion Fatigue Tests.

During the first half of the last decade, mainly in response to the rapid and perhaps the most dramatic development in construction activities in the North Sea, researches on the corrosion fatigue properties of reinforced concrete have been initiated to provide some fundamental understanding to the phenomenon of corrosion fatigue and to examine its potential hazard to the long term strength of offshore platforms.

However, the strategy of corrosion fatigue researches and the reliability of design guidelines which are based on laboratory results has always been a subject of vigorous debate and dispute ever since these series of research had been initiated.

Early discussions[12,49,198,199] were articulated on some major considerations which include the appropriate choice of specimen size, loading regime and test frequency. At early stages, nevertheless, the research details were dictated by the urgent need for early indications for such data were virtually not in existence. For instance, most of the early tests were carried out at high test frequencies (3-6 Hz) despite of the recognition that loading frequency of offshore structures varied from 0.05 to 0.3 Hz. It seems also clear that such decisions are in fact partly influenced by some other knowledge and experience which were gained from tests in air in which

case the test frequency is known to have little influence on fatigue strength. The compromise between urgency, practicability and reliability seems to have been balanced wisely by the research workers and thus offered much help and guidance for recent research and well as the development of future work. In addition, apart from offshore structures, the data obtained are obviously relevant to a large number of structures which experience fatigue loading in hostile environment such as bridge decks and parking structures.

The available research works, however, are still limited and a search of the publications in this subject has revealed some 17 research works during the past 15 years most of which were undertaken in countries bordering the North Sea. Seven of these works were parts of different stages of the concrete in the ocean (C.I.O) programme. A summary of the technical merits of the published work is given in Table (4-1) which provides a clear picture of the gradual change in emphasis as, probably, a result of cumulation of knowledge and experience Table 4.1 indicates the following important features:

1. Early tests were generally conducted at high test frequencies, whereas most of the recent investigations have adopted low frequencies in the range of 0.12 - 0.17 Hz.

2. The main objectives of early tests have been to obtain fatigue endurance, thus the tests were basically performed at sufficiently high stress levels to ensure failure after reasonable test duration. This trend has changed gradually towards obtaining data from long term tests which are more related to serviceability behaviour under moderate to low stress levels.

3. As a result of above 1 and 2, fewer test specimens are tested for a given time with relatively higher costs.

4. Recent investigations place more emphasis on the

electrochemical measurements as a consequence of the increased awareness of the links between the electrochemical and the structural responses of the test element and also due to the improvement and the availability of the monitoring techniques.

5. The influence of the marine environment on the fatigue properties of reinforced concrete has been the main objective of these studies and little has been done to study the effect of other aqueous environments.

4.1.2 Fatigue Properties of Reinforced Concrete in Corrosive Environment.

In general researches have investigated various fatigue properties of reinforced concrete in corrosive environments such that more confident predictions can be made as to the performance of the structural elements in real life and to ultimately develop design criteria under conditions intended to model actual service environments. On the same line the effectiveness of the protective measures were also investigated. The corrosive environment was found to have a crucial influence on several aspects of the fatigue properties of reinforced concrete being dependent on several interrelated factors.

In light of the current knowledge, however, the overall picture can be described under the following major head lines.

Effect of Environment on Endurance.

It is generally recognised that in tests at high frequencies, sea water environment causes a significant reduction in fatigue life compared with exposure to air.

Waagaard[198] presented results which indicated that at maximum stress level equivalent to 0.7 of the compressive strength of the concrete and at a test frequency of 5 Hz, specimens tested in air had a fatigue life which was from 10 to 15 times those tested in sea water under hydraulic pressure. Roper et al[202] and

Hetherington[144] found that at a test frequency of 6.7 Hz, the presence of a corrosive media significantly reduces the fatigue strength and that for beams reinforced with hot-rolled bar, 3% NaCl solution was more aggressive than sea water, in reducing the fatigue strength. Bannister's results[22] on 12 mm diameter Torbar at 3 Hz showed a 34% reduction in fatigue strength at the same number of cycles between sea water and air.

Hajime et al[200] carried out fatigue tests at 3 Hz and indicated that the longer the duration of exposure to the sodium chloride solution the lower the fatigue strength of beams due to corrosion of the bars near the crack opening.

Although Arthur et al[19,79] found a similar reduction in fatigue lives under high-frequency loading conditions in seawater, they further suggested that short-term tests, such as those above-mentioned, may not reproduce the long term effects particularly those effects which are related to the phenomenon of crack blocking. This phenomenon refers to the progressive blocking of the concrete cracks on the tensile side which effectively reduces the stress range of the reinforcement for a constant load range leading to an enhanced fatigue life. Due to the importance of this phenomenon, it will be discussed in more detail in the following section. Nevertheless, a series of researches carried out at Glasgow University[19,79,150,204] have shown that under favourable conditions, crack blocking can improve the fatigue lives of the beams compared with their expected fatigue lives in air. Otherwise, beams which did not develop crack blocking have fatigue lives which are lower than those of air at the same stress range.

On the other hand, the enhancement in fatigue lives due to blocking has not been found in the work reported by Paterson et al.[59,203] In their tests in seawater at 0.1 and 3 Hz cyclic frequency, they indicated inferior fatigue performance in seawater despite of the apparently similar changes towards less severe stress conditions, due to crack blocking.

This difference was attributed to the difference in

the effectiveness of this phenomenon due to dissimilar experimental conditions particularly the degree of exposure to seawater, since in the tests of Paterson et al the water was kept at the level of the tension reinforcement of the full length of the beam (i.e. the tests were of splash-zone conditions) compared with total immersion of the exposed maximum bending moment zone in Glasgow University tests.

To take the effect of blocking into account, Paterson et al modified their S-N curves using the effective stress range instead of the initially applied or intended stress range, the effective stress range = (initial range + final stress range)/2. The changes in the stress range was found to be equal to the change in deflection range. As the beneficial effect of blocking is removed, the new S-N curves showed even more detrimental effect of sea water on the fatigue lives. For instance, at 10^7 cycles the limiting effective stress ranges for directly comparable tests at 3 Hz were approximately 175 N/mm^2 in air and 95 N/mm^2 in sea water, a reduction of 46% in seawater environment.

From directly comparable experimental details, Katwan et al[20] obtained lower fatigue lives in Tapwater and 3.5% NaCl solution than those obtained by Arthur et al[19,79] in sea water. This was attributed to much delayed onset of crack blocking in the former tests which implies that the test beams were subjected to high stress range for relatively longer proportion of their fatigue lives than sustained in seawater tests.

Fatigue failure of the test beams always occurs by the fracture of one or more of the main tensile bars at a point corresponding with a crack in concrete. For long duration tests, crack initiation in the reinforcement takes place at corrosion sites. The crack normally propagates[44,59,150] by striation mechanism with a final fracture occurring by ductile tearing.

Fatigue tests on prestressed concrete carried out by Banerjee et al[204] and Paterson et al[203] have also indicated the occurrence of crack blocking phenomenon and followed generally the same trends as those observed in

reinforced concrete beams.

Effect of Cyclic Frequency.

The effect of cyclic frequency on the fatigue characteristics of the test specimens in corrosive environment is not thoroughly researched (see Section 2.3.5) and only limited data are available.

Arthur et al[79] presented fatigue results of partially immersed beams (short tanks) tested at high stress range which indicated a trend towards a reduction in fatigue life at the higher frequency. For a stress range of 345 N/mm^2 and with less effective crack blocking, the average endurance was 637 x 10^3 cycles for 0.17 Hz compared to 185 x 10^3 for 5 Hz. It should be mentioned, however, that the scatter band of tests at lower frequencies is much wider than tests at high frequency. When the exposed area was doubled (i.e. using long tank) the observed endurance at 0.17 Hz for the same stress range was considerably greater (average of 4.7 x 10^6) than those of high test frequency of 5 Hz with short tank. The enhanced endurance was attributed to the beneficial effect of crack blocking in reducing the stress range.

On the other hand, Paterson et al[59] suggested that at lower stress range, the real time duration of a test in seawater assumes greater importance since for a given number of cycles the exposure of the reinforcement to the corrosive environment is longer for a slower cycling frequencies. This was supported by the observation that in tests at initial stress ranges at or below 200 N/mm^2 the fatigue failure had in fact initiated at corrosion sites. After discounting the effect of crack blocking, Paterson et al tests in seawater at 0.1 Hz gave significantly reduced fatigue endurance compared to testing at 3 Hz.

The Structural Behaviour During Fatigue Loading.

At high test frequency (6 - 6.7 Hz)[44,198,202] researches on the fatigue properties of reinforced

concrete in sea water, under uni-directional bending regime, have indicated structural change similar to tests in air. Initial high reduction in stiffness (increase in deflection range) and crack width was observed which continued at substantially lower rate over the remaining test duration.

It has been observed that tensile cracks on the concrete surface tend to be wider in seawater than in air. The extra crack width arises[22] from the attrition effect of water flowing in and out of the cracks and the hydraulic compression on the reduction of the stress from the maximum value every stress cycle.

Arthur et al[79] reported the same observation for reverse bending tests on beams with the central portion exposed to seawater.

Different behaviour, however, was observed in tests at lower cyclic frequency. Researches at Glasgow University[19,79,150] indicated that after an initial reduction in stiffness and increase in crack width range, beams tested at 0.17 Hz showed progressive increase in stiffness and reduction in crack width range and this trend continued at slower rate until failure point. This change in behaviour was coincided with progressive build up of deposit within the cracks.

Paterson et al[59,201,203] presented results which indicated that an increase in stiffness is possible even at 3 Hz cyclic frequency. Katwan et al[20] reported similar structural change for test at 0.17 Hz for stress levels up to 0.85 of the characteristic yield strength of the reinforcement in tapwater and in 3.5% NaCl solution. The onset of reduction in deflection range and crack opening range, however, was not as early as that observed in seawater test, and this was found to be proportional to the stress level in the reinforcement. Hetherington[44] also reported increase in stiffness in tests in 3% NaCl solution at 0.17 Hz.

The only exception from tests at lower frequency is the single test reported by Waagaard[198] who observed continuous reduction in stiffness in sea water test at 0.2 Hz. It should be mentioned, however, that this particular

test was carried out at very high stress level (≃ 100% of the static capacity of the concrete) with an endurance of only 2330 cycles.

Reverse bending tests at 0.17 Hz have shown structural behaviour which is dependent on exposure condition and environment. Beams with short tank[79] containing seawater and enclosing the central 580 mm showed signs of crack blocking but the fatigue lives were within the scatter of air test results. When doubling the tank length to include the full maximum bending moment zone, reduction in both deflection and crack width ranges were recorded, the percentage of reduction and the point of onset were stress range dependent so that at a stress range of 363 N/mm^2 blocking was virtually non-existent.

Essentially similar conclusions were reached from fatigue tests in tapwater and 3.5% NaCl solution[20] where the reduction in deflection and crack width ranges was only observed at a stress range of 164 N/mm^2 and occurred only after 446 x 10^3 cycles had been applied. It appears that unlike tests in sea water this process has a reduced tendency in water and chloride solution so that tests at higher stress level than 164 N/mm^2 did not show any sign of structural change from that of test in air.

Corrosion Process Under Dynamic Loading.

Non-destructive electrochemical monitoring techniques have only been recently introduced to provide a continuous picture of the change in corrosion activities with time. Work by Hodgkiess et al[150] and Paterson et al[59] in sea water have indicated that the half-cell electrode potentials of the embedded reinforcement, before the application of fatigue loads, were generally in the passive regime at about -0.1 V SCE. These values[20] were close to zero volts (SCE) in tap water and between -0.1 and -0.2 V SCE in NaCl solution. Upon commencement of fatigue loading, an immediate drift in electrode potential to more negative values was recorded indicative of the immediate onset of corrosion and break of passivity due to the easy ingress of seawater at flexural cracks in the

concrete during load cycling. Breaking open of the beams at the termination of the test confirmed that corrosion was of localised nature at and around the intersection of the reinforcing bars with cracks in the concrete.

The maximum negative value of the electrode potential was proportional to the applied stress range and was generally reached after a relatively small proportion of fatigue life had elapsed.

Hodgkiess et al[206] and Katwan et al[20] reported a reversal in the movement of the potential to more positive values after a variable number of cycles and observed that this reversal in potential started after crack blocking had become well established. It was suggested that the reversal in potential may be attributed to the alleviation effects which are produced either by the development of a substantial physical barrier to the ingress of corrodent or by some inhibitive chemical effects. There were, nevertheless, some features which produced strong indications of continued ionic mobility and perhaps significant corrosion rate throughout the entire duration of the tests including the period when blocking is visibly and effectively (as manifested by the structural change and potential reversal) well established.

These indications include, firstly, bars removed from the beams involved in the long running tests[59,150] were found to have suffered serious local attack. Secondly, linear polarisation measurements made on one long running beam[206] just prior to termination of the experiment without beam failure indicated that the corrosion at this late stage was continuing at a significant rate. Thirdly, the colour change in the crack blocking deposit observed in all the tests some of this was in the late stage of tests, such as tap water tests reported by Katwan et al,[20] which indicate continued ionic mobility.

On the other hand, less developed blocking tended to stabilise the electrode potential levels or to reduce the rate of change in the negative direction. Also in the absence of blocking in short duration tests, the potential continued to fall during the entire test duration.

Paterson et al[59,203] did not observe the reversal in

potential but reported stabilised potential at early stages of tests at stress range below 150 N/mm^2. However, the effectiveness of blocking in Paterson's tests was small as mentioned earlier on, therefore, their observations agreed generally with Katwan's et al observations.

Nilson et al[205] in their fatigue tests at 0.12 frequency on totally submerged reinforced concrete specimens observed an initial negative drift in the first months of exposure which was followed by a period of stabilised potentials. With reference to the modified Poubaix diagram,[198] Figure 4.1, they attributed the negative drift in potentials to the oxide transformation as a result of the change in oxygen availability on the steel surface. The interesting feature in their experimental results is that the corrosion behaviour of the specimens was not significantly influenced by the type of loading (no load, static and dynamic loading conditions) and cover thickness (18 to 48 mm). Even the dynamically loaded specimen with crack widths up to 1 mm measured at the concrete surface and exposed to 6×10^6 load cycles showed, rather surprisingly, no sign of localised attack of the reinforcement at the bottom of the cracks despite the easy ingress of O_2-saturated seawater which would have depassivated the steel and caused some initial corrosion even if later the corrosion rate is very low as a result of blocking of cracks and concrete pores. However, only limited corrosion products were found at crack sites on some of the freely corroding dynamically loaded specimens and this was believed to have been formed during the last three weeks of the exposure period when these specimens were raised halfway above the seawater level in the tank to simulate the tidal/splash zone condition. They suggested that the possible formation of a local galvanic cell at the bottom of dynamically loaded submerged cracks seems to be a minor risk and this was considered to be a result of restricted oxygen diffusion in the submerged concrete which is influenced by the precipitation of calcium carbonate and magnesium hydroxide in the cracks and pores. The fact that the process of anodic dissolution

of the steel exposed in the bottom of the crack is cathodically controlled is further confirmed by the drop in the current necessary to polarise the reinforcing steel to a potential of -0.8 V (SCE) from the initial current density of 150 mA/m^2 to only 0.05 mA/m^2 within 3-6 months of the test (total test duration = 24 month). These results are in fact in agreement with results reported by Wilkins[118] which indicated that fully immersed concrete would be an extremely poor cathode. Wilkins, however, suggested that cathodic steel is capable of supplying not more than $\sim$ 0.5 mA/m^2 which is an order of magnitude greater than the value obtained by Nilson et al.

On the other hand, Espelid et al[207] indicated that current densities as high as 3 mA/m^2 have been recorded for cathodically protected submerged reinforcement in a multizone reinforced concrete system under dynamic loading. They suggested that the considerable differences in current density from those obtained for totally submerged systems may be attributed to the availability of oxygen at the steel surface not only by diffusion but also by convection of the pore water and as soon as the possibilities for convection are established, the electrochemical behaviour of submerged reinforcing steel will be altered.

Effect of Different Treatment on Corrosion Fatigue.

Researches have investigated limited factors influencing the corrosion fatigue properties of reinforced concrete. These factors are related either to corrosion or the structural characteristics of the test specimens and can be summarised as follows.

1. The use of cathodic protection[22,203] significantly improves the fatigue resistance and restores the fatigue life of reinforced concrete beams to a value at least equal to its fatigue life in air. This observation clearly confirmed the influence of corrosion on endurance.

2. Galvanising treatment[200] slightly improves the fatigue resistance the beneficial effect, however, will be negligible compared with the remarkable effect of the difference in the deformation on bars. There is, thus, practically no need to consider the effect of galvanising treatment on the fatigue strength of reinforced concrete.

3. Epoxy coating[207] on the reinforcing bars can act as an effective barrier against oxygen diffusion and thus significantly reduces the possibilities of the bars acting as cathodes in the tidal/splash zone area.

4. Coating of the external concrete surface[207] only has a marginal effect on the current drain of the reinforcement in cathodically protected systems.

5. Beams with cold-worked bars exhibit inferior fatigue performance[44,202] compared with beams with hot-rolled bars despite the fact that cold-working increases the tensile strength of deformed hot-rolled bars.

6. Partial replacement of cement by pulverised fuel ash[203] (pfa) has no discernible effect of fatigue life.

7. A limited number[203] of tests suggests that cementitious repairs did not adversely affect the fatigue life but resin repairs might do so.

8. Corrosion of embedded reinforcement can occur about as quickly in internally sealed[169] members as in members of normal concrete, it is thus expected to provide no improvement to the fatigue strength. In addition, the use of light weight aggregate was found to significantly reduce the current drain of the cathodically protected reinforcement under dynamic loading in seawater.

4.2 Crack Blocking.

4.2.1 Definition.

Crack blocking refers to the phenomenon in which concrete compounds at crack sites are able, under favourable conditions, to react with the ambient moisture to produce low-solubility salt deposits and block the cracks. This phenomenon, which was observed in fatigue tests, appears to have similarity to the phenomenon of "crack healing" reported in other circumstances which are related to static loading conditions. The following literature review describes the formation of deposit and the mechanism of effect under both loading conditions.

4.2.2 Literature Review.

Static Loading Condition.

The ability of concrete to heal cracks caused by loading was first observed by Abrams in 1913,[208] he presented the results of load tests on a 12 meter reinforced concrete highway bridge, in which a load of 106 tons was applied when the bridge was 3 months old. This load formed distinct diagonal tension cracks in both ends of the girder. The bridge stood exposed to the weather for 3 years before it was reloaded, upon reloading about 6 times the original load was applied to the girder. It was found in many instances during the application of load that some diagonal cracks which had been previously marked had opened again but at a much higher load than was placed on the bridge in the earlier tests, others did not reopen at all and in some instance new cracks were formed parallel to and near the old ones, it was evident that in being exposed to the weather during three years between the tests many of these cracks had healed in such a way as to form a joint even stronger than the unbroken concrete.

In a later investigation on the compressive strength of concrete Abrams[209] applied the name Autogenous Healing to this phenomenon and later there were further reports of

healing. The ensuing investigations have primarily been concerned with the gain in mechanical properties both compressive and tensile. The aim had been to evaluate the practical potential of this phenomenon to function as an effective natural remedy to visibly damaged concrete elements.

Gilkey[210] carried out an investigation on small mortar and concrete specimens tested for ultimate compressive strength at various ages and retested from one to five times in a period up to eight months. covering variable w/c ratio, curing conditions (wet and dry) and particle size. He observed deposits of salts in and around the cracks, the cracks did not in general disappear. His investigation justified the following conclusion to be made.

1. Autogenous healing follows the same general law of uninterrupted strength gain from continuous moist curing.

2. Specimens salvaged without much visible damage (cracks) often develop later strength approximately 100% of what they would have had without previous tests

3. Perhaps more importantly from the practical point of view, the percentage recovery in strength was mainly a function of the extent of structural damage with greater recovery being associated with specimens less severely damaged.

4. Recovery from damage, however, at early ages is more complete, as is their strength.

Later in other investigation on the tensile healing of standard briquets of mortar 6 cm^2 cross section Gilkey[211] suggested that healing is due to fresh crystalline growth resulting from the resumed or continued normal curing of uncompleted hydration process. The delayed chemical processes probably arise from two causes:

1. natural slowness of the calcium silicate to fully react,

2. slowness of hydration of large particles that are in the vicinity of the fracture, and thus coarser particles conceivably form a reserve supply of unhydrated material available for damage repairs.

He observed that specimens stored in stagnant water heavily charged with calcium hydroxide exhibit similar healing ability to that observed in specimens stored in fresh water which suggests that the conditions of the water (pH) can not be considered a major factor in this process. Other important observations in this study were:

1. healing never occurs in the absence of moisture but a period of dryness seems to have only a suspension effect on the healing activity thus healing will resume upon re-immersion,

2. healing was never observed to be present over an entire fractured area. The outer margin appears to be immune and crystal growth seems to start at some interior point.

3. healing occurred for mixture varying from very dry to very wet and for all ages inspected (upto 2 1/2 years) and it was greater with
   - richer mixtures
   - prolonged curing time
   - early initial test

   and in no case the tensile healing attains in magnitude the full strength at initial test.

Bouge[212] pointed out that physical forces may be expected to aid materially in the healing process by virtue of increasing the solubility of the solid phase. The material dissolved will be precipitated in contact with unstressed portions. He also concluded that the healing action represents a continuation of the hydration

of the hydraulic compounds of the cement supplemented by physical stresses. Thus the compounds formed at the break may be expected to be identical to those formed during the normal course of hydration.

Turner[213] examined the gain in mechanical properties due to healing in tension for small briquets of neat cement and mortar, and in compression for 12.5 x 25 cm in concrete cylinders. He reached essentially similar conclusions in that the gain by healing is related to the initial damage sustained and lesser cracking at an earlier date would reveal much higher healing percentages. Water condition (stagnant or running) appears to have no influence on the results.

Whitlan[214] investigated load-deformation characteristics of healed concrete. A series of concrete cylinder were tested at varying ages and re-tested after further varying periods of curing. He found that moisture and intimate contact of the fractured surfaces are essential for healing to take place, under these conditions healing took place in fractured concrete specimens at all ages examined (3 days to 3 years). Deposits of white crystals were observed at visible cracks and also at various other places. The compression of the healed specimens under re-test took place in the same manner as initial tests and no peculiarities were noticed which suggests the possibility that healing followed the same form as the general hardening process in concrete. The gain in strength, however, was proportional to the period of re-curing.

Strength and deformation characteristics of healed fractured mortar specimens as compared with unfractured specimens were studied by Dhir et al.[215] They observed that the ability of fractured material to heal is reduced when subjected to second fracture. The healed specimens behaved in a more brittle manner than the equivalent unfractured specimens. i.e. the range and extent of nonlinearity of the stress-strain relationship diminished for stresses approaching failure. The ultimate strains of healed specimens were less than those of the equivalent fresh specimens and were even lower for twice healed specimens.

Later in a more comprehensive study Mandy et al[216] investigated the effect of age of concrete, environment, constituent materials and mix proportions on the healing properties of cement paste, mortar and concrete with regard to strength behaviour and the practical implications of this phenomenon. The main findings of this study are summarised in the following.

- Age. Full recovery in strength was observed at all ages employed. Concrete tests at 7 and 28 days gave the greatest strength increase above fresh concrete (not previously tested). Thereafter healed and fresh strengths gradually become approximately equal.

- Environment. Concrete cured in relatively dry air shows greatly reduced healing ability at all ages as compared with moist cured concrete. However, healing does not increase directly with increasing availability of water and there is some optimum minimum humidity level for maximum healing.

- Initial curing. Tests to determine the effect of initial water curing followed by air curing until the time of test indicated that initial curing has relatively little effect on subsequent healing ability at later ages. However, test results have shown that a short period of moist treatment limited to the fracture sites, after initial severe fracturing, can have a marked beneficial effect on the healing ability.

Concrete of all kinds of cement employed showed gradual decrease in healing ability as the age at which the concrete experienced damage increases. Concrete made with Portland cement showed full recovery at 28 days after initial test at 3 days but only partial recovery at 90 days, whereas concrete made with Portland blast furnace (low heat) cement showed full recovery at all ages, Table 4.2, but when initial test is at 90 days its ability to heal is impaired. Low-alkali cement which has relatively more rapid rate of hydration exhibited a very rapid decline in its healing ability with increased age. Table 4.2 indicates that the cements which display the optimum healing at early ages show a greater reduction in their healing ability at later ages which appears to be allied

closely to the normal hydration behaviour of each cement.

Aggregate type has no significant effect on autogenous healing.

Dynamic Loading Condition.

Unlike healing under static loading, the reported investigations were not conducted primarily to obtain data on healing under dynamic loading. In fact all the available information was obtained as by-products and were only confined to reinforced concrete.

Due to the difference in the nature of the influence of the healing phenomenon under this type of loading, the main concern has not been the gain in strength properties but the influence on the structural behaviour and the fatigue lives. In the field of fatigue of reinforced concrete this phenomenon is usually referred to as crack-blocking. It is not absolutely clear when and by whom, the phenomenon of crack blocking under dynamic loading conditions in an aqueous environment was first observed. In any case it appears that the first published reference to this phenomenon was in 1978 in a French report[217], (quoted by Paterson)[59] on fatigue tests on U-shaped concrete members where it was observed that cyclic deflections of the members were reduced on this account. However, more detailed and systematic information have been provided by research carried out at Glasgow University which will be described in more detail in the following:

Arthur et al[19] observed a formation of white deposit at crack sites when concrete beams were fatigue tested in seawater under a uni-directional regime at slow cyclic rates. This observation was coincident with a drop in deflection range from a typical value of about 6 mm to somewhere in the region of 1 1/2 to 2 mm together with the observation of crack width changes. Under similar conditions but at high cyclic rate (5 Hz) this phenomenon was not observed. The formation of the deposits has the beneficial effect of increasing the fatigue life of the test beams as compared with air tests. The mechanism of

this effect as proposed by the authors was that blocking of the cracks prevents the steel in the immersed section of the beam from recovery to the intended lower stress level in the cycle when the load falls to its lower limit. This has the effect of reducing the stress range in the reinforcement and hence moving the immersed section to a regime of reduced severity in terms of fatigue, as shown diagrammatically in Figure 4.2. Dosing the solution with dilute HCl acid to keep the solution pH at a typical value for sea water of (7.8 - 8 Hz) showed seemingly no effect on the blocking process which suggests that the pH value of the surrounding solution would not contribute significantly to the observed blocking. The authors attributed this to the fact that pH within deep fine tortuous crack will be high in any case regardless of the external sea water condition.

In a later publication, Arthur et al[79] reported results of fatigue tests on reinforced concrete under both uni-directional and reverse bending regimes. In uni-directional regimes again a fatigue life of more than ten times the fatigue life of the corresponding air tests was obtained due to the effect of this phenomenon. The deflection ranges started to decrease significantly from the first day of the test and continued until a state of stability was reached after which the crack opening and deflection ranges remained virtually constant. In these tests, the greater proportion of the specimen fatigue life was spent cycling under these substantially less severe conditions, leading to enhanced fatigue lives.

Under the reverse bending regime, although there was evidence of crack blocking, there is no indication of any increase in fatigue endurance. Reverse tests, however, were conducted at high stress ranges. The deposit material was identified to be calcium carbonate ($CaCO_3$) and/or magnesium hydroxide ($Mg(OH)_2$). Blocking did not occur in tests at the higher frequencies of 3 and 5 Hz.

In the same research programme, Hodgkiess et al[150] reported enhanced fatigue lives of reinforced concrete beams under uni-directional regime and 0.17 Hz test frequency in sea water as compared to air tests and

seawater tests at 5 Hz. The deposition process of slightly soluble salts in sea water has been described. It was shown that sea water is close to saturation with respect to $CaCO_3$ and the solubility limit can be reached as a result of slight change in conditions. The dissolution of alkaline substances like $Ca(OH)_2$ from the cement will stimulate supersaturation of slightly soluble salts. At the same load level and test frequency, tests carried out in 3.5% NaCl and tap water showed no sign of crack blocking nor enhanced fatigue endurances. Progressive blocking of concrete cracks was observed in another study on fatigue[204] behaviour of prestressed concrete in sea water with similar effects.

The beneficial effect of blocking on the fatigue lives of reinforced concrete beams under reverse bending regimes was observed in a later phase[206] of the programme. However, no definite explanation as to the mechanism by which crack blocking increased fatigue lives in these circumstances was possible but it was thought to be associated with a consequential reduction of the stress range in the reinforcing bar crossing the cracks.

Results of parallel studies have been reported by paterson and Paterson et al[59,203] on fatigue strength of reinforced concrete in sea water and in air at a test frequency of 0.1 and 3 Hz under uni-directional bending regime. The sea water was replaced whenever the pH reached 8.4. Generally in all seawater tests except those of a few days duration ie. tests at high load level and high frequency. Cracks in concrete were blocked by a deposit which produced structural changes as described earlier. Chemical analysis of the deposits identified magnesium hydroxide $Mg(OH)_2$ (Brucite) as a major constituent, an alkaline reaction product of sea water in contact with cement paste. It was observed[203] that replacement of 20% of cement with pulverised fuel ash (pfa) produced a percentage reduction in deflection range due to crack blocking approximately 60% of that for beams without pfa under similar test conditions. However, this had no adverse effect on the fatigue lives of such beams.

On the other hand fatigue test on reinforced concrete

by Bannister [22] in sea water at cyclic rate of 3 Hz and Roper et al[202] in chloride solution and sea water at 6.7 Hz loading frequency have shown no sign of crack blocking nor different structural behaviour from in air test even after 10^7 cycles ($\sim$ 10 days of test).

4.2.3 Concluding Remarks.

Having reviewed the available information on the occurrence of the blocking phenomenon and its significance under both dynamic and static loading conditions, it becomes apparent that:

1. Blocking can only be expected under certain favourable conditions. These conditions are more fully defined for static loading conditions but less clear under dynamic type of loading.

2. In blocking-conductive conditions, there exist different machanisms of effect depending on loading nature and degree of damage and exposure.

More information is required on the limitations and practical implications of this phenomenon.

4.3 National Codes Recommendations.

Reinforced concrete structures which are subjected to fatigue loading in corrosive environments, such as offshore structures, have generally to satisfy minimum requirements in the guidelines, rules and recommendations provided by different national authorities. These rules will be reviewed with respect to the following parameters:

1. Mix design, cover and crack width limitations.
2. S.N. curves for steel reinforcement.
3. S.N. curves for concrete in compression.
4. Transverse shear capacity.
5. Cumulative fatigue strength.

4.3.1 Mix Design, Cover and Crack Width Limitations.

Guidelines for design of concrete mixes and the required minimum concrete cover to the reinforcement are usually recommended to ensure adequate protection from the external aggressive environment so that the risk of reinforcement corrosion can be effectively limited. These requirements as proposed by different authorities are given in Tables 4.4 and 4.5. Crack width limitations, Table 4.6, also serve the same aims and can generally be achieved by limiting the stress level or the spacing of the reinforcement in the tension zone.

The aforementioned tables indicate that while all codes appear to agree on the parameter which control the durability of reinforced concrete structures, there are considerable differences between them over what would actually constitute durable structure. This is particularly evident in cover and crack width limitations.

4.3.2 S-N Curve for Steel Reinforcement.

DNV recommended the following S-N curve for straight deformed reinforced bars.

$$\text{LogN} = 6.5 - 2.3 \frac{S_r}{\frac{f_y}{\gamma m}} - 0.002\, S_{min}$$

and the endurance limit, f_r, is calculated from

$$f_r = \frac{165}{\gamma m} - 0.33\, S_{min}$$

where N = No. of cycles to failure
S_r = Stress range ($S_{min} - S_{max}$)
S_{min} = Minimum stress
S_{max} = Maximum stress

f_y = characteristic yield strength of reinforcing steel

γm = 1.15

FIP does not provide S-N curve for reinforcement but indicates that fatigue in the reinforcement is not likely to be critical if the stress range in straight deformed bar is less than 140 N/mm^2. ACI also proposed the same stress range limitation for adequate fatigue resistance of the structure. NPD recommendations states that provided no experimental data is available, the endurance limit for straight deformed rebar can be taken as 170 N/mm^2.

Waagaard[38] suggested that the last three rules and recommendations are far too conservative as the cracking limitation of offshore structures ensures predominantly compressive stressed reinforced concrete members with predominantly compressive stress variations under which condition endurance limit is increased.

Recently published design curves, however, acknowledge that there is no fatigue limit for reinforcement in corrosive environments and that a fatigue limit is only relevant to good quality plain bars in air.

The BSC[47] developed modified design curves to take into account the characteristic strength, bar diameter, mean stress, environment and surface conditions including welding.

These are:

$$\text{Log}S = 2.7 - 0.01D - E/9[\text{Log}(N) - 4]$$

and

$$\text{fatigue limit} = (f_y - 3D)(1 - R)/2 \quad \text{for plain bars in air only.}$$

where D = bar diameter in mm.

R = stress ratio (minimum stress/maximum stress) in fatigue cycle.

E = environmental parameter and defined as follows:

E = 1 for bars in air or for corrosion fatigue situation where environmental fatigue crack initiation is precluded.

E = 2 for corrosion fatigue in sea water

E = 2.5 for fatigue of welded or jointed bars.

BSC design curves are based on constant amplitude fatigue tests on 16 mm diameter reinforcing steels in sea water.

The C.I.O. design curves[224] for the splash zone have been recently proposed from which the endurances can be obtained according to the applied stress range as follows:

$$\text{Log}S_r = 3.27 - (\text{Log}N)/6 \qquad S_r > 235 \text{ N/mm}^2$$

$$\text{Log}S_r = 4.3 - (\text{Log}N)/2.8 \qquad 235 \text{ N/mm}^2 > S_r > 65 \text{ N/mm}^2$$

$$\text{Log}S_r = 3.26 - (\text{Log}N)/4.8 \qquad S_r < 65 \text{ N/mm}^2$$

These design curves are obtained from a series of fatigue tests on partially submerged concrete beams with 32 mm diameter bars. Thus it can be safely used for smaller bars of similar steel types. Conditions such as those of fully submerged or cathodically protected beams are likely to be more favourable since these environments are less condicative to corrosion.

The C.I.O. curves for air exposure are.

$$\text{Log}S_r = 3.27 - (\text{Log}N)/6 \qquad 400 \text{ N/mm}^2 < S < 120 \text{ N/mm}^2$$

$$\text{Log}S_r = 2.73 - (\text{Log}N)/11 \qquad S < 120 \text{ N/mm}^2$$

Figure 4.3 compares the DNV rules with BSC (for 12 mm diameter) and C.I.O. curves which, for corrosive

environment, indicates that at high stress ranges BSC gives approximately similar values to the DNV rules whereas the C.I.O. curve is more optimistic. At low stress ranges, however, both BSC and C.I.O. curves give generally more conservative estimations than DNV. Figure 4.3 also indicates that the C.I.O. air curve gives consistently more conservative estimates than the BSC air curve.

4.3.3 S-N Curve for Concrete in Compression.

DNV has specified the following combined Goodman and Wohler curves for submerged concrete members.

$$\text{LogN} = 10.0 \frac{1.0 - \frac{S_{max}}{\alpha . f_K / \gamma m}}{1.0 - \frac{S_{min}}{\alpha . f_K / \gamma m}}$$

where $\alpha = 1.26 - 0.26\ B \leq 1.26$

f_K = characteristic compressive strength of concrete

$\gamma m = 1.25$

and B is the ratio of the simultaneous minimum edge stresses in the concrete section (ie. a value of the flexural gradient across the section).

FIP states that provided the compressive stresses are no greater than those for the several limit states, there is, in general, no need to check further the fatigue condition.

NPD requires the following Wohler curve.

$$\text{LogN} = 12.5 \frac{1 - \frac{S_{max}}{f_c}}{1 - \frac{S_{min}}{S_{max}}}$$

ACI states the following guidelines: the resistance of a structure to fatigue is considered to be adequate if, for frequently recurring environmental loads, the concrete stress is less than $0.5f'_c$; and no membrane tensile stress or flexural tensile stress is more than 1.4 N/mm^2.

4.3.4 Transverse Shear Capacity.

DNV states that for concrete members with one sided lateral shear loading the V-N curve is

$$LogN = 10.0 \frac{1.0 - \frac{V_{fmax}}{V_r}}{1.0 - \frac{V_{fmin}}{V_r}}$$

where V_{fmax} and V_{fmin} are the maximum and minimum shear force

$V_r = V_{cr} + V_{pr} + V_{sr}$

V_{cr} = shear resistance due to concrete and longitudinal reinforcement

V_{pr} = shear resistance due to prestress or axial force

V_{sr} = shear resistance provided by shear reinforcement

The total shear resistance should not taken greater than:

$$V_{max} \leq 0.25 F_{cr}.b.d$$

F_{cr} = Stresses in concrete

where b = breadth

d = depth

For reversible lateral shear loading the shear

capacity of concrete V_{cr} should be ignored in the calculation of V_r.

FIP states no special guidelines against fatigue in shear.

Unlike DNV recommendation, NPD considers each component contributing to the shear fatigue strength separately as follows:

$$LogN = 12.5 \frac{1.0 - \frac{V_{cfmax}}{V_{cr}}}{1.0 - \frac{V_{cfmin}}{V_{cfmax}}}$$

where V_{cfmax} = maximum average shear force carried by concrete

V_{cfmin} = minimum average shear force carried by concrete

ACI states that if shear fatigue loading exceeds the allowable shear on the concrete alone and where the cyclic stress range is more than half the maximum allowable shear in the concrete alone, then all shear should be taken by stirrups.

4.3.5 Cumulative Fatigue Strength.

The cumulative fatigue strength of a structure subjected to random loads can be estimated according to Miners hypothesis. Different Miners numbers have been proposed[38] but a value between 0.2 to 0.5 appears to be appropriate.

DNV states that the cumulative fatigue life may be estimated according to Miners hypothesis as:

$$\sum_{i=1}^{M} ni/Ni \leq 0.2$$

FIP gives no special recommendations to consider random loading.

NPD suggests Miners number of

$$\sum_{i=1}^{M} ni/Ni \leq 1.0$$

ACI indicates that a complete analysis based on the principle of cumulative damage should be undertaken only in the case where the stress limitation check is unsatisfactory or at locations where fatigue resistance is likely to be a serious problem. The analysis should also consider low-cycle, high amplitude fatigue.

Table 4.1 Summary of the Technical Merits of the Experimental Researches on Corrosion Fatigue of Reinforced Concrete.

Year of Publication	Authors	Loading Regime	Test Frequency (Hz)	Reinforcement Details	Beam Dimensions (mm)	Number of Tests and Environment	Objectives	Comments (measurements)
1976	Hajime et al[200]	U	5	One bar, 19 mm Ø	1600 x 200 x 150	24 exposed to spray of 3.5% NaCl soln 36 in air	Effect of exposure and galvanizing treatment on endurance.	Endurance, crack width, no electro-chemical measurements
1977	Waagaard[27]	U	6 (one test at 0.2 Hz)	4 No. 16 mm Ø with central ungrouted 32 mm Ø prestressed bar.	800 x 300 x 120	8 seawater under hydraulic pressure 6 Air	Effect of hydraulic pressure inside the cracks on endurance.	Endurance, crack width, deflection, concrete strain, no electrochemical measurement.
1978	Bannister[22]	U	3	One bar of 12 mm Ø Torbar	2400 x 150 x 100	Seawater	Effect of cathodic protection, lapping, wire fibres on endurance.	Endurance, no electro-chemical measurements
1979	Arthur et al[19]	U	5, 4, 3, 2, 1, 0.75, 0.5, 0.17	Reinforcing cage with 2 - 10 mm Ø Torbars	3000 x 250 x 150	16 Seawater with short tank 3 Seawater with long tank 40 Air tests	Effects of frequency, and exposure on endurance.	Endurance, crack width, deflection, No electrochemical measurements.
1980	Flick et al[169]	U	0.05	2 No. 12 mm Ø	3680 x 203 x 203	Flush of 3% NaCl Solution	Effects of internal sealing on corrosion under dynamic and static loading.	Electrochemical behaviour monitoring including half cell potential and chloride content
1980 1981	Paterson[201] and Paterson et al[59]	U	3, 0.1	One bar 32 mm Ø	3350 x 400 x 200	24 Seawater sub-merged partially 2 totally sub-merged 3 Air	Effects of frequency and exposure on endurance.	Endurance, crack width, deflection, steel stresses and electrode potential.
1981 1982	Hetherington[44] and Roper et al[202]	U	6.7, 0.17	One bar 12 mm Ø	2000 x 380 x 190	21 Air 18 Seawater 11 3% NaCl solution	Effects of different steel type and environment on endurance.	Endurance, crack width, deflection, No electrochemical measurements.
1982	Arthur et al[79]	U	5, 4, 3, 2, 1, 0.75, 0.5, 0.17	Reinforcement cage with 2 - 10 mm Ø Torbars	3000 x 250 x 150	44 Air U 6 Air R 32 Seawater U 5 Seawater R	Effects of frequency, exposure and loading regime on endurance.	Endurance, crack width, deflection, No electrochemical measurements.
1984	Hodgkiess et al[150]	U	5, 0.17	Reinforcement cage with 2 - 10 mm Ø Torbars	3000 x 250 x 150	10 Air 23 Seawater 1 Water 1 3.5% NaCl soln.	Effects of frequency, exposure and loading regime on endurance.	Endurance, crack width, deflection, electrode potentials.
1984	Paterson et al[203]	U	3, 0.1	One bar of 32 mm diameter or 13 mm prestressed strand	3350 x 400 x 200 and 3350 x 252 x 150	4 PFA (seawater) 5 CP " 5 PSC " 8 Repair "	Effect of cathodic protection, repair, PFA and prestressing on endurance.	Endurance, crack width, deflection, electrode potentials.

Table 4.1 Summary of the Technical Merits of the Experimental Researches on Corrosion Fatigue of Reinforced Concrete (Continued).

Year of Publication	Authors	Loading Regime	Test Frequency (Hz)	Reinforcement Details	Beam Dimensions (mm)	Number of Tests and Environment	Objectives	Comments (measurements)
1985	Banerjec et al[204]	U	5, 0.17	12.7 mm prestressed strand	3000 x 250 x 150	26 Air 6 Seawater	Effects of environment on endurance of prestressed reinforced concrete.	Endurance, crack width, deflection, electrode potentials.
1985	Nilsen[205]	U	0.12	Two bars of 12 mm Ø	1000 x 250 x 150 and 1000 x 250 x 120	24 Seawater 8 Dynamic 8 Static 8 Unloaded	Effect of cathodic protection, type of loading and cover on the electrochemical behaviour of sub merged reinforced concrete beams	Electrode potential and polarization curves
1986	Hodgkiess et al[206]	R	5, 0.17	Reinforcment cage with 2 - 10 mm Ø top and bottom	3000 x 250 x 150	6 Air 9 Seawater	Effects of loading regime and environment.	Endurance, deflection, crack width, electrode potential and polarization measurements
1986	Espelid et al[207]	U	-	Layers of bars of 16 mm Ø	Columns of circular cross section, 5 meter length, 0.6 m diameter	8 Partially submerged in seawater	Effect of cathodic protection on the electrochemical characteristics of reinforced concrete columns	Polarization of the reinforcing steel
1987	Katwan et al[20]	U, R	0.17	Reinforcment cage with 2 - 10 mm Ø Torbars top and bottom	3000 x 250 x 150	3.5 NaCl solution 3 R, 3 U Water 6 R, 3 U	Effects of loading regime and environment on endurance	Endurance, deflection, crack width, electrode potential

Note: U = Uni-directional bending regime.
R = Reverse bending regime.
PFA = Pulverised fuel ash.
CP = Cathodic protection system.
PSC = Prestressed concrete.

Table 4.2: Effect of age at first test on the rehealing ability of concrete. (Reference 216).

Cement type	Strength - N/mm^2 Test and retest ages (days)				
	3	7	28	90	180
Ordinary Portland	17.8*	28.6	38.1	34.9	33.7
		25.7*	37.7	41.6	39.8
			36.7*	39.8	38.7
				43.5	41.1
					45.9*
Portland Blastfurnace	12.0*	20.9	32.0	37.6	37.5
		18.3*	34.2	40.5	41.8
			30.6	37.5	39.0
				37.6*	36.9
					39.0*
*Strength of concrete at first test					

Table 4.3: Influence of cement type on autogenous healing (Reference 216).

Cement Type	Age Span	(Healed Strength Change-Fresh Strength Change) %			
		3-28	7-28	28-90	28-180
Ordinary Portland		+ 8.2	+4.6	-4.3	-4.8
Portland Blastfurnace		+ 7.4	+8.0	-6.9	-6.5
Low Alkali		+13.0	+0.7	-8.4	-9.8
High Alkali		+ 9.9	+5.3	-7.3	-9.6

Over the range of test ages employed concretes made with all the cements show the expected gradual decrease in healing ability as the age at which the concrete experiences damage increases. The low heat (Portland blastfurnace cement, however, showed no decrease.

Table 4.4: Recommended Characteristics for Structures in Aggressive Environment.

Authority / Characteristics		BS8110 (218)	BS5400 (219)	ACI 357 (220) Tidal Submerged	DNV (221) Tidal Submerged	FIP (222) Tidal Submerged
Maximum w/c ratio		0.55	0.45	0.45 0.4	<0.45 preferably 0.4	<0.45 preferably 0.4
Minimum cement content kg/m^3		325	320-410* maximum 550	356	400 300	400 300 to 360
chloride content %wt of	RC	0.4	0.06 for sulphate resistance and supersulphated cement 0.35 for 95% of results for Portland cement	0.1	0.3	-
	PSC	0.1		0.06		
C_3A %wt of cement		-	-	4% < but < 10%	5% < but < 10%	<12

* depending on aggregate size
R.C = reinforced concrete
PSC = prestress concrete

Table 4.5: Permissible minimum thickness of concrete cover to reinforcement.

Authority / Location	BS8110 (218)		BS5400 (219)		ACI357 (220)		DNV (221)		FIP (222)	
	Reinforced Concrete (mm)	Prestressed Concrete	Reinforced Concrete (mm)	Prestressed Concrete	Reinforced Concrete (mm)	Duct for post or pre tension	Reinforced Concrete (mm)	Duct for post or pre tension	Reinforced Concrete (mm)	Prestressed Concrete
In air	30		25*		50	75	40	80	-	-
In air and tide zone	50		55*		65	90	50	100	75	100
In seawater	40		55*		50	75	50	100	60	75

* Note: minimum cover to any duct should be $\geq$ 50 mm

Table 4.6: Crack Width Limitations.

Authority	Crack Width Limitations
BS 5440 (219)	Reinforced concrete - 0.1 mm for marine environment. 0.15 mm for seawater spray and de-icing salts. Prestressed concrete - Class 1: no tensile stress permitted Class 2: tensile stress permitted but no cracking Class 3: as for reinforced concrete
BS 8110 (218)	Reinforced concrete - < 0.3 mm Prestressed concrete - Class 1: no flexural tensile stresses. Class 2: flexural tensile stresses permitted but no cracking. Class 3: surface width < 0.1 mm for aggressive environment and < 0.2 for all others.
ACI 357 (220)	No membrane tension is allowed. The edge stress should be limited to 1.4 N/mm^2 flexural tension.
DNV (221)	No membrane tension. The edge stresses are to be limited to the tensile strength of the concrete.
FIP (222)	< 0.3 mm under extreme load condition. For structures required to contain oil, the membrane stress should be less than the tensile stresses necessary for cracking.
NPD (223)	No structural cracking is accepted.

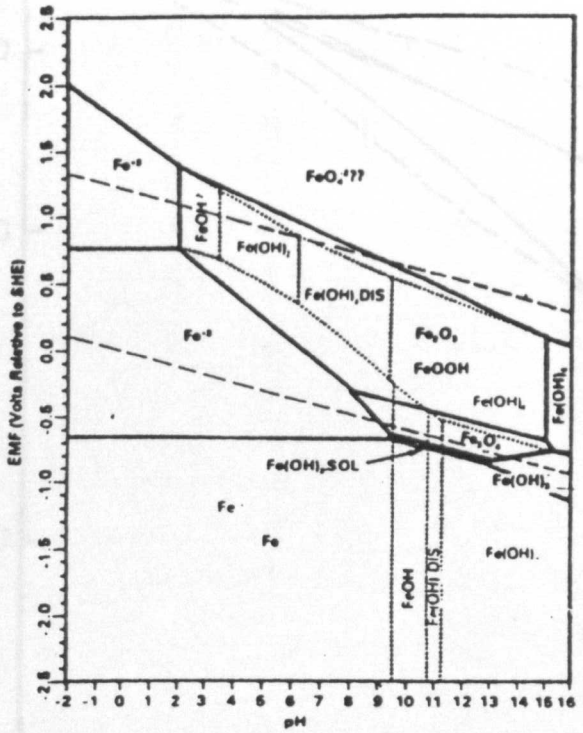

Figure (4-1): EMF-ph diagram for iron as calculated by Siverman (Ref. 198).

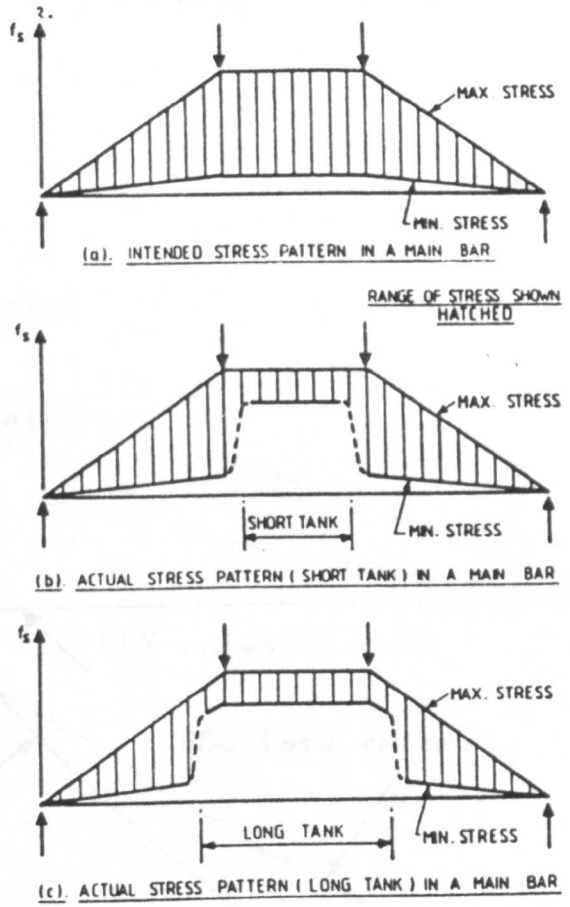

Figure (4-2): Comparison of intended and actual stress distribution (slow, submerged tests, unidirectional bending) (Ref.79).

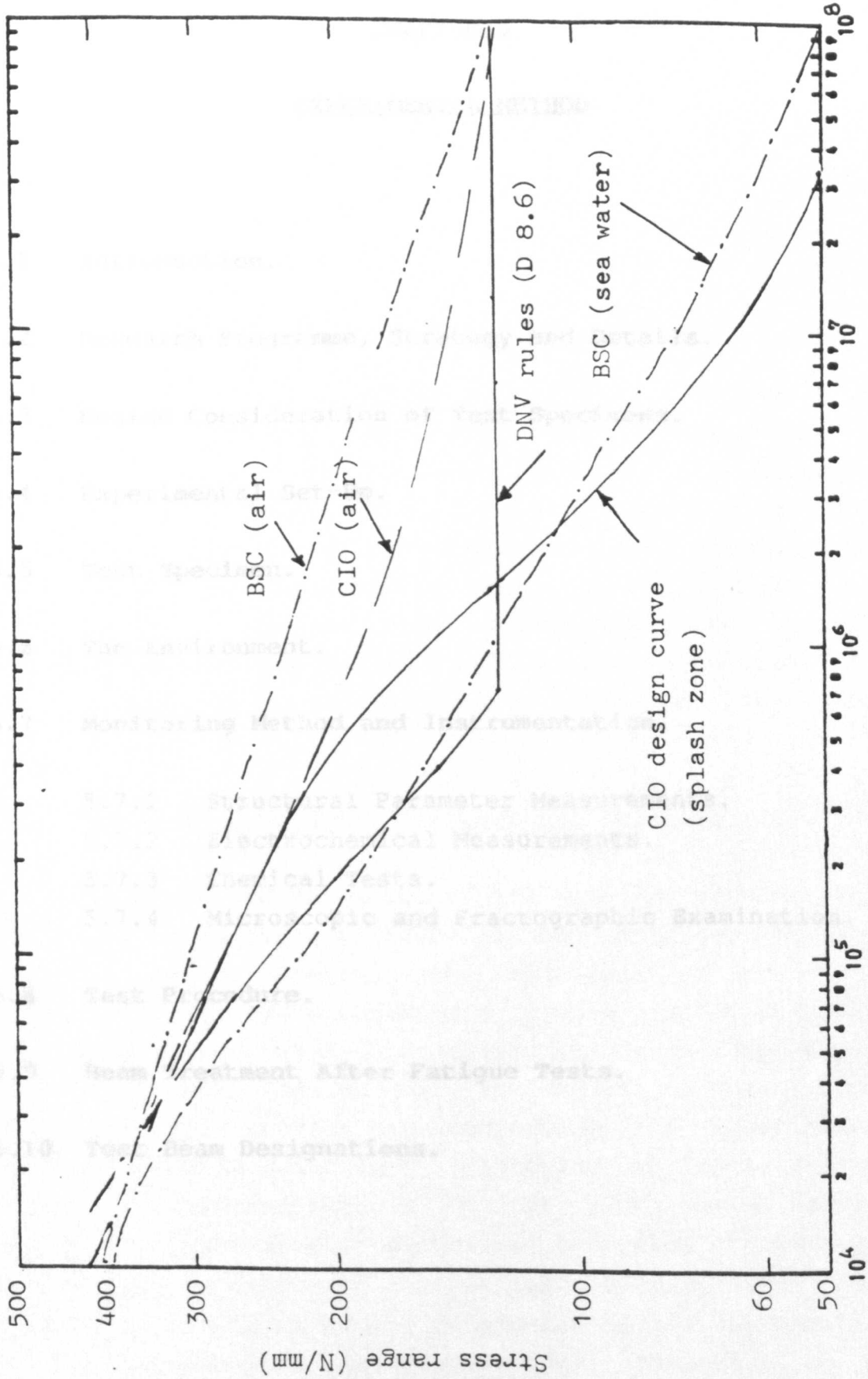

Figure (4-3): Design curves as proposed by different authorities.

CHAPTER 5

EXPERIMENTAL METHOD

CHAPTER 5

EXPERIMENTAL METHOD

5.1 Introduction.

The experimental study was mainly designed and detailed to provide information with respect to the fatigue behaviour of reinforced concrete in corrosive environments under moderate to high loading conditions. This chapter outlines the research programme and describes in detail the experimental setup, the specimens, the instrumentation and monitoring methods used. The detailed description and test methodology of the electrical and electrochemical measurements are presented in other chapters.

5.2 Research Programme, Strategy and Details.

The scope and potential of the problem of corrosion fatigue of reinforced concrete has been outlined elsewhere in this thesis, however, the behaviour of structural elements in hostile environments is more complex and less easily predicted than comparable structure exposed to fatigue loading in an air environment. This poses particular difficulties in converting the experimental data into design criteria by improving or rationalizing existing evaluation methods. On the other hand fatigue tests are notoriously expensive and time consuming, accordingly in corrosion fatigue research programmes many factors should be carefully considered before any decision as to the nature and the experimental variables to be studied can be taken.

Previous fatigue tests on reinforced concrete in corrosive environments have essentially been conducted to provide information about the susceptibility of the structural elements to fatigue failure under the combined effects of environment and heavy structural load, but other different characteristics during fatigue loading were also examined. It is evident that the fatigue life is astochastic phenomenon and a scatter in test results is an inherent property. Fatigue tests on reinforced concrete are not an exception, therefore in order to establish a statistically valid assessment, multiple tests should be conducted at each load level. This consideration poses tremendous experimental difficulties in the field of reinforced concrete particularly when information on the effect of the environment is required which is in turn time-dependent. Past experience suggests that an effective contribution of corrosion to the damage process under this type of loading can only be expected in long running tests ie. at low load amplitude where conventional fatigue damage due to fatigue cracks is not likely to cause failure by its own and this would certainly be the case when the stress levels are below the fatigue limit.

Obtaining full time-covering data (eg. for say 10^8 cycles) under such circumstances is practically impossible due to the time requirement for each test (of the order of several years), therefore the determination of the rate or rates of damage caused by environmental factors over reasonable durations of test by more reliable techniques and the exploration of the possible link between these data and the available body of information to provide ultimately reasonable predictive basis, for the processes prevailed in reality seems highly desirable.

In these particular, yet sensitive, conditions no one factor conclusively bears the major responsibility of damage process, consequently it is only possible for any research programme in this area to cover certain factors and leave the others either for extrapolation or speculation. For instance, any study of the effect of an aqueous solution on either fatigue crack initiation and propagation or on localised corrosion must take into

account the fact that the results are likely to be partially dependent on the loading frequency. The importance of this aspect has been demonstrated in earlier work. As a result in the present study a single test frequency of 0.17 Hz was utilised; this frequency being the same as that used previously for beams tested in sea water, since it represented the observed frequency of extreme storm waves in the North Sea. This then provides a means of comparing the results of this programme with those previously obtained from the sea water work.

A review of previous work on the corrosion fatigue of reinforced concrete led to the conclusion that there were a large number of variables relevant to the conditions under which real concrete structures may be serving which had received virtually little or no attention. One of the uncovered significant variables is the test environment. Since for the vast majority of corrosion fatigue researches, the sea water effect has been the main concern, it is necessary to raise the question of the effects other aqueous environments might have under fluctuating load conditions. Consequently the research programme involves the study of reinforced concrete beams exposed to 3.5% chloride solution and to low total dissolved solids (T.D.S.) tap water.

One of the important aspects of fatigue tests has been the load variation, while environmental loads are completely random in nature with respect to magnitude and order of loading, its simulation involves further practical, economical and analytical difficulties. In this research, however, the simplest form of loading ie. constant load amplitude was employed, thus the loads were applied between constant minimum and maximum values throughout any one test, but different load amplitudes were examined.

Finally the research involved two stages. The first stage was designed to provide more general information and early indication of the effect to be expected. Therefore most of the tests carried out have been at high stress amplitudes under both uni-directional and reverse bending regimes as described in Table 5.1 and 5.2.

The approach adopted in Stage 2 of this research assumes that the role of metal loss or corrosion-related deterioration has more effect on the eventual damage occurring during fluctuating loadings. The experimental interpretation of this statement has been the use of low-amplitude low-frequency fatigue loading with periodical monitoring of the corrosion rate by means of electro-chemical methods. For each of the load levels investigated, the chosen maximum test duration was 5 months. Due to the expected change in some electro-chemical parameters such as Tafel constant during this duration (5 month), which is essential for corrosion rate estimation, and also to provide a means of checking the reproducibility of the test results, another two tests were conducted involving exposures of 1 and 3 months respectively. Static tests were conducted at the same load levels chosen in this stage in order to provide comparative electrochemical and structural data. The test programme of Stage 2 is given in Table 5.3.

During the course of the study, several additional tests were added to the original programme either to provide some particular information or to substantiate others, these tests referred to as complementary tests in Tables 5.1, 5.2 and 5.3.

5.3 Design of Test Specimen.

Corrosion fatigue is a process which prevails when corrosion processes contribute considerably to the total fatigue damage (see Section 2.1). Under these conditions as well as in the majority of air-fatigue failure cases, it is widely accepted that failure will most probably be governed by the fatigue properties of reinforcement. In any case, however, for more realistic assessment of the potential influence of corrosion on the eventual total fatigue failure, the beam resistance to fatigue may heavily depend on the reinforcing steel. The experimental conditions thus, should be set so as to fulfill the following:

1. Corrosion - conductive environment.

2. To allow corrosion damage to play a part other damaging processes eg. pure fatigue effect should not be predominant.

3. To ensure dependency of corrosion fatigue resistance on reinforcing steel, the test specimen must be under reinforced with respect to failure in flexure.

In the same way as the static properties of reinforced concrete elements are related closely to the properties of the component materials, the fatigue properties are also related to them except the rare cases of premature shear and bond failure. Therefore for under-reinforced members failing in bending the fatigue properties are directly related to those of reinforcement, similarly over-reinforced members would fail in compression. Balanced failure would occur at a particular steel content when the steel reaches the yield strength (f_y) and the concrete reaches the extreme compression strain of approximately 0.003 simultaneously. The steel content for balance condition (ρ_b) may be calculated using standard design methods. The type of failure will depend on whether the steel content is less or greater than ρ_b. For the particular material properties, the steel content for balanced failure was found to be equal to ρ_b = 0.05334. While the adopted steel content varied between ρ_b = 0.0069 and 0.0084, the theoretical static failure load being, P = 32 kN. Other factors considered during this stage have been:

1. The size and capacity of the available testing machines and,

2. Similarities in experimental details with other concurrent tests conducted in this department in sea water to provide means of direct comparison with present test results.

5.4 Experimental Set-up.

Loading Configuration and End Support Condition.

Symmetrical two point loading was applied as shown in Figure 5.1 on a span of 2.8 m. The shear span being 1 meter. The test beams were simply supported at both end supports. For uni-directional bending, a small minimum load of 3 kN, corresponding to a steel stress in tension steel of 0.1 f_y, was maintained on each load cycle to prevent backlash and vertical movement upon the release of maximum load.

Horizontal movement was restricted in one end of the beam by a combination of fixed roller and a steel plate with circular groove attached to the beam soffit. Frictionless piece of "PTFE" was put between the two surfaces to facilitate end movements. The other end was arranged to provide free-sliding horizontal movement, Figure 5.2. Loads are transmitted from the machine ram to the beam through 25 x 80 x 150 mm stainless steel plates. To reduce noise during operation, as well as other considerations as will be discussed later, the contact surface were separated by PTFE plates and a rubber plate were put between the beam and the steel plate, Figure 5.3a.

Reverse bending arrangements, Figure 5.3b, are functioning basically in a similar way. Horizontal movement was restricted in one end by a plate of steel with a V-shape groove glued to the beam soffit. The remaining supports were free sliding rollers in horizontal directions, Figure 5.4. The load was applied up and down wards during fatigue loading and transmitted to the beam's top and soffit through steel plates.

Load Calculation.

To relate the applied flexural load to the required force in the tensile reinforcement, the recommendation given in the British Standard BS 18110: Part 1: 1985.

Section 3 may be used for elastic cracked section analysis on the basis of linear strain distribution with a tensile concrete contributing a fictitious triangular stress-block below the neutral axis so as the concrete stress at the level of the tensile steel not exceeds 1.0 N/mm^2. Such an analysis was applied using the following:

1. The chosen steel stresses (eg. $0.7f_y$, $0.75f_y$...etc.) are expressed as a percentage of the specified characteristic proof stress of 460 N/mm^2.

2. The steel stresses calculation was based on the nominal cross section area of 10 mm diameter Torbar. The effective area, however, is about 6% lower than the nominal area so the true stress is about 6% higher than those calculated.

3. An actual modular ratio between the steel and concrete (E_s/E_c) equals to 6.15, Table 5.5 (E_s and E_c were determined experimentally).

Details of the analysis procedure and the formulae used to relate the applied load to the stress in the reinforcement are given in Appendix A. The applied loads were calculated to produce a maximum steel stress in the tensile zone ranging between 0.35 to $0.95f_y$. For uni-directional series, a minimum stress of $0.1f_y$ was set through out the fatigue testing as shown in Table 5.1. In the reverse bending series, the applied loads were in the constant ratio of 1.33 (down):1 (up) thus producing variable steel stresses as shown in Table 5.2.

Testing Machines.

Four simple fatigue machines, Figure 5.5a have been used for uni-directional bending tests. The machines employed a 0.75 kW hydraulic pump-set operating a single-acting ram. The loading was monitored by a strain-gauge load cell mounted in a spherical seat attached to the ram body. Load variation was achieved by means of a pressure

control valve and cycle frequency controlled by a constant speed cam. The wave form of load against time was arranged to be nearly sinusoidal by the adjustment of fine control valves operating on the ram inlet and outlet pipes, and the lower load was controlled by a further flow restriction in the oil return line.

For reverse bending series Losenhausen servo-controlled equipment was used with a demountable packless ram on a loading frame bolted to a hollow testing floor. The machine can also be used for uni-directional bending regime and operates over a wide range of loading frequency, Figure 5.5b.

The Static-Testing Machine.

Static tests were conducted by an other purpose-made setup Figure 5.6 with the same loading arrangements. The load in this case was applied by a hand-operated screw jack by which a constant deflection was maintained through out the test.

Test Frequency.

Fatigue tests, in both bending regimes, were confined to single low loading rate of 0.17 Hz ie. ten application of load per minute.

5.5 Test Specimen.

The present research is concerned with two main variables as described in the test programme "Paragraph 5.2" which are the environment and loading conditions (level and regime), thus the specimens were identical in the overall dimensions and properties unless the loading regime dictated otherwise. The beam design considerations are outlined in the preceding Sections 5.3.

The specimens were concrete beams of rectangular cross section 150 mm in width and 250 mm in overall depth and 3 meter long. For Stage I of the research programme, beams intended for uni-directional bending were reinforced

with two 10 mm diameter Torbars on the tension side with two 8 mm diameter mild steel lacing bars to provide anchorage for the stirrups. Those intended for reverse bending tests had two 10 mm Torbars top and bottom. 6 mm diameter mild steel links were spaced along all but the central 40 cm portion of the beam with concrete cover of 25 mm to the main tension bars. In Stage II of the programme, which was confined to uni-directional bending regime, similar details were used as in Stage I except that the links diameter was 8 mm mild steel instead of 6 mm. This is because the production of the later type was abandoned at the time when Stage II has been started during summer 1986. All reinforcement cages were wire tied. The beams details are illustrated in Figure 5.7.

Concrete Mix Design.

The concrete mix design was made following the procedure described in the Department of Environment report, The Design of Normal Concrete Mixes. The mix consisted of ordinary portland cement, 20 mm uncrushed morainic gravel and zone 2 sand. The coarse and fine aggregate used in the concrete mix were obtained from Hyndford in Lanarkshire. The mix specified max water cement ratio was 0.45 with a characteristic cube strength of 40 N/mm^2 at 28 days. Thus a mix proportion of 1:1.58: 2.91 was used and the proportion per 80 kg of concrete is given in Table 5.4. Other mix details were given in Table 5.5.

Properties of Reinforcing Bars.

10 mm high yield deformed cold twisted bars (Torbars) were used as the main reinforcement. To eliminate variability due to differences in composition and cold working procedure, all the main steel used in the test programme was obtained from a single batch. Random samples were cut from the steel stock and were tested in a Tinius olsen universal testing machine, fitted with s-type electronic extensometer. The tests were carried out in

accordance with the manufacturer's instruction manual. Typical stress-strain curve as obtained from the testing machine is presented in Figure 5.8. Since the yield point for all the bars was not well defined; the yield stress of the bar was taken as the stress at which a line parallel to the initial slope of the curve from 0.2% proof strain intersects the curve. The yield strain was taken as the strain at which the straight line portion when extended, intersects with the yield stress as illustrated in Figure 5.9. The main values of three tests specimens are presented in Table 5.5 which also presents the chemical composition of the reinforcement.

Manufacturing and Curing Process.

An electric pan mixer used to mix concrete ingredient. The mixer consists essentially of a circular pan of 0.04 m^3 capacity fixed in position with two star paddles rotating about its axis and clockwise around the pan circumference. Coarse, fine aggregate and cement were first fed into the mixer and mixed in a dry state for approximately 2 minutes. After having obtained a homogeneous mix, the greater part of the designed amount of water was added, the remaining small amount was withheld until visual assessment made as to the required amount of water to achieve the required workability. The batch mixing time was between 1 to 1:30 minutes.

Reinforcing cages were supported on plastic spacers of the required depth (25 mm) and located in steel moulds, Figure 5.10a-b, concrete was placed in 3 layers of approximately equal depths, each of which received adequate consolidation by means of external vibrator (frequency 50 kHz).

The beam surface was screeded, trowelled and covered with damp sacking for 24 hours and then in laboratory air until time to test. Six samples of concrete 100 x 100 mm cubes and two 150 x 300 cylinders were taken from each day mix to determine the compressive strength and the elastic modules (and the stress-strain curve). A vibrating table was used for the compaction of the controlling specimens.

The specimens were cured under similar curing conditions as those used for the actual test beams. The actual strength of the cubes at 28 days varied between 46-65 N/mm^2. For the majority of the test beams the age at time of test varied between 33-55 days. As a result, the cube strength at the start of the test ranged from 58 N/mm^2 to 70 N/mm^2. The standard deviation being 9.6 N/mm^2. Some of the test beams, as will be described later, were of more than one year old (up to 8 years in a few cases). Consequently the cube strength of these beams varied between 82 to 96 N/mm^2. Stress-strain curves of the concrete were determined according to BS 1881: Part 121: 1983. A typical curve is shown in Figure 5.11.

5.6 The Environment.

Air Tests.

Three static tests and a single fatigue test were carried out in laboratory air. No attempt was made to alter the ambient atmospheric conditions during the fatigue test.

Corrosion Fatigue Tests.

Corrosion fatigue tests were carried out both in tapwater and in a 3.5% sodium chloride solution. Tapwater was drawn from Glasgow public mains supply which is very low in total dissolved solid (TDS). Typical TDS values are in the range 20-50 ppm with sodium and chloride concentration both less than 10 ppm. The results of detailed analyses carried out on the tapwater are given in Table 5.6. The chloride solution was made from commercially available sodium chloride mixed with tapwater in the required proportion. The central 1170 mm long portion of each beam was enclosed in a transparent plastic jacket containing the solution. Due to the profound effect of the jacket length on fatigue life, discussed earlier by Arthur et al.[19,79] The length of the jacket chosen ensured that the whole of the maximum moment region

of the beam was enclosed in the solution which was circulated through the water jacket, passing beneath the beam and through approximately 300 litre storage tank at a lower level. The jacket inlet and outlet was adjusted so as to maintain the water level approximately 15 mm above the top of the beam. The temperature of the solution was usually close to the ambient temperature in the laboratory, i.e. in the range 16-21^{o}C. For good correlation of laboratory tests with natural exposure conditions appreciable increases in pH was prevented and the pH of both solutions was maintained in the range 7.9-8.2 by intermittent dosing with dilute hydrochloric acid into the storage tank. This dosing, however, was only found to be required in the first few days of experiments. In the tapwater tests in Stage II, the water was replaced. twice a week for the first week and then each 10 days. The solution level in each test was kept constant throughout the test duration by adding fresh water to offset any loss by evaporation.

Solution-Metal Isolation.

As mentioned earlier, the solution jacket extends beyond the loading points, under these circumstances complete electric isolation had to be made at the electrolyte - machine ram contact area. For uni-directional tests, this was accomplished by using PTFE plates between the ram and the partially submerged stainless steel plate which transmits loads on the top of the beam. The plates were further isolated from the electrolyte by a non-soluble grease layer so that no metal other than the reinforcing steel was exposed to the electrolyte, Figure 5.3a.

For the reverse bending loading arrangement, due to the inherent difficulty of isolating the machine ram from the electrolyte, the use of stainless steel elements and non-soluble grease coating were the main isolation measures. In Stage II of the programme where electrochemical parameters such as corrosion rates were monitored, it was found that even the small contact

between the deflection measuring clock and the stainless steel stand, which is fixed on the top surface of the beam, can have an effect on the electrode potential of the system. Therefore this was separated by a piece of PTFE as shown in Figure 5.12.

5.7 Monitoring Methods and Instrumentation.

All test beams were instrumented to measure the load and mid span deflection. The determination of other parameters depends on the objective of each individual series of tests. The measurements are categorised according to their nature into four kinds as follows.

5.7.1 Structural Parameter Measurements.

Load Monitoring.

The applied loads were monitored periodically to avoid changes in the initially set fatigue loads which might occur during the test duration. The machine load cells described in Section 5.4 were calibrated either after each two consecutive tests or yearly which ever occurred first. The load monitoring was made using a Peekel strain indicator type CA605 which was also used to calibrate the load cells.

Deflection.

Measurements of beam deflection during the test were made using a dial gauge (0.01 mm div) situated at the mid span of the beam.

Crack Width Measurement.

In ten of the tests of Stage I of the programme, two separate cracks in each beam were monitored. The monitored cracks were inside the jacket zone about 200 to 400 mm from the mid span and were randomly chosen before the fatigue test by applying gradually increasing load until

visible cracks appeared. The cracks were then marked and the load released immediately. Generally the applied load was far less than the intended fatigue load. Crack width measurements were made using linear transducers mounted on the side of the concrete beam at the level of the centre line of the main reinforcement, i.e. at the bottom of the beam for uni-directional tests and at the top and the bottom for reverse bending tests. The body of the transducer was held in perspex brackets adhesively attached to the concrete on either side of the cracks (see Figure 8.5), the movement of the transducer core, which represents the crack width, is displayed on a digital monitor.

Cycle Counting.

The number of cycles elapsed in each test were recorded using a simple electrical counters with a 10 to 1 ratio (i.e. 10 loading cycles moves the counter 1 number) for the losen-nausen system and 1:1 for the other fatigue machines.

Concrete Strain Measurements.

In two dynamic tests and in the air static tests, row of demec points at 100 mm and 200 mm gauge lengths were employed to determine the concrete surface strain and neutral axis depth.

Steel Strain.

Electrical resistance strain gauges were used to measure the strain in steel for static tests in air. The gauges were of the type, student EA.0.6.24012-120. All the strain gauges were connected to a linear voltage processing data logger (Orion A) which directly recorded the strains at each point for each load increment.

5.7.2 Electrochemical Measurements.

Electrode Potential.

The electrochemical potential of the reinforcing steel in the beam for corrosion fatigue tests was measured at regular intervals using a high impedance digital voltmeter capable of reading 0.01 mV in conjunction with a saturated calomel electrode SCE (potential on SCE scale = Potential on Ag/AgCl scale - 42 mV) immersed in the solution adjacent to the beam body. The electrical connection with the reinforcing bars was made via a lifting hook (an extended shear link). The relative position of the electrode inside the jacket has no effects on the measurement potential.

Corrosion Rate Measurements.

See Section 10.2.

IR-Drop and Concrete Resistivity Measurements.

See Section 9.6.

Solution Conductivity.

Measurement of the solution conductivity was made using model 5003 portable conductivity measuring set. The tests procedure was in accordance with the manufacturer instruction manual.

5.7.3 Chemical Tests.

Solution pH and temperature:- The solution pH and temperature were periodically monitored using standard commercial probes.

Dissolved oxygen content:- Dissolved oxygen content was determined using a modified winkler technique.

Deposit chemical composition:- The x-ray diffraction and x-ray fluorescent microanalysis techniques were used

to identify the chemical composition of the deposit material. The tests were carried out at the Geology Department of Glasgow University.

5.7.4 Microscopic and Fractographic Examination.

The concrete surface skin and steel fracture structure were examined using light optical microscope and scanning electron microscopy respectively.

5.8 Test Procedure.

In general, after placing the beam in the testing rig, the water was circulated and the initial measurements are recorded. In Stage I the loads were applied immediately after water circulation whereas in Stage II 5 days of immersion were allowed before load application.

The maximum loads were first applied statically with another set of readings being taken, before setting the machines on the cycling mode, the knobs or values which control the minimum load were set on values slightly more than zero to reduce the possibility of backlash in the loading system at the early stage of cycling.

During the first 10-50 cycles, both maximum and minimum loads are usually brought to their exact values and maintained constant thereafter throughout the test. The structural and electrochemical measurements were taken more frequently in the first week of the test and the first day in particular, then at regular, but wider intervals, for the remaining period of test.

5.9 Beam Treatment after Fatigue Tests.

Fatigue tests were usually terminated when the test beam failed in fatigue or when the test ran for the pre-planned test duration. In both cases the beams were then broken open as quickly as possible after draining the solution from the jacket enclosing the beam, to reveal the nature and the extent of corrosion on the reinforcing bars and also to facilitate removal of the reinforcement cage

for further examination including scanning-electron microscopy and the determination of the corroded area.

5.10 Test Beam Designation.

Dynamic Tests.

The test beams are designated according to their bending regime (U:uni-directional or R:reverse), their intended stress level as a percentage of the characteristic strength of the steel (e.g. 70), and the surrounding environment (N:chloride solution, W:water or A:air) in which the test was carried out.

Thus: MU70W indicates a beam tested in uni-directional bending, with an intended upper stress level of 0.7 f_y, tested in tap-water.

MR75N indicates a beam tested in reverse bending, with an intended upper stress level of 0.75 f_y tested in 3.5% NaCl solution.

MU70A indicates a beam tested in uni-directional bending, with an intended upper stress level of 0.70 f_y and the test was carried out in air.

Stage 2 of the programme involved tests of variable test duration, therefore the test duration in (months) was introduced in the beam designation as a third figure following the load notation, thus

MU605N indicates a beam tested uni-directionally with an upper stress level of 0.6 f_y tested in chloride solution for 5 months.

Static Tests.

Static tests in air involved load cycles of different levels and this was referred to by a four figure number indicating the lower and the higher level of the load cycles employed. Other notations are similar to those described above. Thus:

MR7595SA indicates a beam tested statically (s) in reverse bending in two cycles, the upper intended stresses being 0.75 f_y and 0.95 f_y respectively the test being carried out in laboratory air (A).

In Stage 2 (where time is involved) of the programme, static tests were conducted in chloride solution. The load regime was annotated by (L), other designations being similar to those of dynamic tests, e.g. ML403N refers to a static test in chloride solution with an intended upper stress level of 0.4 f_y and test duration of 3 months. Detailed descriptions of the test and loading conditions will be given for each test beam in the results' Chapters.

Table 5.1: Test Programme;* Stage 1 Uni-directional Bending Regime Series.

Applied load (KN)		Intended Stress (N/mm^2)			Stress Range (N/mm^2)	No. of Tests		
		Maximum		Minimum				
Max	Min	Steel	Concrete	(steel)		Air	Water	3.5% NaCl
21	3	322	16	46	276	1	1	1
22.5	3	345	17.2	45	299	-	1	1
25.5	3	391	19.5	46	345	-	1	1

* One beam tested statically to failure in air with load increments of 21, 22.5 and 25.5 KN respectively.

Table 5.2: Test Programme;* Stage 1 Reverse Bending Regime Series.

Applied load (KN)		Intended Stress (N/mm^2)			Stress range N/mm^2	No. of Tests		
		Maximum		Minimum				
Down-wards	Up-wards	steel (bottom)	concrete (top fibres)	bottom bars		Air	Water	3.5% NaCl
10.5	8	161	9.6	-3.0	164	-	1^{c}	-
14	10.5	212	12.7	-3.8	216	-	1^{c}	-
21.0	16.0	322	19.1	-5.7	328	-	$1 + 1^{c}$	1
22.5	17.0	345	20.6	-6.0	351	-	1	1
25.5	19.5	391	23.2	-7.0	398	-	1	1

c = complementary tests.

* Two beams tested statically to failure in air with load increments of 21.0/16, 25.5/19.5 and 22.5/170, 25.5/21.5 KN respectively.

Table 5.3: Fatigue Test Programme; Stage II.

Environment	Loading regime	Applied load (KN)		Maximum intended stress (N/mm^2)		Stress range N/mm^2	No. of tests			
		Max	Min	Steel in Tension	Concrete in Compression		Test duration (months)			
							< 1	1	3	5
3.5% NaCl	Dynamic	18	3	276	13.7	230	1^c	1	$1 + 2^c$	1
		12	3	184	9.2	138	-	1	1	1
	Static	18		276	13.7	static	-	1	1	-
		12	0	184	9.2	static	-	-	1	-
	No-load	0	0	0	0	0	1	-	-	-
Water	Dynamic	21	3	322	16	276	-	0	1	-
		18	3	276	13.7	230	-	-	-	1
		12	3	184	9.2	138	-	-	-	1

c = complementary test.

Concrete mix design form

Stage	Item		Reference or calculation	Values
1	1.1	Characteristic strength	Specified	40 N/mm² at 28 days; Proportion defective 5 per cent
	1.2	Standard deviation	Fig 3	____ N/mm² or no data ____ N/mm²
	1.3	Margin	C1	(k = ____) ____ × ____ = 5 N/mm²
	1.4	Target mean strength	C2	40 + 5 = 45 N/mm²
	1.5	Cement type	Specified	OPC/~~SRPC/RHPC~~
	1.6	Aggregate type: coarse Aggregate type: fine		UNC UNC
	1.7	Free-water/cement ratio	Table 2, Fig 4	0.46 — Use the lower value
	1.8	*Maximum free-water/cement ratio*	*Specified*	0.45
2	2.1	Slump or V-B	Specified	Slump 50 mm or V-B ____ s
	2.2	Maximum aggregate size	Specified	20 mm
	2.3	Free-water content	Table 3	180 kg/m³
3	3.1	Cement content	C3	180 ÷ 0.45 = 400 kg/m³
	3.2	*Maximum cement content*	*Specified*	____ kg/m³
	3.3	*Minimum cement content*	*Specified*	____ kg/m³ — Use if greater than Item 3.1 and calculate Item 3.4
	3.4	Modified free-water/cement ratio		____
4	4.1	Relative density of aggregate (SSD)		2.6 known/assumed
	4.2	Concrete density	Fig 5	2375 kg/m³
	4.3	Total aggregate content	C4	2375 − 400 − 180 = 1795 kg/m³
5	5.1	Grading of fine aggregate	BS 882	Zone 2
	5.2	Proportion of fine aggregate	Fig 6	32 to 40, Say 35 per cent
	5.3	Fine aggregate content	C5	1795 × 0.35 = 628 kg/m³
	5.4	Coarse aggregate content	C5	1795 − 628 = 1167 kg/m³

Quantities	Cement (kg)	Water (kg or l)	Fine aggregate (kg)	Coarse aggregate (kg)	Σ
per m³ (to nearest 5 kg)	400	180	630	1165	= 2375
per trial mix of 80 ~~kg~~	14	6	21	39	= 80

Items in italics are optional limiting values that may be specified.

1 N/mm² = 1 MN/m² = 1 MPa.

OPC = ordinary Portland cement; SRPC = sulphate-resisting Portland cement; RHPC = rapid-hardening Portland cement.

Relative density = specific gravity.

SSD = based on a saturated surface-dry basis.

Table (5-4):Concrete mix design detail.

Table 5.5: Details of Concrete and Steel.

Concrete		Steel	
Characteristic Cube Strength at 28 days	40 N/mm^2	Tor bar 10 mm diameter	
E_c	34 KN/mm^2		
W/C	0.45	Characteristic Strength	460 N/mm^2
		Yield Stress	528 N/mm^2
Cement Type	O.P.C.	Yield Strain	0.002525
		Young's Modulus, E_s,	209 KN/mm^2
Aggregate	Irregular morainic gravel and sand	Chemical Analysis	
		Carbon	0.28%
Slump	50 mm	Phosphorus	0.017%
		Sulphur	0.035%

Table 5.6: Analysis of Major Components of Tap Water.

Water Constituent	Concentration in ppm
Chloride	6
Sodium	4
Sulphate	5
Magnesium	7
Calcium	4
Potassium	0.7
Silica	1
Aluminium	0.02
Nitrate	0.8
Fluoride	0.01
Iron	0.05
T.D.S.	50
pH	$\simeq$ 8
Conductivity	45 MEG SIEMENS/cm

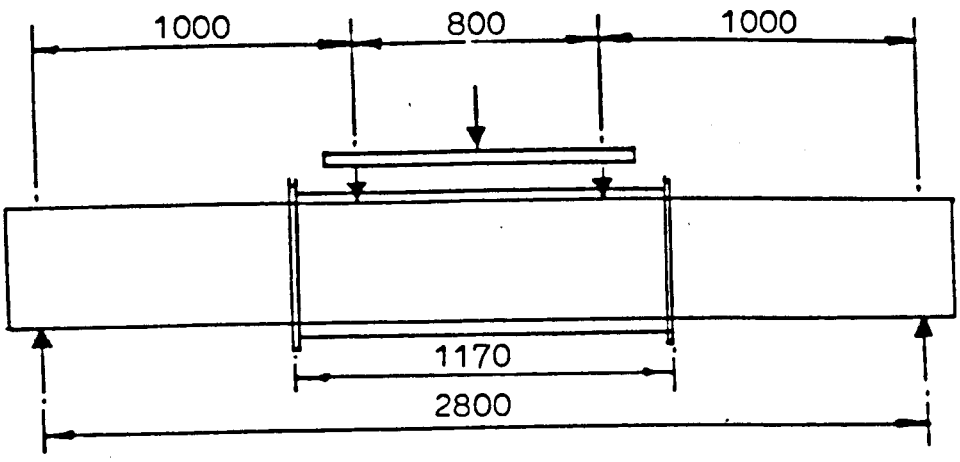

a) Uni-directional bending

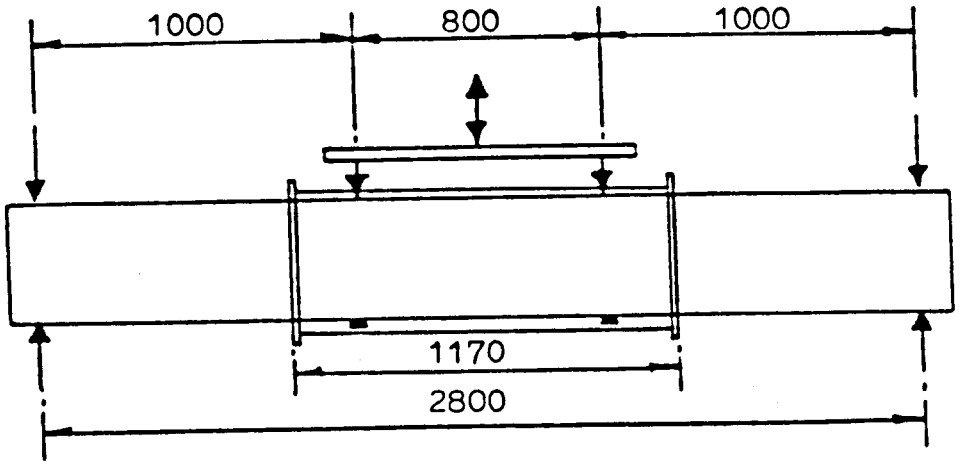

b) Reverse bending

Figure (5-1): Loading arrangement and water-jacket dimensions (mm).

1 PTFE
2 Stainless steel plate
3 Rubber plate
4 Glue

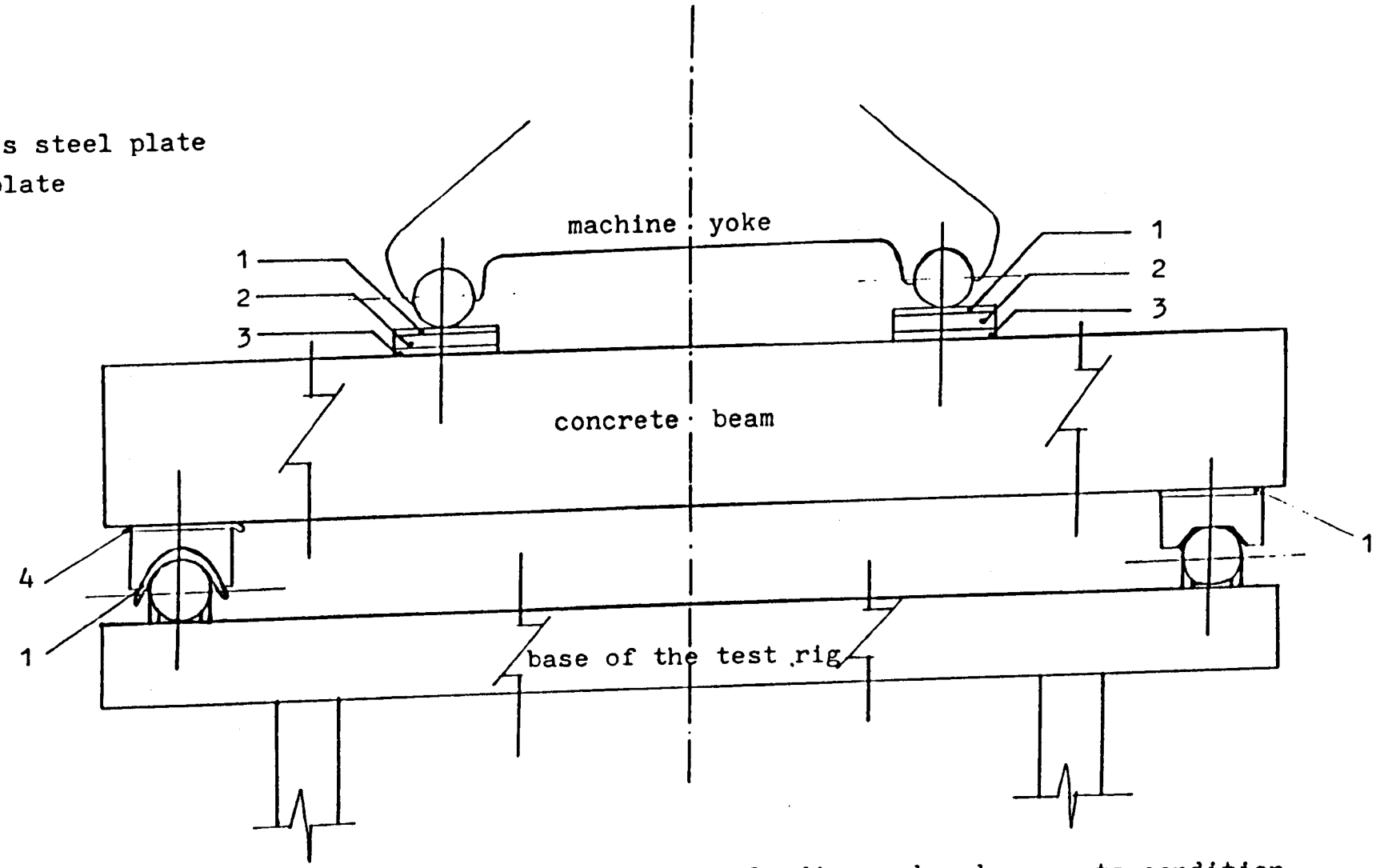

Figure (5-2): Uni-directional bending series;loading and end supports condition.

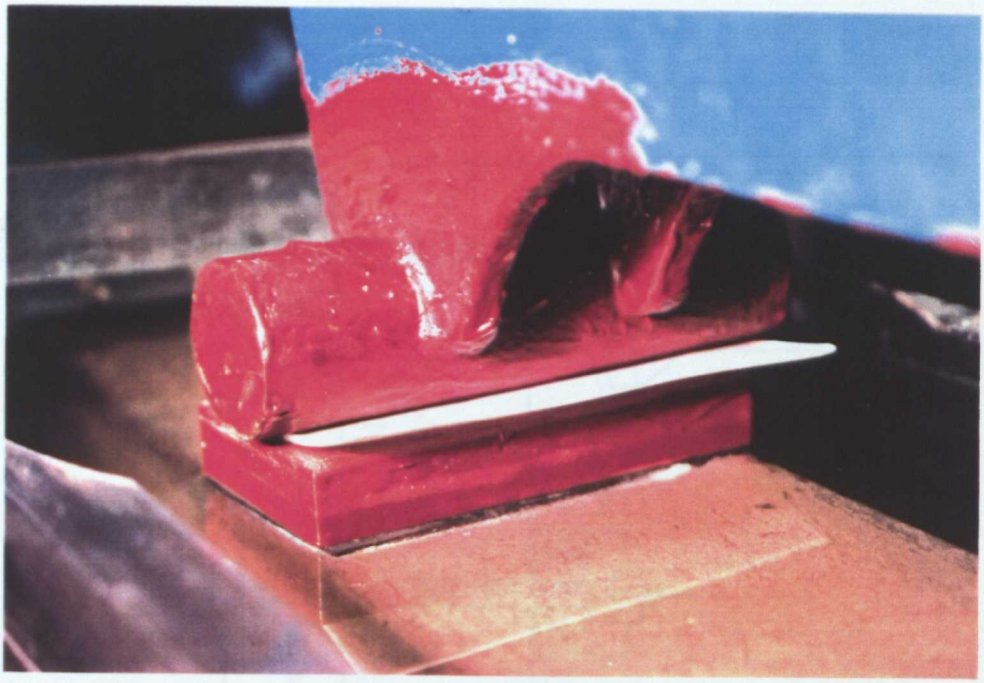

a) Uni-directional bending

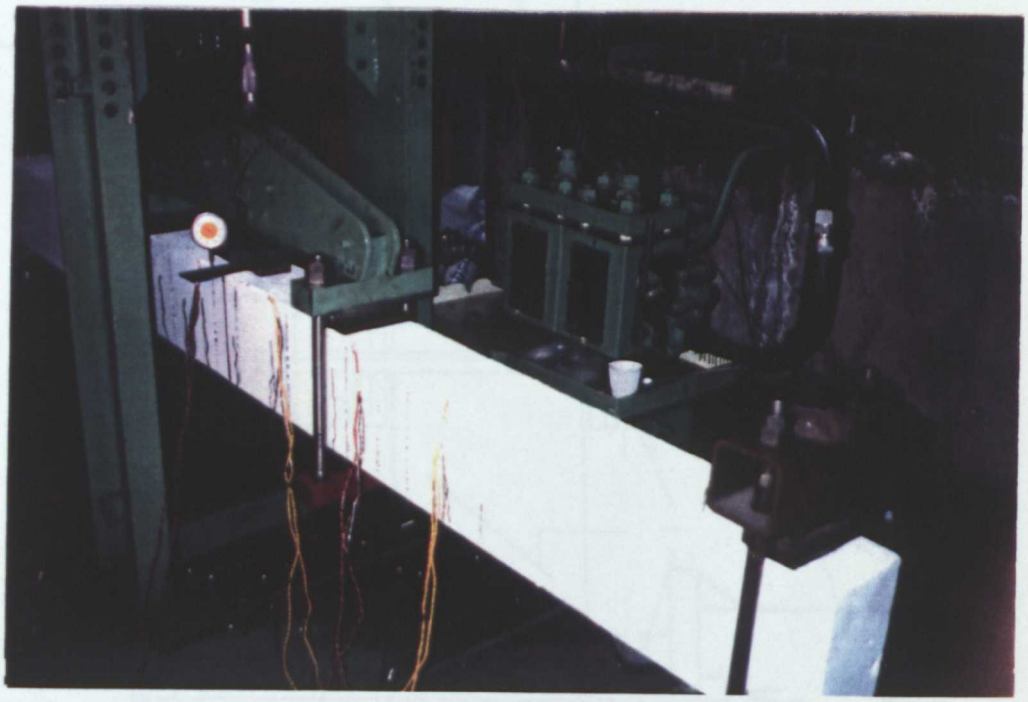

b) Reverse bending

Figure (5-3): Loading arrangement;points of load application.

1 Roller
2 Stainless steel plate
3 Rubber plate
4 V-shape groove
5 Glue
6 Base of test rig

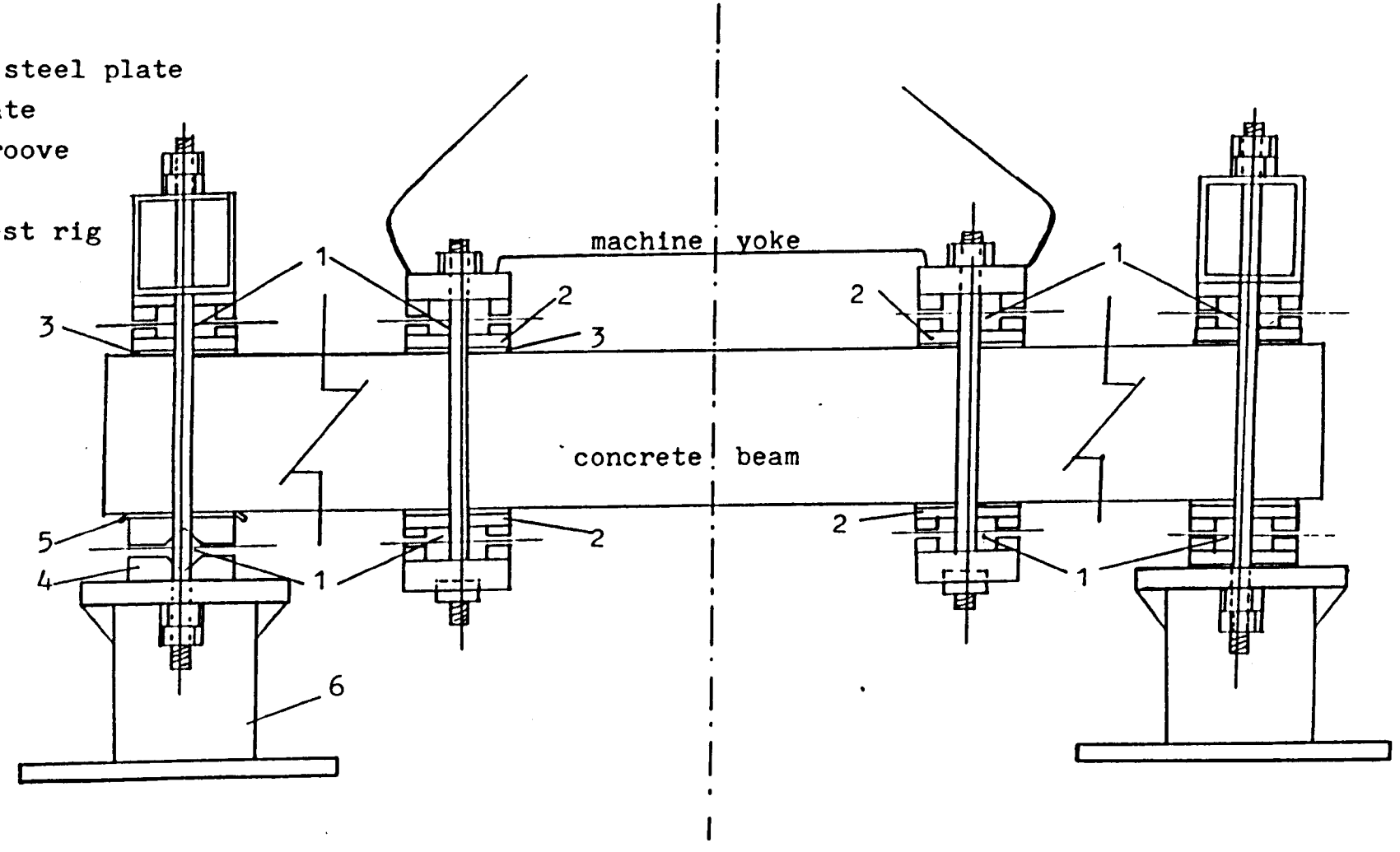

Figure (5-4): Reverse bending series;loading and end supports condition.

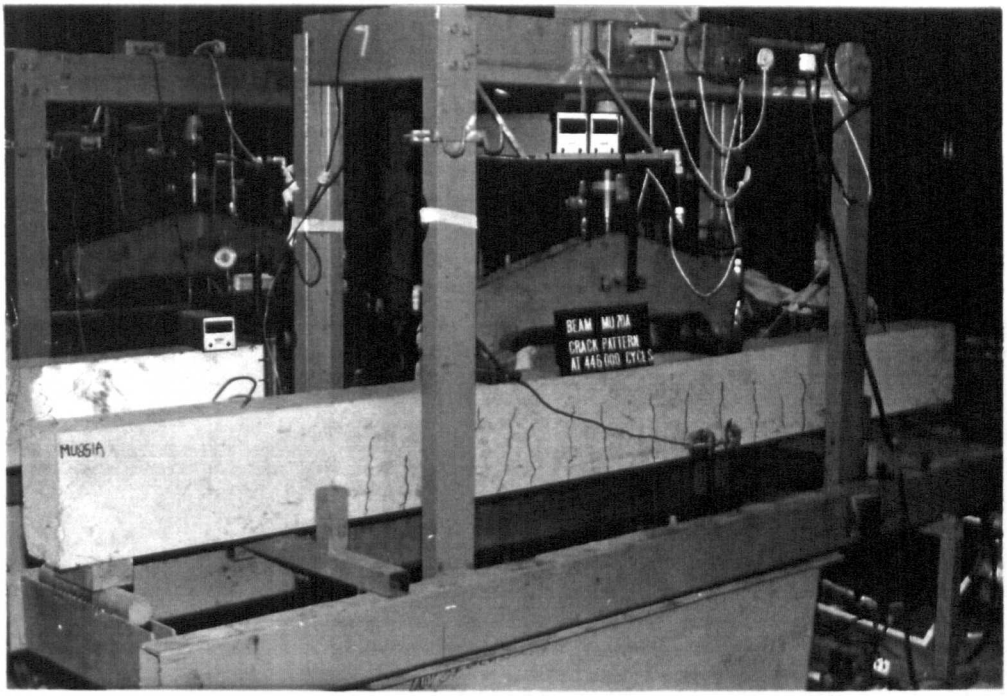

a) Uni-directional bending

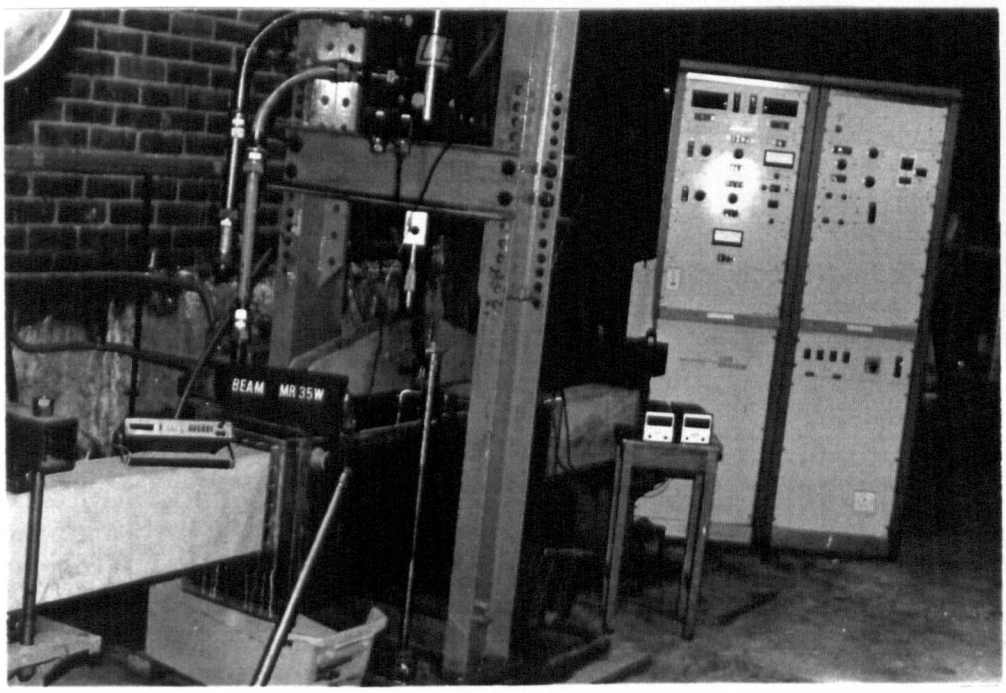

b) Reverse bending

Figure (5-5): Fatigue testing machines.

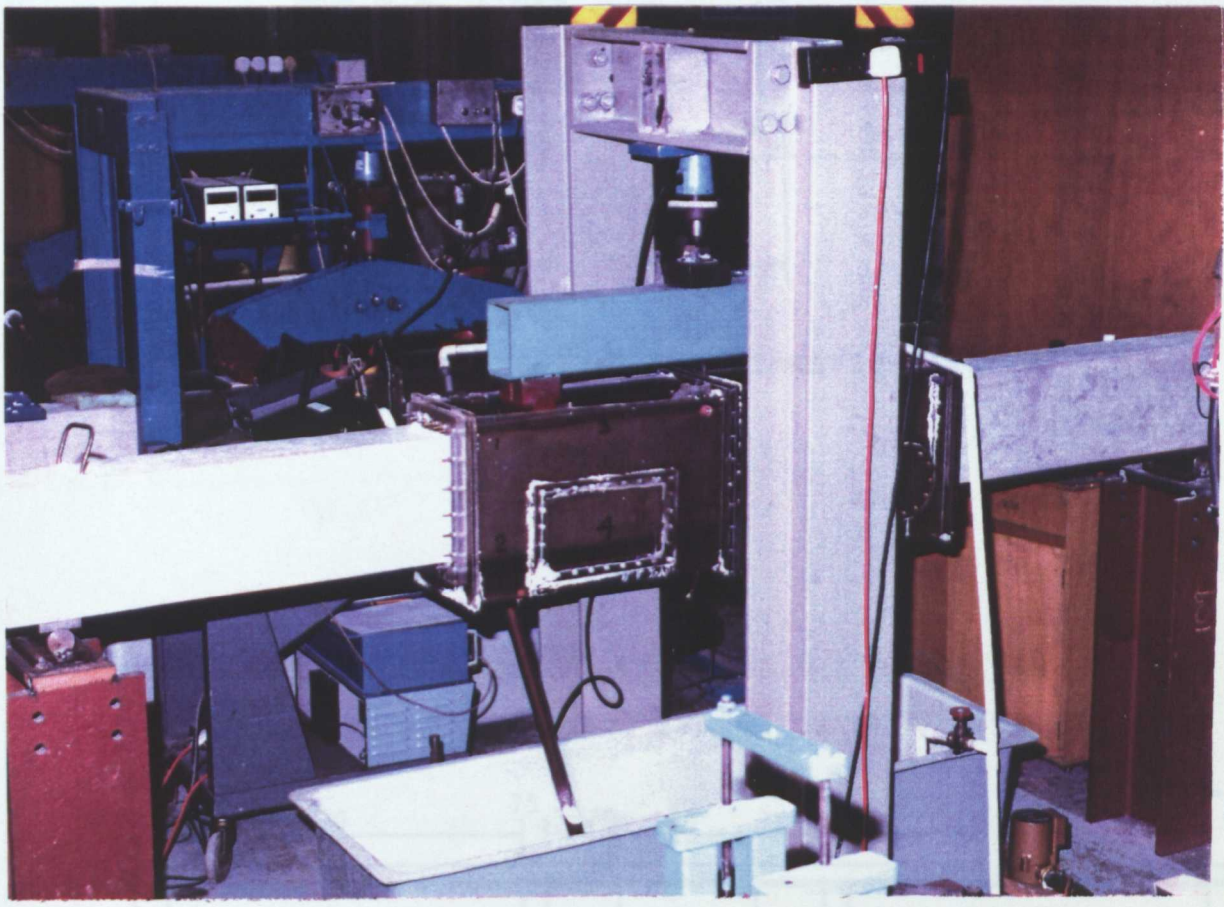

Figure (5-6): Static test set up.

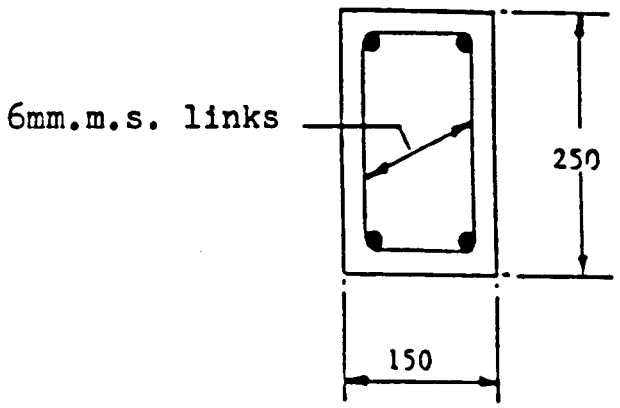

a) Test beam;cross-section (dimensions in mm)

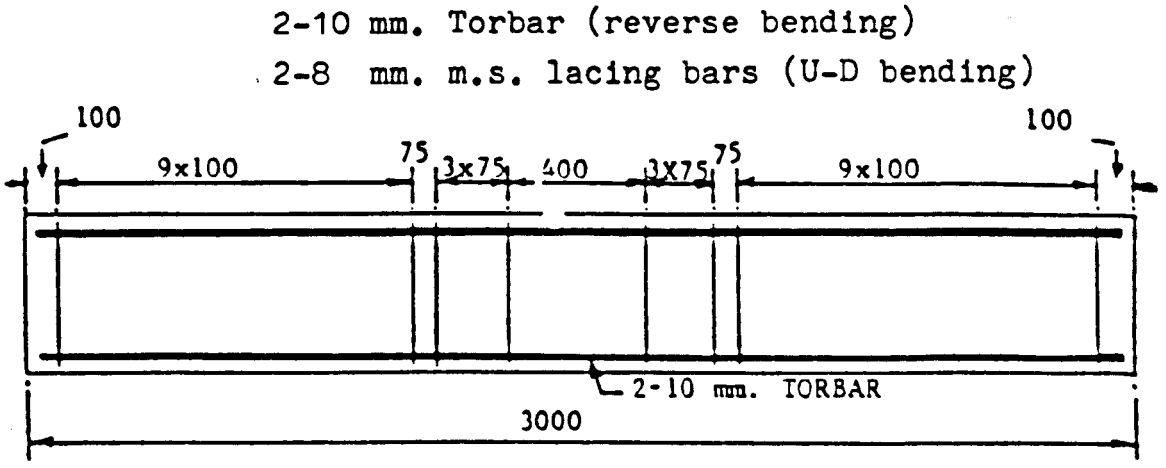

b) Test beam;reinforcement details (dimensions in mm)

Figure (5-7): Test beam;cross-section dimensions and reinforcement details.

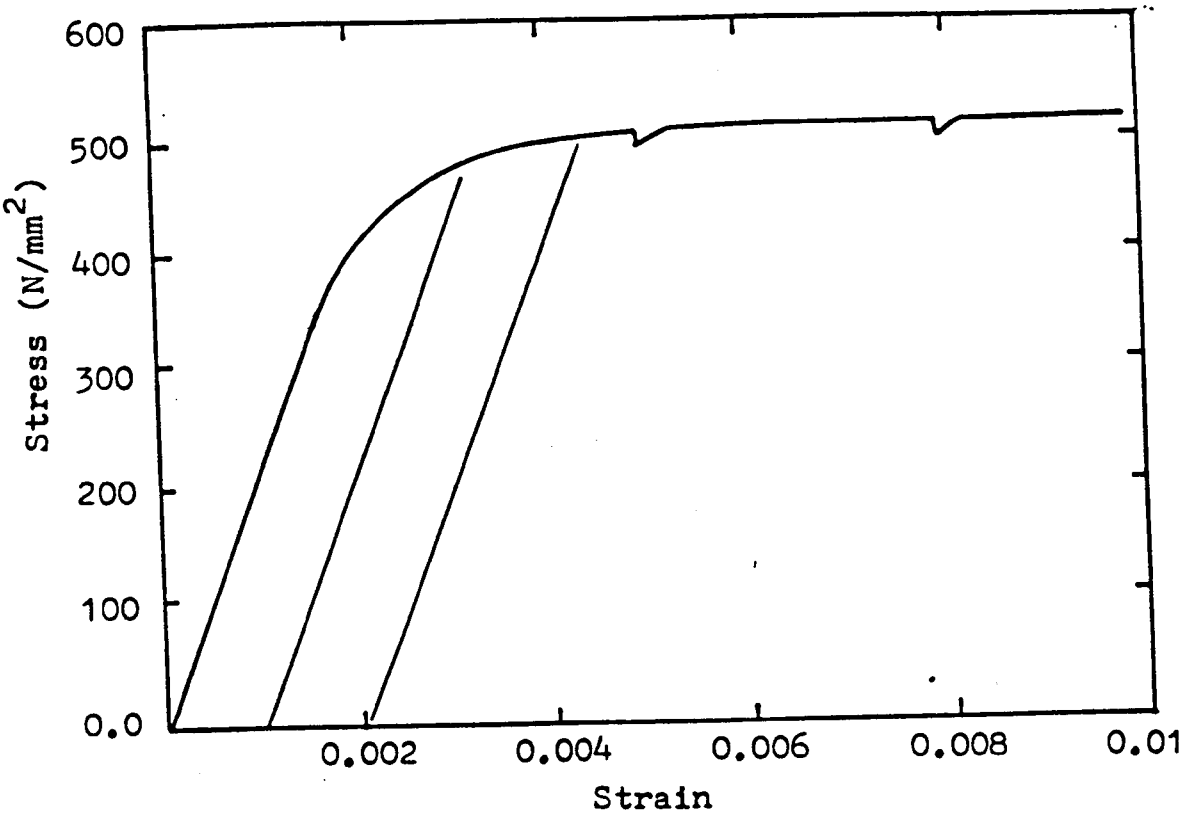

Figure (5-8): Typical stress-strain curve, main reinforcement (Torbar 10mm dia.).

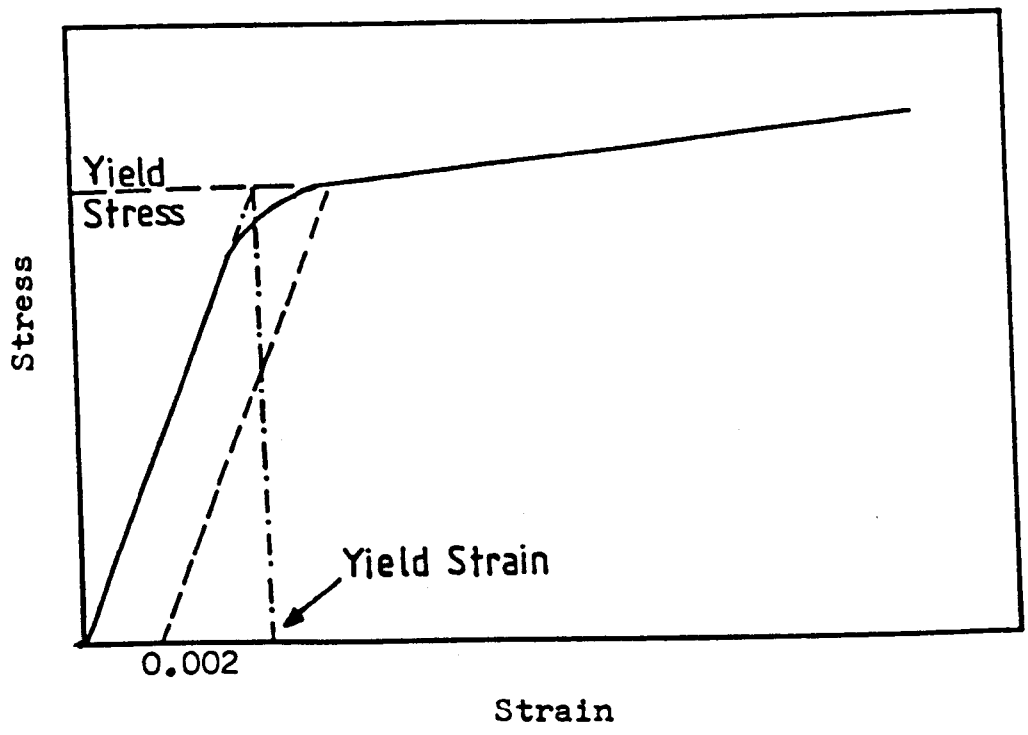

Figure (5-9): Definition of yield stress and strain of steel reinforcement.

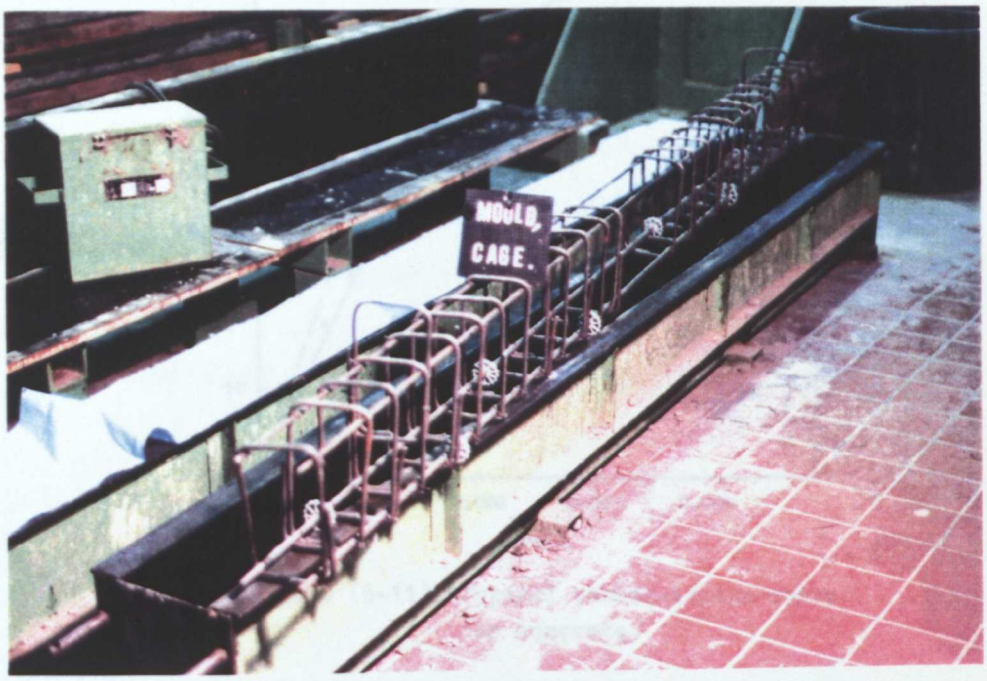

a) Reinforcement cage

b) Reinforcing cage inside the steel mould

Figure (5-10): Test beam;mould and cage .

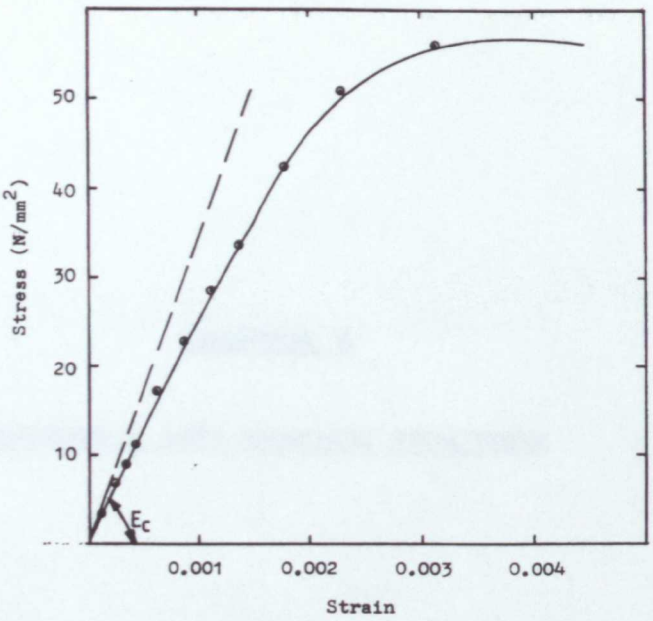

Figure (5-11): Typical stress-strain curve for concrete.

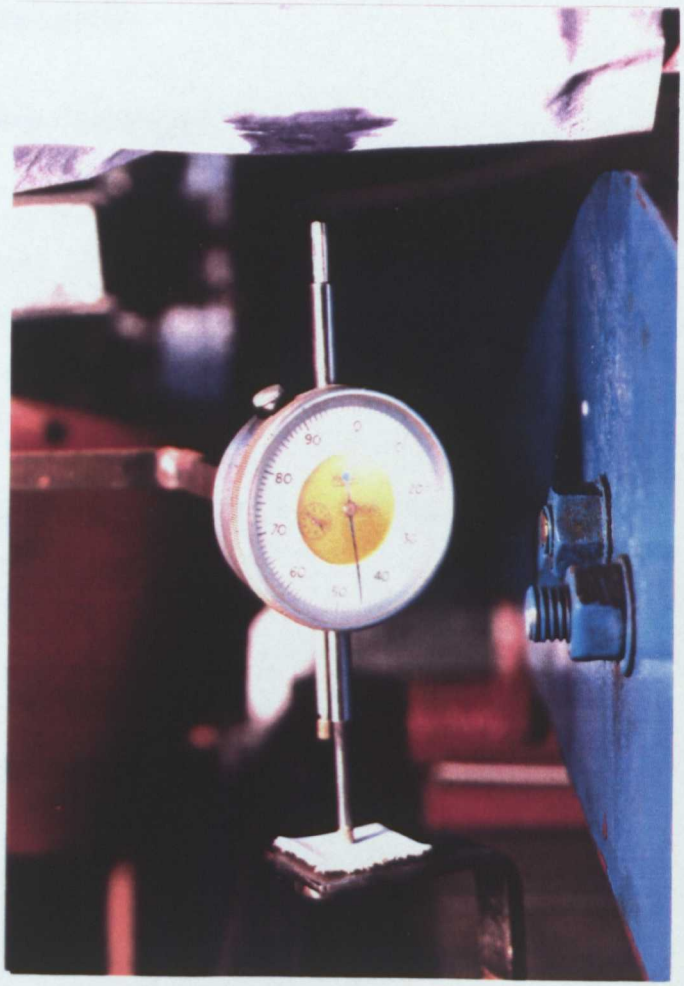

Figure (5-12): Separation of the deflection gauge from the electrolyte system.

CHAPTER 6

ENDURANCE AND SURFACE FRACTURE

CHAPTER 6

ENDURANCE AND SURFACE FRACTURE

6.1 Introduction.

This chapter presents, mainly, results obtained from Stage I of the programme. As described earlier in Chapter 5, tests in this stage were performed at high load amplitude so that early indications could be obtained and used in the more detailed investigation undertaken in Stage II of the programme. As a result of this policy ie. test at high load level, all the test beams have failed in fatigue after varying number of cycles. The only exception has been the single air test which was terminated without failure.

In the following, endurance results, fractographic observations of the reinforcing bars failure surfaces including, when possible, examinations using scanning electron microscope (SEM) and other relevant results will be presented and discussed.

6.2 Endurance.

The number of cycles to failure recorded in various fatigue experiments under uni-directional and reverse bending regimes are presented along with other related data in Tables 6.1 and 6.2.

These are also illustrated diagrammatically in Figure 6.1 in which the endurances are plotted against the max intended steel stress range in logarithmic fashion (note that the four run-outs on Figure 6.1 are results from the Stage II, lower-stress, tests). As described in Chapter

5, the uni-directional tests involved a load cycle set to cause intended stress on the lower rebars cycling from 0.1 f_y (46 N/mm^2) to the designated higher values. In the reverse bending tests, the applied loads were in the ratio 1:33 (down): 1 (up). Thus the maximum steel tensile stress and concrete compression stress were in the lower bars and upper concrete respectively. Recall also that the compression stress in the steel bars was very low (<8 N/mm^2). Table 6.1 indicates that, for uni-directional tests, the beam ages were within the age range that would be practical in real structures to withstand the design loads. On the other hand, most of the reverse bending beams (Table 6.2) were of age exceeding 4 years. The only two low-aged beams in this series were added later to the programme to investigate the age effects on the specimens response to the environment during dynamic loading as will be described in more details in Chapter 8. However, as Figure 6.1 shows, the fatigue lives of these two beams were in essentially the same scatter band as for older beams.

Figure 6.2 indicates that for the same maximum intended stress in the tension bars ie. for the same maximum applied load the tension-compression load application regime is more onerous than the tension-tension condition. Hence the endurances observed in reverse bending tests are lower than in uni-directional loading at the same maximum loading level. It should be pointed out, however, that endurances were not only a function of load in all cases, since for lower load levels, in particular, environmental effects start to play increasingly important role in this respect as will be shown later.

Uni-Directional Series.

In general, at higher load levels corresponding to upper steel stress of 0.75 and 0.85 f_y (stress range of 299 and 345 N/mm^2 respectively), the severity of the environment plays a relatively minor role, probably due to the short test duration which is in turn a consequence

of the more-damaging high load amplitude. Visual observations indicated that these tests exhibited, although to a limited extent, the phenomenon of blocking of the flexural cracks with white deposit during the tests similar to that observed in earlier work[19,79,150] in this department involving sea water.

These observations were later confirmed by other crack opening and deflection measurements. For this loading family, however, the fatigue loading appears so dominant as to restrict the beneficial effects of this phenomenon on endurance and also to eliminate the expected scatter in the number of cycles to failure (between 346,643 to 532,500 cycles) normally encountered in fatigue tests.

Tests at a lower upper stress level of 0.7 f_y (stress range = 276 N/mm^2) show appreciably greater endurances particularly for tests in tap water (1,807,200 cycles compared to 1,076,000 cycles for test in sodium chloride solution). Both tests showed early development of progressive crack blocking accompanied by parallel change in the structural behaviour as indicated by crack opening and deflection measurements.

The air test was terminated after 2,216,700 cycles without failure and was then loaded statically to failure to determine the effects of fatigue loading on the subsequent static characteristics of the beam.

As Table 6.1 reveals, all the unidirectional fatigue failures occurred within the central (water-immersed) constant bending moment part of the beam.

Reverse Bending Series.

Under this loading regime, chloride tests have consistently exhibited lower endurances than tests in tap water. Tests at lower levels corresponding to upper stresses in the tension bars of 0.35 and 0.46 f_y (stress range of 164 and 216 N/mm^2 respectively) have shown considerably higher endurances than for tests at higher load levels. Although the beam ages at the time of test varied over a very wide range (34 to 1846 days), the

results suggest that the beams age has no tangible effect so far as endurance is concerned. No visual sign of the occurrence of crack blocking were observed but test at 0.35 f_y showed structural changes indicative of the initiation of blocking at later stages of test.

6.3 Nature of Failure.

Failure of the beams was always inside the transparent water jacket and in the central constant bending moment zone. Failure occurred either by:

a. Fatigue failure of one bar or,
b. Simultaneous fatigue failure of both bars or,
c. Fatigue failure of one bar followed by ductile fracture of the remaining bar.

Details of failure are given in Table 6.1 and 6.2 and examples of failure in the main bars are shown in Figure 6.3. As indicated in Figure 6.4, usually there were about 8 to 10 flexural cracks in the maximum bending moment zone and 2 to 3 in each shear span. Failure always occurred at one of the major cracks in the maximum bending moment zone.

Premature failure in the shear span, where the stress range is less than the intended stress range, occurred in one beam namely beam MR85N (Figure 8.1) which failed after 6300 cycles. Spalling of concrete was observed at the top of some of the reverse bending beams just prior to failure indicative of high compressive stresses on concrete surface condition probably due to excessive amount of elongation in the tension bars. In both loading regimes no special relationship was observed between the position of failure and the loading level or the number of cycles to failure. Figures 6.4 and 6.5 show the similarity of crack pattern and mode of failure of the static and fatigue specimens for both kind of loading regimes.

6.4 Fractographic Examination.

The examination of failure surfaces is an important approach for describing and understanding various mechanisms and causes of failure. The examinations may, more extensively, be conducted on both macroscopic and microscopic scale since[44] while the tensile strength of reinforcing bar is determined primarily by the macrostructure of the whole section, fatigue strength is particularly affected by the microstructure of the bar surface.

In this study, after each fatigue test, the reinforcement cage from the submerged zone was retrieved the cage then inspected for the existence of cracks other than the fracture cracks and photographed. The fracture surfaces were treated with an inhibited acid solution "clark's solution" to remove the corrosion products and reveal the underlying fractographic features for scanning electron microscopy. This procedure, however, was not always successful as will be shown later.

6.4.1 General Visual Inspection.

Visual inspection revealed that only few cracks existed at sites on the reinforcing bars other than the fracture surface. These visible cracks were observed on certain specimens (beams MU85N, MU85W, MU75W) of Stage I and were completely absent in stage II of the programme.

A crack on an unfailed bar recovered from beam MU85N is shown in Figure 6.6. This crack was situated at the position of the main crack in the concrete opposite to the fracture site of the failed bar. It can be noted that the crack was initiated at the small gap between the longitudinal rib and the transverse rib. The area of initiation clearly suffered a metal loss due to corrosion attack despite the relatively short test duration ($\sim$ 28 days).

Instances of cracking remote from the fracture surface are shown in Figures 6.7a and 6.7b for Torbars retrieved from beams MU75W and MU85W respectively. In both

cases, the cracks were severe and cover almost half the bar perimeter. Unlike the first example, Figure 6.6, these cracks did not initiate at the area between the longitudinal and transverse ribs. Further more it can be noted that, for beam MU75W at least the cracks were initiated at areas of corrosion attack.

6.4.2 Macrofractographic Observations.

No preferential orientation of ribs could be given to the cold-worked torbars encased in concrete. Therefore the characteristics of the bar section cannot be used to indicate the bar orientation with respect to the applied load. For bars under tension, it is assumed that crack initiation takes place at the lower half of the bar perimeter. However, unless identified by S.E.M., the exact position of the initiation zone can not be located in the cases of complete severance of bars. For partially severed bars, the initiation zone may more accurately be estimated. General features of the fracture surfaces have been:

1. Crack initiation had no preferential location with respect to bar ribs.

2. Fracture surfaces exhibited different patterns. Plain-fronted, slant-fronted and irregular surface-fronted fracture surfaces have been observed. In all cases, the fracture process was identified as having three different stage.

   a. The initiation stage: A good example of this stage is shown in Figures 6.6 and 6.7. The crack initiation was observed in some areas of localised corrosion which suggests that the corrosion action is likely to promote initiation process at the attacked area.

   b. The initiation zone propagates into a crack growth zone. This zone normally suffered variable degree

of corrosion, depending on the type of the surrounding solution, most probably due to the coincidence of these surfaces with cracks in the concrete.

c. Immediate ductile fracture occurred when the remaining un-cracked cross section area could not support the applied load. This area is exposed to the surrounding solution for very short period, thus suffered less severe corrosion attack (see Figure 6.3b).

Beam MU75W.

Figure 6.8 shows two patterns of failure which occurred in the main bars of this beam. The top photograph shows the fatigue failure of one of the tension bars in which distinct zones of propagation and rupture can be identified. These are annotated with A and B respectively in Figure 6.8a. In accordance with other observations,[44,202] the shape of the boundary between the two zones indicates that the cracks preferred to propagate across the bar in faster rate in proximity to the surface than towards the centroid. The bar failure occurred at the main concrete crack and was followed by an immediate ductile fracture of the remaining bar at the same concrete crack. The latter fracture exhibited notably small initiation zone as shown in Figure 6.8b.

Beam MU85W.

Failure occurred in one bar only after 346,643 cycles. The failure surface indicates probable multiple initiation mechanism which contributed to the irregularity of the growth zone (Figure 6.9a).

Beam MU85N.

Failure of this beam also occurred due to fatigue failure of one of the tension bars after 397.246 cycles.

Unlike beam MU85W, the crack seems to have initiated on one site of the section and propagated through a smooth growth zone up to the critical stage when eventual failure occurred, Figure 6.9b.

Beam MR70W.

Fatigue failure occurred in one bar after 172,500 cycles of reverse bending. The fracture surface features characteristics similar to those observed in the preceding beam in that the surface exhibited a smooth growth zone followed by ductile failure of the remaining un-cracked section.

6.4.3 Scanning Electron Microscope (S.E.M.)

Attempts were made to examine the fracture surfaces of the reinforcing bars using scanning electron microscope. It was found, however, that most of these surfaces have sustained variable degrees of corrosion attack. Although the corrosion products were removed chemically after the test, in many cases particularly in reverse bending tests and tests in sodium chloride solution it was still difficult to detect any clear structural details on the fracture surface useful for the identification of the fracture mechanism. It was, therefore, only possible to obtain S.E.M. fractographs for limited number of samples. In order to facilitate the description of S.E.M. fractographs of the bars failed in fatigue, additional fracture surfaces from what would be regarded as representative of different failure mechanisms were also examined under S.E.M. These are:

1. Bare Torbar failed in pure-axial tension in air.
2. Torbar from concrete beam failed after static loading in bending in air.

Bare Bar in Pure Tension.

The S.E.M. fractograph shown in Figure 6.11 reveals,

as would be expected, a honey-comb structure characteristics of monotonic ductile failure in carbon steels. The higher magnification of Figure 6.11b shows holes of variable sizes ranging between 1 - 20 μm, these being assumed to have initiated during rising load application at sites of non-metallic inclusion.

Torbar From Beam Subjected to Single Bend Test In Air.

The fracture surface was dominated by a distorted honey-comb structure caused probably by a shear deformation at the time of ductile fracture. Figure 6.12 shows typical structure at the centre of the specimen.

Beam MU75W.

Figures 6.13 and 6 .14 show the S.E.M. fractographs of the fracture surfaces of the two bars (1 and 2) failed in this fatigue test. The corresponding macrographs are presented earlier in Figures 6.8a and 6.8b respectively.

Considering bar 1, most of the fracture surface showed evidence of ductile tearing in a form of honeycomb structure. Typical of such area is shown in Figure 6.13a which also suggests a degree of perhaps uniform corrosion attack occurring on the surface after beam failure but before removal of the bar. Figure 6.13b, which is a magnified view of the central region of Figure 6.13a, shows a rod-like non-metallic inclusion in the largest hole in the centre of the figure.

S.E.M. examination on bar 2 revealed mechanism of failure not found on the surface of the above described bar. A limited featureless region, Figure 6.14a, was observed on the fracture surface of the bar. This area was probably damaged by the ingress of water during crack growth. In another small region near the bar outer surface, an interesting flaky structure was evident as shown in Figure 6.14b. Most of the remaining surface area exhibited the familiar honey-comb structure as shown in Figure 6.14c.

Beam MU85W.

Figure 6.15a is a S.E.M. fractograph of a likely crack initiation site emanating from a rib with a steep cliff down to a flatter region. Figure 6.15b examined the top plateau on the RHS of the above fractograph, virtually on the rib, which reveals featureless structure with globular corrosion product. The flatter region down the cliff (LHS of Figure 6.15a) seems to exhibit honey-comb structure as suggested by Figure 6.16.

Beam MR70W.

Figure 6.17 shows S.E.M. fractograph of typical structure on the fracture surface of a bar from this beam. The structural details are obviously obscured by corrosion product.

6.5 Discussion.

The major problem encountered in the compilation of new data within the framework of the existing information is the fact that any individual research on fatigue of reinforced concrete, for obvious practical difficulties is bound to cover limited variables which are known, or expected to have a profound influence on the fatigue performance of reinforced concrete and its fatigue life in particular. Accordingly comparison of the results of different research programmes is restricted by the fact that the experimental details, specimen geometry and loading regime were designed according to the required information and the available machinery giving rise to different combinations of parameter for different research programmes. Despite these differences, comparison studies are useful in assessing the general trends in fatigue characteristics. A detailed account on the available information on the factors controlling the fatigue performance of reinforced concrete in corrosive media is given in Chapter 4. The following discussion, however, considers the influence of stress range, environment and

loading regime on the fatigue lives of the test specimens and explore the possible link between the present results and other relevant fatigue data.

6.5.1 Mode Of Failure And Fracture Surface.

The test specimens static load carrying capacity is dominated by the steel area as described in Chapter 5. It was expected, therefore, that there is little chance of fatigue failure of concrete before the steel failure. This was confirmed later by the mode of failure observed in all of the test specimens. The fatigue failure, thus, occurred due to failure in the tension bars in side the max bending moment zone. The only exception was that of beam MR85N in which failure occurred in the shear span. It should be pointed out that this particular test was carried out in reverse bending at the highest load level and that the failure occurred at notably early stage of cycling. The relatively premature failure in shear span has also been reported earlier by Hodgkiess et al[206] in fatigue test in sea water under exactly the same experimental details but lower stress range (equivalent to 0.4 f_y). They observed that the failure coincided with the location of a plastic bar spacer, subsequent static test, however, indicated no apparent connection between the position of the spacers and the location of cracks. In any event, beams with adequate static shear capacity are reported[31,74,75,86] to have failed under repeated loading in shear at as little as 30% of their static shear strength.

It seems likely that the unexpected fatigue failure in shear is a consequence of the complex mechanism of accelerated damage in the area of shear crack, triggered probably by the existence of a defect or defects in the concrete tension zone less sensitive to static type of loading.

Fracture Mechanism.

Initiation Stage.

Visual inspections of the reinforcing bars suggested that corrosion attack seems to be an important factor in the crack initiation mechanism. In accord with other reported observations, this factor appears to supersede the mechanical factors[59] (surface geometry) or to reduce the dependency of crack initiation on the pre-existing stress concentration.[44,202]

The corrosion influence on this process is, conceivably, increased as both the exposure time and the severity of the solution increased. The process is also dependent on the loading condition.

Dynamic loading may enhance the effectiveness of this factor as it permits relatively early and easy ingress of the aggressive species to the steel surface. But, on the other hand, the effect of corrosion is greatly diminished in tests at high load level as the latter becomes a predominant factor in initiating fatigue cracks. Corrosion attack, however, is still occurring on these areas, as clearly shown in Figure 6.6 (test at high load level of 0.85 f_y), giving rise to a possible acceleration effect. Another important feature of the initiation mechanism is that cracks can be initiated in other areas than the area of the main crack in the concrete where final fracture occurred as shown in Figure 6.7.

The dominating effect of either of the two factors (corrosion or stress) in the crack initiation process precluded the effectiveness of other factors such as the existence of non-metallic inclusions, Figure 6.13b, as a potential crack initiation sites although their existence in the already initiated cracks may promote speedy crack propagation.

Crack Propagation Stage.

Although the majority of test specimens were not examined under S.E.M. due to extensive corrosion attack on

the fracture surface, those specimens which were examined revealed essentially similar fracture features. These include 1) the dominance of non-corroded honey-comb structure indicative of ductile fracture and 2) the absence of stable crack growth zone which is normally characterized by ductile fatigue striations.

The fact that some of the examined area showed corrosion damage, Figures 6.14a, 6.15b and 6.17, which obscured the underlying fracture surface, produced a degree of uncertaintly as to the actual mechanism of crack propagation. However, the above two features suggests either, case 1: the propagation stage may have covered only limited proportion of the bar cross section area which, together with the initiation site, suffered sufficient corrosion attack so that propagation by striation mechanism could not be observed, this case is presented schematically in Figure 6.18a, or alternatively case 2: propagation stage may have partly been proceeded by ' ductile tearing mechanism through Stage II of propagation and, therefore, could not be distinguished from the final fracture surface due to similarities in surface features as illustrated in Figure 6.18b.

Since in both cases ductile failure is dominant, both cases imply extremely high propagation rate (ie. high ΔK) and consequently, this stage occupied an extremely short period of the fatigue life.

Nevertheless the macrofractographic observations as shown in Figures 6.8 and 6.9 indicated a shape of cross section which is more related to case 2 than case 1, it is interesting to note that bars which had failed in fatigue exhibited approximately equal propagation zone equivalent to $\sim$ 50 to 65% of the cross sectional area. The reduction in area would produce a parallel proportional increase in the stresses of the unsevered area which put the working stresses at or beyond the characteristic yield strength of the reinforcing steel. A simple calculation assuming even distribution of stresses on the remaining steel area including the whole area of the uncracked second bar show the following stresses near failure.

f_y N/mm^2	Original Working Stresses		Approx. Stress on Sound Part of: N/mm^2	
	% f_y	N/mm^2	Total Area	Affected Bar Only
460	0.7 f_y	322	452	757
	0.75 f_y	345	483	811
	0.85 f_y	391	548	919

It should be appreciated, however, that the above table is only a rough indirect estimation of the likely trend of stresses near failure, nevertheless, the table does suggest that fracture of the second bar is not necessary for failure to occur although it may sustain less developed or embryo cracks as is the case, for instance, in beam MU75W (Figure 6.8b). The fact that these second bars often, if failed of course, exhibited a slant fracture typical of tensile failure in static bending of concrete-encased bars and similar to that obtained from static test (compare Figure 6.8b with Figure 6.10b) indicates that failure may have occurred immediately after, rather than simultaneously with, the failure of the remaining steel area to support the beam's dead weight.

Unlike the initiation process, the already high rate of crack growth is less sensitive to the effect of the environment particularly under higher loading conditions. It seems realistic that these observations can be explained in terms of the dominant effects of seemingly sufficiently high fatigue loading employed in this series accompanied by the total dependence of the specimens structural characteristics on the steel area. Under this condition, the high stress range in the reinforcing bars produced confidently safe maximum stress range in the

extreme fibre of concrete from the stand point of fatigue as described earlier in Chapter 5. Thus a relatively small reduction in bar diameter due to a fatigue crack at its early propagation stage would lead to considerable increase in the bar tensile stresses and rapid deterioration in the section load carrying capacity, further propagation and eventual failure. This is illustrated diagrammatically in Figure 6.19 which relates the increase in the stresses of the remaining total unsevered steel area with the percentage reduction in cross section area of one bar, it can be seen that the stresses of test groups of 0.7 f_y, 0.75 f_y and 0.85 f_y attain the characteristic yield strength of 460 N/mm^2 after a reduction in the cross section area of one bar of 60%, 50% and 30% respectively, (which is equivalent to 30%, 25% and 15% of the total steel area). These calculations, however, underestimate the beneficial effect of crack blocking in reducing the stress range which may account for the high actual reduction in cross section area observed particularly at lower load level.

Supportive evidences to the aforementioned observations with regard to the profound effect of the magnitude of the applied fatigue loading on the mechanism of crack propagation were reported by several authors. Using identical experimental details to those used in this study, Hodgkiess et al[150] observed striated regions on the fracture surface of a reinforcing 10 mm Torbars from tests in air at the high upper stress level of 0.85 f_y with endurances comparable to those examined in this study (average of 583 x 10^3 cycles), the fact that the fatigue failure mode of the reinforcing bar exhibited a slant fracture suggests that striated regions were indeed limited to small proportion of the cross sectional area and hence in agreement with the present observations.

On the other hand, Roper et al[202] and Paterson et al [59] observed fatigue crack propagation by ductile striation mechanism in tests at load levels corresponding to 0.52 f_y and 0.42 f_y respectively with endurances of 7.46 x 10^6 and 2.6 x 10^6 which are considerably higher than those of the specimens examined under SEM in this study.

More over there is some indication suggesting the partial dependence of fracture mechanism and propagation stage in particular on reinforcement details as the latter reported results were obtained from fatigue tests on concrete beams reinforced with one bar of a diameter of 24 mm and 32 mm respectively as compared 2-10 mm diameter in the present study. This is so because it was observed, as mentioned earlier, that it is unlikely that both bars undergo the same degree of fatigue cracking thus giving rise to progressive increase in stress in the firstly cracked bar not being proportioned to what would be expected if the beam is reinforced with one bar of area which is equivalent to the area of two 10 mm bars. This aspect is obviously significant from the practical point of view and therefore requires more experimental verifications.

In conclusion, the above discussion suggests that fracture mechanism is dependent on the magnitude of the applied load. For the high stress condition investigated in this part of the study, the propagation stage appears to have proceeded by two different mechanism which are striation and ductile tearing, the latter being unseperable from the final fracture surface. The propagation stage as a whole occupied extremely short period of the fatigue life. Accordingly the fatigue process for high stress conditions regardless of the test environment can be illustrated schematically as shown in Figure 6.20.

Another important aspect is that reinforcement details seem to effect the fatigue performance of reinforced concrete, the initial indications favour the use of smaller number of bars with adequate cross section area. This observation requires more experimental research.

6.5.2 Endurance.

It should be appreciated that this discussion is based, in most of the cases, on endurance results of one beam in each combination of stress range, loading regime

and environment. Also insufficient tests have been carried out to permit an accurate S-N curve to be established particularly with relation to lower load level and tests in air. Due to the long time scales involved, the tests did not, in fact, tend to define the fatigue limit or the long-life region of any of the environmental and loading conditions investigated in this study. Hence the tests were ended either due to fatigue failure or terminated with out failure after approximately 2.3×10^6 cycles. This is also true in Stage II of the programme from which representative results are shown in Figure 6.1.

Crack Blocking.

The build up of white deposits in the concrete flexural cracks was observed in certain loading conditions but not in all. This phenomenon was previously termed "crack blocking". Tests under comparable conditions performed by Arthur et al[19,79] and Paterson et al[59,203] have shown the profound effect of crack blocking on the endurance results in seawater environment. The mechanism of this effect hinges on the fact that the stress range is a controlling factor in fatigue endurance. Blocking of concrete cracks was found to increase the flexural stiffness of the beam and prevent the reinforcement from recovering the intended minimum stress upon removal of maximum load each load cycle, thus producing a reduction in the stress ranges and an increase in the mean stress. The occurrence and degree of influence of crack blocking are dependent in a complex manner on steel stress, environment and test duration. Due to the significant effects of this phenomenon on the overall fatigue behaviour of reinforced concrete, these factors together with other observations made in Stage II of the programme, will be presented and discussed in detail in another chapters (Chapters 7 and 8).

Uni-directional Bending Series.

For the stress ranges investigated in this series

(0.70 to 0.85 f_y), as suggested by fractographic examination, the environmental factors are more effective in the crack initiation process than in the propagation stage. In the high stress range, the stress influence is so dominant that fatigue failure occurs relatively rapidly and therefore the corrosion fatigue endurance in this case is expected to become close to fatigue endurance in air. A comparison with air tests performed earlier by Arthur et al[19,79] under identical test conditions confirmed this conclusion as will be shown in Section 6.5.4.

This situation is evident in tests at load level corresponding to 0.75 and 0.85 f_y where insufficient time elapses for corrosion to become effective as a crack initiation mechanism.

At lower stress range (0.7 f_y), the initially set stress ranges are further reduced due to the intervention of concrete crack blocking. While this tends to prolong the fatigue life, it also permits sufficient time for corrosion attack to become effective thus supersedes the stress as a primarily cause for the initiation of cracks. At this stage the endurance is totally dependent on the fine balance between increasingly alleviated situation in terms of stresses due to crack blocking and the otherwise escalated detrimental effect of the corrosive media allowed for by longer exposure time. The interesting competition between the two factors is demonstrated clearly in tests at 0.7 f_y (stress range of 267 N/mm^2) in air, water and sodium chloride solution (see Figure 6.1). With the exception of the air test, the remaining two tests exhibited comparable reduction in steel stress range, as will be shown in the following chapter, during the test duration particularly during the first 500,000 cycles. However, the aggressive sodium chloride solution seems to cause earlier crack initiation, (it is also probable that this solution increases the rate of crack growth) and consequently earlier failure in fatigue. On the other hand, the mechanism of crack initiation, in the air test is clearly stress dependent. It was observed, however, that, at the time the test was terminated without failure, there was no signs of crack initiation on the

tension bars. This example may further illustrate the role of corrosion attack on the crack initiation process and earlier fatigue failure as tests at, initially at least, the same load level exhibited earlier failure when performed in corrosion-conductive environment.

It should be pointed out, that however clear this trend may have been, statistically reliable conclusions require replicate tests as fatigue properties are inherently vulnerable to scatter.

More definite conclusions may be reached from the tests at the lower levels of Stage II of the programme. Thus, after a maximum of approximately 2.3×10^6 cycles, none of the tests failed in fatigue (stress level of 0.4 and 0.6 f_y in both tapwater and sodium chloride solution), nor did any of them exhibit fatigue cracks upon the termination of the tests, despite of clear signs of early corrosion attack at locations of cracks in the concrete. These observations suggest:

1. The stresses are too low to initiate cracks during the period of the test.
2. The bar section did not suffer, for a maximum test duration of 5 months, sufficient metal loss due to corrosion to raise the local stresses to the critical level for crack initiation.

Accordingly, under such low loading conditions, accompanied by a further decrease in stress range due to blocking, it is possible to speculate that when sufficient time is permitted appreciable corrosion attack would be developed and thus it is likely to be the primary cause of crack initiation and eventual failure.

The practical implications of this conclusion are extremely important and will be discussed later in this thesis after the presentation of other pertinent results.

Reverse-Bending Series.

It is observed from the results that for tests at high upper stress levels corresponding to 0.7 to 0.85 f_y,

fatigue endurances are consistently lower in sodium chloride tests than in tap water (Figure 6.1). This observation appears to conflict with earlier conclusions draw from uni-directional series and raise a question of what effects the environmental severity, in terms of corrosion aggressiveness would have on the fatigue endurance in view of the relatively short period of exposure for appreciable corrosion to take place. The fact that a test in sodium chloride at maximum upper stress level of 0.85 f_y exhibited shear failure may account for the premature failure in this test not observed in the corresponding tap water. For the remaining two stress levels, i.e. tests at 0.7 and 0.75 f_y it would appear that fatigue crack initiation requires less mechanical energy to form in the more aggressive sodium chloride solution than in tapwater and for the same stress level, this implies earlier crack initiation. This effect may be attributed to hydrogen embrittlement or to a mechanism of solution ingress into the concrete cracks. The latter involves an almost immediate attack and easy ingress of the solution to the steel surface through appreciably wide concrete cracks and the subsequent exit under pressure upon load reversal each load cycle with the total absence of crack blocking.

It can be noted that this effect is less pronounced in the corresponding uni-directional test presumably due to more restricted access of the solution through the concrete as a result of a less severe loading condition and the effect of crack blocking.

The above explanation agrees with the general belief and also the findings of other research workers in that a more aggressive environment is likely to produce lower endurances. Nevertheless, in fatigue tests the normal scatter in the results cannot be ignored as a possible explanation particularly when limited data are available.

Fatigue tests in tapwater exhibited a logarithmic linear relationship between stress range and number of cycles to failure. Furthermore, there were indications of crack blocking occurring in a test at the lowest load level which may account for the considerably greater

endurance observed in this particular test.

6.5.3 The Effective Stress Range During Cycling.

When crack blocking is effective, Paterson et al[59] suggest that presenting the endurances against the initial stress range could give misleading impression as they do not represent the complete situation resulting from the progressive reduction in stress range. Thus using the effective stress range (the average of the initial and final stress range), they estimate the underlying S-N curves as a true representative loading history. The resulting curves were, obviously less favourable than those based on the initial stress range since the beneficial effects of crack blocking in reducing the stress range have been removed. Their calculation of the effective stress range were based on the following assumption.

1. The initial stress range does not increase during cycling.
2. The initial stress range commences to decline immediately upon the load application and continued in this trend at a constant rate (linear change) over the test duration until the point of failure.

These assumptions, however, conflict with the actual deflection range changes recorded in this study and, subsequently with stress range changes deduced from these measurements. These measurements, generally, indicate a behaviour dependent on the initial magnitude of the stress range. For tests at higher load levels, where blocking is less effective and late in occurrence, there were appreciable increases in the stress range particularly at the initial stage of test. For the other extreme case where blocking is very influential, most of the reduction in the stress range occurred at a relatively early stage of test.

Thus while, corrections based on these assumptions tend to produce more favourable results for the former

conditions (where crack blocking is absent) this procedure tends to give less favourable results for the latter (crack blocking) conditions as compared with the initial intended stress range. It seems, therefore, that the best estimate of the effective stress range can be obtained by averaging the area under the stress range number of cycles curve (details are given in the following chapter) for each test. This method takes into account the initial increase in the steel stress as well as the non-linear change in this parameter upon the onset of crack blocking.

Using this procedure, the effective stress range was estimated for uni-directional series (in which blocking was observed) and the results are given in Table 6.3 which also include the intended and the average stress range (as used by Paterson) for each test. A comparison between these values for tapwater test is presented diagrammatically in Figure 6.21 which clearly illustrates the influence of crack blocking in changing the shape of the S-N curve and the effect of using different methods in estimating the effective stress range. It can be seen that the use of the original intended stress range produces both conservative (at high stress range) and unsafe (at lower stress level) estimation of the endurances. Also the use of effective stress range (by area under the curve method) to allow for the change in stress range during the test gives safer estimate of life under more realistic lower fatigue loadings than using the average stress range method originally proposed by Paterson et al.[59]

6.5.4 Comparison with Other Available Test Results.

A unique opportunity to evaluate the result and the effect of the environment on the endurance in particular is provided by results from a series of test performed at Glasgow University.[19,79,150,206] These tests were carried out using identical overall specimen details and loading conditions in seawater using different cyclic frequencies including the frequency used in the present research. Other related researches on fatigue of reinforced concrete beams in flexural in seawater and

sodium chloride, which are reviewed in some detail in Chapter 4, involve different experimental details and thus the use of these data for quantitative evaluation is rather difficult if possible at all. However, in an attempt to assess the environmental effects, these results will be compared with currently available design curves for reinforced concrete in sea water proposed by different scientific authorities.

Comparison with Glasgow University Tests at 0.17 Hz.

For uni-directional bending conditions, the results of sodium chloride and tap water are at the lower end of the scatter band of air test endurances reported by Arthur et al[19,79] and are much lower than fatigue lives observed in the sea water tests in the earlier study. For example, for a stress range of 345 N/mm^2 (upper stress = 0.85 f_y) the chloride and tapwater tests had average endurances of 372 x 10^3 cycles while the corresponding seawater tests averaged 3792 x 10^3, an order of magnitude greater.

Limited test results are available for comparison from reverse bending fatigue loading at comparable stress ranges. These results, however, suggest that for high load level, sea water tests exhibited slightly higher endurances than chloride and tap water tests, but considerable differences in endurances were observed in tests at lower load levels. For instance, for stress range of 216 N/mm^2, the tapwater test had an endurance of 0.447 x 10^6 cycles while two of the corresponding seawater tests were terminated with out failure after 13.5 x 10^6 and 8.94 x 10^6 cycles, the third test failed in shear span after 0.6 x 10^6 cycles. On the other hand, comparison with air tests in reverse bending is not possible as no results for the latter at comparable stress levels are available.

Thus for the given test conditions and load levels, the comparison shows that, so far as fatigue endurances are concerned, sodium chloride solution and tap water appear to be more deleterious than sea water and that at high loading conditions, the differences in endurances due

to the type of environment (for tapwater and chloride solution) are greatly diminished. The observed trends are attributed to the change in the structural behaviour of the beams during cycling as a result of crack blocking phenomenon. The much higher fatigue lives observed in sea water for the same initial stress range, can be accounted for by the much earlier onset of crack blocking (as demonstrated by detailed data in Chapter 7) and hence the earlier reduction in stress range. This situation, in fact, means that the fatigue tests in sea water were run under considerably lower stress range than for tests in both tap water and 3.5% sodium chloride solution over larger proportion of fatigue life which renders the type of environment irrelevant for comparison purposes unless these comparisons are made for tests at the same effective stress range as determined by the area under the curve method or when the blocking phenomenon is absent.

In the absence of crack blocking phenomenon, as is the case in reverse bending tests at high load levels, endurances are mainly dependent on the load level and the severity of the environment. This is in accord with results reported by Roper et al[59,201] who obtained lower endurances from tests in 3.5% NaCl solution than in seawater in the absence of crack blocking.

6.5.5 Comparison with Current Design Rules.

To evaluate the endurances results obtained in this study, these results are super-imposed on Figure 4.3, which presents the design curves proposed by different authorities, and represented in Figure 6.22.

It can be seen that, for uni-directional series, all the endurance results fall above the design curves for sea water environment, it should be pointed out that for this series, the endurances were based on the true effective stress range rather than the intended stress range.

For reverse bending tests, two of the chloride tests fall on or slightly below the design curves while all tapwater test results were above the design curves but these were notably near to the C.I.O. design curves. On

the other hand DNV rules is expected to be unsafe for stress ranges below their fatigue limit, this was confirmed by Paterson's et al[59] work.

In general Figure 6.22 indicates that the endurance results obtained in this study fall within the safe zone of the design curves it should be appreciated, however, that:

1. The C.I.O. curve was based on results obtained from tests on concrete beams with single 32 mm diameter torbar and was modified for splash zone exposure conditions and that;
2. BSC design curve was based on results from beams with single 16 mm bars.

Thus, these curves may be expected to give even more safe results when used for the less-severe circumstances of 10 mm Torbar in submerged condition as is the case in this study. Accordingly, the reason for some results being near or below the design curves is not fully understood and may be related to the observation discussed in Section 6.5.1 with regards to the effect of reinforcement details. On the other hand, although the C.I.O. curve takes into account the removal of the beneficial effect of crack blocking, it seems that the trend observed in this particular curve can partly be related to the assumptions made in deducing the effective stress outlined earlier in Section 6.4.3. The observed trend may also be attributed to the fact that no modifications were made for reverse bending series as to the true effective stress range, this is because no experimental evidence are available, as yet, relating the change in deflection range to the change in steel stress range as provided earlier for tests, in uni-directional regime which forms a basis for the stress range modification for tests under the latter loading condition.

If this relation is also valid for reverse bending regime, the effective stress range is likely to be greater than the initial intended stress range for tests at higher load level, thus, put the endurances above the design

curves.

Contrariwise, for test at lower load level (0.35 f_y), the modification of stress range is likely to locate the endurance result within the unsafe regions of the design curves.

Table 6.1: Results: Uni-directional Bending Series.

Environment	Beam Designation	Maximum intended stress (N/mm^2)		Stress range (N/mm^2)	Age at fatigue test (days)	Position of main crack (mm from ℄)	No. of bars cut at failure	Endurance Cycles
		Steel in tension	Concrete in compression					
Water	MJ70W	322	16	276	33	380	2	1,807,200
	MJ75W	345	17.2	299	55	160	2	532,500
	MJ85W	391	19.5	345	56	390	1	346,643
Chloride	MJ70N	322	16	276	37	120	2	1,076,000
	MJ75N	345	17.2	299	33	150	1	400,435
	MJ85N	391	19.5	345	37	390	1	397,246
Air	MJ70A	322	16	276	198	-	-	Stoppped after 2,216,700 cy. without failure

Table 6.2: Results: Reverse Bending Series.

Environment	Beam Designation	Maximum intended stress (N/mm^2)		Stress range (N/mm^2)	Age at fatigue test (days)	Position of main crack (mm from ℄)	No. of bars cut at failure	Endurance Cycles
		Steel in tension	Concrete in compression					
Water	MR35W	161	9.6	164	175	200	2	1,208,000
	MR46W	212	12.7	216	1580	350	2	447,600
	MR70W1	322	19.1	328	1825	100	2	123,000
	MR70W2	322	19.1	328	34	400	1	172,500
	MR75W	345	20.6	351	1811	250	1	72,900
	MR85W	391	23.2	398	1765	220	2	29,900
Chloride	MR70N	322	19.1	328	1862	70	1	34,600
	MR75N	345	20.6	351	1840	280	2	34,400
	MR85N	391	23.2	398	1846	520*	1	6,300

* shear failure

Table 6.3: Uni-directional Series; Intended, Average and Effective Stress Range.

Environment	Beam Designation	Stress Range N/mm^2		
		Intended	Average	Effective
Water	MU70W	276	218	180
	MU75W	299	310	368
	MU85W	345	396	435
NaCl	MU70N	276	235	233
	MU75N	299	299	317
	MU85N	345	379	450

Note: It should be pointed out that the above given effective stress ranges for tests at high load level of 0.75 and 0.85 f_y may be overestimates as the calculations did not take into account the effect of creep of concrete in increasing the deflection of the beams from which these values were deduced.

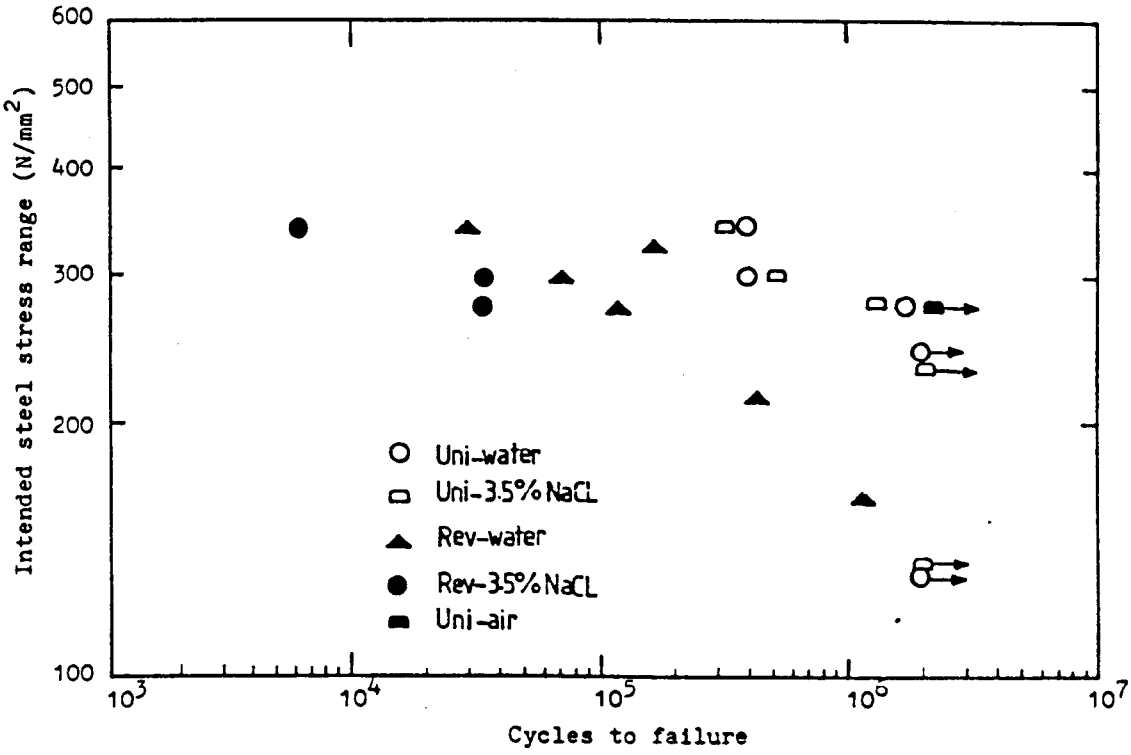

Figure (6-1): Endurance vs. stress range for unidirectional and reverse test beams.

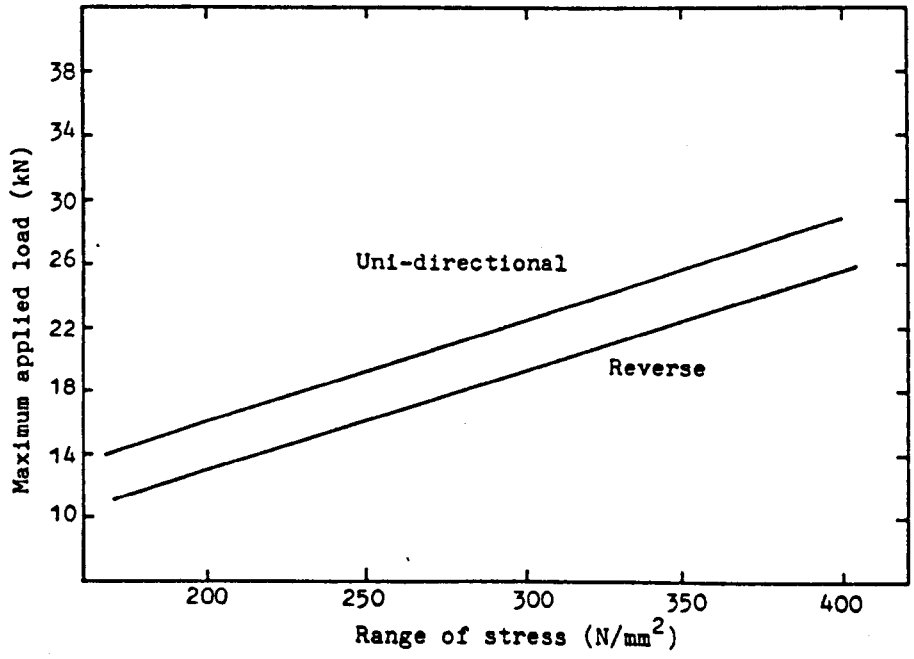

Figure (6-2): Maximum applied load vs. range of stress tension bars.

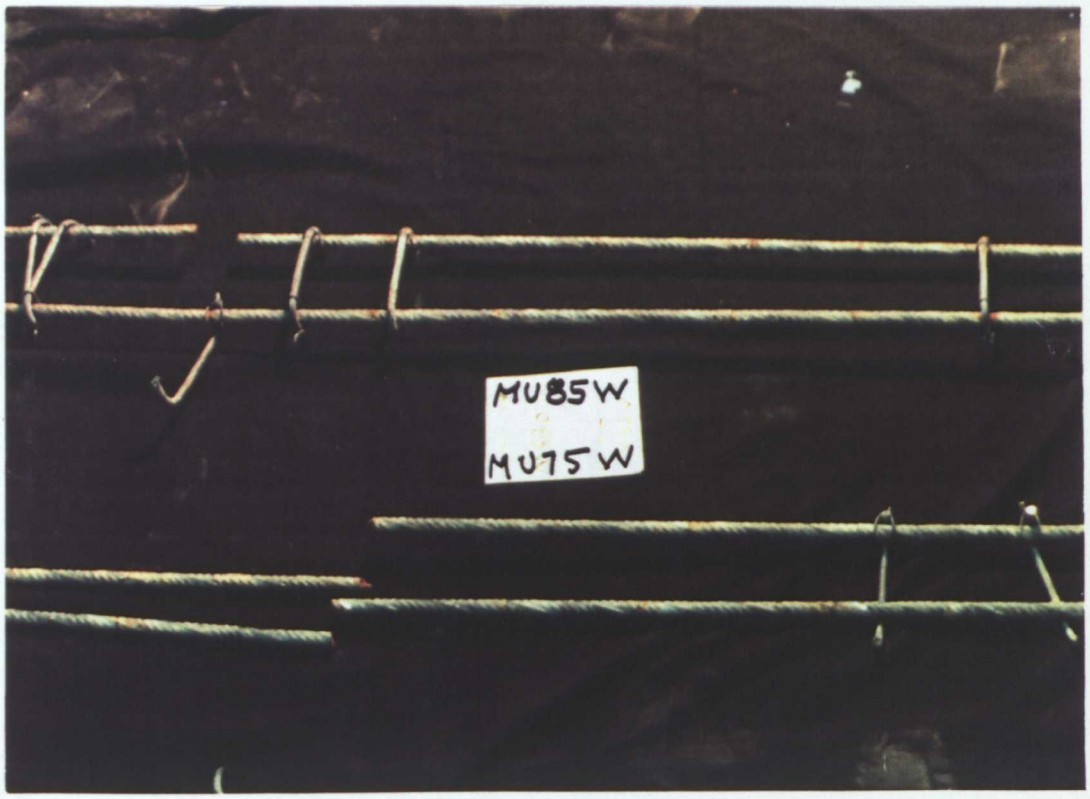

a) MU75W,MU85W

b) MU85W (close-up)

Figure (6-3): Failure in the main tension bars after fatigue test at different load levels.

a) Dynamic test

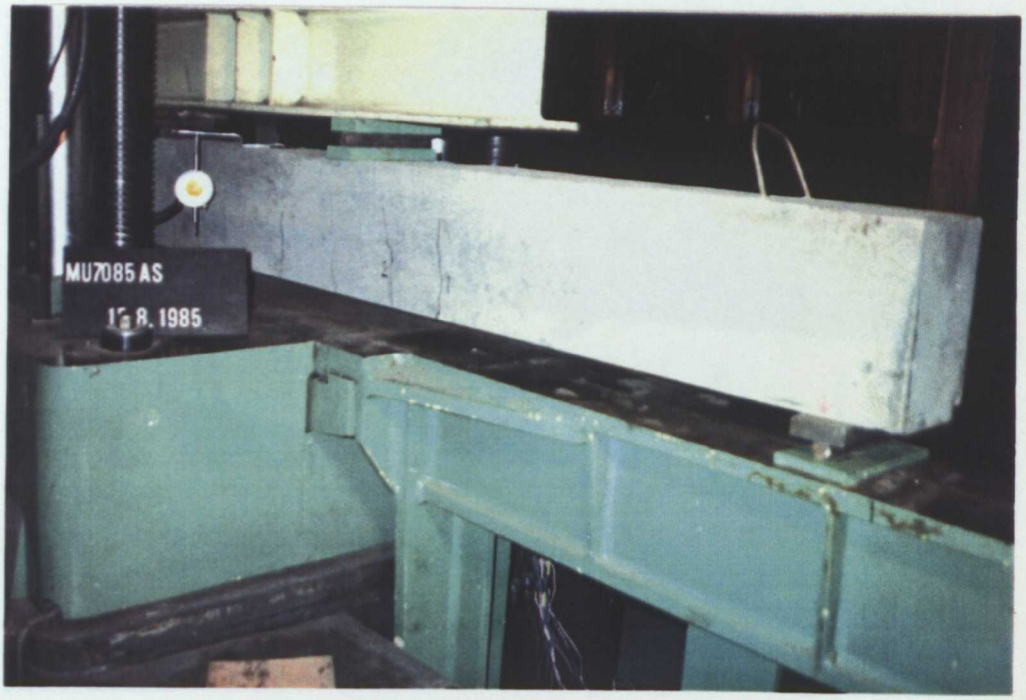

b) Static test

Figure (6-4): Uni-directional series;cracking pattern at failure.

a) Dynamic test

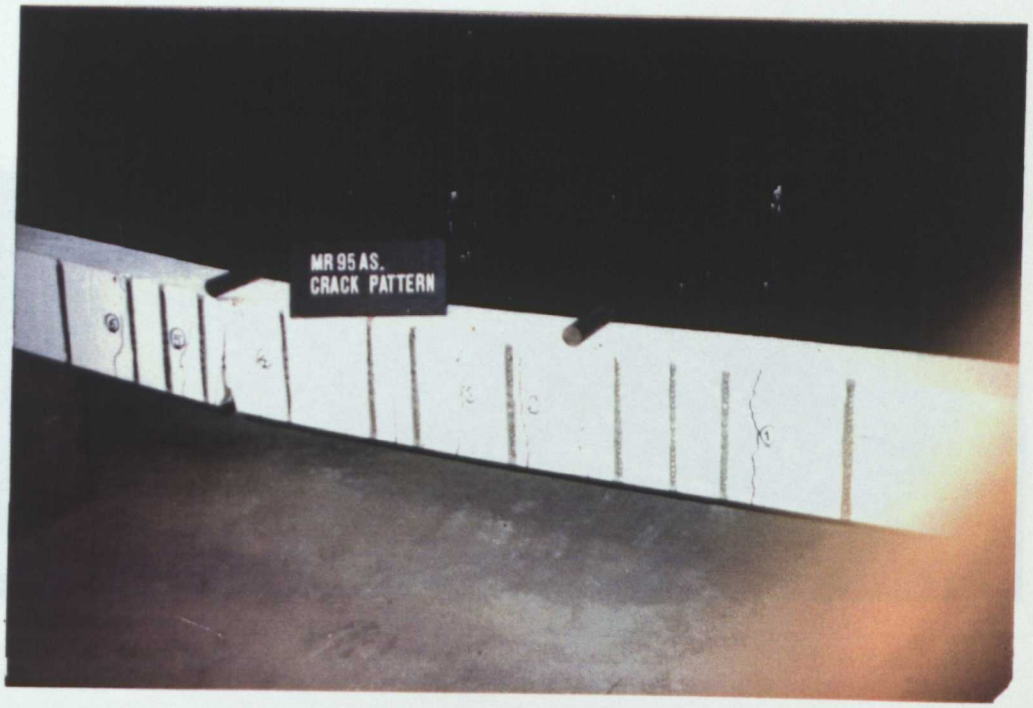

b) Static test

Figure (6-5): Reverse bending series;cracking pattern at failure.

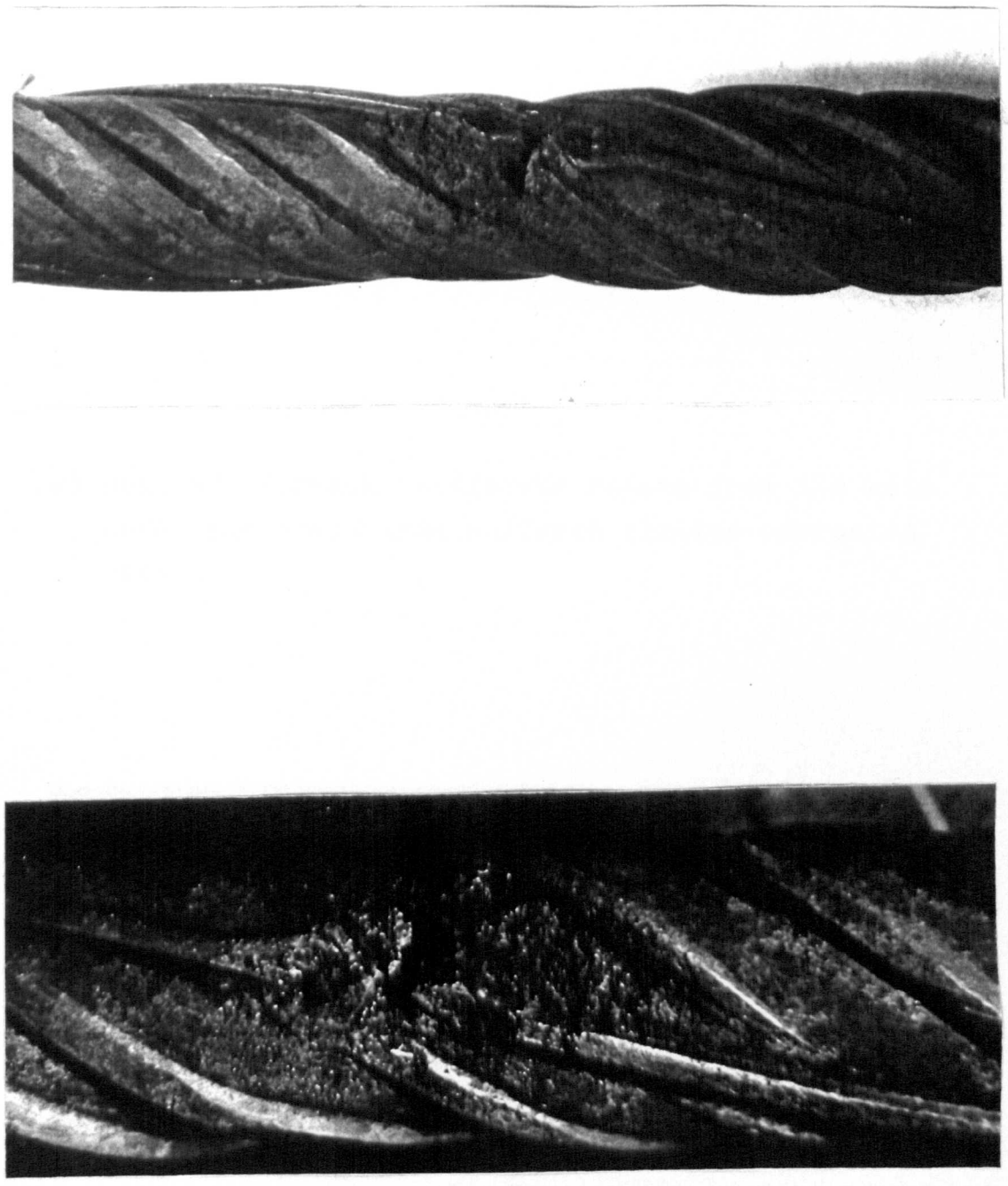

Figure (6-6): Beam MU85N;crack initiation at corrosion attacked area.

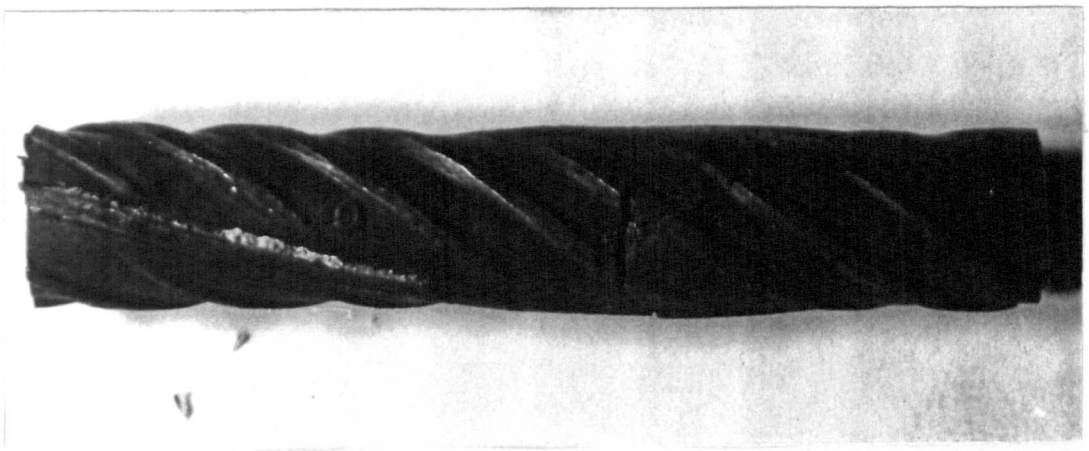

a) Beam MU75W;crack initiation remote from the main crack the crack area suffered limited corrosion attack

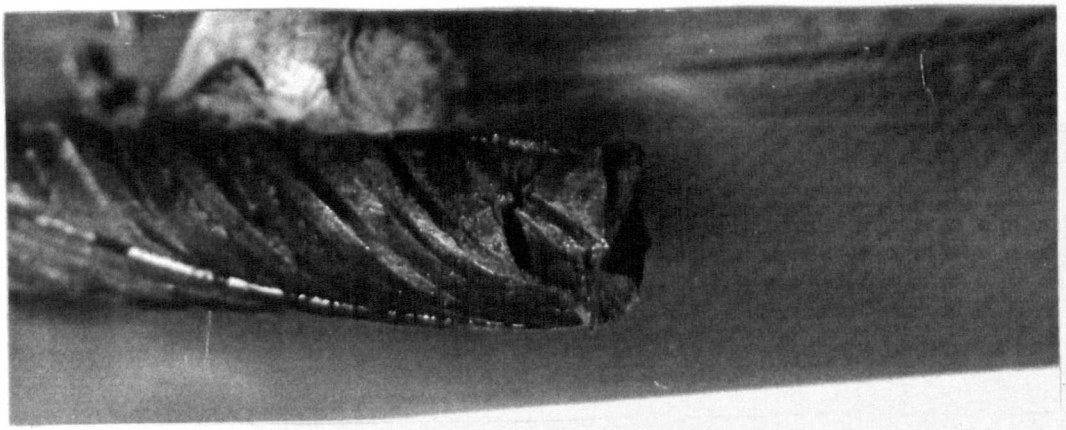

b) Beam MU85W;initiation of new crack near the main crack

Figure (6-7): Crack initiation phase.

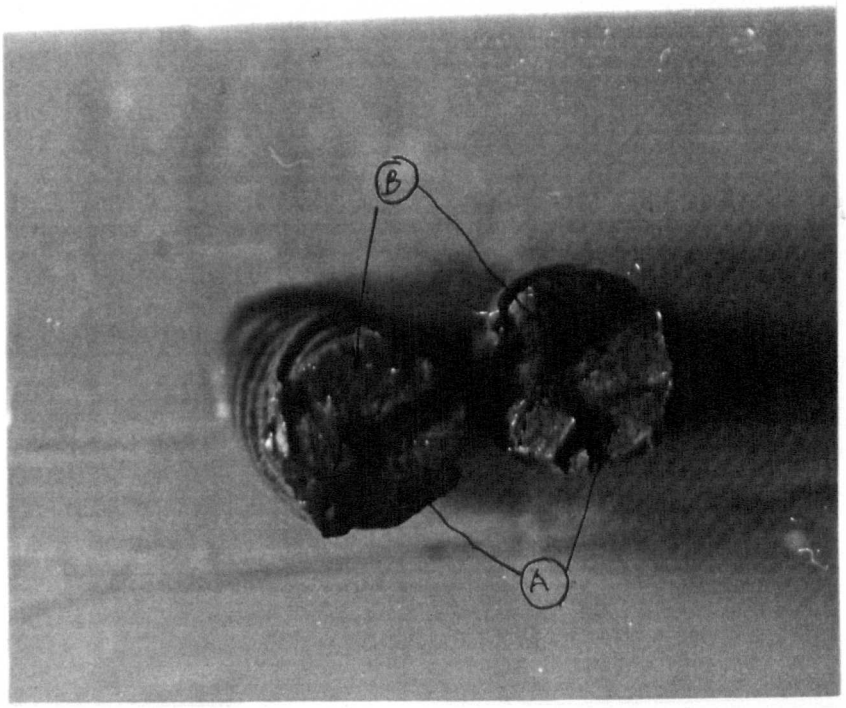

a) Bar 2 fatigue failure

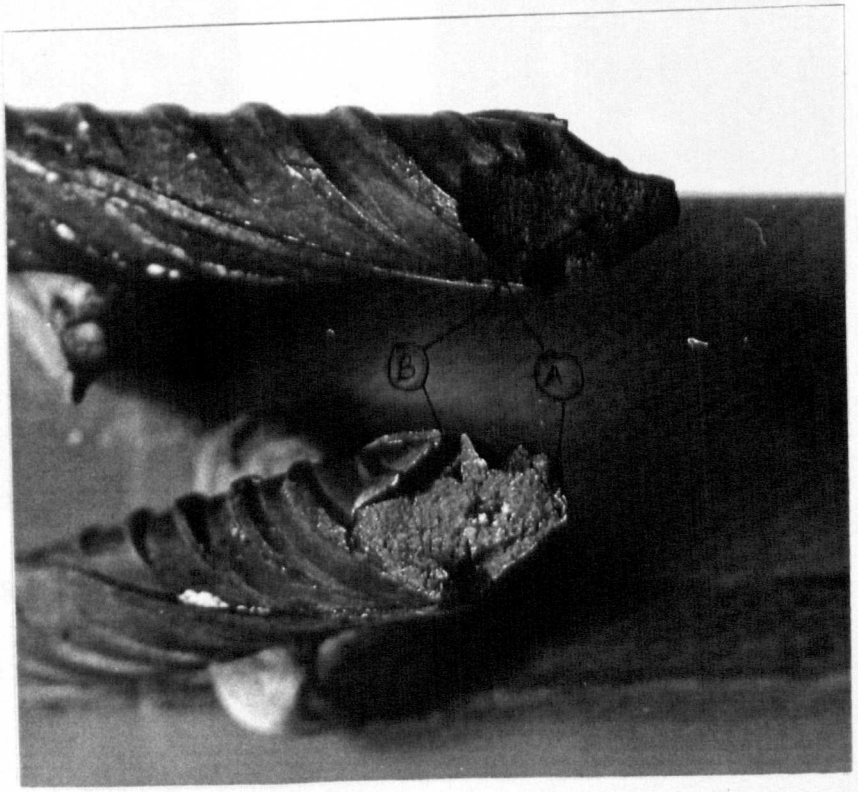

b) Bar 1 ductile failure

Figure (6-8): Beam MU75W;fracture surfaces.

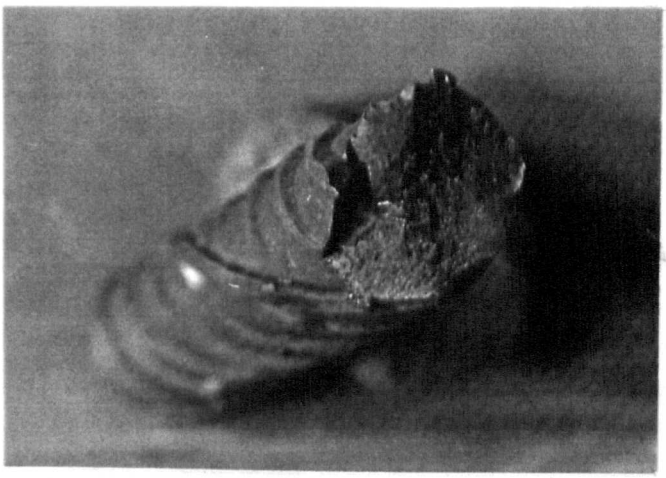

c) Beam MR70W

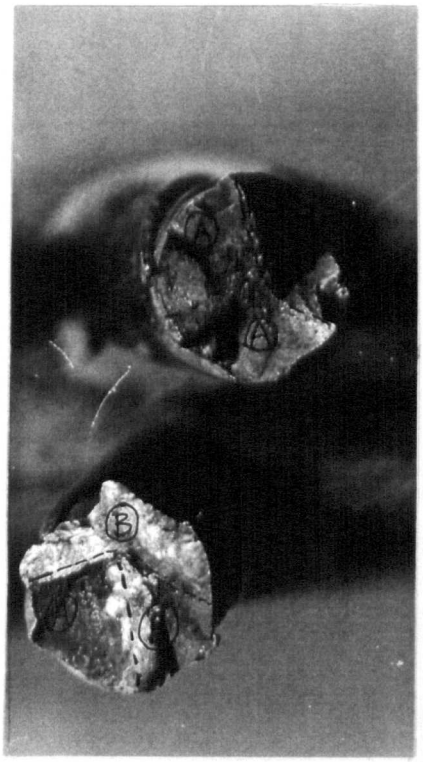

a) Beam MU85W

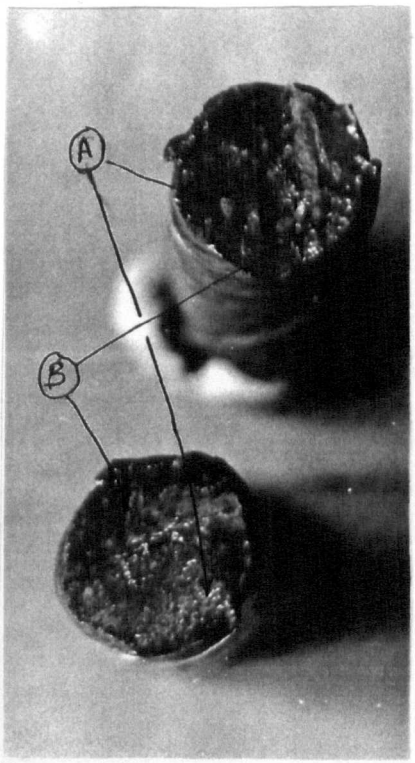

b) Beam MU85N

Figure (6-9): Fracture surfaces for different reinforcement bars failed in fatigue.

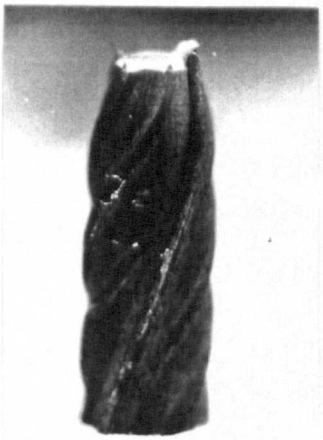

a) Pure tension

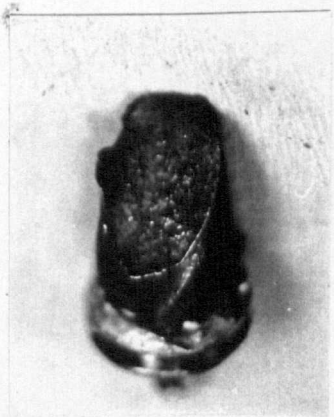

b) Static bending (embedded in concrete)

Figure (6-10): Fracture surfaces for different reinforcement bars failed under static loading.

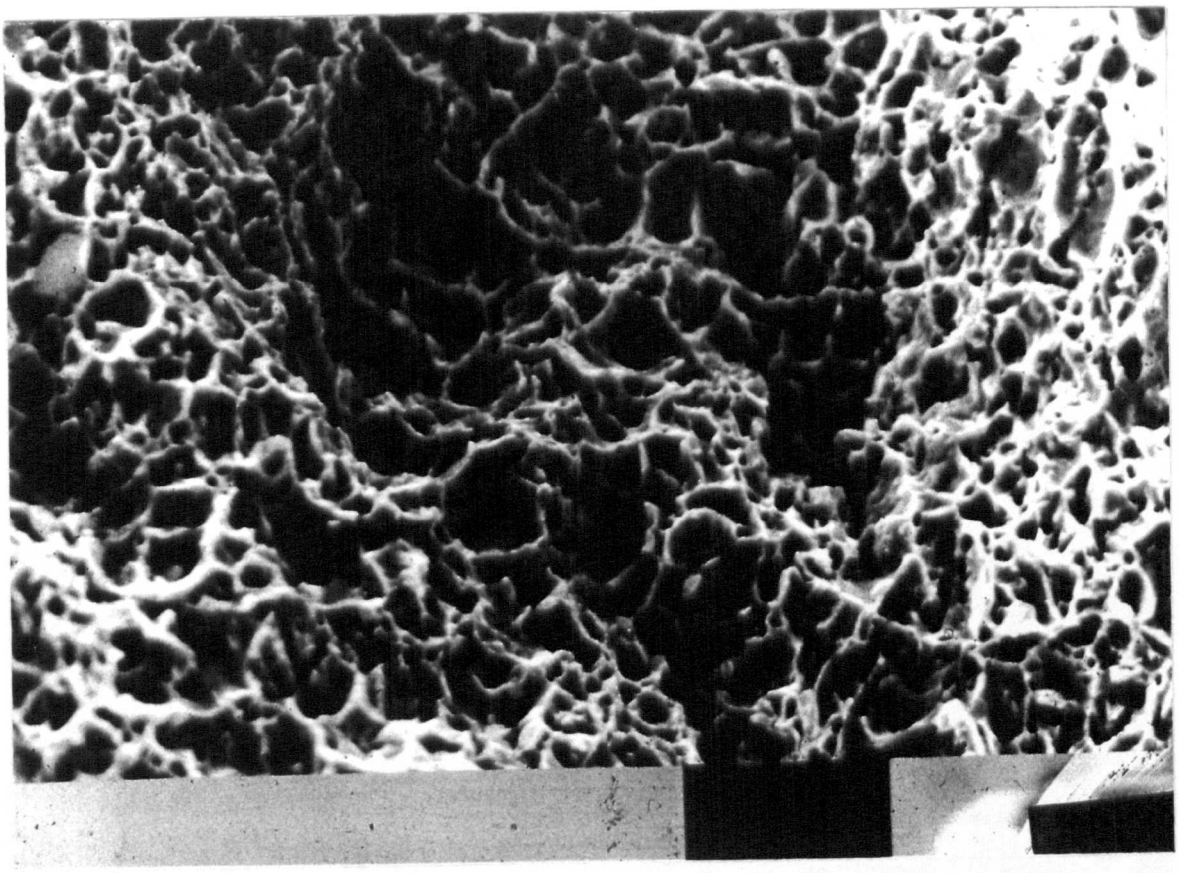

a) X 1k

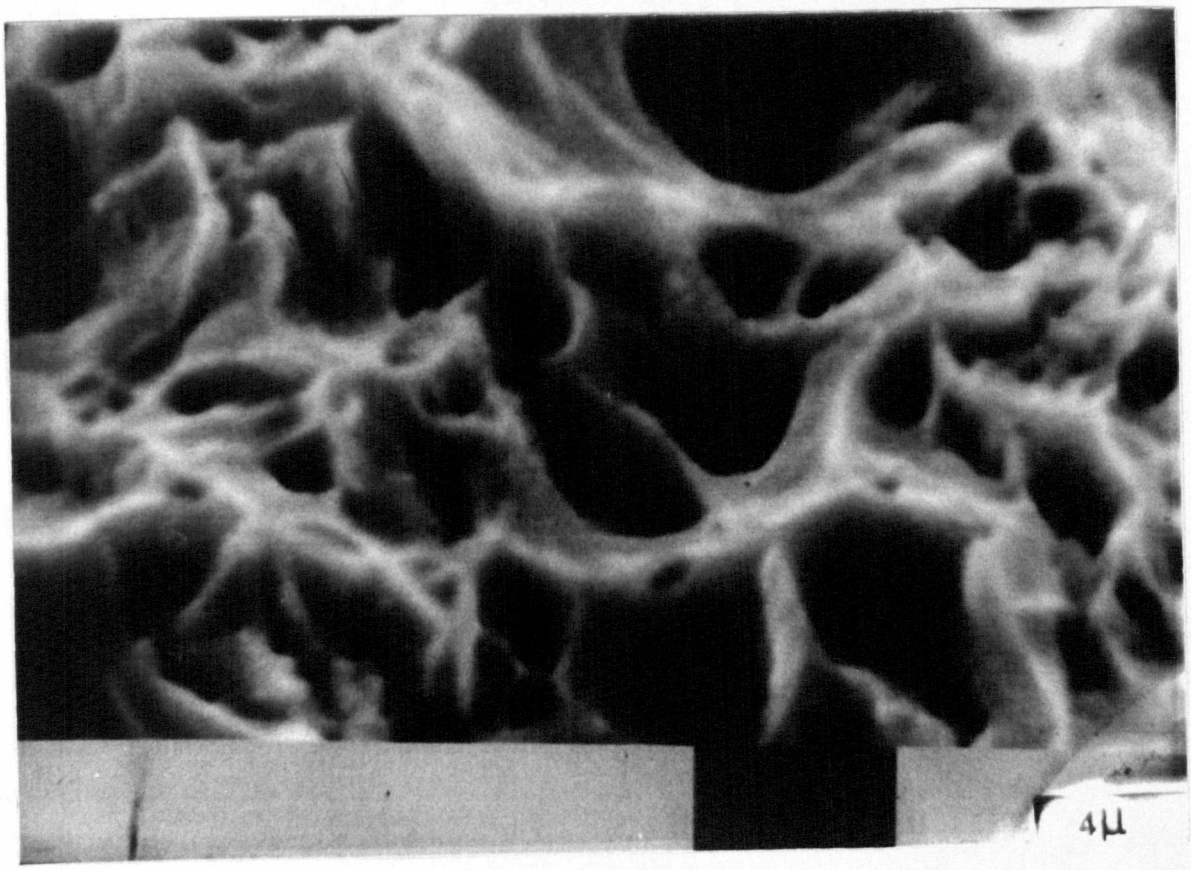

b) X 5k

Figure (6-11): A SEM photographs of the fracture surface of a bare Torbar in axial tension indicating honeycomb structure.

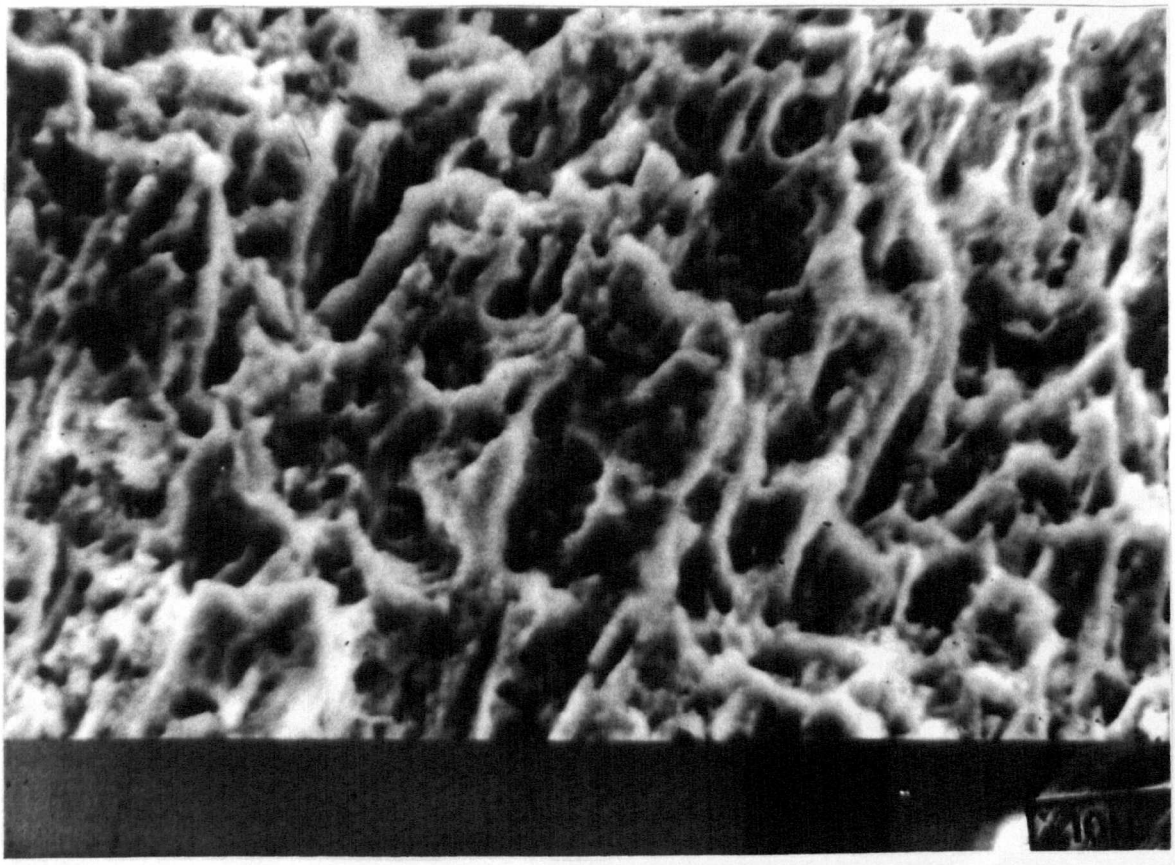

X 2k

Figure (6-12): A SEM photograph of the fracture surface of Torbar from static test in air showing distorted honeycomb structure.

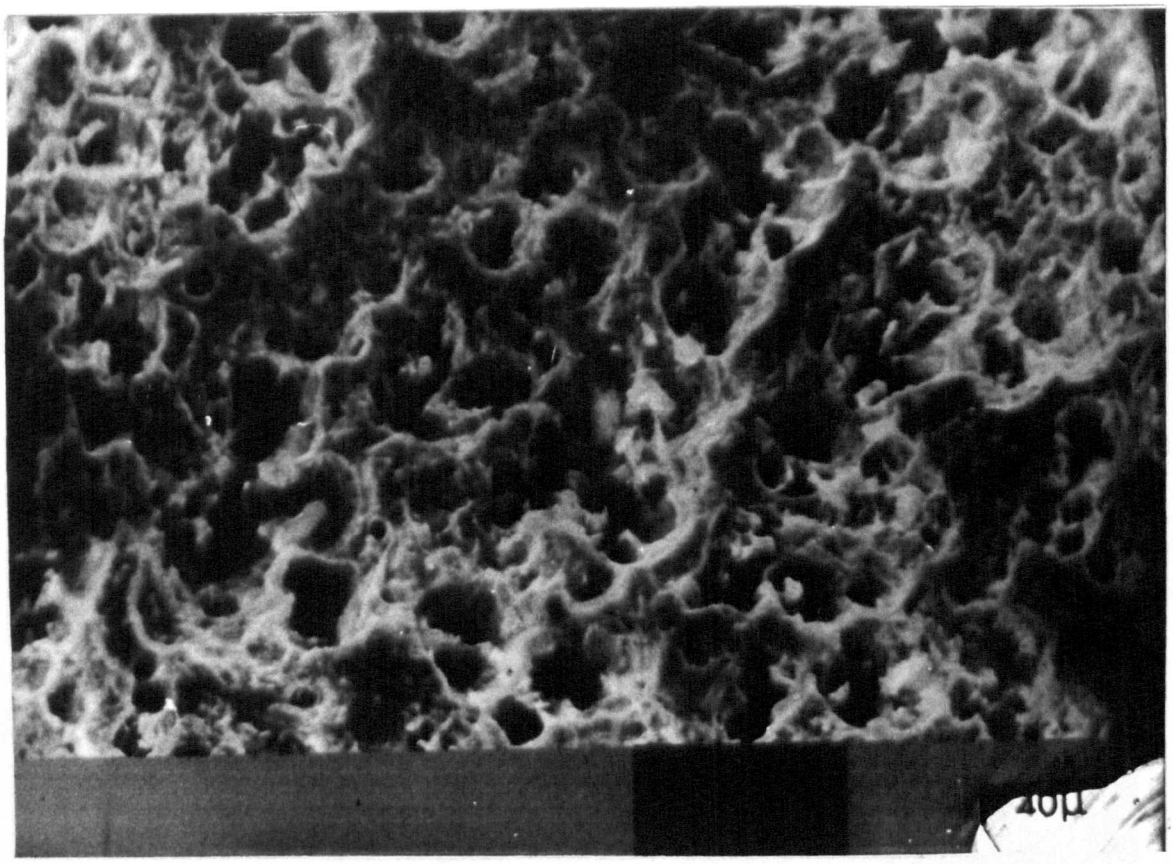

a) X 500

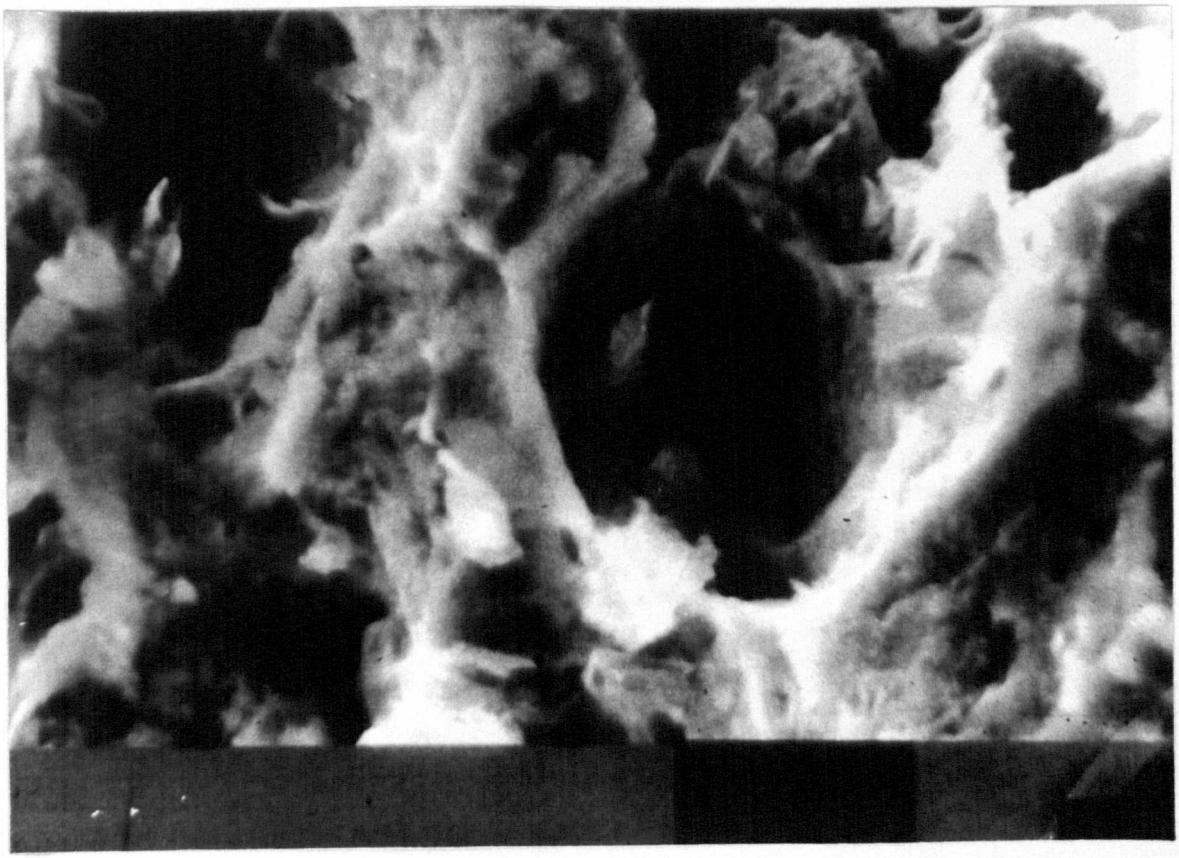

b) X 2k

Figure (6-13): A SEM photographs of the fracture surface of Torbar 1 from beam MU75W showing honeycomb structure.

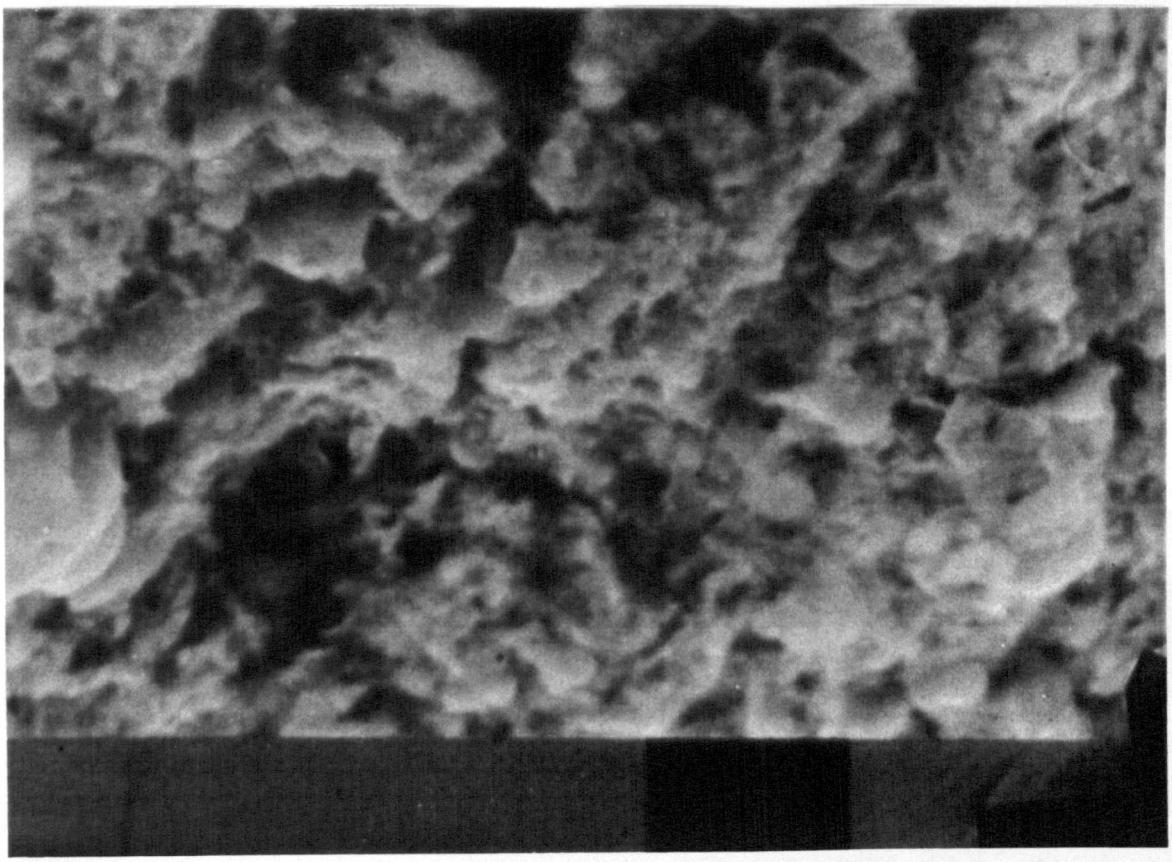

X 2k

Figure (6-14-a): Featureless fracture surface due to corrosion damage.

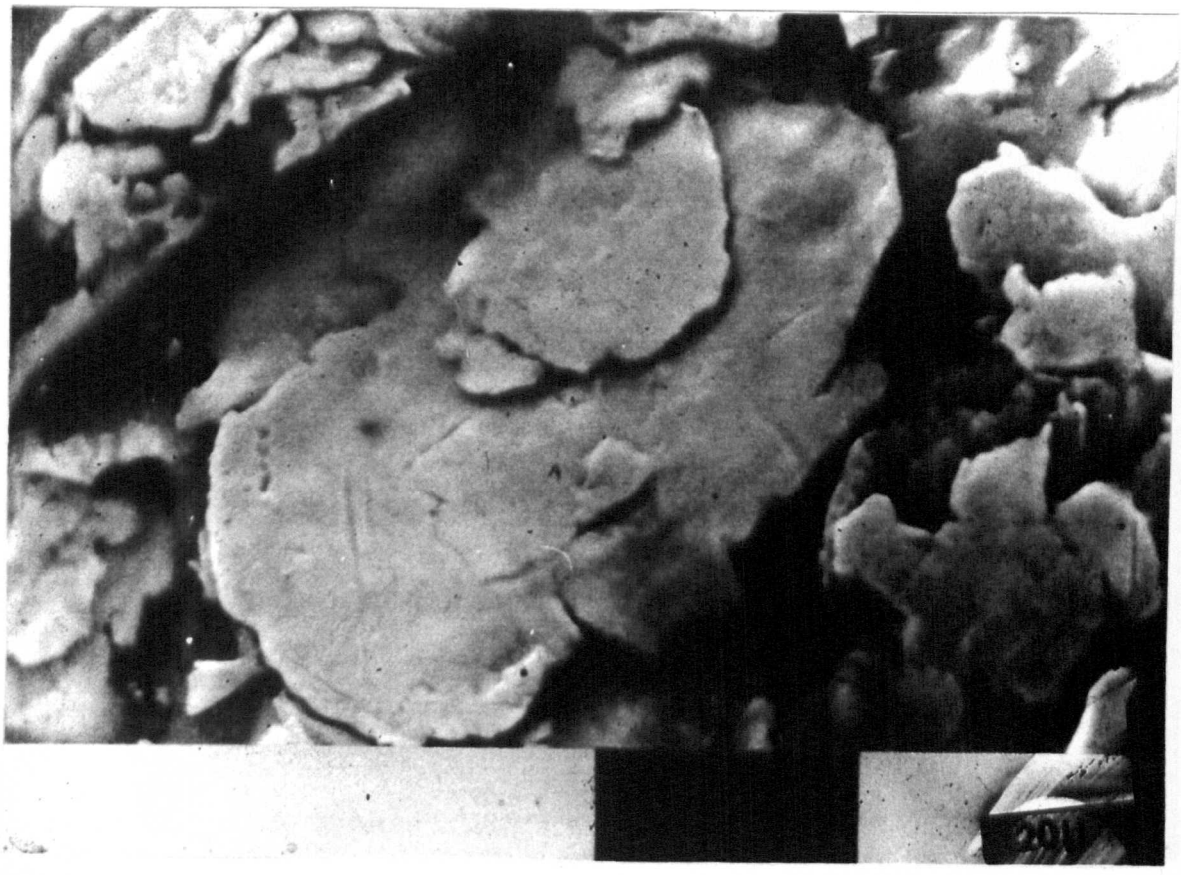

b) X 1k flaky structure

c) X 500 honeycomb structure (ductile fracture)

Figure (6-14): A SEM photographs of the fracture surface of Torbar 2 from beam MU75W.

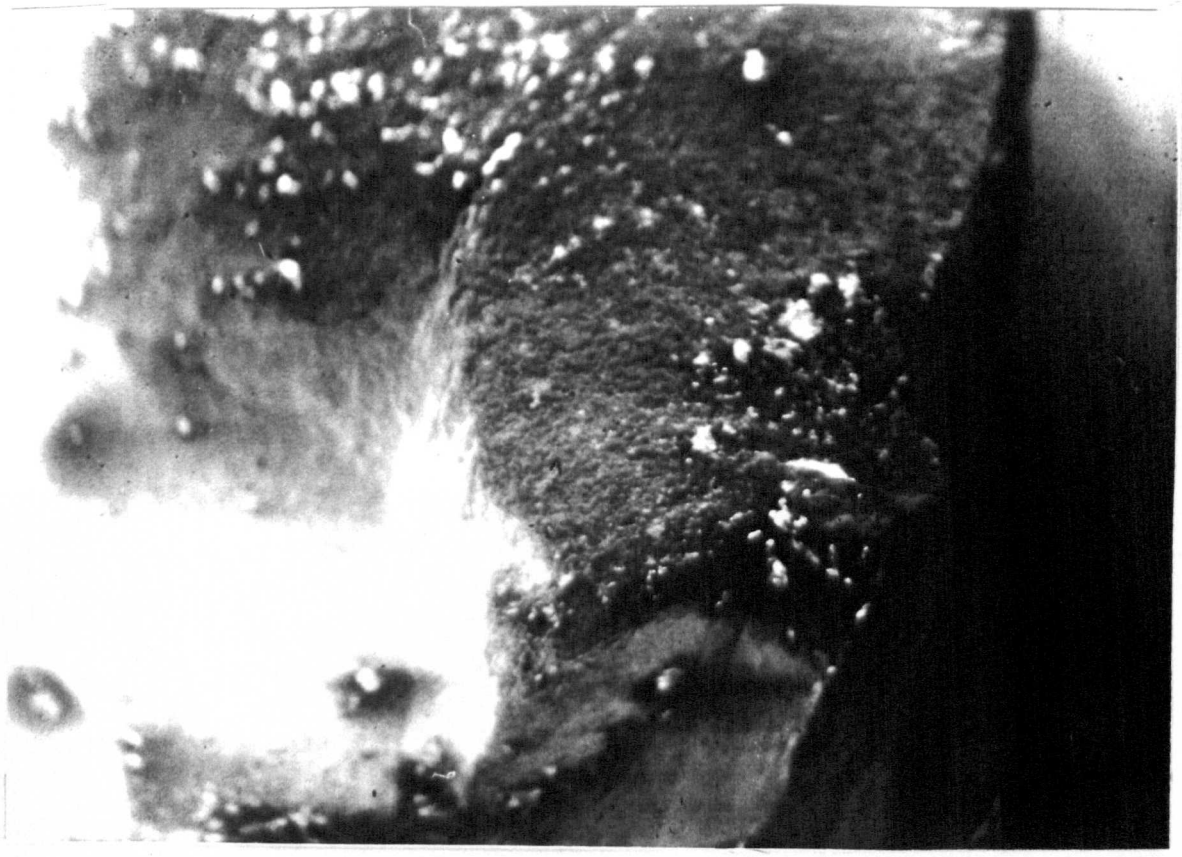

a) X 20 stepped fracture surface

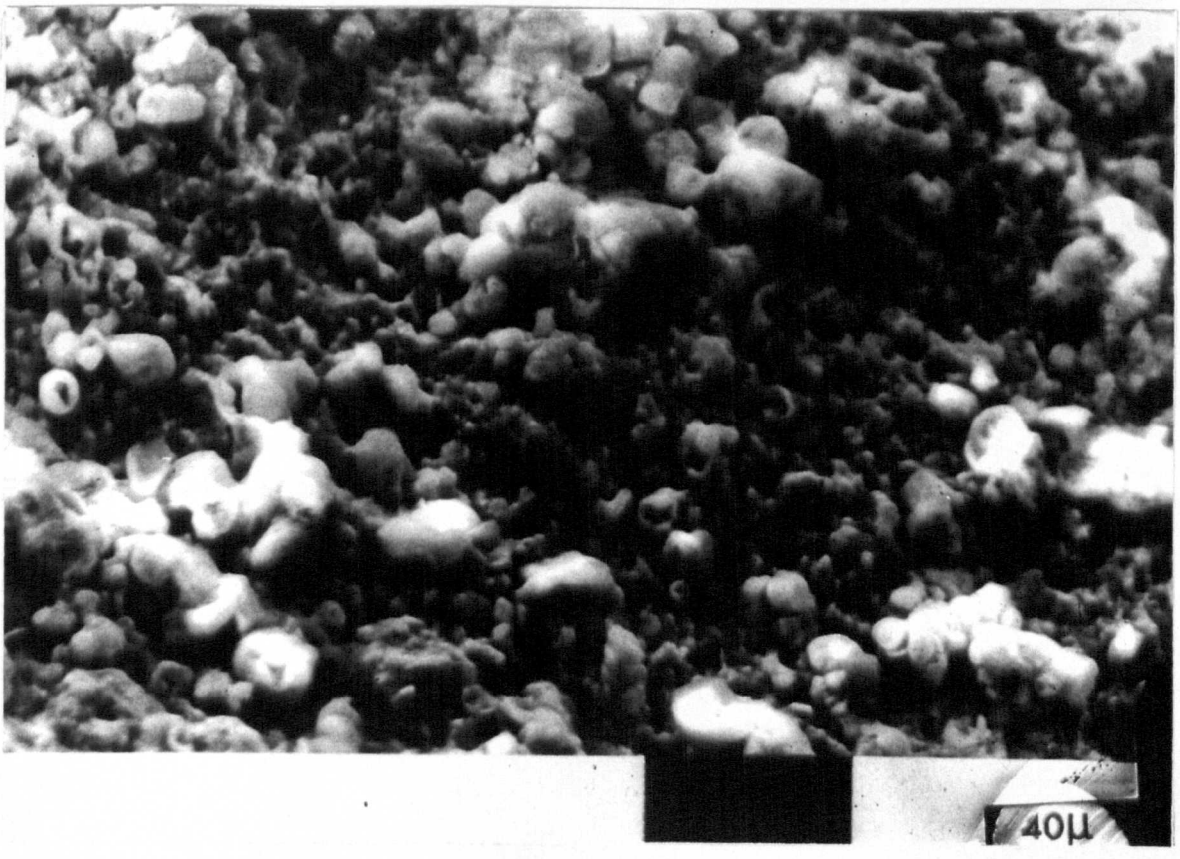

b) X 500 corrosion product on fracture surface

Figure (6-15): A SEM photographs of the fracture surface of a Torbar from beam MU85W.

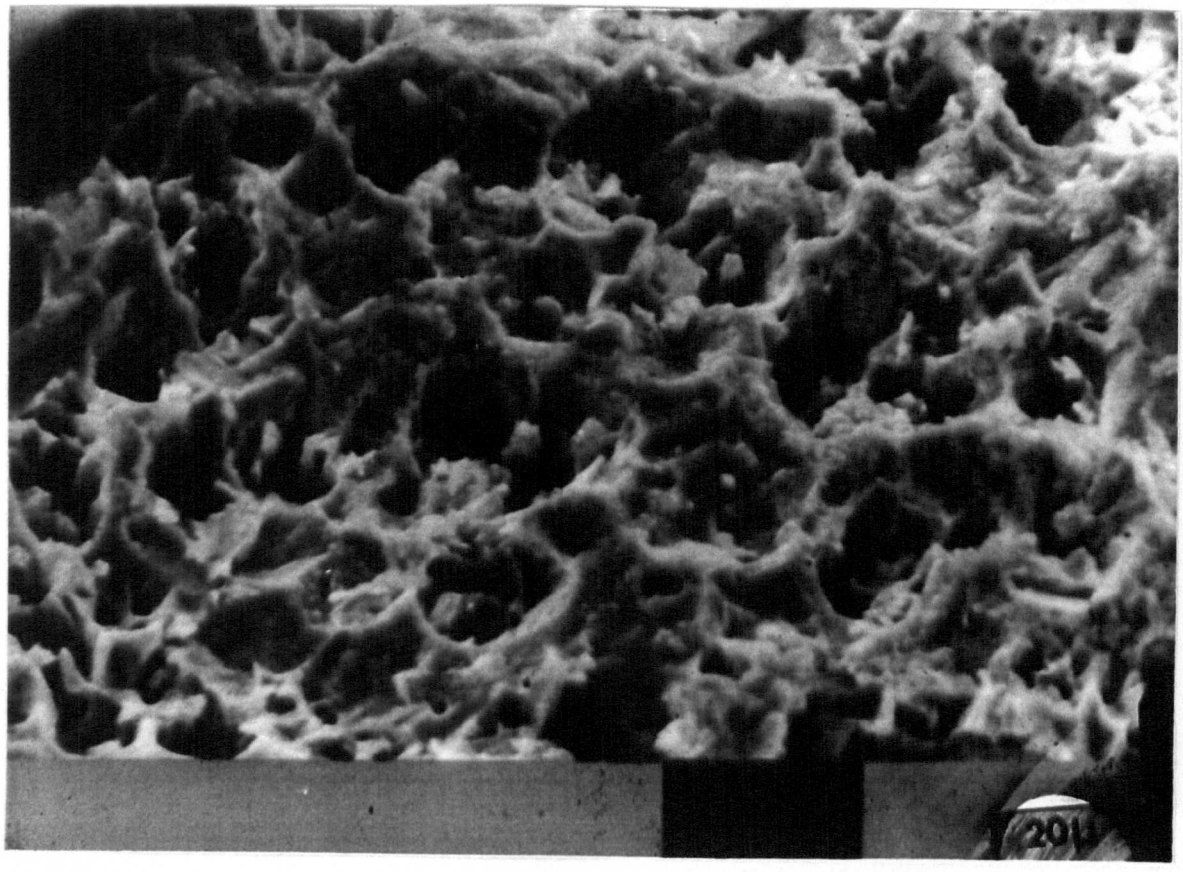

X 1k

Figure (6-16): A SEM photographs of the fracture surface of a Torbar from beam MU85W showing honeycomb structure.

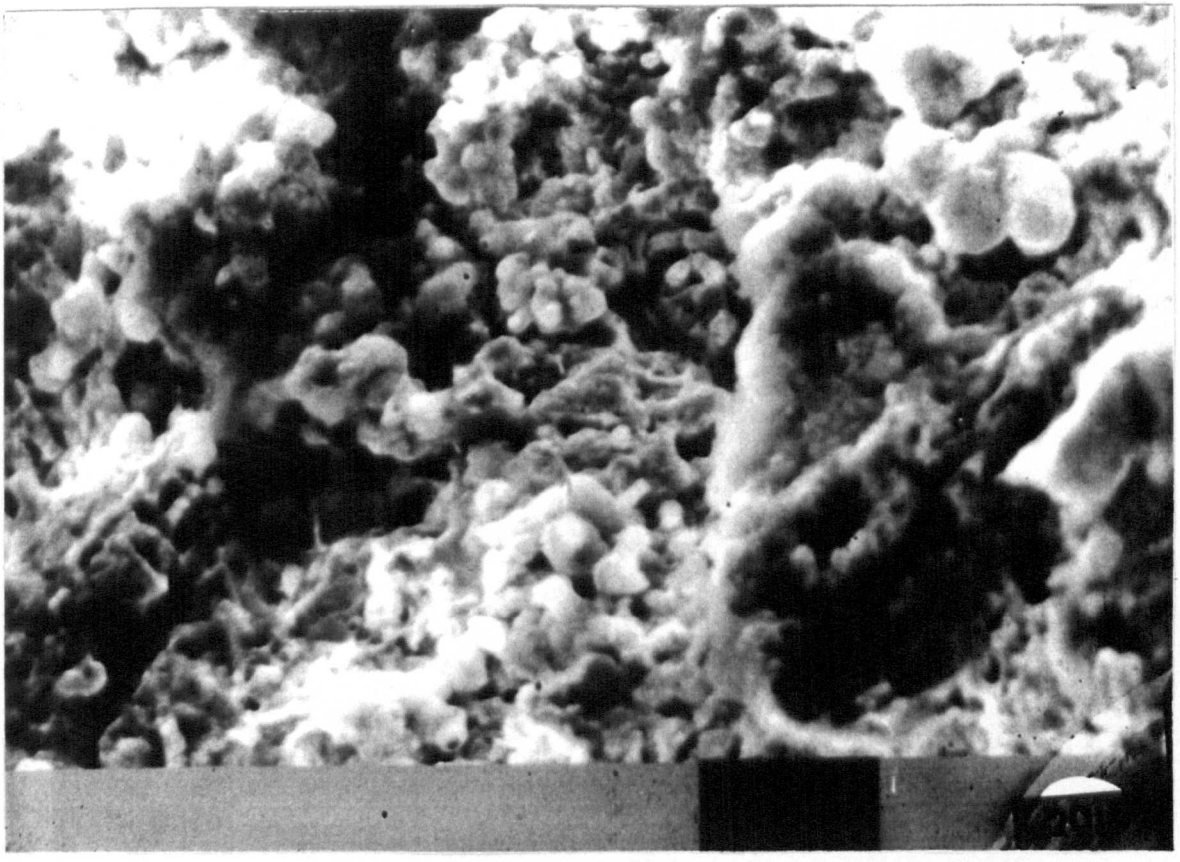

Figure (6-17): A SEM photographs of the fracture surface of a Torbar from beam MR7OW indicating corrosion product.

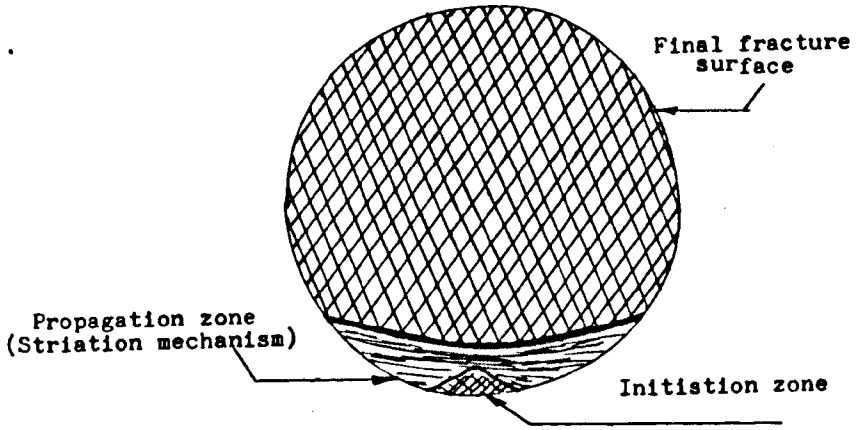

a)Case 1

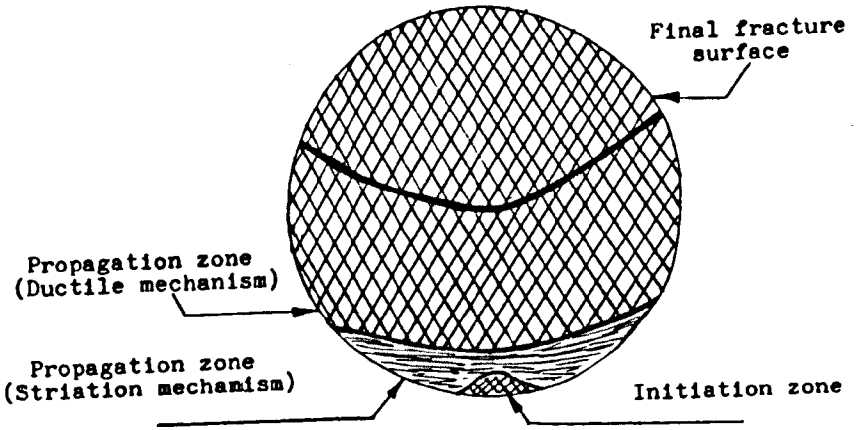

b)Case 2

Figure (6-18): Possible failure mechanisms.

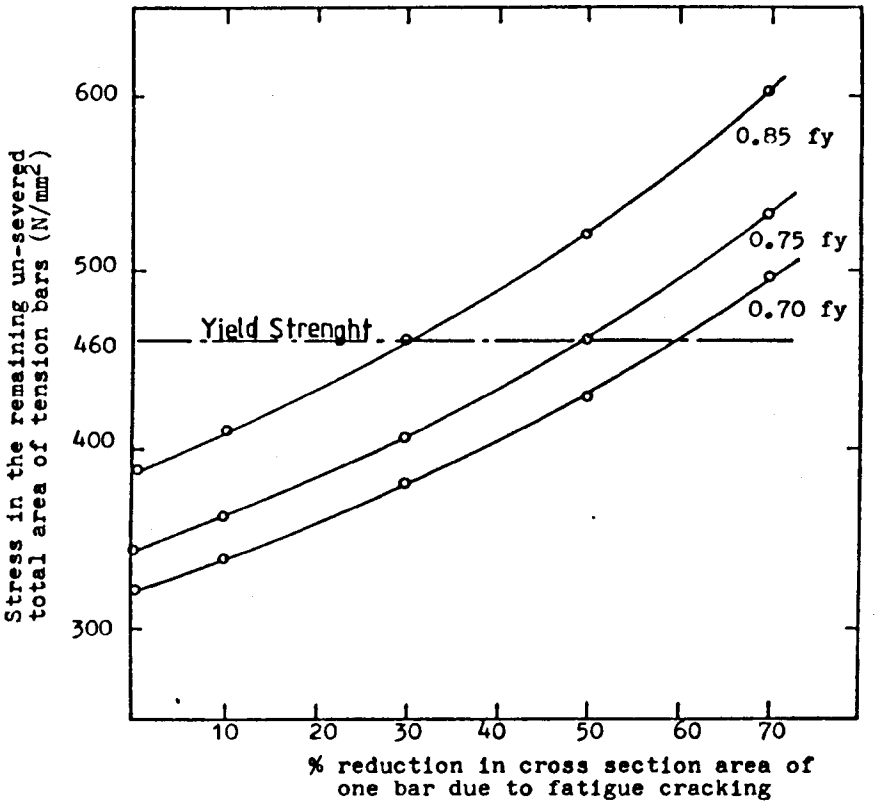

Figure (6-19): Stress-cross section area relationship for different applied maximum stresses.

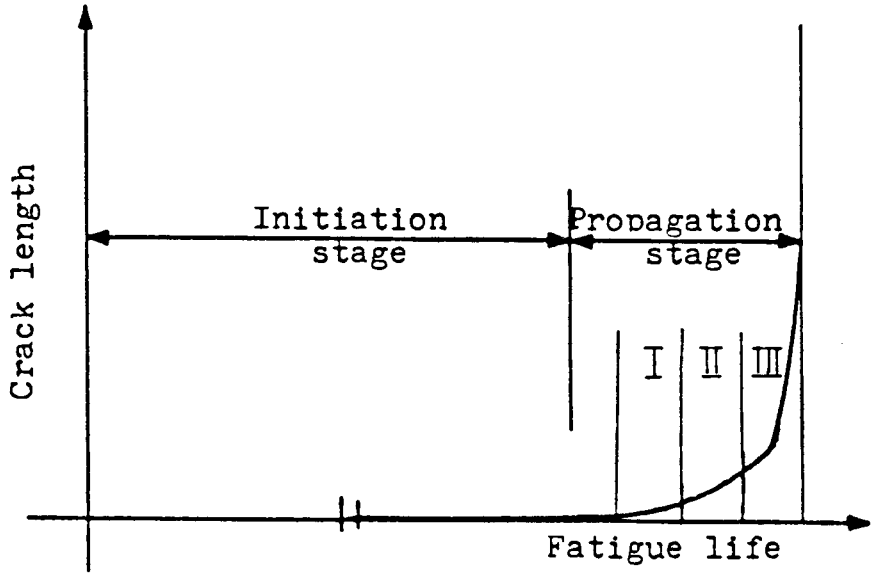

a) Crack length vs. fatigue life

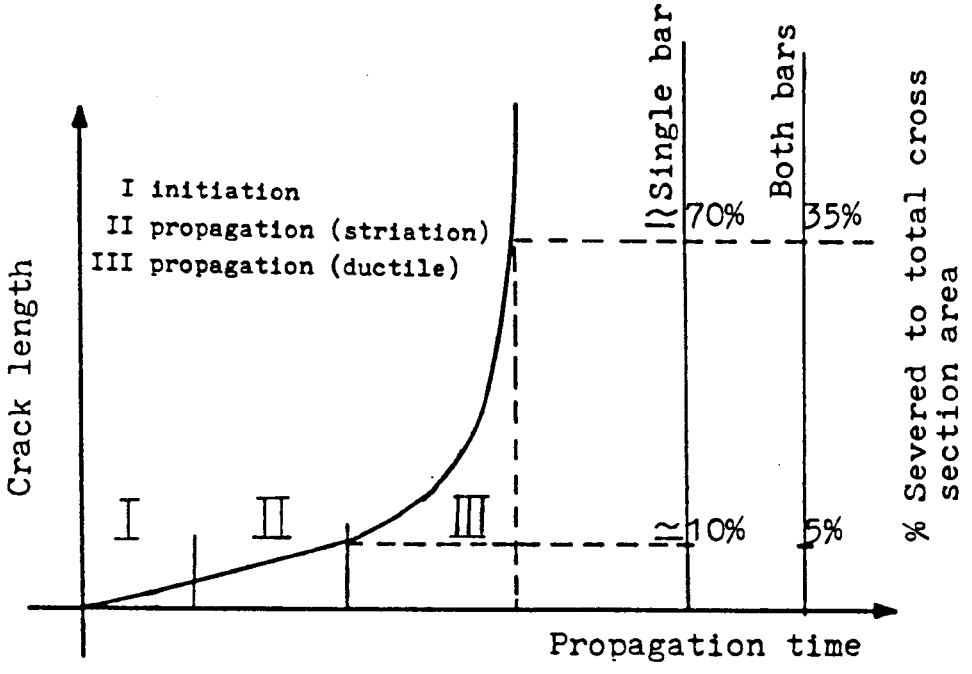

b) Propagation stage

Figure (6-20): Fatigue failure process for high stress conditions.

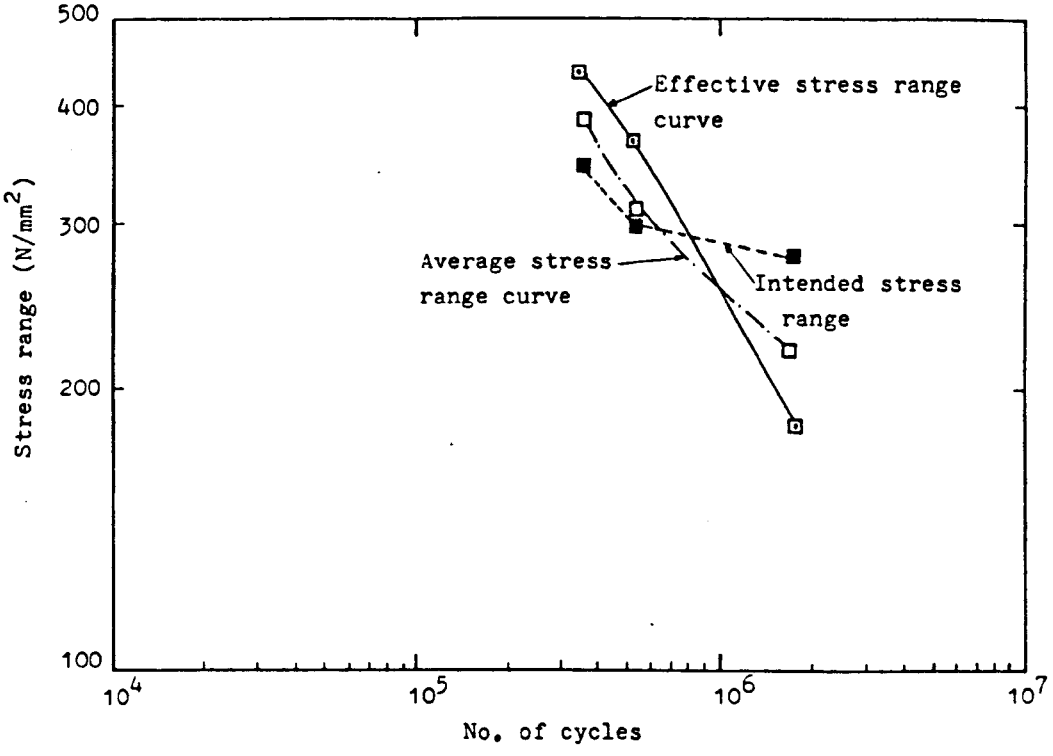

Figure (6-21): Comparison between effective and average stress range curves for uni-directional tests in water.

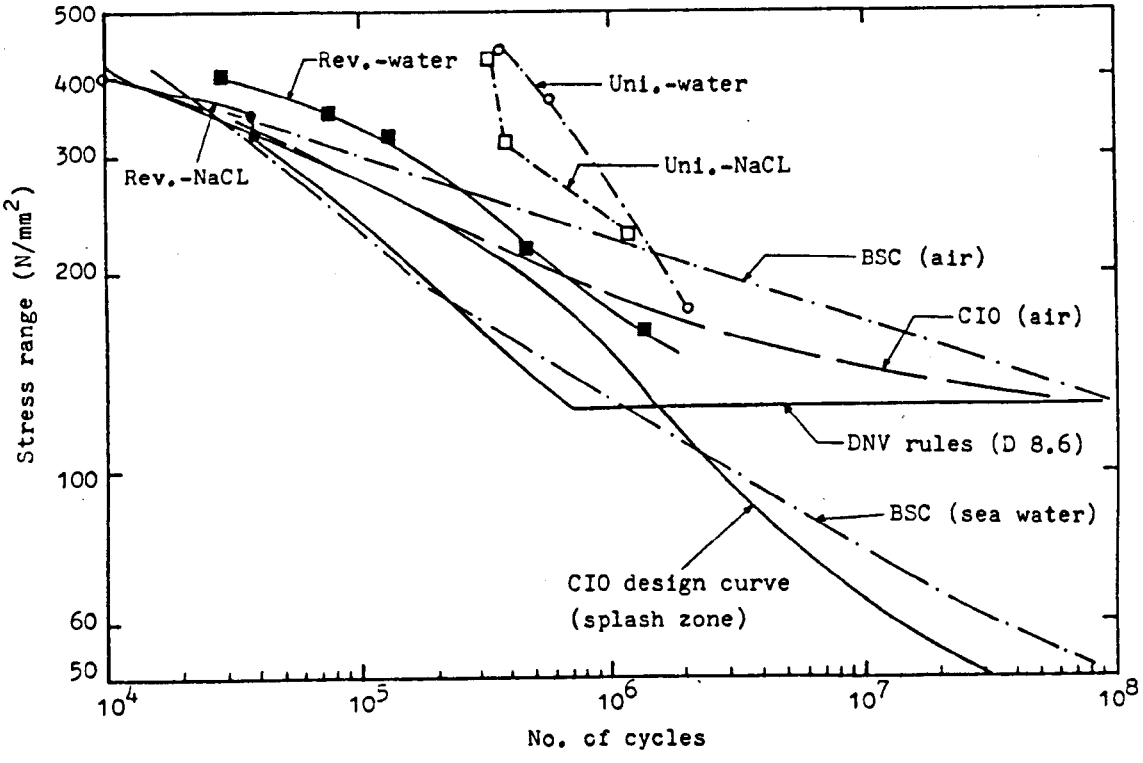

Figure (6-22): Comparison of fatigue endurance with the current design curves.

CHAPTER 7

DYNAMIC RESPONSE OF REINFORCED CONCRETE BEAMS IN AQUEOUS ENVIRONMENT

CHAPTER 7

DYNAMIC RESPONSE OF REINFORCED CONCRETE BEAMS IN AN AQUEOUS ENVIRONMENT

7.1 Introduction.

The results presented in this chapter are mainly concerned with the structural behaviour of the test specimens during cyclic loading.

The results presented in this chapter were obtained from both research stages. In Stage I of the programme, deflection and crack width were monitored. The results, however, indicate that deflection monitoring alone may adequately describe the characteristic change in the beam's response to cyclic loadings. There are several reasons for this conclusion:

First; The similarities in deflection and crack width histories observed during the tests.

Second; In theory, the deflection data may be related directly to steel and concrete stresses and strains more positively than to crack width.

Third; Due to the practical difficulties involved in crack monitoring, only a few cracks can be monitored and these were selected randomly in the maximum bending moment zone. These cracks, clearly do not necessarily represent the maximum nor the average crack width, therefore, in contrast to deflection, crack width data are not a sound basis for quantitative comparison.

Finally; In studies on the corrosion processes, which is the main objective of Stage II of the programme, it is particularly important to eliminate any uncertainties in

electrochemical measurements which may arise form the exposure to the corroding solution of any other metal as would be the case in crack monitoring which involves the immersion of the metallic body of the crack sensor in the solution.

7.2 Crack Propagation in the Concrete.

It has been pointed out that prior to the application of cyclic loading, the beams were first loaded statically to loads corresponding to the maximum steel stress in the high tensile bars used. As the load on the beam was increased from zero, a few cracks (2 to 3) began to be visible at a load equivalent to a steel stress of approximately 0.6 to 0.65 of the characteristic proof strength. The crack lengths varied from approximately 60 to 120 mm. Beyond this stress right up to the maximum intended stress (for beams tested at higher stress levels than 0.6 f_y), the existing cracks slightly widened and very few new ones formed (1 to 2 cracks). These cracks were in the maximum bending movement zone. Upon the application of cyclic loading a rapid increase in both number and length of cracks occurred. Most of the newly formed cracks were inside the maximum bending zone. Beams tested in uni-directional bending, however, show an appreciable decrease in the rate of increase in crack length after approximately 10,000 to 20,000 cycles and crack length was then practically constant for the remaining period of the test. In reverse bending series, although the number of cracks was comparable to that of the former series, the cracks were more extensive. As a result, the upper and lower cracks, induced by reverse movement, were observed to be connected and this in most of the cases occurred at early stage of cycling (see Figure 8.1). The actual cracking patterns, distribution and length at the end of the tests for five representative beams tested in uni-directional bending and one static test in sodium chloride solution are presented in Figures 7.1, 7.2, 7.3. In these figures the individual cracks length are indicated in 'mm' at the top of each crack. A

summary of crack data including the average crack length of representative beams is given in Table 7.1. From these data the following observations may be made.

1. Dynamic loading produced a significantly higher number of cracks and average crack length than a statically applied load.

2. Most of the cracks were formed in the maximum bending movement zone and only in rare cases were cracks observed out side the solution jacket or the central 1200 mm portion of the beam in air tests.

3. For the range of steel stresses investigated, the results suggest that the test duration, type of the surrounding solution and the load level have no effect on the observed number of cracks.

4. The average length of cracks is slightly greater at higher load levels.

5. In contrast to what was observed in static tests, dynamic tests produced fairly uniform crack lengths.

Using an illuminated microscope, with a scale division of 0.01 mm, the crack widths were measured for beam MU605W (dynamic) and beam ML603N (static). The results are given in Table 7.2 from which it can be seen that reasonably uniform crack lengths and widths resulted from cyclic loading whereas much more scattered values were observed in static tests.

7.3 Dynamic Tests.

7.3.1 Uni-directional Bending Series.

Beam Deflection.

The variation of maximum mid span deflection with

number of cycles is shown in Figures 7.4 and 7.5. Figure 7.4 shows the results of Stage I of the programme and also incorporates two representative results for beams tested in Stage II at lower stress levels for comparison purposes. Figure 7.5 presents the same parameter obtained from the multiple tests of Stage II. These Figures indicate the continuous increase in the deflection with number of load cycles with higher deflections being associated with higher stress levels. The start of fatigue loading led to a rapid increase in deflection. For beams which failed in fatigue, for which comparison in terms of percentage fatigue life (N/N_F) can be made, most of the increase occurred during the first 10% of the fatigue life. This trend is described in Table 7.3 and also shown in Figure 7.6 which relates the percentage fatigue life N/N_F to the increase in deflection expressed as a percentage from the initial deflection i.e. D_n-D_o/D_o where D_n, D_o are the deflection at 'n' number of cycles and the initial deflection respectively. (The initial deflections were determined by applying the maximum load statically prior to fatigue loading). However, for these beams and the remainder of the tests beams, the deflection increased in a curved form to about 50 to 100 x 10^3 cycles after which it took a linear form with varying slopes depending on the fatigue load level until either failure occurred or the experiment was terminated. From Figure 7.6 it is interesting to note that the relative deflections at failure are identical for a given stress level irrespective of their fatigue life (N_F). Other important information Figure 7.6 conveys is:

1. The slopes of the linear portions of the curves, which occupy the larger proportion of the fatigue life, are distinctly higher in lower stress levels of 0.4 and 0.6 f_y. For these particular tests the value N_F was assumed to be the number of cycle at which the tests were terminated without failure i.e. approximately 2,150,000 cycles, therefore, the actual slopes are even steeper.

2. The increase in relative deflection is noticeably higher at lower stresses. It appears, however, that there is an optimum stress level for this change to occur, and according to this figure this is observed to be 0.6 f_y.

It should be pointed out that this Figure describes the change in deflection in relative terms whereas the absolute values were directly proportional to steel stress as mentioned earlier.

Range of Deflection.

The range of deflection is defined as the algebraic difference in deflection between minimum and maximum load. As in the preceding section, results from stage I and two representative results of beams at a lower stress level from Stage II are shown in Figure 7.7 while the results of Stage II are presented in Figure 7.8 (which also indicates the reproducibility of the multiple tests conducted under identical test conditions). In the early stages of the test, all tests showed an increase in the range of deflection. However, apart from an air test, these early increases subsequently ceased and were followed by progressive reduction in this parameter. The observed decline in deflection range was coincident with visual observation of progressive blocking of the concrete flexural cracks with white deposit. The formation of this material, composition and the point at which this phenomenon became influential were load and environment dependent and will be discussed in detail in Chapter 8.

Given in Figures 7.9 and 7.10 are the maximum, minimum and range of deflection for different stress groups represented by beams MU75W, MU85W and MU605N, MU405N respectively. These figures show that a rapid increase in curved form occurred initially in both maximum and minimum deflection with a higher rate of increase being associated with maximum deflection values. As a result an increase in range of deflection was observed up to certain points where both maximum and minimum

deflection curves took a straight line form but the minimum deflection rates of increase became faster than the maximum ones due to the increasing influence of crack blocking.

For lower stress levels, Figure 7.10, the maximum and minimum deflections attained, rather early, approximately the same rate of change after which the deflection ranges stabilised at fairly constant values.

Due to the fact that most of the dramatic changes in behaviour in this series (uni-directional) occurred in the early stages of the tests, data presentation on a semi-log graph provides an appropriate way of permitting comparisons. Thus, deflection histories for beams MU70N, MU70W and MU70A (air test) are presented in this manner in Figure 7.11 and 7.12 respectively. Figure 7.12 showed that, for the beam tested in air, the rate of increase of maximum deflection was greater than that of minimum deflection over the whole test duration leading to a continuous increase in deflection range. When comparing Figures 7.7, 8, 9, 10, 11 with Figure 7.12 the change in response to fatigue loading due to environmental interference became clear.

Crack Width.

Crack widths in the concrete showed responses to blocking phenomenon similar to those observed in deflection. Figure 7.13 presents the variation with test duration of the crack opening range for four representative beams tested in tapwater, sodium chloride solution and in air. In three of these beams, two crack were monitored (annotated A and B). This figure indicates that the air test did not show any decline in crack opening range. For the other tests, although different cracks monitored on the same beam exhibited a decline in the crack opening range, indicative of the onset of blocking, these declines were often not coincident. The maximum, minimum and range of crack openings are presented in semi-log form in Figure 7.14 for two long running beams, namely MU70W and MU70N. For comparison with the air

test, where blocking was absent, the same parameters are presented in the same manner in Figure 7.15 for beam MU70A.

Table 7.4 gives the percentage increase in crack width at maximum load after 10% of the fatigue life and the last recorded value before failure (approx 100% of the fatigue life). This table indicates that although some of the cracks showed substantial increase in width during the first 10% of the fatigue life (an increase of about 60%) close to that trend observed in deflection data, some other cracks showed rather different histories in that the increase was proportional to the percentage fatigue life as given in line 2 and 4 of this table. This behaviour is further illustrated diagrammatically in Figure 7.16 which present the relative increase in the maximum crack width over the test duration of two cracks monitored on beam MU70N. Another important aspect shown in this Figure is that the cracks appear to have a dormant period which covered approximation 20-30% of the fatigue life during which very small increases and in some cases slight decreases occurred in the maximum width. the increase, nevertheless, resumed over the remaining period of test. In this respect, it should be pointed out that in both cases ie. dormant and active periods, the influence of crack blocking on the range of crack width was still evident as shown in Figure 7.14 mentioned earlier.

7.3.2 Reverse Bending Series.

Beam Deflection.

Figure 7.17 shows the maximum deflection change during fatigue loading for nine beams tested under this type of loading regime. Generally the deflection was proportional to the applied load with a distinctly lower rate of increase being associated with tests at lower load levels. The increase in the relative deflections for four beams are presented in Figure 7.18 which indicates a similar trends to that observed in the uni-directional series in that a larger proportion of the increase

occurred during the initial stages of the tests. However, in contrast to the former series, in one case (beam MR35N), the relative deflection curve started to decline after approximately 37% of the fatigue life ie. 446,700 cycles but a sharp increase in relative deflection was observed at later stage just prior to failure.

In all the tests except beam MR35W the deflection range exhibited a continuous increase during fatigue loading until failure intervened, Figure 7.19. For the longest-life beam MR35W, however, the increase subsequently ceased and was followed by progressive reduction in this parameter. Again the decline was first recorded after approximately 446,700 cycles and was coincident with the observation of crack blocking. The mechanism by which this reduction occurred was different from that described for the uni-directional series in that it was a consequence of the reduction in both maximum and minimum deflection as shown in Figure 7.20.

Crack Width.

In this series, two separate cracks in each beam were also monitored and due to the reverse movement of the beams during testing, one of the monitored cracks was chosen from the upper part and the other from the lower part of the beam. Figure 7.21 shows the variation with test duration of the range of crack opening for representative beams from different locations ie. lower or upper parts of the beams.

The data presented in this figure indicates a continuous increase in crack opening range until failure for all the beams except in the long endurance beam MR35W which exhibited a steady decline at a relatively late stage. Figure 7.22 examines in some detail the history of two cracks monitored on beam MR70W2. It is interesting to observe some evidence of an early decline in the maximum crack opening for the upper crack (the solid circle). This decline, however, was offset by a progressive increase in minimum values leading to a fairly small rate of increase in the crack opening range. On the other hand

the monitored upper crack showed a small decline at a later stage after which the increase in the crack range apparently ceased. Figure 7.23 presents the same parameter for a crack from the lower region of beam MR35W (this beam was the only one in this series with visible crack blocking) from which it can be seen that the maximum width, induced by downwards load, exhibited a reduction which did not immediately result in a reduction in crack range. A higher rate of reduction in maximum crack width, however, eventually resulted in a steady decline in the range of crack width for the remaining period of the test.

7.3.3 Neutral Axis Position.

Beams MU85N and MU85W were strain gauged on the concrete surface with 6 sets of 12 rows of demec points at 200 mm gauge length. The location of the points allowed the measurement of the concrete strain at 150, 450, 750 mm on either side of the centre line to be made. These locations were identical to those chosen for static tests (see Figure 7.26). To determine the N.A. depth, the concrete surface strain measurements were made at different loading stages starting from static load application prior to fatigue loading up to near failure at 387,600 cycles for beam MU85N. The measurements were made with the maximum load applied statically. The results are presented in Figure 7.24 which, in agreement with visual observations described in Section 7.2, indicates:

1. The initial stage of dynamic loading marked a sharp decrease in neutral axis depth (compare curves 1 and 2 of the lower part of Figure 7.24).

2. The rise in N.A. position continued but was not proportional to the elapsed number of cycles (compare curves 2 and 3 of the lower part of Figure 7.24).

3. At latter stages only a small decrease, 2-3 mm, in neutral axis depth occurred (curve 1 and 2 of the upper part of Figure 7.24).

7.4 Static Tests.

7.4.1 Introduction.

In order to assess the effect of cyclic loading on the behaviour and the load carrying capacity of the structural element it may be necessary to obtain both the static and the dynamic characteristics for exactly identical specimen details and loading conditions. Therefore three beams, one in uni-directional and two in reverse, were tested statically in air to simulate the effect produced by the first loading cycle at each load level. Each test specimen was subjected to static load in the sequence described later in this section and they were all instrumented to provide the required information. The use of strain gauges in these tests provides more accurate determination of the steel stresses developed upon each load application.

7.4.2 Instrumentations and Measurements.

Use was made of an 880 KN universal testing machine Figure 7.25a, for uni-directional test whereas a Losenhausen testing machine originally used for dynamic tests was used for reverse bending tests. Loads were applied and increased from zero at a slow rate up to values calculated to produce the required intended maximum steel stress for the highly tensioned bars (as pre-determined from a cracked section analysis described in Appendix A). The loads were applied starting from the lower load level to eliminate errors which may be introduced due to the hysteresis deformation involved if the tests were started at higher load levels. In an attempt to determine the concrete strain and the neutral axis position the beams were strain gauged by a series of Demec points on the concrete surface. The uni-directional tests beam (MU70855A) was provided with 6 sets of 12 rows of Demec points at 200 mm gauge length as shown in Figure 7.26. The reverse tests beams were provided with 6 sets of

18 rows of Demec points. The loading arrangements, however, prevented access to the second pairs of column (from the centre line), so the gauge length of these two sets was set at 100 mm as shown in Figure 7.27.

24 electrical resistance strain gauges of 20 mm gauge length were attached to the beam's main reinforcing steel in an arrangement shown in Figure 7.28 so that their centre lines were approximately coincident with the centre line of each Demec columns. Using an electronic recorder "Data Logger" continuous recording of strains was traced for each load level examined in this series. The corresponding steel stresses could therefore be calculated using the actual stress-strain curve for the reinforcing steel.

The mid span deflections were measured using a clock dial gauge of 0.01 mm divisions. The crack widths at the centroid of the tension reinforcement were determined using an illuminated microscope with a scale division of 0.01 mm.

Upon completion of tests, the loads were increased until failure occurred. The ages of the beams at the time of test ranged between 69 and 81 days.

7.4.3 Results.

Uni-directional Static Test, (beam MU70855A):

This beam was tested in uni-directional bending. Loads were applied in two cycles in the following loading sequence:

	Maximum downwards load (KN)
First cycle	21, 22.5, zero, 25.5
Second cycle	0.00, 21.0, 22.5, 25.5

A minimum load of 3 KN was applied after the application of each maximum load. During the test steel strain, concrete strain, mid span deflection and crack widths were

monitored. The load was then increased in slow rate until failure occurred at 37.5 KN. The results of this tests are tabulated in Table 7.5a,b,c. Table 7.5a gives the deflection and crack width for the first loading cycles. The monitored cracks were chosen inside the maximum bending moment zone, a comparison of steel stresses obtained both theoretically and experimentally is presented in Table 7.5b from which it can be seen that stress values obtained using the experimentally determined N.A. yielded close values to those determined theoretically using the cracked-section analysis. The actual steel stresses values, however, which may be considered as the values obtained from strain gauges measurements, were approximately 7% higher than the theoretical ones. The steel stress profile up to 75 cm from the beam centre line, thus covering the maximum bending movement, zone is given in Table 7.5c and presented diagrammatically in Figure 7.29 from which it can be seen, as would be expected, that the steel stress decreased as the distance from the centre line increased with higher stresses being associated with higher load levels. The second load cycles produced an increase in stress levels over the whole bar length under examination. Of special interest is the residual stresses at zero load, Table 7.5c indicates that the percentage residual stresses expressed as a percentage from the preceding stress was increasing as the distance from the centre line increases.

Reverse Bending Static Tests (Beams MR70855A & MR7595A):

Due to the reverse movement involved in this kind of test which may cause damage to the attached strain gauges, it was decided to reduce the load cycles sustained by the gauges thereby testing two beams instead of one to provide the required data on the three steel stress levels employed in the main dynamic test series i.e. 0.7, 0.75 and 0.85 f_y.

The loading sequence of these beams was as follows:

Beam	downwards load (KN)		upwards load (KN)
MR70855A	21.0		16.0
	25.5	zero	19.5
MR75955A	22.5		17.0
	28.5	zero	21.5

The beams were then loaded to failure, failure occurred at 42 and 39 KN respectively. The measured deflection parameters are presented in Table 7.6a,b and a summary of results obtained from both beams including the steel stresses along the central 1500 mm portion of the steel bars, neutral axis depths and a comparison between the theoretical and the experimental steel stress is presented in Table 7.7.

Typical concrete strain-beam depth diagrams for N.A. depth measurement are presented in Figure 7.30a,b. It appears from the summary Table 7.7 that the measured steel stresses using the electric strain gauges are considerably higher than the calculated values using the actual N.A. depth. Some of the measurements were even unrealistic it seems, therefore, that the type of gauge used is inappropriate for this kind of loading.

7.5 Discussion.

7.5.1 General.

The serviceability behaviour of structural elements presents the most important aspects of the assessment of the degree of damage experienced during service life. In the area of fatigue studies this consideration assumes an even more important role in indicating the risk of failure. The present study covers a range of steel stresses corresponding to 0.4 to 0.85 f_y of the characteristic proof strength of the high tensile reinforcement bars, which are the most fatigue-vulnerable component in the test specimens (Note: The characteristic proof strength is that proof strength below which 5% of

test results would be allowed to fall). According to B58110: 1985 the allowable steel stress in tension at the serviceability limit state is equivalent to 0.5 f_y for the particular section and material properties employed in this study. Therefore the interesting behaviour of beams tested at lower load level of 0.4 and 0.6 f_y may present realistic boundaries for conditions prevailing in reality. In the following sub-sections, the time dependent behaviour of reinforced concrete beams subjected to fatigue loading will be discussed with special emphasis on the influence of the surrounding environment. The problem of corrosion fatigue, however, is far too complex to be described from these data alone and for comprehensive account of the fatigue effects in aqueous environments to be made, this discussion should be viewed in connection with other discussion sections which appear in the following chapters as well as the final discussion chapter (Chapter 12) in which an attempt to link the various aspects will be presented.

7.5.2 Cracking During Dynamic Loading.

Unlike deflection data, the general trends in cracking during cyclic loading are more likely to be useful than their absolute values in terms of crack width, height and number. Direct quantitative comparison in crack width is not possible due to the random nature of crack distribution and size as well as the small number of cracks monitored due to practical difficulties. However, the data and observations presented in Sections 7.2 and 7.3 showed similar trends in response to the environment to those observed in deflection.

7.5.3 Deflection.

In general, the values of deflection at the maximum load are of more practical importance than the values at lower load level. The fact that maximum deflections increase significantly under the action of repeated loading is well known and has been reported in many

related fatigue researches.[62,68,69,72] Empirical expressions have also been proposed to predict the maximum deflection under this kind of loading. Several reasons were identified for this increase and these were discussed in Chapter 2. Table 7.8 and 7.9 present comparison in deflection parameters obtained from static tests and the latest recorded dynamic values for both loading regimes.

Previous corrosion fatigue researches[19,59,79] underlined the profound influence of the aqueous environment on the electrochemical as well as the structural behaviour of reinforced concrete specimens. Under favourable conditions, the formation of white deposits on the concrete flexural cracks constitutes the most important major event that effectively alters the test conditions in many aspects and certainly the structural one from predictable to less predictable type of behaviour, thus the general available informations which were mainly deduced from tests in air are no longer sufficient to describe the effect of fatigue loading for a given exposure condition where crack blocking is anticipated.

In all cases, the maximum deflections were proportional to the maximum intended steel stresses during the test period as shown in Figure 7.31 in which the maximum deflection vs. the steel stresses at different stages of the tests for the uni- directional series are presented. This figure also incorporates the theoretical deflection, calculated using the procedure outlined in Appendix A, and the data obtained from static tests. It can be noted that the initial increase in maximum deflection increases as the steel stress increases and beyond this stage, i.e. 30,000 cycles in Figure 7.31, the increase was independent of the steel stress. In the uni-directional regime crack blocking does not act opposite to the downwards movement which produces the maximum deflection, as a result, the maximum deflection continued to increase.

For test involving reverse movement, however, the movement restriction in a given direction is expected if the cracks at the opposite part of the beam are being

blocked, thus blocking at the upper cracks would cause a reduction in deflection in the downwards direction and vice versa. Under this loading regime blocking occurred only in beam MR35W in which both the lower and the upper cracks were blocked resulting in reduced deflection in both directions. Figure 7.20 indicates that the rate of decrease in minimum deflection i.e. the upwards movement was considerably faster than the decrease in maximum deflection indicative of more extensive blocking occurring at cracks at the lower part of the beam.

7.5.4 The Concept of Relative Deflection.

As described in Sub Sections 7.3.1 and 7.3.2, the increase in the maximum deflection expressed in terms of relative deflection was proportional to the fatigue life. Considering uni-directional series, for higher applied loads corresponding to 0.7, 0.75 and 0.85 fy the increase in the relative deflection was interrupted by the beam's failure with a maximum increase in the relative deflection ranging between 30 and 65%. This suggests that for beams already subjected to a substantial stress level where the initial deflections are relatively high only a small increase in maximum deflection due to cyclic loading is possible before failure and, perhaps more importantly, for a given load level, the beam failures occurred at different maximum deflections in relation to their fatigue life. The variation of relative deflection, however, with the cycle ratio (N/N_F) is independent of the number of cycles to failure.

For lower load level (0.4 and 0.6 f_y), although similar trends were observed, the difference, in relative terms, between the initial and final deflections is high. Clearly for the same amount of increase in deflection the relative deflection is higher for lower initial deflections than for higher. The time required to reach the critical stage and the eventual failure is equivalent to the fatigue life. The deflection change, thus, follows the expression:

$$D_f = D_o + \frac{dD}{dN} N_F \qquad \ldots 7.1$$

where D_f = maximum deflection at failure (fatigue life dependent).

D_o = the initial maximum static deflection which may be calculated using one of the existing methods.

$\frac{dD}{dN}$ = the rate of increase in deflection with number of cycles and according to Figure 7.6 its value is constant for a given stress level.

N_F = No. of cycles to failure.

In case of reverse bending, under favourable conditions for the development of crack blocking, the maximum deflection decreases beyond a certain point and hence the above predictive basis is no longer valid.

In any event, however, describing the fatigue behaviour and the eventual failure in terms of maximum deflection would underestimate the fact that the endurance is stress range dependent and this is particularly important in tests in an aqueous environment because of the expected change in stress range during cyclic loading and the effect of corrosion. The latter being more pronounced in low stress conditions.

7.5.5 Range of Deflection.

The mechanisms by which the deflection range changes are described in Subsections 7.3.1 and 7.3.2. This phenomenon was previously observed in fatigue tests conducted in seawater and considered as a significant factor in controlling the fatigue life. The cyclic stiffening, as it is sometimes called, is now a well known phenomenon. The present research examined a wide range of load levels in two less investigated environments, namely tapwater and sodium chloride solution. Consequently,

together with the available information from studies on fatigue in flexure in seawater, it appears that some definite conclusions may be made as to the conditions for the occurrence of this phenomenon and the limits to its occurrence. These aspects will be discussed in detail in the following chapter. Nevertheless despite the awareness of the causes its effectiveness still requires more attention and one of the major obstacles that prevents the introduction of the beneficial effects of crack blocking as a design criterion is that it is not possible to predict the extent of its effectiveness. In the following an attempt is made to analyse its effect qualitatively: As described previously, regardless of the environment and the magnitude of the initial stress range, the initial stage of cyclic loading marked a dramatic change in structural behaviour. A stable condition, however, was attained after a relatively short period of load application, i.e. 10,000 to 20,000 cycles and the tests proceeded under a condition of approximately constant cracks length and number together with a small rate of increase in deflection keeping the neutral axis depth at almost constant value. The possible contribution of concrete below the neutral axis to the tensile resistance is also drastically eliminated and reaches an eventual small constant level, yet unknown, at the end of this stage. The analysis of the section during the test is complex and certainly differs from that normally assumed for static loading conditions. However, it is safe to assume that the fatigue behaviour is entirely governed by the tensile steel.

Table 7.10 compares the deflection under statically applied load before and after different numbers of load cycles. These data assert the primary role of dynamic loading in producing both instantaneous and cyclic dependent deformation. However, although the maximum deflection (when no blocking occurs in the upper cracks) is not affected by crack blocking, the minimum deflection is particularly sensitive to it which upsets the assumed link between the load and the stress level. The load range was continuously monitored and remained substantially

unchanged throughout each test but the stress range was changing in line with the increase in minimum stresses as a result of the beam's failure to recover its original position upon the release of the maximum load.

As indicated earlier in Chapter 2 and 4, few data are available on the actual change in maximum stresses during dynamic loading. These include the work by Jagdish[65] and Bishara[66] who conducted fatigue tests in air on simply supported beam at 3 Hz and reported an increase in maximum steel stresses by 7% most of the increase occurred during the early stage of the tests. In more relevant research Paterson et al[59] fatigue tested an instrumented beam in seawater at a cyclic rate of 0.1 Hz and found that after an initial increase in both maximum deflection and maximum steel stresses their values remained substantially constant throughout the remaining test duration. Of special interest in what they found is the very close relationship between the reduction in steel stress range and the deflection range due to crack blocking. The relationship can be written as follows:

$$\frac{D_{r,n} - D_{r,o}}{D_{r,o}} = \frac{S_{r,n} - S_{r,o}}{S_{r,o}} \qquad \ldots 7.2$$

where $D_{r,n}$, $S_{r,n}$ are the deflection and stress ranges at a given n number of cycles respectively.

and $D_{r,o}$, $S_{r,o}$ are the initial deflection and stress ranges

However, in deducing the maximum and minimum steel stress variation during the tests using this relationship they assumed a constant maximum steel stress equivalent to the corresponding initial intended values with continuous increase in the minimum steel stress values.

In the respect, in generalising this important conclusion one should be aware of the fact that the aforementioned relationships is valid for the stable period during the test, in other words the relationship

should be dealt with more conservatively in describing the acute change in deflection occurring at the early stages which is not necessarily accompanied by parallel proportional changes in minimum steel stresses. Nevertheless, this conclusion is very useful in giving insight to the change in steel stresses in the absence of actual stress measurements and, therefore, was used in deducing the variation of steel stresses with test duration after the necessary modification described in the following sub section.

7.5.6 Change in Steel Stresses During Dynamic Loading.

Figure 7.32, 7.33 and 7.34 present the variation in deflection range (from experimental data) and steel stress range (calculated from Equation 7.2) with the test duration for the uni-directional series of Stage I and representative tests from Stage II. Except for the few cycles, where residual stress upon the release of maximum stress each load cycle may be appreciable, it seems rational to assume that during the period from the start of the test up to the reversal in deflection range, i.e. when crack blocking starts to be influential, the minimum steel stress is reasonably constant at its original intended value. Therefore the change in range of deflection reflects primarily the increase in maximum steel stress. However, beyond the point of inflection, which also marked the start of stable conditions, the maximum stress values are expected to be fairly constant and instead a progressive increase in minimum values starts to occur due to crack blocking. This assumption is made in calculating the increase in maximum steel stress which is indicated between parenthesis on the curves of each beam in these figures. In comparing these figures some interesting features are identified, these are:

1. Tests at higher stress levels of 0.75 and 0.85 f_y: tests in both tapwater and sodium chloride solution exhibited a comparatively late decline in steel stress range. The stress ranges, however, were higher than

the initial values throughout the test duration. The increase in maximum stress ranged between 15 and 35% with higher increases being associated with higher initial stress levels.

2. Tests at a stress level of 0.7 f_y: air tests exhibited continuous increase in stress range. Both tapwater and sodium chloride tests exhibited an early decline in steel stress range curves with higher reduction being associated with tapwater tests the increase in maximum steel stress ranged between 8 and 16% and the maximum decrease in the range of steel stresses was 45% and 30% respectively.

3. Tests at lower steel stresses of 0.4 and 0.6 f_y: the increase in maximum steel stress ranged between 4% and 9%. The percentage reduction in steel stress range was higher in tapwater than in chloride solution. For tests at 0.4 f_y this percentage was 35% and 16% respectively. Higher reduction was observed in the tests at 0.6 f_y.

The deduced data presented above is in broad agreement with the observation made on crack blocking in that:

1. The beneficial effect of crack blocking is diminished in tests at higher load levels due to the lower rate of stress range reduction.

2. The significantly greater amount of crack blocking deposits observed in tapwater tests resulted in greater reductions in stress range than those involving sodium chloride solution. This in turn, can be rationalised in terms of increased solubility of salts in solutions of higher salinity as is discussed in more detail in Chapter 8.

7.5.7 Comparison with Tests in Seawater.

Directly comparable results from parallel research at Glasgow University conducted in seawater under identical test conditions[19.79.150] are presented in Figure 7.35. This figure shows the change in deflection and steel stress ranges for 3 beams tested at load levels corresponding to 0.4, 0.6 and 0.85 f_y. These beams were all terminated without failure after 30.5 x 10^6, 35.6 x 10^6 and 13.32 x 10^6 cycles respectively. When comparing with other results conducted in tapwater and sodium chloride solution, it is clear that blocking is more fully developed in seawater than the other two environments due mainly to the observed earlier decline in deflection and stress curves (in most cases within the first several hundred cycles) and to the ensuing high rate of decrease in these parameters. The greater proportion of this change occurred within the first 100,000 cycles and as a result the tests were proceeded under appreciably lower steel stress ranges up to the termination of the tests.

The more rapid initiation and occurrence of crack blocking in seawater in comparison with 3.5% NaCl solution (which has about the same total salt content as normal seawater) and water is understandable in view of the Ca^{2+}, Mg^{+2} and bicarbonate/carbonate contents of seawater. Again this will be discussed in some greater detail in the following chapter.

7.5.8 Hypothesis for the Change in Steel Stresses under Dynamic Loading in Aqueous Environment.

Evaluation of the experimental results of this study, as well as other studies, the works of Arthur et al[19.79] and Paterson et al[59,203] in particular, led to the following hypothesis for the effect of environment on the actual steel stresses under cyclic loading. The cyclic loading causes a rapid increase in deflection and crack width and height which may be attributed primarily to the increase in bar slip at crack locations due to bond deterioration at concrete steel interface as well as the

progressive elimination of the possible contribution of cracked concrete below the neutral axis to tensile resistance. This change results in an increase in the maximum steel stresses over its initial intended value. This increase is proportional to the original value. For loading conditions more realistically related to service loading this increase was found not to exceed 10%. Meanwhile the minimum steel stress exhibits an initial increase in a form of residual tension stresses upon the release of the maximum load which rapidly decrease during the first few cycles and levels off at the minimum intended steel stress. This stage is marked S_{min1} in Figure 7.36.

Under favourable conditions, crack blocking effectively intervenes and produces a decline in the deflection range due to the inability of the beam to recover its minimum deflection upon unloading to the minimum load level on each load cycle. In this stage the change in deflection range is approximately in agreement with the change in steel stress range. Since the maximum steel stress is stabilised, the change in steel stress range is due principally to the increase in minimum steel stress.

Thus blocking produces a decrease in stress range, tending to prolong the fatigue life, although the corresponding increase in the mean stress acts in the opposite way.

The significant conclusion from the afore described changes is that this phenomenon effectively changes the loading regime from constant amplitude loading to multiple stage variable amplitude testing, in terms of steel stresses, Figure 7.36, with stress cycles varying in magnitude, number and order, i.e. variable peak-constant trough in the first stage to constant peak-variable trough in the following stages. The sequence in which repeated loads of different magnitudes are applied has a considerable influence of fatigue life, but it is difficult to predict.

According to the test results, tapwater is more effective, particularly at lower load level, than sodium

chloride solution in reducing the steel stress range due to crack blocking. Sea water, however, produces significantly higher changes than both other environments due to the same phenomenon, and as mentioned earlier, these relative effects of environment are due to solubility effects to be discussed in Chapter 8.

7.5.9 Comments on the Change in Steel Stresses During Cycling.

The mechanism of structural change during cyclic loading as summarised in the preceding section indicates an interesting case in that, as a result of fatigue loading, a time-dependent increase in the maximum steel stresses appeared to develop a constant moment condition of the tests. This observation, however, is clearly in breach of the equilibrium equations as deduced from the elastic theory assumptions, although both the maximum applied steel stresses, as indicated by strain gauge measurements, and the maximum steel stresses during cycling are, mostly, within the elastic region of stress of the Torbars.

According to the elastic section analysis, the tensile strength of concrete may be ignored if a crack has commenced at the extreme tension fibre. Consequently, the increase in crack lengths and the subsequent rise of the N.A. would cause proportional increase of the lever arm of the internal resisting couple which would result, for constant applied moment, in lower tensile stresses in contrast to the actual observations. Clearly such a decrease in the maximum stresses during dynamic loading is not possible as fatigue failure in tension would, most probably, involve an increase in maximum steel stresses.

However in the absence of actual steel and concrete stress measurements, an attempt to determine the causes for this phenomenon will be highly spectulative. Therefore, further detailed investigations are obviously required to determine, more accurately, the complex internal change in section properties during cyclic loading. In this respect, detailed monitoring of steel and

away from the cracks during the test, although still practically difficult, can provide vital informations which help for better understanding of the problem.

Table 7.1: Summary of Crack Data for Typical Beams.

Beam Designation	Environment	Loading Regime	No. of Cracks	Average Length of Cracks (mm)	Test Duration (Months)
MJ405W	Water	Dynamic	10	141	5
MJ601N	NaCl		10	162	1
MJ605N	NaCl		12	145	5
MJ605W	Tap Water		11	164	5
MJ75W	Tap Water		11	176	1
MJ85	Tap Water		11	168	1
MJ70A	Air		14	167	5
ML603N	NaCl	Static	6	112	3

Table 7.2: Crack Width and Length for Beam MJ605W and ML603N.

Crack No.	Beam MJ605W Cracks		Beam ML603N Cracks	
	Length (mm)	Width (mm)	Length (mm)	Width (mm)
1	170	0.1	80	0.1
2	172	0.155	150	0.13
3	182	0.102	50	0.02
4	125	0.130	120	0.08
5	185	0.118	150	0.10
6	175	0.135	120	0.12
7	185	0.124		
8	175	0.140		
9	45	0.08		
10	197	0.102		
11	190	0.125		

Table 7.3: Increase in Maximum Deflection During Fatigue Life for Uni-directional Testing Beams.

Beam Designation	Initial maximum deflection (mm) 1	Last recorded maximum deflection before failure (mm) 2	Increase in maximum deflection after 10% of fatigue life (%) 3	Increase in maximum deflection just before failure (%) 4	Col. 3/Col. 4 (%)
MJ70A	7.00	10.73	38.2	53	72
MJ70N	6.27	9.91	51	58	88
MJ70W	5.85	9.60	49	64	77
MJ75N	8.10	10.91	24	34	70
MJ75W	9.00	12.0	25	32	80
MJ85N	8.58	12.17	31	42	74
MJ85W	9.45	13.33	32	41	78

Table 7.4: Increase in Maximum Crack Width During Fatigue Life for Beam MJ70N and MJ70W.

	Beam Designation	Initial maximum crack width (mm) 1	Last recorded maximum crack width before failure (mm) 2	Increase in maximum crack width after 10% of life % 3	Increase in maximum crack width before failure % 4	Col.3/Col.4 % 5
1	MJ70N (A)	0.144	0.338	73	135	54
2	(B)	0.135	0.428	37	217	17
3	MJ70W (A)	0.118	0.288	83	144	57
4	(B)	0.131	0.714	67	545	12
5	MJ85N	0.111	0.273	88	146	60

Table 7.5a: Static Test Results - Beam MU7085SA. Deflection and Crack Width Measurements.

Load (KN)	Deflection (mm)			Crack width (mm)*	
21.0	Max	Min	Range	Crack No: 1	Crack No: 2
21.0	7.1	2.63	4.47	0.3	0.21
22.5	8.2	2.82	5.33	0.45	0.38
25.5	9.42	3.13	6.29	0.55	0.50
37	Failure				

* For 2 randomly chosen cracks from the central maximum bending moment zone, the readings represent the width at the level of tension steel bars.

Table 7.5b: Static Test Results - Beam MU7085SA: Comparison of Steel Stresses Measured by Different Methods.

Load	Maximum Steel Stress (N/mm^2)				N.A. Depth (mm)	
(KN)	Theoretical (cracked-section analysis)	Deduced from experimental N.A. values	Deduced from strain gauge measurements		Theoretical	Experimental
			1st cycle	2nd cycle		
21.0	322	331	346	381	53.5	51.0
22.5	345	354	361	399	53.3	49.0
25.5	391	401	424	436	52.6	48.0

Table 7.5c: Static Test Results and Beam MJ7085SA. Electric strain gauge measurements.

Load (KN)		Average Steel Stress (N/mm^2) Distance from ℄ (mm)		
		150	450	750
First Cycle	21	346	271	215
	22.5	361	309	260
	0.0	135 (37%)	128 (41%)	116 (45%)
	25.5	424	370	299
Second Cycle	0.0	119 (28%)	131 (35%)	111 (37%)
	21.0	381	340	264
	22.5	399	354	279
	25.5	436	386	305

* Values in parentheses are the percentage of the steel stress remaining at zero load relative to the previous maximum stress values.

Table 7.6a: Static Test Results - Beam MR7085SA: Deflection Measurements.

Load (KN)		Deflection (mm)			
Downwards	Upwards	First cycle	range	second cycle	range
21.0		7.88		8.16	
	16.0	-2.35	10.23	-2.54	10.70
25.5		9.24		9.48	
Zero				2.59	
	19.5	-4.25	13.49	-4.57	14.05
42.0		Failure			

Table 7.6b: Static Test Results - Beam MR7595SA. Deflection Measurements.

Load (KN)		Deflection (mm)	Range of deflection (mm)
Downwards	Upwards		
22.5		8.31	
zero		3.10	
	17.0	3.08	11.39
28.5		12.20	
zero		3.45	
	2.15	5.34	17.54
39		Failure	

Table 7.7: Static Test Results - A Summary of Results for Reverse Bending Static Tests.

Load (KN) downwards	Average steel stress (N/mm^2) Distance from midspan in (mm)			N.A. Depth (mm)	Steel stress N/mm^2	
	150	450	750		Theoretical	from experimental N.A. value
21.0	411	291	175	52.1	322	330
22.5	433	312	187	56.0	345	357
25.5	472	341	291	49.0	391	399
28.5	676	462	357	48.0	437	445

Table 7.8: Comparison of Deflections for Uni-directional Static and Dynamic Tests.

		Deflection (mm)			Applied Load (KN)	
		Max.	Min.	Range	Max.	Min.
Static test		7.10	2.63	4.47		
Dynamic tests	Water (1,758,700 cycles)	9.60	7.24	2.36	21.0	3.0
	NaCl (1,076,000 cycles)	9.91	7.29	2.62	(0.7 f_y)	
Static test		8.20	2.87	5.33		
Dynamic tests	Water (532,500 cycles)	12.0	6.82	5.12	22.5	3.0
	NaCl (399,590 cycles)	10.91	6.22	4.69	(0.75 f_y)	
Static test		9.42	3.13	6.29		
Dynamic tests	Water (344,305 cycles)	13.33	6.98	6.35	25.5	3.0
	NaCl (385,500 cycles)	12.17	6.93	5.24	(0.85 f_y)	

Table 7.9: Comparison of Deflections for Reverse Static and Dynamic Tests.

		Deflection (mm)			Applied Load (KN)	
		Max.	Min.	Range	Max.	Min.
Static test		8.16	-2.54	10.7		
Dynamic tests	1. Water (160,070 cycles)	11.29	-4.64	15.98		
	2. Water (116,500 cycles)	12.11	-7.09	19.20	21.0	-16.0
	NaCl (28,600 cycles)	11.57	-6.83	18.40	(0.7 f_y)	
Static test		8.31	-3.08	11.39		
Dynamic tests	Water (71,200 cycles)	12.28	-6.42	18.70	22.5	-17.0
	NaCl (27,980 cycles)	9.81	-7.89	17.70	(0.75 f_y)	
Static test		9.48	-4.57	14.05		
Dynamic tests	Water (25,800 cycles)	15.15	-6.20	21.35	25.5	-19.5
	NaCl (4,700 cycles)	14.8	-6.98	21.78	(0.85 f_y)	

Table 7.10: Effect of Cyclic Loading on the Static Deflection.

Beam Designation	Loading Description	Max Deflection (mm)
MU85W	Statically applied load before cycling	9.45
	Statically applied load after 72,000 cycles	11.33
	Under cyclic loading after 72,000 cycles	11.42
MU85W	Statically applied load before cycling	8.58
	Statically applied load after 99,000 cycles	12.66
	Cyclic loading after 99,000 cycles	12.87

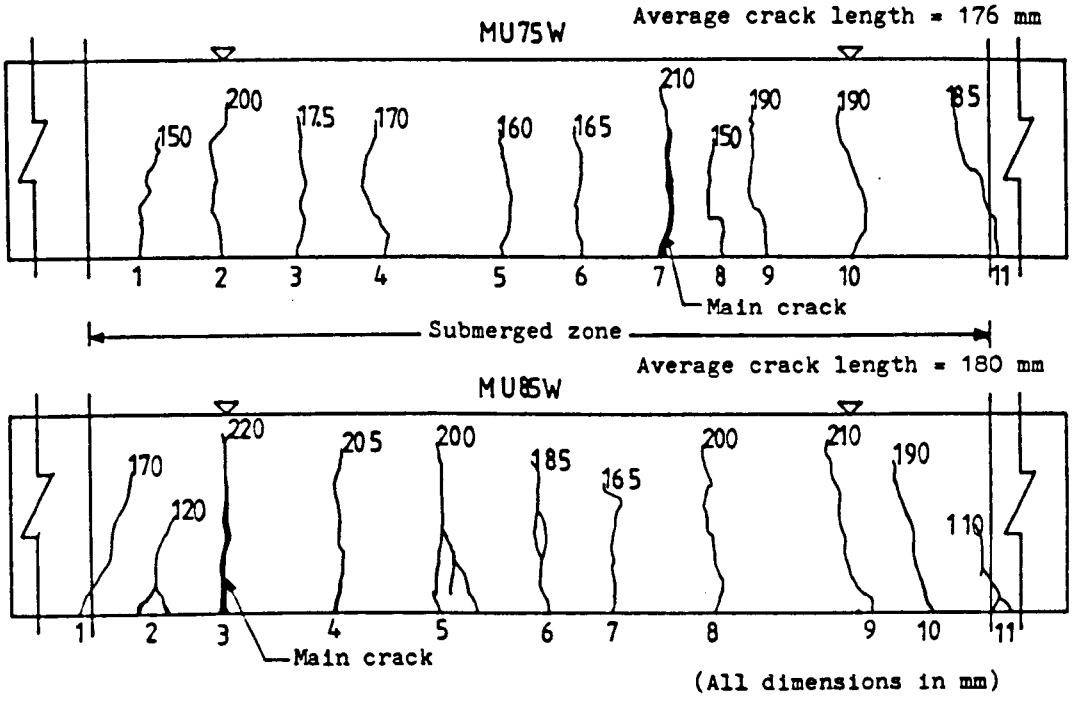

Figure (7-1): Actual crack pattern;beams MU75W and MU85W.

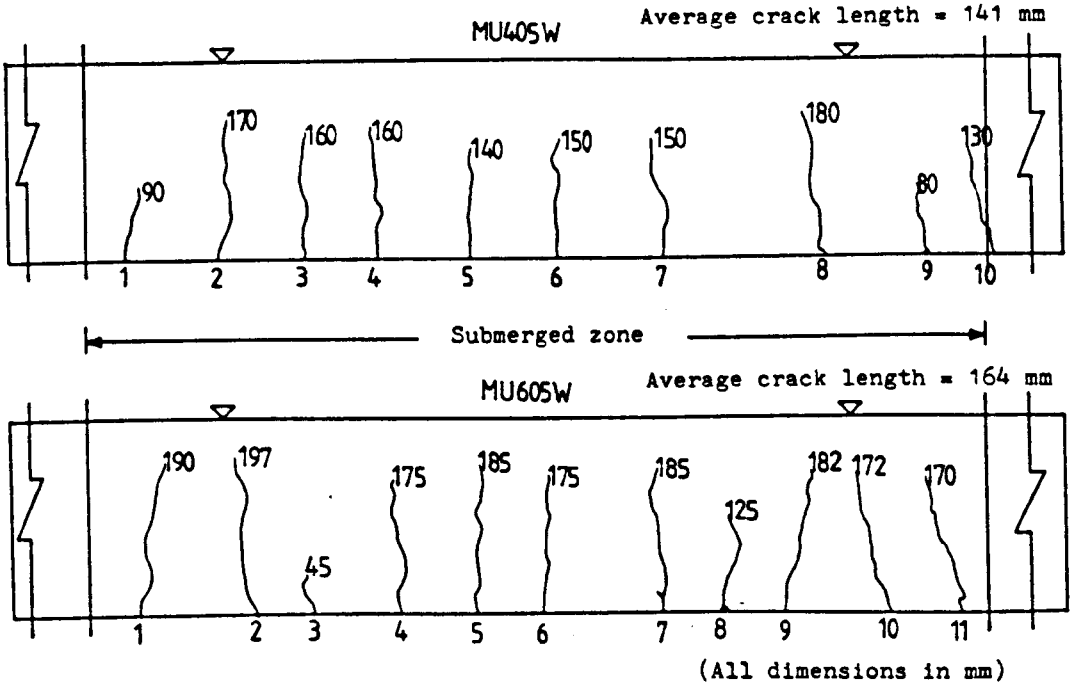

Figure (7-2): Actual crack pattern;beams MU405W and MU605W.

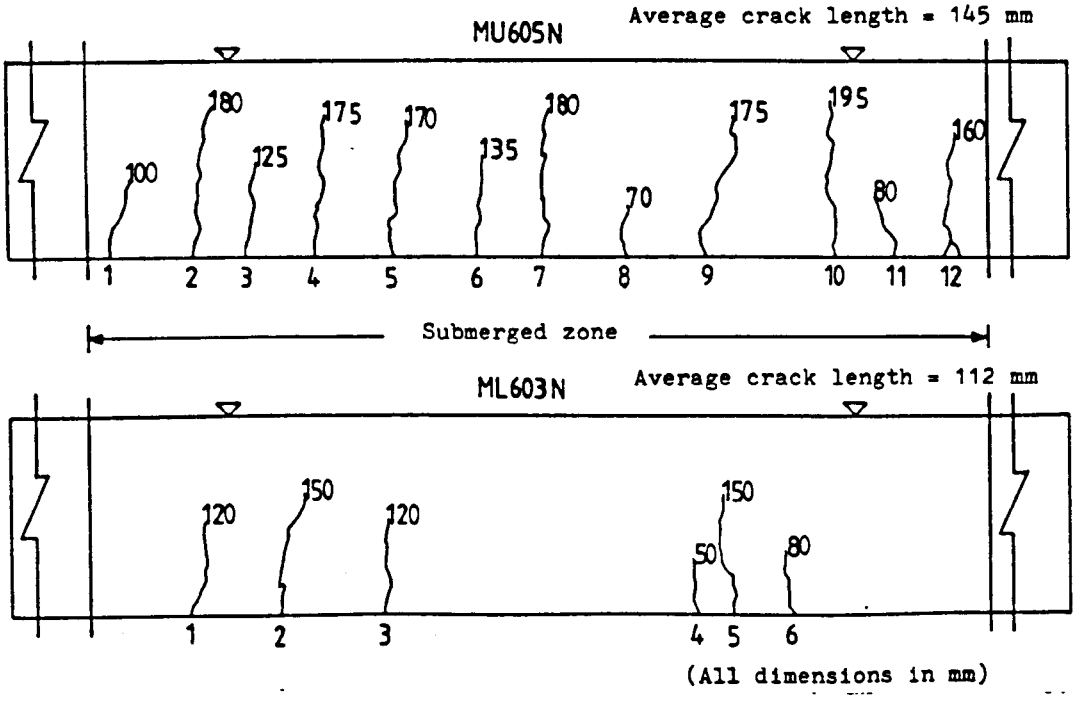

Figure (7-3): Actual crack pattern;beams MU605W and ML603N.

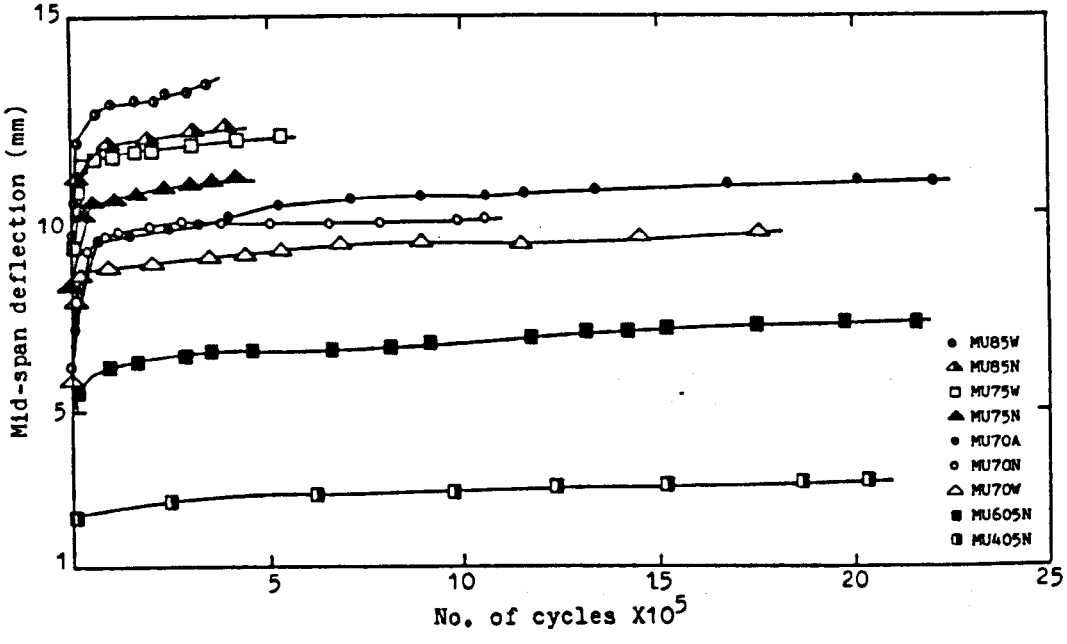

Figure (7-4): Uni-directional test series;maximum deflection vs. No. of cycles.

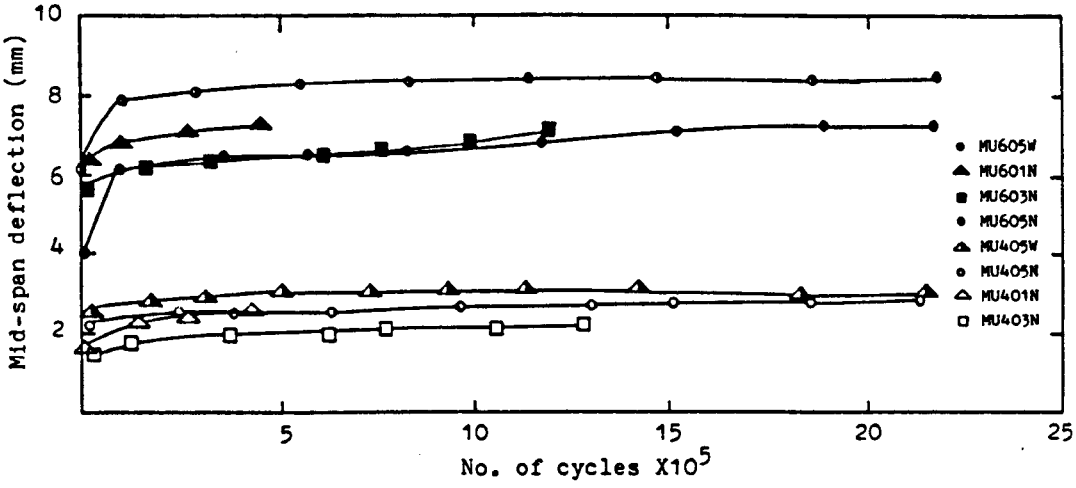

Figure (7-5): Uni-directional bending series;stage II,maximum deflection vs. No. of cycles.

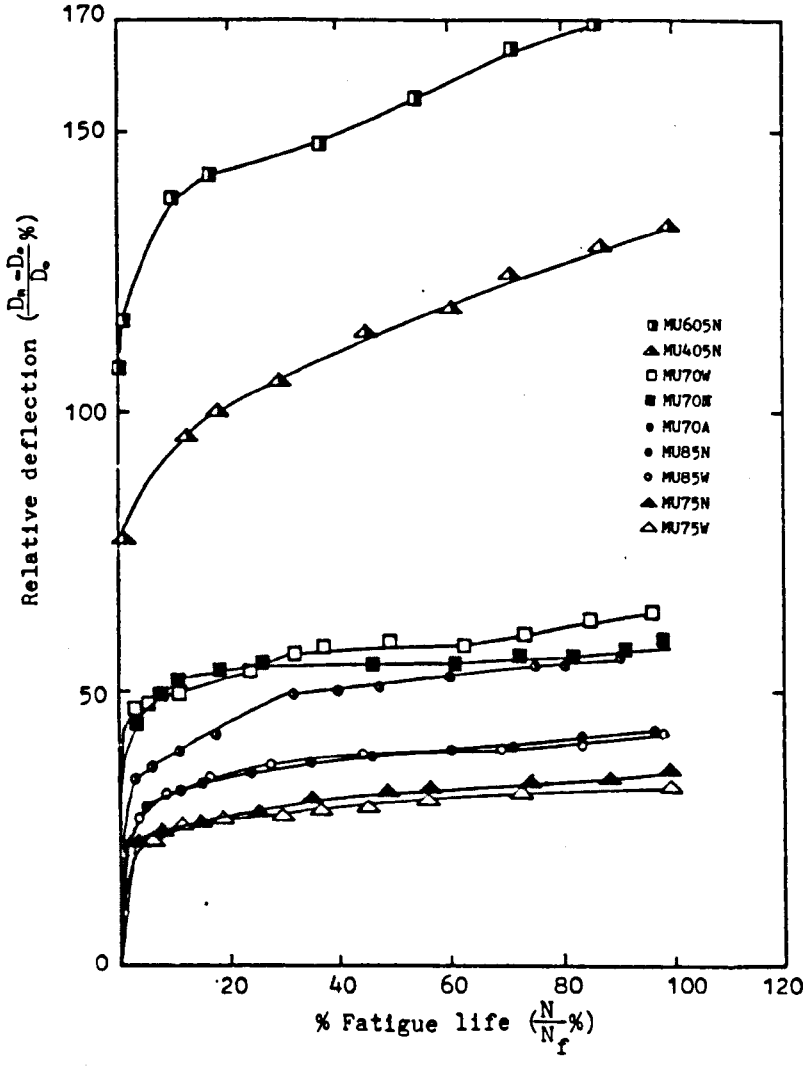

Figure (7-6): Uni-directional bending series; percentage increase in deflection vs. % fatigue life.

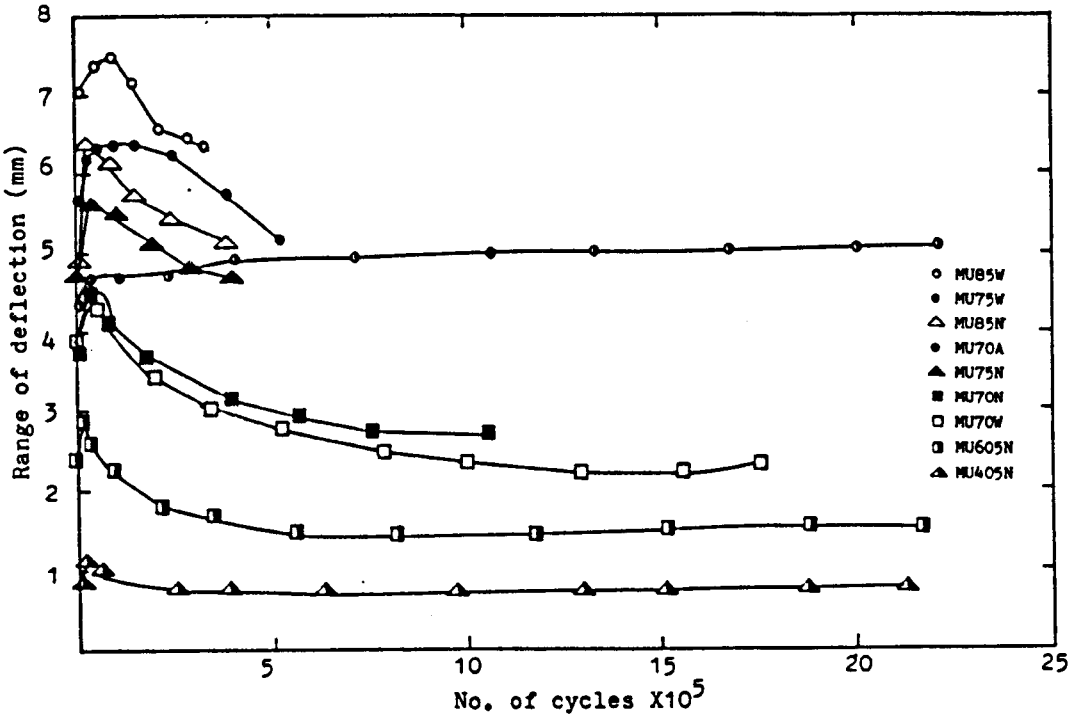

Figure (7-7): Uni-directional bending series;range of deflection vs. No. of cycles.

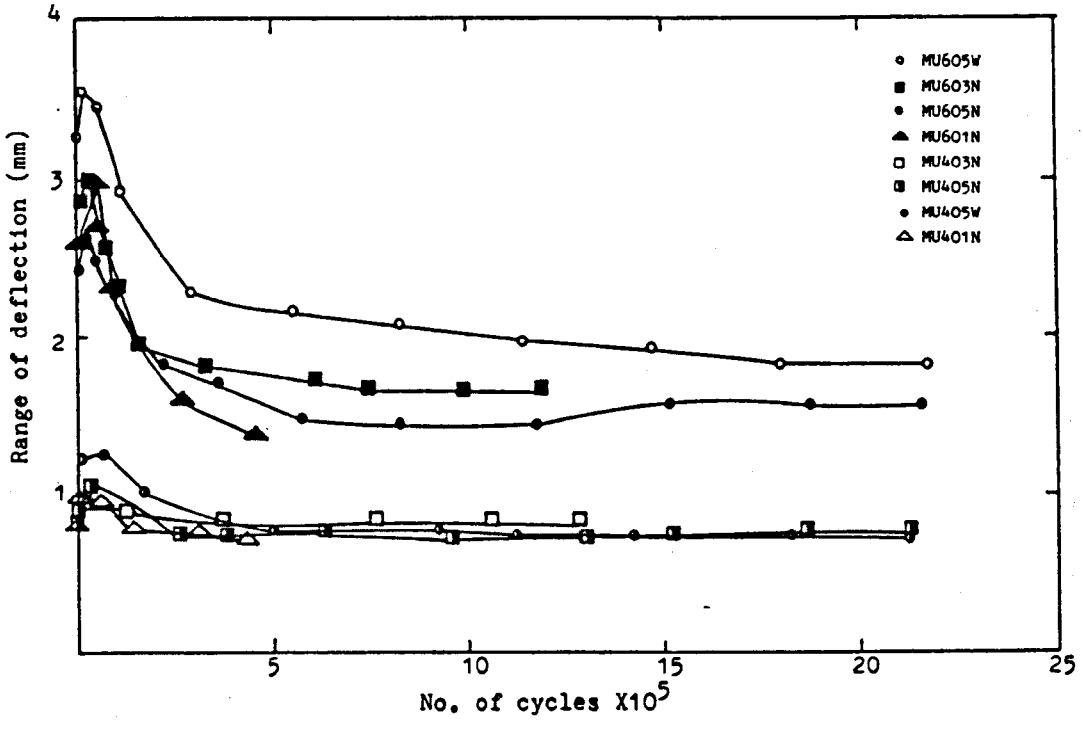

Figure (7-8): Uni-directional bending series;stage II,range of deflection vs. No. of cycles.

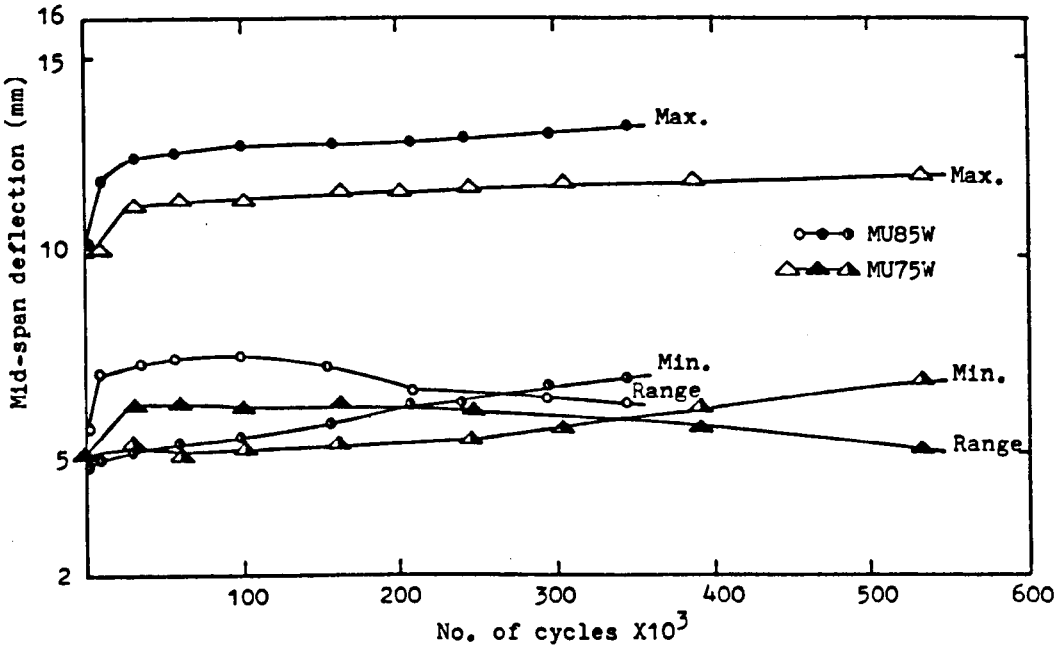

Figure (7-9): Uni-directional series;maximum,minimum and range of deflection for beams MU75W and MU85W.

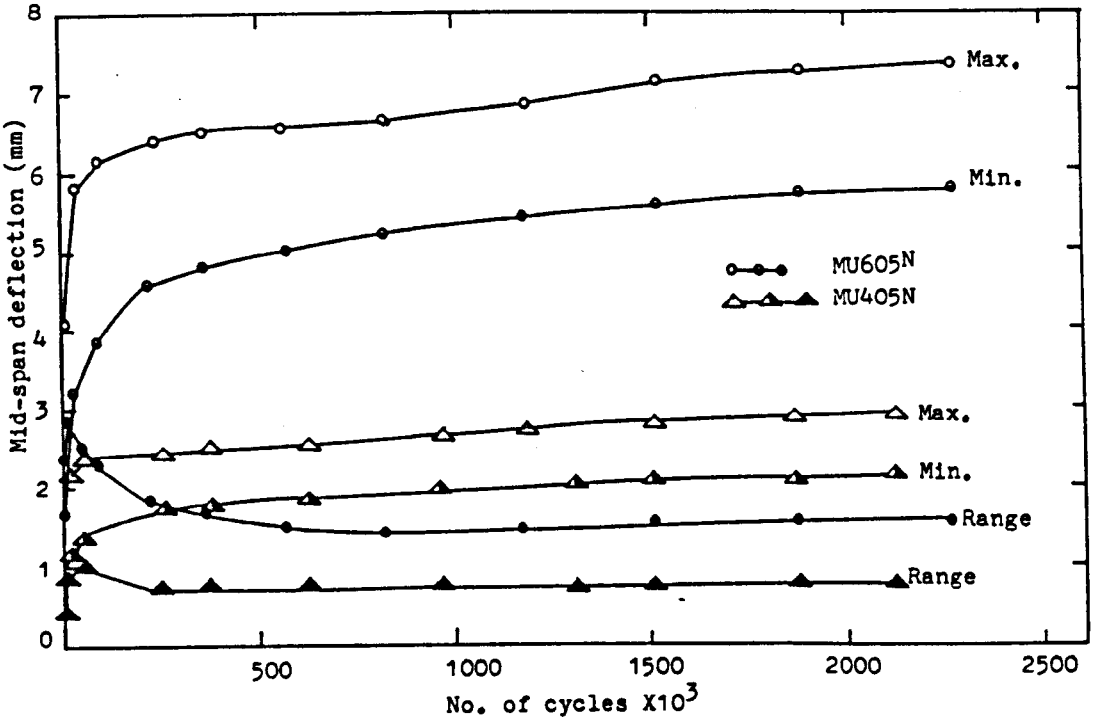

Figure (7-10): Maximum,minimum and range of deflection for beams MU605N and MU405N.

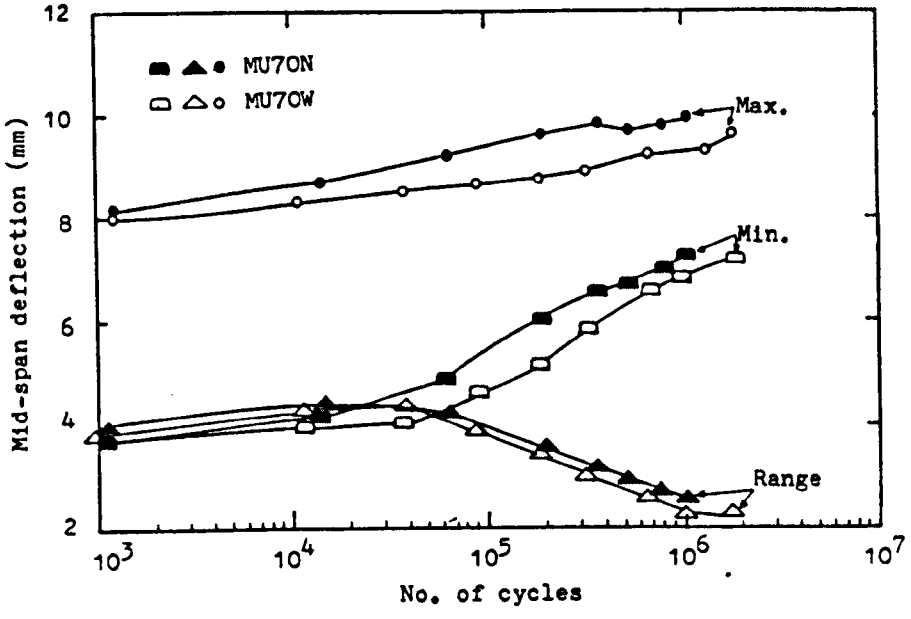

Figure (7-11): Beams MU7OW,MU7ON maximum,minimum and range of deflection vs. No. of cycles.

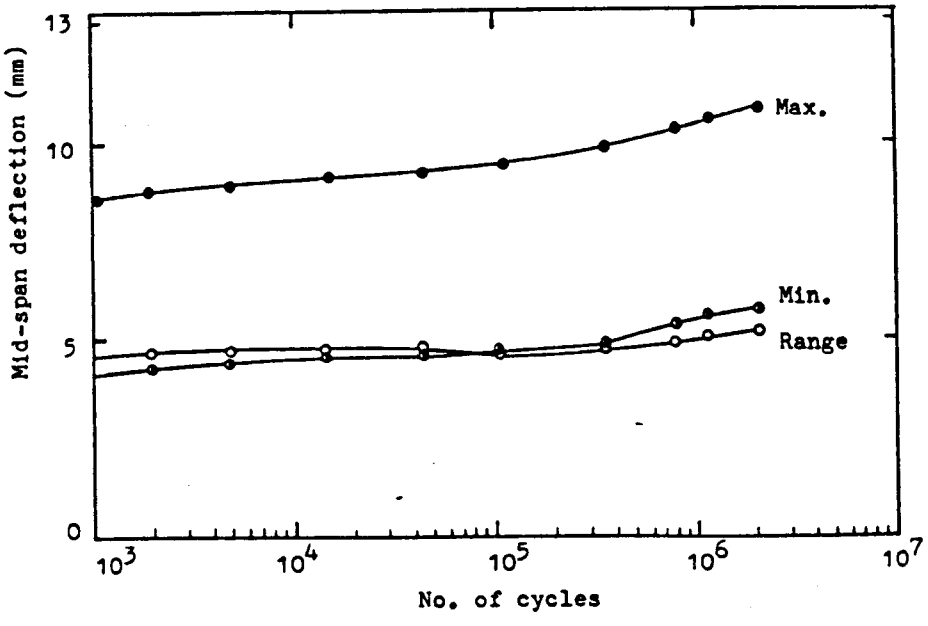

Figure (7-12): Uni-directional bending series;beam MU7OA in air,maximum,minimum and range of deflection.

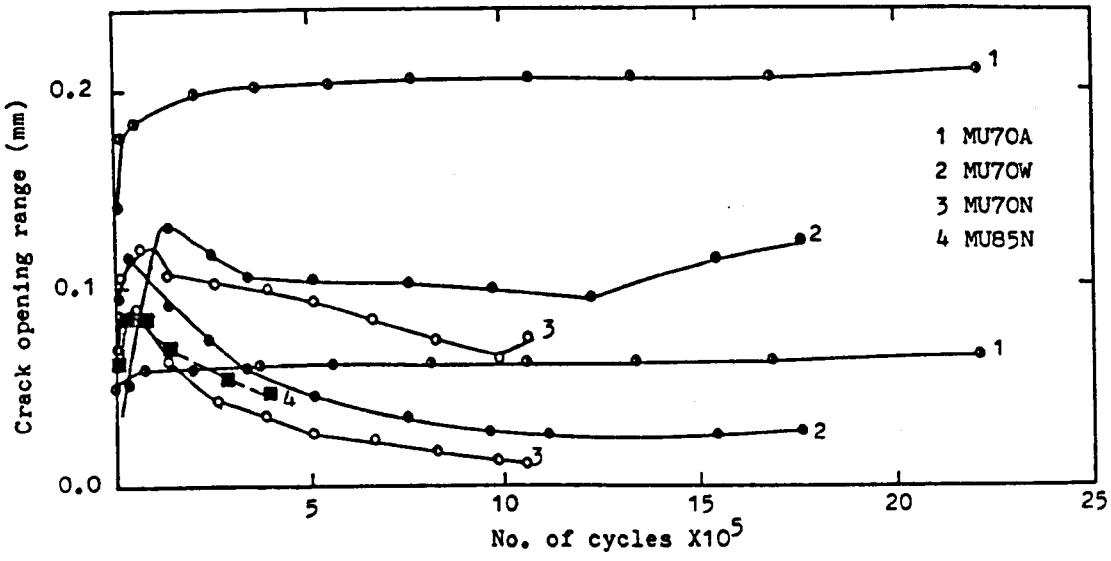

Figure (7-13): Uni-directional series;crack opening range vs. No. of cycles.

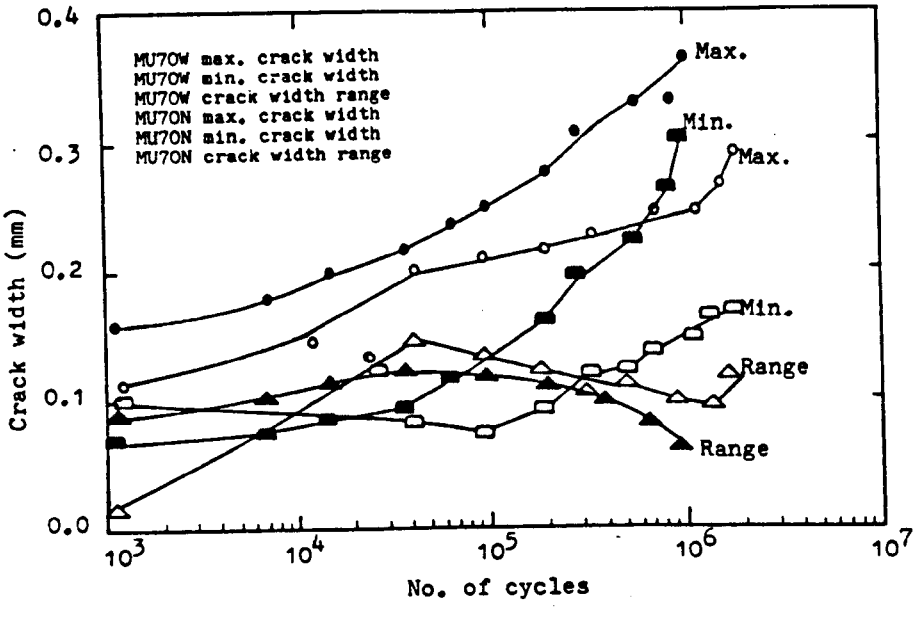

Figure (7-14): Beams MU7ON,MU7ON maximum,minimum and range of crack width vs. No. of cycles.

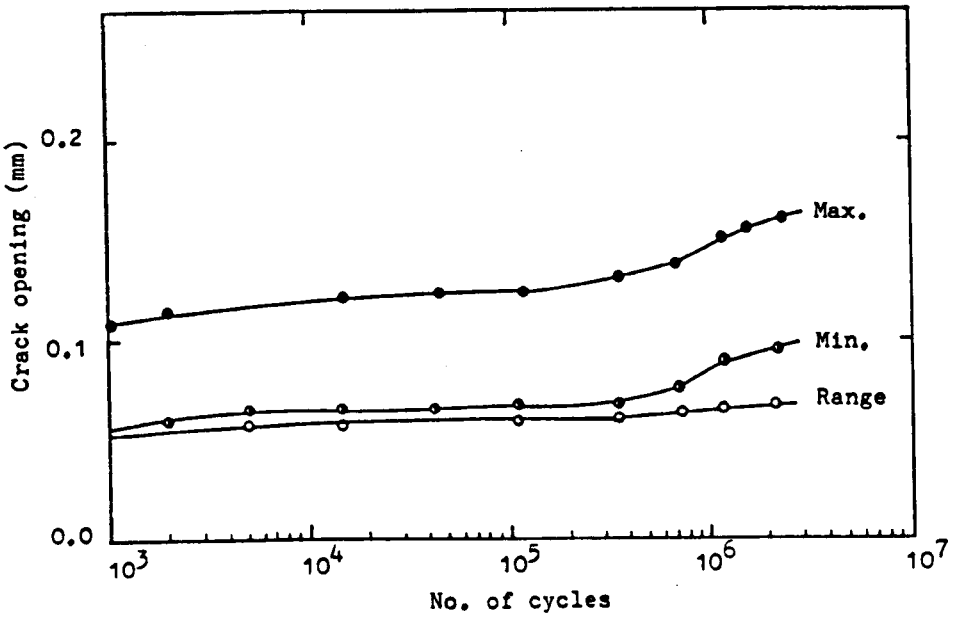

Figure (7-15): Uni-directional bending series, maximum, minimum and crack opening range for beam MU70A.

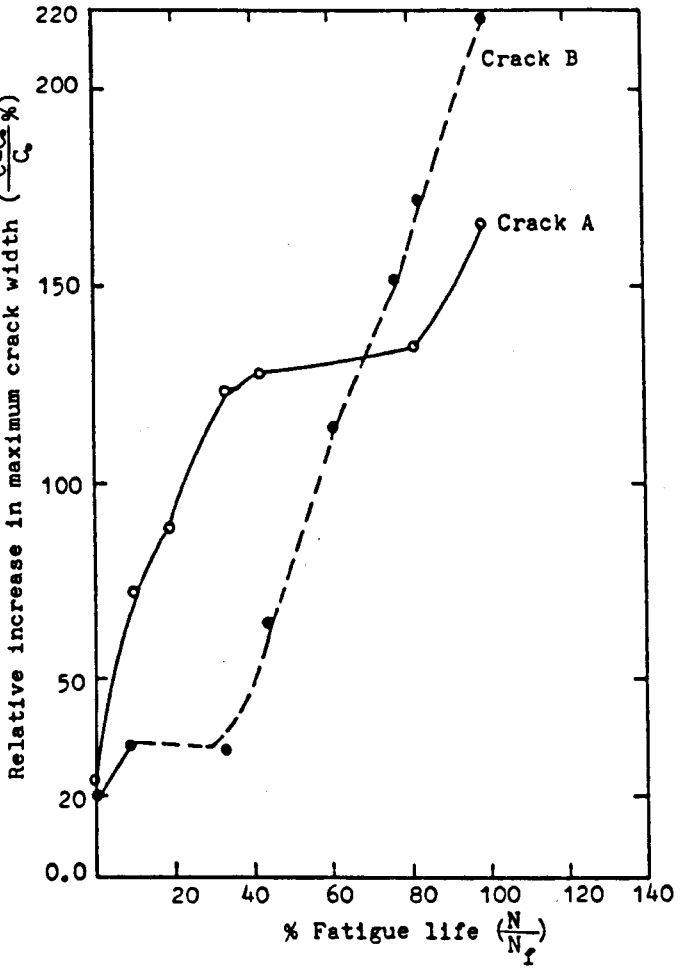

Figure (7-16): Uni-directional series; beam MU70N, relative increase in maximum crack width vs. % fatigue life.

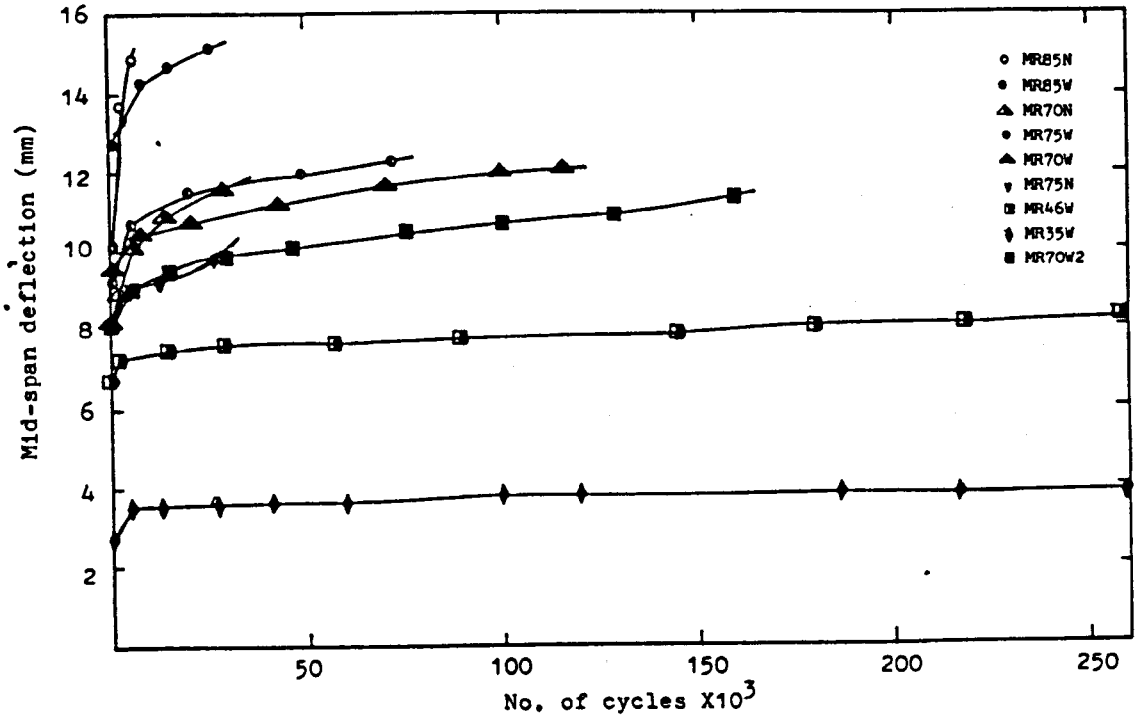

Figure (7-17): Reverse bending series;maximum deflection vs. No. of cycles.

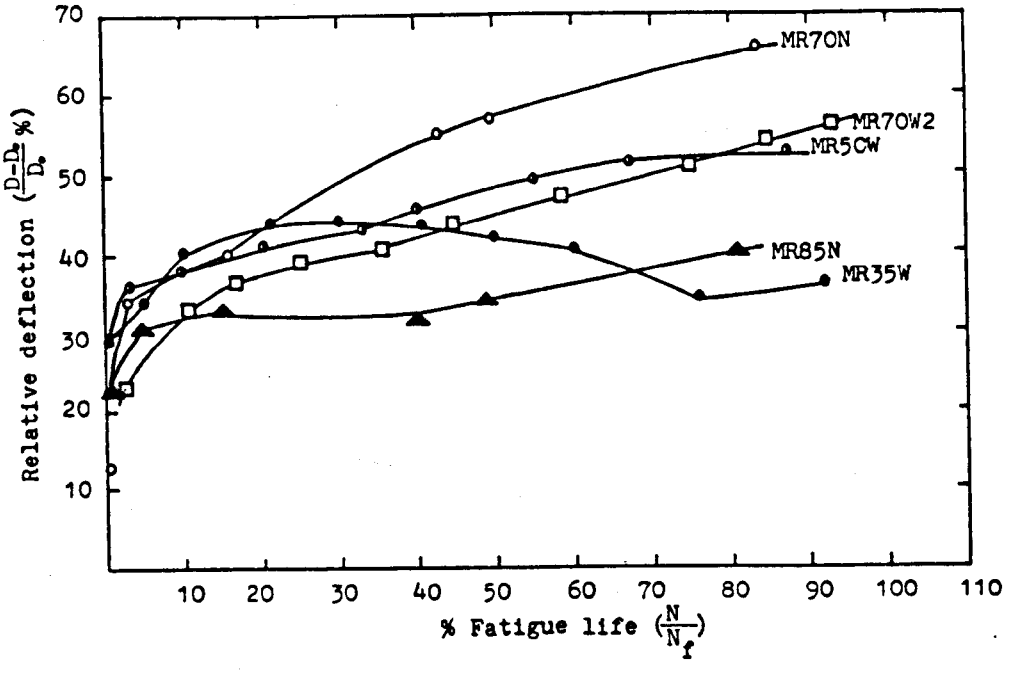

Figure (7-18): Reverse bending series;relative deflection vs. percentage fatigue life.

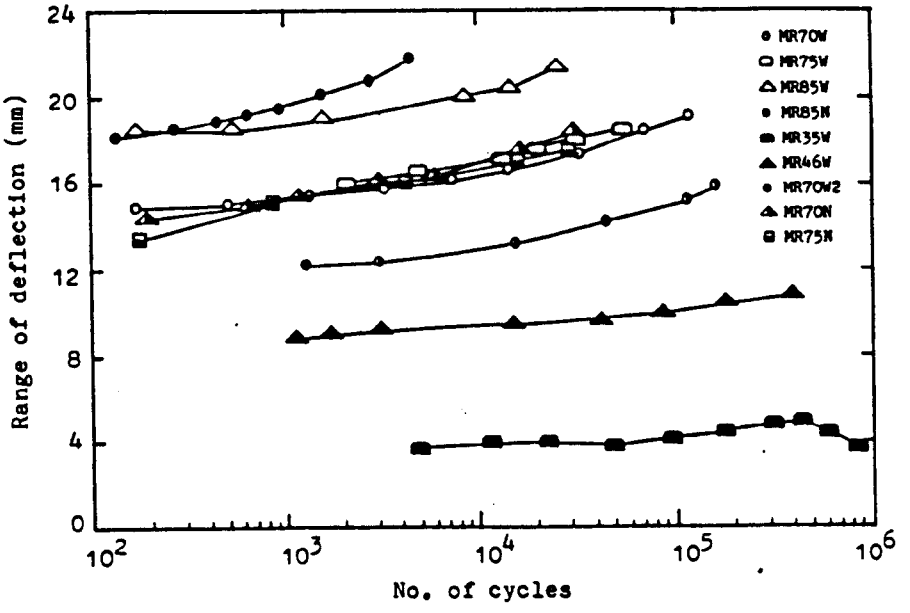

Figure (7-19): Range deflection vs. No. of cycles for reverse bending tests.

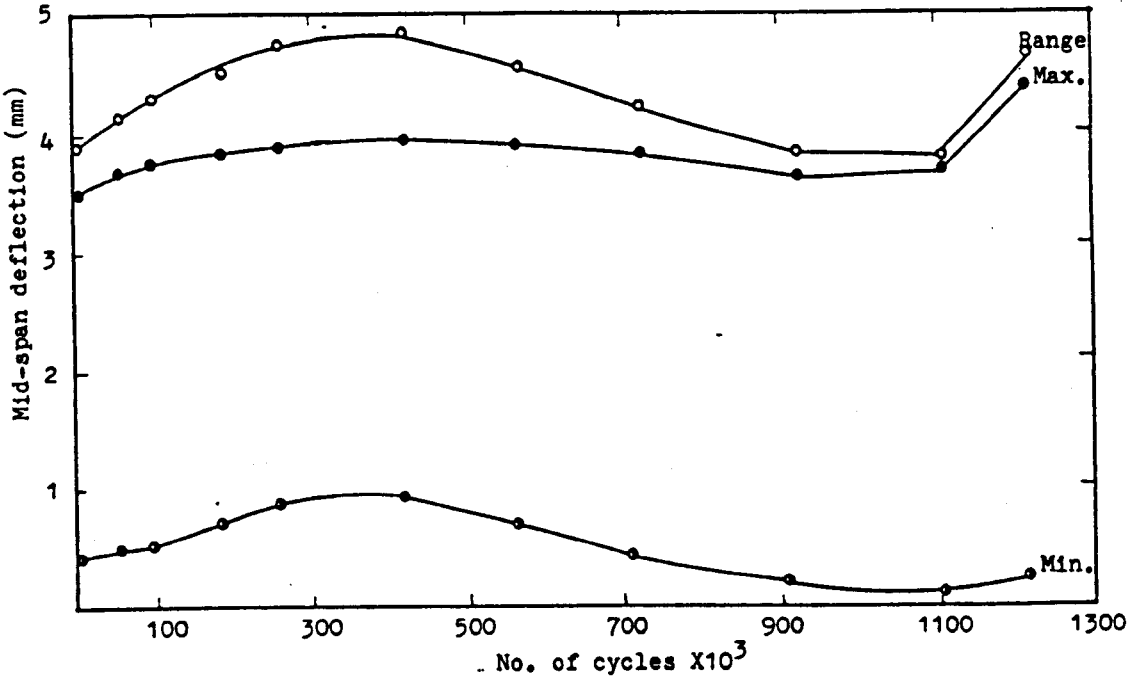

Figure (7-20): Reverse bending series;for beam MR35W maximum,minimum and range of deflection.

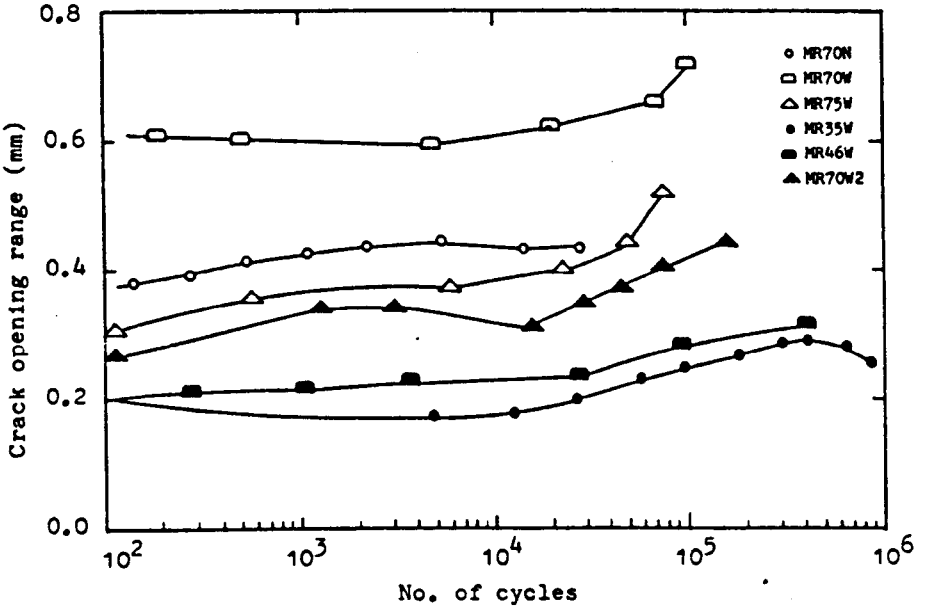

Figure (7-21): Crack opening vs. No. of cycles for reverse bending tests.

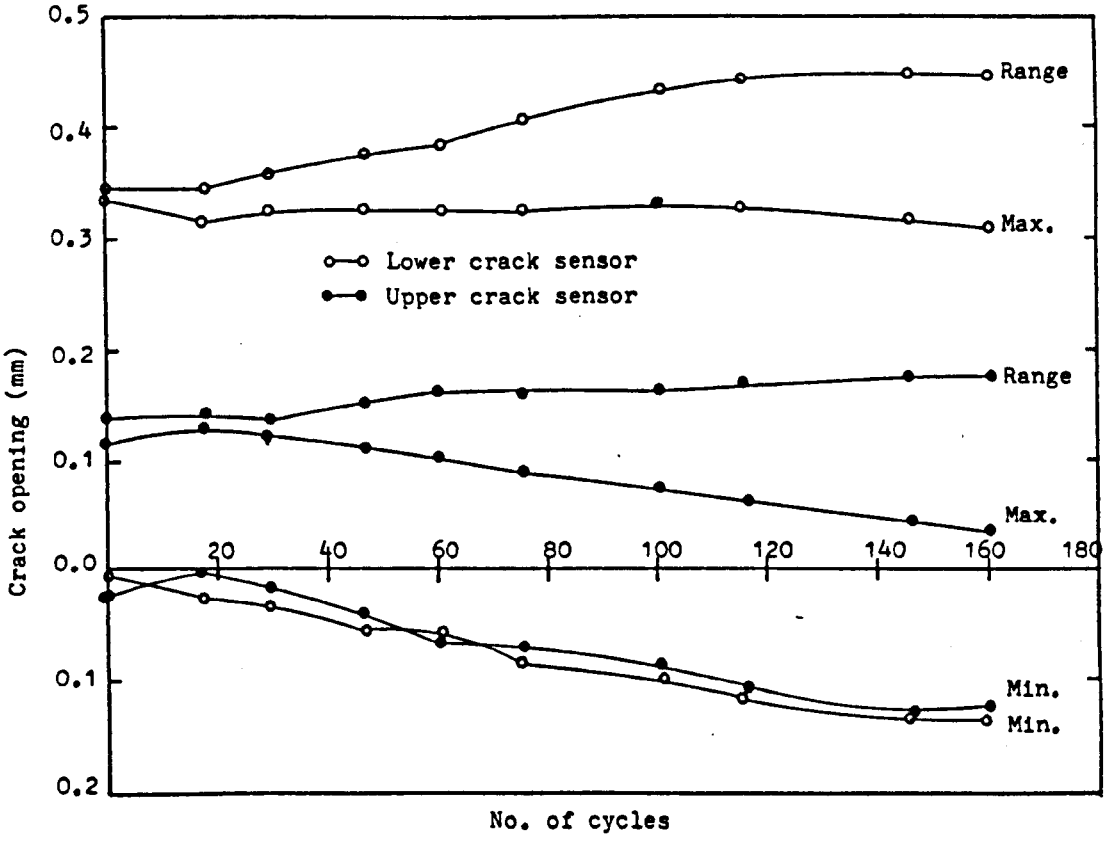

Figure (7-22): Reverse bending series;maximum,minimum and range of cracks opening for beam MR70W2.

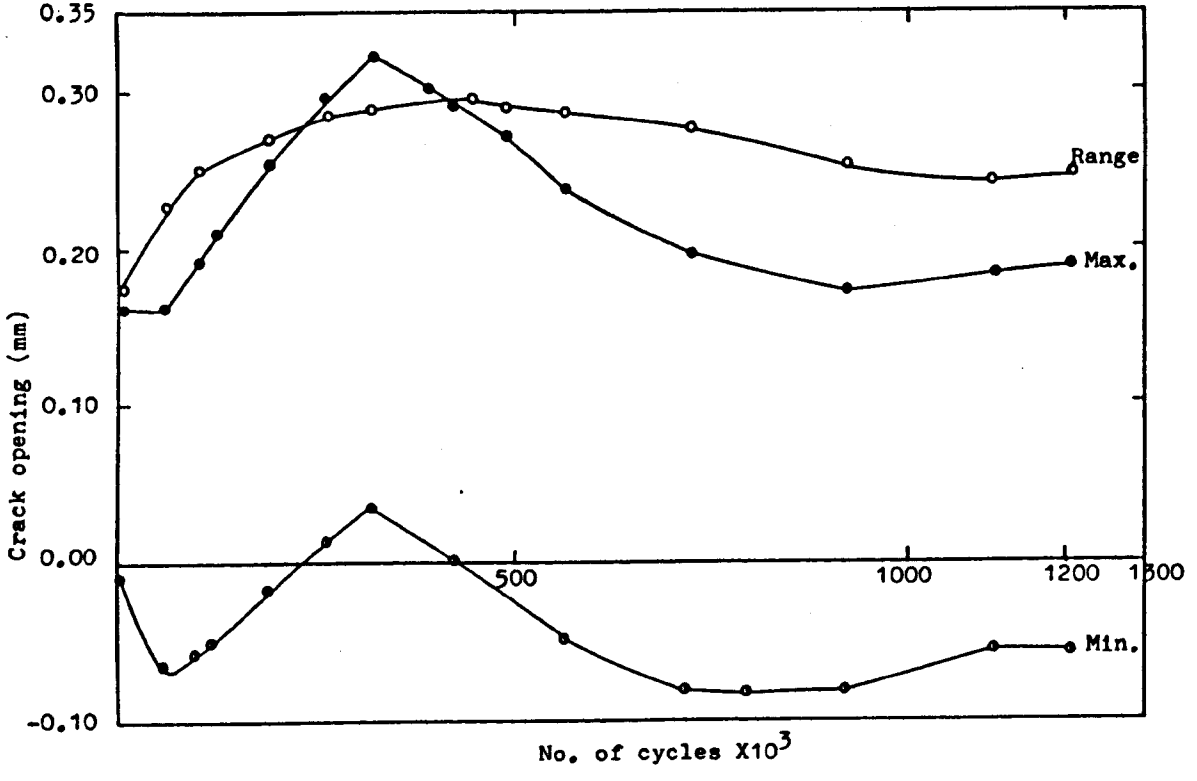

Figure (7-23): Reverse bending series for beam MR35W maximum,minimum and range of crack opening (lower crack sensor).

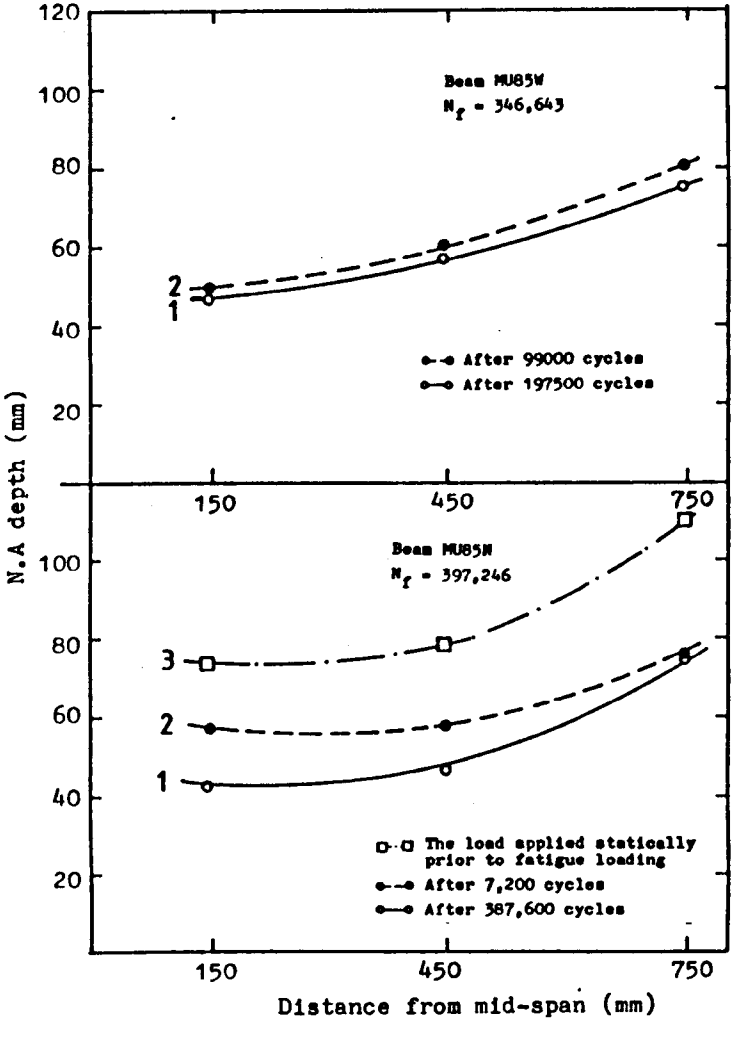

Figure (7-24): Profile of the neutral axis at different stages of cycling for beams MU85W and MU85N.

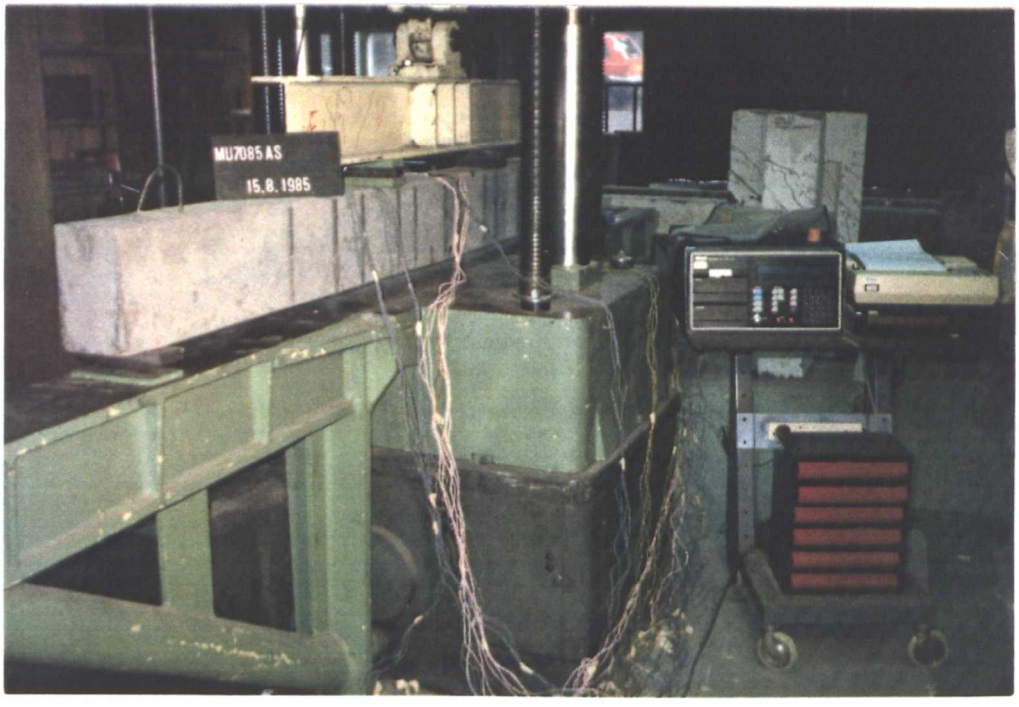

a) Uni-directional bending

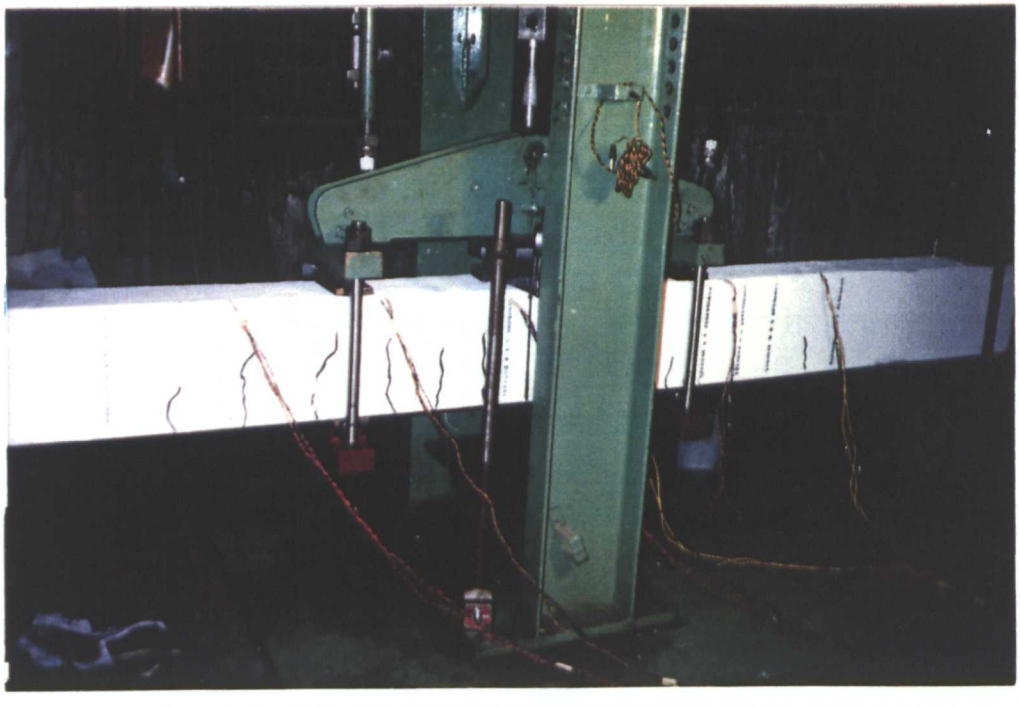

b) Reverse-bending

Figure (7-25): Static tests loading arrangements and instrumentation.

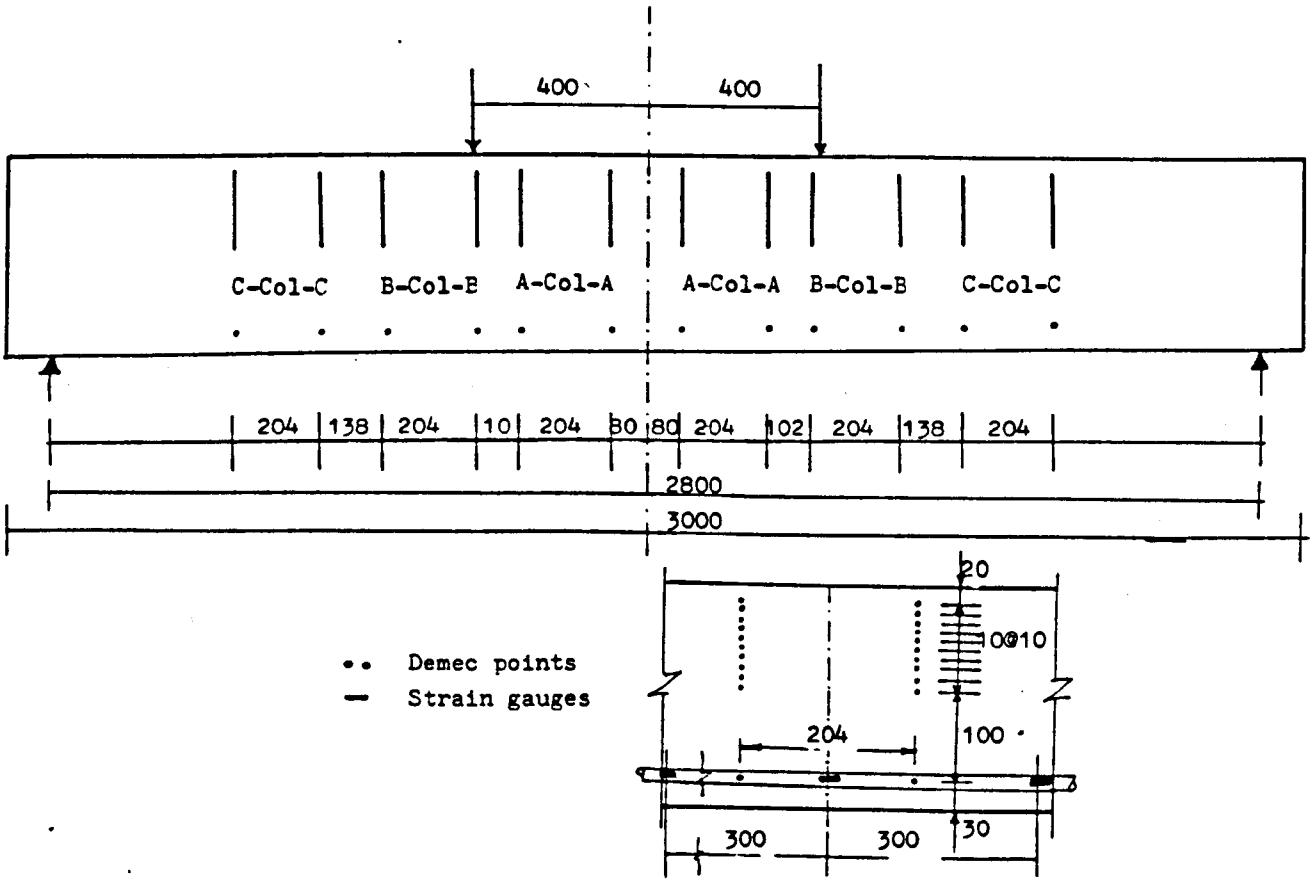

Figure (7-26): Static tests-unidirectional bending test beam,details and distribution of Demec points column on concrete surface and the relative position of steel strain gauges.

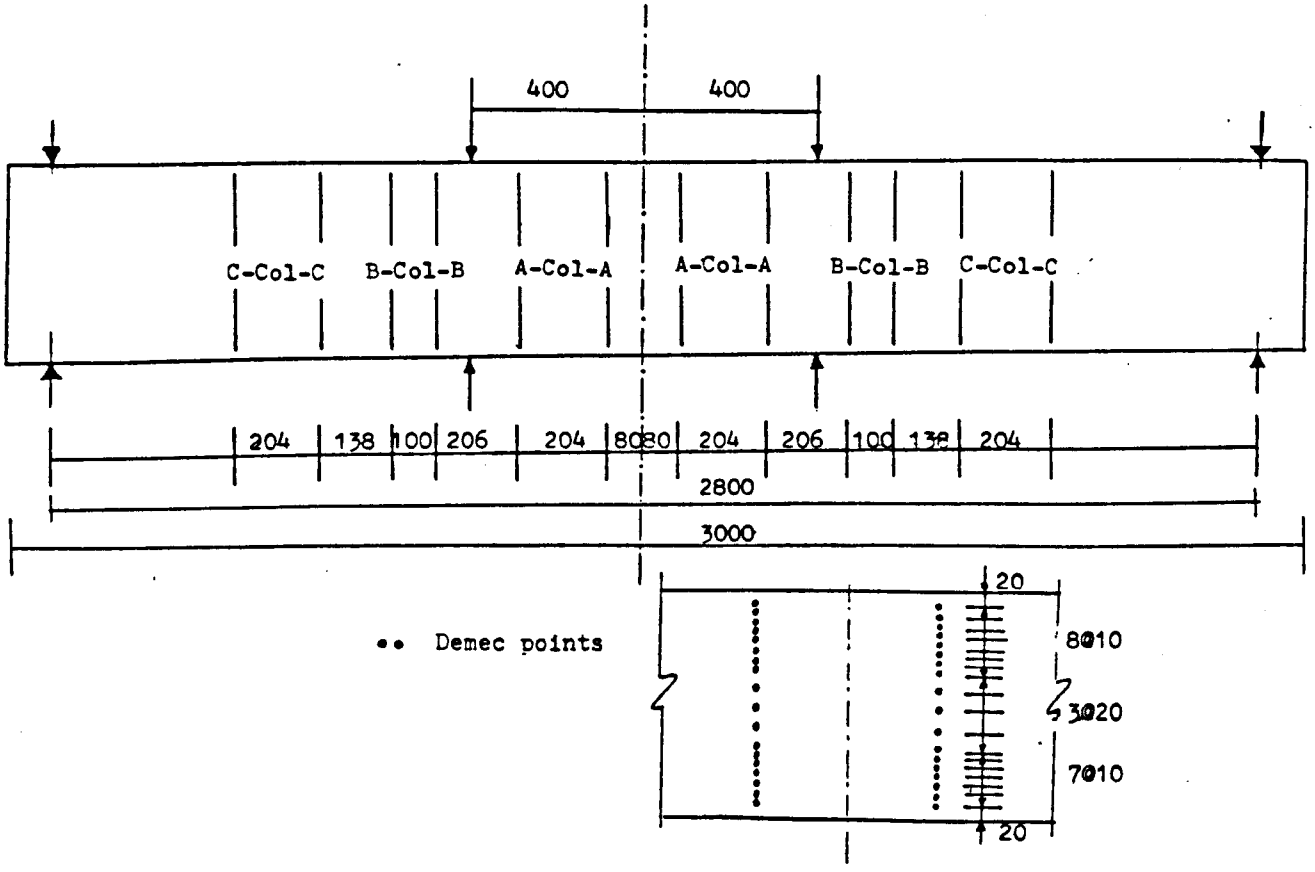

Figure (7-27): Static tests-reverse bending test beams;details and distribution of Demec point columns on concrete surface.

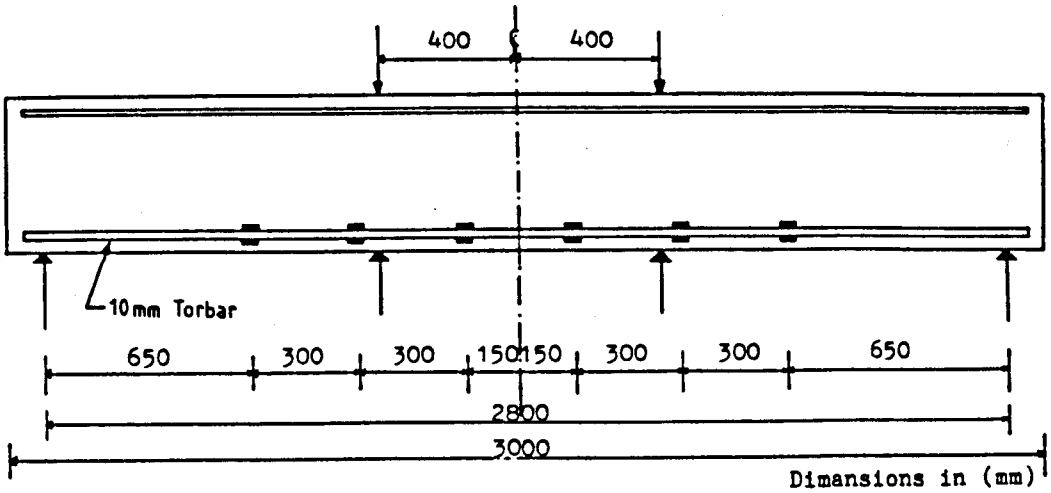

Figure (7-28): Static tests;locations of strain gauges on the tension Torbars (strain at each location is determined from the average of 4 gauge readings).

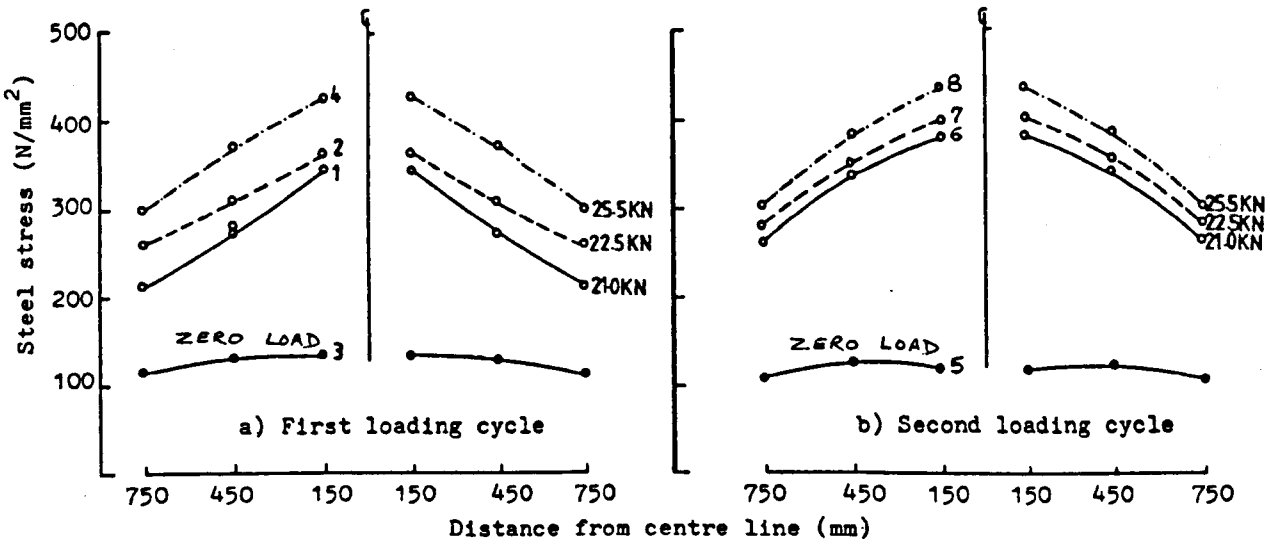

Figure (7-29): Uni-directional static test;steel stress distribution

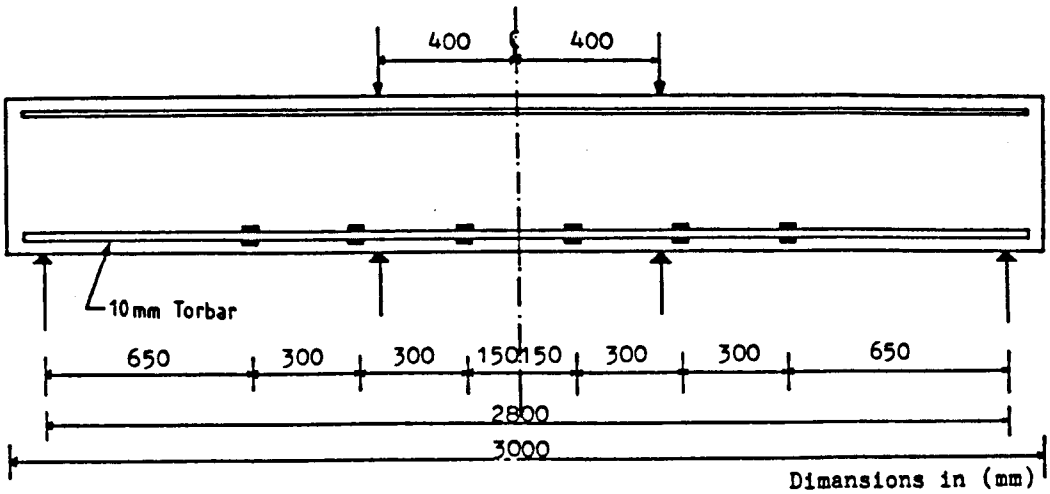

Figure (7-28): Static tests;locations of strain gauges on the tension Torbars (strain at each location is determined from the average of 4 gauge readings).

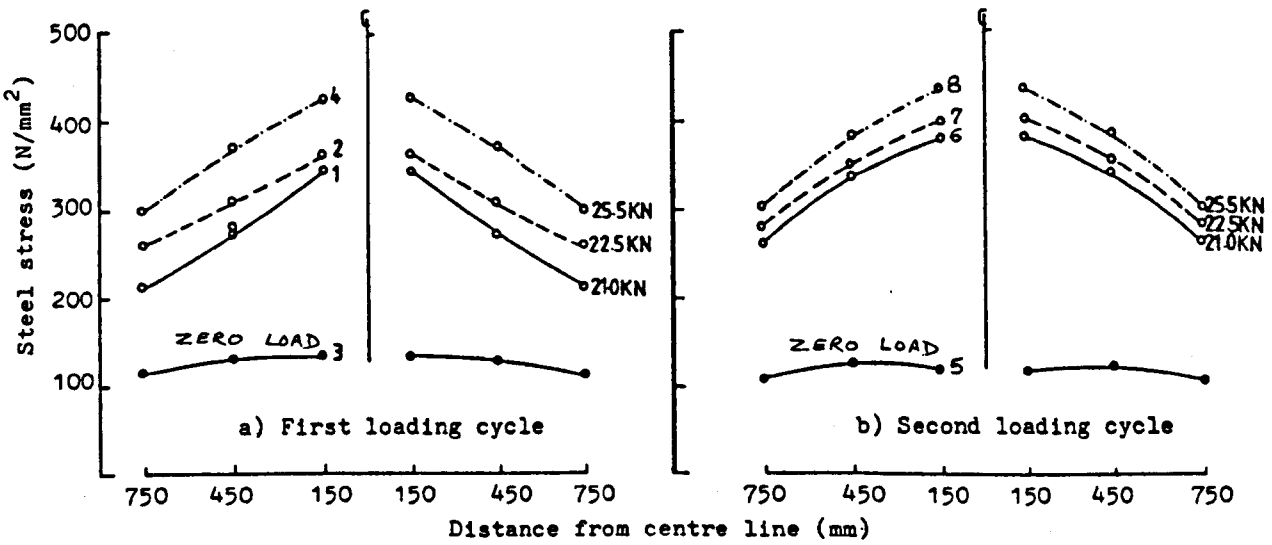

Figure (7-29): Uni-directional static test;steel stress distribution

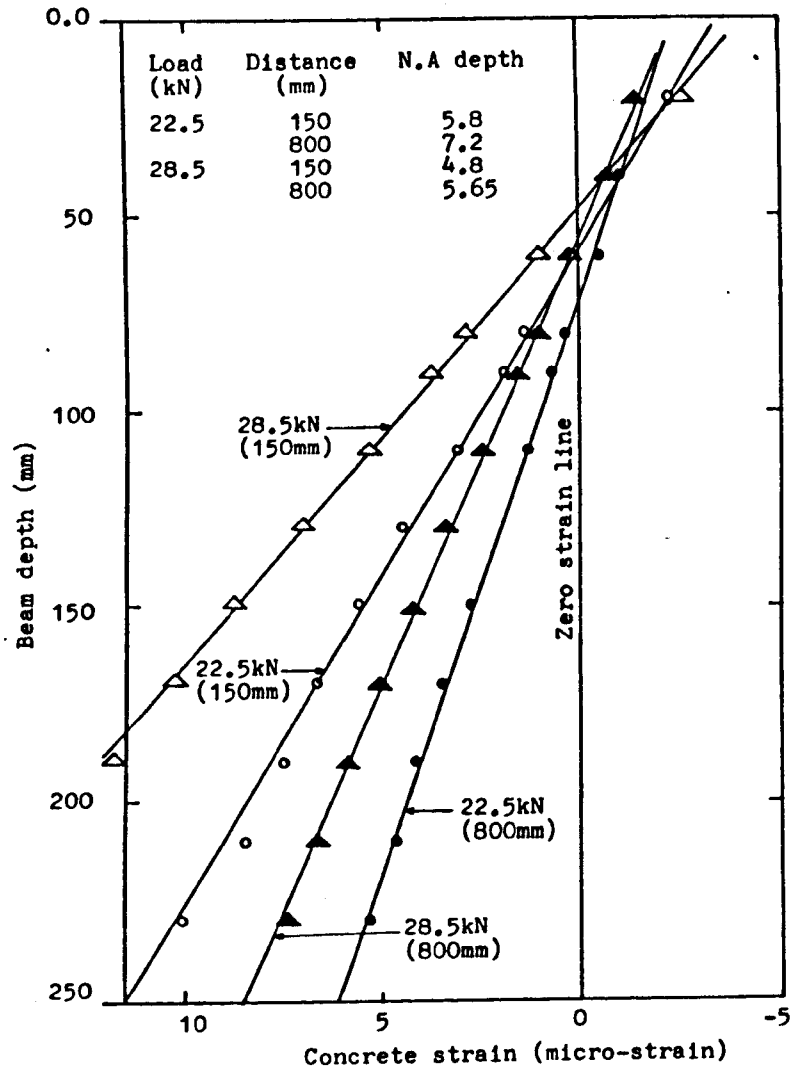

Figure (7-30-a): Beam MR7595SA;N.A depth at 150 and 800mm from the beam centre line for applied loads of 22.5 and 28.5 kN.

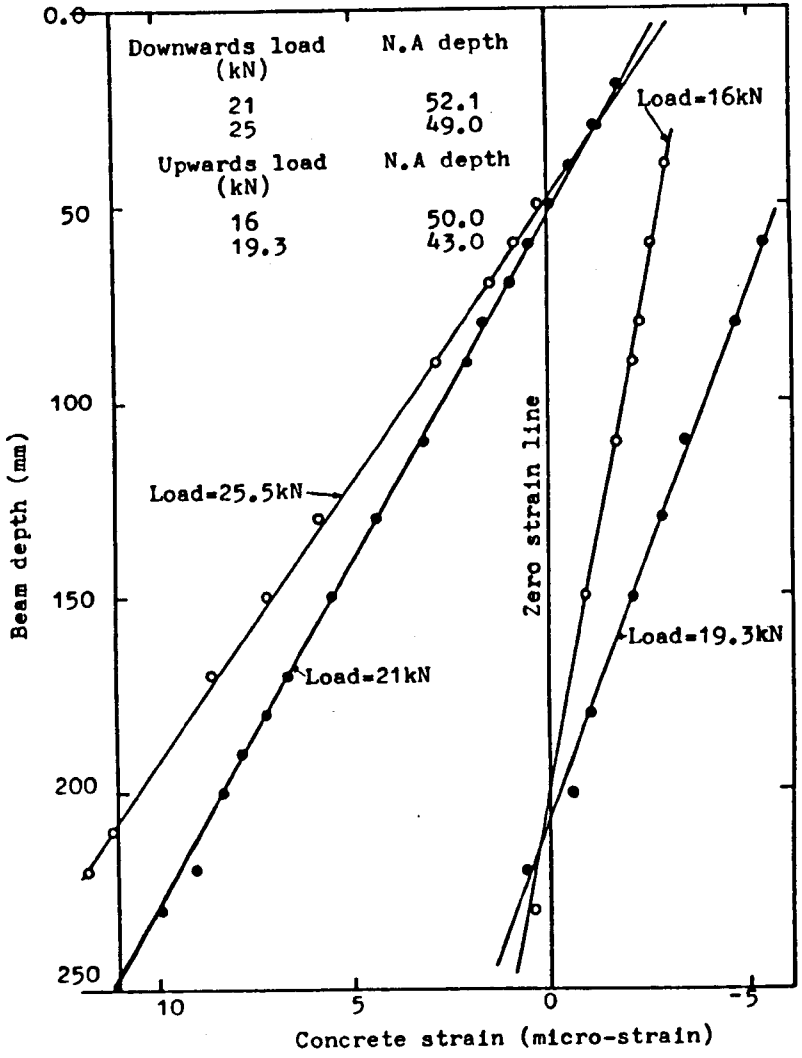

Figure (7-30-b): Beam MR7085SA;N.A depth at 150mm from the beam centre line of up and downwards load of 21,25.5 and 16,19.3 kN respectively

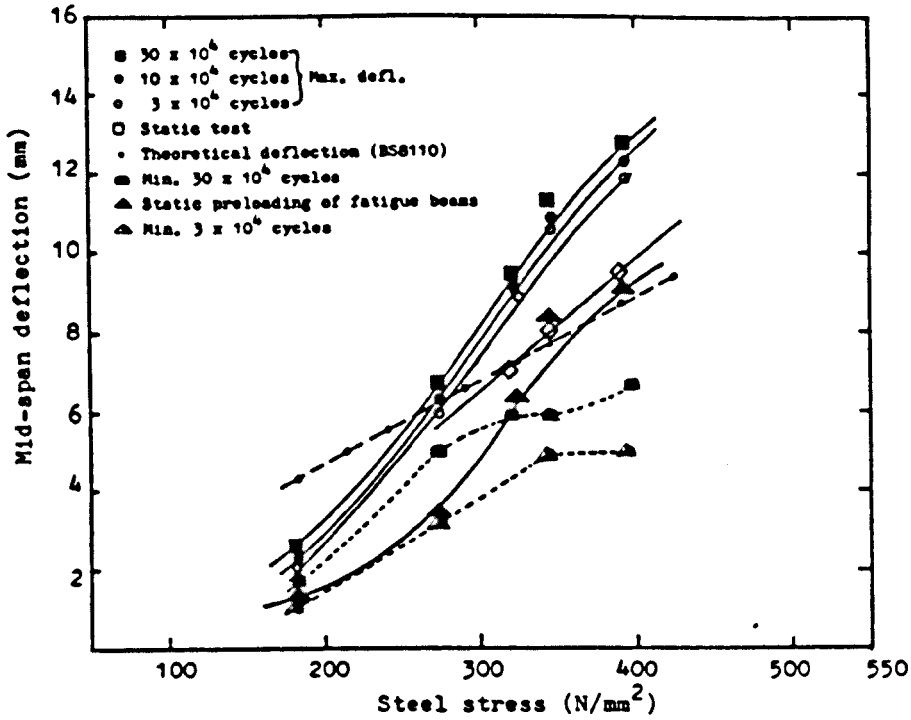

Figure (7-31): Uni-directional bending series;effect of of loading on deflection-steel stress relationship.

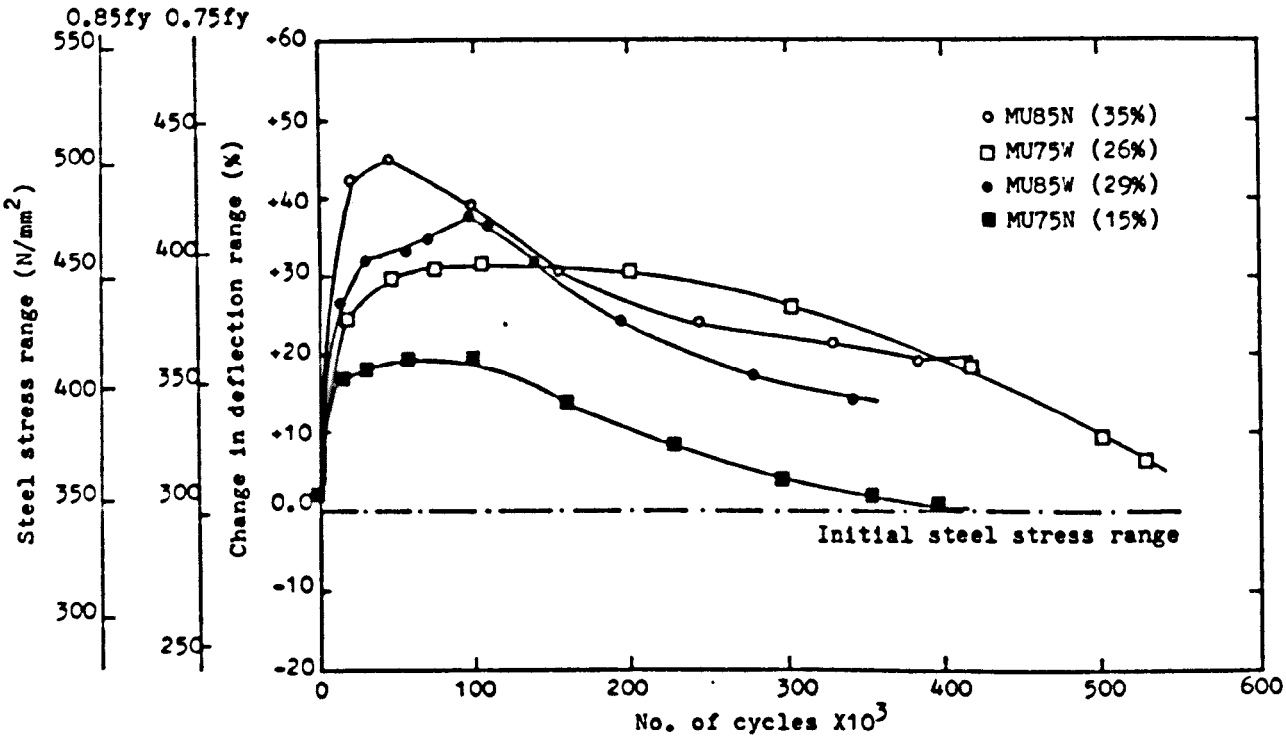

Figure (7-32): Change in steel stress range and deflection range vs, No. of cycles for beams MU75W,MU75N,MU85W and MU85N.

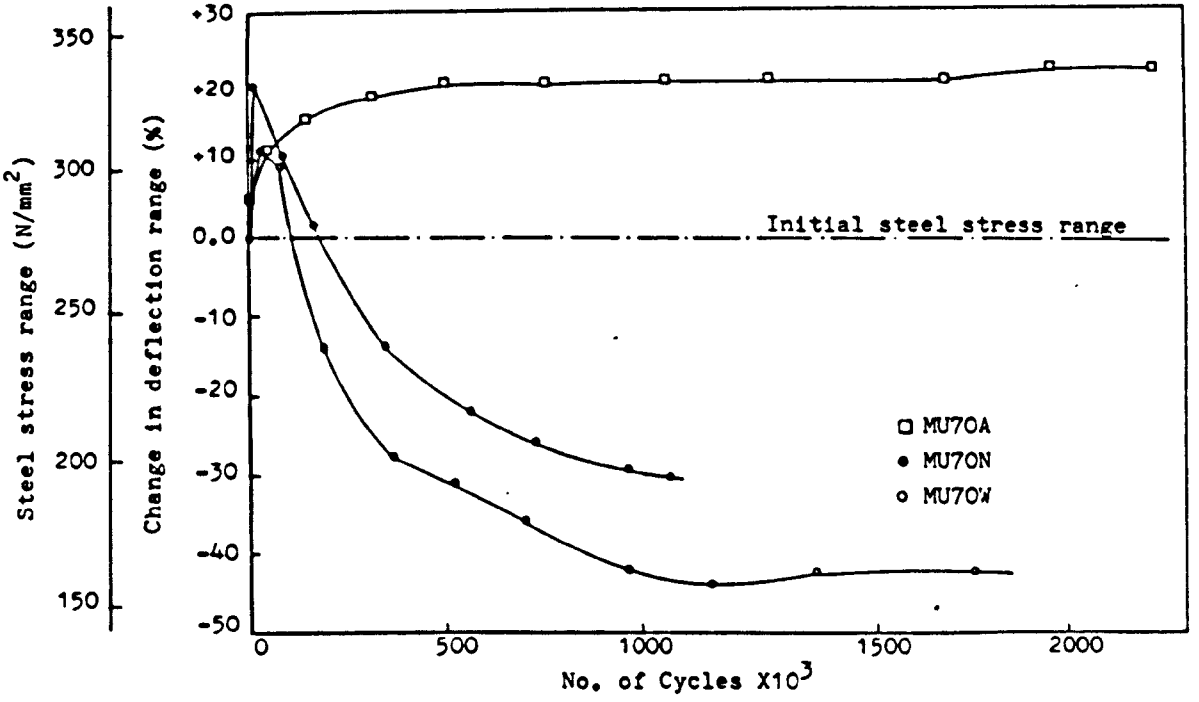

Figure (7-33): Change in steel stress range and deflection range vs. No. of cycles for beam MU70N,MU70W and MU70A.

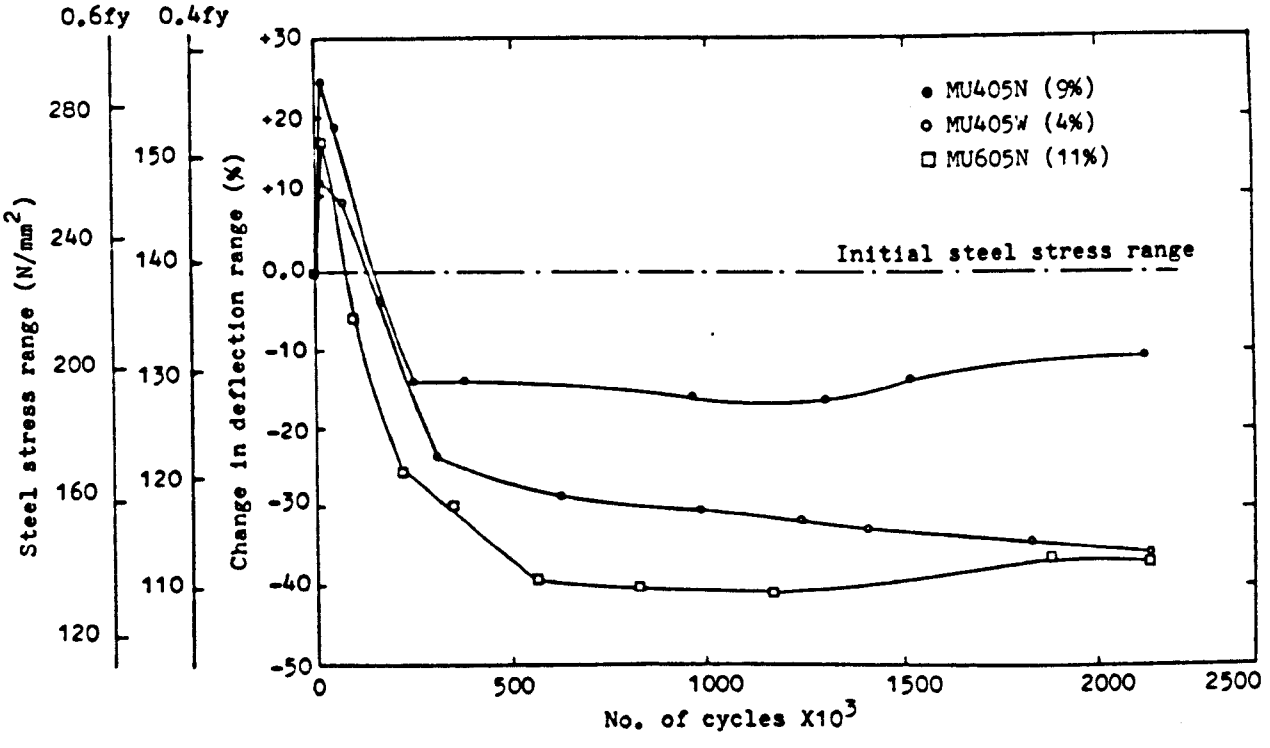

Figure (7-34): Change in steel stress range and deflection range vs. No. of cycles for beams MU405N,MU405W and MU605N.

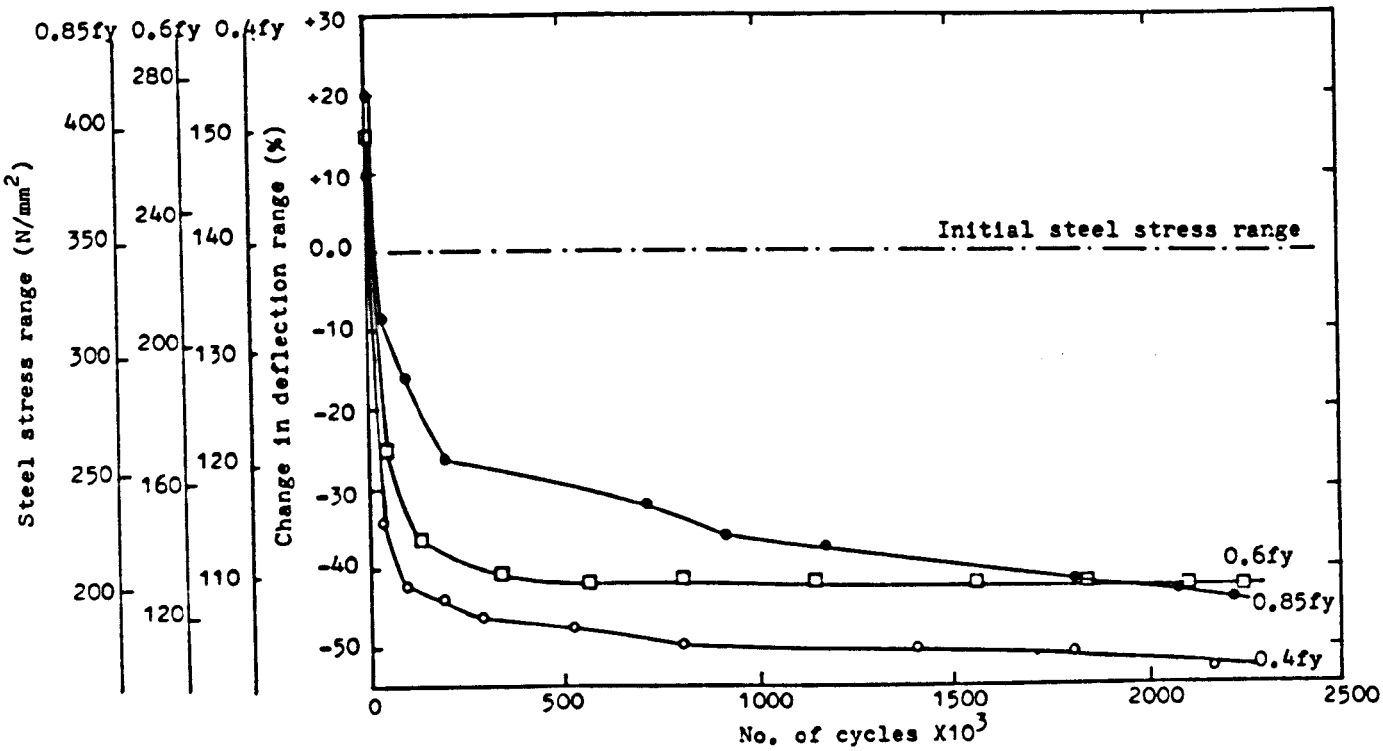

Figure (7-35): Change in steel stress range and deflection range vs. No. of cycles;tests in seawater at different load level (data from Glasgow University research).

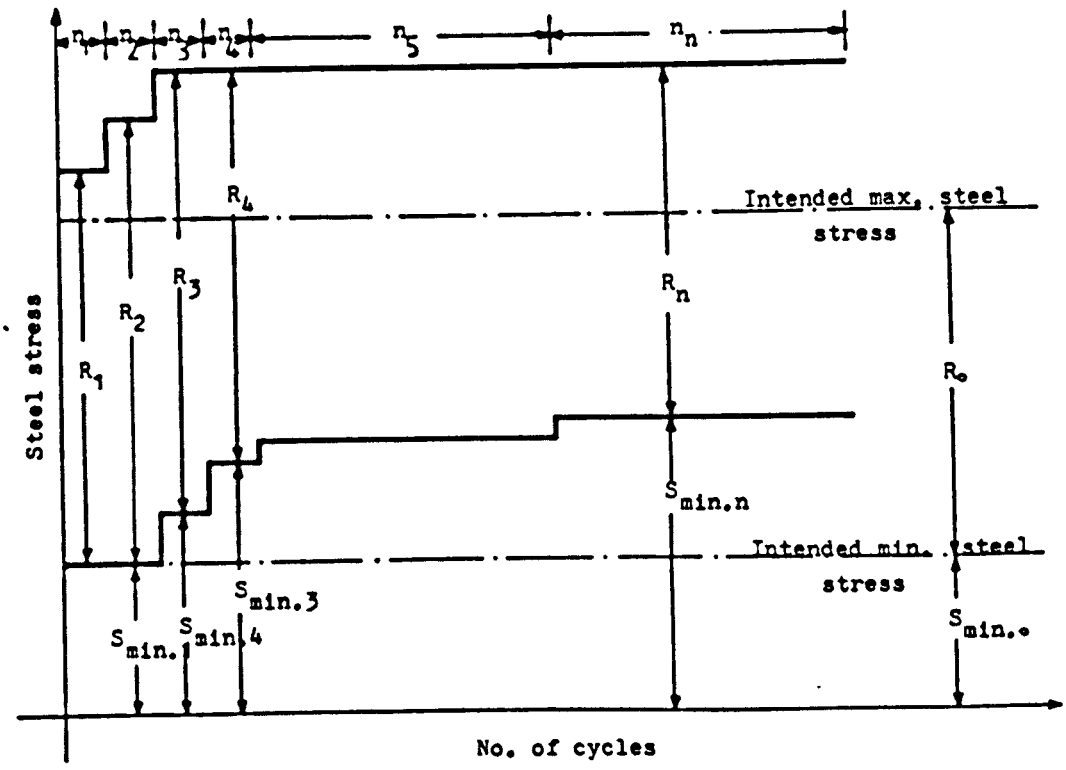

Figure (7-36): Change in loading sequence as compared with the initial intended stress range as a result of crack blocking.

CHAPTER 8

CRACK BLOCKING OF CONCRETE FLEXURAL CRACKS

first recorded for both uni-directional and reverse bending tests, these tables will be described in the following sections.

8.2 Reverse Bending Tests.

Initially 6 beams were tested under this kind of loading, 3 beams in each test environment. For a stress range in the highly tensioned bars ranging between 328 to 398 N/mm^2 neither visual sign of blocking at crack sites nor reduction in deflection and crack opening range were observed (Figure 8.1). However, some deposit was observed in the first crack outside the tank. It should be pointed out that the age of these beams at the start of the test were between 4 and 5 years and the tests were of relatively short duration, from 6300 to 123000 cycles. Therefore it was decided to extend the tests to cover three more other conditions in water. These conditions were as follows:

- Young beam at high load level, MR70W2
- Young beam at low load level, MR35W
- Old beam at low load level, MR46W

Table 8.1b indicates that blocking occurred only in the lowest load level (MR35W) in water environment and after approximately 446,700 cycles.

8.3 Uni-Directional Tests.

8.3.1 Tapwater Environment.

Blocking occurred in all the tests for the various load levels under consideration, however, difference in stress level produced some appreciable differences in blocking response in terms of the amount and development of deposits as well as their initiation time i.e. the number of cycles after which this phenomenon becomes effective.

0.75 and 0.85 f_y Load Level.

Blocking was mainly confined to the upper regions of concrete flexural cracks. The amount deposited was relatively small (Figure 8.2) also the reductions in deflection range and crack opening range were relatively late (Table 8.1a).

0.70 and 0.6 f_y Load Level.

Blocking initiated at the upper region of the cracks and extended downwards the crack mouth. At early stages of the tests, larger amounts of deposit material were accumulated at the upper regions of the cracks, Figure 8.3a, but later this trend disappeared, earlier in fact for lower load level than for higher one, and no particular relationship was apparent between the amount of deposit and the relative position along the crack length, (Figure 8.3b,c) and large amounts of deposit was found even at the beam soffit (Figure 8.4). The amount of deposit increased with time, see Figures 8.3a,b,c and Figures 8.5a,b, i.e the elapsed number of cycles up to a certain point (approximately 700,000 - 900,000 cycles) beyond which the increase was halted and the material started to undergo a colour change, Figure 8.3c.

0.4 f_y Load Level.

The blocking material was small in amount and late in effect on the structural behaviour of the beam as compared with the preceding group, Figure 8.6a. However, unlike the 0.75-0.85 fy group, the deposit covered all the length of the crack as well as the beam soffit, Figure 8.6b.

8.3.2 Chloride Environment.

Generally the amount of deposit formed at crack sites was small but was able to produce slightly earlier structural change than the tapwater tests. Higher load level tests (corresponding to steel stress of 0.75 and

0.85 f_y) showed blocking limited only to the upper regions of the cracks whereas the second load group (0.6 and 0.7 f_y) showed complete closure along the whole length of the cracks. Unlike tapwater tests the blocking material was rather uniformly distributed over the cracks length and the deposits increase with time was small Figure (8.7a,b,c). Colour change was also observed at later stages, Figure (8.7b,c). With regard to the lowest load level (0.4f_y) the blocking was at its minimum, Figure 8.8a and batches of reddish-brown soft deposit was seen at different positions at the upper parts of the beams away from the flexural cracks, Figure (8.8b).

8.3.3 Tests on Old Beams.

Two beams were tested in sodium chloride solution at age of 1 and 8 years respectively at a load level corresponding to steel stress of 0.6 f_y. In both cases blocking was observed at early stages, Figure 8.9a,b and caused early reduction in structural parameters. After 916,650 cycles beam MU60N87 was subjected to an incremental increase of load. As a result small increases in crack length occurred upon each incremental increase. Concurrently the formation of deposit re-commenced and rapidly blocked the newly added length of the cracks.

8.3.4 Static Tests.

These tests were limited to sodium chloride environment for load levels corresponding to steel stress of 0.4 and 0.6 f_y. For lower load level the cracks were very small and difficult to detect.

Under this condition blocking was completely absent at the surface of the concrete beam, Figure 8.10a. For higher load levels a very small but detectable amount of deposit was observed to form at some concrete cracks, Figure 8.10c, in both cases, however, patches similar to those observed in chloride-low load dynamic tests were observed, Figure 8.10b.

8.4 Development of Surface Skin.

Upon draining the solution after each test, for both exposure conditions (water and chloride), it was possible to observe a thin surface layer (approx. 100-150 μ) of small crystalline structure developing on the exposed surface of concrete. A piece of concrete including the surface, Figure 8.11a, was recovered from a beam exposed to chloride solution for 5 months, and examined and photographed under a light optical microscope. The photomicrograph is shown in Figure 8.11b; the left part of the surface shown in this Figure was scratched to provide better contrasted image of the developed layer. Using the same microscope, Figure 8.11c was obtained for fresh concrete to provide a visual comparison of the concrete surface before and after exposure.

The formation of the surface layer was observed to be uniform over the concrete surface area except the crack sites. Samples of the skin layer-material were taken for examination for chemical composition.

8.5 Deposit Identification Tests.

Ten samples of deposits were scraped from the surface of the submerged cracks, cracks outside the solution jacket and surface skin of the submerged part of the concrete beam and analysed for their chemical composition using x-ray diffraction and x-ray fluorescent techniques. The sample preparation and analysis was carried out at the Geology Department of Glasgow University.

Six samples were run on a Philips x-ray diffractometer 1010, the optimum test conditions used were as follows.

- 40 kV and 20 Mamp
- Tube; cu-K alpha radiation
- Filter; Ni
- Counter; Geiger counter
- cps; 1 x 10^3
- paper speed; 10 mm/min

The samples location were as described below.

Beam	Sample Location
MU70N	Deposit from the submerged cracks
MU85N	Deposit from the submerged cracks
MR35W	Deposit from the submerged cracks
MR46W	Deposit from cracks outside the jacket
MU60N8Y	Deposit from cracks outside the jacket
MU605N	Surface skin

The x-ray diffraction patterns for these samples are given in Figure 8.12a,b,c,d,e,f respectively. For submerged cracks, in both kinds of solution as well as surface skin sample, the deposit analysis revealed major peaks corresponding to the K-α x-ray emissions of calcium carbonate together with smaller peaks of minor impurities such as dolimite $MgCa(CO_3)_2$ and silica SiO_2, emanating probably from the subjacent concrete, and halite NaCl, Figure 8.12a,b,c.

Analysis of deposits from cracks situated outside the jackets yielded different characteristics depending on the test environment. While water tests revealed similar patterns as those obtained for submerged deposit described above, deposits from chloride tests revealed major peaks of Halite (NaCl) and smaller amount of calcite ($CaCO_3$).

The XRF technique was used to quantitatively analyse three more deposit samples from submerged cracks in water and chloride solution as well as one sample from the red-brownish patches shown in Figure 8.8b. Prior to examination, the samples were crushed to pass 100 μ mesh. The results are given as a percentage by weight of each existing element in Table 8.2 which excludes elements of low atomic number such as hydrogen, oxygen and carbon. This analysis confirmed the XRD results in that calcium compound is the major constituent of the deposit, the

analysis also showed that iron oxide is the major element of sample IV with 9.76% of SiO_2 and 8.67% of Na_2O.

8.6 Discussion.

Concrete is able to block or heal load-induced cracks under a wide range of environmental exposure and loading conditions. If the predominant nature of loading is static the healing material acts as a binder across the crack thus fracture may occur at cracks other than the initial ones which have healed. In contrast dynamic loading can be instrumental in consolidating the material deposited in the cracks and hence increasingly affects the movement pattern of the concrete element. As a result of this the assumed direct link between load level and stress in steel is no longer reliable and the consequences for fatigue lives follow as described elsewhere.[10,11,15] In this context perhaps the most important aspect of the occurrence of this phenomenon has been the initiation time after which it becomes effective. The environmental conditions of this study may be summarised as followings:

1. When test solution pumped around the test beam, pH of the solution increased to 10.5-11.5.

2. In order to carry out the experiments at approximately constant pH, the pH was controlled as follows:

   For NaCl tests, by adding dilute HCl as required. Calculation showed, that this only very slightly altered the Cl^- concentration compared with the Nominal 3.5% NaCl. Additions of acid were only required for the first few days of tests (3-4 days).

   For the tapwater tests, acid was added in stage I of the programme. In Stage II, however, pH was controlled by changes in the water. This was done typically on

second day and then approximately weekly. The reason for this practice is to avoid possible effect of increased Cl^- ions concentration due to dosing on the corrosion phenomenon which was studied extensively in Stage II of the work.

3. In corrosion fatigue tests, evidence of initiation of concrete-cracks blocking was obtained both visually and indirectly (via reduced beam deflection range) after 2-8 days testing. The onset of crack blocking was load dependent but, for identical loading conditions, was slightly earlier in NaCl solution than in tapwater. Table 8.3a,b and Figure 8.14 compare the point of initiation of blocking, defined as a time at which a reduction in deflection range has been started.

4. Subsequently, the deposition appeared to be at a faster rate in tapwater than in NaCl solutions.

8.6.1 The Mechanism of Crack Blocking.

For precipitation of deposits to be possible the aqueous solution in question must be supersaturated at least locally at the deposition site with respect to the particular deposit. In other words the ions activity product (IAP) of the pertinent ionic species present in the solution must exceed the thermodynamic solubility product (K_{sp}). The degree of saturation $S(=IAP/K_{sp})$ is probably the most important parameter governing the likelihood of precipitation. The relevant compounds pertaining to crack blocking have been $CaCO_3$ and $Mg(OH)_2$ for sea water and as demonstrated in the present work, $CaCO_3$ for both chloride solution and water.

The precipitation reactions can be written as:

$$Ca^{2+} + (CO_3)^{2-} = CaCO_3 \qquad \ldots 1$$

and

$$Mg^{2+} + 2(OH)^{-} = Mg(OH)_2 \quad ...2$$

thus the solubility equilibria are

$$K_{sp_{(1)}} = a_{Ca^{2+}}\, a_{(CO_3)^{2-}} \quad ...3$$

$$K_{sp_{(2)}} = a_{Mg^{2+}}\, (a_{(OH)^{-}})^2 \quad ...4$$

the activity a = fC where

where f is the activity coefficient
c the concentration at the solubility limit

then if

$$K_{sp_1} \leq [a_{Ca^{2+}}\ a_{(CO_3)^{2-}}]$$

and

$$K_{sp_2} \leq [a_{Mg^{2+}}\ .\ (a_{(OH)^{-}})]$$

here a is the activity of the pertaining ionic species present in the solution.

Then the degree of saturation $S \geq 1$ and unless this requirement is satisfied, precipitation of these compounds can not occur.

In this work and in both test solutions, ie. tapwater and NaCl solution, the origins of the ionic constituents responsible for the observed $CaCO_3$ deposit were:

1. Dissolved Ca^{2+} ions resulting from dissolution of $Ca(OH)_2$ in the early stages of exposure of the beam to the test solution.

2. Carbonate ions arising from the equilibration between

CO_2 gas in the atmosphere and dissolved CO_2 in the water:-

$$CO_2(g) = CO_2(aq)$$

A small proportion of this dissolved $CO_2(aq)$ hydrolyses to carbonic acid, H_2CO_3:-

$$CO_2 + H_2O \text{ ---> } H_2CO_3$$

and, in turn, H_2CO_3 dissociates yielding bicarbonate ions:

$$H_2CO_3 \text{ --> } H^+ + (HCO_3)^-$$

and especially at high pH, the $(HCO_3)^-$ can produce carbonate ions:-

$$(HCO_3)^- \text{ --> } (CO_3)^{2-} + H^+$$

As the two above equations indicate, the concentration of both $(HCO_3)^-$ and $(CO_3)^{2-}$ in a solution at equilibrium depends on the solution pH (but the equilibrium concentration of $CO_2(aq)$ and H_2CO_3 are constant with pH).

In particular it can be demonstrated (see Appendix II) that for carbonate ions:

$$-\log_{10} a_{(CO_3)^{2-}} = 21.6 + 2\ pH \qquad \text{at } 25^oC$$

where $a_{(CO_3)^{2-}}$ is the activity of $(CO_3)^{2-}$ ions (effective concentration which is not necessarily equal to real concentration).

Consequently, in the experiments in this work, the sequence of events leading to crack blocking with $CaCO_3$ was as follows:

In the early stages of exposure, $Ca(OH)_2$ dissolved in the test solution (demonstrated by the rise in pH towards 10.5-11.5). This furnished the Ca^{2+} ions for the subsequent, typically 2-7 days of fatigue loading depending upon the test condition as described later,

deposition of $CaCO_3$ within cracks and on the external surfaces. The initial dissolution of $Ca(OH)_2$ and subsequent deposition of $CaCO_3$ were possible essentially because of the lower solubility of $CaCO_3$ compared to $Ca(OH)_2$ since:

K_{sp} for $CaCO_3$ = 4.6×10^{-9} at 25°C
K_{sp} for $Ca(OH)_2$ = 5.01×10^{-6} at 25°C

The idea that the addition of sufficient $Ca(OH)_2$ to water will cause $Ca(CO_3)$ to precipitate, has been discussed elsewhere[225] and in the Appendix II there is a detailed thermodynamic analysis which demonstrates that, at the experimentally-controlled pH levels of about 8.5 and assuming prior dissolution of $Ca(OH)_2$ more or less to its limit of solubility, the solubility of $CaCO_3$ is clearly exceeded thus allowing deposition to occur.

Similar crack blocking was observed in an earlier experimental study[79,150] in seawater but crack blocking in seawater was detected much sooner. For example, in three tests conducted at 345 N/mm^2 intended stress amplitude, the deflection ranges were observed to commence their decline as crack blocking initiated at between 11,000 and 13,000 cycles as opposed to more than 70,000 cycles in the NaCl and tapwater environment studied in the present work. This quicker deposition in seawater is due to its significant Ca^{2+}, Mg^{2+} & $(HCO_3)^-/(CO_3)^{2-}$ contents. Indeed it is possible to show that normal ocean seawater is essentially saturated with $CaCO_3$ at normal ambient temperatures. It consequently follows that such an aqueous medium would be expected to very rapidly attain sufficient $CaCO_3$ supersaturation (adjacent to a concrete surface) via increases in its normal calcium concentration of around 1×10^{-2} mole/litre and/or increase in $(CO_3)^{2-}/(HCO_3)^-$ ratio at raised pH values.

In the present work (see Tables 3a,b) there were indications of a somewhat earlier detection of crack blocking in the NaCl solution than in tapwater. However, in the phase I test, these differences were small compared to scatter in replicate experiments. Moreover, in the

phase II experiments, the normal practice of replacing the tapwater after 2 days would essentially cause tests in tapwater to be 2 days behind the NaCl tests in terms of establishing conditions for $CaCO_3$ precipitation and this "time lag" more or less wipes out any differences in the detectable onset of crack blocking between the two solutions.

At this point it is worthwhile discussing the relevance of the observations on blocking in the two test solutions to practical situations of fatigue loaded reinforced concrete members in corrosive environments. Clearly in circumstances where the concrete was subjected to a steady flow of continuously replenished water, crack blocking by $CaCO_3$ deposition might not be expected as the dissolved lime would be continuously swept away from the concrete surface. On the other hand, more stagnant conditions would be more alkaline to the circumstances prevailing in the tests undertaken in this work. Indeed, in such practical circumstances, crack blocking might occur even easier than in these experiments on account of the probable attainment of solution pH levels nearer 11-12 than the 8.5 maintained in the experiments. Higher pH means higher $[a_{Ca}2 \times a_{CO_3}2-]$ ion activity products and hence higher degrees of over saturation of $CaCO_3$. The pH dependency of the precipitation process has been described earlier by Hodgkiess and Arthur[206] who assessed the effect of temperature and pH upon the tendencies towards the production of deposits in seawater. Their study showed the dramatic effect of pH upon the saturation of seawater with both $CaCO_3$ and $Mg(OH)_2$ as illustrated in Figure 8.13 in which the concentration product $[C_{Ca}2+ \times C_{CO_3}2-]$ and $[C_{Mg}2+ \times (C_{OH}-)2]$ are plotted against pH values. Their conclusions have been that the effect of a localised increase in solution pH within pore water and cracks outweighs any moderate temperature effects and hence the seawater is supersaturated with respect to the two compounds over the temperature range investigated.

Another observed feature of the crack blocking was that once its occurrence had been detected, there was a faster rate of subsequent build-up of deposit at cracks

(observed both visually and via beam deflection) in tapwater as compared with NaCl solution. This is more pronounced in beams tested at the optimum-blocking load level i.e. loads corresponding to the upper steel stress of 0.6 and 0.7 f_y (compare Figure 8.4 with Figure 8.8). This feature might have been caused by a slightly lower degree of oversaturation of $CaCO_3$ inside cracks in the NaCl tests as a result of somewhat lower crack-interior pH caused by the local presence of corrosion products from the rebar. In support of this postulation it can be said that:

1. A local build-up of Fe^{2+} ions (or of Fe^{3+} ions but these were not evident in the lowO_2 conditions within partially-blocked cracks) can produce H^+ ions by hydrolysis reactions such as:

$$Fe^{2+} + H_2O \text{ --> } (FeOH)^+ + H^+$$

2. Subsequent examination of bars removed from beams after tests revealed evidence of more severe corrosion at concrete crack sites in beams exposed to the NaCl solution but not in tapwater.

3. Deposition rates from aqeous solution are often found to be proportional to the degree of supersaturation of the depositing compound.

However, despite the above arguments, it must be readily admitted that proof of this postulation would require local pH determination within concrete cracks. To the writer's knowledge, these have not been done by anyone although some indirect evidence of lowered pH local to corroding rebar within concrete were obtained by Grimes et al.[146]

8.6.2 Nature and Level of the Applied Load.

Under reverse bending conditions, it does appear that this process has a reduced tendency, and therefore takes

longer, to become established. A possible explanation for this trend might have been the effect of the hydro-dynamic conditions within the cracks since in beams subjected to reversal of loading the gradual accumulation of deposit material within the cracks may be inhibited by the complete closure of the cracks on each load cycle. It may also be that rather similar hydraulic pressure effects in washing out deposited material from the cracks, might have accounted for the delayed onset of crack blocking in the only case of blocking observed in the lowest load reverse loading condition (MR35W) and at the two uni-directional higher stress ranges (corresponding to steel upper stress level of 0.75 and 0.85 f_y) in comparison with lower stress ranges (0.6 and 0.7 f_y).

This effect may also be responsible for the absence of deposits at the lower parts of the cracks outer surface despite its existence in the upper parts of the cracks (for 0.75 and 0.85 f_y uni-directional tests). However it is worth mentioning that this does not mean in any case the absence of deposit at the internal lower part of the cracks its self since deposit does exist at the internal surface of the crack as shown in Figure 8.15 which indicates the internal blocking under extreme hydraulic condition of test at a maximum load level corresponding to 0.85 f_y and also indicates that healing starts from interior points. A good example on the effect of hydraulic pressure is shown in Figure 8.3a,b which indicates the initial accumulation of deposit material at the upper parts of the cracks where the pressure is at its minimum, Figure 8.3a. However, when blocking becomes effective it reduces the free passage and the pressure of water inside the cracks, and the ensuing accumulation process becomes independent of the relative position along the crack

The available data as well as the experimental evidence from this study suggest that the effects of dynamic loading on crack blocking depends on:

a. <u>The Rate of Load Application (Frequency).</u>

Although this effect is not fully investigated, the

limited data available from fatigue tests in sea-water[79,150,201,203] indicate that at low frequencies such as 0.1 and 0.17 Hz. Concrete exhibits greater blocking ability than at higher frequencies such as 3 and 5 Hz.

b. The Load Level.

This controls the crack width i.e. the exposed internal surface area, the hydraulic pressure inside the cracks and the pore pressure in the vicinity of crack surface. The conditions at higher dynamic loading have been described earlier in this section, however, at lower dynamic loading levels as well as in static tests, a smaller internal exposed area is available, the degree of expulsion of free lime in concrete through the cracks is minimal and mass transfer and water movement are more restricted. Therefore beams under these conditions experienced an appreciably smaller amount of blocking than those of the former case. It has been observed that the blocking ability of concrete was enhanced under dynamic loading in comparison with static-type of loading. This may be attributed to the increased solubility of the solid phase of the material inside the cracks due to the mechanical destruction and grinding effect provided by this type of loading. Fatigue loading also provides greater internal surface area of the cracks available for blocking reactions.

The above discussion suggests that there is no unique relationship between load level and the amount or more accurately the effectiveness of crack blocking. It is rather suggestive of the existence of an optimum level of dynamic loading at which the phenomenon of crack blocking is at its maximum and at which change in structural behaviour towards less severe conditions would occur at the earliest possible time. The optimum dynamic load level for blocking was found to lie somewhere between load levels corresponding to upper stress levels of 0.6 and 0.7 f_y as shown in Figure 8.14.

The results therefore clearly indicate that for saturated conditions blocking can occur even when the

cracks are active and subject to movement. In fact, in some cases, these conditions promote rather than retard the progress of crack blocking and the absence of tensile stress across the crack is not necessary for the blocking process to proceed.

8.6.3 Age at the Start of Test.

As stated earlier, the test program covers a wide range of concrete beam's age, from 33 days to approximately 8 years and considering the reduction in deflection range as a reasonable indicator of the initiation and growth of blocking material to an effective extent in addition to visual inspections, it would appear that under favourable dynamic conditions of loading level and frequency, concrete is able to block cracks over the whole age range considered in this study as shown in Table 8.1a. Crack blocking probably takes place beyond this period but this was the limit of the experimental work. Interestingly older beams (MU601Y and MU60N8Y) exhibit even earlier blocking than other younger beams under similar test conditions.

The cement compounds that are mostly responsible for strength properties of portland cement are tricalcium silicate (C_3S) and dicalcium silicate (C_2S). Of these the former reacts with water at such a rate that with ordinary mixes and moist curing it is completely hydrated between 3 and 12 months. The dicalcium silicate reacts more slowly, becoming conspicuous only after about a month and continuing for some years. On a weight basis both silicates[228] require approximately the same amount of water for their hydration but C_3S produces more than twice as much $Ca(OH)_2$ as is formed by the hydration of C_2S. The rate of hydration decreases continuously so that even after a long time there remains an appreciable amount of unhydrated cement.

The principal products of this hydration are, as well as crystalline calcium hydroxide, tricalcium aluminate hydrate, calcium sulphoaluminate and amorphous hydrated calcium silicate. Other material in small amount may also

be present. As the test beams were of identical mix proportion and cured the same way, it would be expected then that older beams would have:

- lower hydration rate
- less unhydrated cement
- more calcium hydroxide content

Therefore in attempts to draw conclusions, crack blocking may occur in either or both of the following processes.

Direct Process.

The dissolution of some of the readily available $Ca(OH)_2$ by the action of the surrounding solution, thus increasing the ionic activity product in the solution and allowing precipitation as described earlier (Sub-Section 8.4.1).

Indirect Process.

The re-commencement of the natural hydration process in the presence of abundant water at crack internal surfaces. The new hydration product of $Ca(OH)_2$ at the concrete-solution interface then behaves as in the above "direct process" to produce deposit or it may become carbonated where exposed to air or carbonated water.

It seems likely, however, that both factors contribute, but to different degree, to the formation of blocking material with the possibility of the "direct process" being more predominant particularly for more mature beams.

8.6.4 Effect of Blocking on the Structural Behaviour of the Test Beams.

This is discussed in Chapter 7.

8.6.5 Effect of Blocking on Corrosion of Steel.

This is discussed in Chapters 10 and 12.

8.6.6 Surface Skin.

It has been demonstrated that concrete exposed to sea water may develop a surface skin producing marked reduction in permeability of concrete. The skin typically[23] consists of a layer of brucite ($Mg(OH)_2$) of around 30 μm thickness overlain by a thicker but more slowly developing layer of aragonite. In the present study, it was also found as stated in the deposit identification section that the chemical composition of the skin material was identical to that of the crack blocking material (namely, $CaCO_3$), from which one may envisage the development of surface skin as a special case of the blocking process with its distinct characteristics and effects. One of these is the limited but uniform source of deposit i.e. from the surface and very small hair cracks. Due to the fact that the concrete surface is the most treated area during curing and full hydration is likely to be achieved, the direct process of precipitation is the predominant process in these areas. At crack sites, the source of blocking material differs in nature and quantity, in nature since it comes from the less hydrated areas and in quantity because the internal exposed area for a given surface crack area is high compared with a similar uncracked area, thus blocking at crack sites is more conspicuous than at other areas.

8.6.7 Deposition Outside the Jacket.

Deposition usually occurs on the first crack in the concrete outside the jacket. Concrete outside the jacket, however, exhibits some degree of saturation which decreases as the distance from the jacket increases. Thus water may reach the external cracks by some internal paths. The nature of the seeping water is expected to influence the composition of deposit material. For

chloride solution the greater part of the solution reaching the crack may evaporate leaving a salt residue (NaCl) in place and some of the remaining water reacts with the concrete constituents and CO_2 in the surrounding air to produce $CaCO_3$ (calcite). The same is true for tapwater tests, where some of the water reaching the crack evaporates whereas the remaining portion is consumed in the formation of the deposit following the same mechanism mentioned above. Clearly no salt residue can be formed in this case.

8.6.8 Brownish-Red Deposit.

This kind of deposit was only observed in the highly aggressive exposure conditions of the chloride solution, and at lower load levels. The fact that this material is very soft explains why it would not be expected to be observed in active situation afforded by high amplitude dynamic loading. This observation substantiates the importance of having dense, well compacted concrete so as to reduce the internal paths and increase the concrete resistivity. This phenomenon appears to be confined to dormant conditions, such as the upper parts of the beam, and thus was not observed near crack sites. It should be pointed out that the chemical composition of this material is not merely iron component since tangible amounts of SiO_2 and Na_2O were found and this presumed to be originated from some concrete constituents and aggregates in particular.

Table 8.1-a: Blocking Phenomenon - Uni-directional Bending Series.

Environment	Programme Phase	Beam designation	Intended stress range in (N/mm^2)	Age at start of test (days)	No. of cycles when reduction first recorded	
					in deflection range	in crack opening range
Water	II	MU40SW	138	45	101.2×10^3	N.M.
		MU60SW	230	45	42.5×10^3	-
		MU70WN	276	55	72.4×10^3	-
	I	MU70W	276	33	44.1×10^3	41.1×10^3
		MU75W	299	55	119.1×10^3	N.M.
		MU85W	345	56	99.6×10^3	73.1×10^3
Air	I	MU70A	276	198	No reduction	
NaCl	II	MU40IN	138	49	55×10^3	N.M.
		MU40SN	138	45	67.5×10^3	-
		MU40SN	138	49	47.5×10^3	-
		MU60IN	230	79	28×10^3	-
		MU60SN	230	57	39×10^3	-
		MU60SN	230	49	28.7×10^3	-
		MU60N1Y	230	419	22.8×10^3	-
		MU60N5Y	230	2740	19.2×10^3	-
	I	MU70N	276	37	39.6×10^3	45.3×10^3
		MU75N	299	33	91.3×10^3	N.M.
		MU85N	345	37	72.0×10^3	83.6×10^3

N.M. - Not Measured

Table 8.1b: Blocking Phenomenon - Reverse Bending Series.

Environment	Programme Phase	Beam designation	Intended stress range in steel (N/mm^2)	Age at start of test	No. of cycles when reduction first recorded	
					in deflection range	in crack opening range
Water	I	MU35W	164	175	446.7×10^3	490.8×10^3
		MR46W	216	1580		
		MR70W1	328	1825		
		MR70W2	328	34		
		MR75W	351	1811	No change	No change
		MR85W	398	1765		
NaCl	I	MR70N	328	1862		
		MR75N	351	1840		
		MR85N	398	1846		

Table 8.2: Chemical Analysis of Deposits.

Elements	Percentage by weight			
	MU603N I	MU605W II	MU405W III	MU405N IV
SiO_2	1.22	1.09	0.64	9.76
TiO_2	0.04	0.03	0.03	0.01
Al_2O_3	0.46	0.24	0.29	0.32
Fe (total)	0.73	0.33	0.43	45.98
MnO	0.03	0.02	0.03	0.03
MgO	0.43	0.44	0.28	0.32
CaO	53.47	46.77	54.59	0.31
Na_2O	0.00	0.52	0.00	8.67
K_2O	0.05	0.06	0.06	0.00
P_2O_5	0.04	0.09	0.12	0.08
Total	56.47	49.59	56.47	65.48

I, II, III - white deposit
IV - red-brown deposit

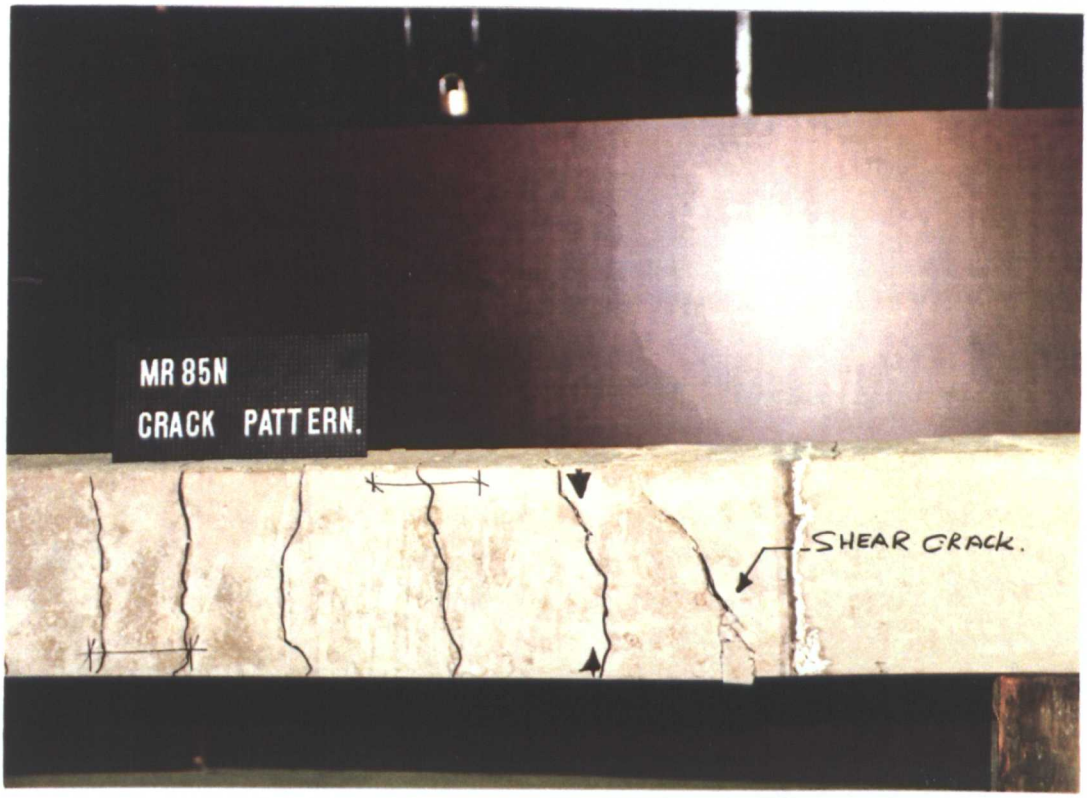

Figure (8-1): Blocking phenomenon;reverse bending test (MR85N).

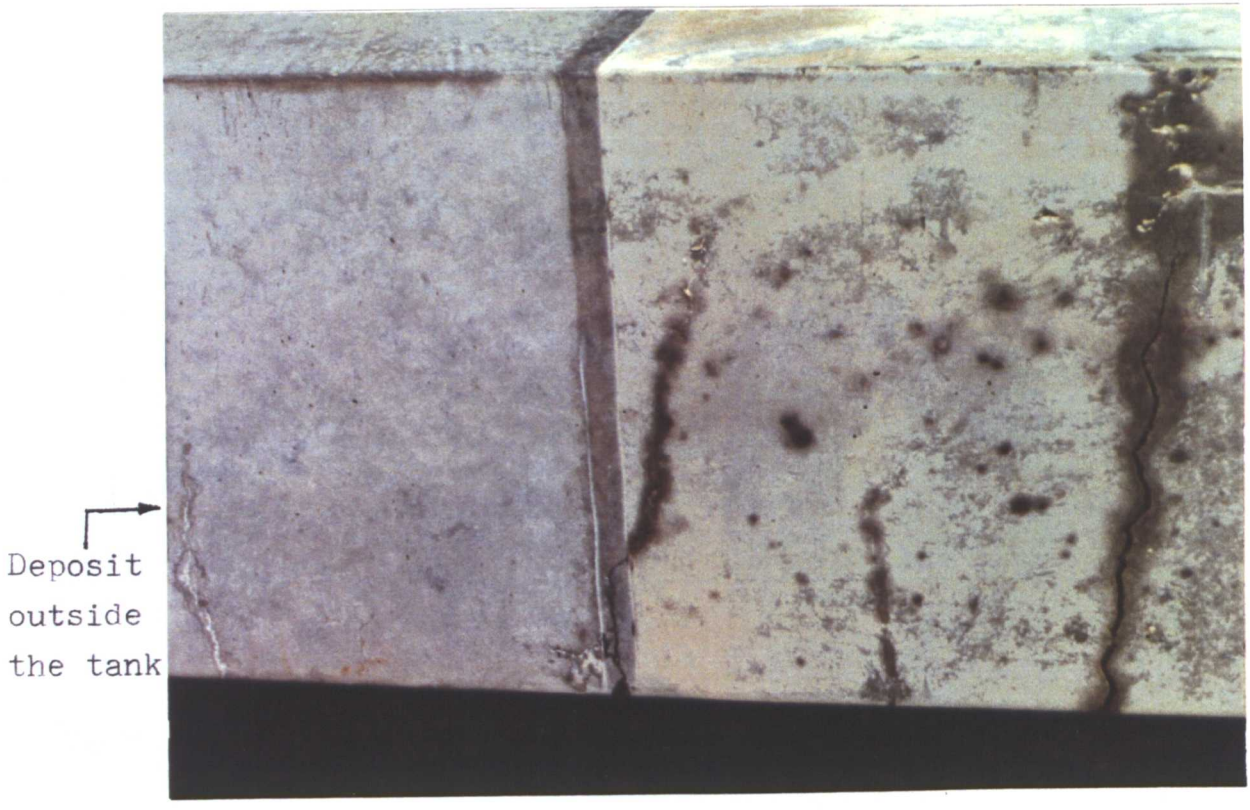

a) Blocking in and outside the jacket

b) Blocking at the upper region of the cracks

Figure (8-2): Blocking phenomenon;water test beam MU85W.

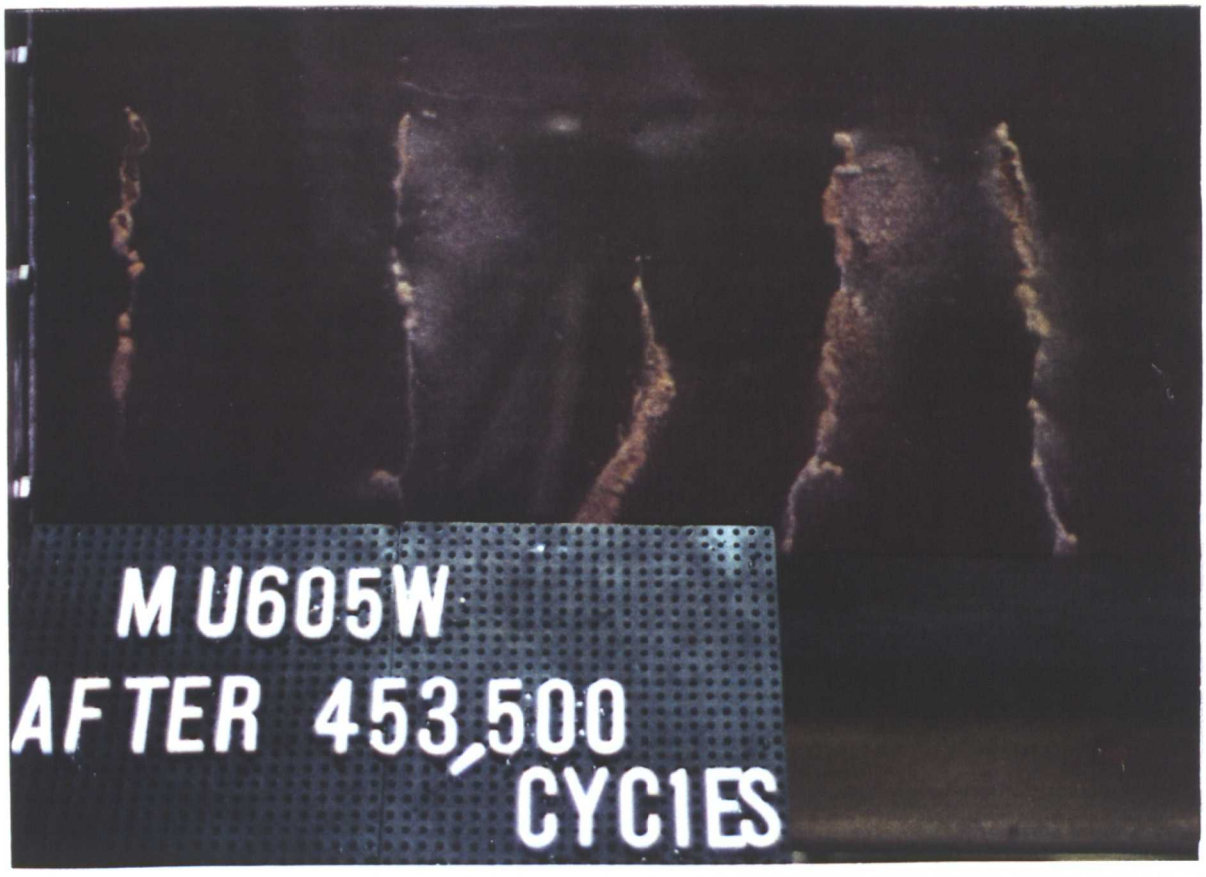

Figure (8-3-a): Blocking after 453500 cycles

Figure (8-3-b): Blocking after 898000 cycles

Figure (8-3-c): Blocking after 2160000 cycles

Figure (8-3): Blocking phenomenon;developement of blocking in water environment;beam MU605W.

Figure (8-4): Blocking phenomenon;blocking at beams soffit;beam MU605W.

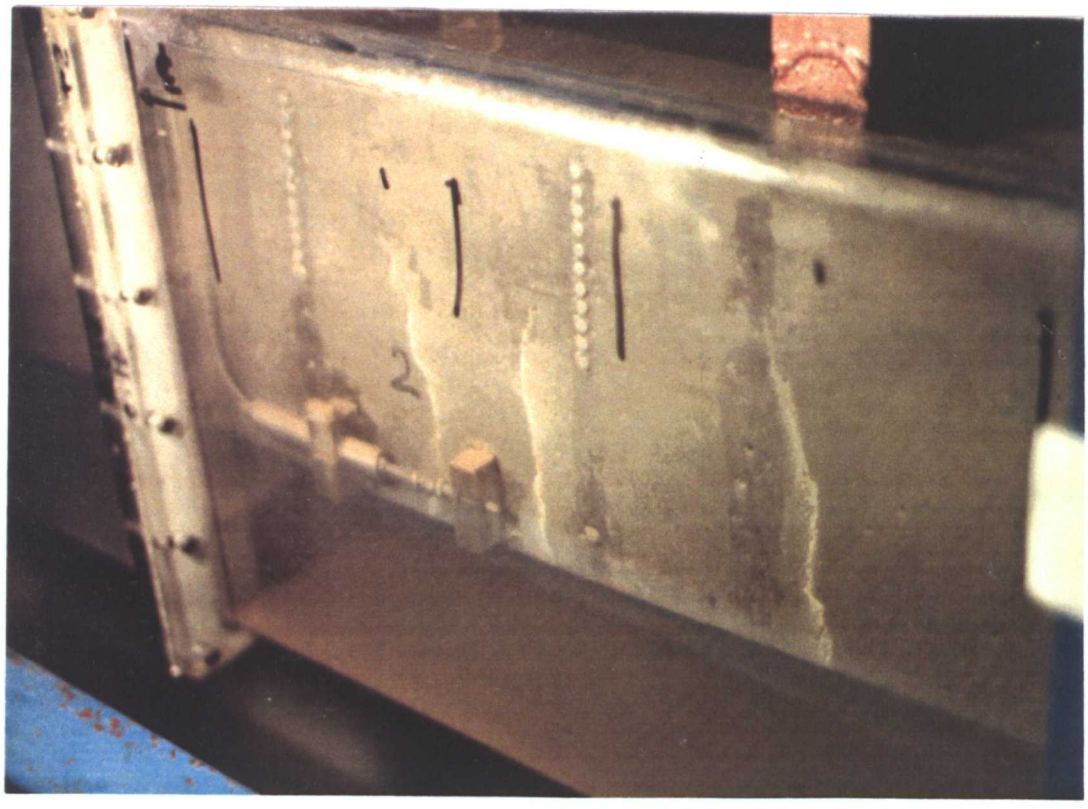

a) Blocking after 220000 cycles

b) Blocking after 691000 cycles

Figure (8-5): Blocking phenomenon;beam MU70W (the figure also shows the transducer for crack width measurements).

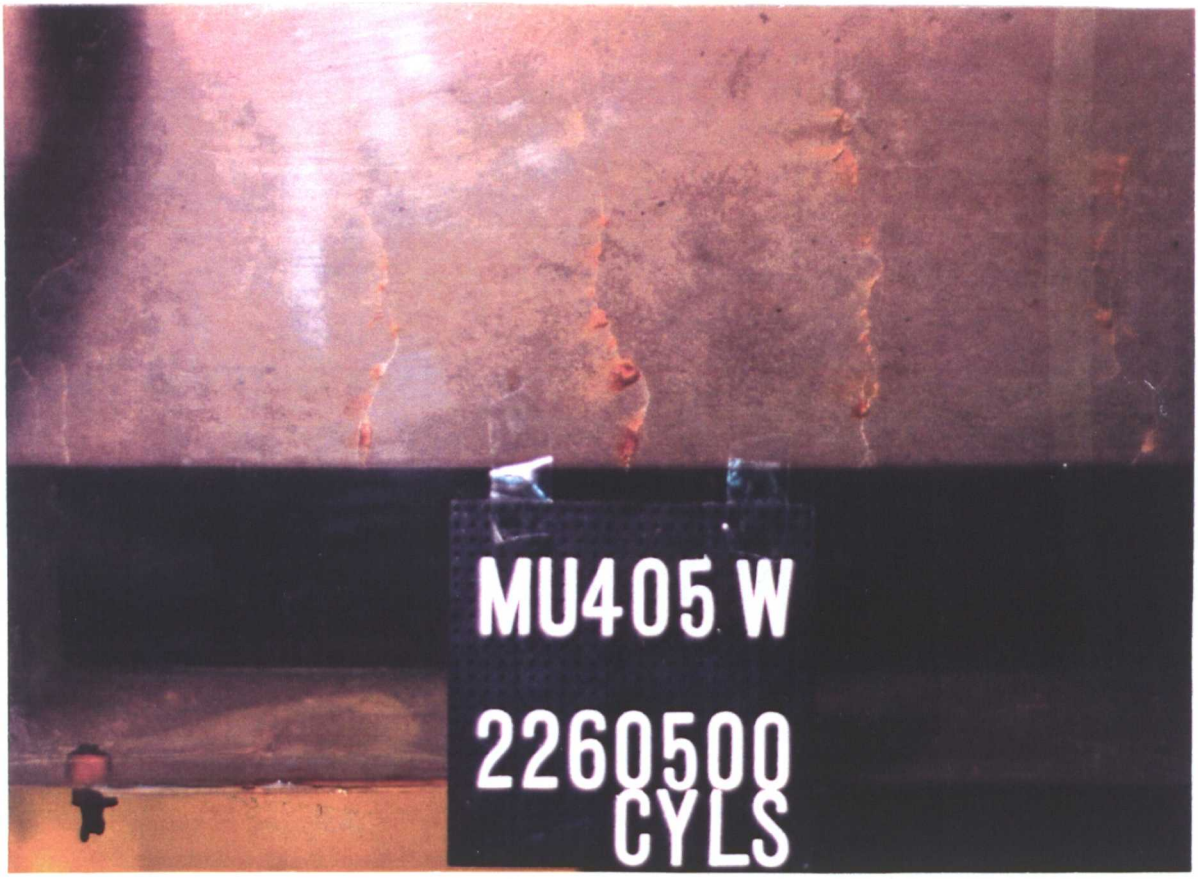

a)

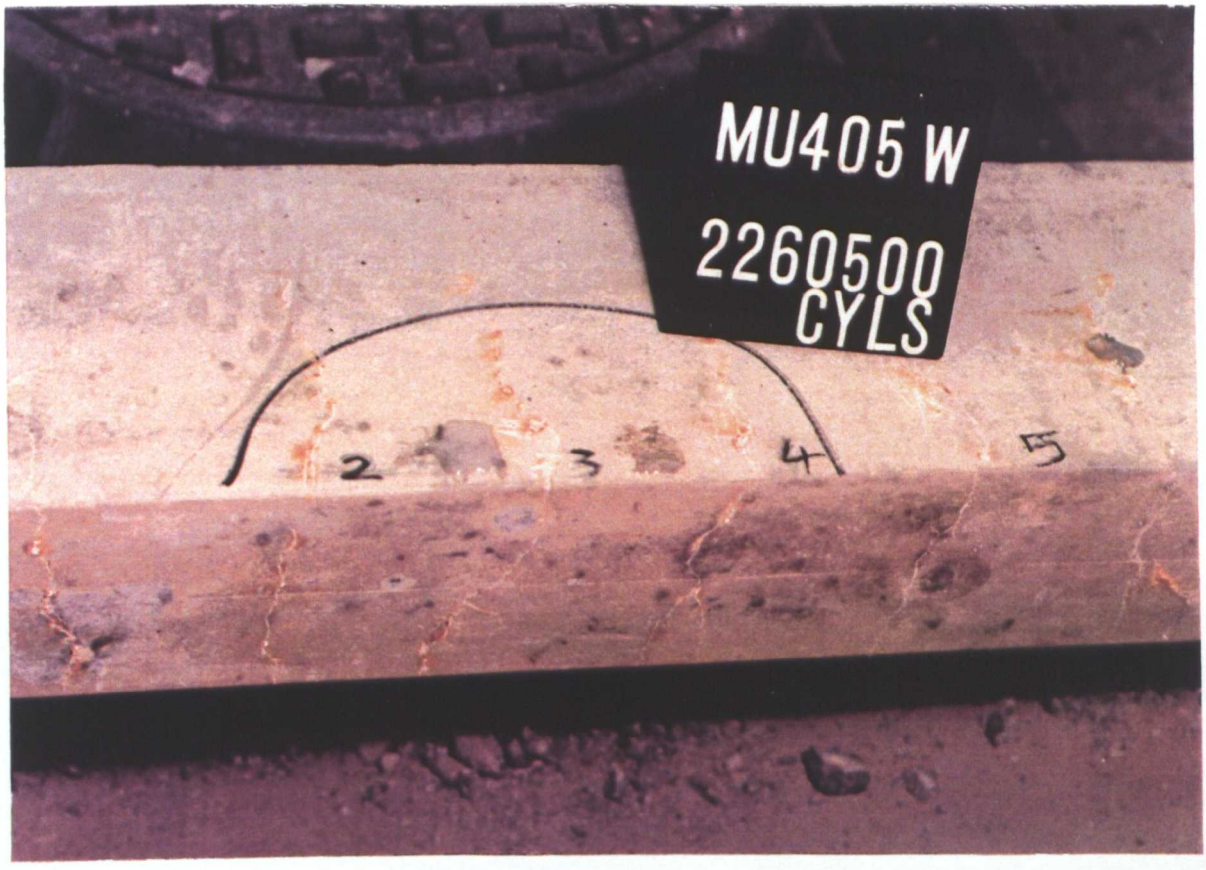

b)

Figure (8-6): Blocking phenomenon;water test at lowest load level beam MU405W.

Figure (8-7-a): Blocking after 423000 cycles

Figure (8-7-b): Blocking after 1669000 cycles

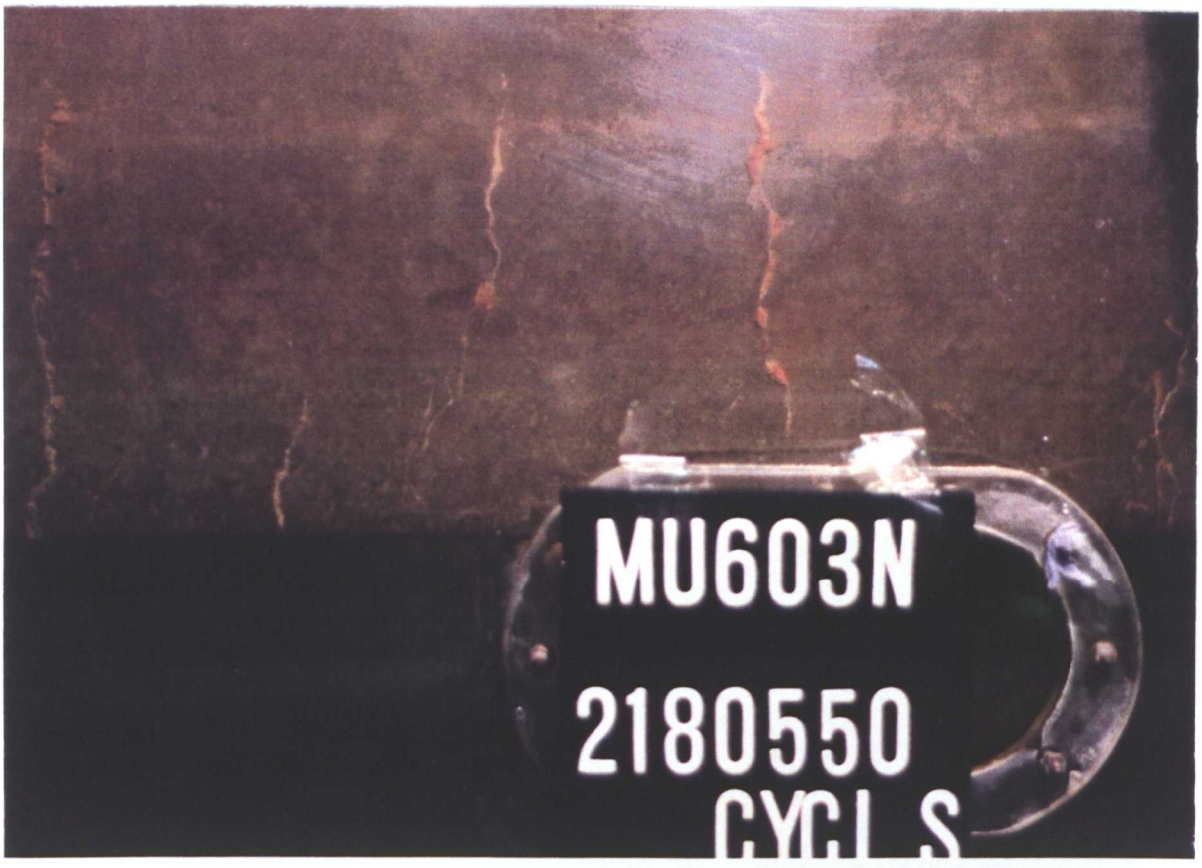

Figure (8-7-c): Blocking after 2180550 cycles

Figure (8-7): Blocking phenomenon;developement of blocking in chloride environment;beam MU605N.

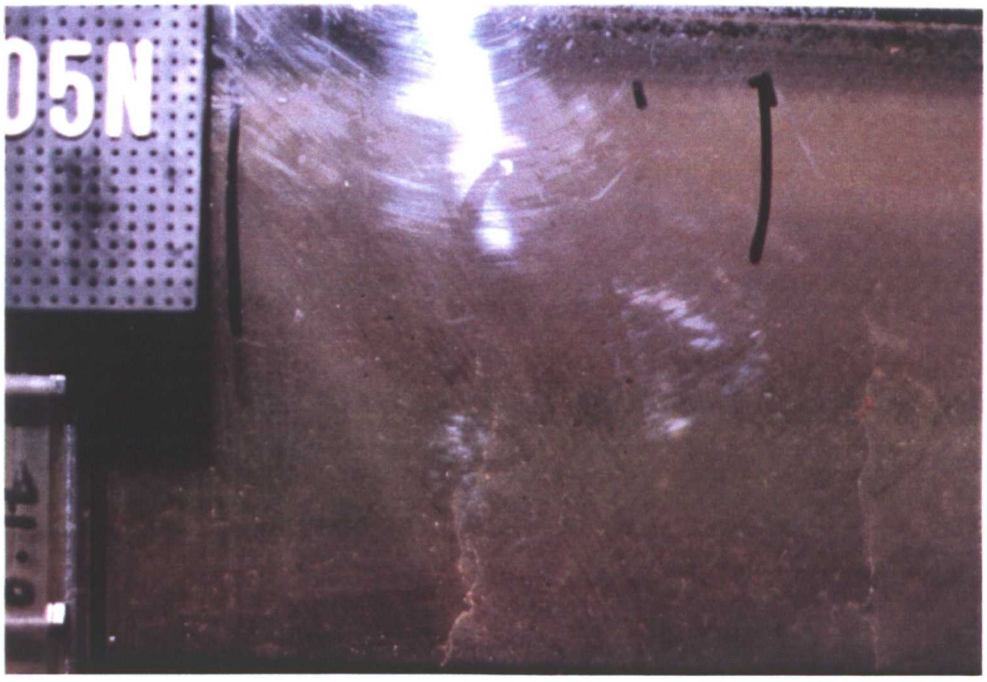

a)

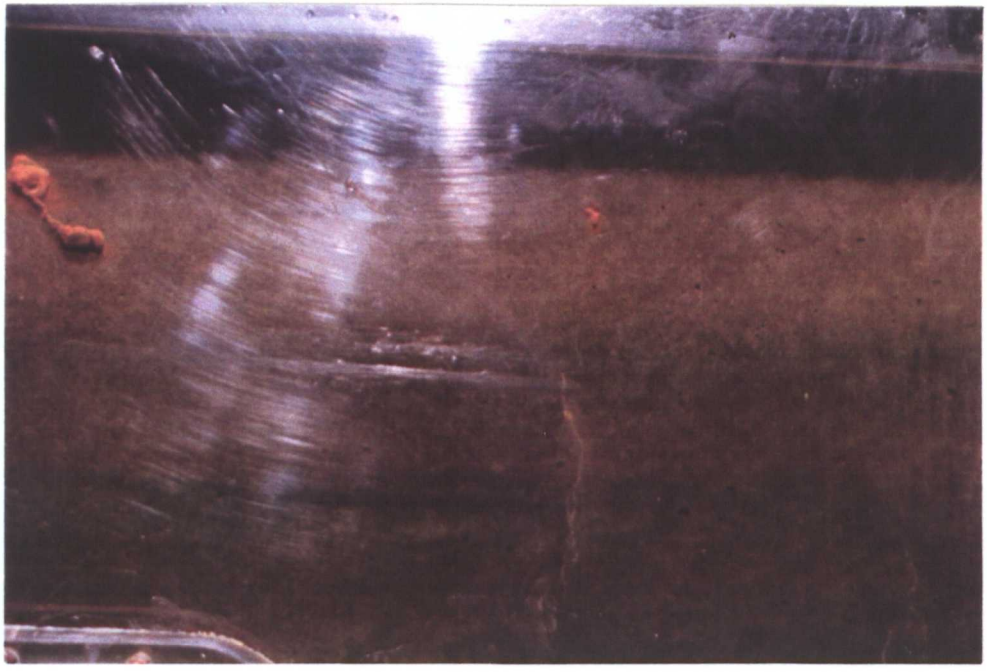

b)

Figure (8-8): Blocking phenomenon;chloride test at the lowest load level;beam MU405N

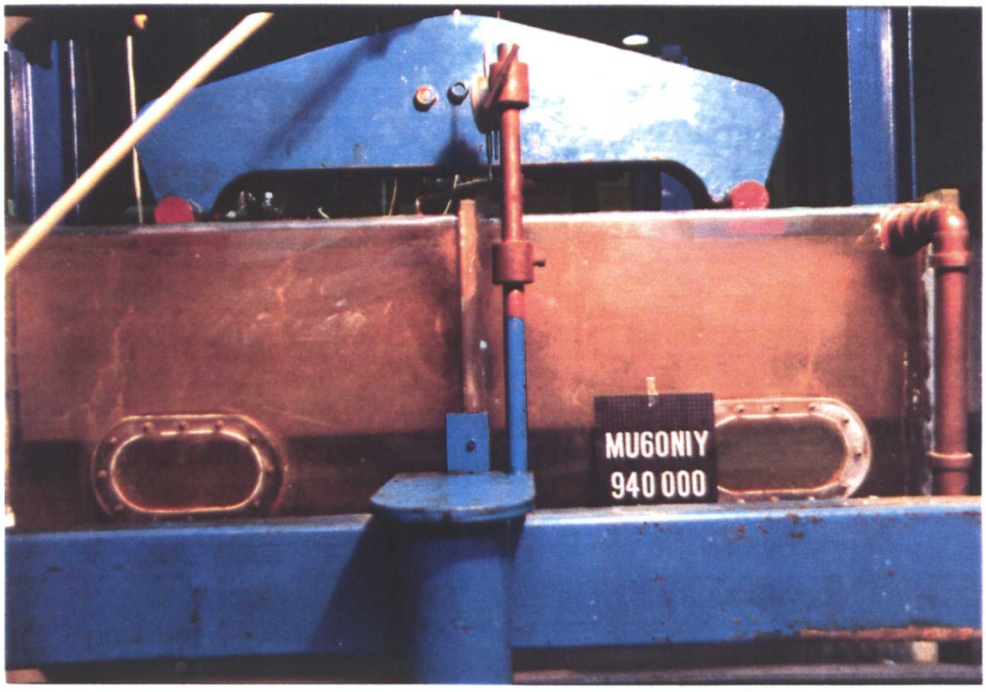

a) One year old

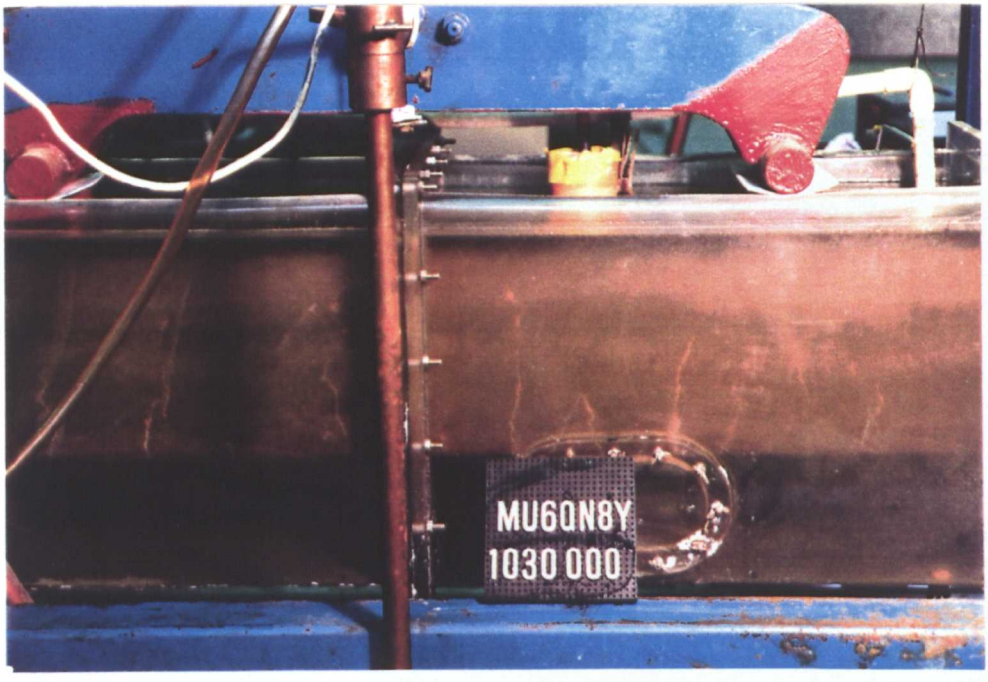

b) Eight years old

Figure (8-9): Blocking phenomenon;blocking for older beams in chloride solution;beams MU6ON1Y and MU6ON8Y.

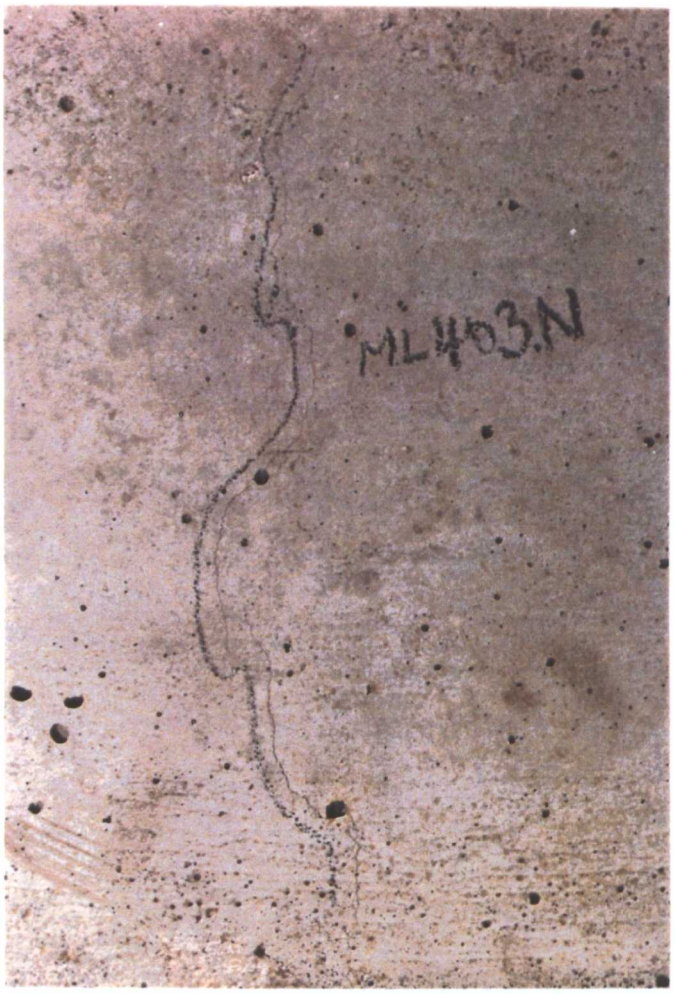

a) Absence of blocking ML403N

b) Reddish-Brown batches ML403N

Figure (8-10): Blocking phenomenons static test at the lowest load level in chloride solution; beam ML403N.

c) Small amount of blocking;beam ML603N

Figure (8-10): Blocking phenomenon;static tests in chloride solution;beams ML403N and M1603N.

a) A concrete piece after 5 months exposure to chloride solution

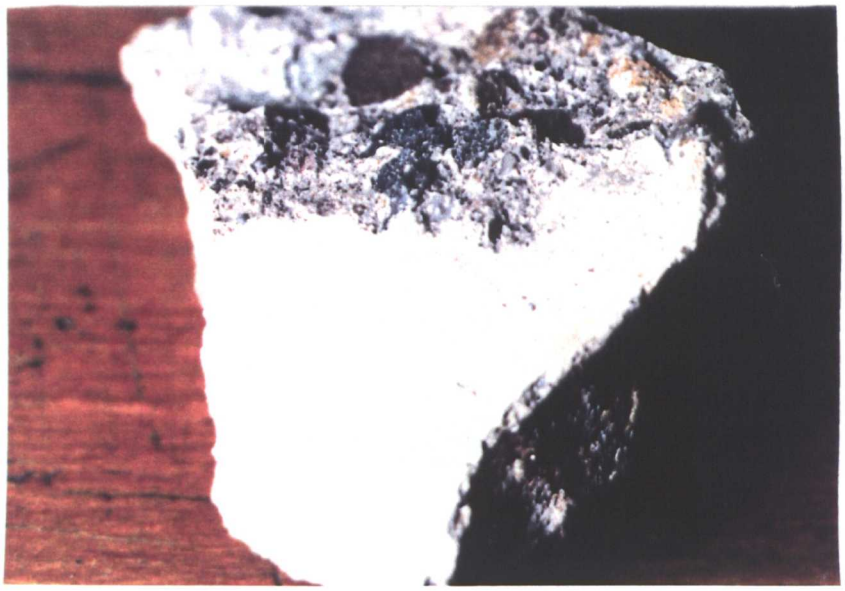

b) Part of fig. a under microscopic examination

c) Concrete piece before exposure

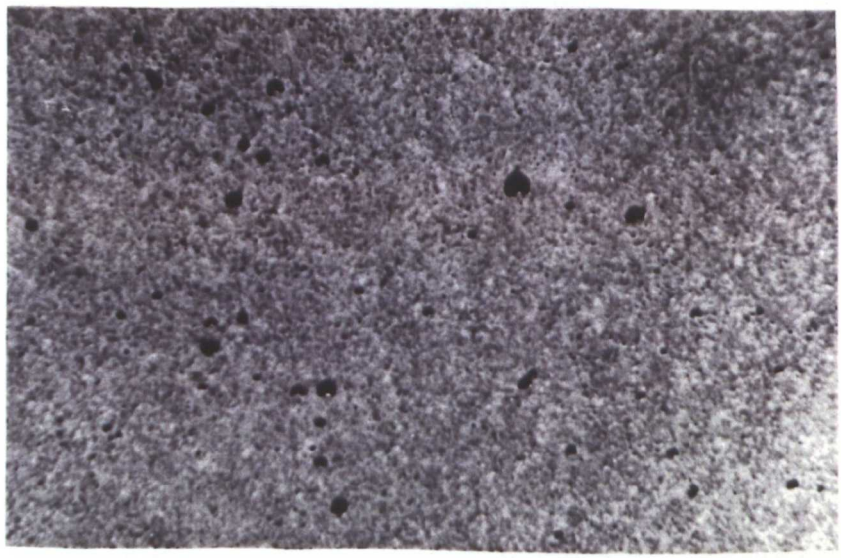

Figure (8-11): Surface skin;beam MU605N.

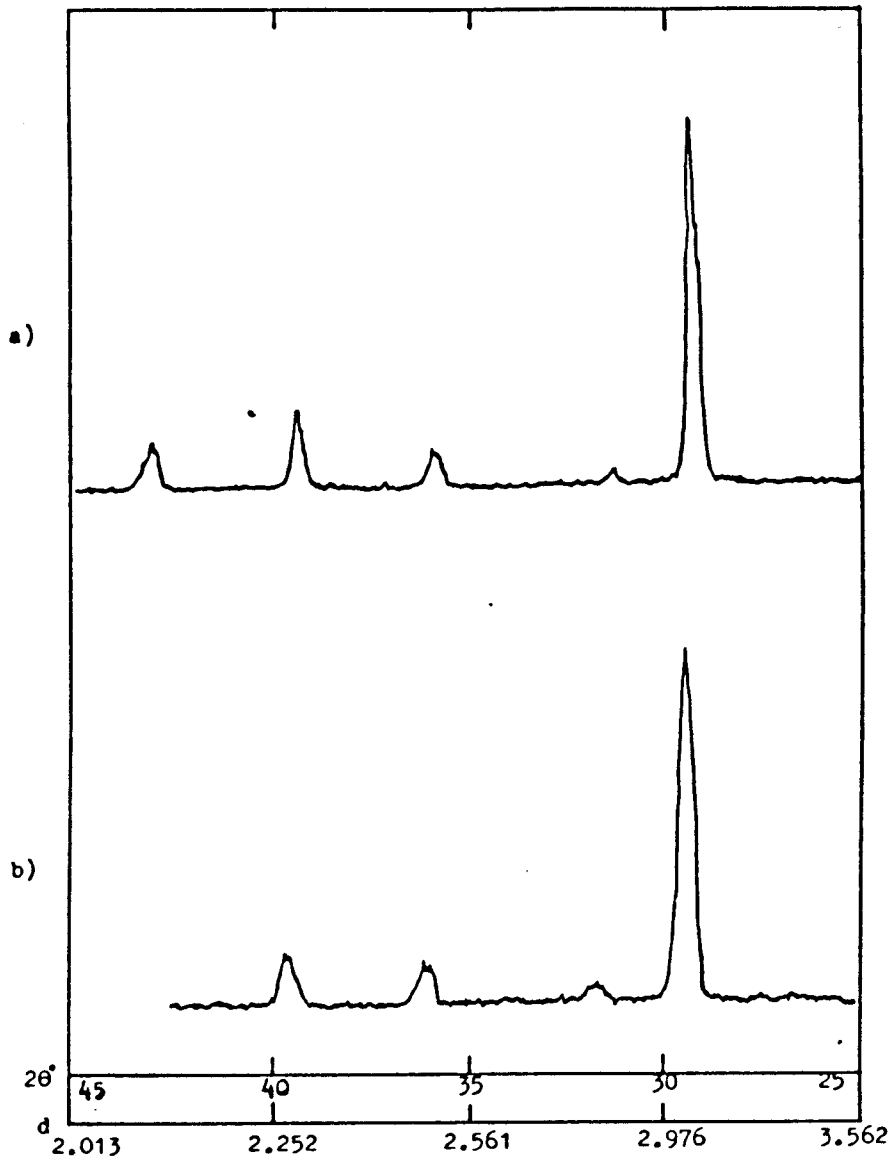

Figure (8-12): Blocking phenomenon;XRD-pattern for deposits from;a: Beam MU70N;submerged cracks.
b: Beam MU85N;submerged cracks.

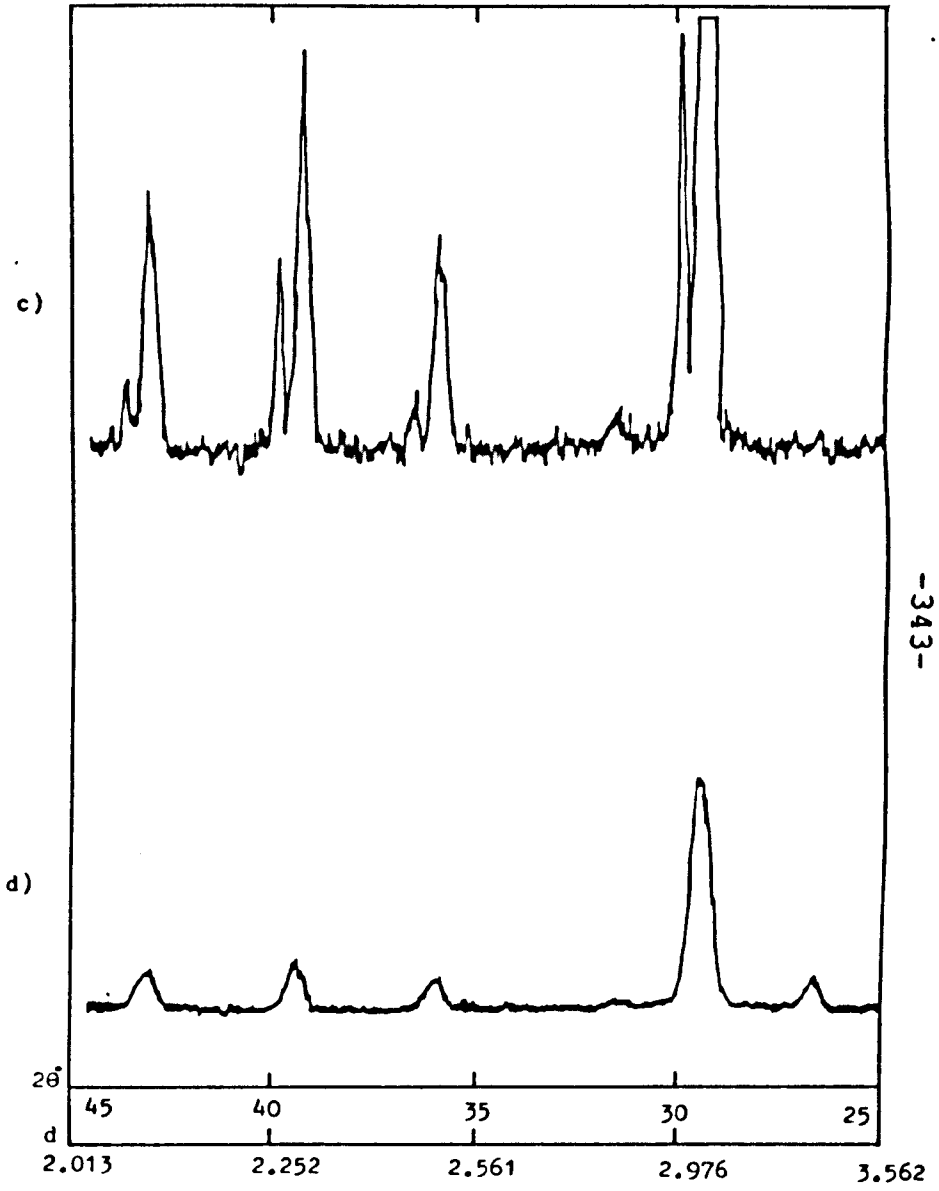

Figure (8-12): Blocking phenomenon;XRD-patter for deposit from; c: Beam MU35W;submerged cracks.
d: Beam MH46W;cracks outside the solution jacket.

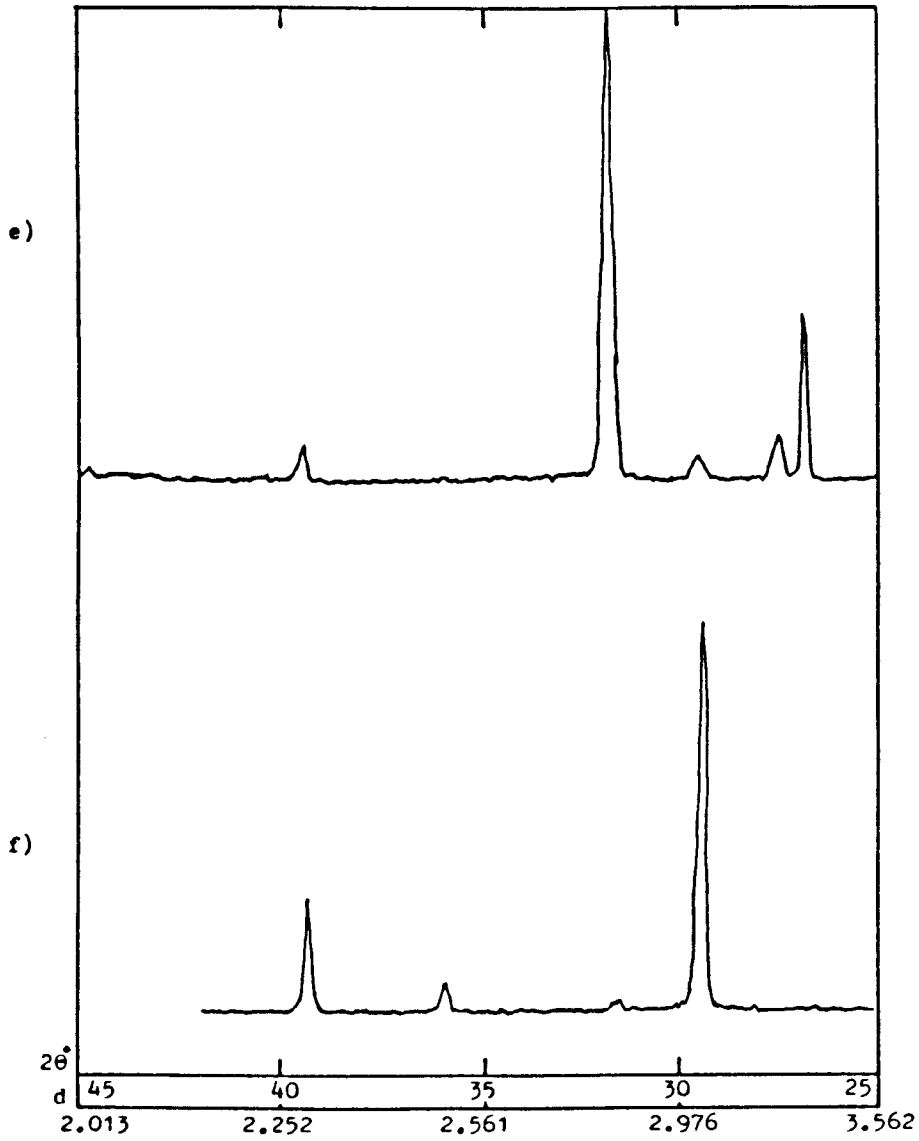

Figure (8-12): Blocking phenomenon;XRD-patter for deposit
from e: Beam MU60N8Y;cracks outside the
solution jacket.
f: Beam MU605N;concrete surface
skin inside the solution jacket.

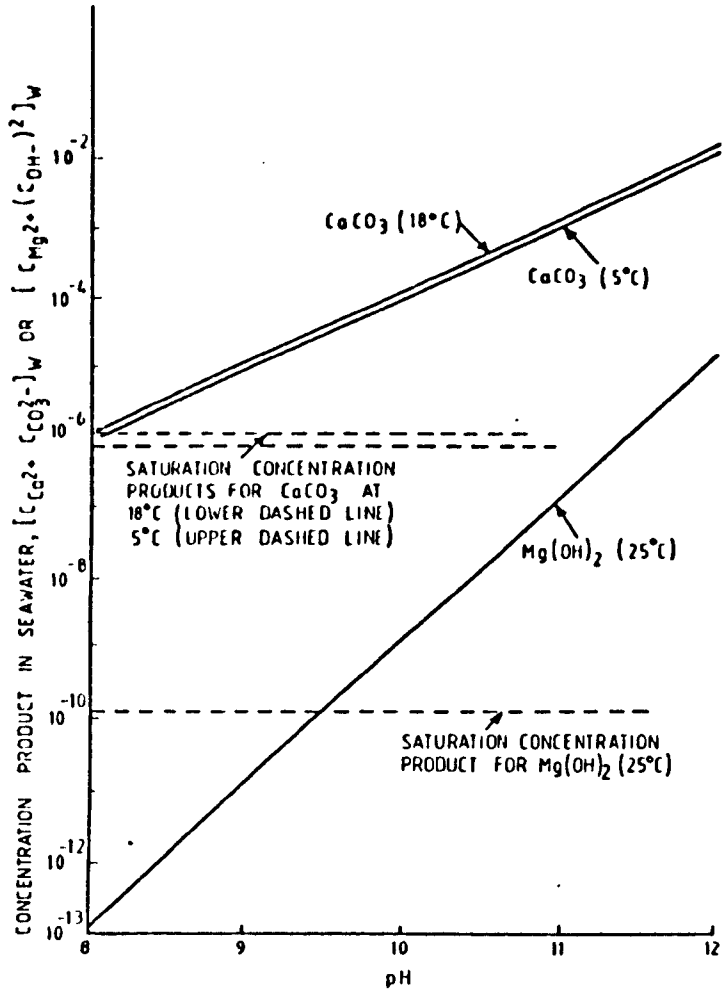

Figure (8-13): Effects of temperature and pH on solubilities of $CaCO_3$ and $Mg(OH)_2$ in seawater solution (Ref.206).

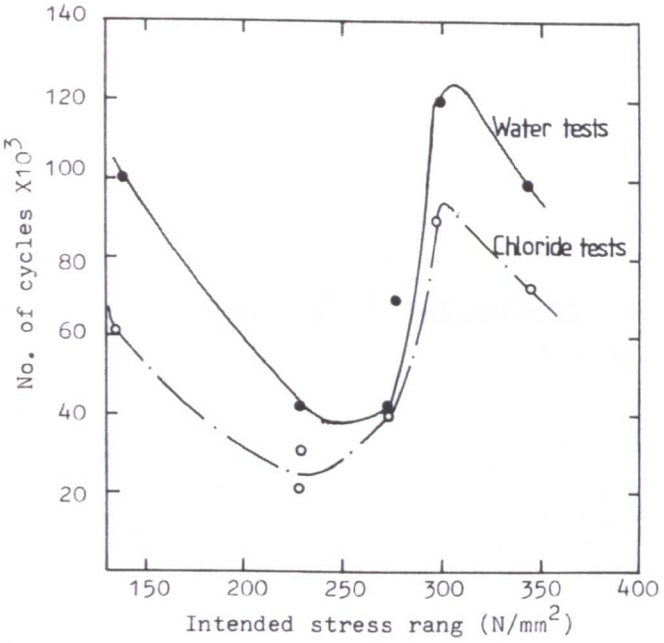

Figure (8-14): Blocking phenomenon;intended stress range vs. No. of cycles at which reduction in deflection range first recorded (Unidirectional bending).

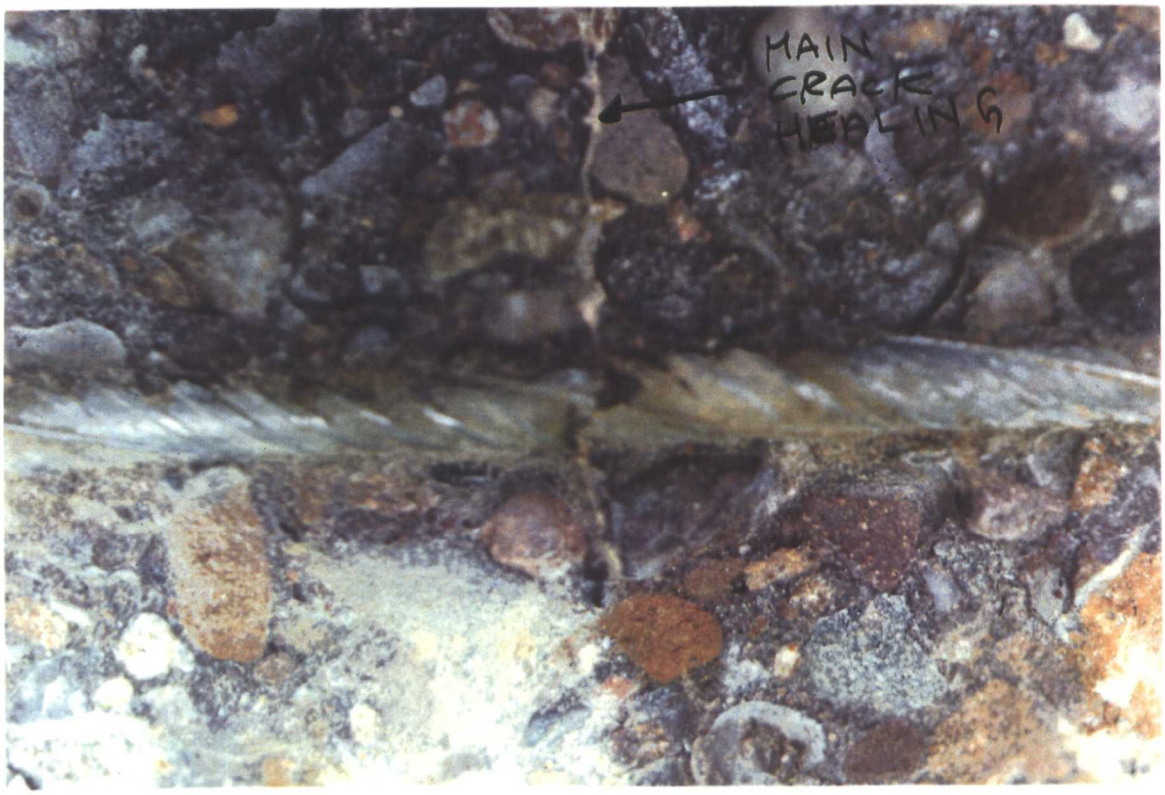

Figure (8-15): Blocking phenomenon;blocking at the interior part of the cracks;beam MU85W.

CHAPTER 9

CONCRETE RESISTIVITY MEASUREMENTS (EXPERIMENTAL DETERMINATION OF IR-DROP)

CHAPTER 9

CONCRETE RESISTIVITY MEASUREMENTS (EXPERIMENTAL DETERMINATION OF IR-DROP)

9.1 The Problem.

The electrochemical measurements using the linear polarisation method were initially made with the IR-Drop effects being allowed for by separate single measurement of the concrete resistance. This was accomplished by applying an A.C. voltage of 16V, 50 Hz between the embedded steel and the counter electrode. However, this practice was abandoned for the following reasons.

1. The application of a voltage across the system which is high when compared with the corrosion potential may perturb the electrochemical measurements. This was confirmed by monitoring electrode potential during measurements as an immediate one direction change of ~420 mV was recorded and this remained at a new level during the voltage application. The electrode potential, however, returned to approximately its original value within 6 seconds after the A.C. current was cut off.

2. Separate measurements require their own arrangements and instrumentation thus increasing the time required for each set of measurements.

3. It was not clear at that time whether there is or not, for the condition studied, any difference between the electrical response to A.C. and D.C. source of

voltage, also if there is any dependence of the resistance value on the applied voltage since the potential shift during polarisation represents a very small proportion of the applied voltage for resistance measurements.

4. The resistance value obtained from single measurements is generally considered less accurate than its value being determined from a slope of a line through several points.

The above mentioned points may result in an erroneous estimation of the resistance especially when the ratio of polarisation resistance to the electrolyte resistance i.e. R_p/R_s is small as in the case of active corrosion. It may therefore be appropriate to determine the IR-drop by applying the same amount of potential shift (10 mV) as is applied during polarisation measurements and to adopt the same kind of voltage (i.e. D.C.).

One of the direct methods[39,40] for eliminating the IR-drop effect is the so-called positive feedback method which is provided in many recent commercial potentiostats as an electronic compensation phase facility. Unfortunately, however, with a complex current multipath of the saturated system under study, this method has proved troublesome and very delicate despite the use of an oscilloscope to detect the compensated resistance. This has been the case with the two potentiostats available for this research.

Preliminary experiments supported by theory have shown the possibility of the application of the current interruption technique (see Section 3.4) to provide a good degree of accuracy in determining the voltage drop across the electrolyte. The fact that the use of this technique needs virtually no extra instrumentation and is thus time saving made this technique more attractive for further examination to establish its validity and limitations in comparison with other conventional methods for resistance determination. This has partly been promoted by the lack of information in this specific area

and the unknown effect of the application of conventional methods on the electrochemical condition of systems involving reinforcing bars in a state of active corrosion.

In response to this an experimental program was undertaken for concrete resistance determination to provide information with regard to:

1. The potential use and limitation of the current interruption technique as an experimental tool to determine the electrolyte contribution to the voltage during the electrochemical measurements (L.P.M.).

2. Provide a comparison between different method of measurement under identical test conditions.

3. The effect of different measuring methods on the electrochemical condition of a system involving reinforcing bars undergoing active corrosion.

9.2 Scope of the Tests.

The experimental program includes measuring the concrete resistance by 5 different methods which are:

Method No.1 Current interruption technique
Method No.2 A.C. measurements
Method No.3 D.C. measurements
Method No.4 Constant alternating current techniques
Method No.5 16V alternating 50 Hz voltage

The electrode potential of the reinforcing steel v.s. S.C.E. was monitored during and after each set of measurements.

9.3 Test Specimen.

Beam MU60N8Y was chosen as the test specimen using which different measuring technique were examined. The beam was 2740 days of age at the time of fatigue testing. Reinforcing details, concrete mix, curing and loading

regime were as described elsewhere in this thesis.

9.4 Test Conditions.

After a 5 day period of saturation in chloride solution, the beam was fatigue tested in uni-directional loading regime. Previous experience indicates that, for a chloride test, a period of fatigue loading would cause a reduction in resistance of about 25% of its pre-loading value after which the decrease would continue at a very low rate followed by a slight increase after blocking began. Therefore the measurements were made after about 95,000 cycles (approximately 7 days). The tests lasted two days during which the change in resistance with time can be considered too small to introduce any error in comparison level.

9.5 Important Considerations and Measurements.

For the various methods used, a voltage of a given magnitude was applied between the embedded steel via the lifting hook and a copper counter electrode positioned in the solution in contact with the beam at a level of the main steel bar, Figure 9.1.

Due to the fact that the application of an external voltage to the reinforcing steel has a polarisation effect, the reinforcement was connected to the negative terminal of the power supply (unless otherwise required) so that the steel would be polarised cathodically during measurements. This practice effectively reduces the influence of voltage application on the electrochemical condition of the system since, as a large number of polarisation measurements conducted in this research have indicated, the effect of cathodic polarisation on the corrosion state of the reinforcement has a much more transitory nature than anodic polarisation.

A simple electric circuit similar to the type shown in Figure 3.28 was used to conduct resistance measurements for all but measuring method No.1. In general measurements were made by applying a voltage across the system

generated by the corresponding power supply and measuring the current flowing by means of a multimeter (SOLARTRON 7045). The half-cell electrode potential of the reinforcing steel via a saturated calomel electrode was monitored throughout the measurements by a separate voltmeter (Thurlby 1905a) with logging facilities. To double check the instantaneous change in Ecorr, an x-y plotter (Rinkadenki Model RY-101) was connected in parallel to the measuring voltmeter which was set at suitable voltage and time scales. Method No.1 was conducted using the potentiostat as will be explained later.

9.6 Test Results.

9.6.1 Current Interruption Technique.

Section 3.4.4 outlines the concept of this technique. In this research the measurements were essentially conducted by step shifting the half-cell potential (via SCE) of the system by controlled amounts (typically $\pm$ 10 mV) by means of a potentiostat (Thompson Ministat E-series). The potential shift was kept constant over the required length of time with continuous observation or data logging the flowing current at suitable intervals. The voltage application rate and amount were controlled by a voltage scan generator (Wenking Model VSG72). The current was then interrupted by switching off the circuit and the instantaneous voltage recorded as well as the current just before its interruption. The resistance was then obtained by Ohms' law:-

$$R_s = \frac{\text{voltage drop}}{I} = \frac{E_p - E_i}{I} \qquad \ldots 9.1$$

where R_s = System resistance
E_p = Polarization potential
E_i = Interruption potention

The instantaneous voltage drop was recorded by means

of either a data logging voltmeter (Thrubly 1905a) capable of storing 3 readings per second which were called out later or alternatively by using a data logger capable of storing 10 readings per second with print out facilities. Which ever was used the data logger was connected in parallel to the x-y plotter to trace the electrode potential behaviour after the release of the controlled potential shift.

It was found that the immediate sharp drop in half-cell potential occurred during approximately 0.6 sec after which the potential changed at a considerably lower rate. This behaviour is illustrated by a typical 530 Orion Data logger print out shown in Figure 9.2 and the electronic recorder plots shown in Figures 9.3, 9.4, 9.5.

To determine the accuracy of this method, resistance values were determined from 3 different potential shifts (5, 10, 15 mV) applied both anodically and cathodically, each of which was imposed on the system for various lengths of time (1, 5, 10 minutes).

Table 9.1 shows the resistance value computer for each of the 18 cases. Figures 9.3, 9.4, 9.5 show the electrode potential behaviour after current interruption for different amount of cathodic shift and time of application.

From these data it can be seen that:

1. The resistance remains constant at about 9 Ω (Table 9.1) independent of the amount of shift (5, 10, 15 mv), the direction of shift (anodic or cathodic) and time of application (1, 5, 10 minutes).

2. For a given time of application the amount of instantaneous potential drop increases as the amount of shift increases, Figures 9.3, 9.4, 9.5. Also for a given amount of potential shift the instantaneous drop increases as the time of application decreases. However, these effects were offset by the flowing currents which produced a constant value of resistance

3. The half-cell electrode potentials restore greater

proportions (70 - 100%) of its original value after approximately 5 - 15 minutes. The lower the amount of shift the faster recovery observed, also for the same amount of shift the shorter the time of application the faster the recovery. This effect is much more apparent in 10 and 15 mV shift than 5 mV shift.

9.6.2 A.C. Measurements.

The A.C. measurements were made using a circuit shown in Figure 3.28. The power was supplied by an oscillator (Farnell LFP/1) providing sine and square waves from 10 Hz to 1 MHz with maximum output of up to 12 v peak to peak.

Resistance was measured using both kinds of output over frequencies of 10, 15, 100 Hz, 1, 5, 20 kHz for sine wave and 10, 150 Hz, 1, 10 20 kHz for square waves.

Measurements at higher frequencies than 20 kHz would require more sophisticated measuring devices than the ones available. According to past experience,[187,192] however, the range of frequencies examined was considered sufficient to provide reasonable accuracy of the measurements of concrete resistance and to the electrochemical response of the system to this kind of voltage.

Results.

The results are shown in Tables 9.2, 9.3, 9.4 and Figures 9.6, 9.7, 9.8 from which the following remarks can be made.

1. For both kinds of output examined, the higher the frequency the lower is the value of concrete resistance obtained, the effect of frequency has been remarkable at the lowest frequency of 10 Hz. The change in E-I slope with frequency is more gradual above 50 Hz (see Table 9.2).

2. The resistance, Figure 9.8, ranged from 14.4 Ω to 12.9 Ω for sine wave and 13.8 - 11.6 Ω for square

wave for frequencies of 50 Hz and 20 KHz respectively. Apart from the lowest frequency (10 Hz) the application of square wave resulted in slightly lower resistances than those obtained from sine wave particularly at high frequency as shown in Figure 9.8.

Polarisation Effect.

Figures 9.6, 9.7 show the E-I curves intercepting the voltage axis at points near to the origin. However E-I curves for a frequency of 10 Hz of both kinds of output intercept the voltage axis at about 0.55 volt. This polarisation effect can also be seen in Table 9.3 in the form of a comparison between the resistance values determined from single measurements without allowing for the intercept value and the resistance after making the allowance. It can clearly be observed that the value from a single measurement after the allowance for the interception value is in good agreement with the value determined from the slope of the E-I line. The degree of error is lower the higher the applied voltage. Table 9.4 shows a similar kind of comparison for the highest frequency (20 KHz) which indicates a good correlation between single measurements resistance value and the slope of the E-I line except in the case of applying extremely low voltage in which case the very low polarisation (0.084 V) becomes effective.

Effect on Half Cell Potential.

The half-cell electrode potentials were monitored throughout the measurements. With sine wave output, apart from measurements at the low frequency of 10 Hz, the electrode potential was slightly changed upon the application of voltage. The maximum change has been 3 mV in the case of 50 and 100 Hz and for other cases the change was less than 2 mV. In all cases, however, the potential returned to its original value immediately upon the release of the applied voltage.

On the other hand, greater changes in the electrode

potential were observed in square wave measurements. For frequencies 1, 10 and 20 KHz the potential remained virtually constant during voltage application up to about 3 volts after which a sharp change was detected and found to be dependent on the frequency as shown in Table 9.5.

Table 9.5 indicates, rather surprisingly, that at a given applied voltage higher frequencies produced higher changes in the electrode potential.

For 10 Hz frequency, in both kinds of output the electrode potential fluctuated exactly at the same frequency as the impressed voltage (10 cycle/min). The range of fluctuation slightly increased as the impressed voltage increased with a parallel increase in the electrode potential, as illustrated schematically in Figure 9.9.

9.6.3 D.C. Measurements

A Weir 423D Model D.C. power supply was used for these measurements. Data from the impressed voltage and the corresponding current produced the curve shown in Figure 9.10. It can be seen that the curve follows the behaviour described earlier by Monfore[185] and Hausmann[190] (see Section 3.4.4) in that the initial part of the curve exhibited a small current flow up to certain applied voltage after which an entirely different voltage-current function is obtained (the right portion of the curve). With the assumption that any other circuit resistance is negligible, the resistance of concrete is equal to the slope of the linear portion of the curve which equals 12.8 Ω.

Polarisation Effect.

The effects of polarisation of the resistance measurements were examined using the same approach adopted in the preceding section. A comparison between different resistance parameters is given in Table 9.6. This shows that the polarisation effect is substantial at lower voltage ranges (column 3,5) and this decreases as the

impressed voltage increases i.e. with the decrease of E_p/E_a ratio. It is clear that polarisation does have a considerable effect even in the case of high impressed voltages.

Effect on Half-Cell Potential.

Table 9.7 and Figure 9.11 show the relationship between the impressed voltage and a change in the electrode potential. The significant feature conveyed by these data is that the electrode potential changes have been substantial compared with the initial corrosion potential (-0.468), the slope of the line $\Delta E_a/\Delta E_p$, where ΔE_a and ΔE_p are the change in the applied voltage and the electrode potential respectively, equals 1.9 which implies a one direction change of more than 0.500 V SCE in electrode potential per 1 volt of the impressed voltage. Upon the interruption of the circuit current, an instantaneous drop in the electrode potential from -6.224 V SCE to -1.448 V SCE was recorded, Figure 9.12. The greater proportion of the initial value of the electrode potential was restored after approximately 1.5 hours.

9.6.4 Constant Current Technique.

A testing device was built in the Department of Civil Engineering using the circuit initially developed at Birmingham University as described in Reference 191 and shown in Figure 3.32. The device was further developed to enable measurements of wider range to be made, thus instead of having two ranges of measurements of 0.1 mV/Ω and 1 mV/Ω the measurements were extended to include the ranges of:

5 mV/Ω, 10 mV/Ω, 15 mV/Ω, 20 mV/Ω

This was accomplished by increasing the passed constant current peak-peak through the measured system. With the current constant, the voltage developed across the system is directly proportional to its resistance.

Table 9.8 presents resistance measurements which indicate that the increase in the applied constant current would cause a parallel increase in the voltage measured across the electrode, accordingly the resistance values ranged from 40.3Ω to 25.3Ω . This is also shown in Figure 9.13. Thus after an initial sharp drop in resistance value as a function of the applied current, the change became less steep with almost linear relationship. If the linear relationship is also valid for values beyond 20 mamp, the resistance would reach the value of 10Ω if 40-50 mamp constant-current applied.

Effect on Electrode Potential.

Upon switch on and switch off of the constant current, there were transient shifts of E_{corr} as shown in Figures 9.14 and 9.15. For a given applied constant current, although the magnitude of shift is the same, the detailed form of the transient shifts were somewhat different during switch on and switch off with longer duration being associated with the latter. Also as indicated in Table 9.9 and Figure 9.16 the magnitude of shifts were proportional to the applied constant current.

A part from the transient, the electrode potential did not change during the measurements. This may be attributed to the comparatively low applied voltage as well as the alternating nature of the applied current.

Polarization Effect.

Since the resistance was determined from a single measurement at each level of applied current, the effect of polarization cannot be quantified. However, the change in resistance value with the magnitude of the applied current suggests the existence of this phenomenon. On the other hand, the high value of resistance obtained by this method as compared with high frequency A.C. measurement indicates that the polarization effect is probably considerable.

9.6.5 16 V Alternating 50 Hz Voltage.

In these measurements, a constant A.C. voltage of 16V is applied across the specimen as described in Section 9.6.2. Therefore a single value of resistance can be obtained from each measurement. Several measurements were made and an average value of 11.6 Ω was obtained.

Upon application of the voltage, the electrode potential changed from -0.5325 to -0.9555 (volt-SCE) and remained at this new potential over the time of application.

The electrode potential, however, regained its original value within 6 seconds after the release of voltage. The instantaneous change in E_{corr} on switch off was 0.360 V SCE.

For the same reason given in the preceding case, (Section 9.6.4) the polarization effect can not be quantified. Nevertheless, the transitory change in electrode potential value indicated a limited degree of polarization or perhaps a small E_p/E_a ratio which controls the error in resistance measurement and, therefore, the resistance values obtained fall close to those obtained from high frequency A.C. measurements.

9.7 Discussion.

In the preceding sections it was mentioned that the existence of the IR-drop in the polarisation potential is undesirable since it gives an unsafe prediction of the polarisation resistance. This is particularly so when the polarisation resistance R_p is small in which case the small amount of voltage drop can substantially affect the measurements. The IR-drop may be eliminated if the current due to polarisation or potential required to overcome it is simply subtracted from the total value of current or potential respectively.

Apart from method No.4 the other measuring technique employed in this investigation have yielded very close values of resistance. The principal dissimilarities have been the response of the system under measurement to each

measuring technique with respect to polarisation and change in the electrochemical condition of the reinforcement.

9.7.1 Resistance and Resistivity.

The IR-drop can reasonably be considered as a resistance of the media through which the polarisation current travels under a given condition and length of travelling route.

It seems fairly clear that it is the resistance rather than the resistivity of the media that controls the amount of drop to be subtracted from the R_p value during a linear polarisation measurement. Resistivity, thus provides bulk indication without considering the temporal variation, which is crucial from corrosion point of view. Nevertheless while it may provide the most appropriate basis (as compared to resistance) for describing the physicochemical transformation undergone by hydraulic material from the moment it comes in contact with water until transformation practically ceased[10,12,13,22,28] it's reliability in quantifying the role of concrete on the corrosion of reinforcement is open to question. Consider for instance a concrete specimen with an artificial crack, which may cause serious consequences as far as the passivity of the reinforcement is concerned. Under dry or partially moist but not saturated conditions the value of resistivity may be equal to that of the un-cracked concrete or even greater despite the defects in the protective cover.

On the other hand, for saturated concrete the resistivity is most probably unaffected by cracks even though the cracks provide an effective least resistance line for the electrochemical circuit, thus promoting premature influence by the surrounding environment.

It would be argued, therefore, that for partially saturated concrete the local resistance assesses more realistically the susceptibility of reinforcement to corrosion than does the resistivity. Resistance being a function of the preferential path for the corrosion

current which is by definition the least resistive one and which closely simulates the situation prevailing in real structures where current is transmitted by only a small proportion of the cross-sectional area. However, for fully saturated concrete, due to the geometry effect of small area of cracks compared to uncracked concrete, cracks are unlikely to produce considerable change in resistance which means that even resistance becomes less reliable approach to assess the corrosivity of the system.

Thus, the wide variation in data relating resistivity and corrosion may at least partly by attributed to this basic concept of measurement. Another possibility may have been the effect of reinforcement amount and arrangement in addition to the possible error which arises from the uncertainties in estimating the area of concrete through which the applied current travels.

Consequently, in the experimental work in this chapter, the comparison was based on the resistance values.

9.7.2 Conduction Through Reinforced Concrete.

The physical and equivalent electrical model for conduction through concrete described in Chapter 3 can not readily be assumed for conduction through reinforced concrete. This is mainly because the effect of reinforcement is as to provide additional conductive path with almost zero resistance. The effect of reinforcement on the resistance has not been fully researched. Hope et al[151] experimentally investigated this effect and provided data showing that the reinforcing steel that falls within the field of influence of the measuring probes will reduce the measured value of the resistance. The field of influence was found to be approximately a sphere with radius equal to half the depth of the reinforcing steel.

During the corrosion process the electrical conduction by reinforcing steel forms an integral part of the electrochemical circuit. However, in the electrochemical measurements this contribution is particularly

evident since the current is, in fact, forced to travel through the reinforcement in the required direction. It can be inferred therefore that the previous conduction model is only valid in the distance between the counter electrode and the reinforcement which clearly means that the resistance to polarization current is mainly afforded by the latter, ie. concrete cover.

Cracks which occur can be considered as another resistive element in the conduction model the amount of which depends on the size and geometry of the cracks, Figure 9.17. On the other hand in saturated reinforced concrete where corrosion of the reinforcement is probable the 'cracks' resistance is slightly lower than the pore solution resistance leading to slightly lower overall resistance because, although the crack will have inherently lower resistance than uncracked concrete, it represent very small proportion of the total surface area of concrete.

Therefore the electric conduction model shown in Figure 9.17 agrees well with the general theory which indicates the effect of cover to reinforcement on corrosion of the uncracked concrete as it increases the length of the conducting paths. This model also indicates that in saturated condition, the resistance is unlikely to be effected significantly by cracks despite the fact that it provides easy ingress of the corroding species and oxygen which makes corrosion highly probable.

9.7.3 Comparison Between Different Methods.

Most of the published work is mainly confined to the use of D.C. and sine wave A.C. techniques and generally indicates the superiority of the latter.

Apart from these techniques, however others were given virtually no attention. The current interruption technique was underestimated as a useful technique to determine the voltage drop due to the concrete resistance during electrochemical measurement particularly in cases where other methods are either inaccurate or need extra instrumentation and special arrangements.

A summary of the results obtained in this investigation is given in Table 9.10. Apart from constant alternating current, low frequency sine and square wave A.C. methods, the other methods yielded relatively close resistance values with the lowest values obtained from the current interruption technique and A.C. 20 kHz square wave.

The evaluation of the test results and consequently the test method can be accomplished better by examining the effect of such relevant phenomena as polarization and half-cell electrode potential during measurements. The basis of this approach relies on the fact that transmission of corrosion current in nature is not associated with instantaneous drastic changes in other electrochemical characteristics of the system.

9.7.3.1 Polarization Effect During A Resistance Measurement.

It was shown (Section 3.4.4) that it is recommended that the resistance be determined from the slope of the linear portion of the E-I curve, since single measurements may include a polarization element as described in Section 3.4.4. In such a case the resistance is:

$$R = \frac{E_a - E_p}{I} \qquad \ldots 9.1$$

where E_a = is the applied potential
E_p = is the polarization potential

Therefore a single measurement may not give the real resistance unless the polarization potential is very small or subtracted from the applied voltage.

The theoretical approach to assess the polarization effect in this study can be described as follows:

The percentage error (%ε) in the calculated value due to polarization may be expressed as:

$$\% \varepsilon = \frac{R_A - R_C}{R_A} \qquad \ldots 9.3$$

where R_A = The apparent resistance (without considering polarization effect)

$$= \frac{E_a}{I}$$

R_C = The corrected resistance

$$= \frac{E_a - E_p}{I}$$

$$\text{thus} \quad \% \varepsilon = \frac{\frac{E_a}{I} - \frac{E_a - E_p}{I}}{\frac{E_a}{I}} = -\frac{E_p}{E_a} \times 100 \qquad \ldots 9.4$$

Equation 9.4 indicates that the error in resistance due to polarization is equal to the ratio of the polarization potential to the applied voltage, Figure 9.18. Alternatively, a small error would be expected if the applied voltage is sufficiently large even for systems with high polarization effect. In this case, however, the electrochemical stability should be considered.

This approach has been successfully used to assess the polarization effect as can be seen in Tables 9.3, 9.4 and 9.6 which proved helpful in providing a reasonable basis as to which method is the most appropriate. Moreover the calculations confirmed other's[185,190] conclusions in that the polarization potential is equal to the intercept on the E-axis of the linear portion of the E-I curve, as can be seen when comparing columns 4 and 5 of Tables 9.3 and 9.6.

9.7.3.2 Changes in Half-Cell Electrode Potential.

The change in electrode potential is a consequence of the polarization effect, and thus, is critically dependent upon the kind of impressed voltage as well as its amount.

This effect is substantial in D.C. measurements where the polarization potential is considerable (1.9 V) for which the following relationship relating the applied potential and the half cell potential was obtained.

$$E_a = 1.9\ E_{corr} - 0.325 \qquad ...9.5$$

substituting $\Delta E = E_{corr} - E'_{corr}$

and $\Delta E_a = E_a$

then $$\Delta E_a = 1.9\ \Delta E_{corr} + 0.568 \qquad ...9.6$$

where E'_{corr} = the initial potential before voltage application = -0.468 V SCE

With A.C. measurements, it was found that sine and square wave yield nearly identical values of resistance (Table 9.2) with slightly lower values given by the latter at higher frequencies.

However, rather surprisingly, the effect on electrode potential was dissimilar in that the sine wave current produced almost negligible change (for the range of voltage applied) whereas change as high as 17 mv was recorded for the square wave case, this effect seems to be dependent on the applied voltage and frequency, since beyond a certain voltage barrier (3 volts) the change in electrode potential was directly proportional to the current frequency. However, it is not possible at this stage to provide a convincing explanation as to why such dissimilarities in effect on the potential exist and this aspect, therefore, requires further investigation.

In the same context, it is important to emphasise that a polarization effect does exist when A.C. voltage is applied even at high frequency. However, this effect is frequency dependent so that at frequencies above 10kHz it becomes negligibly small as compared with D.C. measurements.

The constant current technique consists essentially

of an A.C. 50 Hz square wave constant current operating at low impressed voltage (maximum ~ 0.5 volts) which implies considerable polarization effect for the particular test condition in this research. The theoretical way of avoiding polarization effects in this technique which is based on delaying the voltage measurement until the capacitance is fully charged using a two sample and hold circuit, seems inapplicable when used for a complex full scale saturated specimen despite its apparent efficiency when used for small carefully controlled specimens such as those described in Ref. 191. Attempts to increase the amount of constant current (ie. the voltage) to reduce the polarization effect will render the measuring device equivalent in effect to 50 Hz A.C. method at higher applied voltage (method 5).

The main shortcoming of method 5 is that it requires the application of a high voltage which may alter the electrochemical equilibrium of the system particularly in the case of an actively corroding system or when the time of application is increased.

9.7.3.3 Current Interruption Technique.

Although this method is in practical use for the determination of the ohmic component of the applied potential for cathodically protected systems, particularly for buried pipe lines, it is rarely considered in the literature to be an efficient method to estimate the ohmic resistance during electrochemical measurements.

This may be partly because other techniques, such as electronic compensation, are considered sufficient to provide the required information, or perhaps the ohmic resistance is so small to produce no tangible error in the polarization measurements and is thus left unmeasured.

The use of electronic compensation in the present investigation has been troublesome and inaccurate. However, the use of any other method inevitably implies the requirement of extra measuring devices and special arrangements and thus increases the time required for each test.

As mentioned in the earlier sections, a good correlation has been observed between the results obtained by this method and those of the D.C. and high frequency A.C. methods. Also the continuous decrease in the resistivity value as the current frequency increases made it possible to postulate that the resistance values at higher frequencies than 20 kHz would probably amount to the value obtained from this technique. Moreover the unique consistency of the results obtained from different amounts of shift and times of application increases considerably the reliability of this method. Other important merits of this technique are:

1. The measurements can be made without changing the system equilibrium since no separate potential shift is required.

2. It provides the amount of resistance at the very time the polarization measurements are made, and thus totally excludes the spatial effects which may be vital in some cirumstances.

3. The measurement is based on the resistance concept rather than resistivity and the current travelling route is similar to the one followed during polarization measurements.

9.8 Summary.

Concrete resistance is critically dependent on the test method, concrete quality, degree of saturation, temperature, chloride ions, and the presence of reinforcing steel as well as on other factors. The test results as well as theoretical considerations suggest that the specimen size and the complex combination of cracks, local flaws, moisture and reinforcing steel can be crucial to the extent that generalization of assumptions drawn from simple systems may be hazardous. In this context it was shown that even the basic concepts of the measurement methods should be carefully considered as possible

additional source of variations and sometimes wrong conclusions. This was described in the discussion of resistance and resistivity aspects.

The presence of reinforcing steel necessitates the modification of the conduction model which provides ultimately more evidence of the decisive role of concrete cover.

Different measuring techniques were examined and an evaluation criterion was suggested and based on:

1. Polarization effect during resistance measurement
2. Change in the electrochemical condition of the system and therefore of changes in E_{corr}

It was found that the polarization effect on the resistance value is mainly controlled by the value of the ratio E_p/E_a.

The experimental work described in this chapter highlights the potential use of the current interruption technique as an accurate method in determining the ohmic resistance through a complex system where other methods were either inaccurate or expensive and time-consuming. It should be pointed out, however, that it is generally believed that this kind of measurement can include capacitance effects as the double-layer on the steel surface becomes charged up and discharged. But the fact that the IR-drop values obtained by this technique, ie. current interruption technique, are lower than those estimated by other methods indicates that such effect seems negligible for the particular test conditions examined in this study. Consequently, this method was used through out this research programme for various specimens and different exposure conditions to determine the ohmic resistance of concrete during linear polarization measurements whenever these measurements are possible.

Table 9.1: IR-drop Technique: Potential Shift, Time of Application and Resistance.

Electrode Potential Shift (mV)		Resistance (Ω)		
		Time of Application		
		1 min	5 min	10 min
5	C	8.85	8.94	8.7
	A	9.09	8.98	9.12
10	C	9.16	8.9	8.7
	A	8.7	8.73	8.98
15	C	8.67	8.73	8.73
	A	8.85	8.79	8.94

C = cathodic measurements.

A = anodic measurements.

Table 9.2: Frequency-Resistance Relation for A.C. Measurements

Frequency Hz	Resistance (Ω)	
	Sine Wave	Square Wave
10	30.8	33.3
50	14.4	13.8
100	13.8	-
500	13.3	-
1000	13.3	13.3
5000	13.3	-
10000	13.14	11.9
20000	12.9	11.6

Table 9.3: A.C. Resistance Measurements and Percentage Error Due to Polarisation Effects (Frequency = 10 Hz). Sine wave.

Applied Voltage (volts) (1)	Current (Mamp) (2)	$R_1 = \frac{E}{I}$ (3)	$R_2 = \frac{E_a - E_p}{I}$ (4)	* $R = \frac{\Delta E}{\Delta I}$ (5)	% Error $\frac{(R_1 - R_2)}{R_1} \times 100$ (6)	$\frac{E_p}{E_a}$ (7)
1.04	14.1	74.28	35		52.9	52.9
2.600	65	40	31.54		21	21
3.200	85.8	37.3	30.9	30.8	17	17
4.00	116	34.5	29.7		14	14
5.00	145	34.48	30.7		11	11
6.050	175	34.6	31.4		9	9
7.100	208	34.13	31.5		8	7.7
8.300	244	34.61	31.75		6.6	6.6

V_p = p voltage drop due to polarisation effect = 0.55 volts

* from plotted graphs.

Table 9.4: A.C. Resistance Measurements - Percentage Error in Resistance from Single Measurements as Compared with the Slope of V-I Curve. (Frequency = 20 KHz).

Applied Voltage (volts) (1)	Current (mamp) (2)	$R_1 = \frac{V}{I}$ (3)	* $R = \frac{\Delta V}{\Delta I}$ (4)	$\frac{R_1 - R}{R} \times 100$ % error (5)
0.202	9.12	22.2		42
0.502	40.3	12.5		3
1.00	80.5	12.42		3.8
			12.9	
2.003	161.3	12.42		3.9
3.011	241	12.49		3.2
3.504	280	12.51		3.0
4.020	321	12.52		3.0

* From plotted graph.

Table 9.5: Change in Half-Cell Potential Upon the Application of 5 V A.C. (Square Wave).

Frequency	Change in E_{corr} (mV)
50 Hz	2
1 kHz	6
10 kHz	15
20 kHz	17

Table 9.6: D.C. Resistance Measurements and Percentage Error Due to Polarisation Effects.

Applied Voltage (volts) (1)	Current (mamp) (2)	$R_1 = \frac{E}{I}$ (3)	$R_2 = \frac{E_a - E_p}{I}$ (4)	$R = \frac{\Delta E}{\Delta I}$ * (5)	$\frac{R_1 - R_2}{R_1}$ (%) (6)	$\frac{E_p}{E_a}$ (%) (7)
1.014	5.5	184	-	-	-	-
2.011	38.4	52.4	-	-	-	94.4
3.054	88.0	34.70	13.11		62.2	62.2
4.00	162.0	24.70	12.34	12.8	50.0	47.5
5.095	246.0	20.70	12.98		37.3	37.3
6.028	314.5	19.20	13.12		31.7	31.5
7.03	395.0	17.80	12.97		27.1	27.0
8.12	485.0	16.70	12.82		23.2	23.4
9.18	570.0	16.10	12.78		20.6	20.7
10.02	632.0	15.85	12.85		18.9	18.95
11.61	756.0	15.35	12.84		16.4	16.2

E_p = 1.9V

* from plotted graph.

Table 9.7: D.C. Resistance Measurements: Applied Voltage, Current and the Electrode Potential.

Applied Voltage (Volts)	Current Mamp	Ecorr Volts (SCE)
0.47	3	-0.468
1.00	5.5	-0.476
2.00	38.4	-1.126
3.00	88	-1.686
4.00	162	-2.296
5.00	246	-2.820
6.00	314.5	-3.240
7.00	395	-3.736
8.10	485	-4.336
9.20	570	-4.896
10.00	632	-5.346
11.60	756	-6.226

Table 9.8: Constant Current Technique: Applied Current (PK-PK), Voltage and Resistance.

Applied Current (mamps)	Voltage (mV)	Resistance (Ω)	
0.1	3.8	38	
	4.1	41	40.3
	4.2	42	
1.0	27.5	27.5	
	26.6	26.6	27.2
	27.6	27.6	
5.00	161.6	32.32	
	142.0	28.4	30.6
	156.0	31.2	
10.00	295.8	29.6	
	290.0	29.0	29.1
	287.0	28.7	
15.00	422	28.1	
	406	27.1	27.4
	403	26.9	
20.00	527.0	26.4	
	480.0	24.0	25.3
	510.0	25.5	

Table 9.9: Constant Current Technique: Immediate Change in Electrodde Potential Upon Switch Off the Applied Current at Different Levels.

Applied Current (mamps)	Change in Electrode Potential vs S.C.E. (mV)
0.10	± 0.5
1.00	± 7
5.00	± 18
10.00	± 36
15.00	± 50
20.00	± 70

Table 9.10: Summary of the Test Results Obtained by Different Techniques.

Measuring Technique		Resistance (Ω)
Current Interruption		8.9
A.C. sinewave	10 Hz	30.8
	50 Hz	14.4
	20 KHz	12.9
Squarewave	10 Hz	33.3
	50 Hz	13.8
	20 KHz	11.6
D.C.		12.8
Constant Alternating Current	0.1 mamp	40.3
	20.0 mamp	25.3
16 volts	50 Hz	11.6

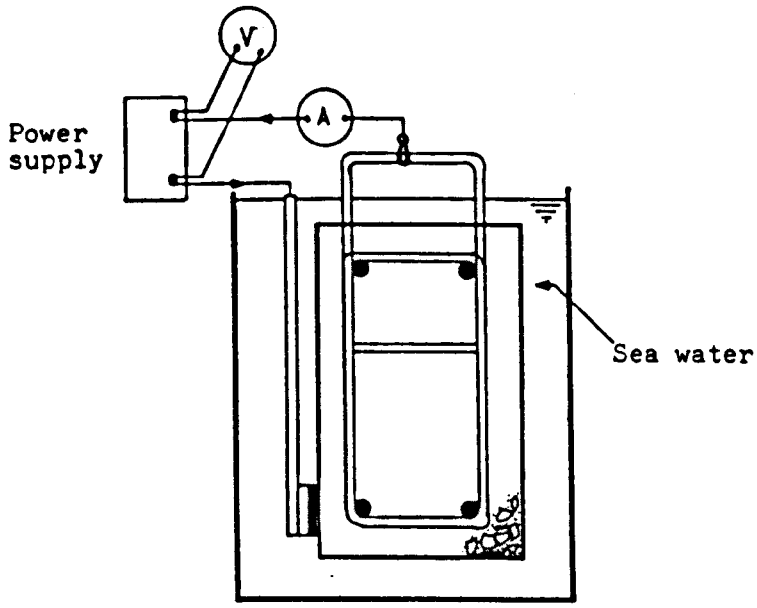

Figure (9-1): Typical circuit during resistance measurements.

Potential and time			Current
S T 1 18:36:35.9			
C 197 0.38741 Vdc	:		C 199-0.24731 mAd
D T 1			
S T 1 18:36:36.2			
C 197 0.38742 Vdc	:		C 199-0.24653 mAd
D T 1			
S T 1 18:36:36.5			
C 197 0.38742 Vdc	:		C 199-0.24661 mAd
D T 1			
S T 1 18:36:36.8		Before current interruption	
C 197 0.38742 Vdc	:		C 199-0.24683 mAd
D T 1			
S T 1 18:36:37.1			
C 197 0.38741 Vdc	:		C 199-0.24612 mAd
D T 1			
S T 1 18:36:37.4			
C 197 0.38741 Vdc	:		C 199-0.24643 mAd
D T 1			
S T 1 18:36:37.7			
C 197 0.38741 Vdc	:		C 199-0.24581 mAd
D T 1			
S T 1 18:36:38.0			
C 197 0.38741 Vdc	:		C 199-00.0003 mAd
D T 1			
S T 1 18:36:38.3		After current interruption	
C 197 0.38841 Vdc	:		C 199-0.000292 mAd
D T 1			
S T 1 18:36:38.6			
C 197 0.38853 Vdc	:		C 199-0.000295 mAd
D T 1			
S T 1 18:36:38.9			
C 197 0.38863 Vdc	:		C 199-0.000294 mAd
D T 1			

Figure (9-2): 3530 Orion data logger print out showing the electrode potential and the current before and after current interruption (beam MU605N at 694,250 cycles).

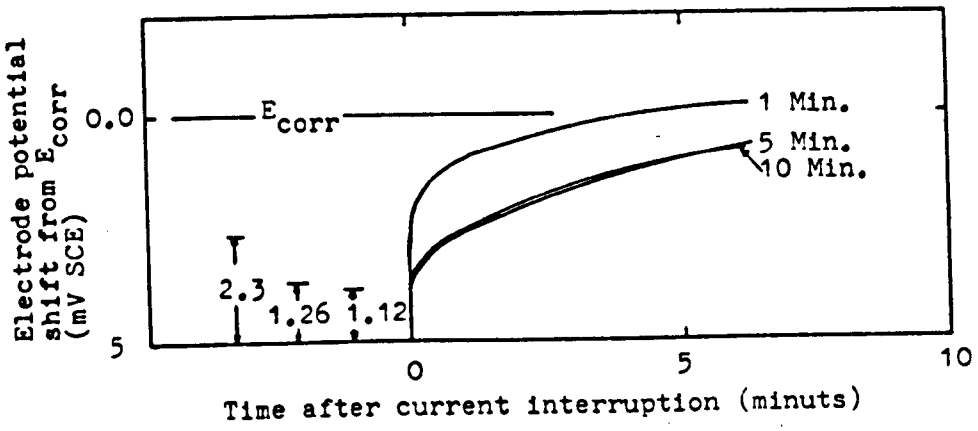

Figure (9-3): Change in electrode potential upon current interruption after cathodic shift of of 5mV for 1,5 and 10 minutes.

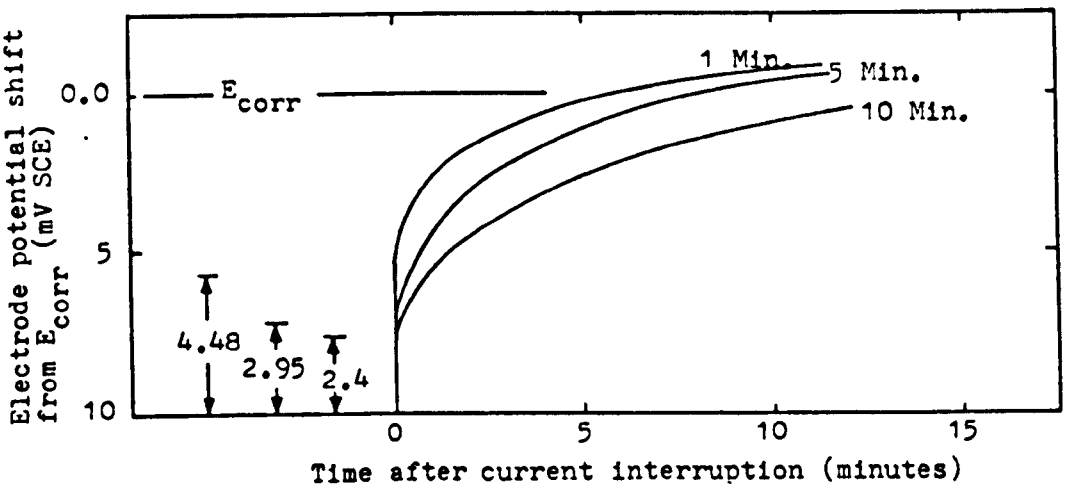

Figure (9-4): Change in electrode potential upon current interruption after cathodic shif of 10mV for 1,5 and 10 minutes.

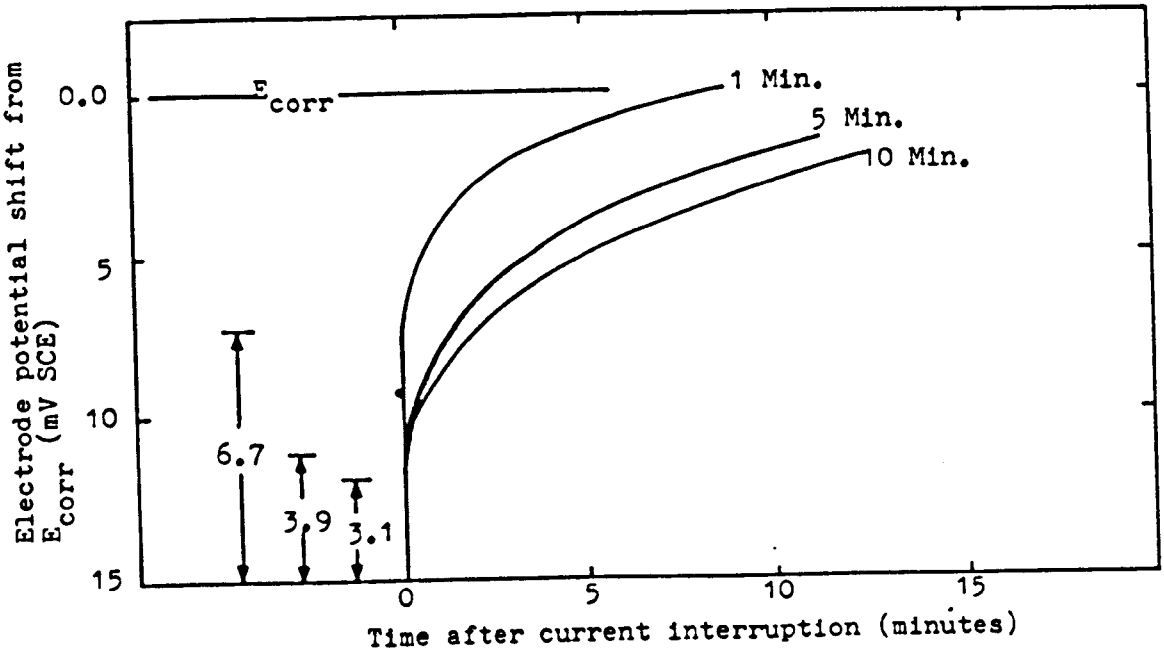

Figure (9-5): Change in electrode potential upon current interruption after cathodic shift of 15mV for 1,5 and 10 minutes.

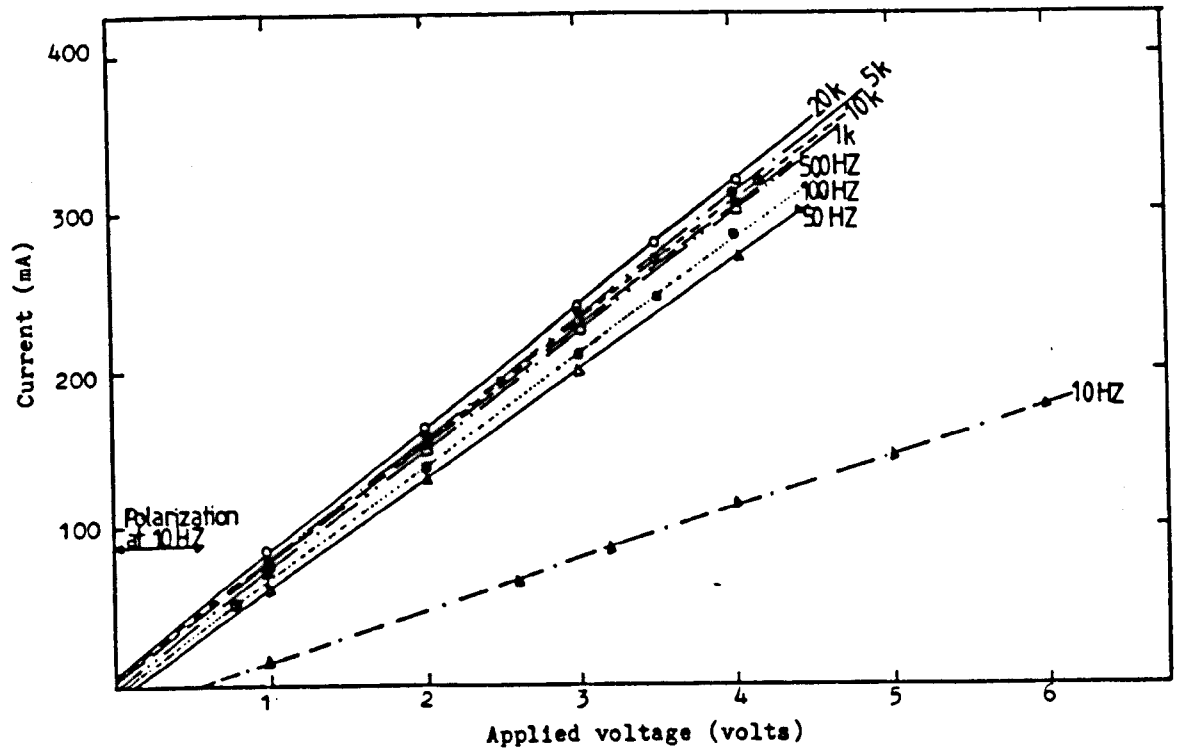

Figure (9-6): A.C resistance measurement;applied voltage vs. current for different current freqencies (sine-wave).

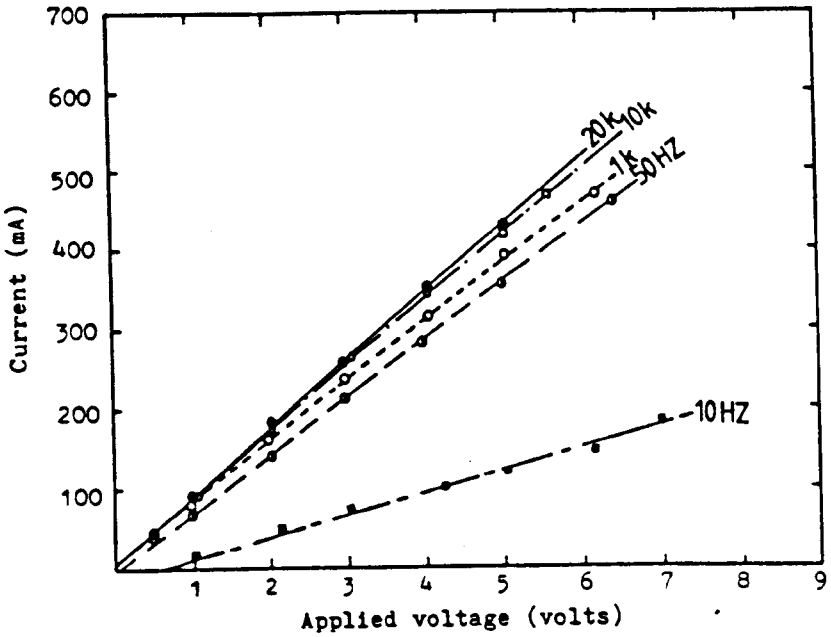

Figure (9-7): A.C resistance measurements;applied voltage vs. current for different current frequencies (square-wave).

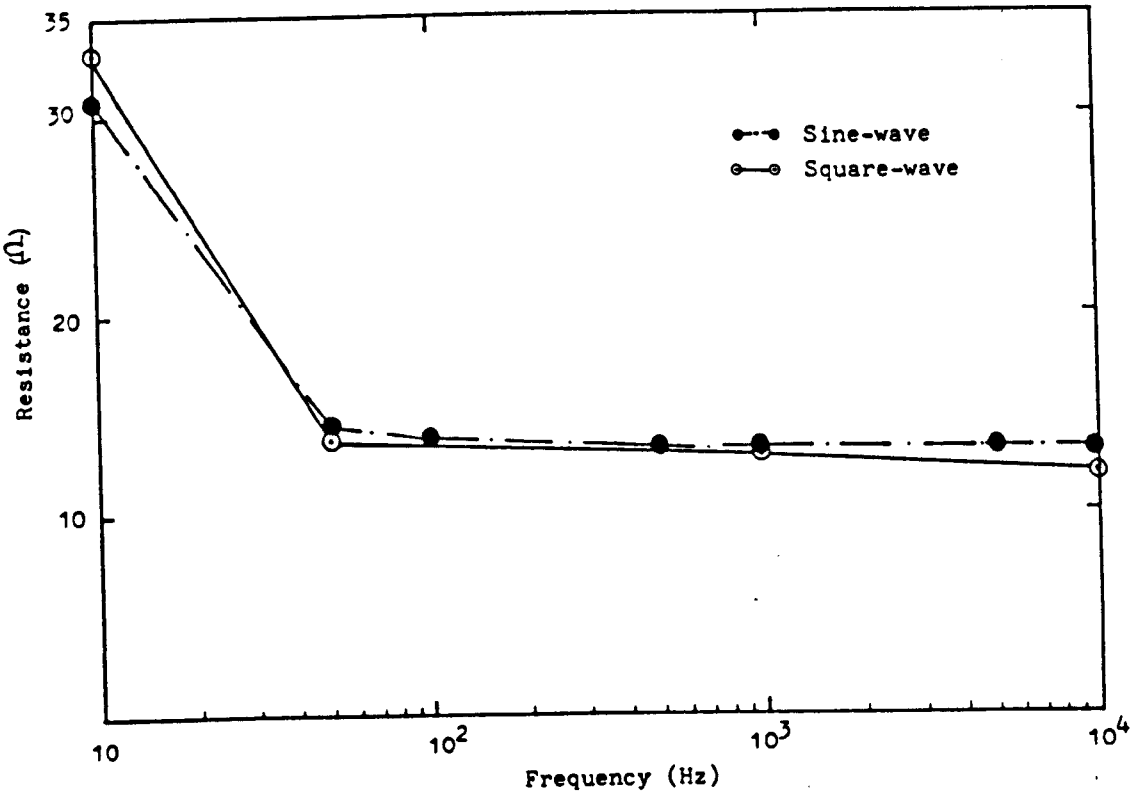

Figure (9-8): A.C measurements;frequency vs. resistance.

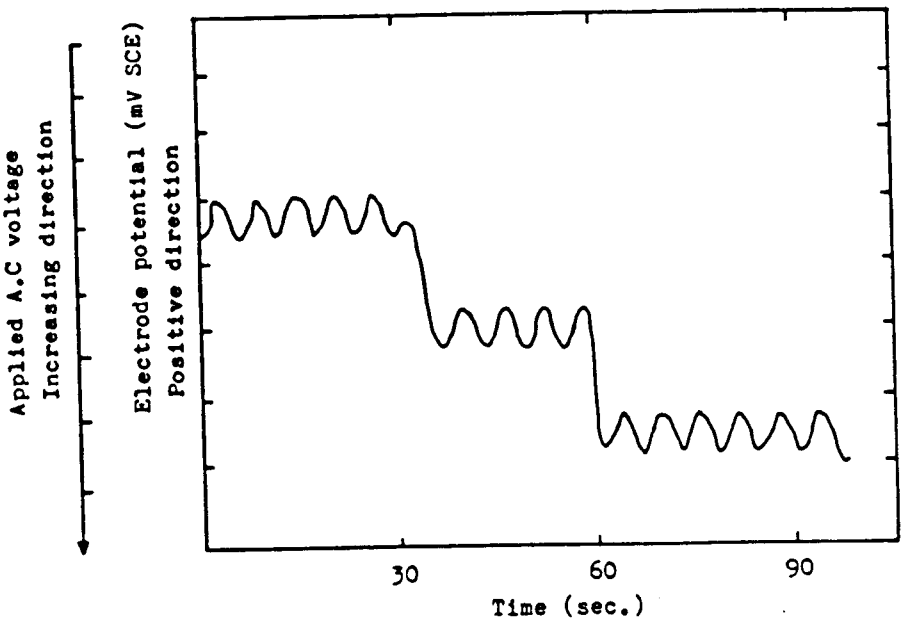

Figure (9-9): Schematic illustration of the flactuation of the electrode potential upon the application of 10Hz A.C voltage (sine and square-wave forms).

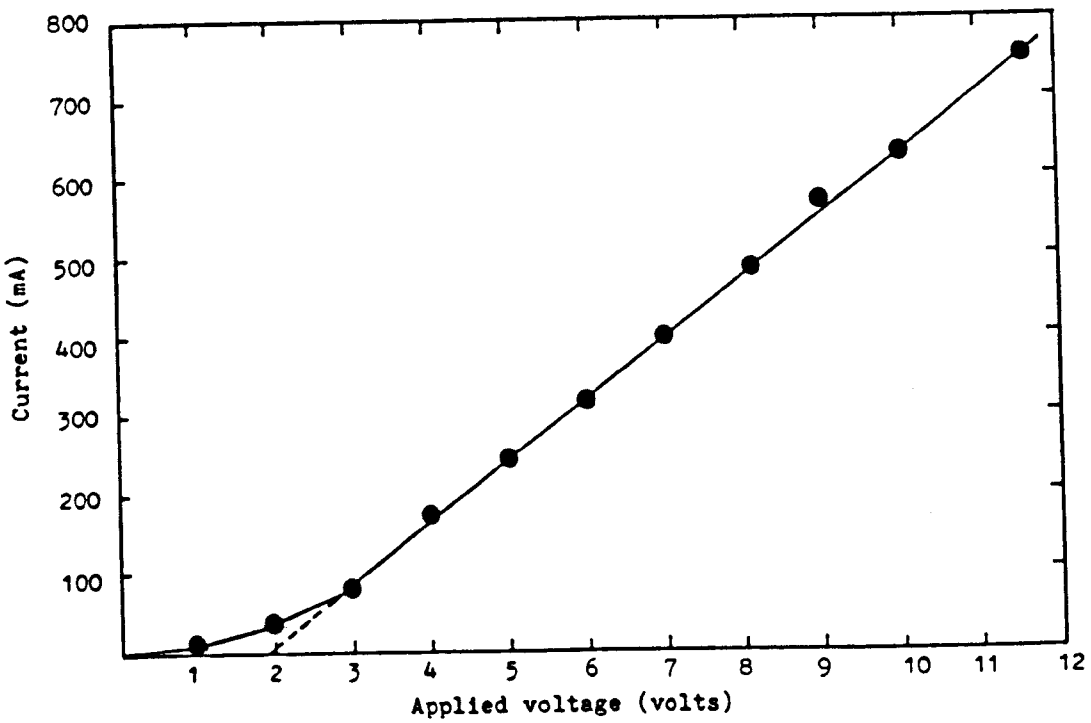

Figure (9-10): D.C resistance measurements;applied voltage vs. current.

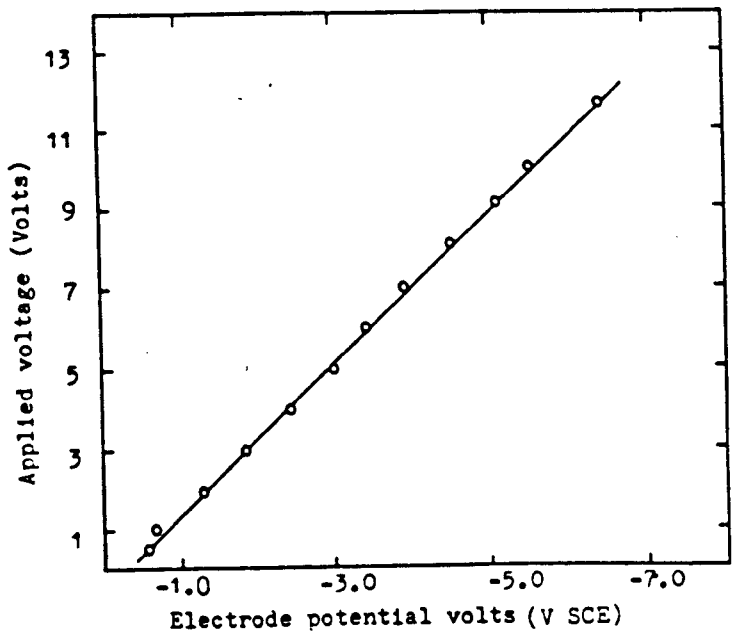

Figure (9-11): Effect of the applied D.C voltage on the corrosion potential of the embedded steel.

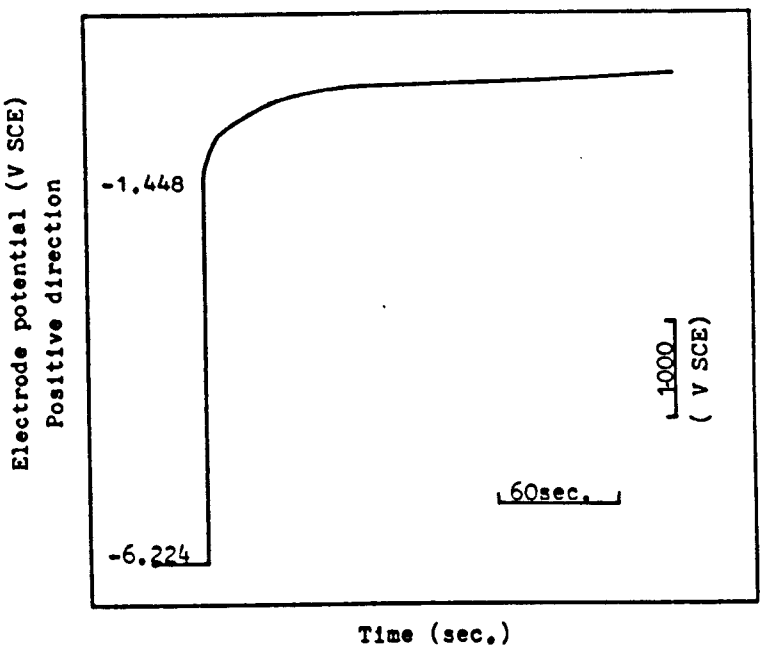

Figure (9-12): Electrode potential immediate drop upon the cut off of the applied D.C voltage.

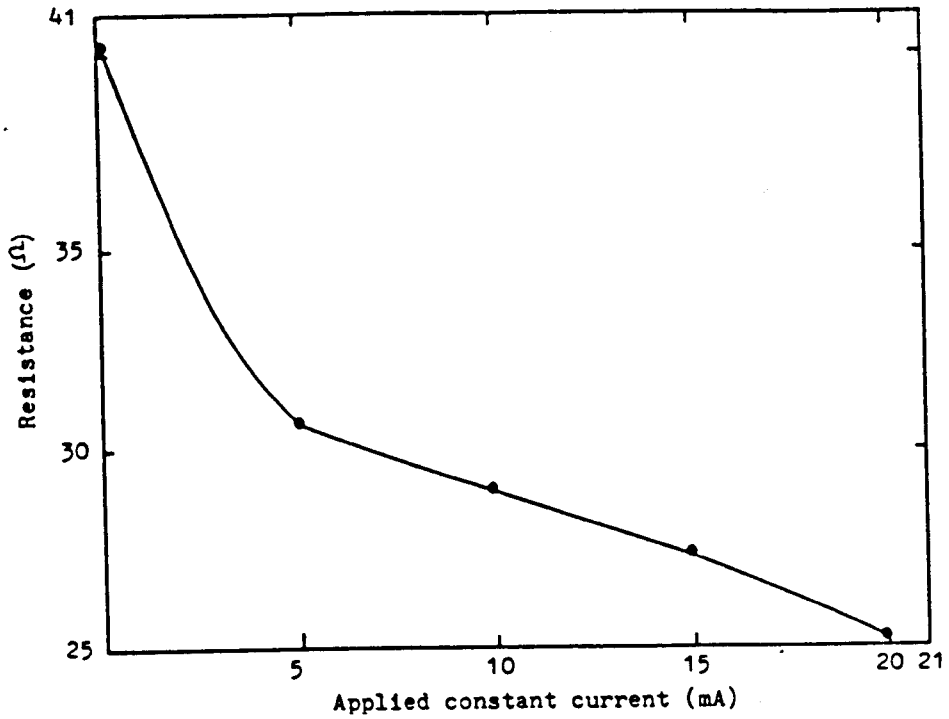

Figure (9-13): Constant current techniqe;applied constant current vs. resistance.

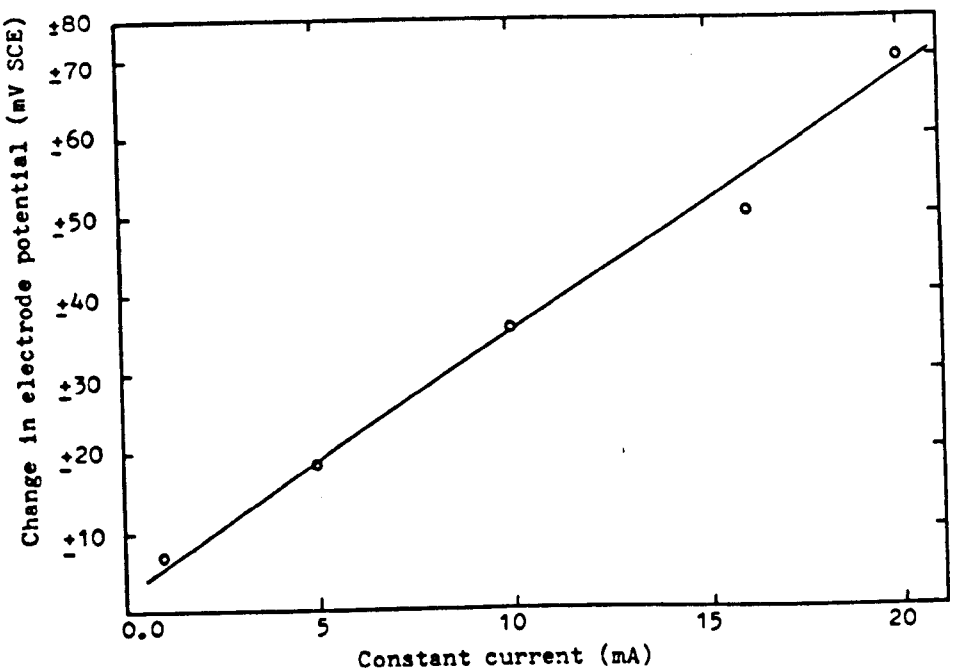

Figure (9-14): Constant current technique;immediate change in electrode potential upon cut off the applied current at different levels.

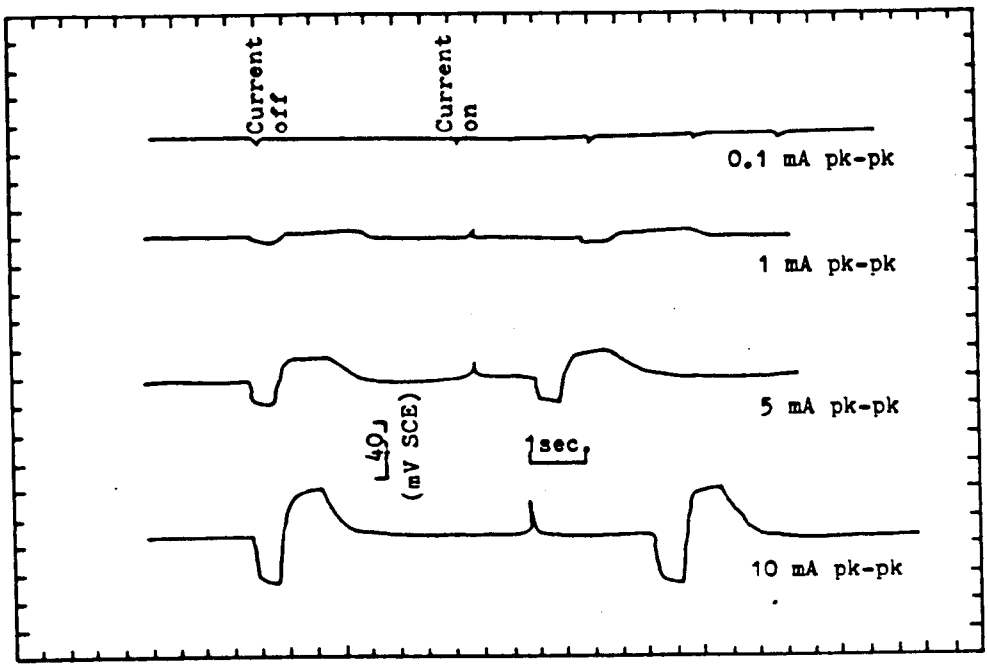

Figure (9-15): Constant current techniqe;corrosion potential response to switch off and on of the constant current generator.

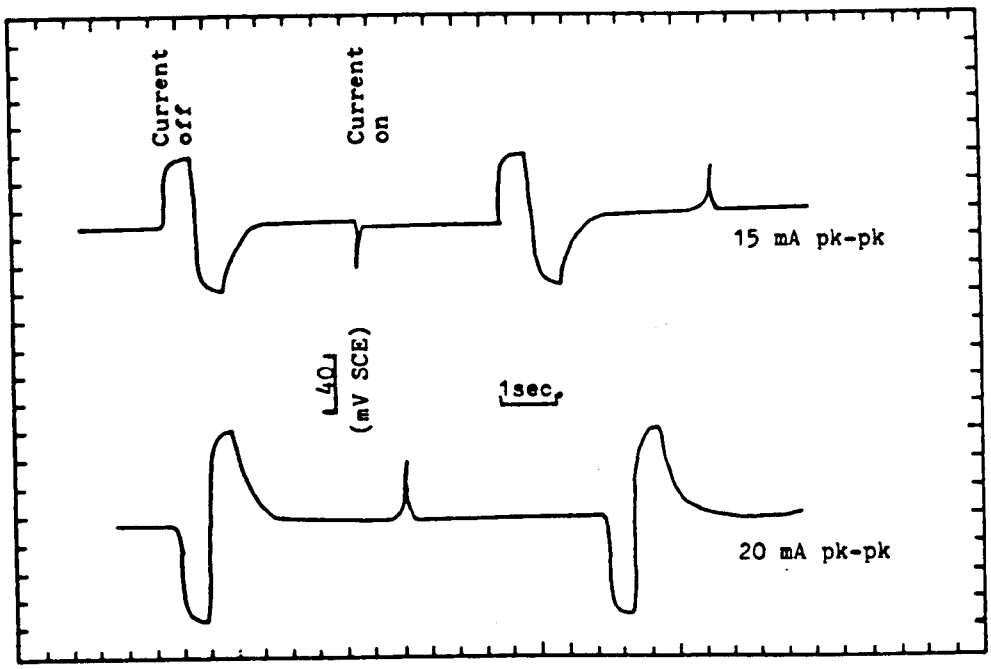

Figure (9-16): Constant current techniqe;corrosion potential response to switch off and on of the constant current generator.

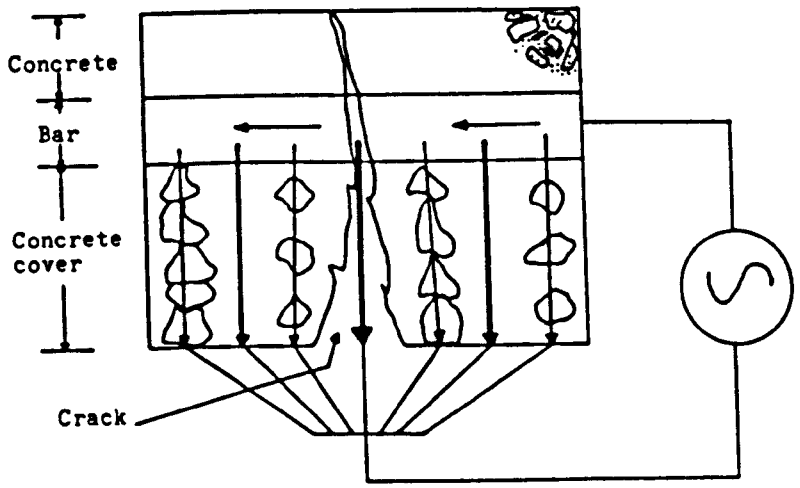

Figure (9-17): Conducting paths of cracked reinforced concrete.

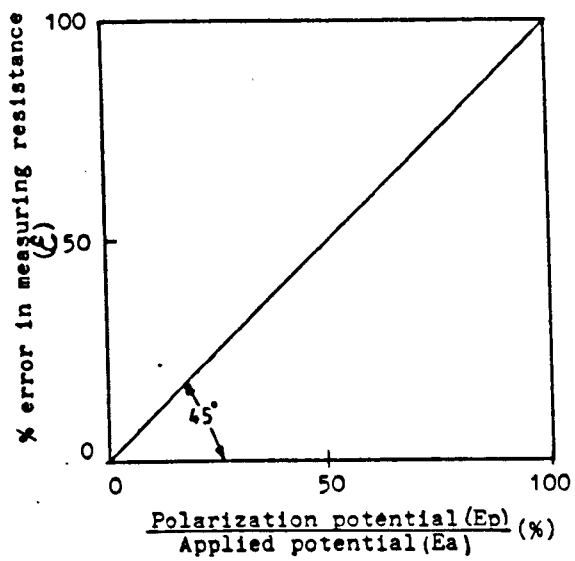

Figure (9-18): Dependence of error in measuring resistance upon the ratio of polarization to the applied potential.

CHAPTER 10

THE ELECTROCHEMICAL BEHAVIOUR OF REINFORCED CONCRETE UNDER DYNAMIC LOADING

CHAPTER 10

THE ELECTROCHEMICAL BEHAVIOUR OF REINFORCED CONCRETE UNDER DYNAMIC LOADING

10.1 Introduction.

The effect of dynamic loading on the electrochemical characteristics of reinforced concrete specimens were monitored during the test duration together with other static tests for comparison purposes. The monitoring technique, however, varied from conventional electrode potential measurements to the more elaborate polarisation measurements. At the conclusion of each test a destructive examination was carried out to determine the nature and the extent of corrosion and for further microscopic examination when appropriate as described in Chapter (6). Early measurements clearly demonstrated that not only the electrochemical characteristics of the test specimens that have changed due to the loading history but it also affected the measuring technique which made it absolutely necessary to further investigate in some details, as a separate line in this study, the factors affecting the measurement accuracy and other related technical aspects.

These factors, the test procedure, the measuring technique and the main electrochemical results of this study will be presented and described in this chapter.

10.2 Corrosion Rate Measurements.

10.2.1 General.

The Stern-Geary method (linear polarisation method)

was used in this study to determine the instantaneous corrosion rates during the tests. The theoretical basis of this method is described in detail elsewhere in this thesis (Chapter 3); accordingly the corrosion current is determined by the formula:

$$I_{corr} = \frac{B_a B_c}{2.3(B_a + B_c)} \cdot \frac{1}{R_p}$$

However despite the fact that standard laboratory methods are useful for polarisation studies, the direct adoption of these methods in reinforced concrete area introduces considerable amount of uncertainties. It was evident at preliminary stages of this study that the utilisation and the interpretation of the obtained data are highly dependent on the particular system conditions, suggesting that test criteria applicable on one system may be different for the others. Under these circumstances, a careful study of all test variables is required to minimize the possible error. The interpretation of the electrochemical data for reinforced concrete system seems to depend on:

1. The environment including the effect of IR-drop.
2 Loading conditions.
3. Specimen geometry and reinforcement configuration.

This section will be devoted to the experimental technique and the factors influencing the accuracy and the interpretation of the test results. (Recall that corrosion rate measurements were conducted in Stage II of the program in which two load levels corresponding to 0.6 and 0.4 f_y were investigated).

10.2.2 Polarisation Techniques.

One of the important merits of this method is that it allows obtaining corrosion rate-time data not available from other methods. This is mainly due to the limited shift in the electrode potential involved in the

measurement which does not produce significant alteration in the nature of the corroding surface under examination. While this is an easy and quick technique, it requires the knowledge of the Tafel slopes B_a and B_c for accurate determination of corrosion current, these values need to be assumed or measured in a separate experiment.

However, past experiences have shown that not only the corrosion rate but also the Tafel constant may vary with time and thus considerable error may result if corrosion rate is determined assuming constant values of Tafel constants. On the other hand, true Tafel behaviour is not evident until polarisation current of the order of several times the corrosion current are applied which implies the requirement of a marked shift from the corrosion potential (E_{corr}). Under such conditions the subsequent corrosion behaviour may be affected for some time after the polarisation has been discontinued. This consideration has been the primary reason to prohibit periodical determination of Tafel constant during the tests. Therefore for the present research, a full polarisation curves were only determined prior to the determination of each test.

The probability of changes in the electrochemical condition, however, increases with exposure time and would be particularly expected under severe situations, hence for longer running tests a single determination of Tafel constant may not provide representative values.

Moreover, the experimental set-up in this work was rather complex in terms of loading conditions and reinforcement configuration (in relation to earlier work on small concrete cubes without loading). Even with earlier simpler set-ups used by others, a wide range of B values (36-120 mV/decade) have been reported. Consequently the possibility of changes in Tafel constants over extended test periods were thought to be significant and led to the necessity of having information about the change of B values with time.

In order to accomplish this, it was decided to have multiple tests (see Chapter 5) each of which is meant to provide information that covers particular periods under

test for particular load levels and exposure conditions.

Using the experimental B values, the corrosion rates were determined from polarisation resistance data. These data were estimated cathodically and anodically during the test duration by two ways:

a. Potentiodynamically: at a sweep rate of 6 mV/min and a scanning range of 10 mV.
b. Potentiostatically: by imposing a potential step of 10 mV and obtaining a current as a function of time over a duration of 10 mins.

In addition, the corrosion current was estimated by back extrapolating Tafel slopes at the end of each test. The correlation between the results obtained by the three methods will be discussed later under another heading.

10.2.3 Instrumentation.

The polarisation measuring setup, Figure 10.1, consists of:

1. The potentiostat type "Ministat E series" which functions basically as a sophisticated D.C. voltage generator that allows a single potential of the sample to be fixed at any desired value relative to suitable reference electrode dipped into the electrolyte.

2. A voltage scan generator type "Wenking model VSG 72". This instrument controls the range and the rate of potential shift produced by the potentiostat.

3. Potential-measuring instrument: A Thurlby 1905a high input impedance ($10^9\Omega$) multimeter was used and was connected to the voltage terminal of the potentiostat.

4. Current-measuring instrument: a 7045 digital multimeter was used for this purpose. The current follower of the potentiostat, however, was connected to 100 Ω shunt according to the manufacturer instructions so

that the current was measured as a voltage multiplied by an appropriate conversion factor.

5. Reference electrode: a saturated calomel electrode was used as a reference electrode. This type of electrode is considered durable, reliable and commercially available. Precautions were taken according to the manufacturers instructions to maintain the electrodes in proper conditions. During measurements, the electrode was placed in the solution in the vicinity of the beam surface.

6. Auxiliary electrode: a 25 x 25 x 2 mm copper plate attached to a piece of wood was used as an auxiliary electrode. During measurement the A.E. was situated inside the water jacket at the level of the lower reinforcement and usually in contact with concrete surface (although it was observed that close contact with the beam did not affect the results in comparison with measurements with the electrode sitting in the solution beside the beam).

7. A x-y chart recorder to obtain direct plots of the measurements if necessary.

A schematic circuit diagram for polarisation measurements is shown in Figure 10.2.

10.2.4 Test Procedure.

1. Connect the beam reinforcement via a lifting hook to the working electrode (W.E.) terminal of the potentiostat. Connection to the hook may be made by a compression type clamp, direct welding or via a screw terminal welded to the hook.

2. Place the auxiliary electrode (A.E.) and the reference electrode (R.E.) in side the solution jacket as described in the preceding sub-section and connect them to the A.E. and R.E. terminals of the

potentiostat respectively.

3. Turn the setup on with the potentiostat at isolate mode and record the open circuit potential (E_{corr}) when becomes stabilised, this was usually attainable after 5 to 10 mins.

4. Adjust the internal voltage of the potentiostat to match the measured potential.

5. Choose the rate and the range of scanning.

6. Set the direction of scanning (anodic or cathodic).

The test starts when the potentiostat is set to the "run" mode. For potentiodynamic sweep measurements, E_{corr} is first displaced cathodically (-10 mV) with the measurement of the corresponding current. The anodic scan starts upon completion of the cathodic one and certain waiting time to allow for E_{corr} to restore its original values (typically 5-20 minutes, being dependent on the test condition). The polarisation resistance R_p then is the average of the slopes of both the cathodic and the anodic curves plotted on a linear scale.

The potentiostatic measurements involve a step shift of E_{corr} by approximately 10 mV using very high rate of scan, e.g. 1 V/min on the voltage generator controlling panel. The polarisation resistance R_{pt} at a given time of potential shift application equals:

$$R_{pt} = \frac{\Delta E}{\Delta I_t}$$

where I_t = the current at time t of shift application.

The anodic and cathodic values are averaged to obtain the polarisation resistance at the time of measurements.

Figure 10.3 shows an example of a complete measurement cycles indicating the controlled change in E_{corr} and its natural recovery to the original value before measurement.

10.2.5 The Experimental Determination of Tafel Slopes.

The Tafel constants B_a, B_c were obtained experimentally using the so-called extrapolation method. During measurements the specimens were polarised cathodically and anodically, using a scanning rate of 6 mV/min for a potential shift (over potential) of approximately 100 mV, and measuring the flowing current through the external circuit. In some experiments, however, in order to obtain the limiting diffusion currents the scanning continued (for up to 500 mV over potentials) except for a few anodic polarisation tests conducted under high-load conditions (see later).

Since the steel areas which function as an anode or a cathode in the corrosion cell are unknown for the system under investigation, the values of the current I in A rather than the current densities I_{corr} in $\mu A/cm^2$ were used in the graphical solution of Tafel slopes. Thus on a semi-logarithmic paper, the current I and the over potential were plotted on the logarithmic x-axis and on the linear y-axis respectively.

Generally at a location of typically more than 30 mV over potential the E-logI values formed a straight line relationship and remained so for further "variable" amount of over potential before taking an exponential form of change and/or reaching the limiting diffusion currents. The portion of overpotentials from zero to this point (where E-logI form a straight line relationship) usually exhibit E-I straight line relationship from which the R_p values at the time of measurement may be obtained from the first 10 mV shift. To obtain the Tafel constants, the straight line portions on E-logI plot are extended in direction of E_{corr} so that the length of the line passes through at least one cycle of current. The Tafel slopes B_a and B_c are the voltage change for one cycle of current on the anodic and the cathodic lines respectively.

The extrapolated lines intersect at a point of a line of corrosion potential and the projection of this point on the x-axis gives the corrosion current I_{corr} at the time

of measurements.

It should be appreciated, that there are some problems in defining the linear portion of the curves hence in some cases this relationship was only valid over a limited range of overpotentials. This aspect and others such as the compensation of IR-drop will be discussed later in this chapter.

10.2.6 Factors Affecting Polarisation Measurements.

a. Loading Regime and Load Level.

Figures 10.4a and b shows the potentiodynamic polarisation curves for measurements conducted during cycling for different load level. Figure 10.4c shows this type of measurement with the average load applied statically. The variation in current with time upon the application of $\pm$ 10 mV potential step is shown in Figures 10.5a and b. It is clear, therefore, that in both kind of measurements the effect of loading is apparent as a fluctuation of constant amplitude in phase with cycling and this effect is more pronounced in tests at higher load level than in the lower. Due to the fact that the potentiostat is essentially potential controller during these kind of measurements, i.e. the potential is kept unaffected by load variation, the current is the only parameter that influenced by cycling as indicated in Figure 10.6a and b, which presents a plot of the variation during measurements of the current and the potential separately. These examples indicate that the change in the exposed area of steel at the site of a concrete crack each load cycle is accompanied by change in the flowing current which is proportional to the applied load. The effect of this factor on the measured value of R_p is rather more pronounced in potentiostatic measurements than in potentiodynamic measurements. For the latter kind of measurement, it was observed that the slope of the line connecting the peaks is reasonably close to the slope of the line connecting the troughs. The average of these values is almost identical to the slope of the

polarisation curves obtained with the average load applied statically during measurement, Figure 10.4. This observation suggests that a short period of static application of load interrupting cyclic loading does not have significant effect on the electrochemical condition of the reinforcement and also indicates that it is possible to obtain reasonably accurate results when conducting polarisation measurements at either loads (maximum or minimum) when applied statically. This conclusion was confirmed when comparing potentiostatic measurements obtained under static application of minimum, average and maximum load consecutively as shown in Figures 10.7a and b which present the results obtained from two tests at load level equivalent to 0.6 f_y at different number of cycles. The potentiodynamic measurements and the IR-drop are also given in these figures which indicate negligible differences. Further the recovery of E_{corr} after potentiodynamic measurements at different level of statically applied load is given in Figure 10.8 which also shows identical response of E_{corr} to the load level after each measurements.

Accordingly, it was decided to conduct the polarisation measurements with the average load being applied statically thus avoiding the possible error in observing the fluctuating current without affecting the accuracy of these measurements.

b. Effect of IR-drop and Environment.

The effects of the electrolyte resistance on the accuracy of the electrochemical measurements and the method used to determine the IR-drop were discussed extensively in Chapter 9. It was evident at the early stage of the tests that the instrumental elimination (positive feed-back) of the IR-drop is unsuccessful presumably due to the multiple current path of the system under investigation and instead the so-called the current interruption technique was used after an experimental verification.

On the other hand, unlike tests in sodium chloride

solution where potentiodynamic measurements yielded consistently linear relationship, measurements in tapwater showed erratic E-I relationship. Potentiostatic measurements also exhibited the same nature so that Rp values cannot be estimated with any degree of accuracy from such measurements. However, whereas this trend continued over the whole test duration of beam MU405W (i.e. 2,138,000 cycles), a linear E-I relationships were obtainable from potentiodynamic measurements on beam tested at higher load level (MU605W) after approximately 210,000 cycles and continued for the remaining period under test.

Therefore, to obtain the limitation of the polarisation technique with respect to the electrolyte conductivity, a special test was carried out at higher load level (MU70WN) in which the test beam was subjected to an environmental change, in terms of chloride concentration, during cyclic loading. Since the test includes the examination of some other variables, it would be more appropriate to describe the test results at a later stage in this chapter.

c. The Effect of Scanning Rate.

Gonzalez et al[90,104] have reported good agreement between gravimetric weight loss and electrochemical weight loss estimated potentiodynamically using a sweep rate between 5-10 mV/min. Apart from this team work, no data was reported on the effect of sweep rate on the accuracy of the electrochemical measuring techniques in reinforced concrete, but some other workers[163,229] generally confirmed the validity of Gonzalez et al conclusion. Therefore the potentiodynamic measurements were generally conducted using a sweep rate of 6 mV/min. However, the effect of scanning rate has been examined for three different cases. Figures 10.9, 10.10 and 10.11 give the variation in polarisation resistance with the scanning rate and the time of step application of $\pm$ 10 mV for beams MU605N (after 915,000 cycles), ML603N (after 90 days of exposure) and beam MU605W (after 1,257,250 cycles)

respectively. Note that R'_p values are plotted; i.e. polarisation resistance values corrected for IR-drop.

These Figures indicate the following:-

1. R'_p decreases, resulting in higher corrosion rate, as the sweep rate increases.
2. R'_p increases with time after the application of the 10 mV step and tends to level off earlier in beams of low corrosion activity (i.e. of high R'_p).
3. In sodium chloride tests, a sweep rate of 6 mV/min and a waiting time of 60 sec after $\pm$ 10 mV step give almost coincident values. Whereas in a tapwater test a sweep rate of 9 mV/min and 90 sec waiting time give equal values of R'_p.
4. Steady state condition after step measurements is also affected by the severity of the surrounding environment. Thus for tests in sodium chloride solution, a potentiostatic steady state R'_p are associated with a potentiodynamic measurements at low sweep rate of 2 to 3 mV/min while in tapwater the corresponding sweep rate was 6 to 7 mV/min.

d. Waiting time After a Step Application of Potential.

The waiting time may be defined as a time after the application of a step potential necessary to obtain the stationary I required to calculate accurate R_p. The stationary I is usually obtained from a steady state portion of I-time curve. However, this condition may not always be obtainable giving rise, to an apparently high time constant.

The time for recording R'_p after the step application chosen at the beginning of this study was 3 to 5 min, but it was necessary to increase the measurement time to 10 min as will be reasoned later in this section. Figure 10-12, 10-13 and 10-14 present I_{corr} variation with time after application of step scan estimated cathodically and anodically for beams at various stage of test and load

level in sodium chloride solution. Consideration of these figures reveals some interesting features which may be summarised as follows.

1. Before load application: i.e. during the saturation period (Figure 10.12), the steady state was achieved after relatively short time so that reasonably accurate estimation of I_{corr} can be obtained from I taken after 1 to 2 min. Anodic measurements gives approximately 9% lower values of I_{corr} than the cathodic ones.

2. Test at higher load level (Figure 10.13): Measurements made at early stage of cycling (Figure 10.13a) showed continuous increasing difference with time between I_{corr} values obtained anodically and cathodically. After 10 minutes, there was more than 30% difference between these values. The diversion is mainly attributed to a continuous decrease in anodic values whereas the cathodic values achieved a steady state condition after approximately 4 min. Other important difference has been the evolution of E_{corr} from the polarised potential after the test has been discontinued, while E_{corr} recovered its original value within 3 minutes after the cathodic step, this was only possible 20 minutes after anodic step.

   At intermediate stage, Figure 10.13b, the observed differences between the anodic and the cathodic measurements were diminished and the time required for E_{corr} to recover its original value after polarisation was 18 and 15 minutes respectively. This trend was even more pronounced in later stages, shown in Figure 10.13c, where virtually identical values of I_{corr} were obtained from both measurements, the time required for E_{corr} recovery was 25 and 22 minutes after the anodic and the cathodic steps respectively. Also, under this condition, I_{corr} tends to stabilise earlier than the preceding stages.

3. Tests at lower load: Figure 10.14, exhibited quite

different characteristics in that, although consistently low I_{corr} was obtained from anodic measurements particularly at early stages of the test, similar anodic and cathodic response was evident. The time required to achieve the steady state condition was between 6-8 minutes. The time necessary for E_{corr} to recover its original values was 12,14 and 18 minutes at 41250, 259800 and 426443 cycles respectively.

The common characteristic observed in this series of tests was that the differences between I_{corr} values obtained anodically and cathodically is least under short time of application i.e. within the first minute. According to the preceding sub-section these values were identical to those obtained from potentiodynamic measurements at a sweep rate of 6 mV/min regardless of other test variables.

This fact is illustrated in Figure 10.15 which present the variation of corrosion current with test duration for beam ML403N. It is clear from this figure that a) similar shape of I_{corr}-time curves were obtained using different measuring techniques, b) different waiting time produced similar relationships, the only difference is their position with respect to I_{corr}. For instance the relationship:

$$I_{corr_{(t1)}} = 1.32\ I_{corr_{(t10)}}$$

where $I_{corr_{(t1)}}$ and $I_{corr_{(t10)}}$ are the corrosion current measured after 1 and 10 minutes of potential step holds always true for this particular test result.

The correlation between the variables of the measuring techniques may be more clearly identified when incorporating other data namely those extrapolated from Tafel plots. At this stage, however, the afore presented experimental evidences justify the following conclusions.

1. It is possible to choose either techniques as a basis for comparative evaluation with no risk of having erroneous conclusions.

2. For potentiostatic measurements, since various waiting time produced qualitatively similar I_{corr}-time of exposure curves and only varying in the actual corrosion rates, any single waiting time may be chosen for comparison purposes.

10.3 Results.

Various electrochemical parameters were monitored for a total of 31 beams tested under variable combinations of load, environment and test duration including 3 static tests. The results also include limited measurements made on sea water tests from concurred test programme conducted in this department.

10.3.1 Electrode Potential.

These measurements were made as described in Section 5.7.2.

Saturation Period and Initial Stage of Load Application.

Figure 10.16 presents the immediate development of the electrode potentials (vs. SCE) of the embedded steel upon contact with the surrounding solution. The potentials moved sharply towards more negative values and tend to stabilise within few hours (minutes in some cases) then remained practically unchanged or at very slow rate of change during the remaining saturation period (approximately 5 days) before the application of loads. Despite the fact that all the beams were made from similar mix design and no load was applied at the time of measurements, the rate by which their electrode potential developed as well as the final attained values were not similar and scattered over a wide range of potentials. For instance the potential varied in some cases (e.g. sodium chloride series) as much as 233 mV (-0.1 to -0.333V). Beams exposed to tapwater exhibited appreciably less negative values. However, the application of loads, dynamic or static, induced further changes towards more negative values, which led to considerable reduction in the observed variation in E_{corr} for a given load level.

The newly attained potentials were load dependent, thus the amount of change was proportional to the magnitude of load, the higher the load amplitude (0.6 f_y series) the higher the change observed. The effect of load was less pronounced in the case of static tests. The changes observed during the first day of load application are given in Table 10.1 and schematically illustrated in Figure 10.17.

Variation of E_{corr} in Phase with Cycling.

Several examples illustrating the change in E_{corr} in phase with load cycles are given in Figure 10.18, 19 and 20 which were reproduced from plots of a chart recorder. These figures indicate that load fluctuation between the minimum and maximum values have produced a parallel fluctuation in E_{corr} with more negative values being associated with maximum loads. The range of fluctuation was found to be dependent on load level, type of solution and time, i.e. the elapsed number of cycles. Figure 10.18 presents periodic E_{corr} monitoring during cyclic made on beam MU60N7D (sodium chloride test) after 120,1400,13250, 41700 and just before the termination of this particular test after 68,500 cycles. It is interesting to note that the fluctuation range increased from the initial value of 0.75 mV to 1.75 mV after 13,250 cycles after which the range exhibited a progressive decrease. At later stages for test at the same load level, the E_{corr} fluctuation range dropped to as small as 0.16 mV as shown in Figure 10.19b which presents measurements made on beam MU603N after 995,000 cycles. However, under the same environmental condition but lower load level (0.4 f_y), the fluctuation in E_{corr}, although present, was extremely small at about 0.07 mV. Tests in tapwater exhibited irregular patterns of change in E_{corr}, Figure 10-20, with different fluctuation ranges the maximum of which was about 2 mV for the case presented in this Figure.

E_{corr} Variation During the Tests.

The electrode potential changes from the point of load application up until the end of the tests for dynamic tests under both loading regime are shown in Figures 10.21,22,23,24, and 25. The results of two static tests in sodium chloride solution are also incorporated in the last two Figures. These results represent the available data apart from two special tests namely beam MU70WN and NU6ON8Y which, due to their special treatment will be described in another convenient place in this chapter. Consideration of the curves presented in the above mentioned figures show.

a. Reverse Bending Tests.

The results of this series are shown in Figure 10.21. It can be seen that E_{corr} moved rapidly to more negative values during the early stage of the tests and continued in this trend over the whole test duration. The only exception was observed in the case of beam MR35W which exhibited a reversal in E_{corr} towards less negative values at a later stage of the test (approximately 10^6 cycles). The rate of change in E_{corr} was appreciably higher in sodium chloride solution that in water. In this series, the load level did not seem to have a controlling influence on the rate of change in E_{corr} and the maximum negative values attained during the test.

b. Uni-directional Tests.

Tapwater tests: Figure 10.22 shows the variation in E_{corr} with test duration obtained from water tests at different load levels from both programme stages. It can be observed that the curves declined to more negative values followed by a reversal to the opposite direction with the exception of beam MU85W which showed continuous decline due presumably to the short time of this test. In contrast to the preceding case, the load level seems to have a profound effect on both the maximum attained

negative E_{corr} values and the points after which E_{corr} sustained a reversal in direction.

Chloride solution tests: Figure 10.23 shows the E_{corr} changes during the test duration for chloride tests carried out at higher load level in Stage I of the programme, it also incorporates two low load tests from Stage II for comparison. It can be seen that the dependency of E_{corr} values on load level was only apparent in tests carried out at load level corresponding to ≤ 0.7 f_y which also exhibited a reversal to less negative values after different exposure time, again dependent on load level. On the other hand, tests, conducted at load level corresponding to > 0.7 f_y, showed higher negative values and tended to level off at later stage. No reversal, however, in direction was observed during the time scales involved in these higher load experiments. Results of multiple tests at lower load level of 0.4 and 0.6 f_y as well as their corresponding static tests are given in Figures 10.24 and 25 respectively. The indications from these figures may be described as follows:-

0.4 f_y series: The E_{corr}-No. of cycles curves moved slightly (10-35mV) to more negative values for the first 2-3 days ($\sim$30-40 x 10^3 cycles) of the test then rose up in the noble direction in similar manner i.e. very slow rate. In later stages, however, the potential seems to have stabilised at constant values. At this load level, the loading regime (static or dynamic) does not seem to have remarkable effect on E_{corr} values and the curves shape are essentially similar. Nevertheless, the potential tended to stabilise at earlier stages in the case of static loading.

0.6 f_y series: the E_{corr} change over the test duration follows the same trend observed for high level conditions mentioned earlier in that a considerable decline in E_{corr} values occurred followed by reverse movement but at slower rate after $\sim 10^5$ cycles. Although similar E-time curve was obtained from static tests, the latter exhibited significantly more positive (approximately 150 mV) potentials.

10.3.2 Potential Profiles.

More detailed potential surveys were made at intervals of approximately 75 mm along the upper surface of the beams. The surveyed area includes both the immersed and the exposed portions of the beam. The potential measurements involved using a high impedance needle-voltmeter ($10^{13}\ \Omega$), the readings were read off through another digital voltmeter connected in series with the measuring voltmeter. A clean piece of cloth wetted with 3.5% chloride solution was used as an electrical junction to provide electrical continuity between the electrode porous plug and the concrete surface. Attempts to obtain measurements on water tests were unsuccessful due to considerable fluctuations in the readings.[173] Thus the data presented in this sub-section were obtained from tests in sodium chloride solution. Figure 10.26 shows the potential profiles for beam MU401N taken after 181,000 and 426,500 cycles, constant values were obtained inside the solution jacket (the central 1170 mm) whereas a rather steep potential gradient towards less negative values was observed in the exposed area. This figure also shows that the change in E_{corr} values with number of cycles (curve 1 and 2) in areas exposed to air was not proportioned to the change observed in E_{corr} inside the solution jacket.

Figure 10.27 presents the potential profile for beam MU403N after 1,289,000 cycles. During measurements the water level inside the jacket was maintained so that the upper 5 cm of the beam was exposed to air. The curve indicates that:

- E_{corr} values inside the jacket are unequal
- These values are more negative than E_{corr} values with the beam totally immersed inside the jacket.

Figure 10.28 shows the potential profiles at a different number of cycles for beam MU603N from which it can be noted that the change in E_{corr} inside the jacket produced proportional change in its values at the air-

exposed portion of the beam.

10.3.3 Corrosion Rate Measurements.

Using the technique described in Section 10.2.4, the corrosion rates were determined periodically at suitable intervals over the test duration. Past experiences have shown that the most dramatic changes in the structural parameters as well as the electrode potentials occurred during a relatively short period after the application of cyclic loading which suggests that the corrosion rate might exhibit similar behaviour. Consequently, more frequent measurements were taken during the first week of the test and then usually more widely separated for the remaining period of the test (approximately twice a week) unless special reasons dictated otherwise. Linear polarisation measurements provided the polarisation resistance R'p free from the IR-drop due to the electrolyte resistance. However converting this value to the instantaneous corrosion current I_{corr} requires the knowledge of the proportionality constants B which were determined at the end of the tests for reasons outlined earlier in Section 10.2.5. Therefore, it may be more appropriate to describe the characteristics of Tafel plots before presenting the corrosion-time data which are dependent upon values derived from them.

Tafel Plots.

Typically a 100 mV shift from E_{corr} both anodically and cathodically was applied during measurements in accordance with the method outlined in Section 10.2. The results are presented diagramatically in Figure 10.29 to 10.43 and are summarised in Table 10.2 which may be described as follows.

a. Dynamic Tests.

Figures 10.29,30,31 and 10.32,33,34,35 show the Tafel plots of fatigue test conducted in sodium chloride

solution at a load level corresponding to 0.4 and 0.6 f_y respectively. Interpretations of some of the anodic curves is difficult because of the occurrence of a limiting current at about 1620 $\simeq$ μamps. This is discussed in more detail in the discussion section of this chapter but the B_a values most affected by this phenomenon are indicated in Table 10.2 and in Table 10.6 (see later).

It can be seen that the B value is load dependent and that for a given load level, the test duration has almost negligible effect on this value despite some variation in the values of B_a and B_c as shown in Figure 10.36 and 10.37. It should be pointed out, however, that the effect of test duration is more pronounced on the values of B_a than B_c.

For tests at higher load level, the extrapolated currents showed continuous decrease with time but this trend was less clear in tests at lower load level (0.4 f_y). Perhaps the most important difference between the two load levels has been the attainment of a constant anodic limiting diffusion current of $\simeq$1620 μA obtained in higher load tests after a relatively small amount of shift, for tests up to 3 months in particular.

In both loading conditions (0.4 and 0.6 f_y) distinct difference between the anodic and the cathodic constants was observed indicating different response to both directions of polarisation. On the contrary, tests conducted in tapwater for 5 months at 0.4 and 0.6 f_y load levels, Figure 10.38 and 39, showed similar response to the anodic and the cathodic polarisations resulting in approximately identical Tafel constants. Moreover, the effect of load level on B values was more defined in tapwater than in sodium chloride tests.

b. Static Tests.

Figure 10.40,41,42 and 43 are Tafel plots for static tests in sodium chloride solution under different load level and test duration. Figure 10.40 shows a Tafel plot of beam ML60IN after 5 days exposure before load application. This plot may be regarded as a representative

of the initial condition of sodium chloride series at the end of the saturation period before the application of load.

Figure 10.41 is the Tafel plot of a static test at lower load level (ML403N) after 90 days of static loading. In this test the polarisations were continued anodically and cathodically until limiting currents were reached, at 1620 μA and 11,100 μA respectively. This figure also demonstrates the effect of the an uncompensated IR-drop on the shape of the polarisation curves.

Figures 10.42 and 43 present the same plot for two beams under higher static loads after an exposure time of 40 and 90 days respectively.

The observations of the attainment of a constant anodic and cathodic current in some of the Tafel-plot determinations was a subject of further experimental study the result of which will be presented in the discussion part of this chapter.

Corrosion Current-Time Data.

The determination of the variation of corrosion rate with test duration presents the primary objective of this chapter. After a series of considerations cited earlier, the corrosion rate-time curves were drawn on the basis of potentiodynamic (6 mV/min sweep) measurements. These measurements were considered as the most appropriate for relative comparison. In the discussion section of this chapter, the use of this data to deduce the absolute value will be discussed in light of the available experimental evidences. The corrosion rate results are presented, according to the maximum applied load and the surrounding environment, in Figures 10.44,45 and 46. The currents on the curves on these figures were calculated using a single B value for each beam as given in Table 10.2. Figure 10.44 presents the variation with test duration of the corrosion rate for tests conducted in sodium chloride solution at lower load level of 0.4 f_y, under both fatigue and static loading conditions. It is interesting to note that, at this load level and under such aggressive

environment, dynamic loading does not seem to have any significant effects over static loading conditions and this was particularly evident after approximately 450,000 cycles or an equivalent of ~31 days of static loading. The shapes of the curves, which were identical, indicate a sharp increase in I_{corr} at early stage of load application followed by a steady decline up to about 400,000 cycles after which the curves tend to level off for the remaining period of test. Further, this series results fall in a narrow band indicating good reproducability of results.

Results from test at higher load level, Figure 10.45, demonstrate a marked effect of dynamic loading on the corrosion rates as compared with static loading at the same maximum load. The shapes of the corrosion rate curves, however, for both cases exhibited the same behaviour and were similar to those of lower load tests. Thus the application of load produced a sharp increase in I_{corr} followed by a reduction, but at slower rate than at the lower load level. The stable state, that is the eventual level off, became evident after approximately 800,000 cycles.

Comparison between the two figures shows that, apart from a very early stage of exposure, the corrosion current in the static test at high load level (0.6 f_y) fall in the same range as those observed in the tests at the lower load level. On the other hand, dynamic loading at 0.6 f_y produced approximately 3 times the rate observed in lower load series.

Measurements on beams tested in tapwater were troublesome (see Section 10.2.6) and were only possible after more than 200,000 cycles at higher load level (beam MU605W) as shown in Figure 10.46. This figure thus lacks information about the early behaviour upon load application. Nevertheless, the remaining available data showed comparatively steady condition with a corrosion rates falling in the range of results obtained from chloride tests cyclically loaded at lower load level.

10.3.4 Corrosion Rate-electrode Potential Relationship.

Figures 10.47,48 and 49 examine the relationship between the corrosion current (I_{corr}) and the electrode potential (E_{corr}) for sodium chloride tests at load level of 0.4 and 0.6 f_y.

Figure 10.50 presents the same relationship for the single tapwater test for which these results are available. The line drawn on each figure is an approximate eye-fitted regression line drawn to facilitate the description of the plotted data. Figures 10.47 and 48 indicate reasonable relationship between I_{corr} and E_{corr} for each individual group of results. For the lower load level (Figure 10.47) the fitted line describes this relationship within an accuracy of $\pm$18% for more than 90% of the data points. For higher load level (Figure 10.48) the accuracy is even better at $\pm$15% for 90% of the data points. Thus, the relationship may be expressed by the equations of the lines as follows:

for 0.4 f_y series $\quad I_{corr} = 1.835\ E_{corr} - 2.791$
for 0.6 f_y series $\quad I_{corr} = 8.700\ E_{corr} - 2.036$

Figure 10.49 incorporates these two lines in their actual positions which clearly indicate the different relationships between E_{corr} and I_{corr} for different test situations. It would appear, therefore, that although apparently a definite relationship may exist between the corrosion rate and the electrode potential, this relation is more likely to be confined to each individual case of particular loading and exposure condition and any attempt to generalise these relations for other different systems would involve a great degree of averaging and approximation.

In the tapwater test (Figure 10.50) the data points exhibited larger scatter around the regression line (> 30%). It seems likely that E_{corr}/I_{corr} relationship would be even less clear under lower loading level to the extent that only rough indications can be obtained under such conditions. It should be appreciated, however, that

the limited data available from water tests precluded any conclusive remarks to be made.

10.3.5 The Evolution of the Electrode Potential After Polarisation Measurements.

The electrode potentials of the embedded steel were monitored after the polarisation tests and compared to the pre-polarisation values in order to evaluate the effect of various amounts of shift in potenial applied during the polarisation measurements on the subsequent corrosion process. Some of these data are presented through Figures 10.51 to 57.

Figure 10.51 and 52 provide the E_{corr} recovery for representative conditions after an anodic polarisation of 10 mV potentiodynamically (at 6 mV/min sweep rate), and potentiostatically (for 10 min time of application) respectively. In these Figures, the corrosion currents at the time of measurements are given for each curve. Figure 10.51 indicates the capability of the embedded steel to restore larger proportion of its original values within 10 minutes after a sweep scan. This may be attributed to a gradual change in potential during a sweep together with the relatively short time of polarisation (the total application time approximates 1:30 minutes) as well as the moderate corrosion rate of the specimens.

On the other hand, Figure 10.52 covers a wide range of corrosion activenesses at the time of measurements (I_{corr} = 80 µA to 1990 µA). Under the polarisation condition presented in this figure i.e. anodic step polarisation maintained for 10 minutes, it can be noted that the system of relatively very low corrosion current (beam MNS00N) with I_{corr} = 80µA) is more susceptible to suffer relatively important alteration in Ecorr than those having high corrosion rates. Continuous monitoring of E_{corr} for beam MNS00N showed that after 12 hr there was more than 2.5 mV change (more positive) from the original E_{corr} value compared with almost complete recovery after 10-12 min for other conditions given in Figure 10.52.

Figures 10.53,54,55,56 and 57 show the recovery

behaviour of E_{corr} after greater amount of shift applied during the experimental determination of Tafel slopes. Figures 10.53,54 and 55 present results obtained from sodium chloride tests and indicate that larger proportion of E_{corr} was recovered after about 20 minutes and almost complete recovery was achieved after approximately 1 hour. It can be seen that the rate of change after cathodic shift was faster that the after anodic shift. Figure 10.56 shows the change in E_{corr} after 100 mV shift in both directions for beam MU405W (I_{corr} = 150 μ A), it can be noted that E_{corr} recovered its original value after approximately 6 hours from cathodic polarisation. However, the E_{corr} recovery after the anodic polarization in this beam exhibited rather peculiar trends in that the original value of E_{corr} was reached relatively quickly ($\underset{\sim}{}$1 hr) but E_{corr} continued subsequently a negative drift for several hours (and to an extent of $\underset{\sim}{}$-70 mV) before commencing a gradual, slow return towards the original E_{corr} value. This result indicates that the anodic polarisation in tapwater causes significant change in the electrochemical characteristics of the reinforcement/ environment system which takes more than a day to be "recovered".

Figure 10.57 presents another interesting behaviour pertaining to system exhibiting passive behaviour (I_{corr} = 80 μA), which shows that longer time was required for E_{corr} to restore its original value. After anodic measurements, 36 hours required to return to within 3 mV (more positive) of the original E_{corr}. Cathodic polarisation on the other hand showed more transient effects than the anodic one. After both kind of polarisation, however, E_{corr} did not "cross over" the pre-polarisation potential.

The afore presented results suggested that, it is likely that in active corrosion condition, the corrosion rate has little effect on the degree of alteration in the electrochemical condition as a result of E_{corr} shift during polarisation, but marked effect on the subsequent corrosion process may be expected if the corrosion rate is extremely small as in the case of beam MU405W. For system thought to be in passive state, however, it can be

speculated, supported by the experimental observations, that although long time may be required to restore the original E_{corr} values, the corrosion processes are less likely to be significantly affected.

In either cases the risk of considerable alteration diminishes as the amount of polarisation reduces and is negligible for the 10 mV shifts. Also the polarisation in the cathode direction is less effective than the anodic one for a given amount of shift in E_{corr}.

10.3.6 Test of Special Nature.

10.3.6.1 Beam MNS00N, With No Links In The Central Portion.

During the course of this investigation, it became evident that there appeared to be an important effect of concrete cover on the pattern and extent of corrosion. The most evident indication of this kind of effect was the observation after the completion of experiments of a higher proportion of the total corroded area occurring on links. It is worth mentioning that in the beam portion exposed to the surrounding solution, the protective concrete cover to reinforcement is reduced from 25 to 17 mm due to the presence of 8 mm diameter links. However, the effect of cover is expected to be more pronounced in uncracked concrete in which the concrete cover presents a barrier whose effect will obviously be in proportion to the concrete cover. The cover effect consequently necessitated some limited work towards the end of the project in order to provide some indications on the development of the corrosion process under increased protective cover. To achieve this objective, a test beam was exposed to sodium chloride solution without loading for approximately one month. The beam details and reinforcement configuration were identical to those used in the main series with the crucial exception of the absence of links in the central 1800 mm portion of the beam. During the test, electrochemical measurements were made including the Tafel slopes at the end of the test.

Upon initial exposure to the surrounding solution,

E_{corr} moved immediately to the negative direction and achieved the value of -0.100 mV SCE after approximately 10 minutes and remained at this value for the remaining month under test. Potentiodynamic polarisation measurements made at different intervals provided approximately constant R'p values of 464 with a corresponding relatively low IR-drop of $\sim 7\,\Omega$. The Tafel plots determined at the conclusion of the experiment are shown in Figure 10.58 which indicates much steeper anodic and cathodic plots and hence a higher B value (64) and extremely low corrosion current of 79 μA compared with B = 21 and I_{corr} = 252 μA for beam under identical exposure conditions, but with normal reinforcement configuration (Table 10.2 and Figure 10.40). The behaviour of E_{corr} after polarisation measurements for this beam is given in the proceeding sub-section. Breaking the beam open upon completion of the test revealed no sign of corrosion on the embedded reinforcement.

10.3.6.2 Test on Old-Aged Beams.

Two beams were fatigue tested in sodium chloride solution under uni-directional bending regime at an age of approximately 1 and 8 years. The primary objective of these tests, designated MU60NIY and MU60N8Y respectively, was to examine the ability of old concrete beams to heal their flexural cracks during loading. Early in the tests, both beams indicated the possession of this phenomenon (see Section 8.3.3). However, the tests were continued for further period to monitor the electrochemical behaviours of the beams.

In addition, the test condition of beam MU60N8Y was modified during the test for experimental necessities as will be described with the results presented below.

Beam MU60NIY.

This beam had been cracked during handling before the start of the test, the only visible crack extended over the whole depth of the beam at a width of approximately 0.1 mm. The beam was cycled for 940,000 cycles before the

termination of the test. Figure 10.59 presents the variation with test duration of the electrode potential, the corrosion current and the range of deflection. (The corrosion current were calculated from R'p values determined potentiostatically at steady state. As usual the initial stage of the test marked a sharp change in E_{corr} followed by a stable period after ~300,000 cycles which continued for further 600,000 cycles from which a slight reversal to less negative values was observed. The range of deflection and the corrosion current followed essentially the same trend. In the measurements of I_{corr}, the proportionality constant B = 41 was used which was experimentally estimated from Tafel plot at the end of the test and given in Figure 10.60.

A comparison with results from other tests conducted under similar experimental condition, i.e. 0.6 f_y series, indicates distinct differences in the values and the rate of change in E_{corr} and I_{corr} despite similar structural behaviour. This discrepancy suggests the accidental cracks as a principal cause for the observed behaviour.

Beam MU60N8Y.

During the course of this test, the electrochemical noise technique (ECN) was developed and ECN measurements were taken for this beam as will be described in Chapter 11. Later it was decided to increase the maximum load incrementally to provide apparently variable conditions in order to examine the sensitivity of this technique (ECN). Thus the load was increased in increments equivalent to 0.05 f_y each of which was maintained for a certain period of test. The first increase was made after approximately 920,000 cycles as shown in Figure 10.61, also given in this Figure are the variations during the test of E_{corr}, I_{corr} and the range of deflection under the test condition which may be described as a variable amplitude fatigue loading. Figure 10.62 presents the Tafel plot at the end of the test from which, B value was found to be equal to ~43. The initial stage of the test showed similar structural and electrochemical behaviours as those

observed in previous 0.6 f_y series. The incremental increase of load, however, produced apparently transient effect in these parameters so that the original trends of change before each incremental load had been applied were resumed after relatively short time with persistent move towards the original values. In addition, the B value obtained at the end of the test (with load level of 0.75 f_y) was very close to those values obtained with a load level of 0.6 f_y despite the differences in their loading history.

Moreover, Figure 10.61 shows the dependency of the changes in the electrochemical parameter on the change in the range of deflection. Thus for the particular case examined in this test it seems that the increase, or more precisely the incremental increase, of load is unlikely to produce significant change in the electrochemical characteristics of the test beam and that the observed changes were of transient nature. It should be appreciated, however, that the incremental increase was gradual, thus precluded any sudden and considerable change and that the load was increased after appreciable period of test when the electrochemical conditions of the beam reached its stable state. Therefore the observed behaviour can not be generalised, and this test in fact poses more questions than it solves, some of these questions are:

1. What effect would the increase of load produce if it occurred during the early stage of test when conditions were changing relatively rapidly.
2. The effect of load increase in greater increments e.g. 0.1 or 0.2 f_y.
3. The effect of load increase if the initial load is lower than 0.6 f_y such as 0.4 f_y, in addition to the effects of loading sequence.

Accordingly more experimental data are required in this important area.

10.3.6.3 Short Duration Tests.

Short tests were carried out in sodium chloride solution on two beams designated ML601N and MU60N7D to provide B values representative of conditions of exposure before loading and the initial stage of fatigue loading respectively when various structural and electrochemical conditions were changing rapidly. For beam M1601N, the B value was determined after 5 days exposure to the solution. Since no permanent change in E_{corr} was observed after this measurement, the test was continued under static load corresponding to 0.6 f_y for one month at the end of which another Tafel measurement was made before the termination of the test. In the case of beam MU60N7D, Tafel measurement was made after 68,000 cycles ($\sim$4 days) after which the test was terminated.

Tafel plots of these tests were previously described in sub-section 10.3.3.

10.3.6.4 Test Under Environmental Change.

Following the difficulties experienced during polarisation measurements on beams tested in tapwater, it was decided to undertake special test to investigate the effect of the solution conductivity on the electrochemical behaviour of the embedded reinforcement as well as the limitations and the accuracy of the polarisation method as a corrosion rate measuring technique. To accomplish this objective, a beam was fatigue tested at high load level corresponding to a steel stress of 0.7 f_y and subjected to variable exposure conditions over the duration of test. The environmental changes were achieved by an incremental increase in the percentage by weight of sodium chloride salt in the solution starting from zero to 3.5% in four steps. The conditions examined and the corresponding test duration, expressed in number of cycles, were as follows:

Step	%.NaCl	No. of cycles
I	zero	616,800
II	1%	45,600
III	2%	42,700
IV	3.5%	477,190
	Total =	**1,182,290**

In order to prevent any artificial increase in the solution conductivity of the stage of 0.0% NaCl, no attempt was made to modify the pH of the solution by intermittent dosing with dilute HCl. Instead the pH of the solution was pulled down from typical initial rise to the value of pH = 10.9 by periodic replacement of the tapwater. This was found to be required only during the first week of step I. The electrochemical behaviour of the beam was monitored during the test as well as the solution conductivity at suitable intervals. Details of the test environmental history is given in Figure 10.63 which also indicates the number of cycles at which Tafel parameters were experimentally obtained.

Conductivity Measurements.

Table 10.3 and Figure 10.64 present the conductivity measurements at different sodium chloride concentration which enables the following comments to be made.

1. The increase in chloride ions concentration did not produce tangible change in the pH of the solution.

2. The conductivity increased as the chloride concentration increased.

It was observed that the solution conductivity rose immediately upon the application of salt and remained unchanged during the rest of the test duration under the new chloride concentration. This change in the conductivity was not accompanied by a proportional

reduction in IR-drop values as determined by a current interruption technique during polarisation measurements. Thus the addition of 1% NaCl produced an immediate drop in IR-drop from 15.1 to 6.62Ω but further addition of NaCl salt seems to have limited effect on this value. In other words a solution conductivity beyond 1.46×10^4 μmhos will produce little or no effect on the IR-drop.

The Variation of E_{corr} During the Test.

Figure 10.65 shows the variation of the electrode potential with test duration, it also shows the change in deflection range and the test interval under each chloride concentration in the solution. During the first stage (tapwater), as expected, the potential moved steadily towards more negative values followed by seemingly stable stage before a reversal towards less negative values. The application of 1% sodium chloride salt to the solution produced an immediate change to more negative direction and continued in this trend but at lower rate of change during the following additions of salt. This figure therefore seems to suggest that further increase in salt concentration beyond 1% served only in continuing the proceeding trend without immediate dramatic change. During the last stage (3.5 NaCl), however, E_{corr} showed a reversal in direction similar to that observed earlier in the test.

On the other hand, deflection range curve showed an initial increase up to approximately 48,000 cycles from which a progressive reduction in this parameter was observed, subsequent changes in salt concentration had no effects on both the direction and the rate of change in deflection range.

Tafel Slope Determination.

Figure 10.66 shows the Tafel plot obtained after 605,200 cycles during stage I when no chloride salt was added. Figures 10.67 and 68 present the same plot obtained during Stage III with 3.5% chloride salt after 754,600 and

1,182,290 cycles respectively. These figures clearly indicate the profound effect of the environmental change on the shape of the polarisation curves.

It should be pointed out however, that the Tafel slopes were difficult to be obtained since, due to limiting current effects, the linear portion of the polarisation curve is very limited. Constant limiting anodic and cathodic currents of 1,612 and 11,120 μA were also obtained in these measurements.

Polarisation Measurements.

Linear polarisation measurements were made during each of the test stages both potentiodynamically and potentiostatically from which the following observations were made:

Tapwater - Stage I.

During this stage which covers 616,800 cycles, the polarisation measurements were troublesome due mainly to the lack of linearity in E-I relationship during potentiodynamic measurement and the continuous fluctuation in current when conducting the measurements potentiostatically. The random nature of fluctuation has also been observed in electrode potential change in phase with load cycling as described earlier in Section 10.3.1 and shown in Figure 10.20. At the end of this stage the effect of sweep rate on polarisation measurements was investigated, the scanning rates examined were 2,4,6,8,12, 16 and 20 mV/min.

The E-I relationship as obtained from the x-y plotter are presented in Figures 10.69 and 70, the corresponding Rp values were determined from an average eye-fitted lines passing through the polarisation curve. Figure 10.71 shows the I-time relationship obtained from a step of 10 $\pm$m V which indicates that the current achieved a steady state after approximately 1 minute Figure 10.72 summarised these results and presents the corrosion current obtained by different methods from which it can be seen that current

obtained using a scanning rate of 2mV/min gave almost identical values to those obtained from back extrapolation of Tafel plots and from potentiostatic measurements at steady state.

Finally, the trends in E_{corr} after polarisation measurements are given in Figure 10.73. The potential after anodic scan went slightly more negative than the original E_{corr} (by 1-2 mV after 20 minutes) in a way similar to, but to lower extent, that observed for water test after Tafel measurements shown in Figure 10.56. On the other hand, the potential recovery after cathodic scan showed a return towards the original E_{corr} but after 20 minute, it was still 2-4 mV more negative than the original value. The shape of the curves, however, suggests that measurements at higher scanning rate are associated with earlier recovery in E_{corr} and less alteration from the original E_{corr} before polarisation.

Addition of Salt.

The application of sodium chloride to the solution immediately improved the polarisation measurements to a large extent and, consequently, clear E-I relationship was observed. Figure 10.74 presents potentiodynamic measurements, made at a scanning rate of 6 mV/min after only 3 hrs from the application of 1% of NaCl. This particular measurement gave R'_p value of 33 i.e. less than one half its value before the salt application had been made. This large change in R'_p however, did not produce an equivalent change in the corrosion current since it was partially offset by the reduction in B valve (see Figure 10.63). 3 days later, under the same 1% NaCl, the R'_p dropped to about half the value after 3 hrs as given in Table 10.4. Further increase in salt concentration slightly improved the linearity of E-I curves with practically no change in IR-drop. B values are only available for Stage I of this test, (Figure 10.63), consequently, presenting the data in terms of corrosion current might be rather unreliable because of changing environment.

10.3.7 Corrosion Pattern and Extent.

Upon completion of each test, the beams were broken open to determine the pattern and extent of corrosion. Breaking the beams up revealed, for both aqueous environments and for all stress levels, that corrosion was present at sites coincident with the position of flexural cracks in the concrete beam, Figure 10.75a.

In cases where the beams were kept under water after the termination of the tests, until immediately prior to breaking up the concrete, black corrosion products were observed in certain positions on the bars, Figure 10.75b.This is indicative of a restricted supply of oxygen to the corrosion site, and on exposure to air the black product changed, within about 20 minutes time, to the familiar reddish-brown rust colour.

The total corroded area for each test beam was determined from the reinforcement cage recovered from the central portion of the beam including the submerged area and the areas of cracks outside the jacket. Figures 10.76a and b show two examples of reinforcement cages recovered from beam MU605N and MU70WN respectively, with clear indications of localised corrosion on the main bars as well as the links coincident with crack sites.

Table 10.5 presents the total corroded area measured for various conditions in Stage II of the programme, from which the following remarks can be made.

1. Larger proportion of the corroded are was observed in shear links rather than the main bars.

2. The total corroded are was proportional to the load level, static or dynamic.

3. For a given maximum load level and test duration, greater amount of corroded area was found in beams tested under fatigue type of loading than the static loading particularly under high load level.

4. Under dynamic loading, the test duration seems to have

negligible effect on the corroded area. Under static loading, however, the limited data available, shows evidence of time effects on the measured corroded area.

5. A beam tested at 8 years of age showed appreciably less corroded area than the beams of lower age despite the higher load levels (Figure 10.61) experienced at later stages.

6. The environment seems to have little effect on the total corroded area.

Different examples of corrosion attack obtained from various conditions are presented in Figures 10.77 to 81. As might have been expected, the most severe metal penetration due to corrosion was observed in NaCl tests. Typical attack is shown in Figure 10.77. Also not unexpectedly, deeper corrosion was observed after dynamic tests in NaCl (Figure 10.77) than in the case of beams subjected to static loading when the attack on the embedded steel was relatively shallow (Figure 10.78).

Figure 10.79a shows a typical area of corrosion observed on the tension bars of beam MU70WN. The tiny corrosion spots around the main area probably indicates a propagation stage by pits formation mechanism.

Corrosion on the links of the reinforced cage recovered from the same beam is shown in Figure 10.79b which clearly shows the formation of thick white layer on the attacked area of links. The same phenomenon was also observed in other tapwater test at lower load level corresponding to 0.6 f_y (MU605W) as shown in Figure 10.78b. The corrosion attack in these cases seems to remove the white layer leaving instead porous corrosion layer of variable thickness, the corrosion attack, however, was shallow in all cases. However, no sign of the formation of such a layer was observed in the attacked area on the main bars of the aforementioned tests shown in Figure 10.79a and 80b. This is also true for the corrosion pattern observed in the links as well as the main bars for

water test at the lowest load level and all chloride tests as shown in Figures 10.77,78 and 81.

The above described observations provide a possible indication of a rather complex, load-dependent, corrosion process in low-TDS water. However, this detailed phenomenon was of relatively small practical importance compared to the observation in all cases studied in tapwater of extremely shallow attack on embedded steel.

10.3.8 Measurements on Seawater Tests.

Concurrent research work in this department provided an opportunity to obtain some directly comparable data as to, primarily, the influence of the environmental factor and to obtain some corrosion rate data on very long running tests. The research is concerned with the behaviour under fatigue loadings in seawater of essentially identical reinforced concrete beams and loading configuration to those investigated in this study. Thus five different loading and exposure conditions were selected as a basis for comparison, these may be put into three different categories according to the test condition as follows:

Category 1: Long Jacket - Uni-directional Tests.

The solution jacket was identical to those used in this research and covers the central 1170 mm of the beam. Two beams were examined under this category which were:

Beam CF103: The beam was fatigue tested in uni-directional bending at a load level corresponding to 0.4 f_y. At the time of measurement, this beam was cycled for 33.8×10^6 cycles ($\sim$6 1/2 years).

Beam CF100: The beam was fatigue tested in uni-directional at a load level of 0.6 f_y for 35.6×10^6 cycles ($\sim$6 3/4 years).

Category 2: Long Jacket - Reverse Test.

Beam CF144: This beam was fatigue tested in reverse bending at a load level corresponding to 0.46 f_y downwards and 0.34 f_y upwards for 6.7 x 10^6 cycles ($\sim$1 1/4 years).

Category 3: Totally Submerged Tests.

Measurements were made on two beams which were totally encased in a seawater jacket along their entire length including the end supports. The beams histories are:

Beam 1TS: The beam was fatigue tested in reverse bending at a load level in both directions of 0.4 $f_y\downarrow$ /0.34 $f_y\uparrow$. At the time of measurements the beam was subjected to approximately 11 x 10^6 cycles ($\sim$2 years).

Beam 2TS: The beam was exposed to sea water for nearly 2 1/2 years without loading.

Polarisation measurements including the determination of Tafel plots were made on the above mentioned beams, it should be appreciated, however, that these measurements were made after relatively long period of test giving rise to the possibility of attaining a stable electrochemical conditions similar to those observed in earlier reported results (Section 10.3). Thus periodic measurements for a given test condition, at this stage would be expected to produce close results. This expectation was confirmed when comparing the results of two polarisation measurements made on beam CF100 at an interval of more than 10 months. Thus using B value obtained at the end of the test, the corrosion current was 1303 μA as compared to 1278 μA after 10 months of cycling. The corresponding E_{corr} was -0.4845 and -0.4854 V SCE respectively.

It seems likely, therefore, that firstly after long exposures, "steady-state" condition may become established

so that any single measurement may represent the electrochemical condition of the test beam for a far longer period of test than it appears to represent, and secondly, although no direct evidence is available on this respect, that the Tafel constants are also expected to exhibit the same trend.

Figure 10.82 to 86 present the Tafel plots for the selected conditions, the results are also summarised in Table 10.6. These results show:

Category 1: Figures 10.82 and 83.

Limiting anodic and cathodic currents of 1612 and 11,100 μA were attained after different over-potentials. These limiting currents are identical to those obtained in sodium chloride tests. The limiting current on the anodic polarisation was too close to E_{corr} for an anodic Tafel range to be evident but this was not the case on the cathodic scan from which Tafel behaviour would be clearly seen.

Category 2: Figure 10.84.

The anodic and cathodic constants are essentially the same, in this test an anodic limiting diffusion current of 1621 μA was also achieved but after greater amount of over- potentials than the proceeding cases. The test was not continued to obtain the cathodic limiting current.

Category 3: Figure 10.85 and 86.

These tests are particularly interesting for comparison as they provide a case where all the concrete body is saturated, hence, different combination of anodic to cathodic area are expected as compared with partially encased beams. Figure 10.85 shows a good example of the effect of the un-compensated IR-drop on the shape of Tafel plots, it also indicates that both, the anodic and cathodic limiting currents are comparable to those previously obtained from partially exposed beams.

Figure 10.86 provides the results of submerged beam with no load and indicates considerably higher value of B_a and little effect of IR-drop on the shape of Tafel plot. This test was not continued to obtain the limiting currents. The comparison of these results with other tapwater and sodium chloride results will be further discussed in the discussion part of this chapter.

10.4 Discussion.

The different electrochemical parameters monitored during the tests which are presented in this chapter reflect the effect of different test conditions and loading regimes investigated in this study. The discussion part of this chapter will be devoted on the technical aspect of the measuring techniques, the interpretation of electrode potential measurements as well as the corrosion rate results. The last section of this discussion presents an attempt to develop a new look at the mechanism of corrosion for dynamically loaded and partially exposed reinforced concrete element.

10.4.1 The Accuracy of Linear Polarisation Method (LPM).

The correct determination of corrosion rate by means of linear polarisation method is limited by several factors. These factors were described earlier in Chapter 3, which clearly demonstrate the crucial influence of the electrochemical characteristics of the corroding systems on the accuracy as well as the choice of the appropriate technical conditions. From the technical point of view, the correct corrosion rate is directly dependent on the accuracy in determining both the proportionality constant B and the polarisation resistance Rp free from an IR-drop. In this study, there have been some technical difficulties in obtaining the B value, this together with other relevant theoretical considerations will be discussed in Subsection 10.4.5. However, the use of linear polarisation method for the determination of the R_p value requires careful consideration of the most accurate sweep rate and

waiting time for potentiodynamic and potentiostatic measurements respectively.

Most of the measuring techniques are provided by several options to help lessen the practical difficulties that arise from measurement on widely varying experimental details and corrosion activity. The results presented in Figures 10.9, 10.10 and 10.11 indicate that the value of R_p is sensitive to the change in scanning range for the former technique and waiting time for the latter. These figures also indicate that different relationships between Rp curves were obtained for different tests of variable corrosion state. The observed behaviour is, in fact, in agreement with what Gonzalez et al[90] have previously suggested in that the relationship between R_p values and the technical variables, namely sweep rate and waiting time, must be established initially for every unknown corroding system. Further, however, they suggested that the sweep rate must be chosen within the range where R_p achieves a constant value and that the correct waiting time for potentiostatic measurement is the one which gives identical R_p value to that obtained potentiodynamically from the constant region of R_p curve. It should be pointed out, that in their tests the constant regions of R_p curves obtained by both methods were coincident (see Figure 3.22).

The results presented in Figures 10.9, 10.10 and 10.11, however, differ in a number of aspects from those obtained in the work of Gonzalez et al.

Firstly: these results indicated a continuous change in Rp' values with the change is scanning rate over the range between 2 to 20 mV/min (note that Gonzalez et al observed constant R'_p value over the range between 2.5 and 10 mV/min). As shown in Figure 10.87 the rate of change in the R'_p was dependent on the IR-drop value with more gradual change being associated with systems of lower IR-drop. However, the shape of the curves suggests that constant R'_p independent on the sweep rate might just be obtainable at higher scanning rate particularly with systems exhibiting lower IR-drop.

Secondly: the region where potentiodynamic

measurement showed a tendency to level off was not coincident with stable region on the potentiostatic curve. On the contrary the differences between Rp values obtained by these technique continued to increase as they, apparently, approach the assumed constant region, this is particularly true for system with low IR-drop. Thus the region of approximately constant R_p of a given measurement is coincident with the rapidly changing region on the other.

It seems likely that the observed differences between the present work and that reported by Gonzalez et al are related to the substantial differences in test conditions. The latter study were conducted on much simpler and smaller specimens comprising steel bars embedded in mortar at considerably lower corrosion rate 0.01 $\mu A/cm^2$ as compared to 2-15 $\mu A/cm^2$ obtained in this study.

On the other hand, the problem of the accuracy of measurement becomes even more complicated due to the absence of actual metal loss based on gravimetric measurements upon which different techniques may be evaluated.

It should be appreciated, however, that these delicate relationships are more related to the absolute value of the corrosion rate than the relative values. Since it seems rational to assume that different response to a constant degree of electrochemical alteration will reflect changes in the corrosion rate for a given specimens details. The only limitation to this general statement is the case where a given measuring condition can not produce meaningful results such as the measurement made on beam MU405W.

The absolute values, on the other hand, are less clearly defined. It seems, as suggested by Figures 10.9, 10 and 11, that whereas it may be possible to obtain the correct scanning rate or waiting time for a given system, the use of the same combination may produce different values for other systems of substantially different characteristics. Nevertheless, important information, may be gained from Table 10.7 which compares the corrosion currents estimated (at the same exposure time) from

different techniques including the back extrapolation of the Tafel plots. It is interesting to note that potentiostatic measurements at a steady state condition give very close values to those obtained from the Tafel back extrapolation method for the majority of measurements including seawater tests. Most of the cases presented in Table 10.7 give agreement between these two estimated current values of within $\pm$10%. There is indication, however, of a tendency in some cases for potentiostatic measurements to either overestimate or underestimate the corrosion current as can be seen in the case of beams MU603N, MU60N7D, CF103 and ITS. It should be pointed out that such differences may be attributed to some uncertainties in obtaining the accurate B values used in determining the corrosion current for these particular beams (except the case of beam MU603N) as indicated in Tables 10.2 and 10.6 and also discussed in Section 10.4.5. Further, in case of overestimation, the real steady state value may have not been achieved at the time of measurement (i.e. after 10 minutes) as will be discussed further in the following subsections.

The correlation between polarisation resistance and Tafel extrapolation or weight loss data has been reported as generally good.[108] In the present study, although not supported by gravimetric metal loss data, it can be assumed that extrapolation method is likely to produce more realistic estimation of the corrosion rate. This is because each measurement usually examined the response of the corrosion system over a relatively large overpotentials (typically $\simeq$ 100 mV) in both directions and thus minimises the possible error arising from estimating the corrosion state of the electrode from limited overpotentials near E_{corr} which are particularly susceptible to the environmental effects, such as the IR-drop, and also to difficulties in measurements due to low current flowing through the outer electric circuit.

Accordingly, the appropriate sweep rate would be that which produces R_p value equivalent to that obtained from steady state potentostatic measurements. Further it is interesting to note that for systems exhibiting high

corrosion rate (Figures 10.9 and 10.10) the accurate R'_p is obtainable by extrapolation to low sweep rate. This observation is generally in agreement with that reported by Fontana[227] who discussed various measuring techniques and suggested, for small-amplitude cycle voltammetry (SACV) technique, that the true R_p could be obtained by plotting R_p-sweep rate curves and then extrapolating to zero sweep rate resistance. It should be appreciated, however, that his suggestions were obtained from substantially different corroding systems than those investigated in this study.

The above discussion allows the following general rules to be recommended for the appropriate choice of the technical variables which are likely to produce the correct comparison basis in terms of absolute and relative values.

1. If comparison in relative terms is required, either techniques may be used provided that the initially adopted scanning rate or waiting time is maintained constant throughout the investigation. (Thus in this study a constant sweep rate of 6 mV/min is used throughout the tests and used for relative comparison).

2. In the absence of gravimetric data, a relationship should be established initially between R_p values obtained by different sweep rates and waiting time. Then the subsequent measurements may be made potentiodynamically using the scanning rate which gives identical values to those obtained potentiostatically at a steady state condition. The R_p relationships, however, should be obtained for each system of different condition or when the condition for each individual systems changes substantially during the test.

3. Allowance should be made of the effect of IR-drop on R_p values.

Finally, despite the numerous factors which worked against the successful application of the linear polarisation method, the present study has in fact, enhanced the reliability of this method and extended its application to include more complicated systems such as those investigated in this study. This is indicated by a comparison between the experimental results and the actual pattern and extent of corrosion observed upon completion of the test. These aspects will further be discussed elsewhere in this section.

10.4.2 Potentiodynamic Measurements.

The appropriate sweep rate for use in measurement on reinforced concrete is not clearly defined in the literature as outlined earlier. The only available guidelines are those of Gonzalez et al[90] who suggested a sweep rate between 2.5-10 mV/min to give sufficiently accurate estimation of R_p. Further they indicated that a sweep rate (K) must be such that the time to apply ΔE = 10 mV is about 5-6 times the time constant (τ). The latter guideline was based on theoretical consideration of an inert Randle circuit.

Accordingly:

$$K^{-1}\Delta E = 5\text{-}6(\tau) \qquad \ldots 10.1$$

where

$$\tau = \frac{CR_eR_p}{R_e + R_p} \qquad \ldots 10.2$$

C = Capacitance
R_e = Electrolyte resistance

and for systems where $R_p >> R_e$

$$\tau = CR_e \qquad \ldots 10.3$$

For the corroding systems with very low corrosion rate, that is with high C and R_p values, Equation 10.3

applies as usually $R_p >> R_e$. For the present work, however, Equation 10.2 is more relevant to the corrosion state of the beams as R_e, in some cases, could reach 50% of R_p.

It was observed that R_e, for a given test condition, increases only slightly with test duration and therefore is not expected to cause changes in the required K value during the tests. Consequently, the change in K value, if required, is mainly controlled by the changes in C and R_p. Nevertheless, as suggested by column 2 and 3 of Table 10.7 and also Figure 10.15, there are indications that the change in corrosion rate of few times does not change the initial relationship between potentiodynamic and potentiostatic measurements. Thus for the range of corrosion activity examined in this study, there is no need to modify the sweep rate during the tests to provide the required accuracy (in relative terms). This would be expected if the change in R_p is compensated by a change in C value to give a constant τ which controls the sweep time.

Table 10.8 gives the appropriate sweep rate (K) for different corroding systems together with other electrochemical parameters. The values of K given in this table were deduced using the criteria outlined earlier in the preceding subsection. It can be seen that for a given environment slower sweep rate is associated with lower corrosion rate. This is in agreement with what Gonzalez et al have suggested in that to avoid errors, the sweep rate should be slower the lower the corrosion rate. Further, this table indicates that the R_e value has far greater influence on the sweep rate than that of R_p. This is particularly evident in the case of tapwater tests which exhibited greater variation in R_e and K values.

Unfortunately, C values for real corroding systems is difficult to be obtained experimentally although it may be estimated using A.C. technique which requires expensive equipment and computational power for the elaboration of data.

It should be noted that the process of choosing the appropriate sweep rate is also influenced by other

considerations. As shown in Figure 10.73, very slow sweep rate increases the possibility of electrode perturbation particularly after anodic measurements despite the small applied ΔE. Meanwhile increasing the sweep rate will result in lower R_p as shown in Figures 10.69 and 10.70, thus overestimates the corrosion rate. (However, for the extreme case, that is very fast sweep rate the R_p value becomes of doubtful value because it approaches the value of R_e as indicated previously in Figure 3.22). These figures also indicate that for tests in low conductivity electrolyte, the increase in sweep rate did not result in improving the linearity of E-I curve. Thus R_p measurements is particularly sensitive to electrolyte conductivity and an addition of 1% NaCl results in significant effect on the linearity of this kind of measurements (see Figure 10.74).

Moreover, it was observed that potentiodynamic E-I curves exhibited an initial low current region (tail) extending over variable overpotentials both anodically and cathodically (Figure 10.4). This kind of behaviour has also been reported by several workers and believed to have been introduced by the voltage drop due to polarisation effect (as described in Chapter 9) and electrolyte resistance. This is so because this voltage drop is relatively considerable compared to the applied potential at early stage of measurement. To avoid this source of error different methods have been proposed as shown in Figure 10.88.

In this study, however, the R_p value was obtained from the slope of the linear portion of the polarisation curve.

Finally, the procedure of conducting potentiodynamic measurements, described earlier in Section 10.2, is different in some aspects from that recommended by the American Standard ANSI/ASTM G59-78. According to this specification a step of ΔE is applied cathodically and the new electrode potential is scanned back anodically up to ΔE more positive to the corrosion potential. R_p then is the slope of the curve at E_{corr}.

A comparison between E-I curves obtained by both

methods is presented in Figure 10.89 which indicates essentially similar R_p value. It should be pointed out, however, that the procedure adopted in this study is more time consuming as it is necessary to allow E_{corr} to restore its original value after the first cathodic measurements before scanning the reverse direction. Nevertheless, this procedure was adopted as it provides more information as to the response of the system under measurement to each kind of polarisation separately.

10.4.3 Potentiostatic Measurements.

The accuracy of this kind of measurements hinges on the correct waiting time before measurement. The waiting time must be long enough for the transitory component of the current to disappear, longer time, however, will increase the possible diffusion process and may transform the electrochemical characteristics of the system. This delicate relationship is illustrated schematically in Figure 10.90 which traces the changes in measured current I_m as a function of waiting time and the corresponding change in the electrode potential responsible for such changes. This figure examines a special case of anodic measurement and may be described as follows:

Region A-B: represents the electrochemical condition before the potential shift. The corrosion process in this region is occurring at the initial potential $E^i_{corr} = E^{act}_{corr}$ and I_{corr} (directly immeasurable). The step shift of potential ΔE is applied at point B which produces an immediate high current flow through the outer electric circuit. Thus the measured potential changes from E^i_{corr} to E_m and

$$E^i_{corr} + \Delta E = E_m \qquad \ldots 10.4$$

Region B-C: exhibits progressive decay in I_m towards the original I_{corr}, thus in this region $I_m > I_{corr}$. Meanwhile E_m remains unchanged and, if the polarising supply was switched off, the specimen potential would

change to a value E^{act}_{corr} which at this stage would be equal to E^{i}_{corr}. Thus:

$$\Delta E_{real} = \Delta E_{imposed}$$

$$E^{i}_{corr} = E^{act}_{corr}$$

Region C-D: where the correct waiting time starts and finishes. Consequently the measured current $I_m = I_{corr}$, and the characteristics of ΔE and E_{corr} remain unchanged as in region B-C.

Region D-E: where the waiting time is longer than the correct one and electrochemical transformations starts to occur. Thus:

$$\Delta E_{real} < \Delta E_{imposed}$$

and

$$E^{act}_{corr} = E^{i}_{corr} + C\,\Delta E \qquad ...10.5$$

where the factor C takes the values $0 < C \leq 1$

Accordingly

$$I_m < I_{corr}$$

The electrochemical change is proportional to the time in excess of the correct waiting time and this is allowed for by the factor C in Equation 10.5. The maximum change in E_{corr} occurs at the end of this region where C = 1 and therefore:

$$E^{act}_{corr} = E^{i}_{corr} + \Delta E \qquad ...10.6$$

At this stage the flowing current in the outer circuit approaches zero. $I_m = 0$ and possibly:

The new corrosion current:

$$I^{act}_{corr} > I^{i}_{corr}$$

It should be pointed out that E^{act}_{corr} may exceed the value $E^{i}_{corr} + \Delta E$ if more time is allowed. On the other hand, if the current is interrupted at any point in the regions B-C and C-D, E_m will most probably recover its original value, E^{i}_{corr}, which existed before the start of the measurements. As indicated in Figure 10.5 extremely low corrosion rate system, where the steady state condition is achievable after very short time (30-45 secs), is particularly sensitive to small increase in time in excess of correct waiting time.

As mentioned earlier in this section, it was found that regardless of the corrosion rates, measurements at steady state conditions have yielded very close values to those obtained from extrapolation method. However, few exceptions were observed in systems exhibiting high corrosion rate, this can be related to the waiting time necessary to obtain the correct R_p value. Referring to Figures 10.13 and 10.14, it is clear that, unlike lower corrosion rate conditions, measurements on high corrosion rate conditions exhibited continuous decay in current with time, also the response to anodic polarisation is quite different from that of the cathodic one. This is particularly evident in the case of the more active conditions presented in Figure 10.13a. It should be appreciated, that the maximum waiting time used was 10 minutes and thus it seems likely, for this particular example (beam MU60N7D), that different steady state value may be obtainable (which is closer to the extrapolated Tafel value) had the waiting time increased. Moreover, for such cases when substantially different anodic and cathodic behaviour is obtained, it is recommended to determine R_p from the anodic measurements rather than the average value of both measurements as corrosion is primarily concerned with the anodic process.

Finally as shown in Table 10.8, the results indicated considerably lower waiting time for tests in tapwater (1-2

minutes) than tests in chloride solution (5-10 minutes). That is longer waiting time to achieve a steady state has always been associated with active corrosion conditions. This observation agreed with the observations made by other research workers[104,163] and can probably be explained according to the theoretical considerations discussed by Gonzalez et al.[104] They indicated that the waiting time necessary to obtain a given error:

$$\frac{I^{o}_{tr}}{I_{\infty}}$$

in the steady state corrosion rate increases with increasing values of the ratio:

$$\frac{R_p}{R_e}$$

where I^{o}_{tr} is the transitory component of the current for t=0

I_{∞} is the stationary component of the current.

Thus if R_p/R_e = 2 (beam MU605W) an error < 10% requires that I_{tr} = 5% I^{o}_{tr} and if R_p/R_e = 10 (beam MU605N) then for the same amount of error I_{tr} should be 0.6% I^{o}_{tr} and thus more time is required for the latter situation. It should be noted, however, that the rate of decay in the measured current is a complex function of R_e, R_p and C, the therefore the ratio between the waiting times of any two situation is not equal to the corresponding ratio of the values of R_p/R_e.

10.4.4 The Behaviour of Electrode Potential.

General.

The exposure of reinforced concrete to corrosive environment is known to cause changes in potentials towards more negative values. These values depend on several factors which are generally related to those

influencing the corrosion rate. For specimens with low moisture content, however, the measured E_{corr} is also sensitive to the location of the reference electrode during measurement. Grimaldi et al[228] indicated that the scatter in E_{corr} for adjacent sections of one sample can reach 233 mV. This characteristic is explainable in terms of the properties of concrete which are not homogeneous throughout the whole volume and which, therefore, influence corrosion of steel heterogeneously. It is evident, thus, that the measured potential of the reinforcement relates to a rather narrow area of the steel where localised corrosion occurs.

In fully immersed situations, the electrolyte has a very much higher conductivity than the concrete and no significant potential difference will be measurable at the concrete surface, as the resistance path is short-circuited by the electrolyte, although localised corrosion is occurring.

Accordingly, in the present study, the measured E_{corr} at any given time was constant for the immersed portion of the beam and independent on the location of the reference electrode. This was the case for both kinds of solutions (i.e. tapwater and chloride solution) despite the considerable difference in their conductivities. Outside the jacket, however, the E_{corr} value showed dependency on location as shown in Figures 10.26, 27 and 28 and this may be attributed to differences in concrete resistivity as a result of different degree of water saturation.

E_{corr}-Corrosion Rate Relationship.

Electrode potential measurements are nowaday widely used for assessing the condition of steel embedded in concrete. Although, qualitatively, it is certain, as numerous studies have indicated, that the corrosion rate is high at more negative values of E_{corr} and low at more positive potentials. However, no kinetic conclusions can be drawn from E_{corr} values with out a great risk of error. The result of this study generally confirmed this observation as shown in Figure 10.49 which includes E_{corr}-

I_{corr} relationships for different test conditions. Despite that, each individual test condition did in fact show analogous displacements of E_{corr} and I_{corr}, and thus good correlation, particularly in chloride tests as shown in Figure 10.47 and 10.48.

However, there are some indications that in certain conditions even qualitative assessment is not possible on the contrary it may indicate completely different conclusion. Consider, for instance, the potential development of beam MU405W shown in Figure 10.22. If potential monitoring is made at any stage after 500,000 cycles, then, according to the American Standard ANSI/ASTM C876-77 given earlier in Chapter 3, there is a probability of 90% that corrosion is not occurring. Whereas the full history of the beam would indicate different conclusions and this was later confirmed when this particular beam was broken open which showed the occurrance of corrosion. The main conclusion, in this respect, is that in the absence of superficial signs of corrosion of the embedded steel, reliable qualitative evaluation using potential data hinges on a proper foreknowledge of the electrochemical history of the structure.

E_{corr} During Saturation Period.

The development of the electrode potentials upon contact with the surrounding solution indicated a complex behaviour which is responsible for the widely scattered values. Consistently less negative potentials were associated with tests in tapwater. Chloride tests, however, showed a behaviour which suggests a dominant effect of concrete cover in terms of both thickness and quality.

An increase in concrete cover (due to the absence of links in the immersed portion) of beam MNS00N produced a clear effect on the initial (uncracked) value of the potential compared with beams of identical mix design and manufacturing process but with links. Thus, without links, E_{corr} was no more negative than -0.100 V SCE (values typical of passive behaviour) in comparison with beams

containing links which exhibit early more negative E_{corr} values in the range of -0.200 to -0.300 V SCE (indicative of some loss of passivity).

Less negative potentials ($\sim$-0.100 V SCE) were also developed by beam MU60N8Y (8 years old at the time of test) despite containing shear links.

These two examples clearly illustrate the decisive influence of concrete cover on the electrochemical characteristics of reinforced concrete under no-load conditions. According to the test result, this effect may be described as follows:-

The potential reflects the properties of the steel/concrete interface and this clearly is dependent upon the local environment at that interface. In cases where the bulk external environment is NaCl, the arrival of Cl^- ions at the embedded steel surface will promote local breakdown of the passive oxide film on the steel. This localised loss of passivity would be expected to be associated with a shift in electrode potential to more negative values.

Clearly the electrolyte diffusion is not uniform and is dependent on the distribution of pores in concrete cover. Also, due to shorter distance from concrete surface, there is greater probability for earlier diffusion to the links than the main reinforcement. It is apparent that the diffusion of the electrolyte and hence of chloride through the 17 mm cover (for link-containing beams) requires relatively short time i.e. $\sim$12 hrs, so that essentially constant E_{corr} has been maintained during the remaining no-loading period ($\sim$5 days). Therefore, for the same quality of concrete cover, an increase of 8 mm to the cover would be expected to produce a rather significant increase in the time for Cl^- ions to reach the embedded reinforcing bars because of the parabulic time dependence of diffusion processes. This factor might have accounted for the maintenance of passivity (as evidenced by the maintenance of relatively positive E_{corr} values of -0.100 V SCE) throughout the 30-days, no-load period of beam MNS00N.

However, a further contributory factor to this improved corrosion behaviour of beam MUS00N is likely to

have been provided by the change of cover thickness having an additional effect in producing enhanced concrete quality. This of course is practically feasible as the less congested reinforcement details allows better compaction efficiency and thus better concrete quality. Some support for this proposition is provided by the IR-drop measurements. These reveal that this beam (MNS00N) exhibited an IR-drop due to cover resistance which is slightly greater than those measured for ordinary beams during saturation period (the resistance of 6.7Ω for the former as compared to 4.5 for the latter).

Further support for the idea of concrete quality contributing to the corrosion behaviour of the beam prior to loading was provided by the potential measurements from the "old" beam MU60N8Y. Accordingly, the observed less negative value of E_{corr} measured for this beam is readily explicable in terms of higher quality of cover as a result of progressive hydration process of cement compounds due to age effect. The improved quality of cover limits the effect of the originally existed defects with an increase in the IR-drop due to an increase in concrete resistance ($\Delta 10\,\Omega$).

The concrete quality may affect the corrosion process in two ways. Either by limiting the oxygen supply to the steel area or by reducing the Cl^- ions diffusibility. However, Tafel plots obtained during no-load condition of beam ML601N (Figure 10.40) and no-link beam MUS00N (Figure 10.58) indicates an important feature in that the cathodic process, which is assumed to be O_2-reduction reaction, is in both cases activation polarisation controlled. This implies that the oxygen availability and diffusibility are not the rate determining steps, but higher B_c value observed for no-link beam indicates that the O_2-reduction reaction is affected by the concrete cover and this may be attributed to different activation polarisation for O_2-reduction on passive-oxide covered rebar compared to that on depassivated steel. It seems likely, therefore, that the observed change in corrosion activity due to increase in cover is explainable in terms of different Cl^- diffusibility and its controlling effect on the anodic

reactions as a result of improved concrete quality and increased resistivity.

The above discussion is generally in disagreement with observations made by Wilkins et al[229] who attributed differences in E_{corr} behaviour for different specimens, in saturated condition, to the differences in oxygen diffusion coefficient. Also, rather interestingly, they noted that the development of E_{corr} in fresh water took similar patterns and values as those of seawater and concluded that the presence of chloride salts was not a significant factor in their specimens. However, the obvious dependency of the initial development of E_{corr} (under no-load condition) on environment observed in the present study (i.e. much more negative potential in chloride solution compared to tapwater), indicates a very important feature with regards to the correlation between the behaviour of real structures, as more closely simulated in this study, and the behaviour of small specimens of completely different concrete/steel area ratio and greater possibility of strict quality control. This important remark has also been appreciated by Wilkins et al.[229] They indicated, however, that the flux of oxygen to the reinforcement of any real structure will be much less than that found in their cylindrical specimens and the rate of steel corrosion in negative active condition would be expected to be correspondingly low being limited by the arrival of oxygen at the steel surface.

The observed discrepancy between Wilkins et al conclusion and those drawn in this study concerning the role of concrete cover may be attributed to considerable experimental differences particularly in the specimen size and reinforcement details. Also, it seems that oxygen diffusion is substantially influenced by the manufacturing defects, such as improper compaction, which are particularly expected in real structures than small laboratory-made specimens.

The Effect of Load Application on E_{corr}.

The immediate decrease in potentials upon the

application of load is indicative of breakdown of passivity at concrete cracks. This is supported by visual observation of corrosion at such sites after the tests. Referring to Figures 10.17 and Figures 10.21 to 10.25. The behaviour of E_{corr} after the application of load and during the remaining period of test after this point is dependent on a combination of factors which are greatly influenced by the load level. Higher load level (e.g. 0.6 f_y series) induces wider cracks and thus allows easier access of the solution to the steel reinforcement. Since the potential is related to small exposed area, the amount of change in potential will be dependent on the crack width. Under such circumstances the influence of the factors which previously controlled the potential under no-load conditions is greatly diminished. Accordingly, the initial scatter in E_{corr} before loading, due to different availability of Cl^- and oxygen at steel/ concrete interfaces, is also reduced. Similarly, lesser influence of load on E_{corr} would be expected for lower load level, as shown by the development of the electrode potential for 0.4 f_y series given in Figure 10.17, which indicates that, in the early stages of loading the potential values are still probably partially controlled by the general concrete cover rather than being dominated by the presence of cracks.

There is clear indication that the values of E_{corr} are proportional to the exposed steel area at early stage of the test with more negative values being associated with larger corroded area (compare Table 10.5 and Figures 10.22 through 10.25). This effect, however, seems to be valid up to certain load level (equivalent to 0.7 f_y) above which the potentials do not seem to be further affected by further increases in loading levels (Figures 10.21 and 10.23). At these higher-load conditions, it might be that the magnitude of corrosion has reached such a level that the supply of O_2 to sustain the cathodic reaction becomes restricted by concentration polarisation effect. However, this proposition could only be confirmed by a programme of tests at higher loads than were involved in detailed corrosion studies in this work. This idea of

higher corrosion currents leading to O_2-reduction concentration polarisation will be returned to later in this chapter.

10.4.5 Corrosion Rate Measurement.

Tafel Plots.

Tafel plots provide particularly interesting informations on the electrochemical characteristics of the test specimens which can be used with greater confidence in describing the corrosion kinetics at the time of measurements. This is because, as outlined earlier, these plots examine the specimens' response over wider range of overpotentials than those applied during the linear polarisation measurements. The reason that make this measurement valuable however is, unfortunately, the same reason which prevents this kind of measurement to be made frequently. Since there is always a risk of perturbation of the corroding electrode and the subsequent change in the corrosion process after the relatively considerable potential shift involved during the determination of such plots. This is particularly so in beams exhibiting low corrosion rate in which, after an anodic Tafel polarisation, E_{corr} usually returned to more negative potentials than the pre-existing E_{corr} as shown in Figure 10.56, and in beams in a passive state in which the potential sustained certain long-term changes in the direction of measurement (anodic or cathodic). In both cases, however, the cathodic measurements are much less perturbative.

Despite a number of methods which have been previously proposed for the direct estimation of the corrosion rate, using electrochemical data near the corrosion potential, without the knowledge of the proportionality constant B, the experimental determination of Tafel plots seems indispensable for better understanding of the corrosion process. It should be emphasised that the Tafel plots are not only valuable in obtaining the B value. Indeed, considering the range of B

value obtained in this study (between 30 and 82 mV/decade for high and low corrosion rates respectively), this value can be guessed at with acceptable degree of error using the corresponding range between 26 to 52 mV/decade proposed by Gonzalez et al[104] which is widely used in corrosion studies of reinforced concrete. For example, a Tafel-determination will also yield a value of I_{corr} directly from back extrapolation to E_{corr}. Also significant information might be derivable from the shape and the Tafel slope of the individual anodic and cathodic curves.

Such information can not be deduced from the B value and is valuable in describing the kinetics of the reactions particularly the effect of factors such as the concentration polarisation and resistance polarisation on the corrosion process.

In this context, an important Norwegian study,[205] which examined the polarisation curves for passive steel embedded in concrete, has indicated that these curves alone should not be used to assess the corrosion rate of the reinforcement. This is mainly because, these curves partly reflect the oxide transformations on steel surface which involve a release of electrons not related to the anodic dissolution of the steel reinforcement. This behaviour was explained with reference to the Siverman modification of the pourbix diagram as mentioned earlier in Chapter 4. It should be pointed out, however, that the present investigation involves different corrosion state i.e. active corrosion is occurring at crack sites and that the related potentials observed are more positive than those reported in the Norwegian study and consequently these alternative reactions are not expected.

For steel embedded in concrete, the linear relationship between overpotential and log current or current density, that is the Tafel region where the corrosion process is controlled by activation polarisation, is often difficult to be obtained due to the two interfering phenomenons, concentration polarisation and the IR-drop effect. However, in the present study, where the specimens were fully saturated with an

electrolyte with good conductivity, these factors are generally less influential.

The Tafel plots given in this chapter were drawn after an allowance of an IR-drop has been made. The IR-drop (η_R) due to electrolyte resistance R_e is a linear function of the flowing current (I_m) between the specimens and the counter electrode following the relationship.

$$\eta_R = I_m \times R_e$$

Thus at a given time of measurement the effect of IR-drop increases with an increase in the values of the measured current and can be removed with relative ease by knowing R_e. The effect of the un-compensated IR-drop can cause:

Firstly: distortion in the polarisation curve with considerable reduction in the linear portion of the curve.

Secondly: error in the Tafel slope.

Upon removal of the effect of IR-drop, the shape of the polarisation curve will be dependent on the degree of concentration polarisation. The overpotential due to concentration polarisation is a function of the relevant diffusion limiting current I_L and becomes significant when the polarisation current approaches 0.1 I_L. This effect is characterised by a curvature in the polarisation curve, for severe concentration condition, the linearity in the curve can be completely absent.

There is some evidence of this phenomenon from the cathodic curves of tests at high load level (0.7 f_y) as shown in Figures 10.67 and 10.68 and in the cathodic curves of long running tests in seawater, Figure 10.82 and 10.85. On the other hand, some polarisation curves exhibited an important feature in that a fixed, but unequal, anodic and cathodic limiting current have been achieved in a number of widely varying test conditions (i.e. different load level, exposure and environment). This feature was first observed in the anodic curve of

chloride tests at high load level (0.6 f_y series), thus a limiting anodic current of 1620 μA was achieved in this series and tests of different duration varied in the anodic overpotential required to attain this stage. This behaviour was initially regarded as a genuine characteristic of the test specimens and the environment. To gain further information about this phenomenon, the polarisation measurements in selective tests of substantially different conditions were continued both anodically and cathodically until the limiting currents have been reached. Examples of these are given in Figures 10.41 and 10.60. These figures indicate that a fixed anodic and cathodic limiting currents of 1,620 μA and 11,200 μA have been obtained in both cases. The fact that these currents are unequal complicates the picture and perhaps enhanced the opinion that this behaviour may be related to the test condition, the reinforcement details and the environment in particular, examined in this study.

Nevertheless, additional measurements made on long running tests in seawater have consistently produced the same limiting current despite substantially different test conditions from those of the chloride tests. The latter results provoked an extensive experimental investigation to determine whether the observed behaviour is a genuine characteristic of the test specimens or due to some unknown instrumental limitations. The examined variables and the findings of this investigation are given in the following section.

The Determination of the Source of the Limiting Currents.

The experimental verification involved the use of different size and type of counter electrode, different specimen and testing equipment as follows.

a. Changing the area of the auxiliary electrode (A.E)

This case was examined to check if the anodic polarisation currents had possibly been limited by the rate of the cathodic reaction on the auxiliary electrode.

Severe concentration polarisation for a particular reaction on the A.E. may result in limiting current which may continue for variable overpotential until the potential of the A.E. changes to allow different electrode reaction to occur (it is postulated that our tests did not continue to reach this condition). For this reason a copper auxiliary electrode with an area of 125 cm^2 was used instead of the original 6.25 cm^2 electrode. The polarisation measurements however, produced the same limiting currents as shown in Figure 10.91 and, therefore, the area of A.E. was excluded as a possible source of error.

b. The Use of Different Type of Electrode.

To eliminate the effect of this factor, a 125 cm^2 stainless steel auxiliary electrode was used instead of the copper electrode. The measurements revealed virtually identical anodic and cathodic curves as obtained with the standard copper auxiliary electrode with the same limiting currents.

c. Polarisation Measurements on Bare Steel Bar.

10 mm diameter Torbar 400 mm in length was polarised anodically and cathodically in both tapwater and 3.5% sodium chloride solution using a copper auxiliary electrode of 125 cm^2 area. Surprisingly, the same limiting currents were obtained.

The obvious conclusion from this series of experiment, therefore is that some unknown instrumental limitations existed in the potentiostat which only allowed certain maximum currents to pass. The situation was clearly obscured by the fact that the maximum anodic and cathodic currents are unequal. Thus, it was considered possible that the two observed, different limiting currents were due to genuine concentration polarisation effects of:

a) the O_2- reduction reaction (cathodic curves).

b) some form of anodic concentration polarisation (anodic curves) due to restriction in removal of anodic products when crack blocking was established.

In addition, due to the limited number of tests in which this phenomenon was observed, it did not attract much attention at early stages of this study.

This conclusion, i.e. the instrumental limitation, was further confirmed when performing another series of measurement using a different potentiostat. As will be shown in the following, the new potentiostat did not show any current limitations. However, there was no reason to believe that the Tafel plots obtained from the earlier-utilised potentiostat would be in any way invalid at currents lower than the two instrumentally-controlled limiting values. Nevertheless, it was considered prudent to confirm this by carrying out a number of Tafel-plot determinations on relevant beams using the second "current unlimited" potentiostat.

For this purpose, polarisation measurements were made on beams from concurrent research program underway at Glasgow University including beam 2TS which was previously monitored using the old equipment and beam MU608N which was subjected to approximately 3.5×10^6 cycles in 3.5% NaCl solution at a load level equivalent to 0.6 f_y. The results are as follows.

Beam 2TS.

Using the new potentiostat the polarisation curve was obtained and presented in Figure 10.92. A comparison between this figure and Figure 10.86, which shows the same plot of the same beam obtained approximately 4 months earlier using the old potentiostat, indicates almost identical Tafel constants and extrapolated corrosion current.

To provide further checking and to avoid the effect of time interval between measurements, although expected to be limited due to the no-load condition of the test, the cathodic polarisation curve was determined using the

old equipment one day after the first measurement. As indicated in Figure 10.29 the polarisation curve also provided very similar B_c and I_{corr} values to those obtained using the new potentiostat. (B_c = 25 and 260 mV/decade, I_{corr} = 500 and 490 μA respectively).

Beam MU608N.

Figures 10.91 and 10.93 show the polarisation curves obtained using the old and the new potentiostat respectively with a time interval of one day between these measurements. The figures clearly indicate almost identical cathodic curves (with B_c = 221 and 230 mV/decade respectively) over the whole parts up to the limiting currents and very similar I_{corr}. (1450 and 1390 μA).

The above tests confirm clearly that the instrumental limitations are only effective at and beyond the aforementioned limiting currents. This confirmed that the data obtained from the cathodic Tafel curves in this work were unaffected by the instrumental cathodic limiting current essentially because of the relatively high magnitude of the latter.

On the other hand, the much lower instrumental anodic limiting current caused uncertainty in establishing the activation-controlled anodic region in some tests. The tests from which there was some uncertainty in the estimation of B_a (and hence of B) are clearly evident from the examination of the Tafel plots presented in this thesis and are listed below:-

Tests in chloride solution: MU60N87D, MU601N, MU60N1Y, MU70WN (after the addition of salts).

Tests in seawater: CF100, CF103, CF144, 1TS.

The Ba values of these tests were roughly estimated and indicated by an asterisk in Tables 10.2 and 10.6.

It should be emphasised that the error in B_a values is unlikely to produce considerable error B value

particularly when the value of B_c is accurately determined. For instance, an error in estimating B_a for beam MU60N7D of $\pm$ 100 mV/decade can produce an error in B value of approximately 8 mV/decade which is quite acceptable error in relative terms.

Finally, the above discussion does underline the significance of cautious preliminary investigation on the possible instrumental limitations which might be very difficult to identify but could lead to erroneous conclusions and wastage of time.

10.4.6 Corrosion Process in Partially Submerged Structures.

Influence of Exposure Condition.

The corrosion of reinforcing steel in concrete results from an electrochemical process accompanied by anodic and cathodic reactions. In the anodic reaction, iron is transferred into the solution as hdyrated iron ions with two electrons left in the reinforcing steel. Thus:

$$Fe = Fe^{+2} + 2e^{-}$$

These two electrons are available to participate in the cathodic reaction. In the alkaline environment of concrete, oxygen reduction reaction is operative according to the reaction:

$$O_2 + 2H_2O + 4e^{-} = 4(OH)^{-}$$

In order for corrosion to proceed, there must be a complete electrical circuit and this is achieved by a flow of electrons and ions between the anodic and the cathodic areas. In many cases, especially in reinforced-concrete structures, these areas are unequal, but the corrosion current is common to both the anodic and cathodic reactions. These reactions are interdependent and either or both may control the rate of corrosion reaction. If the

corrosion process is cathodically controlled, then the rate determining step will be the oxygen diffusion and availability. Thus two types of corrosion cells may exist corresponding to the prevailing condition, these are the microcell and the macrocell. Particularly related to the latter type, the popular theory attributes the occurrence of corrosion to differential concentration cell caused by non-homogeneity of concrete and its environment. Differences in pH, oxygen and chloride content are primary sources of cell potential. Accordingly the corrosion cell model is often described in the form:

	Low pH	| |	High pH	
steel	High Cl^-	| |	Low Cl^-	steel
(anode)	Low O_2	| |	High O_2	(cathode)

For the particular test conditions investigated in this study, the mechanism of corrosion before and after the application of load is dependent on the exposure condition. Referring to Figure 10.94 the exposure condition of the test beam may be described as follows:

Air exposed parts: The parts of the beam which is exposed to air constitute two areas:-

A1: which exhibit substantially low degree of water saturation, greater availability of oxygen (undissolved) due to high permeability to air, and high concrete resistance. Therefore, this area is extremely poor supplier of a cathodic current to fuel any anodic reaction occurring elsewhere on the steel reinforcement.

A2: is relatively wet area with lower resistivity and good supply of oxygen. In this region, air diffuses into the pores and oxygen dissolves in the capillary water. The oxygen concentration is greater where the water saturations and, probably to less extent, the salt concentrations are lower. Potentially, this area can act as an efficient cathode but is substantially dependent on the relative degree of saturation of concrete. Some work[147] has indicated that areas with less than 70-80% RH are generally of high resistance and consequently their contribution to the corrosion process is very limited.

The submerged portion A3: is fully water-saturated with low resistivity, low availability of O_2 and higher Cl^- content. Most of the oxygen involved in cathodic reactions in this region is probably provided by air originally trapped during concrete casting together with the oxygen content of the water which initially saturates the concrete although some of this air is consumed during the development of a passive film. Thus in principle the submerged steel in this region can act as an anode particularly at cracks and points of defects in the concrete cover but is possibly subjected to severe concentration polarisation of O_2-reduction reaction especially over the long exposure periods typical of this investigation (and of practical structures).

Cracks and points of defect allow relatively easy and rapid penetration of the surrounding solution. Accordingly the major effect of loading is to form cracks in the concrete cover which makes the concrete beam more heterogeneous and creates a complex electrochemical condition particularly with regard to the prevailing mechanism of corrosion and the subsequent rate of metal loss.

Mechanism of Corrosion in Partially Submerged Condition.

The corrosion process is greatly influenced by the environmental and structural conditions. The latter is dependent on the loading level, loading regime and manufacturing process. Although this work was primarily concerned with the effects of loading on the corrosion process all the experiments commenced with a period of no-load condition. During this period evidence of slow negative drift in potential was much lower in tapwater than in chloride tests. Figure 10.16 indicates that tests in tapwater exhibit passive behaviour and it was not possible to obtain satisfactory polarisation measurements at this stage in tapwater (and even after fatigue loading had commenced), due to low solution conductivity. In chloride solution, however, measurements including Tafel plots indicated, in agreement with previous workers

findings[149] the crucial influence of concrete cover and its quality in controlling the corrosion activity via restricting Cl^- ions ingress which was the main factor responsible for depassivating the embedded steel. It has been demonstrated that, for the particular test conditions studied in this investigation, O_2 supply is by no-means the controlling factor (direct evidence can be obtained from various Tafel plots which indicate that for a given potential shift the flowing current is greater for cathodic polarisation than the anodic one).

Most of the dramatic change, however, occurs upon fatigue loading. In good quality concrete the effect of loading is often likely to be predominant factor and for a given environmental condition the prevailing mechanism of corrosion will be dependent on the initial crack size and the development of these cracks during the life time of the structure.

In small cracks, dissolution of $Ca(OH)_2$ may occur giving rise to an alkaline pH which promotes passivity which in turn counteracts the effect of increased availability of O_2 and Cl^- ions content. On the other hand if the cracks are wide and the solution flows more easily into and through them, $Ca(OH)_2$ may be leached away from these sites and neutral or slightly acid conditions attained which favours corrosion. The ensuring process, however, is dependent on whether microcells or macrocells are involved in the prevailing process and this is controlled by the following provisions:-

1. The availability of oxygen at crack sites.
2. The development of different electrode potential of steel at these sites with respect to the adjacent passive steel.
3. The cathodic process elsewhere (i.e. availability of O_2 and relative area of non-active regions).
4. Concrete resistivity effect which opposes the corrosion current.

The first provision implies that O_2 is necessary at cracks for corrosion to occur by a microcell mechanism.

Experimental evidence has been reported by other research workers to support the idea that when O_2 supply to crack sites is sufficient, the corrosion process will occur by a microcell mechanism. For example, Boyde et al[114] examined the differential areation effect in simulated concrete environment (saturated $Ca(OH)_2$ solution) with 3.5% NaCl. In their valuable investigation two electrically connected electrodes were used with nitrogen bubbled through the anode and air bubbled through the cathode. Despite the fact that their set-up clearly facilitated a macrocell process more than an actual concrete environment would, they measured greater metal loss of the air bubbled electrode. (This electrode is considered as a cathode according to the popular macrocell model). Basically similar observations have also been reported by Hausmann[116].

Provision two implies that the potential difference between the anode and the cathode is the most important cause of macrocell corrosion because it represents the electromotive force for this type of corrosion. The latter is generally considered true but very few experimental results are actually reported to support it. From these is the important study conducted by Okada et al.[230] In their study they monitored the steel potential at crack sites and measured the macrocell current flowing between these areas and the steel in the uncracked area. The test specimens were of variable concrete quality. They observed that:-

1. Due to ingress of Cl^- ions, the potential at crack locations moved towards more negative values.

2. In good quality concrete and when the crack width is wider than 0.1 mm, the potential difference increased with increased crack width.

3. A decrease in the potential difference caused a decrease in the measured macrocell current.

The potential difference is critically dependent upon

the presence of Cl^- ions, Hausmann[116] observed that in the absence of chloride ions no significant difference in potential existed between steel in oxygen and no oxygen condition.

Provisions 3 and 4: imply that even in the presence of a high potential difference between anodic and cathodic sites, the macrocell process can be severly limited by the cathodic reaction at the cathodic site due to the limited availability of oxygen and/or the high resistivity of the concrete between the anodic and cathodic sites. These situations would clearly favour microcell reactions, but it should be pointed out that, a limited supply of O_2 to cathodic sites can be counteracted by a large cathodic: anodic area ratio provided the concrete is not of very high resistivity and sufficient electromotive force is provided.

According to the above-mentioned provisions and evidence, the corrosion process for various conditions examined in this study, after the application of loads, can be described as follows.

Tests in Tapwater.

Slow steel depassivation occurs due to slow leaching of $Ca(OH)_2$ during loading which eventually lower the local pH at cracks. The degree of depassivation is dependent on the applied load which controls the crack width. Thus:

a. Potential goes more negative faster at higher loads (Figure 10.22).
b. Ditto for reverse bending tests (Figure 10.21).

Both a and b imply more solution interchange between cracks and exterior and thus faster leaching and depassivation. Also dissolved oxygen becomes more readily available at these sites in comparison with other uncracked areas.

Due to the lower solution salt content, uncracked areas of concrete exhibits high resistivity and the particular absence of Cl^- ions means that the potential

difference between these areas and the cracked areas is much lower than their chloride tests counterparts. The situation favours a local microcell process and renders the mass of the submerged concrete an uneffective cathode to fuel the anodic dissolution at crack sites. The corrosion attack at cracks, thus, it most probably controlled by:

- The availability of O_2 at the cracks to support the local anodic reactions and/or
- The passivity of steel due to the absence of Cl^- ions and the local pH.

Both possibilities are obviously crack-width dependent i.e. load level dependent.

The characteristics of the Tafel plots for water tests given in Figures 10.38 and 10.39 suggest that due to the absence of concentration polarisation phenomenon on the cathodic polarisation curves, the rate of ionic dissolution is not cathodically controlled by the availability of O_2 and that the process is likely to be controlled anodically as indicated by the domination of activation polarisation on the anodic curves. Tafel plots also demonstrate the effects of crack size in that lower corrosion current and higher values of B_a and B_c are associated with test at lower load level. This is also indicated by different corrosion currents calculated for tests in water at different load level as given in Table 10.2.

Further, the corrosion pattern upon completion of tapwater tests reveals clear evidence which suggests that corrosion proceeded by pitting mechanism (see Figures 10.79,80) in which small central anode initiated and surrounded by a passive steel in the crack which acts as a cathode where the locally available oxygen is consumed. The corrosion attack as well as the penetration rates determined experimentally for water tests at different load level indicate extremely small metal loss which excludes any possibility of considerable macrocell activity.

Test in Chloride Solution.

Under this condition, cracks permit easy ingress of both Cl^- ions and dissolved O_2. Cl^- ions can break down the passive film and thereby can cause local change in potential to more negative values and thus promote potential differences with the surrounding (more positive-potential) passive steel. Meanwhile oxygen becomes more available than in other uncracked areas. The differential exposure thus involves:

	possible low pH	| |	high pH	
cracked area	high Cl^-	| |	low Cl^-	uncracked area
	high O_2	| |	low O_2	

The question therefore arises on to whether this situation will lead to corrosion at crack sites by microcell or macrocell mechanisms. Such corrosion via a differential-oxygen macrocell is clearly not consistent with the relative O_2 contents summarised above. Indeed the latter by themselves would favour a cathodic crack and anodic uncracked-zone situation but this is overridden by the effect of Cl^- ions causing depassivation and an immediate negative drift in crack potential.

A 'chloride -driven' macrocell caused by the negative move in crack potential in relation to the pre-existing, uncracking potential, is possible in the early stages of fatigue loading. However, such a macrocell would further require reasonably low-resistance paths, partly through the concrete, and the concrete may not be sufficiently saturated in these early stages for this situation to prevail. For the alternative mechanism, involving microcells at the crack sites, to facilitate finite corrosion rates, sufficient oxygen must be available within the cracks.

Tafel plots indicate that this is the case since, as suggested by cathodic Tafel curves for 0.4 f_y and 0.6 f_y dynamic and static tests (and even the Tafel plot of chloride-no load test, Figure 10.40), the O_2-reduction

reaction is totally controlled by activation polarisation at relatively substantial potential shifts, indicative of probably negligible cathodic contribution of the areas far from the cracks to the corrosion process at crack locations. Other important evidence which suggests that the locally available O_2 at cracks is sufficient to support the corrosion process at cracks is given in Table 10.9 which provides information about the current densities (I_{corr}/corroded area) at the end of the tests. This table indicates that in all cases, the current density is lower than the limiting current density of O_2-reduction reaction, which is considered[87] in the range between 40-60 $\mu A/cm^2$.

Further, if considerable macrocell reactions are operative, then it would be expected that A2 in Figure 10.94 would act as an efficient cathode to the anodic areas in the submerged portion of the beam. The actual observation, however, did not support this expectation as, in both tapwater and chloride tests, corrosion occurred at locations inside A2 indicative of local corrosion activity.

Accordingly, the potential differences between different areas of the beam as shown by the potential profiles given in Figures 10.26 and 28, although indicative of different local conditions can not be used safely to describe the possibility of macrocell process.

Therefore, during the initial period of exposure, it is suggested that significant macrocell corrosion is unlikely. The cracking process may merely, if of sufficient size, promote microcell corrosion and the corrosion process is controlled by the anodic activation polarization being dependent on the cracks geometry and the chemical condition inside the cracks. This hypothesis is supported by the Tafel plots conducted at various period of tests (up to 5 months) which show clearly higher values of B_a than B_c. In other words, for a given test condition and for a given potential shift, the flowing cathodic current is greater than the anodic one which means that the possible cathodic reaction is greater than that actually required to support the anodic reaction.

During this period the mechanism of corrosion is possibly sensitive to local changes at cracks such as, for instance, crack blocking.

However, the initiation and the slow development of corrosion causes gradual negative drift in the potential of steel at cracks with the corresponding increase in the potential difference with respect to other passive steel in the uncracked concrete. This increase in potential difference would depend on the uncracked regions remaining essentially unchanged. In this respect, Wilkins[229] has reported negative drifts in the potential of passive steel in concrete submerged in seawater but over variable time scales from specimen-to-specimen sometimes involving some years of exposure. It is thus postulated that a macrocell process may then start to contribute progressively to the overall corrosion activity being supported by adequate potential differences and reduced concrete resistivity due to increased degree of saturation which promotes current flow from adjacent areas acting as a cathode to fuel further corrosion process, possibly at accelerated rate due to progressive increase in the cathodic/anodic area ratio. The rate determining step at this stage may be the concentration polarization of oxygen reduction reaction (this would result in higher B_c value compared to B_a) and the concrete resistivity. The latter factor is dependent on the degree of saturation and the macrocell distance between the anode and the cathode.

The possible change in corrosion mechanism can be described with reference to Figure 10.95 which schematically illustrates the relationship between the potential difference between active and passive steel and the corrosion rate with respect to the prevailing mechanism of corrosion. This figure indicates that during t_1 the corrosion rate is small being anodically controlled with gradual increase in the potential difference. In this period the cathodic process is activation polarization controlled but if the applied external potential, during a Tafel cathodic plot, is considerable, then adjacent areas may be involved and thus concentration polarization starts to affect the process as shown for

instance in Figure 10.67. This particular example shows that the bulk of concrete body and/or the oxygen supply at cracks can support higher cathodic current than actually consumed at the corrosion potential (E_{corr}) if high potential difference is applied to force the reactions of the freely corroding systems in the required direction. Similarly, for systems sustaining high corrosion rate, concentration polarization effect on the cathodic curve would be expected with out the need for external potential if greater cathodic support is required from uncracked area in which O_2 diffusion is restricted.

Therefore, it is clear that the time after which concentration polarization becomes effective on the shape of the cathodic polarization curve is approximately the time required to reach the macrocell state ie. t_1. Accordingly the length of t_1 time is dependent on:

1. The load level which control cracking and exposure to external environment.

2. The time required to develop sufficient potential difference necessary for macrocell process.

Experimental evidence to back this hypothesis can be deduced from the Tafel plots given in Figures 10.67,68,82 and 83. The effect of loading in promoting early macrocell process is shown in the first two figures which are the Tafel plots of beam MU70WN at load level equivalent to 0.7 f_y in chloride solution. These figures show early effect of concentration polarization as compared to the corresponding fatigue tests at lower load level (see Figures 10.31 and 10.35), they also indicate that this effect starts earlier in the more active condition presented in Figure 10.67.

The early concentration polarization effects in tests at high load level can be attributed to the localised corrosion at cracks which becomes so active to necessitate either the involvement of cathodic areas outside the cracks or higher rate of oxygen supply at the cracks after relatively low overpotential during a Tafel measurements.

On the other hand, it should be noted that the accessibility of oxygen to the steel surface could be influenced by the phenomenon of crack blocking and the development of surface skin on the concrete surface. But these factors are unlikely to produce different cathodic curves for these particular measurements since blocking and surface skin are well developed at the time of the first measurement, shown in Figure 10.67, so that extra test duration did not contribute significantly to their effects.

The effect of test duration in developing the macrocell condition is clearly observed in long-term unidirectional fatigue tests in seawater. The Tafel plots of two cases are given in Figures 10.82 and 10.83 which indicate that the concentration polarization effect on the cathodic curve is evident after only 20-50 mV over potential as compared to more than 100 mV for short term tests conducted in chloride solution at the same load level. At such a late stage and in the cases of high corrosion rate when the local oxygen supply at cracks is not sufficient to support the corrosion activity, black corrosion product is obviously expected and B_c values becomes higher than B_a (Table 10.6 gives indication for the latter expectation for long running tests).

However, long term reverse tests in seawater did not show effective concentration polarization, Figures 10.84 and 10.85. This may be attributed to the extensive cracking due to severe loading regime which allows sufficient oxygen availability capable of supporting the local anodic dissolution at crack sites. This example also suggests that crack blocking, which is well established in this test, has less effect on the oxygen supply to the crack sites, as indicated by the absence of cathodic concentration polarization. On the other hand, in uncracked beams, Figures 10.40 and 86, the corrosion process is totally controlled by activation polarization of the anodic reactions which are presumably occurring at points of defects on the concrete cover for which the local cathodic supply is apparently sufficient.

According to the above discussion, it seems that the

effect of the size of the submerged area on the corrosion process is only expected in certain conditions when it becomes necessary for the set up of macrocell condition and this is critically dependent on the degree of cracking and the concrete quality of the possible cathodic area. This probably explains why the cathodic Tafel constants are variable and the observation that totally submerged beams exhibited in fact very close values of B_c to that obtained for partially submerged conditions (Table 10.2 and 10.6).

The above discussion indicates that the macrocell process is usually associated with high corrosion rate systems and involves generally concentration polarization effect on the cathodic plots. There is indication (see Table 10.9), however, that this process is likely to cover limited macrocell distance, probably in the order of few centimeters on both sides of the crack as this small distance can supply considerably high cathodic current to support high corrosion rate.

The mechanism proposed herein is simply hinged on the development of potential in the initially exposed area which under certain conditions can cause serious metal loss and risk thereafter the integrity of the structure. It should be born in mind that this behaviour is very complex and could not simply predicted from the actual potential measurements. These measurements can reflect the corrosion process only at the initial stage of corrosion attack ie. during microcell stage. In fact at this stage (could be months under dynamic loading) good correlation between the potential and the corrosion current was observed for each individual test condition (as described earlier in Section 10.3.4). If microcell corrosion is the predominant process then the potential of the steel at cracks is independent of the more positive potential at uncracked area. Thus the immediate fall in potential upon loading reflects the effect of early ingress of solution at cracks and subsequent local depassivation. Meanwhile the potential of steel at uncracked areas is expected to remain constant or changing to more negative value at very slow rate. This is so

because:

1. Negligible macrocell O_2-consumption
2. O_2 consumption to maintain the passive oxide is very small

It is realistic, thus, to expect that the change in E_{corr} during microcell process, reflects merely the changes at microscale at crack sites. This is particularly sensitive to:

1. The structural changes (deflection and deflection range) which change the micro-exposure by decreasing the cathodic/anodic area ratio at cracks thus producing lower corrosion activity (see Chapter 12), and/or

2. The crack block phenomenon which can cause more severe anodic polarization either due to more restricted movement of the solution and the corrosion product to and from the cracks or by producing changes in the local chemistry ie. activation polarization. Tafel plots, however, indicate clearly that the corrosion process at microcell stage is controlled by anodic activation polarization (B_a always higher than B_c) and thus the second possibility is favoured. As a result O_2 availability at cracks is not the controlling factor.

When macrocell process becomes effective, the measured potentials could not be easily interpretated essentially because it becomes a complex function of galvanic coupling between the cracked and uncracked areas. This is obviously changing with time. Before going any further, it is important to point out that the potential difference necessary for macrocell process may be less than that required at earlier stages due mainly too complete concrete saturation and reduced resistivity.

There is a possibility now of change in potential of uncracked areas to more negative values due to increased

consumption of O_2 in macrocell corrosion. However, evidence from this study and previous work in seawater, suggest continued severe metal loss after long exposure period indicative of maintained sufficient potential difference between these areas.

On the other hand, the potential of steel at cracks can possibly acquire more negative value, due to increased ionic activity and spread of corrosion, or stabilised. In any event the measured (solution) potential is a mixed potential of cracked and uncracked areas in very complicated manner and thus could not be related to the corrosion state of the reinforcement (the potential difference between active and passive steel is also less predictable as shown in Figure 10.95). Evidence on this postulation can be deduced from a comparison between the corrosion currents and potentials of beams MU605N and MU608N, (Figures 10.35 and 10.93). The first beam showed a behaviour typical of microcell condition with decreased corrosion rate whereas the second beam shows indication of increased corrosion activity as indicated by high corrosion rate obtained after approximately 8 months of dynamic loading. The comparison indicates that whereas both beams exhibit very close potentials, the corrosion current of beam MU605N is almost half that of beam MU608N. This observation substantiates the idea that the potential values are not good indications of the state of corrosion of embedded steel if corrosion process is occurring at macrocell scale as is probably the case when microcell corrosion is operative.

Probably the most supportive evidences on the above proposed mechanism are those deduced from the actual corrosion rate measurements as well as the corrosion pattern and extent observed at the end of the tests.

Based on the corrosion rate measurements, simple calculations of the average penetration rate in mm per year were carried out, using Equation 3.10, and given in Table 10.5. These values are remarkably close to the penetration rate of 0.26 mm/year reported by Hodgkiess et al[231] for a bare carbon steel in non-turbulent seawater. This clearly suggests that, for the time scale of most of

the tests in this work steel at cracks behaves in a way similar to a discrete bare steel bar in the solution with microcell process being a predominant mechanism of corrosion.

On the other hand, metal losses for longer exposures in this and earlier work are much greater. For instance, the considerable metal loss observed in long running fatigue tests on reinforced concrete beams also reported by Hodgkeiss et al[206] is readily explainable in terms of the establishment of macrocell process following the mechanism previously described.

Similar interesting examples of severe corrosion attack are those provided by measurements and observations made towards and at the actual termination of the fatigue tests of beams CF100 and CF144. These beams were under fatigue loading for approximately 7 and 1.5 years respectively. In beam CF100 considerable metal loss was observed particularly at shear links, Figure 10.96, in some locations the corrosion attack had dissolved all the shear reinforcement for more than 100 mm length and left behind a black residue. The corresponding Tafel plot given in Figure 10.83 shows substantial concentration polarization effect on the cathodic curve.

Corrosion attack was less severe in the case of beam CF144 as indicated in Figure 10.97, a corrosion penetration of more than 3 mm was observed at sites outside the solution jacket, (recall that the Tafel plot of this test given in Figure 10.84 showed limited concentration polarization effect).

Table 10.1: Electrode Potentials - Effects of Loading.

Loading regime	Environment	Beam designation	Electrode Potentials (mV SCE)	
			At the end of saturation period (5 days)	After one day of load application (≃ 12,000 cycles)
Dynamic Loading	NaCl solution	MU401N	-316	-351
		MU403N	-280	-281
		MU405N	-167	-288
		MU602N	-155	-455
		MU603N	-215	-452
		MU605N	-237	-376
	Water	MU405W	-24	-51
		MU605W	-36	-186
Static loading	Nacl solution	ML403N	-333	-361
		ML601N	-324	-332
		ML603N	-272	-308

Table 10.2: Results of Tafel Plots.

Loading regime	Environment	Beam designation	Tafel constants mV/decade B_a	B_b	B	I_{corr} (μA)	E_{corr} (mV) SCE	Time (days)
Dyanamic Loading	NaCl Solution	MJ401N	209	144	37	520	-376	30
		MJ403N	316.5	140	42	340	-231	90
		MJ405N	261	152	41.7	390	-236	150
		MJ60N7D	268*	176	46.2	1320	-501	4
		MJ601N	244*	165	43	1190	-481	30
		MJ603N	268	174	46	920	-418	90
		MJ605N	230	182	44	710	-362	150
		MJ60N1Y	198*	178	41	2500	-582	66
		MJ60N5Y	192	201	42.7	780	-433	108
	Water	MJ605W	157	156	34	235	-279	150
		MJ405W	372	373	81	150	-006	150
		MJ70WN	282	238	56	450	-415	42W
			-	215	-	2600	-592	42W + 10N
			-	Not obtainable			-572	42W + 40N
Static Loading	NaCl Solution	ML403N	177	172	38	515	-352	90
		ML601N	268	150	42	362	-316	40
		ML601N	199	147	37	320	-279	90
No Load		ML601N	200	103	29.6	350	-313	5
		MN500N	335	261	64	79	-102	30

* less reliable values because of limiting anodic current.

Table 10.3: Conductivity Measurement: Beam MJ70WN.

Environment	Conductivity μOhms x 10^3	pH	IR-drop
Tapwater	0.01	8.6	-
Solution Surrounding the beam before the addition of salt.	0.36	8.6	15.1
Solution with 1% NaCl:			
3 hrs after addition	14.2	8.6	6.55
3 days after addition	14.6		
Solution with 2% NaCl:			
3 hrs after addition	27	8.65	5.9
3 days after addition	27		
Solution with 3.5% NaCl			
3 hrs after addition	43	8.6	5.00
4 days after addition	44		

Table 10.4: Polarisation Measurements, Beam MJ70WN.

Sodium Chloride Concentration	No. of Cycles	R'_p	E_{corr} (mV SCE)
1%:-			
3 hrs after addition	619,800	33.02	-461
3 days after addition	660,000	15.82	-550
2%:-			
3 hrs after addition	665,400	14.42	-550
3 days after addition	699,900	10.7	-576
3.5%:-			
3 hrs after addition	706,300	10.51	-576
4 days after addition	754,600	7.9	-594
16 days after addition	1,182,290	11.2	-577

Note: Polarization resistance (R_p) and corrosion current (I_{corr}) given in the tables and figures of this chapter are the average of the anodic and cathodic polarization measurements unless stated otherwise.

Table 10.5: Areas of Corroded Steel.

Loading Regime	Environment	Beam designation	Time (days)	Corroded Area (cm^2)			Penetration mm/year
				Links	Main bars	Total	
Dynamic Loading	NaCl solution	MJ401N	30	24.7	1.5	26.2	0.228
		MJ403N	90	13.8	2.0	15.8	0.254
		MJ405N	150	21.7	2.4	24.1	0.167
		MJ60N7D	4	56.61	15.2	71.81	0.212
		MJ601N	30	116.0	3.8	119.8	0.135
		MJ603N	90	62.6	19.5	82.1	0.160
		MJ605N	150	41.0	57.5	98.5	0.111
		MJ60N1Y	66	115.8	5.2	121.0	0.238
		MJ60N8Y	108	51.6	7.1	58.7	0.153
	Water	MJ405W	150	190.0	2.0	21.0	0.082
		MJ605W	150	128.0	15.3	143.3	0.02
		MJ70WN	42W+40N	152.4	16.0	168.2	-
Static Loading	NaCl solution	ML403N	90	10.15	0.00	12.15	0.346
		ML601N	40	14.3	0.8	15.1	0.277
		ML603N	90	26.5	1.0	27.5	0.202
No Load		MN500N	30	0.00	0.00	0.00	-

Table 10.6: Sea Water Tests - Results of Tafel Plots.

Loading regime	Beam designation	Tafel constants mV/decade			I_{corr} (μA)	E_{corr} (mV SCE)	Time (years)
		B_a	B_c	B			
Uni-directional bending	CF103	179*	140	34.2	1500	-498	6 1/2
	CF100	156*	154	33	1800	-485	.6 3/4
Reverse bending	CF144	305*	302	66	1070	-433	1 1/4
	1TS	235*	180	44	1020	-594	2
No-load	2TS	680	225	74	550	-464	2 1/2
		735	255	82	500	-420	3

* less reliable values becuase of limiting anodic current.

Table 10.7: Estimation of Current by Different Measuring Techniques.

Beam designation	Current (μA)					1/5 %
	Extrapolated Tafel plot (1)	Sweep scan (6mV/min) (2)	Step Scan			
			1 min (3)	5 mins (4)	Steady State (5)	
MJ401N	510	725	742	577	539	95
MJ403N	340	506	520	320	320	106
MJ405N	390	664	648	368	368	106
MJ601N	1190	2161	2220	1695	1320	90
MJ603N	920	1656	1664	1248	1109	84
MJ605N	710	1095	1114	843	741	96
MJ60N7D	1320	2155	2734	2270	1837	72
MJ60N8Y	780	1950	2022	860	724	108
MJ605W	235	449	509	238	238	99
ML403N	440	534	505	407	407	108
ML601N	252	315	340	257	257	98
	362	502	510	420	392	92
ML603N	320	428	440	304	304	105
MN500N	79	138	165	77.5	67	118
CF103	1500	2073	2565	1514	1357	110
CF100	1800	3515	3685	2116	1740	103
CF144	1070	2497	2623	1453	1218	88
ITS	1020	3470	3790	1333	812	126

Table 10.8: Sweep Rate and Waiting Time with Respect to the Electrochemical Characteristics of the Test Beams.

Environment	Beam Designation	i $\mu A/cm^2$	R_p	R_e	R_p/R_e	K mv/min	Waiting Time (min)
Tapwater	MJ605W	3.5	68	35	2	6-7	2
3.5 NaCl Solution	MJ603N	11.2	120	7	17	2-3	6
	MJ605N	9.2	50	5.2	10	1-2	7

Table 10.9: Corrosion Current Density for Various Test Beams.

Beam Designation	Corroded area (cm^2)	Corrosion current (μA)	Current density ($\mu A/cm^2$)
MJ401N	26.2	510	19.4
MJ403N	15.8	340	21.5
MJ405N	24.1	390	16.2
MJ60N7D	71.8	1320	18.4
MJ601N	119.8	1190	9.9
MJ603N	82.1	920	11.2
MJ605N	98.5	710	7.2
MJ60N1Y	121.0	2500	20.7
MJ60N8Y	58.7	780	13.2
MJ405W	21.0	150	7.2
MJ605W	143.3	235	1.6
ML403N	12.2	575	42.2
ML601N	15.1	362	24
ML603N	27.5	320	11.6

Figure (10-1): Polarization measuring setup.

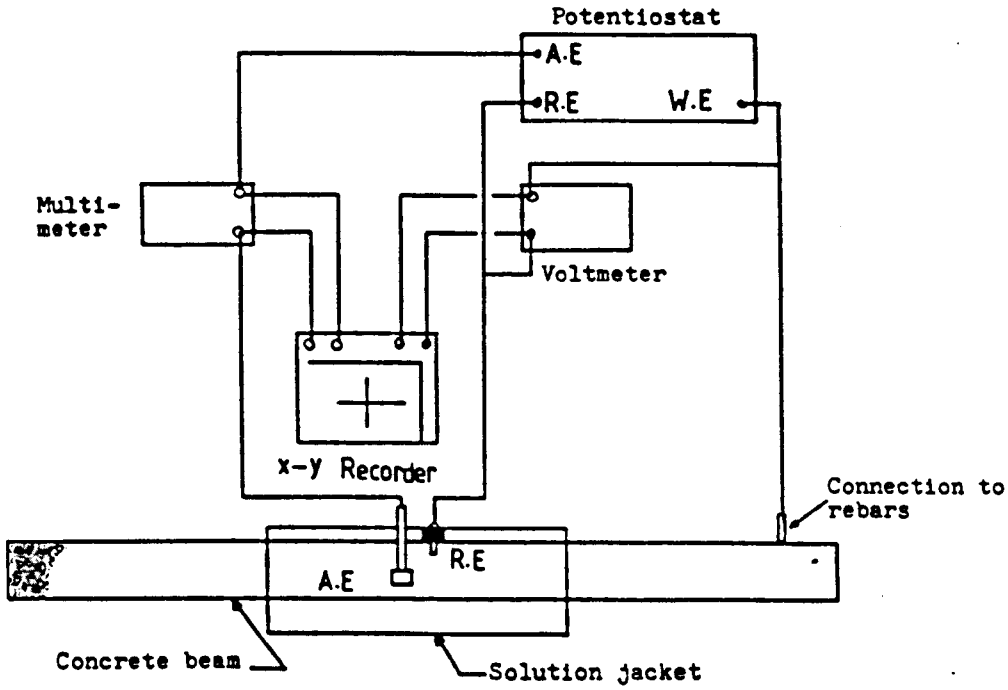

Figure (10-2): Schematic for polarization measurements.

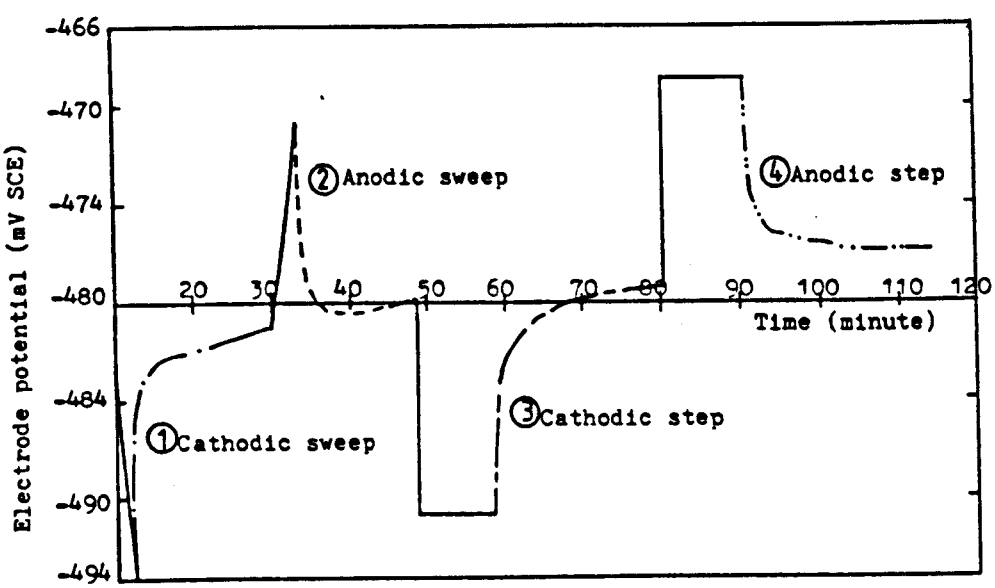

Figure (10-3): Typical E_{corr} - Time relationship during electrochemical measurement (beam MU601N at 447,620 cycles).

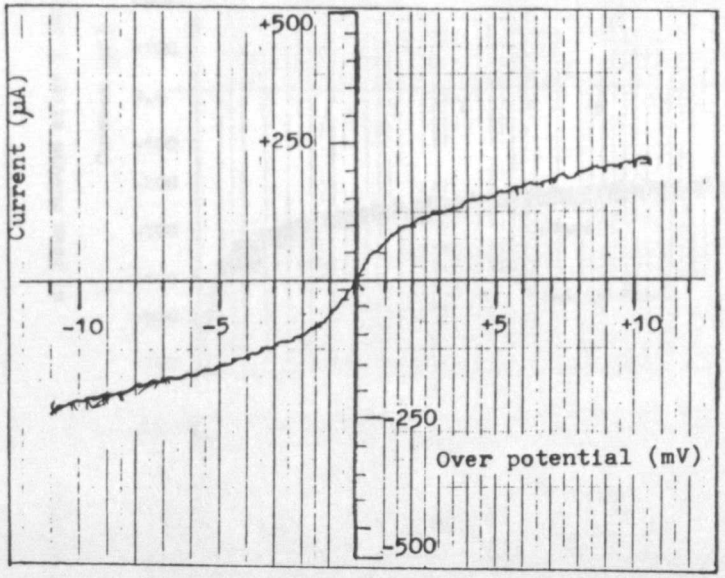

Figure (10-4-a): Polarization curve during cycling;beam MU405N after 2,121,000 cycles.

b)

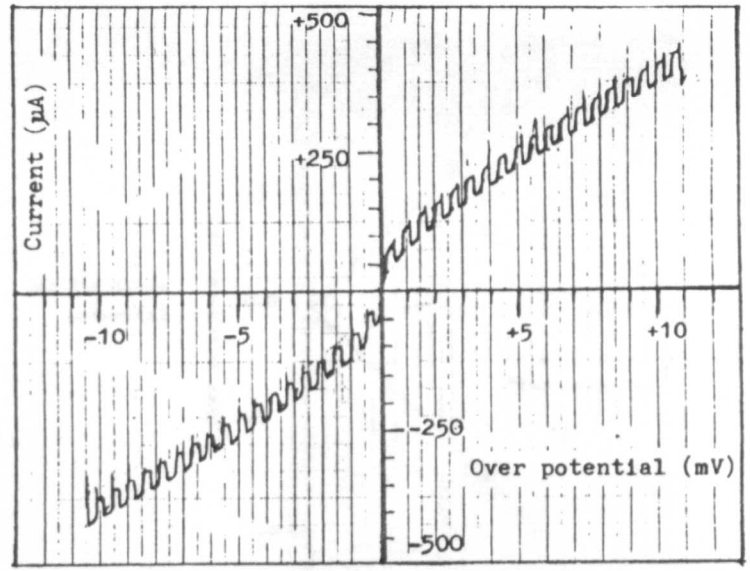

c)

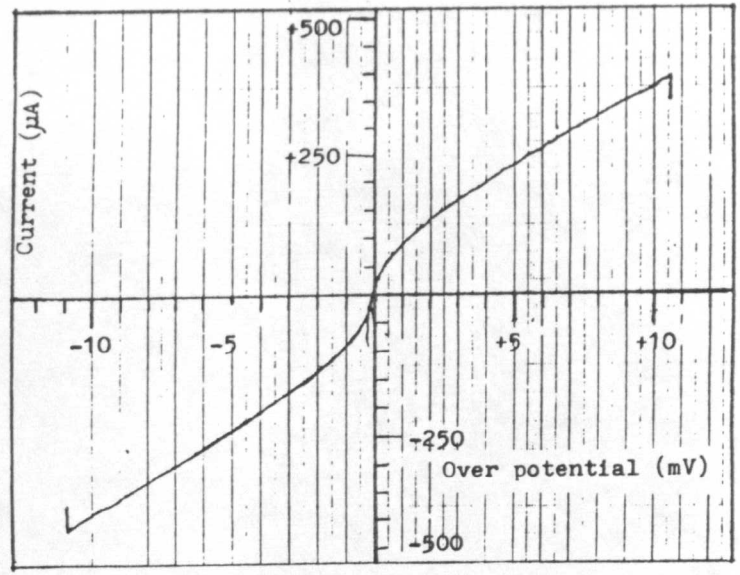

Figure (10-4-b,c): Polarization curves;beam MU603N
b) During cycling
c) With average load applied statically after 1,076,000 cycles.

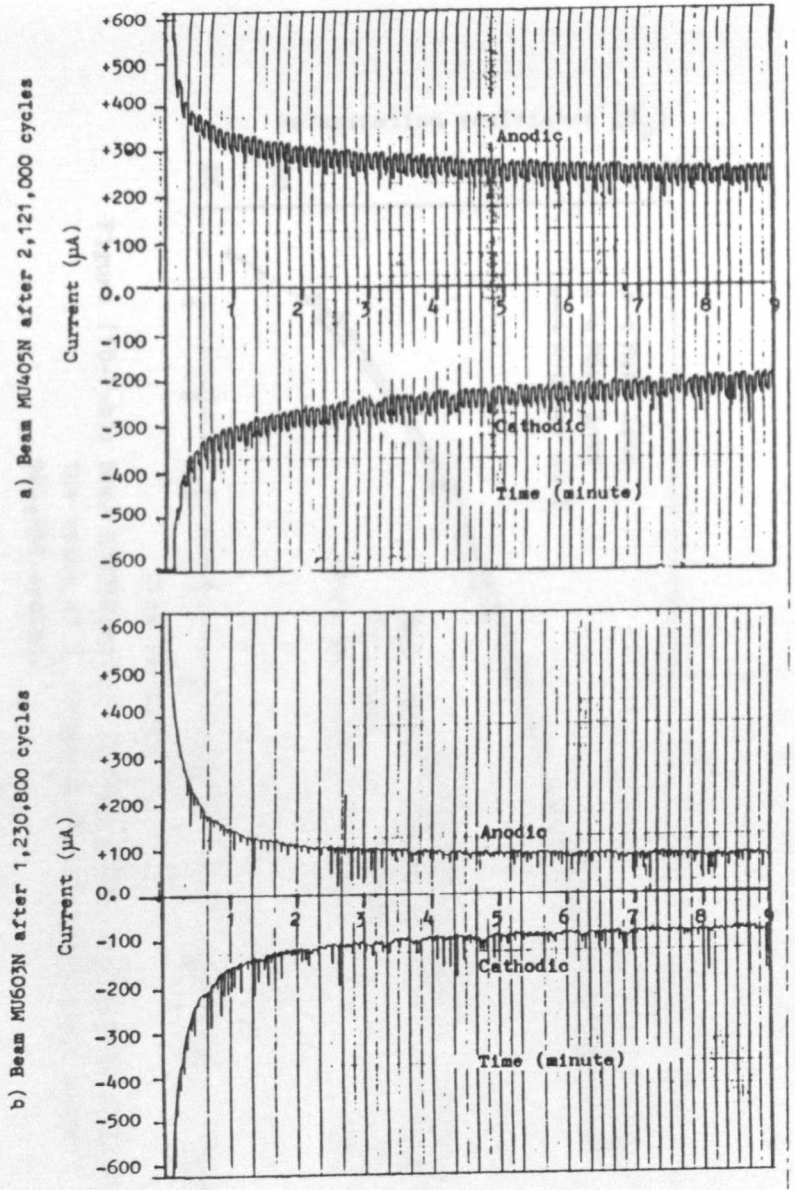

Figure (10-5): Potentiostatic measurement;current-time relationship during cycling.

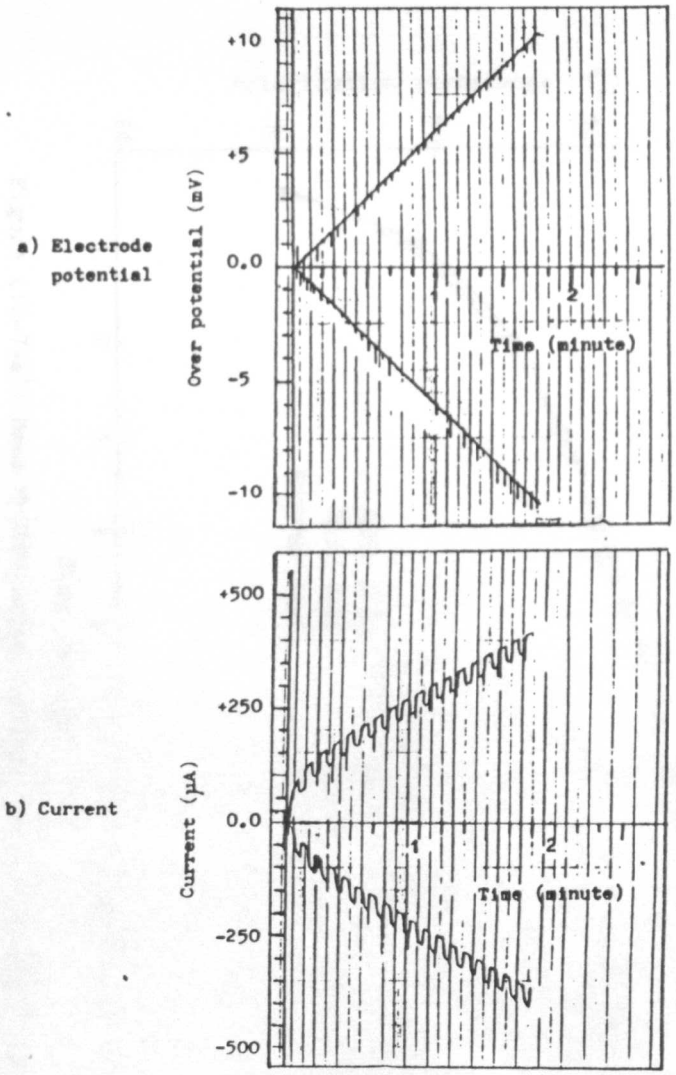

Figure (10-6): Electrode potential and current vs. time during potentiodynamic measurements, beam MU603N after 1,076,000 cycles.

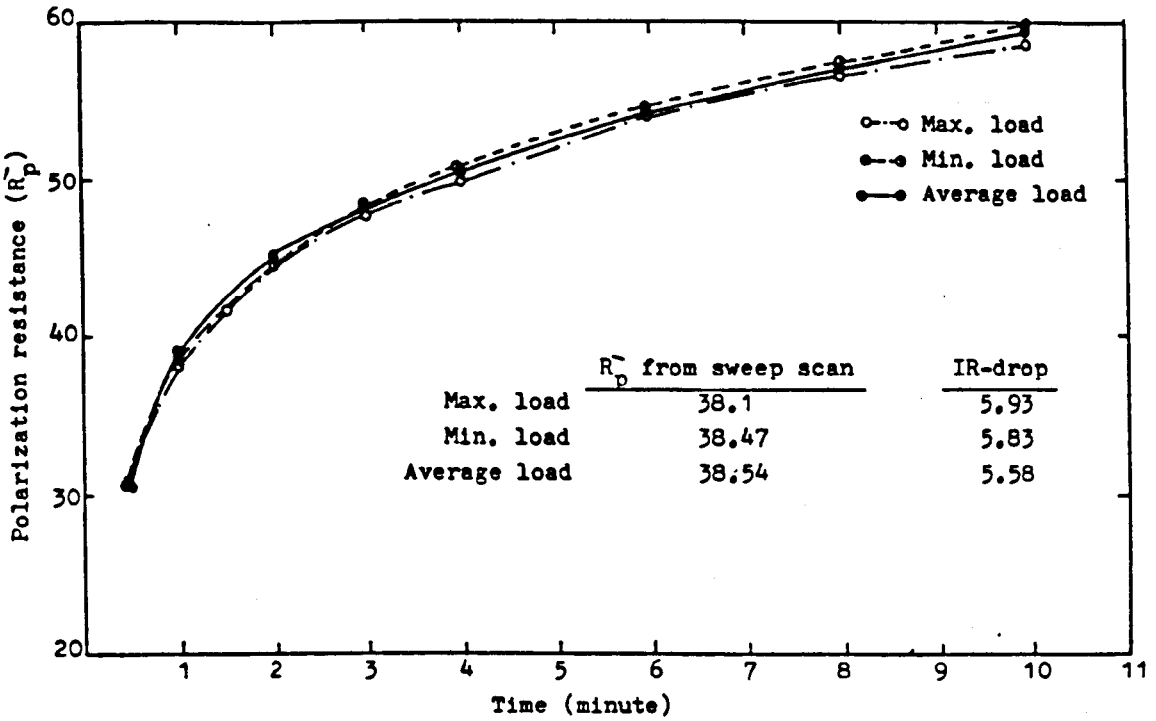

Figure (10-7-a): Beam MU605N;effect of load level (statically applied) on the value of $\tilde{R_p}$ obtained potentiostatically after 2,168,700 cycles.

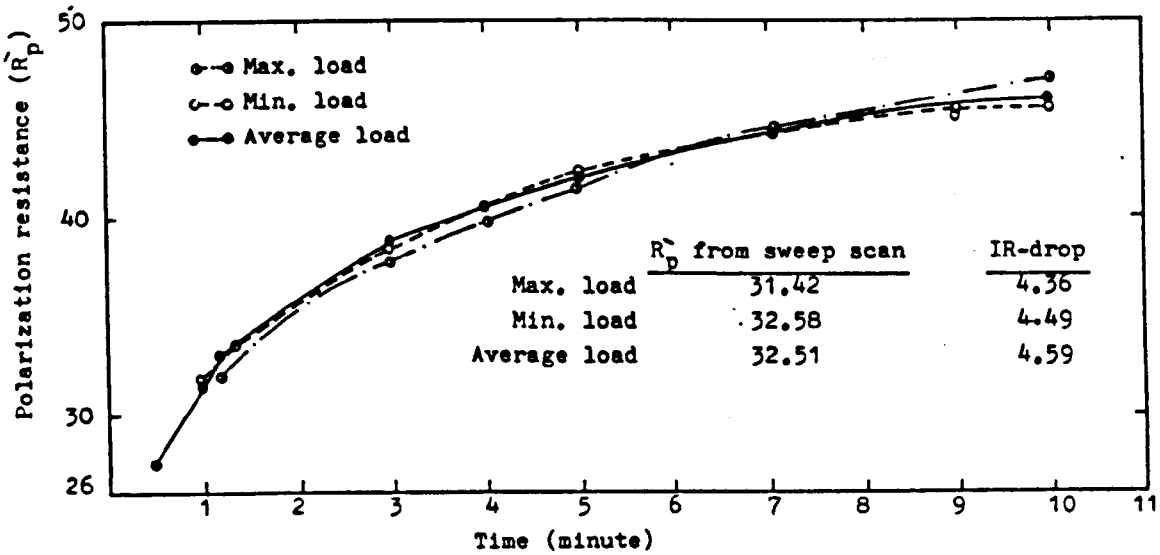

Figure (10-7-b): Beam MU603N;effect of load level (statically applied) on the value of $\tilde{R_p}$ obtained potentiostatically after 424,850 cycles.

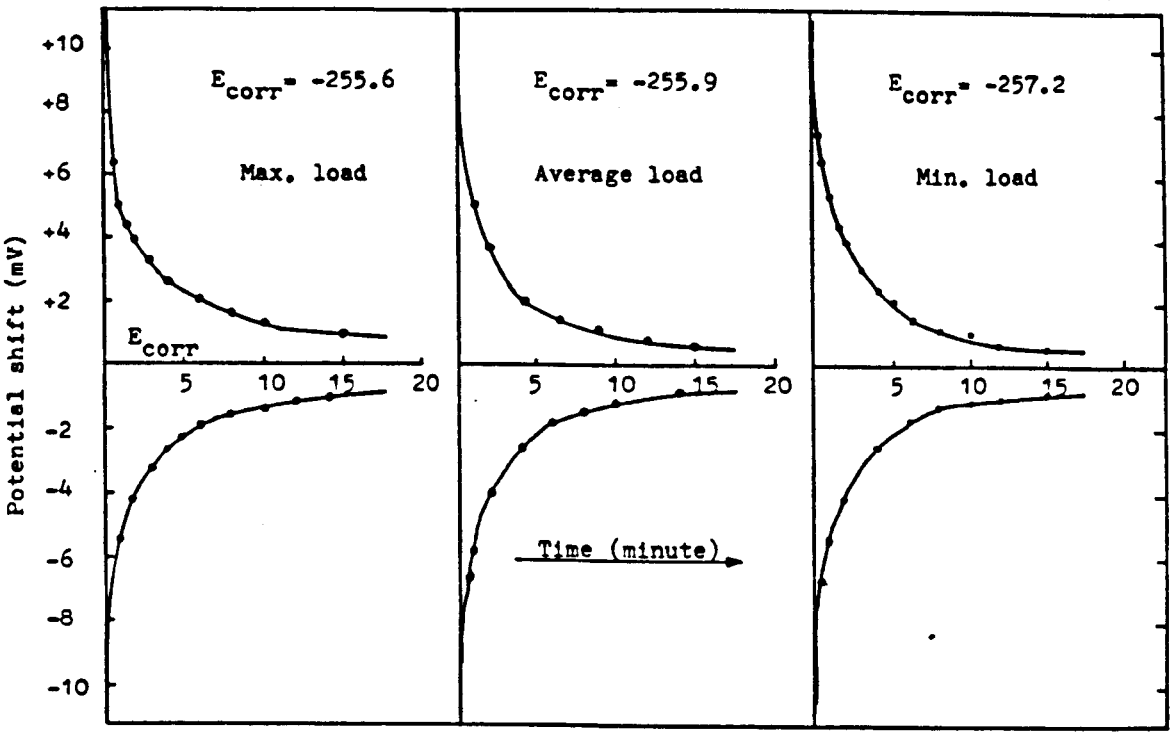

Figure (10-8): Electrode potential evolution after potentiodynamic measurements;beam MU405N at 1,360,250 cycles.

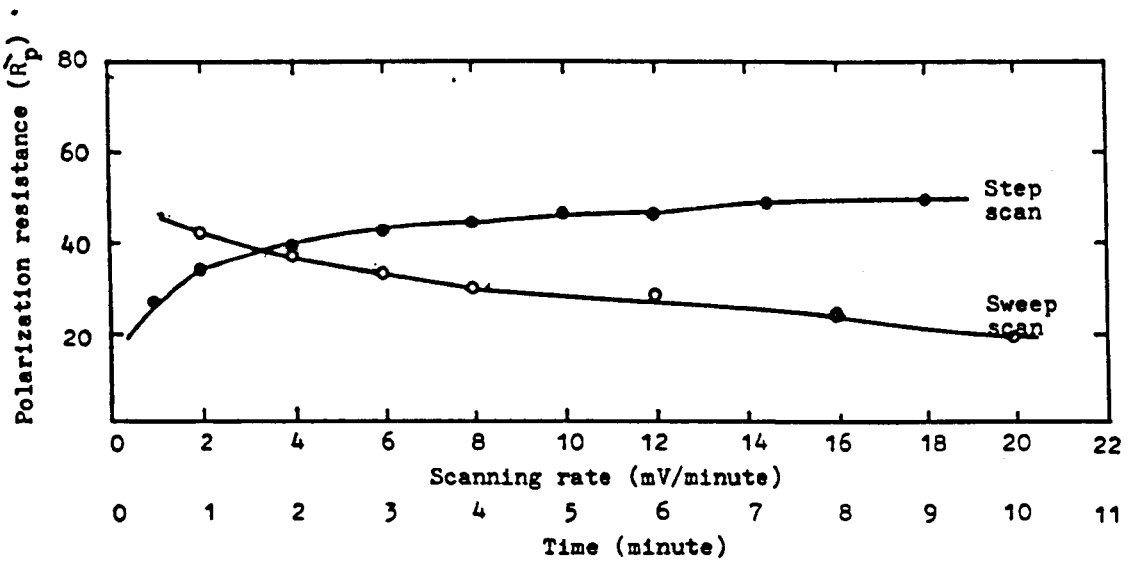

Figure (10-9): Beam MU605N;the veriation of R_p as a function of polarization sweep rate and step scan after 915,600 cycles.

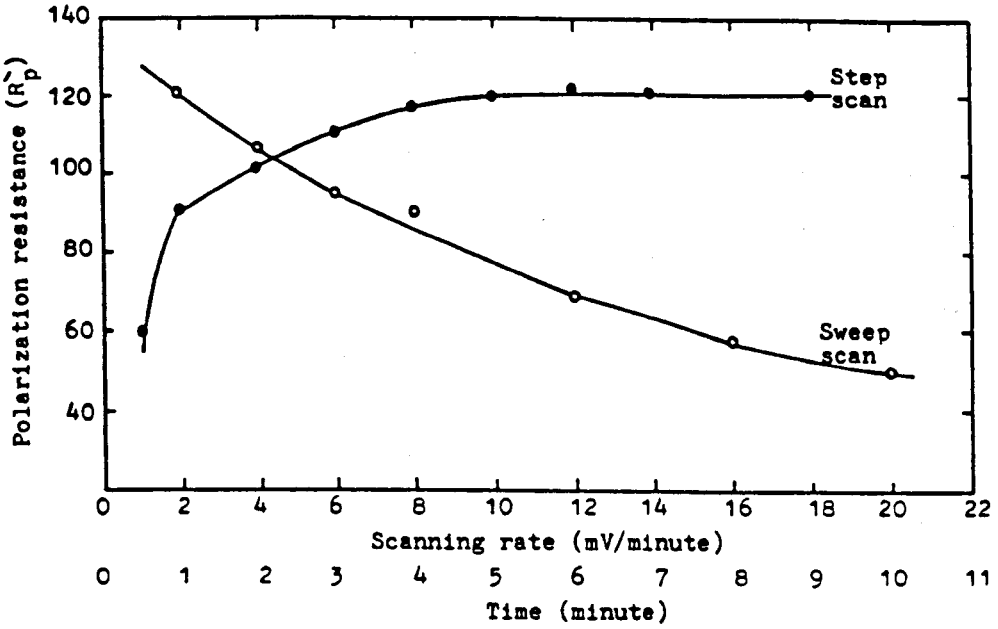

Figure (10-10): Beam MU603N;the variation of R_p^- as a function of polarization sweep rate and step scan after 90 days exposure.

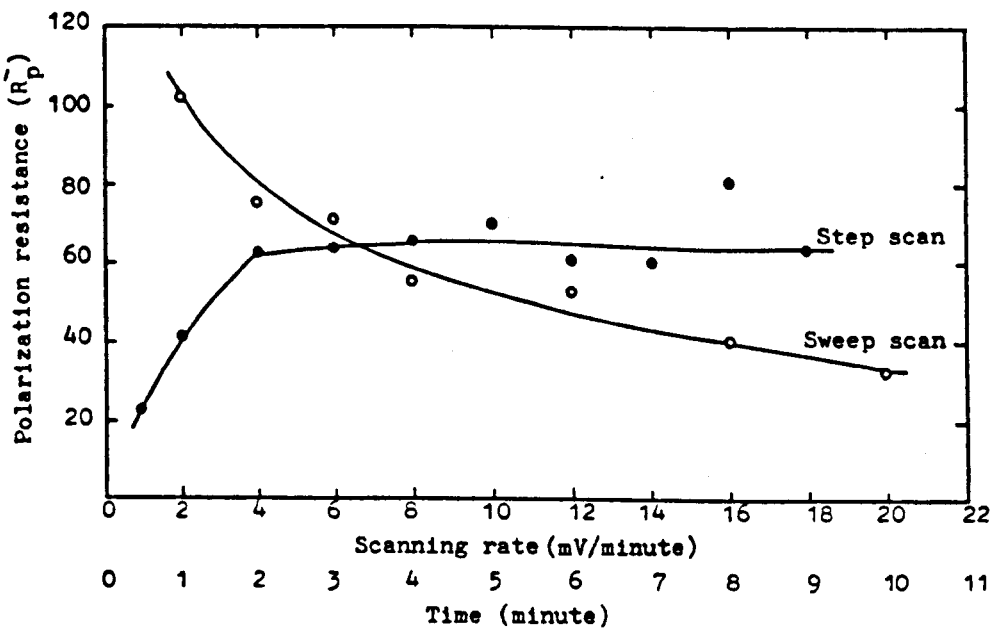

Figure (10-11): Beam MU605W;the variation of R_p^- as a function of polarization sweep rate and step scan (after 1,257,250 cycles)

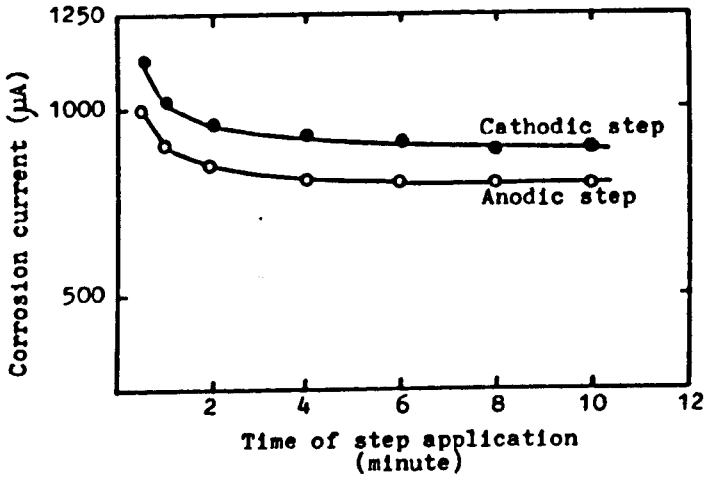

Figure (10-12): I_{corr} variation with time of step application of ∓10mV for beam MU401N before load application.

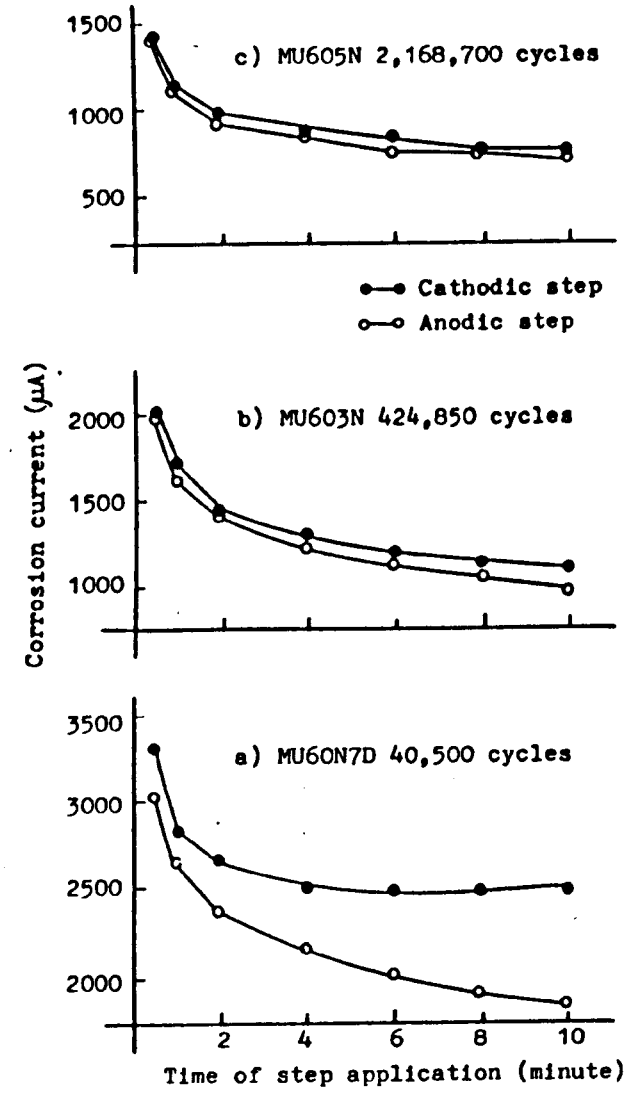

Figure (10-13): I_{corr} variation with time of a step application of ∓10mV for beams at different stages of test.

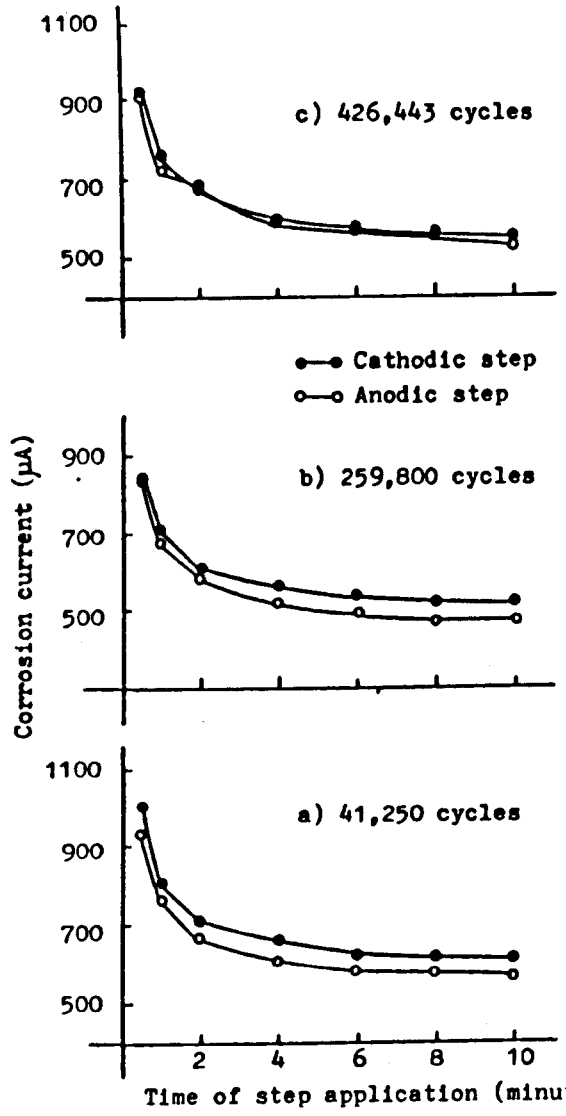

Figure (10-14): I_{corr} variation with time of a step application of ∓10mV for beam MU401N at different stages.

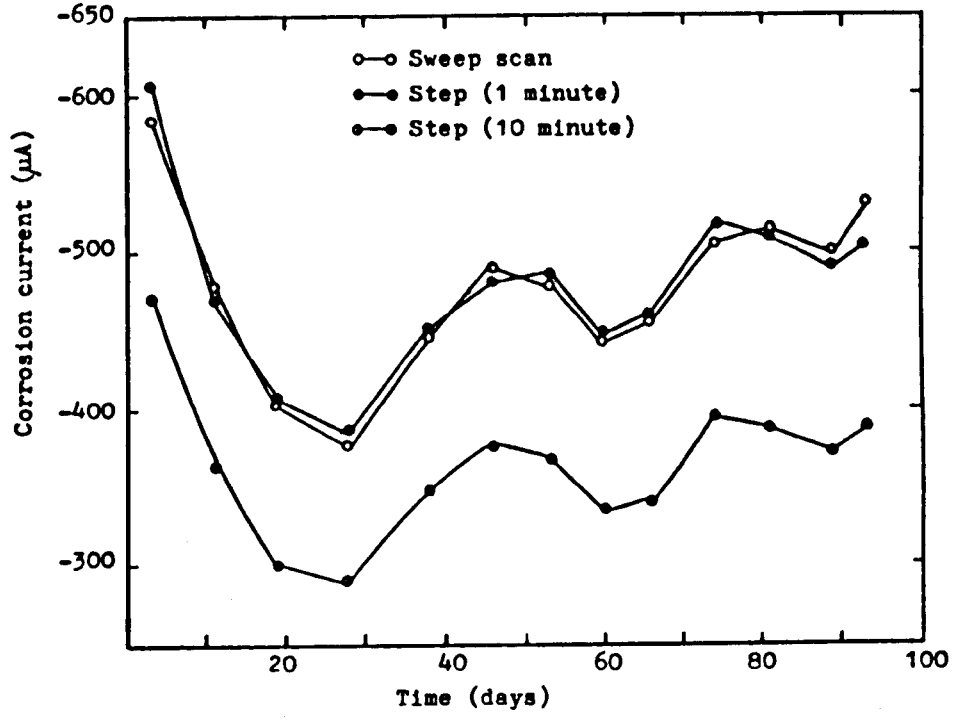

Figure (10-15): Beam ML403N;comparison between I_{corr}-Time curves obtained from different methods of measurement.

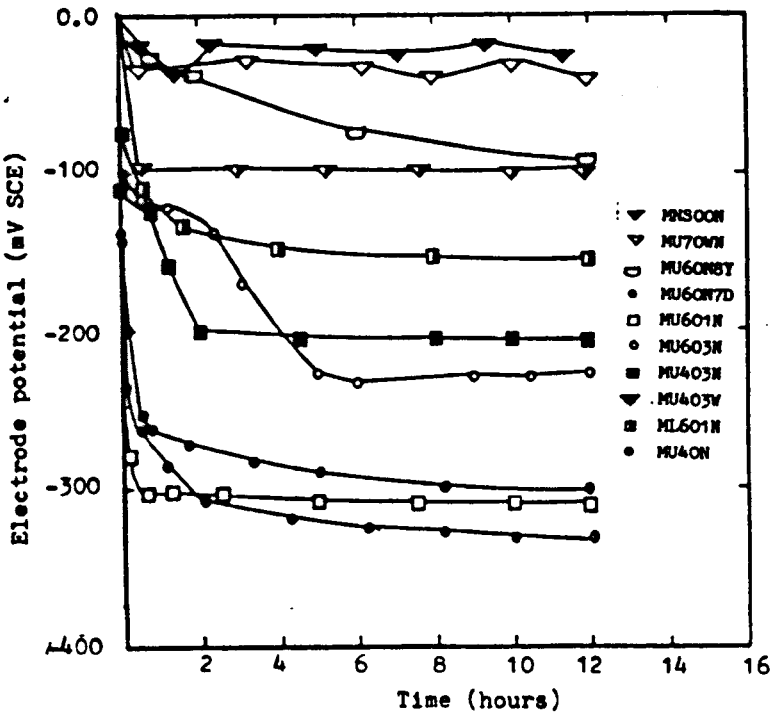

Figure (10-16): Electrode potential variation with time upon exposure to the solution (before load application).

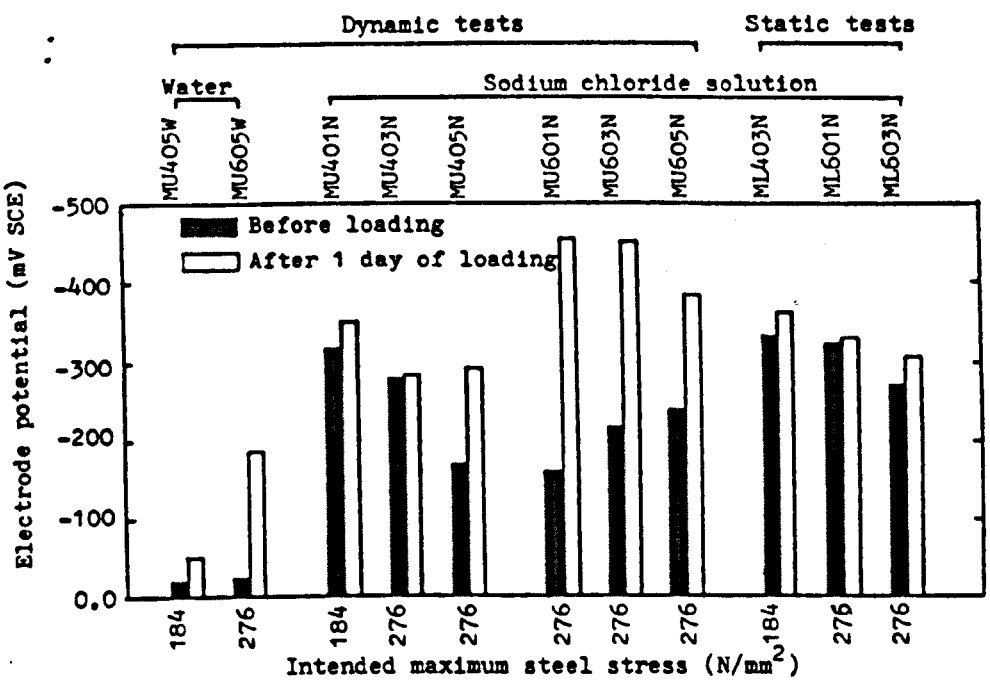

Figure (10-17): The effects of loading on the values of the electrode potential.

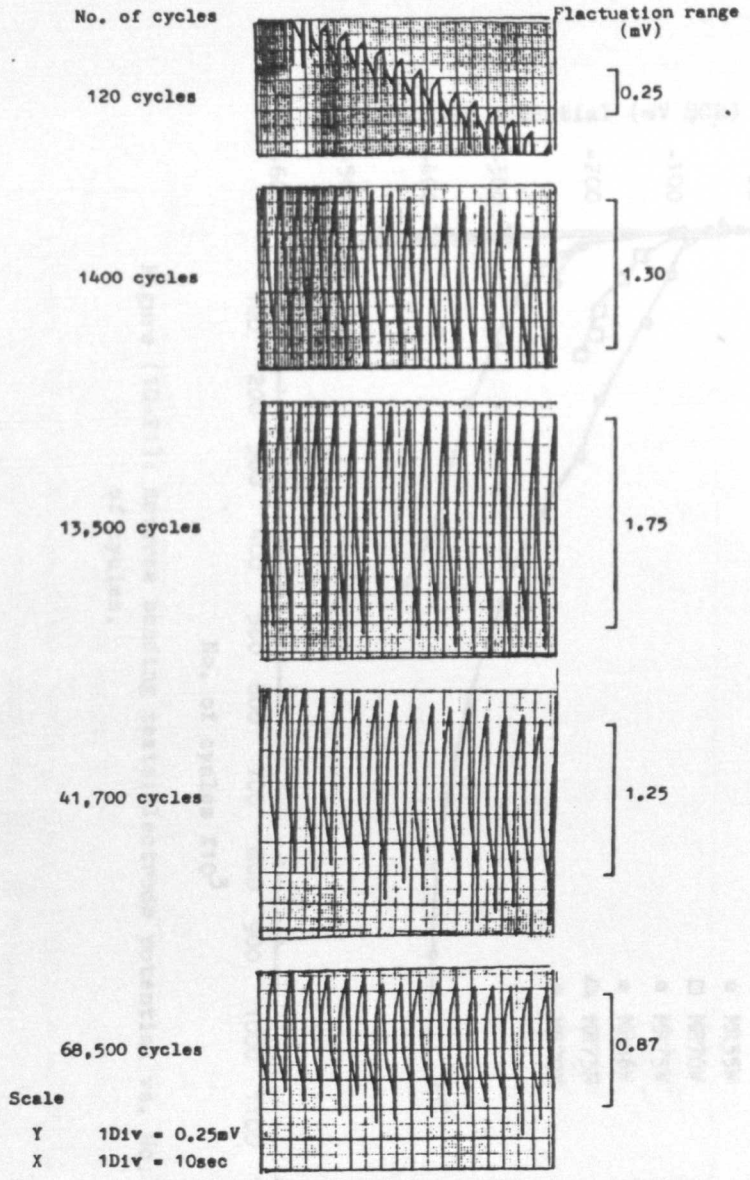

Figure (10-18): Variation in E_{corr} in phase with cycling; beam MU6ON7D.

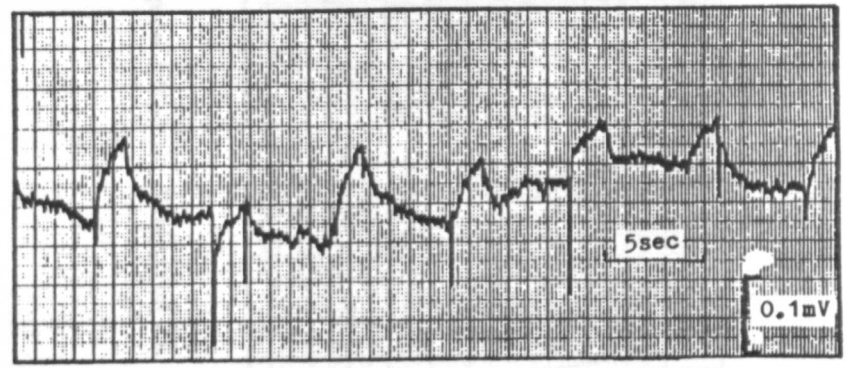

a) Beam MU401N after 429,100 cycles

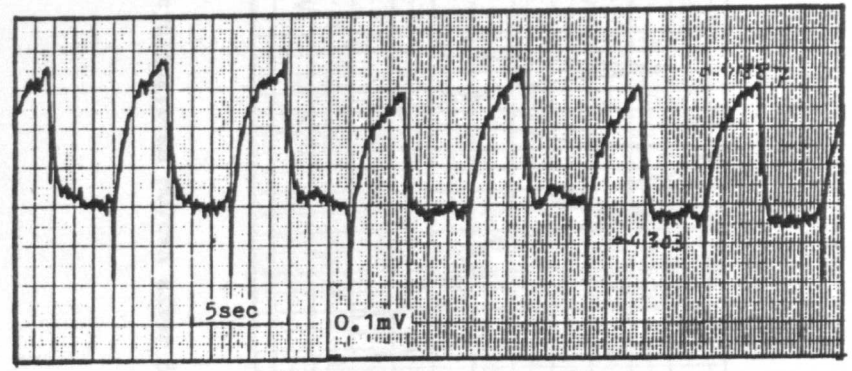

b) Beam MU603N after 994,500 cycles

Figure (10-19): Variation in E_{corr} in phase with cycling.

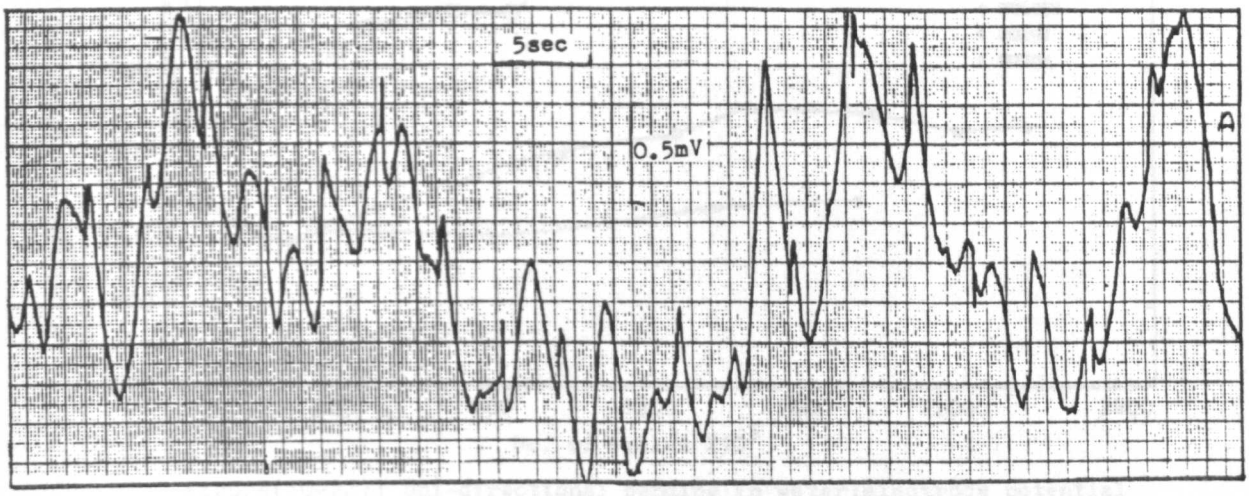

Figure (10-20): Variation in E_{corr} in phase with cycling;beam MU7OWN after 521,400 cycles.

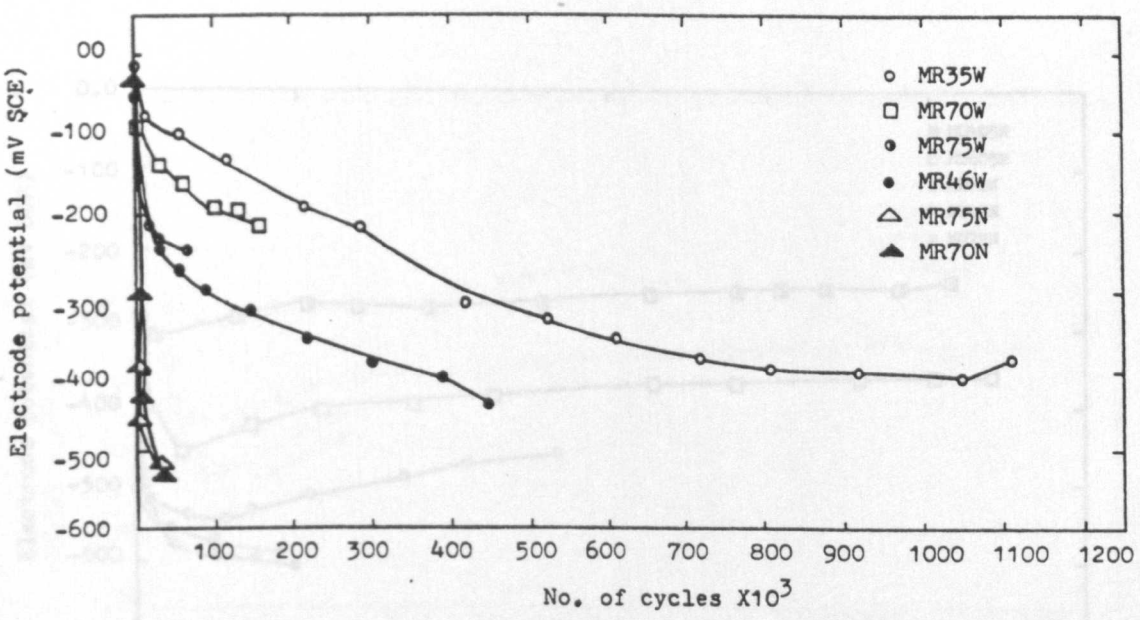

Figure (10-21): Reverse bending tests;electrode potential vs. No. of cycles.

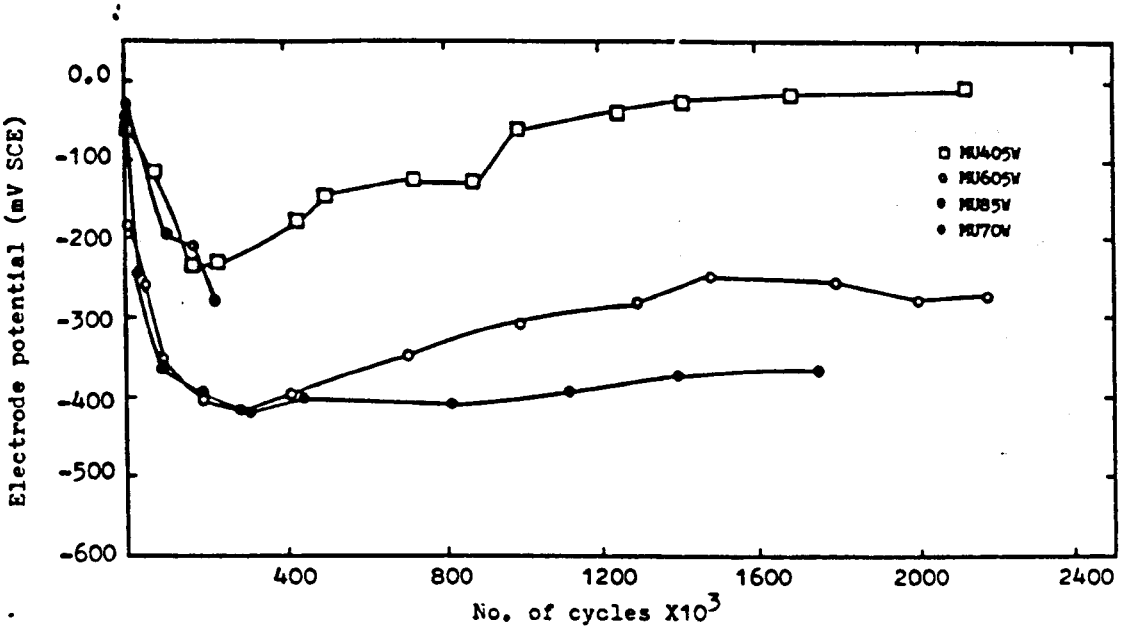

Figure(10-22): Uni-directional bending in water;electrode potential vs. No. of cycles.

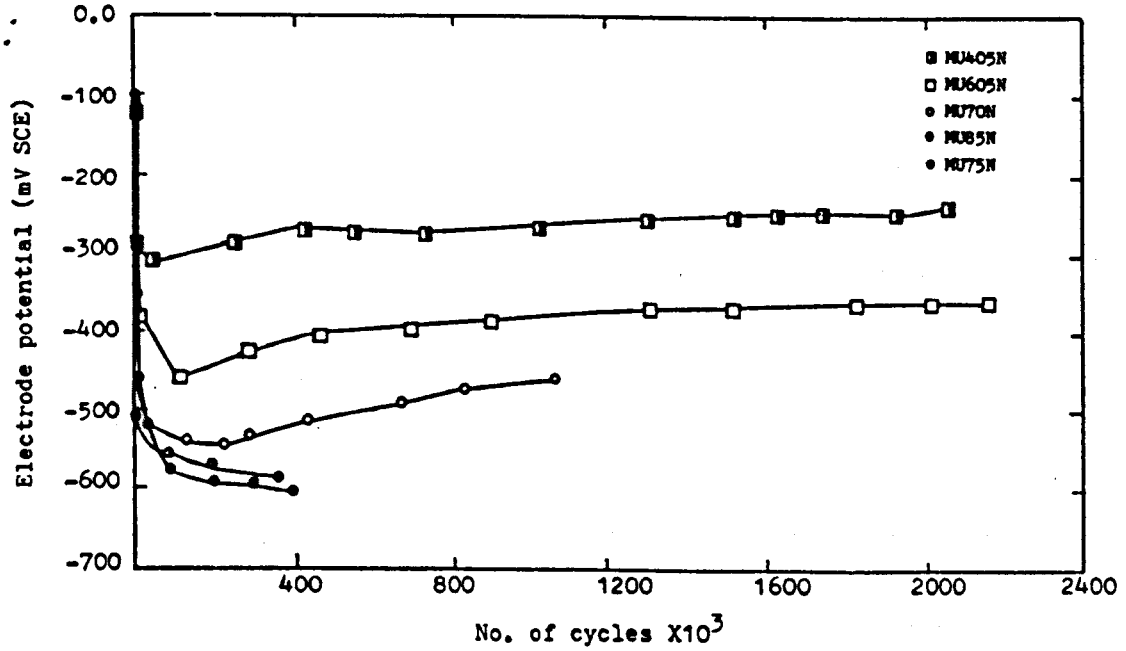

Figure (10-23): Uni-drectional bending tests in chloride solution; electrode potential vs. No. of cycles.

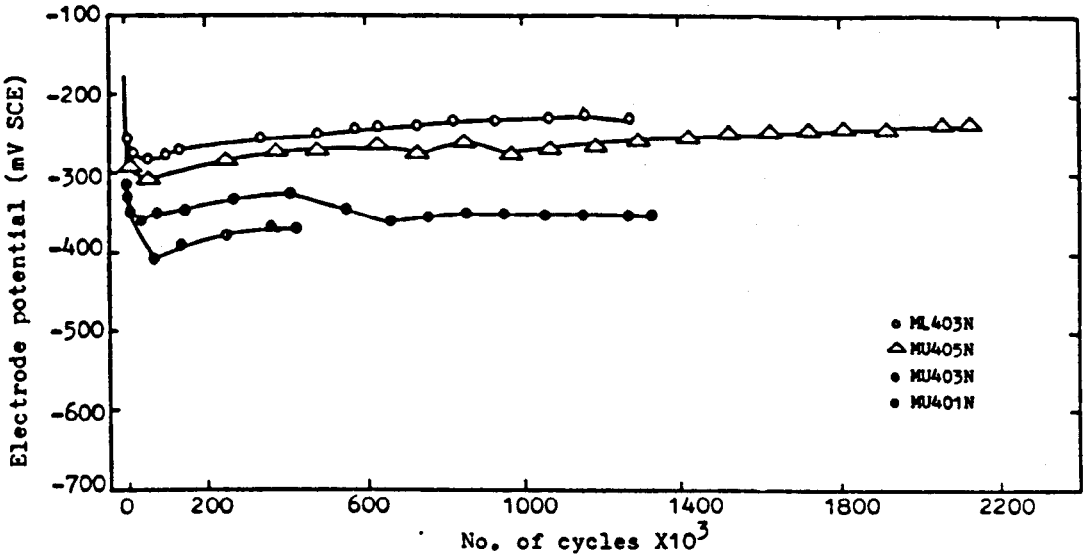

Figure (10-24): Electrode potential vs. No. of cycles for 0.4fy_ chloride series.

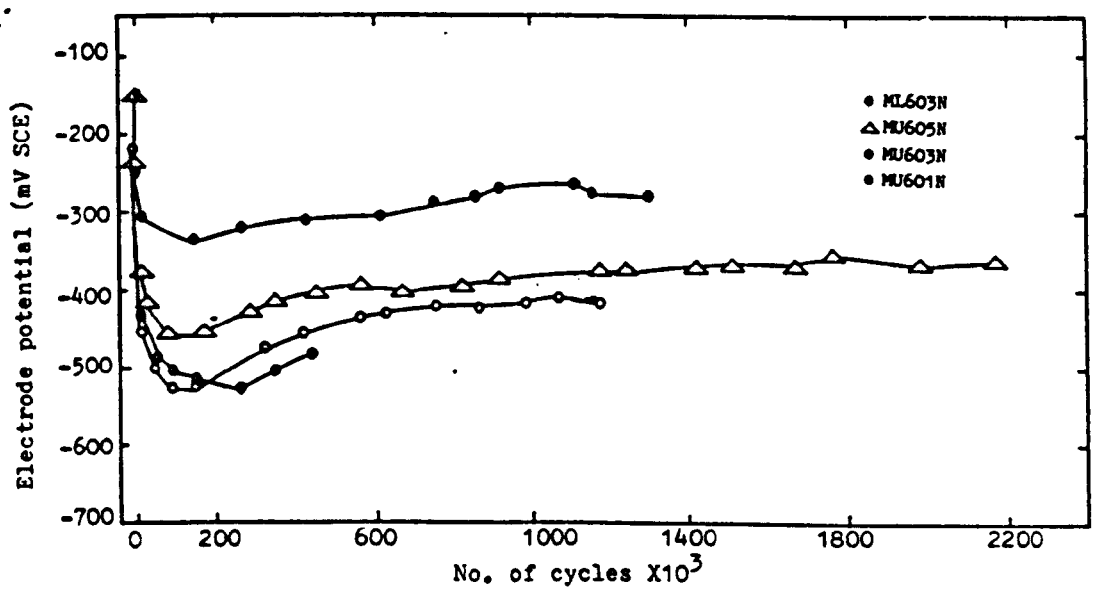

Figure (10-25): Electrode potential vs. No. of cycles for 0.6fy_ chloride series.

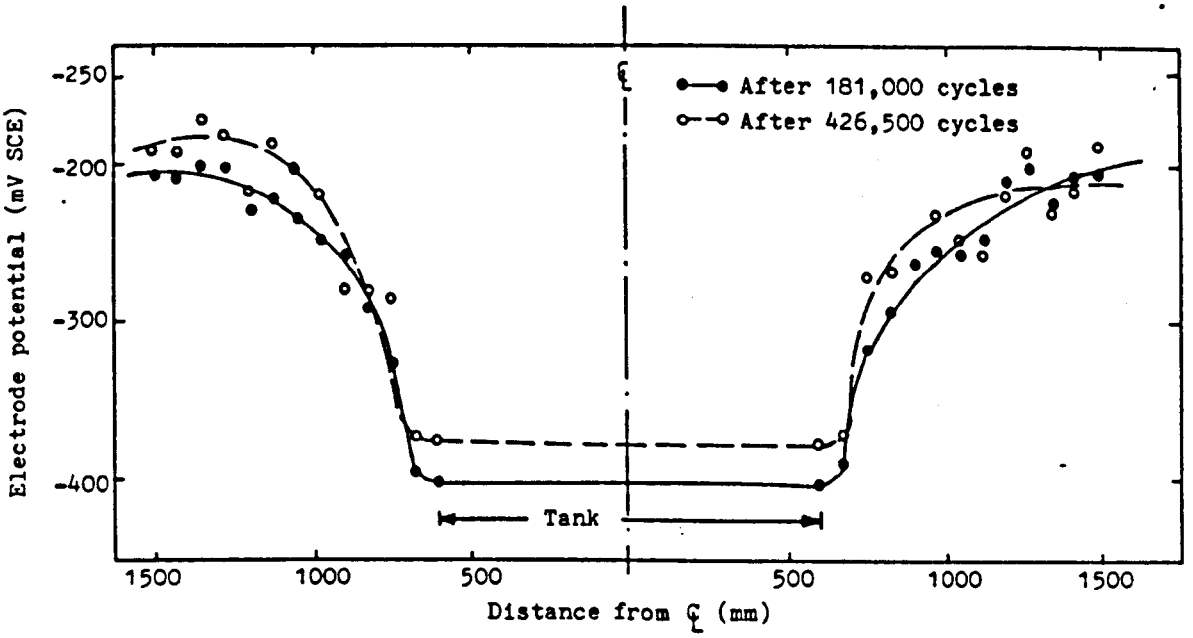

Figure (10-26): Beam MU401N;potential profile along the top of the beam at different No. of cycles.

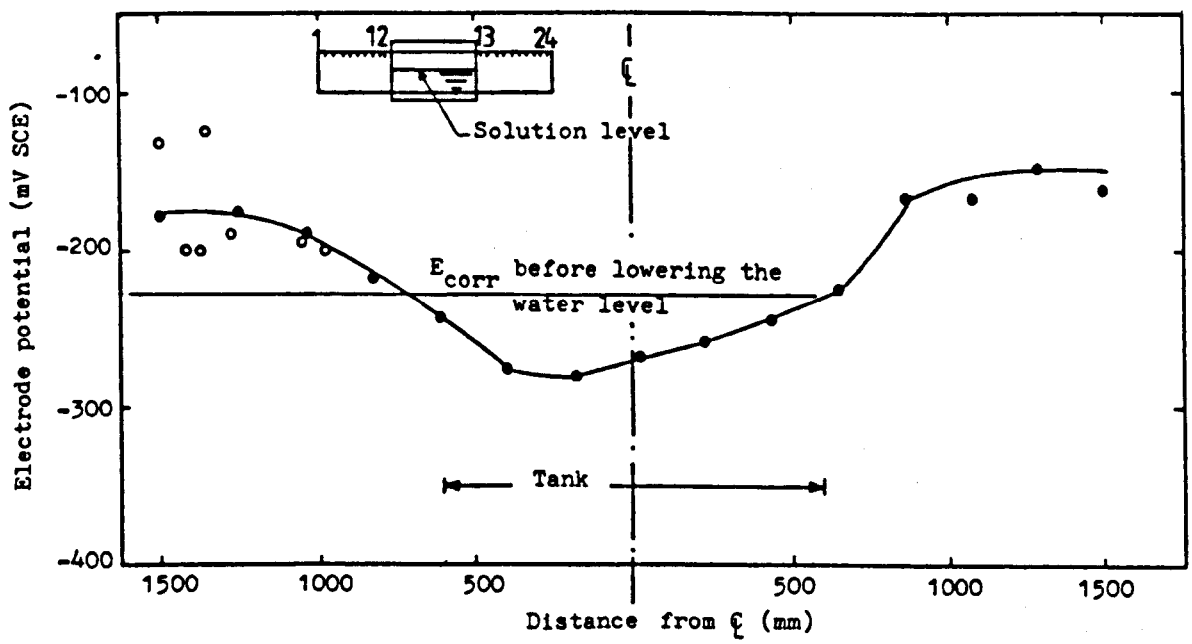

Figure (10-27): Beam MU403N;potential profile along the top of the beam at the end of the test (1,280,000 cycles).

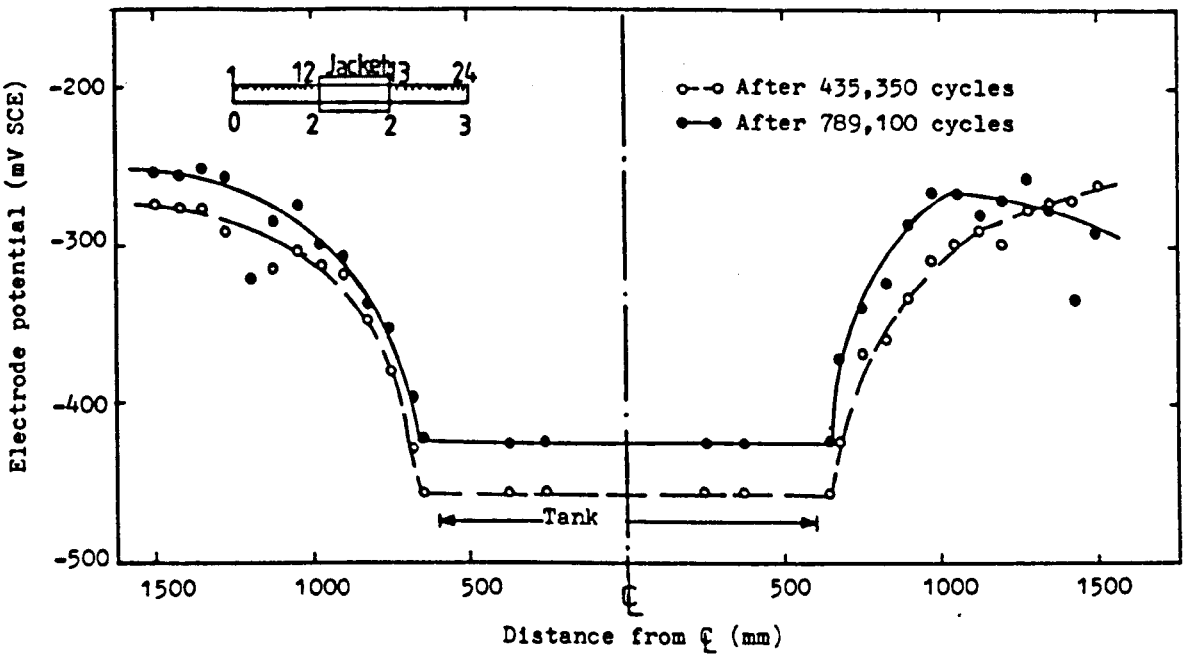

Figure (10-28): Beam MU603N;potential pofile along the top of the beam at different No. of cycles.

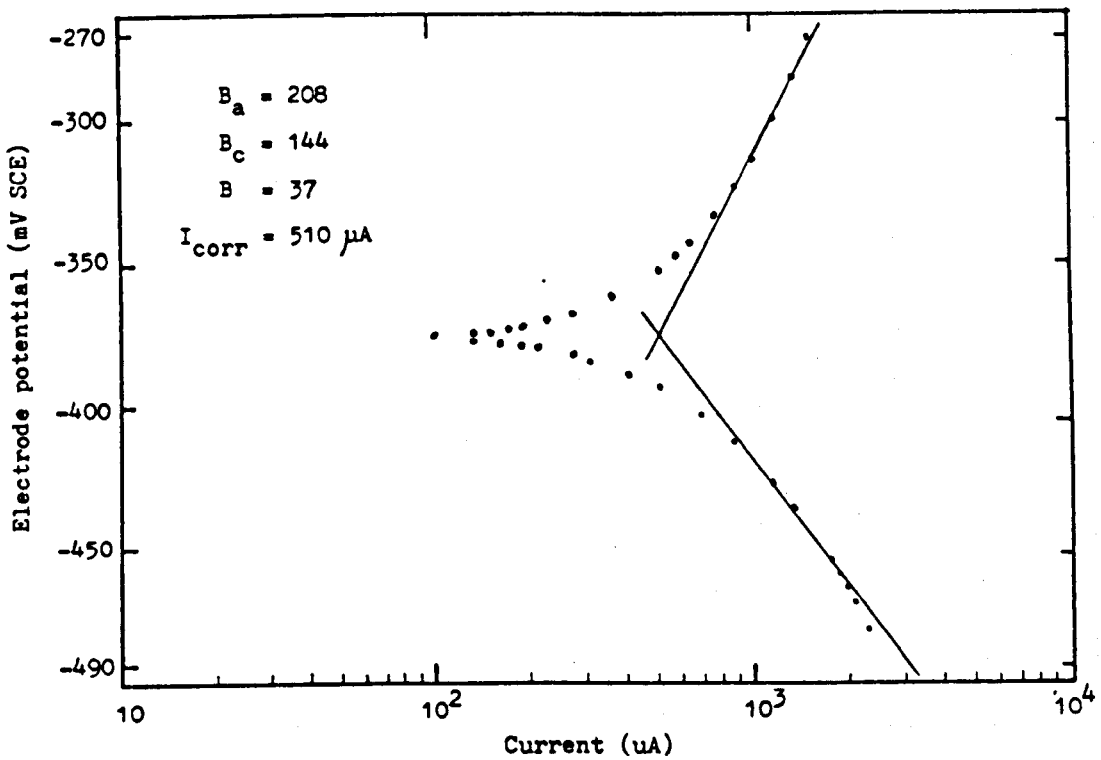

Figure (10-29): Tafel slopes;beam MU401N after 426,450 cycles.

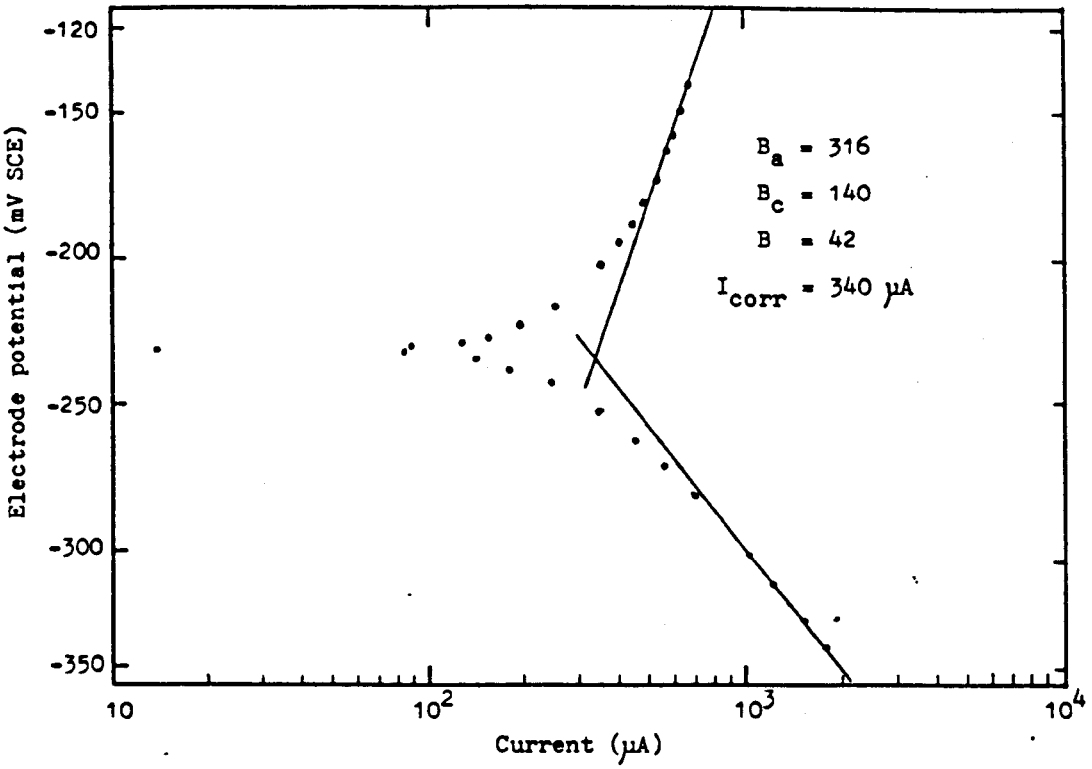

Figure (10-30): Tafel slopes;beam MU403N after 1,280,000 cycles.

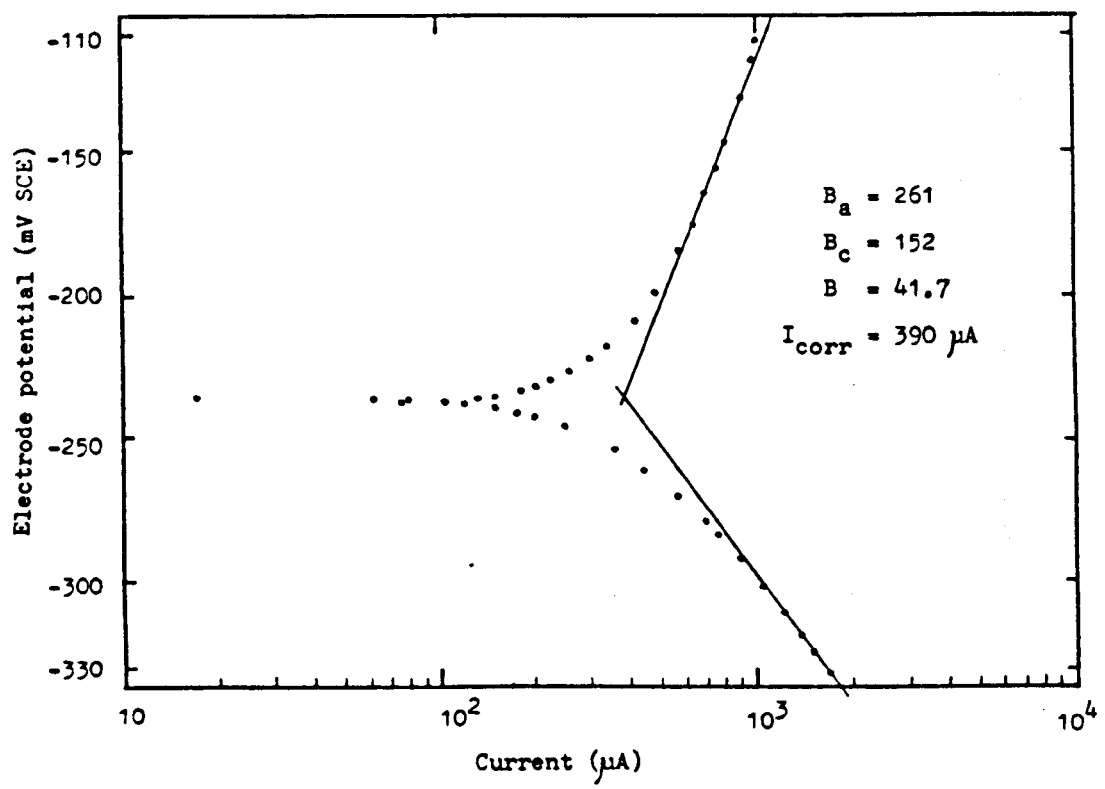

Figure (10-31): Tafel slopes;beam MU405N after 2,132,150 cycles.

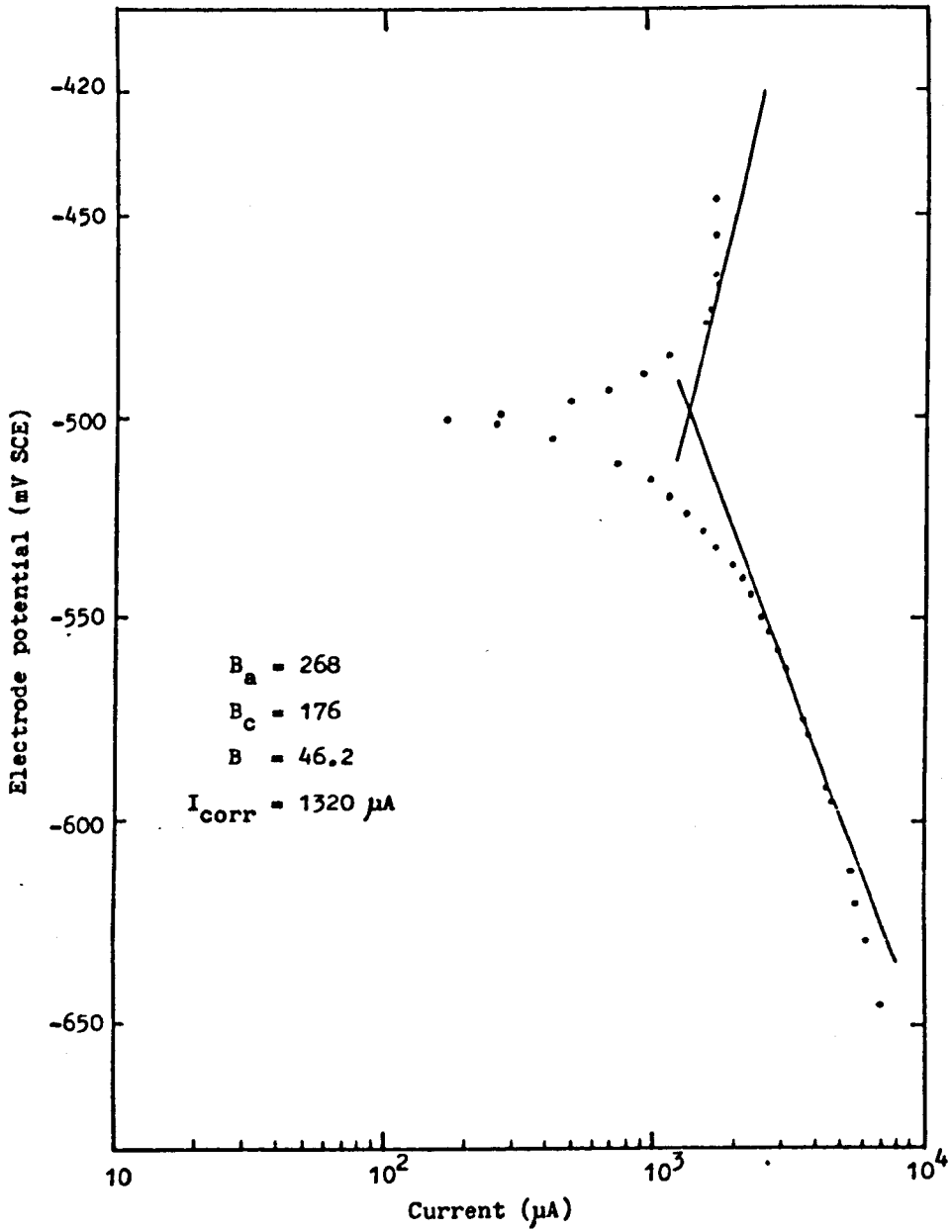

Figure (10-32): Tafel slopes;beam MU60N7D after 40,500 cycles.

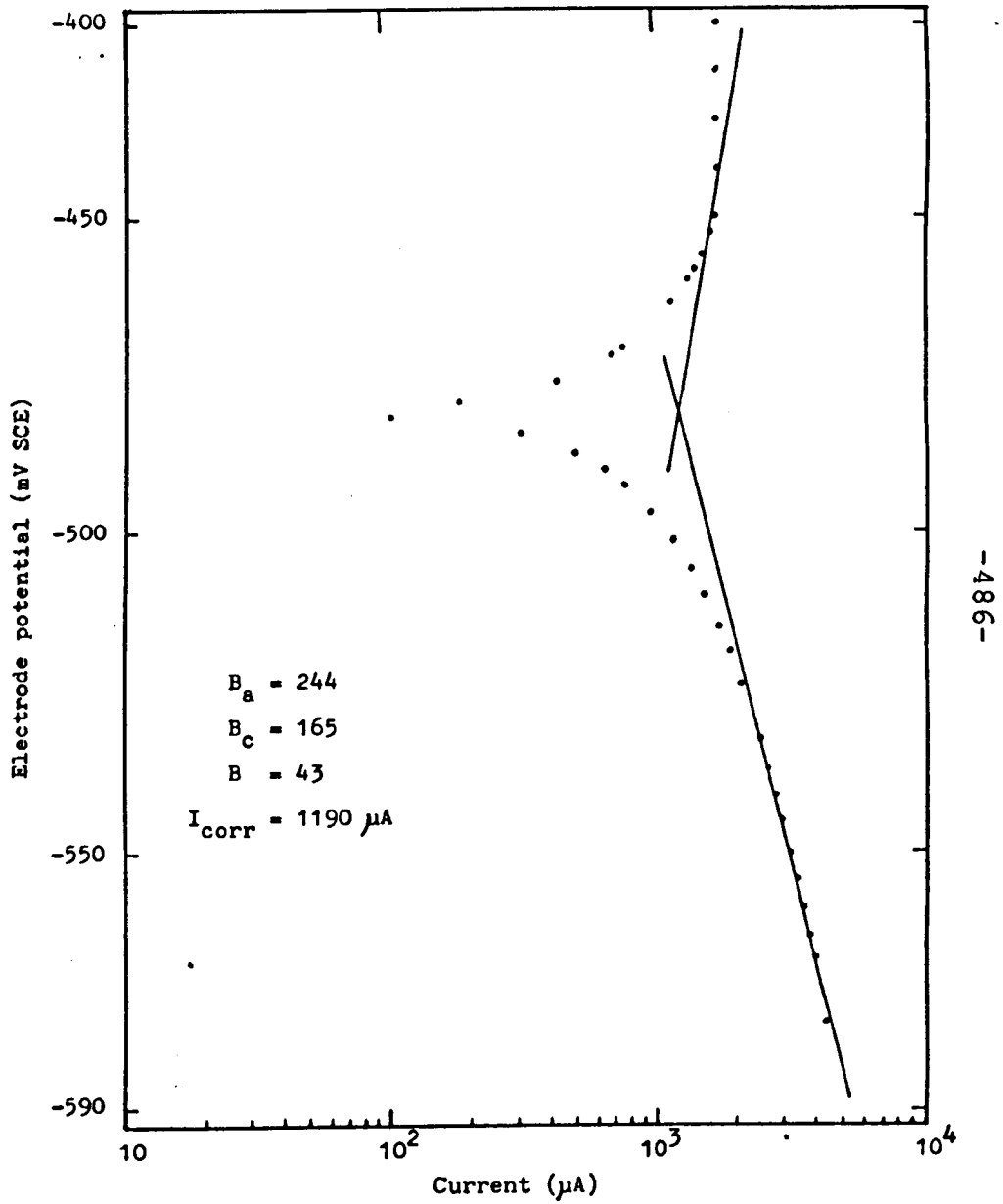

Figure (10-33): Tafel slopes;beam MU601N after 449,800 cycles.

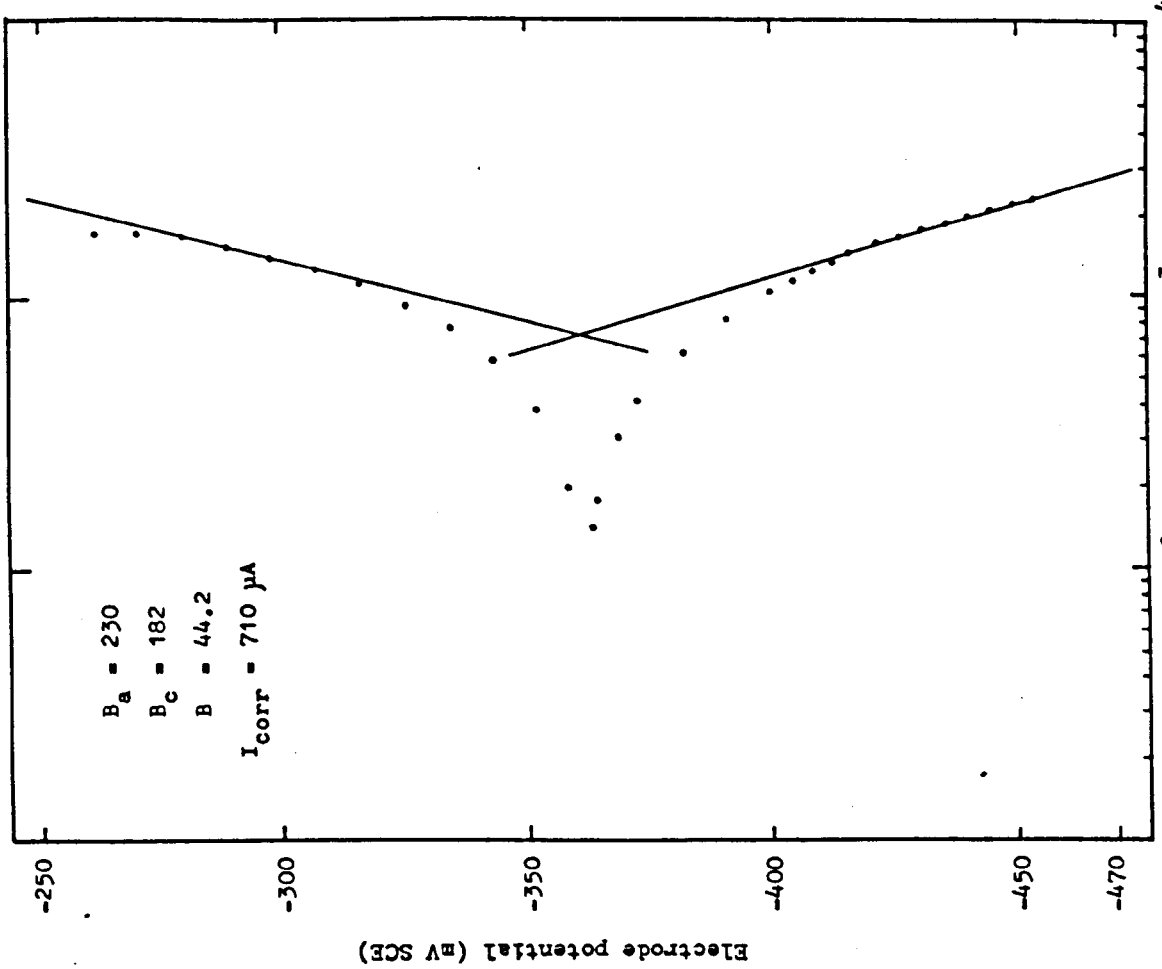

Figure (10-35): Tafel slopes;beam MU605N after 2,183,100 cycles.

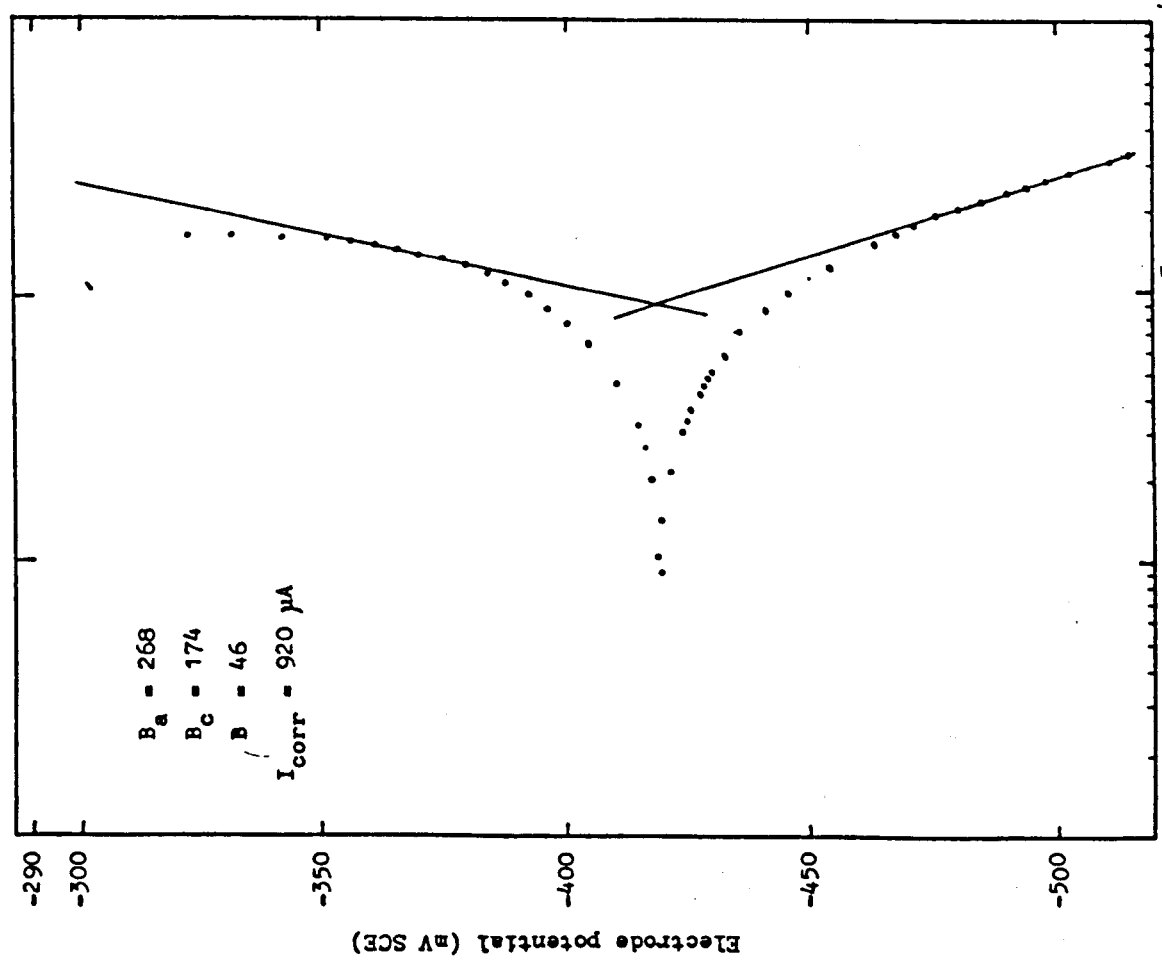

Figure (10-34): Tafel slopes;beam MU603N after 1,290,500 cycles.

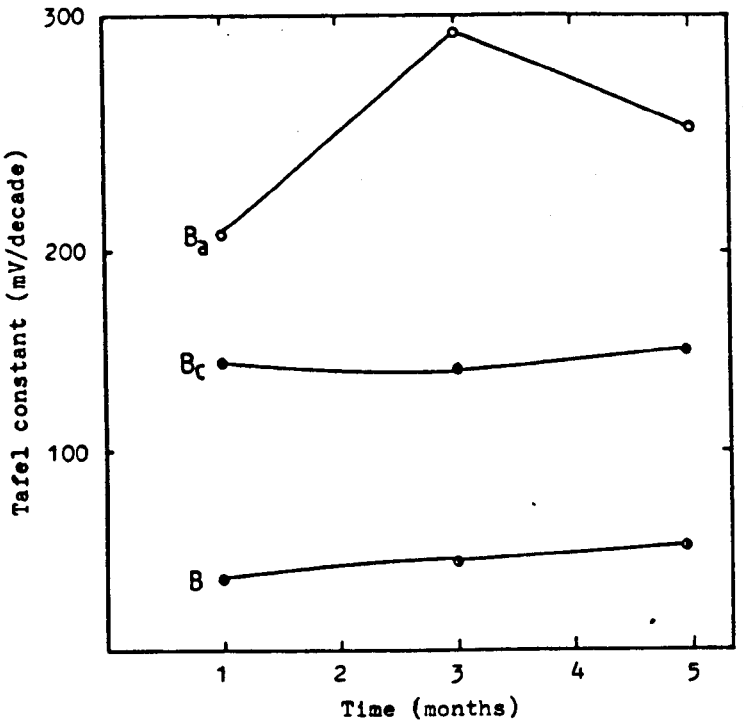

Figure (10-36): Chloride tests-0.4 fy series, Tafel parameter vs. time.

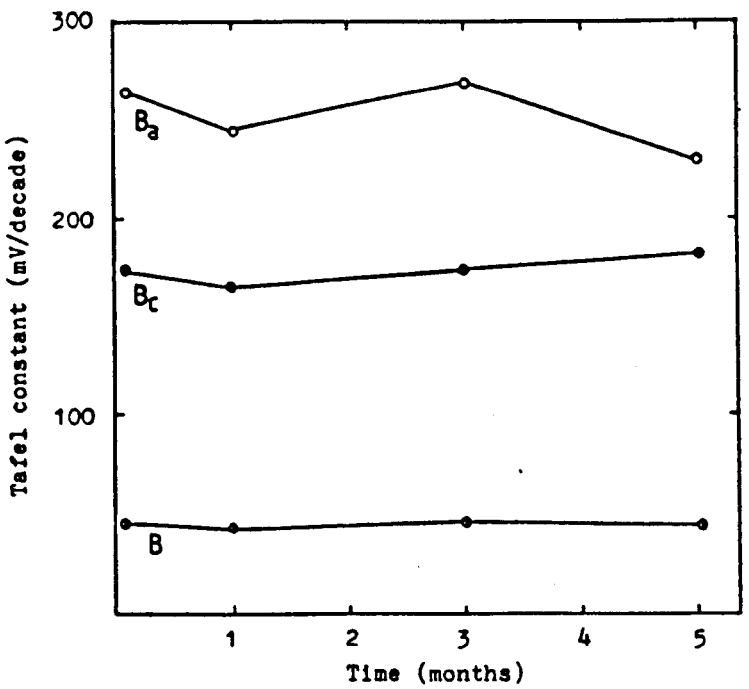

Figure (10-37): Chloride tests-0.6 fy series, Tafel parameters vs. time.

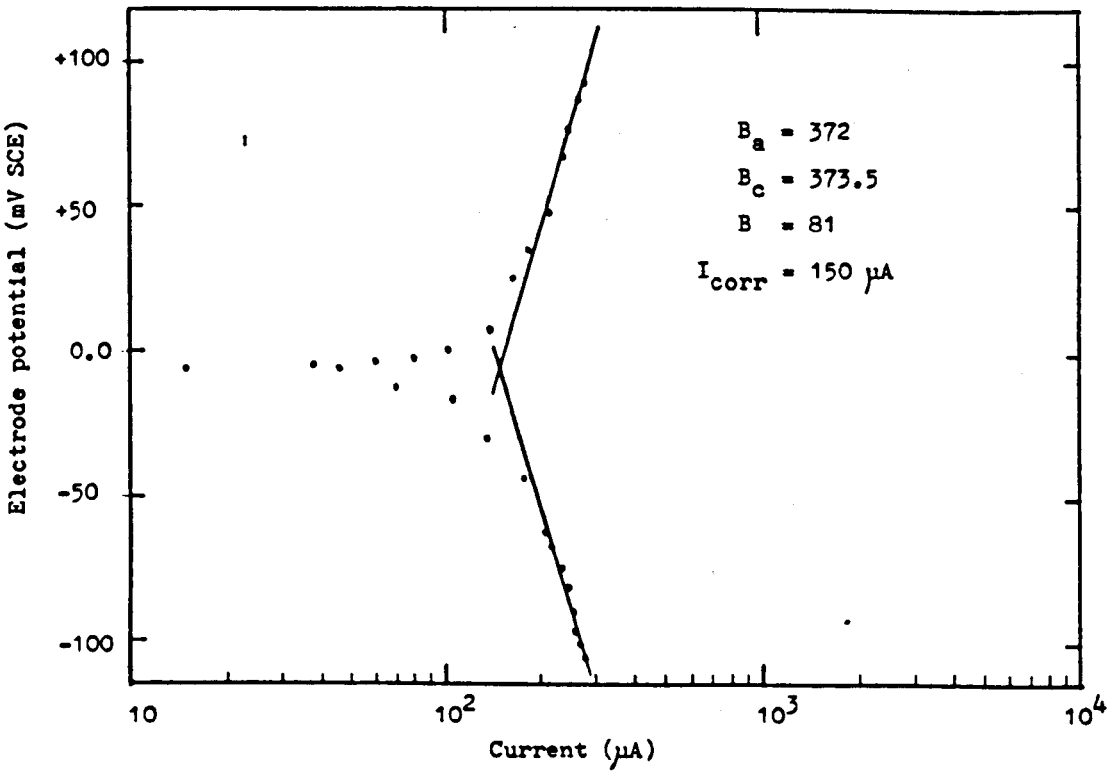

Figure (10-38): Tafel slopes;beam MU405W after 2,188,100 cycles.

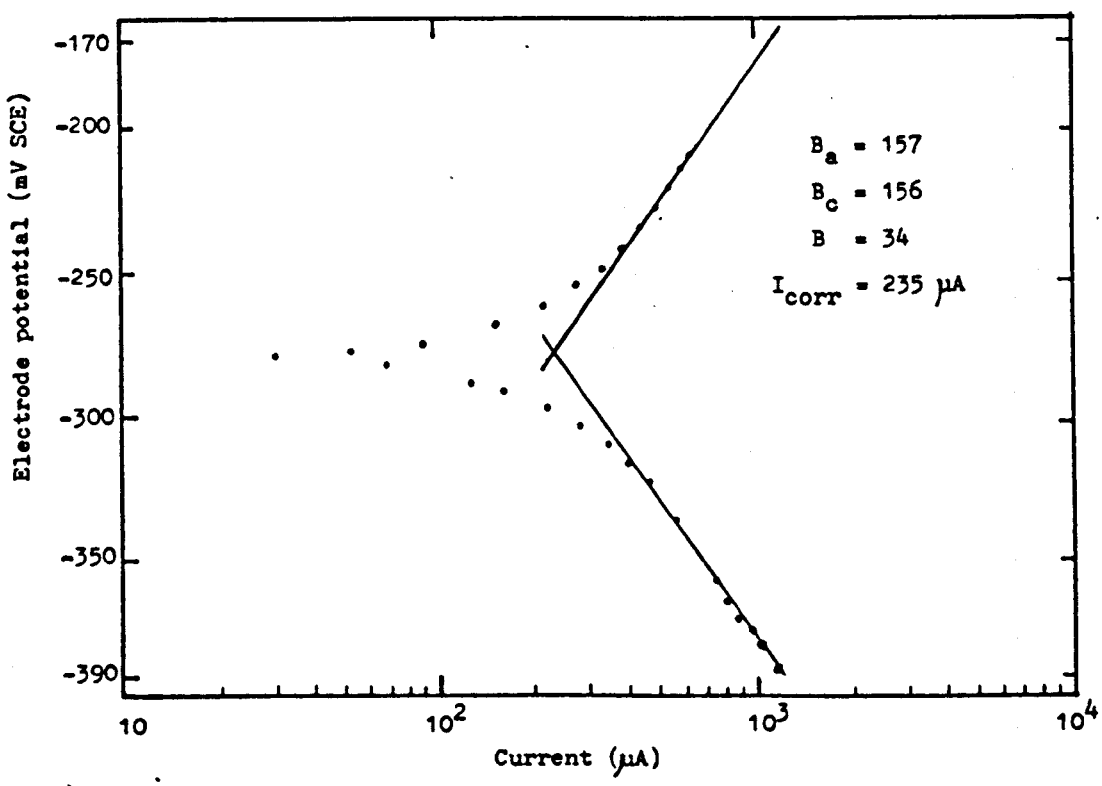

Figure (10-39): Tafel slopes;beam MU605W after 2,182,750 cycles.

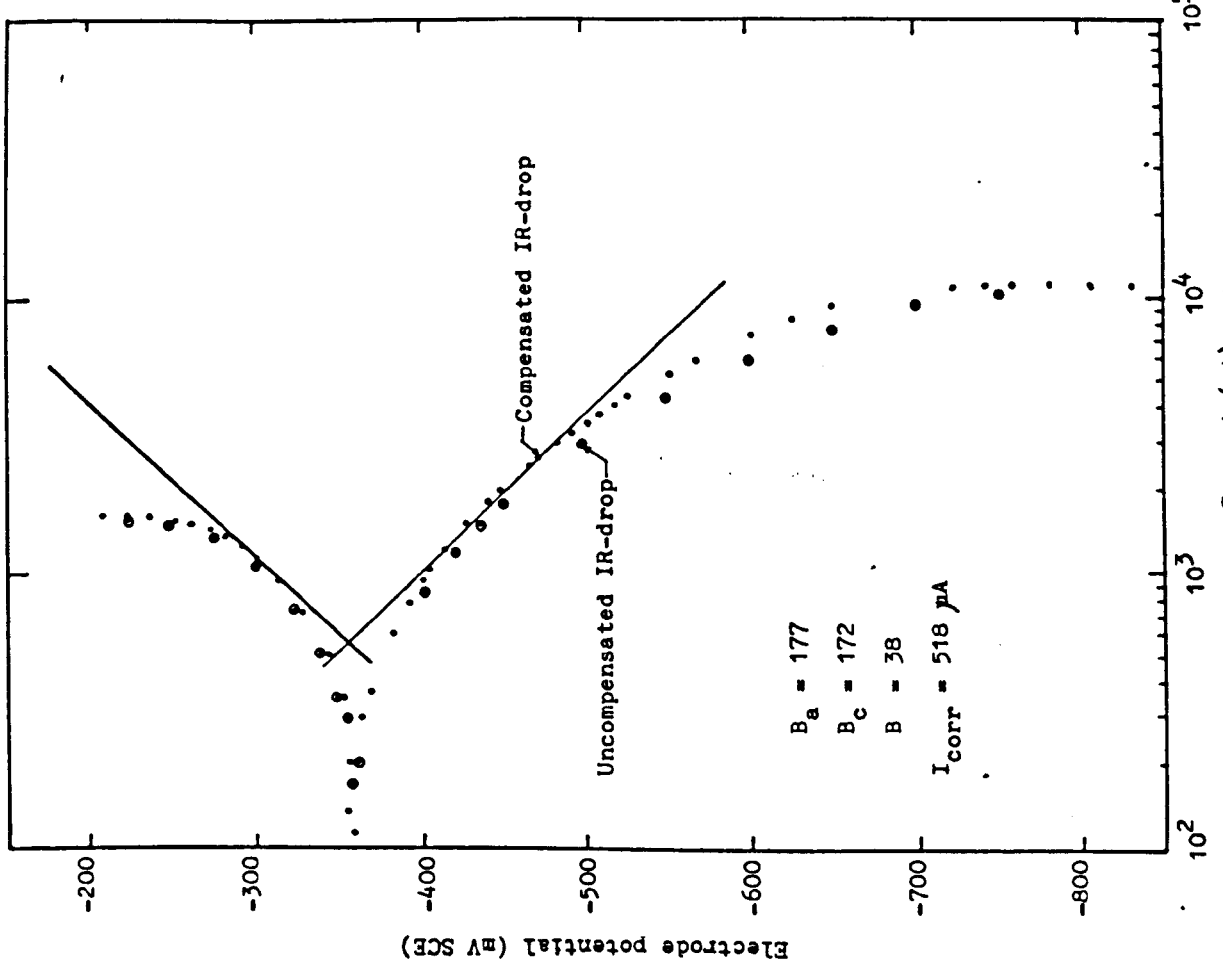

Figure (10-41): Tafel slopes;beam ML403N,static loading for 90 days.

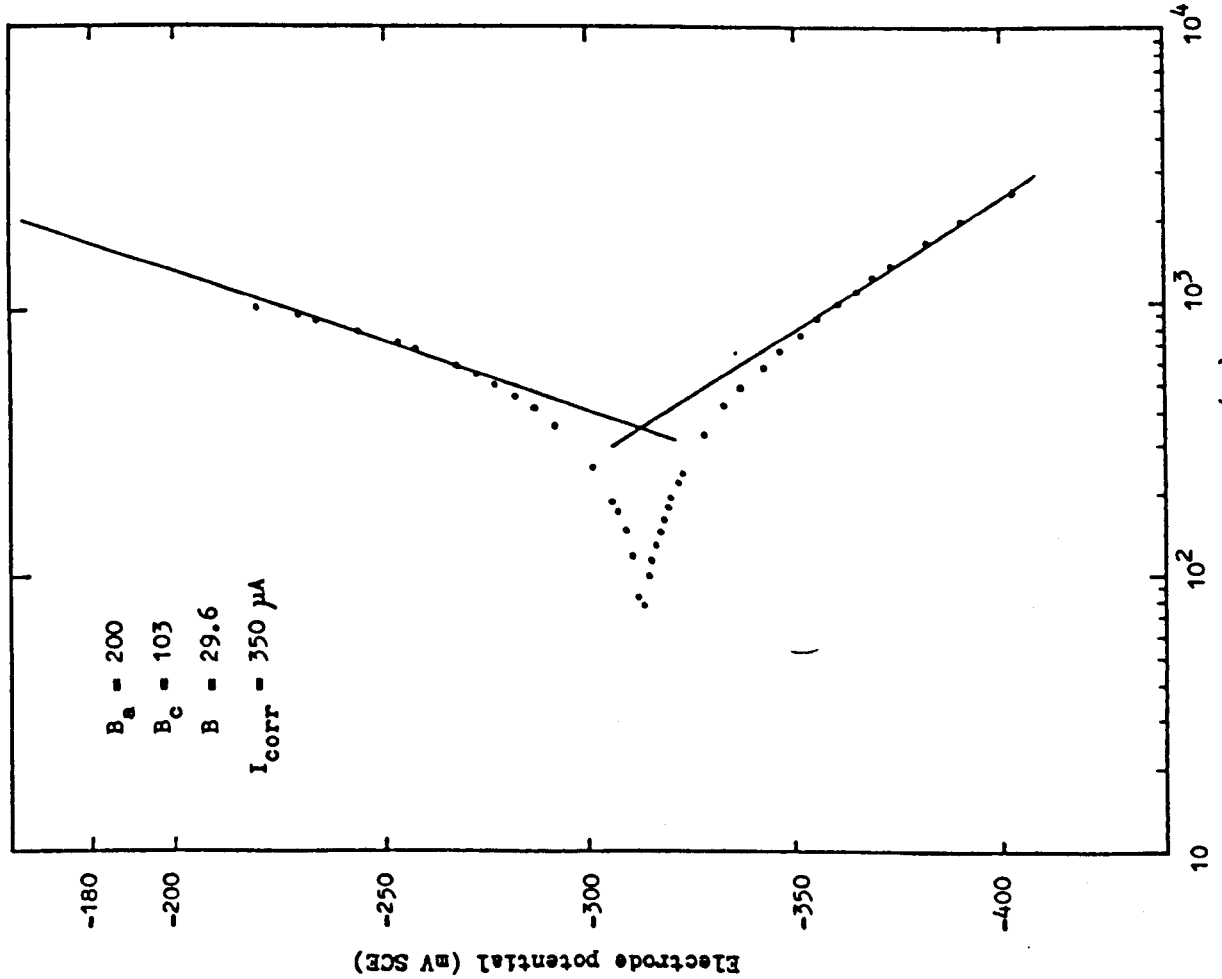

Figure (10-40): Tafel slopes;beam ML601N,5 days exposure without loading.

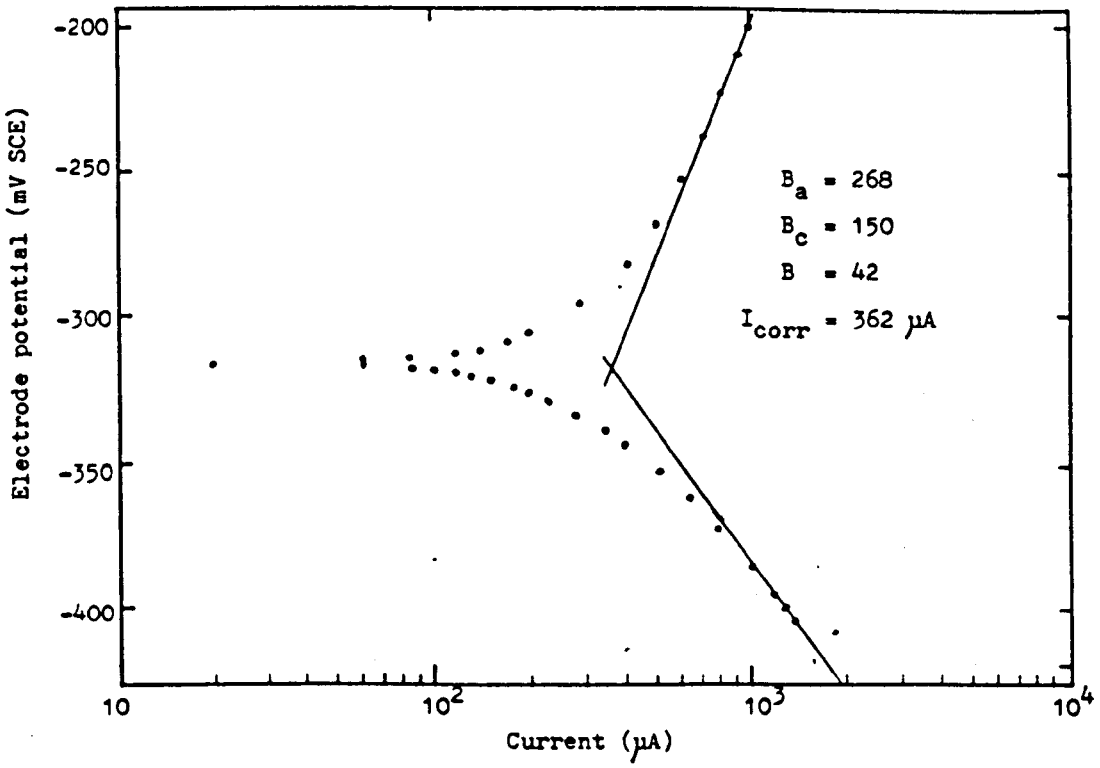

Figure (10-42): Tafel slopes;beam ML601N under static loading for 40 days.

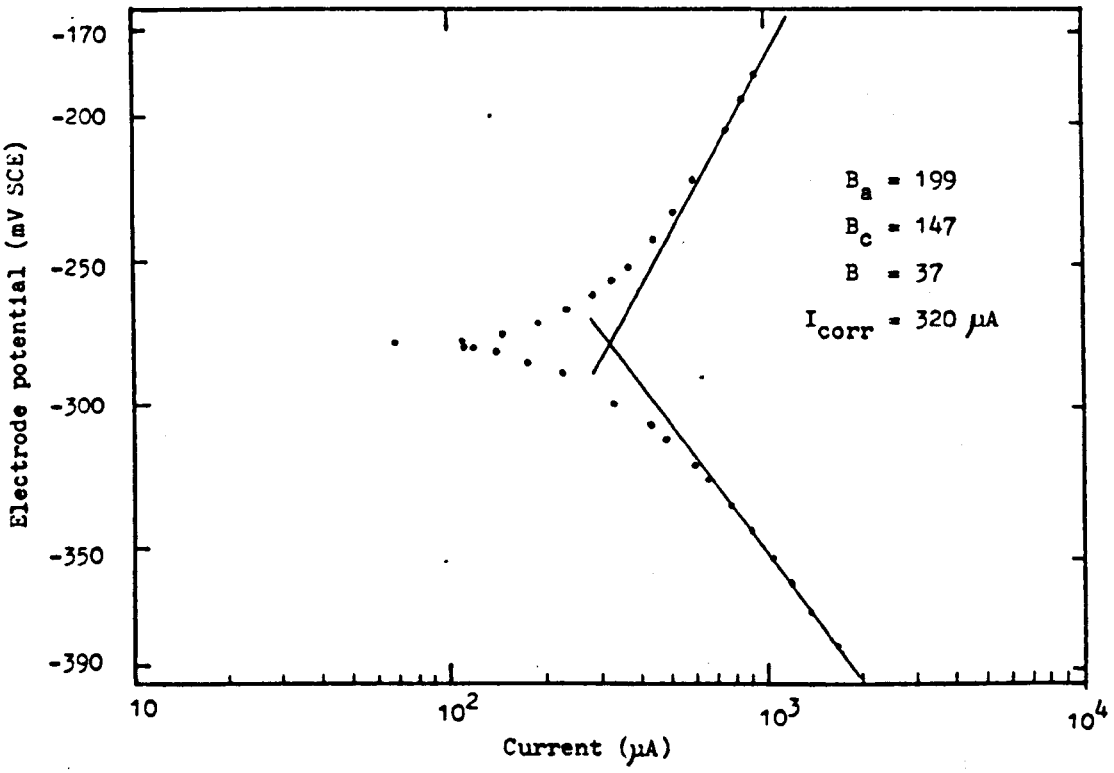

Figure (10-43): Tafel slopes;beam ML603N under static loading for 90 days.

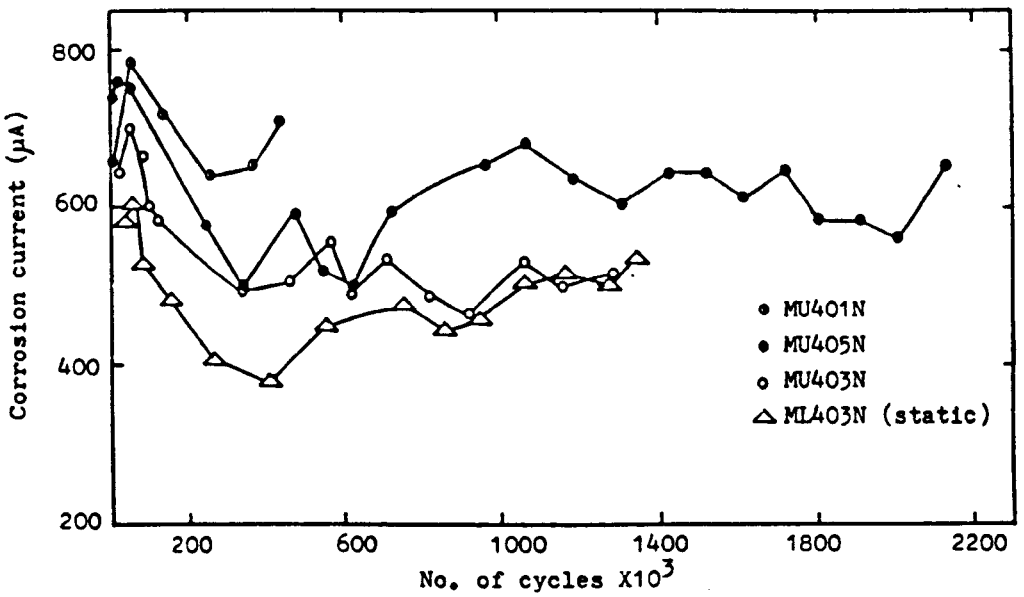

Figure (10-44): Chloride tests-0.4fy series;corrosion current vs. No. of cycles (potentiodynamic measurement).

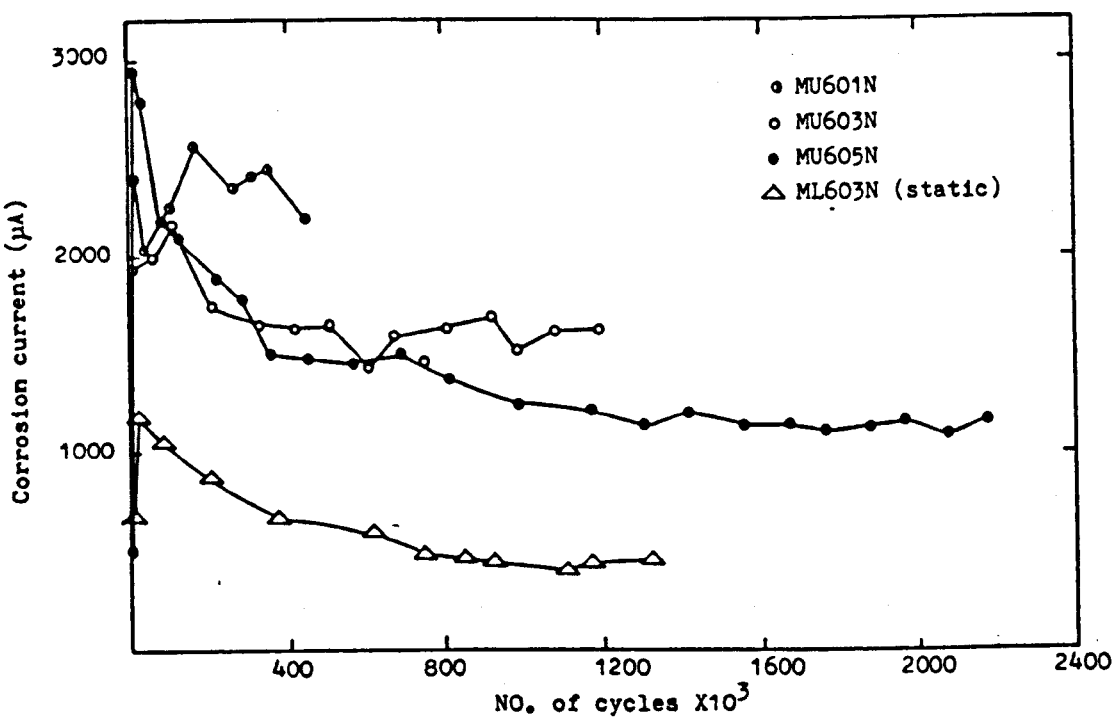

Figure (10-45): Chloride test-0.6fy series,corrosion current vs. No. of cycles (potentiodynamic measurement).

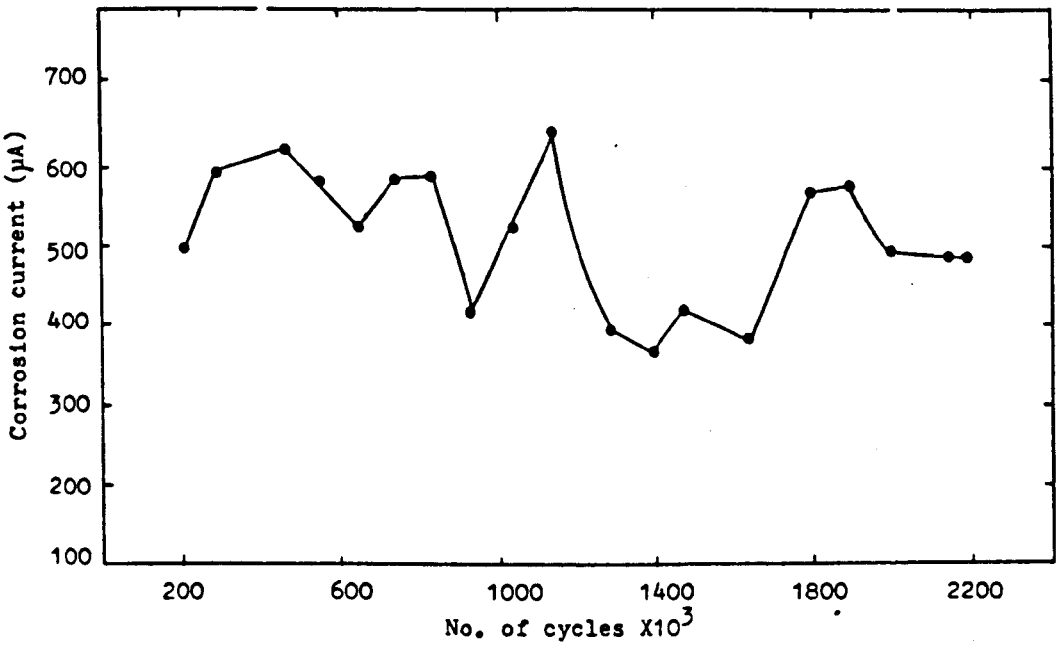

Figure (10-46): Tapwater test-0;6fy ,corrosion current vs. No. of cycles for beam MU605W (potentiodynamic measurt).

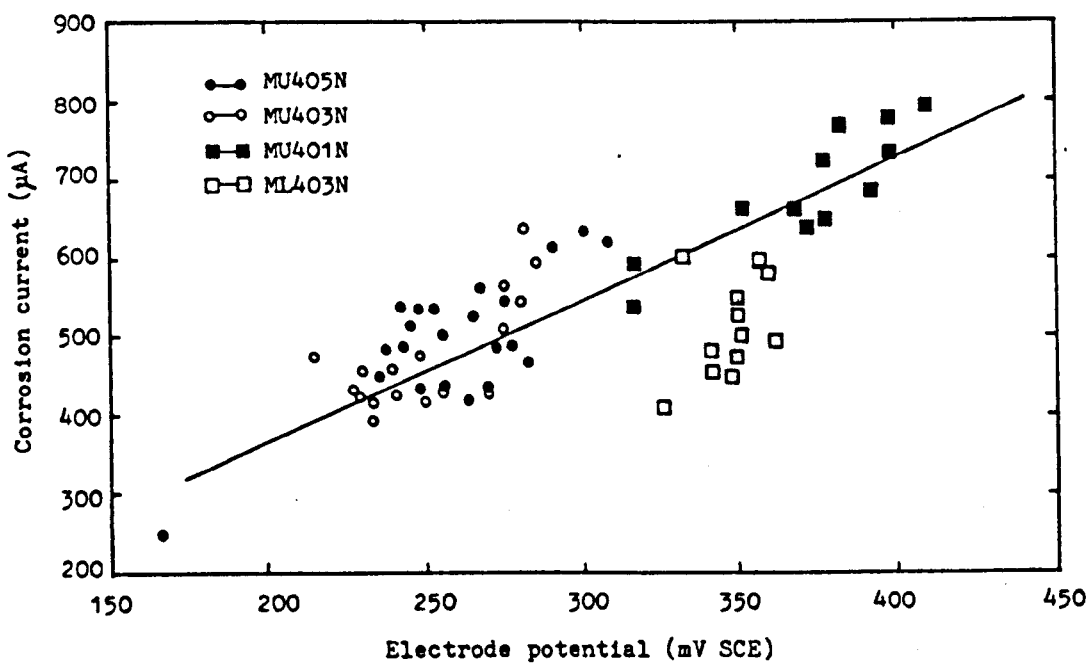

Figure (10-47): Chloride tests-0.4 fy series,corrosion current vs. electrode potential.

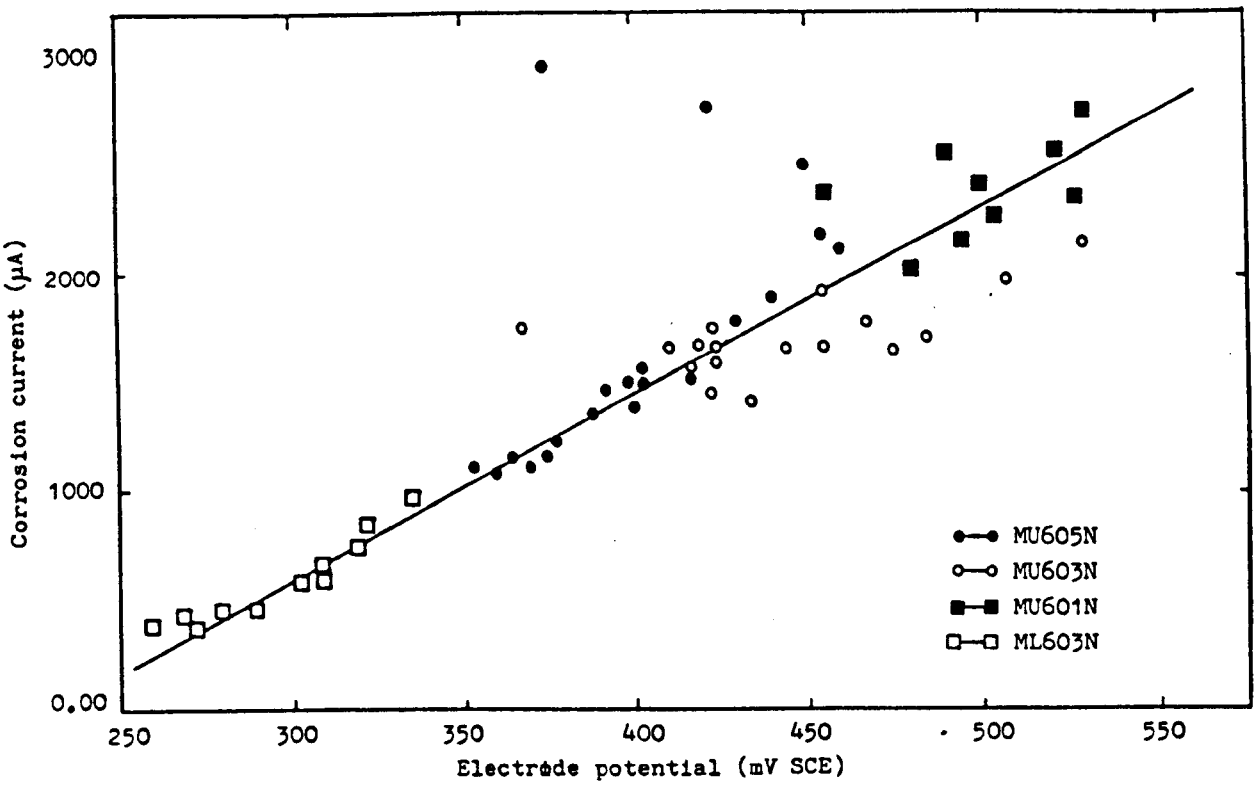

Figure (10-48): Chloride test-0.6fy series,corrosion current vs. electrode potential.

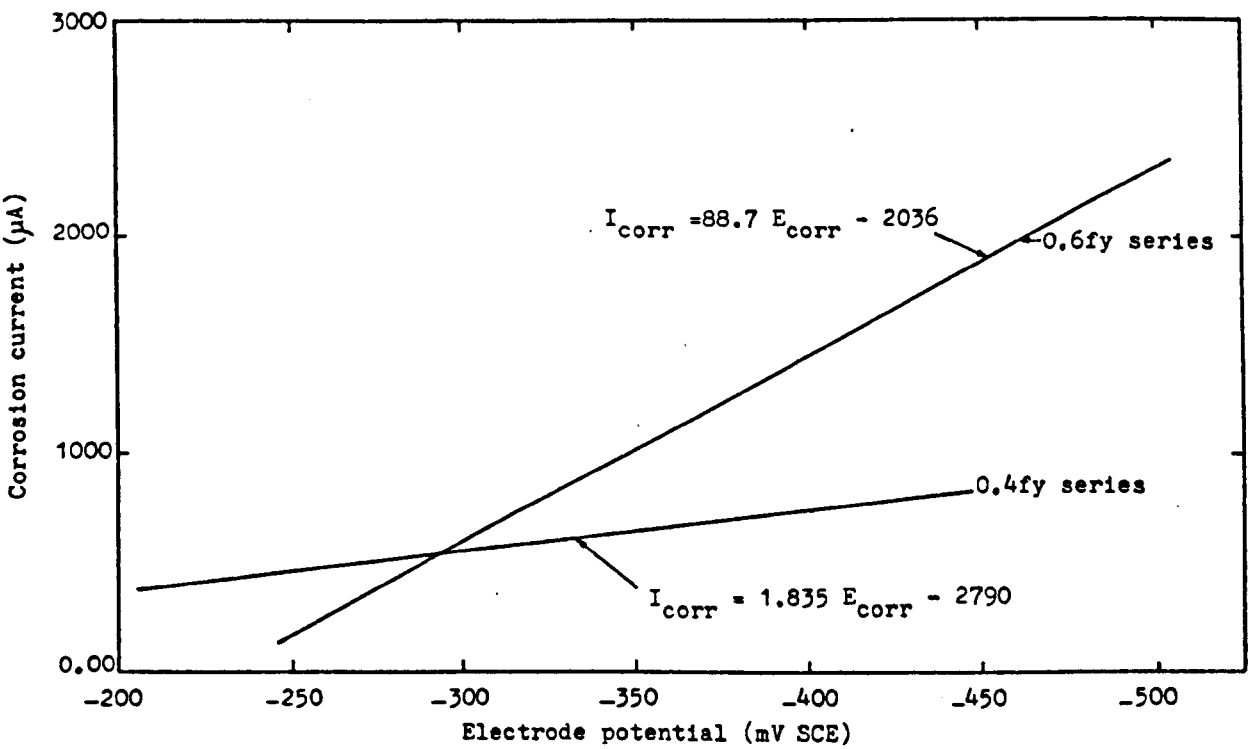

Figure (10-49): Chloride tests;effects of load level on I_{corr}-E_{corr} relationship.

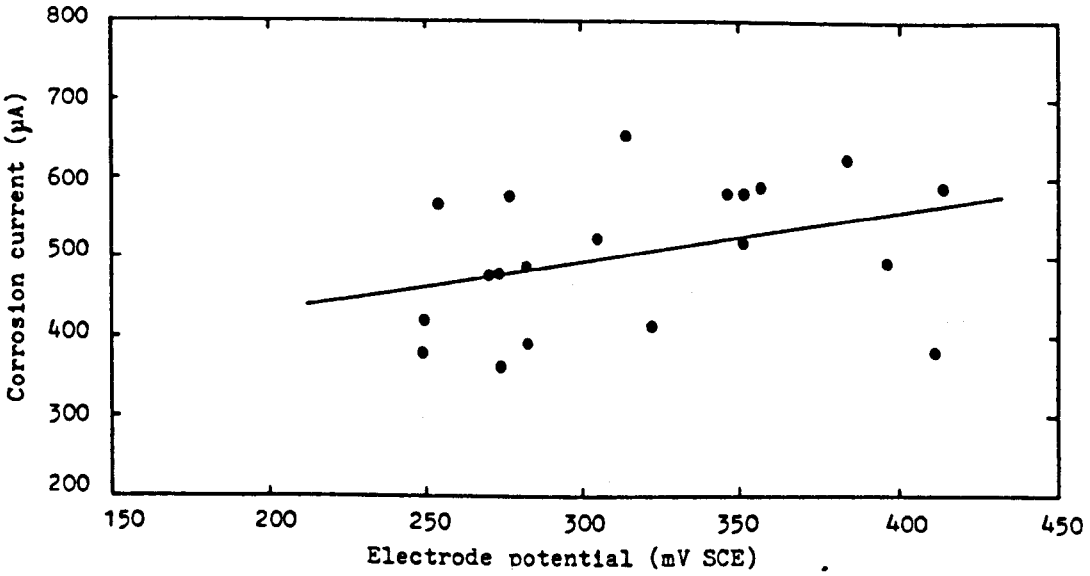

Figure (10-50): Tapwater test;corrosion current vs. electrode potential (beam MU605W).

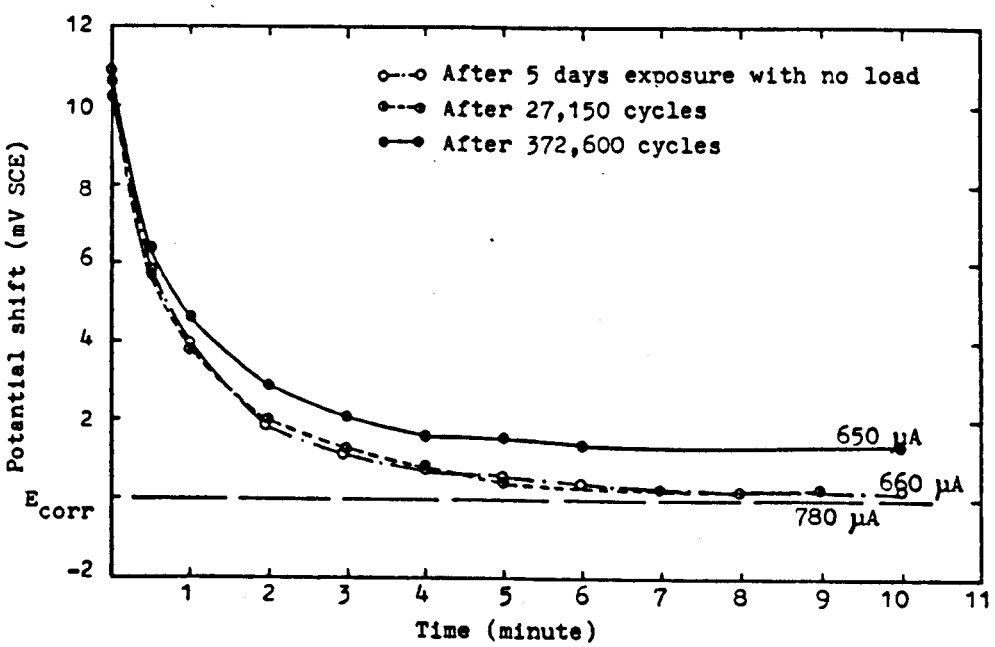

Figure (10-51): E_{corr} recovery after anodic potentiodynamic sweep at different stages of test (beam MU401N).

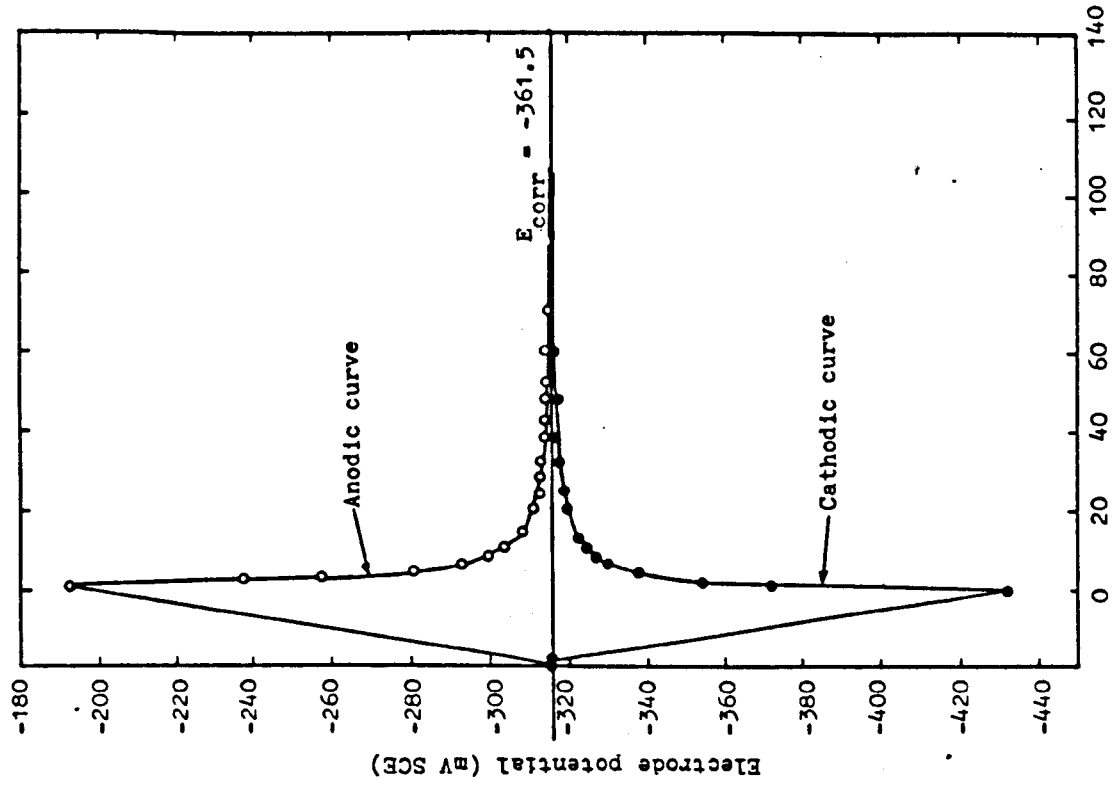

Figure (10-53): Beam ML601N;E_{corr} recovery after anodic and cathodic shift (sweep) during Tafel slopes determination.

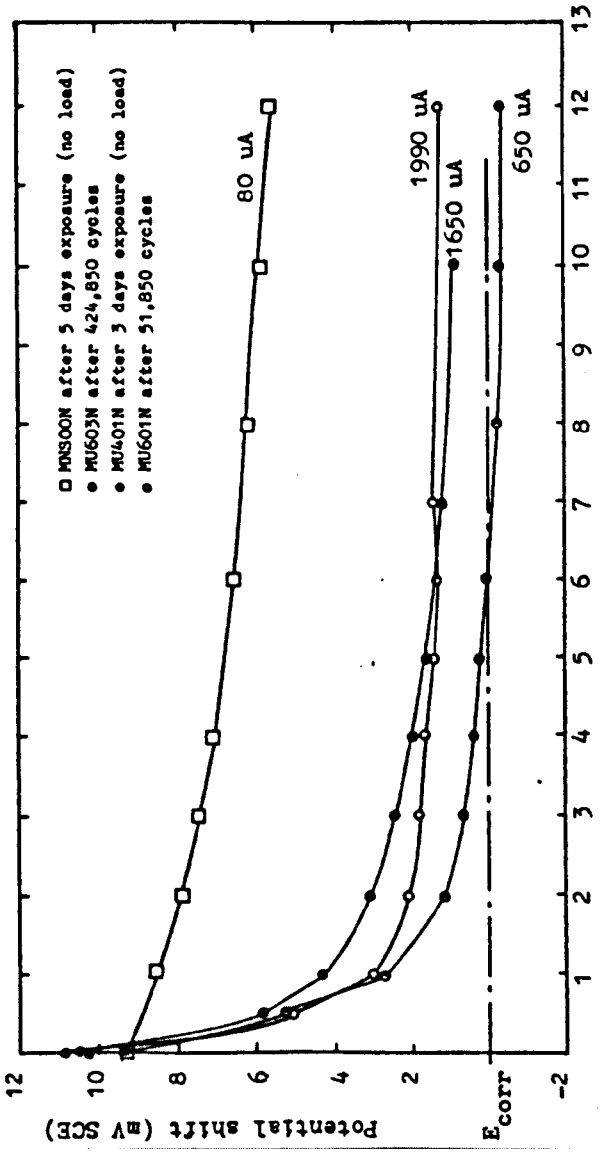

Figure (10-52): E_{corr} recovery after anodic potentiostatic step at different conditions for various test beam.

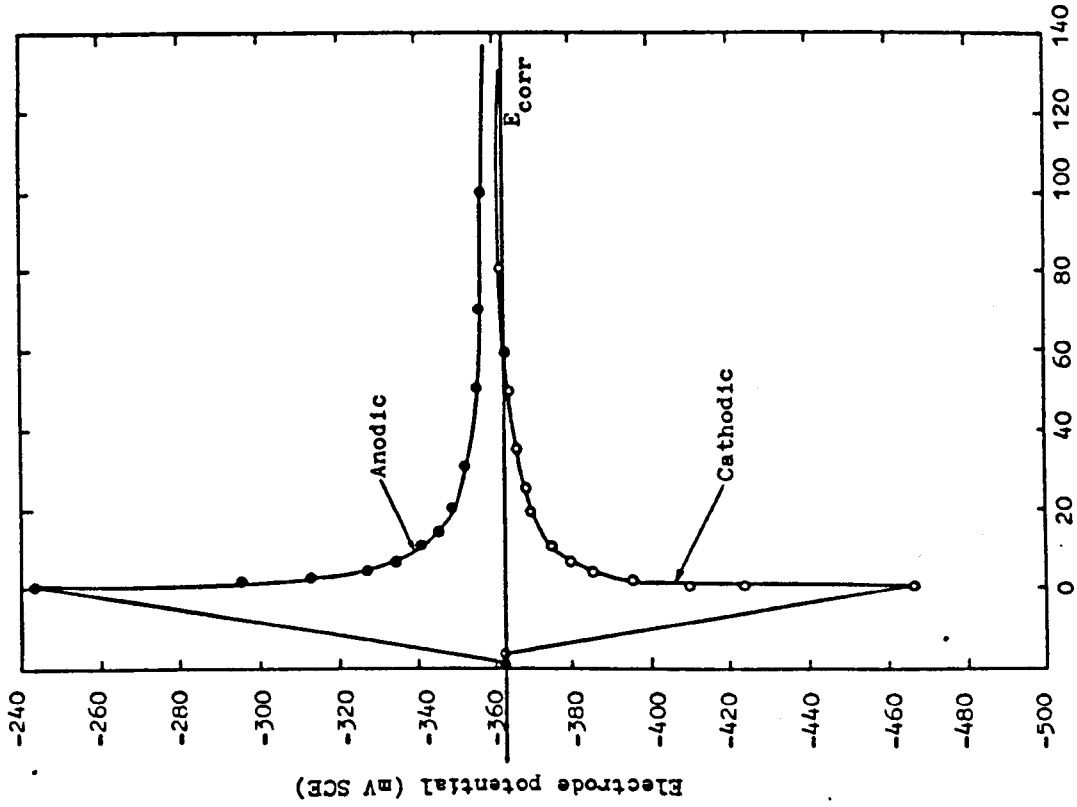

Figure (10-55): Beam MU605N;E_{corr} recovery after anodic and cathodic polarization during Tafel plots determination.

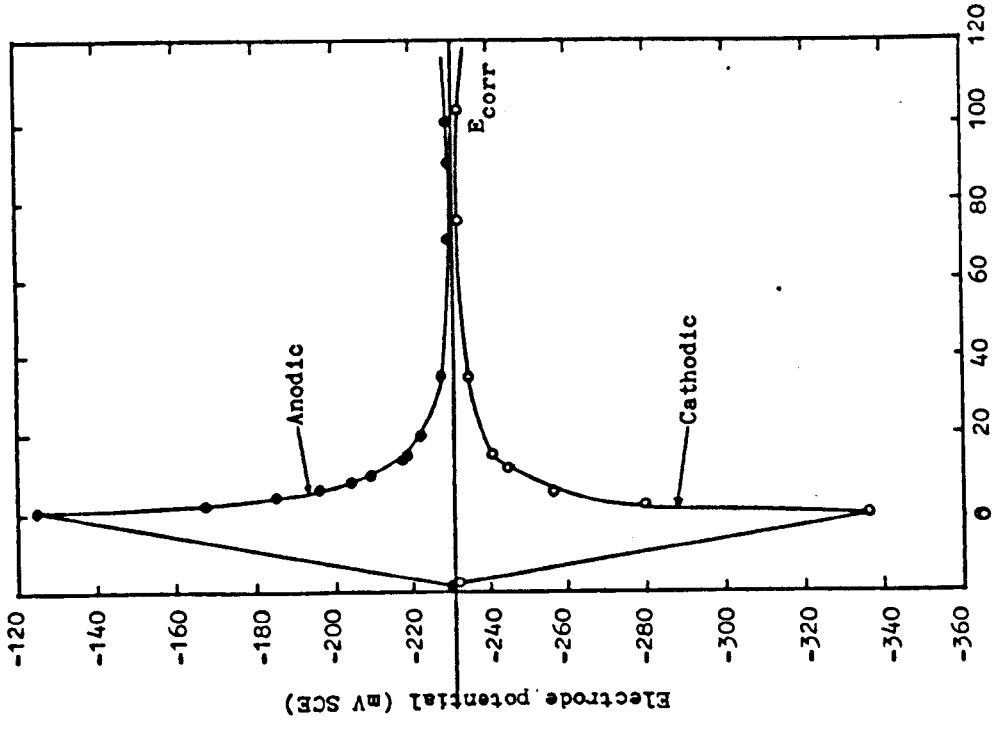

Figure (10-54): Beam MU403N;E_{corr} recovery after anodic and cathodic polarization during Tafel plots determination.

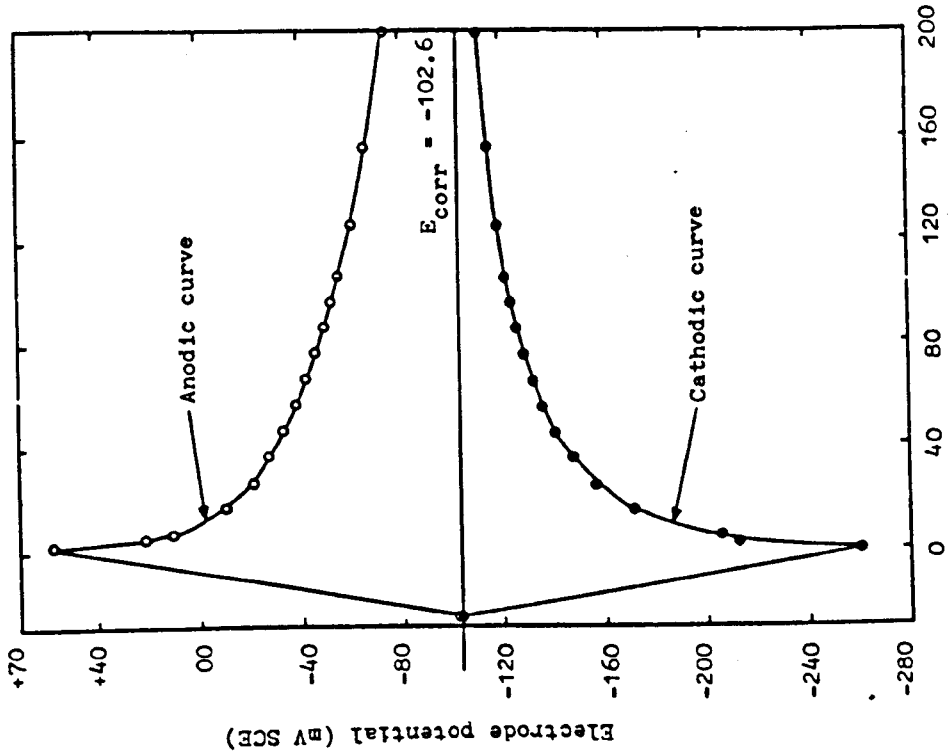

Figure (10-57): Beam MNSOON;E_{corr} recovery after anodic and cathodic shift (sweep) during Tafel slopes determination.

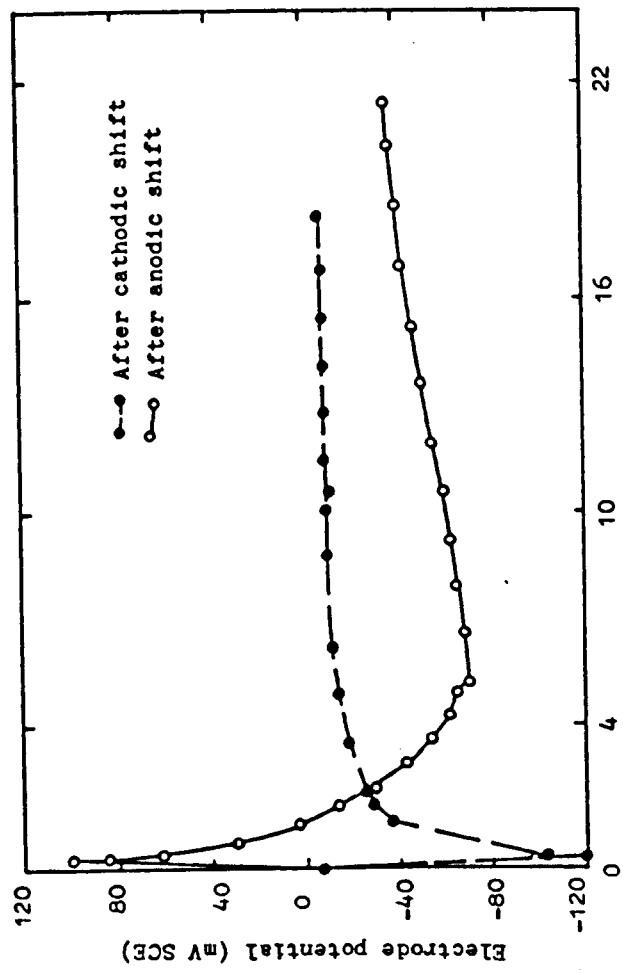

Figure (10-56): Beam Mu405W;E_{corr} recovery after anodic and cathodic polarization during Tafel slopes determination.

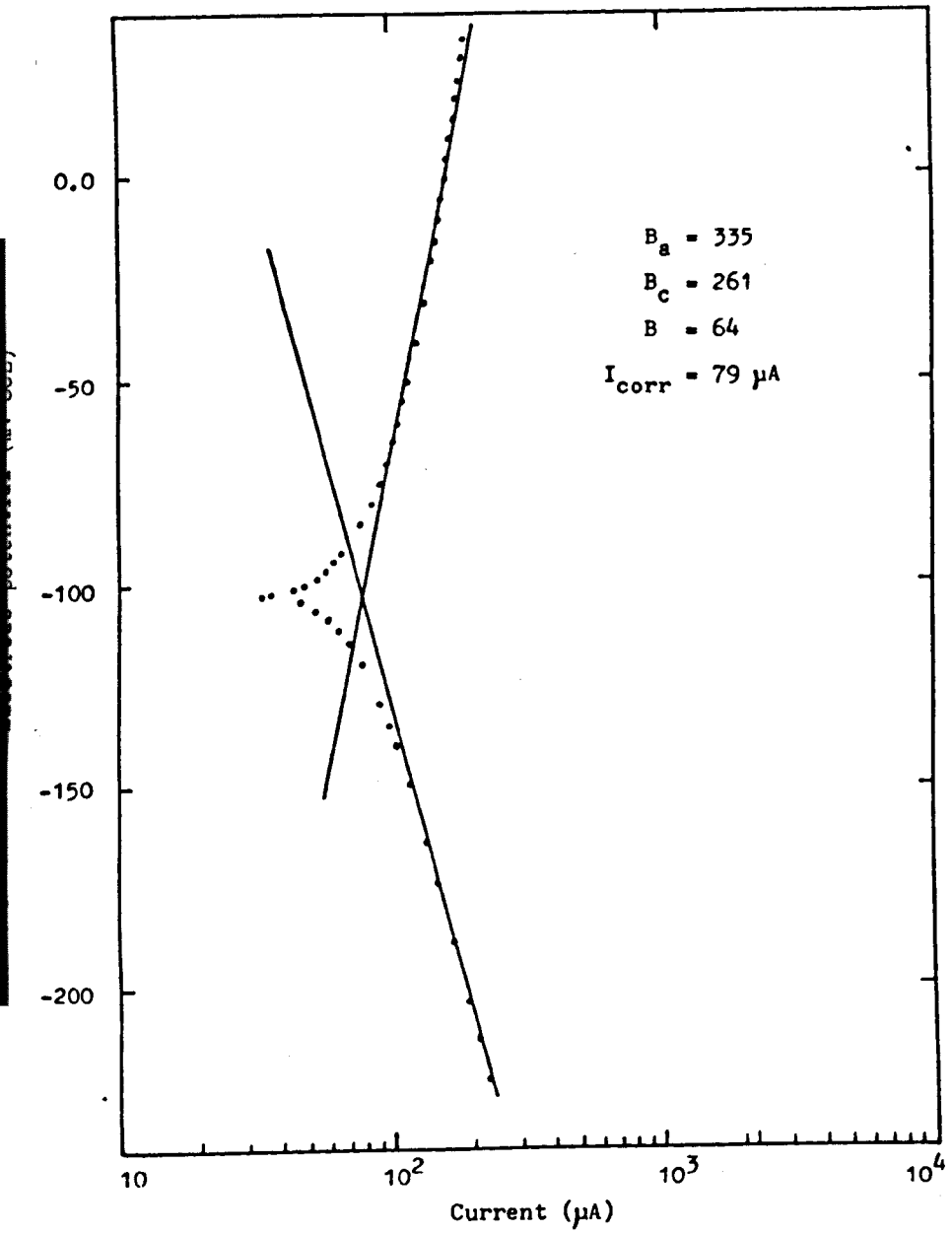

Figure (10-58): Tafel slopes;beam MNSOON,exposed to sodium chloride solution for 25days with no load applied

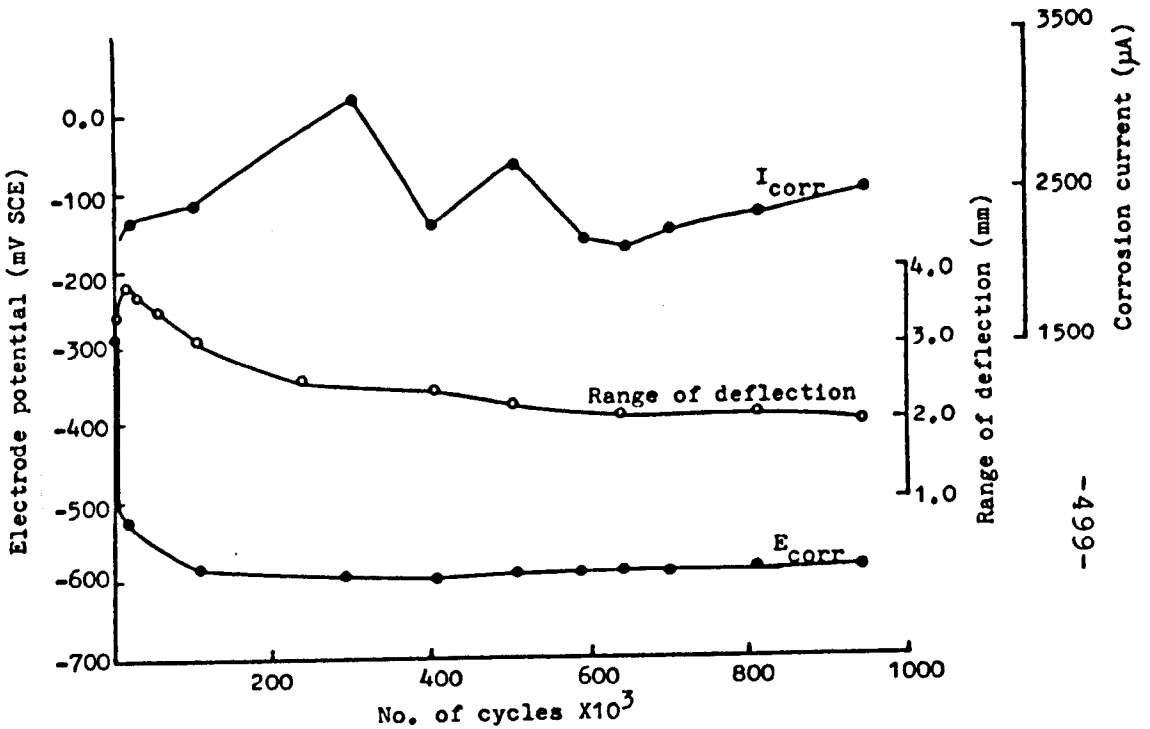

Figure (10-59): Beam MU601N1Y;the variation of electrode potential and corrosion current (determined potentiostatically at steady state) with No. of cycles.

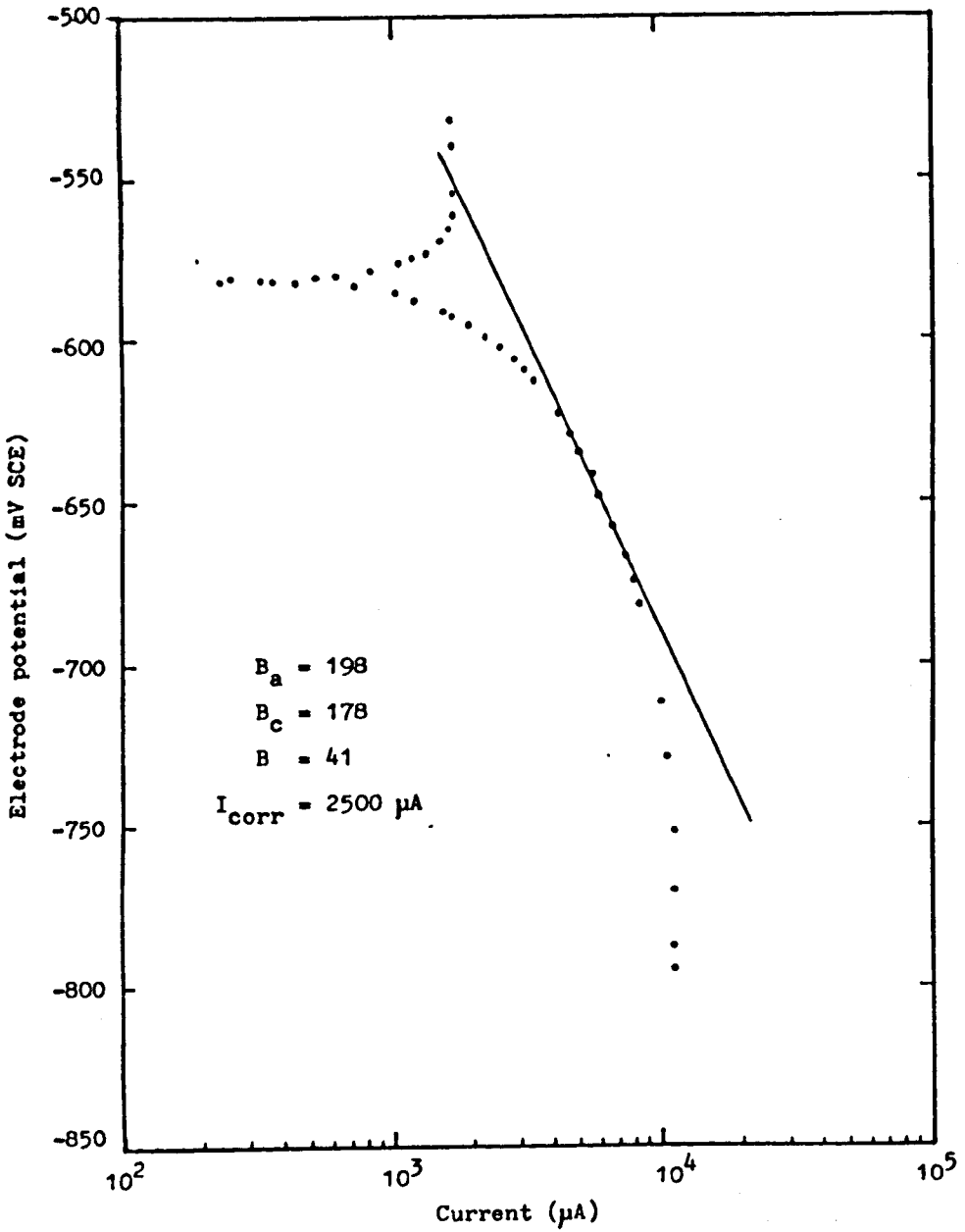

Figure (10-60): Tafel slopes;beam MU6ON1Y after 939,750 cycles.

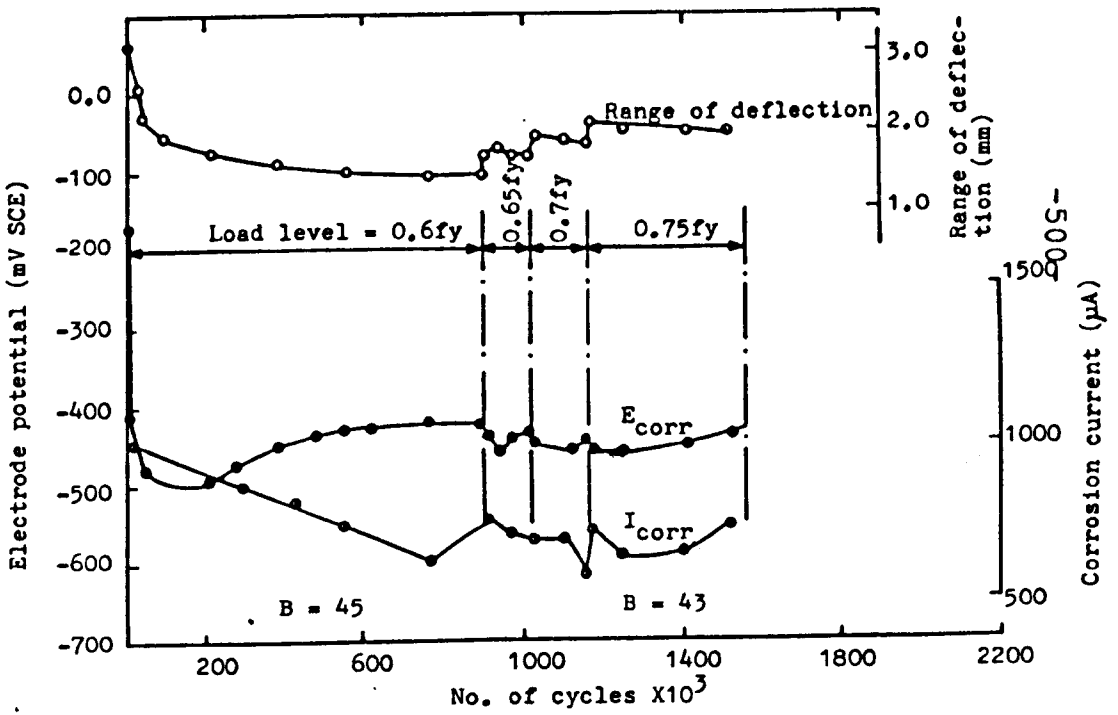

Figure (10-61): Beam MU6ON8Y;the variation of electrode potential and corrosion current (determined potentiostatically at steady state) with No. of cycles.

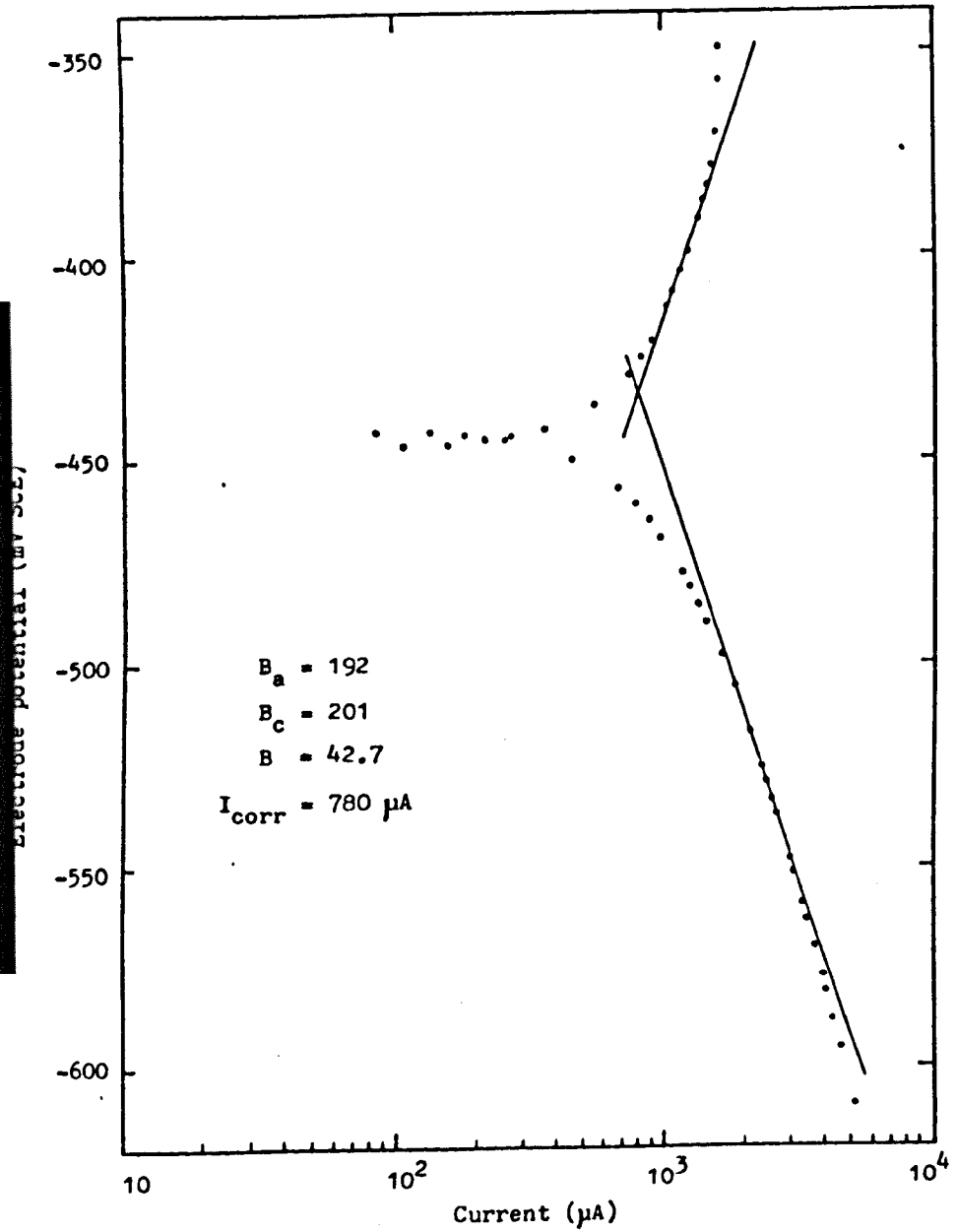

Figure (10-62): Tafel slopes;beam MU6ON8Y after 1,511,800 cycles.

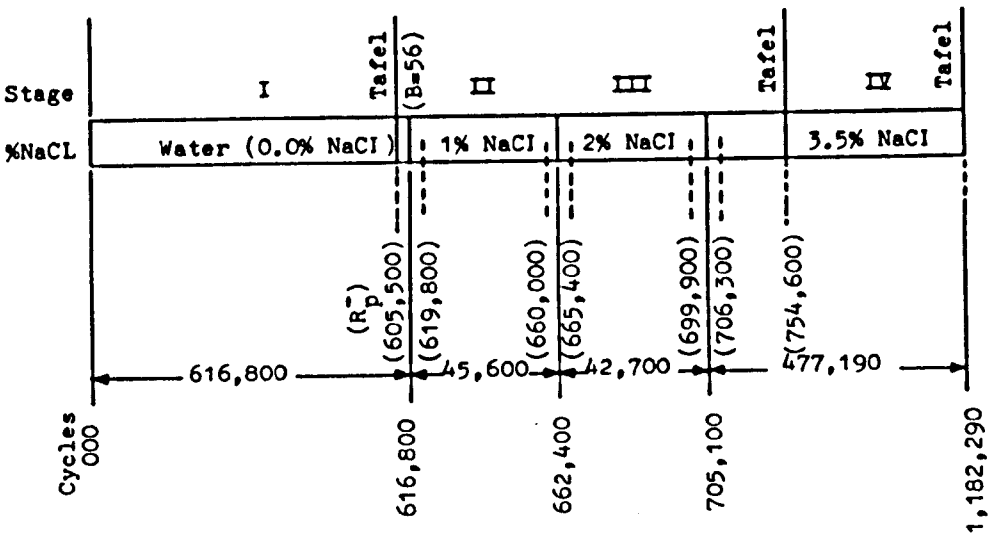

Figure (10-63): Beam MU7OWN;environmental history and polarization measurements.

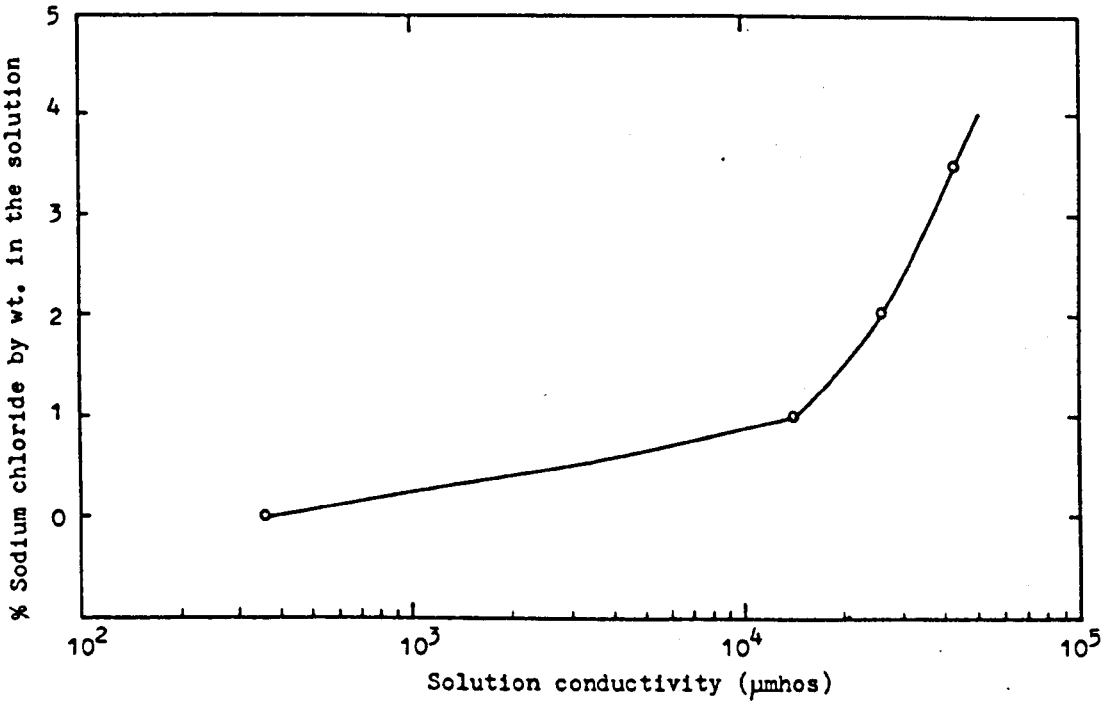

Figure (10-64): Solution conductivity for different chloride content.

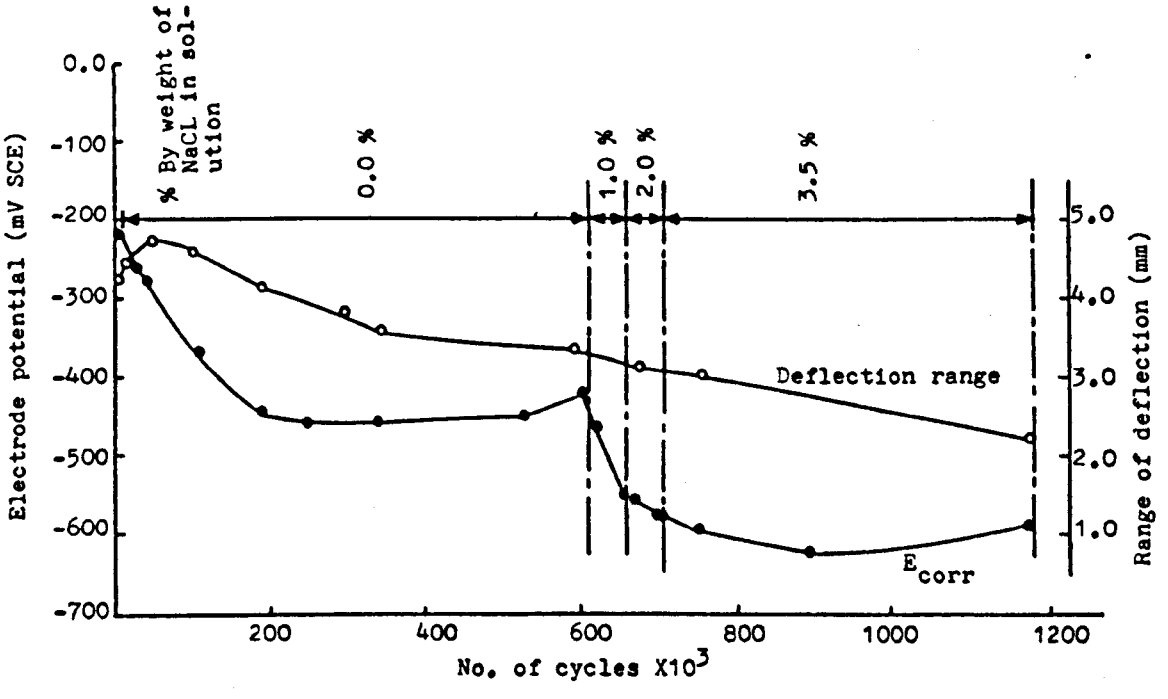

Figure (10-65): Beam MU7OWN;the variation of electrode potential and deflection range with No. of cycles.

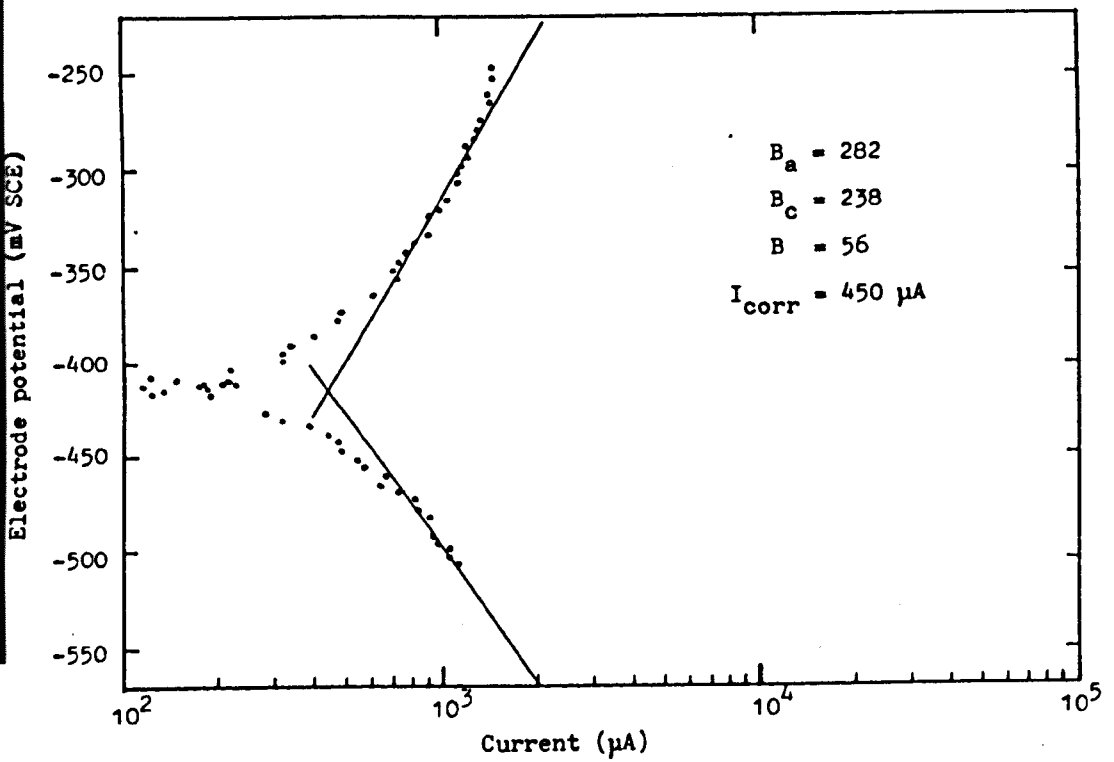

Figure (10-66): Tafel slopes;beam MU70WN,after 605,200 cycles in water.

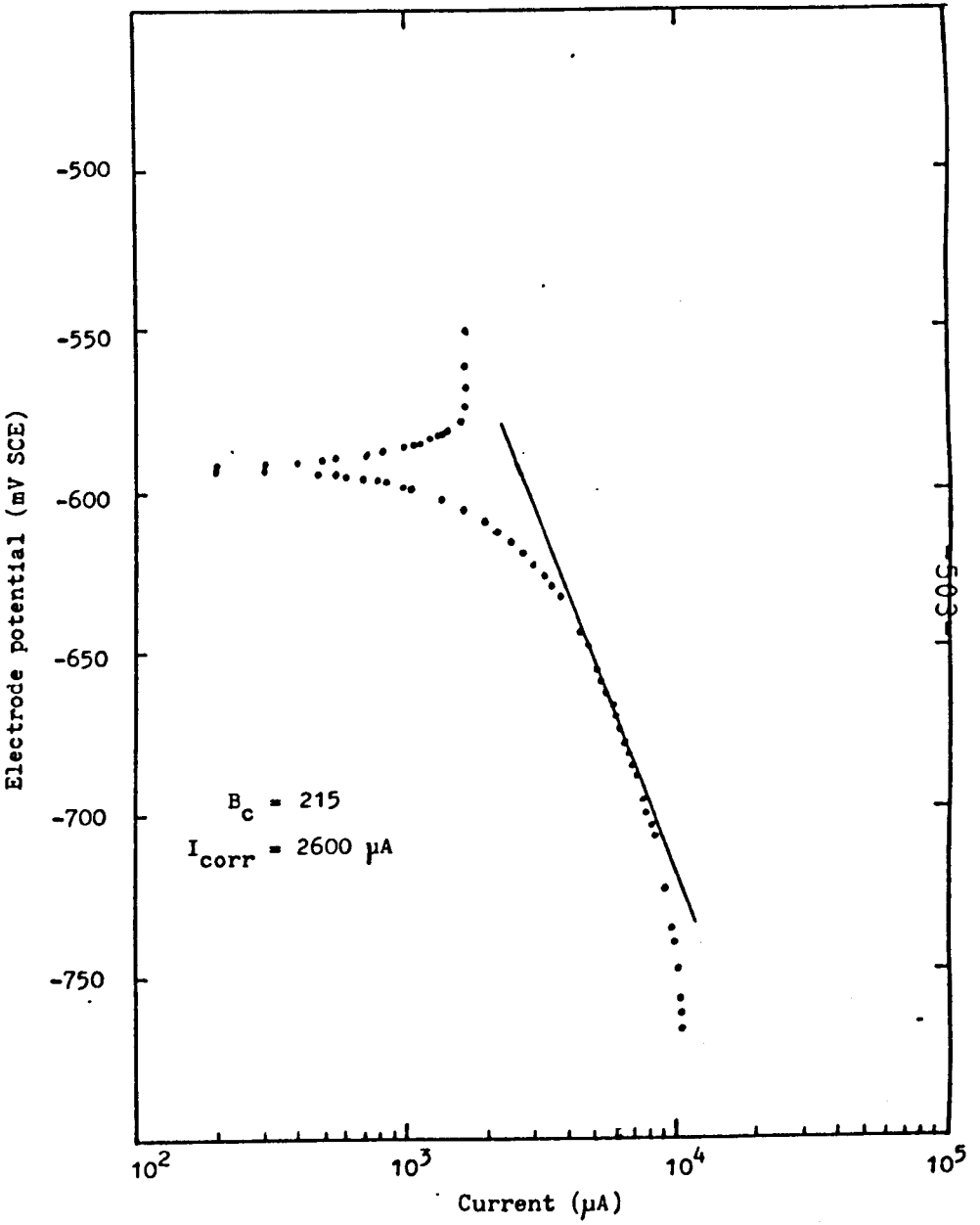

Figure (10-67): Tafel slopes;beam MU70WN,stage IX after 754,600 cycles (3.5 NaCl solution).

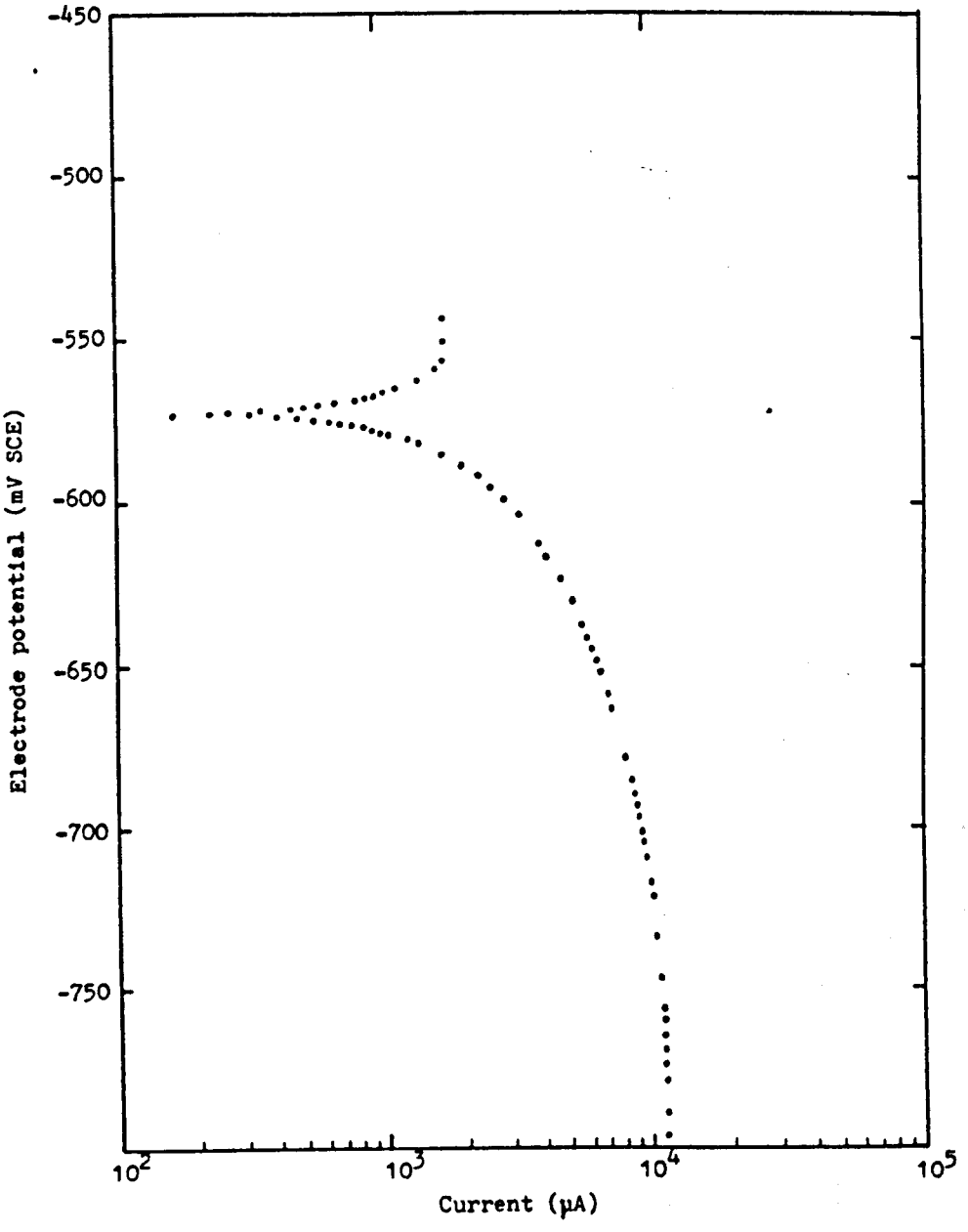

Figure (10-68): Tafel slopes;beam MU7OWN after 1,182,290 cycles in 3.5% NaCL solution.

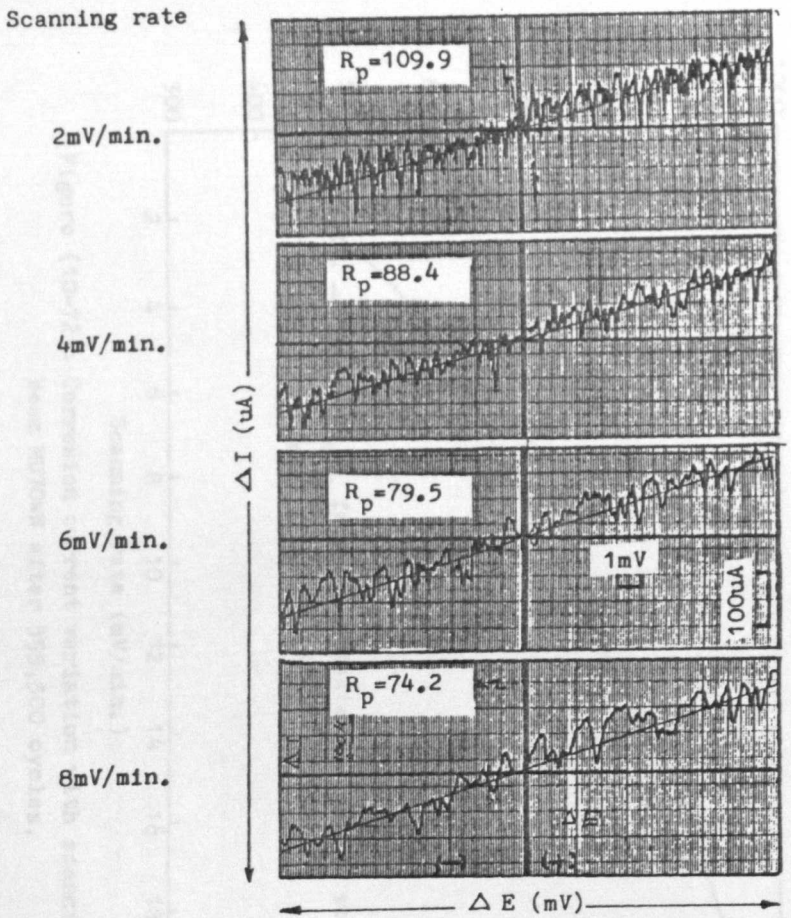

Figure (10-69): E-I relationship at a scanning rate of 2,4,6, and 8mV/min.;beam MU7OWN, stage I,after 595,500 cycles.

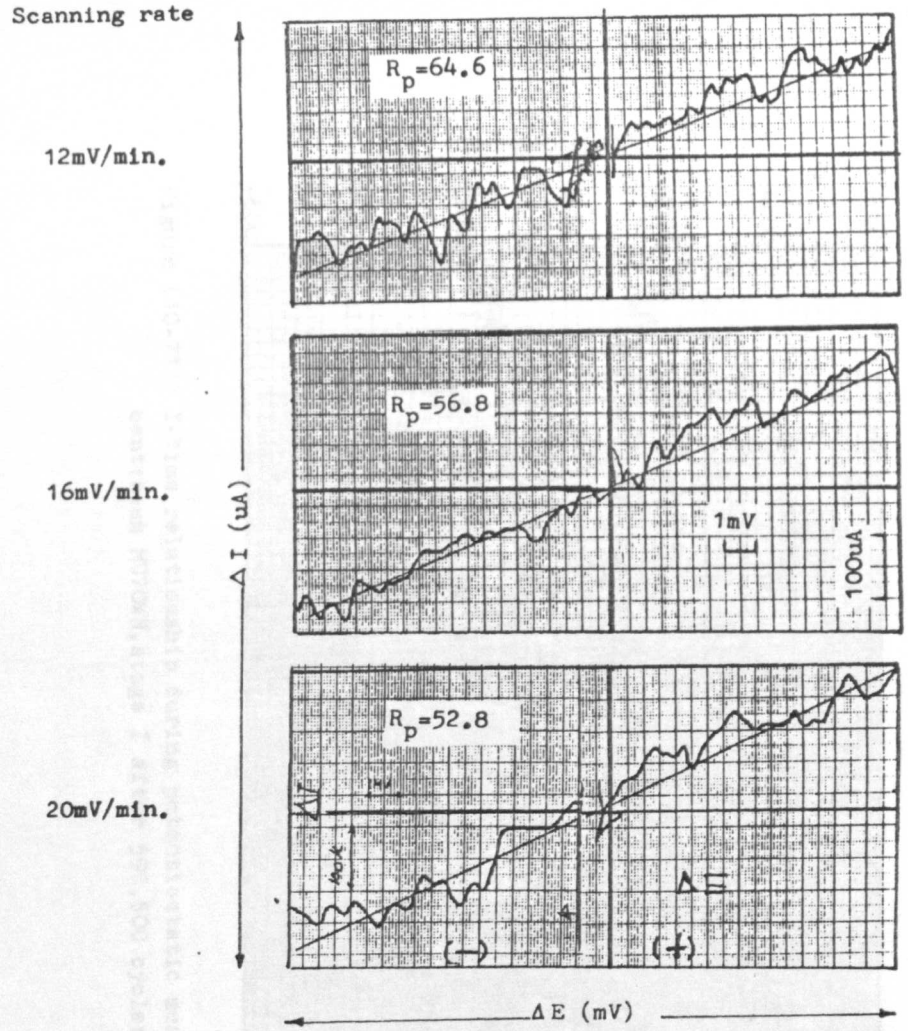

Figure (10-70): E-I relationship at a scanning rate of 12,16 and 20mV/min.;beam MU7OWN,stage I after 595,500 cycles.

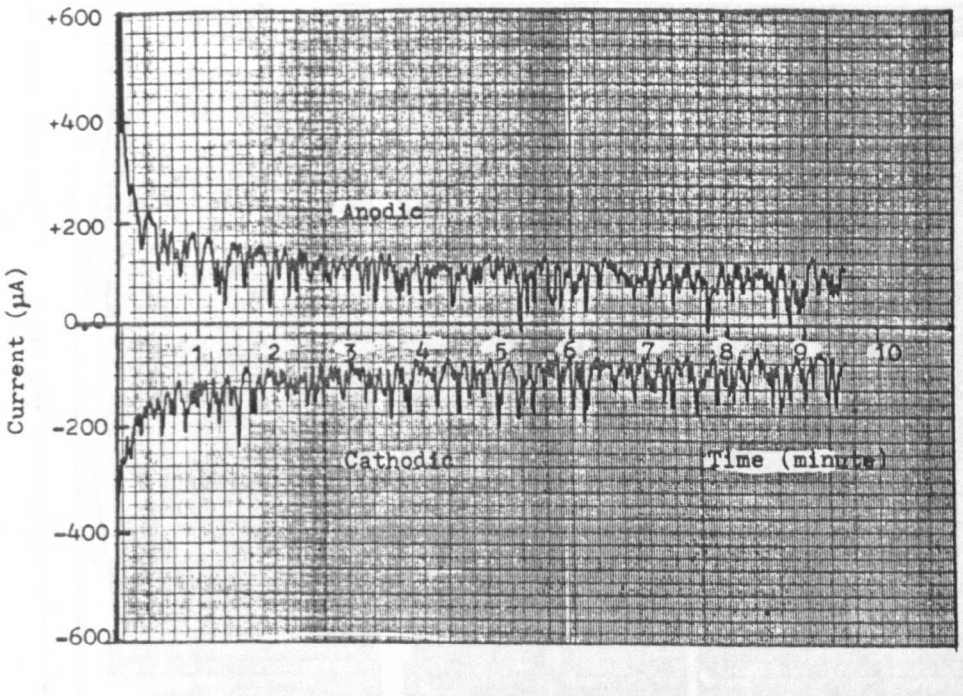

Figure (10-71): I-Time relationship during potentiostatic measurement;beam MU7OWN,stage I after 595,500 cycles.

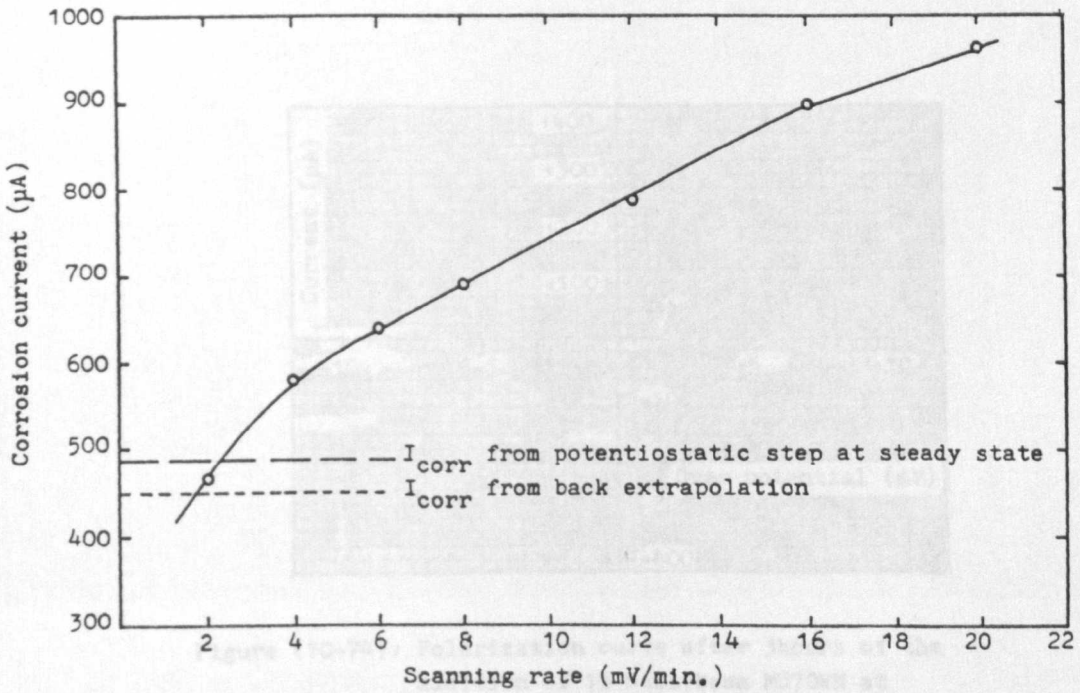

Figure (10-72): Corrosion current variation with scanning rate; beam MU7OWN after 595,500 cycles.

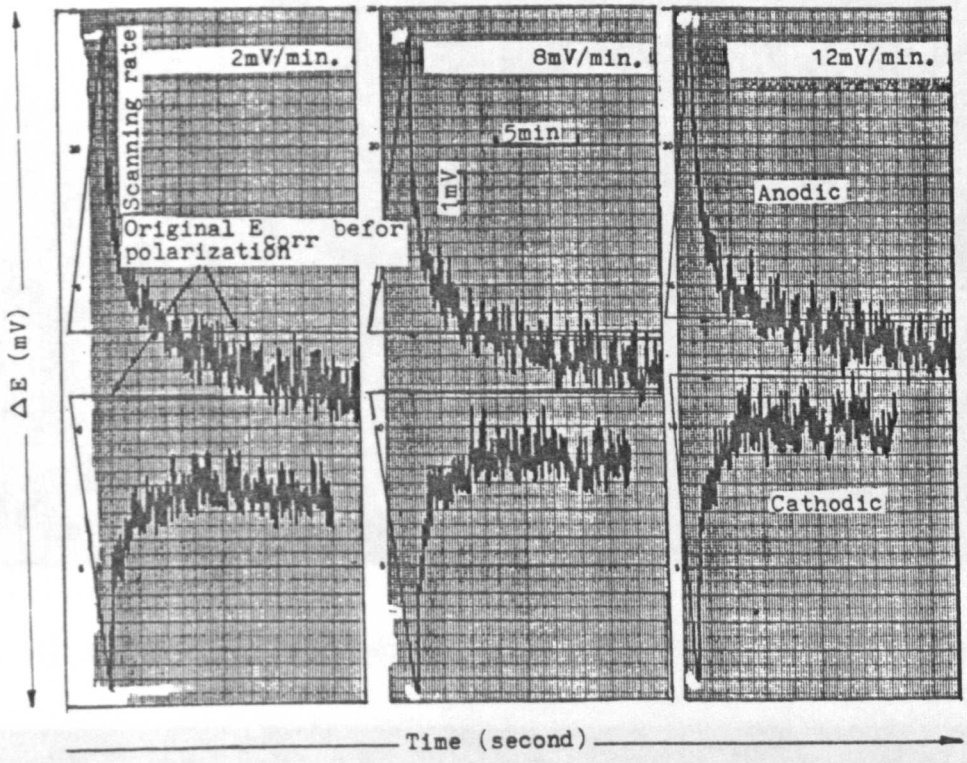

Figure (10-73): E_{corr} recovery after polarization measurement at different scanning rate;beam MU7OWN,stage I after 595,500 cycles.

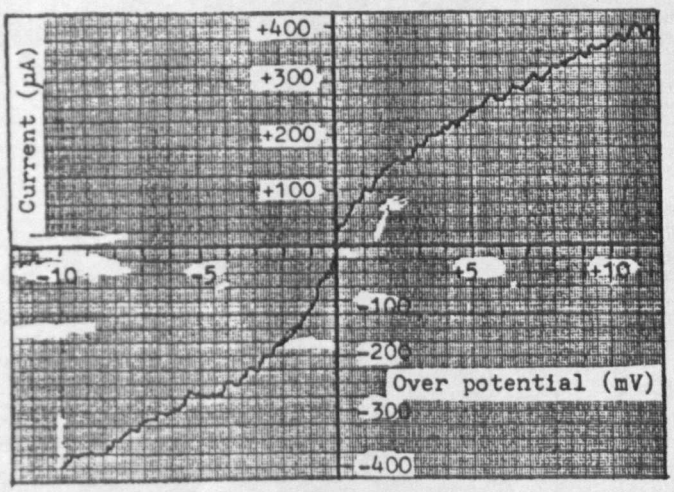

Figure (10-74): Polarization curve after 3hours of the addition of 1% NaCL;beam MU7OWN at 619,800 cycles.

a) corrosion at concrete crack sites (beam MU85W)

b) Black corrosion product (beam MU605N)

Figure (10-75): Corrosion pattern and extend.

a) Beam MU605N

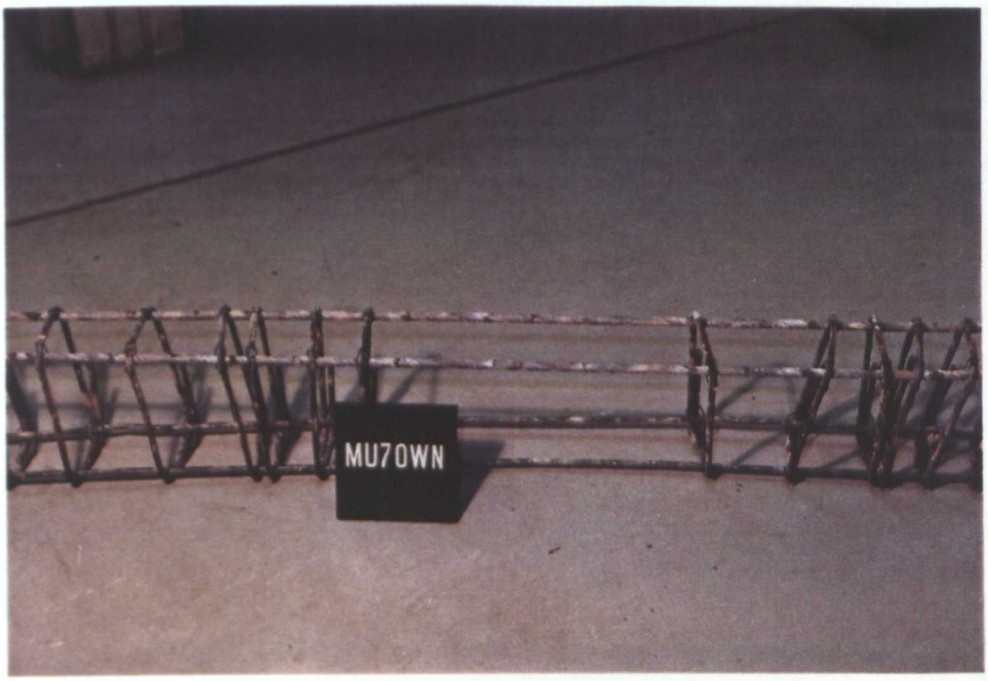

b) Beam MU70WN

Figure (10-76): Localized corrosion on reinforcement cages.

a)

b)

Figure (10-77): Localised corrosion;beam MU605N.

a)

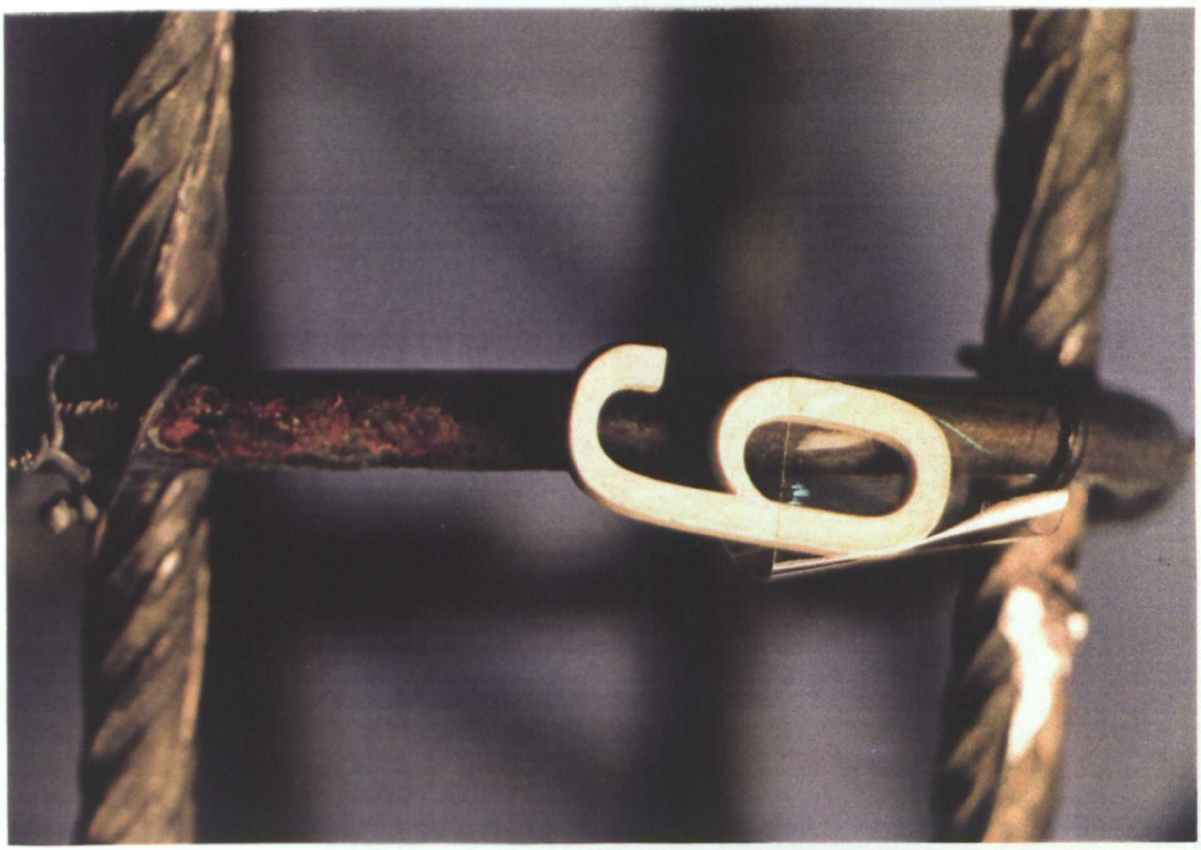

b)

Figure (10-78): Loalised corrosion;beam ML603N.

a)

b)

Figure (10-79): Localised corrosion;beam MU7OWN.

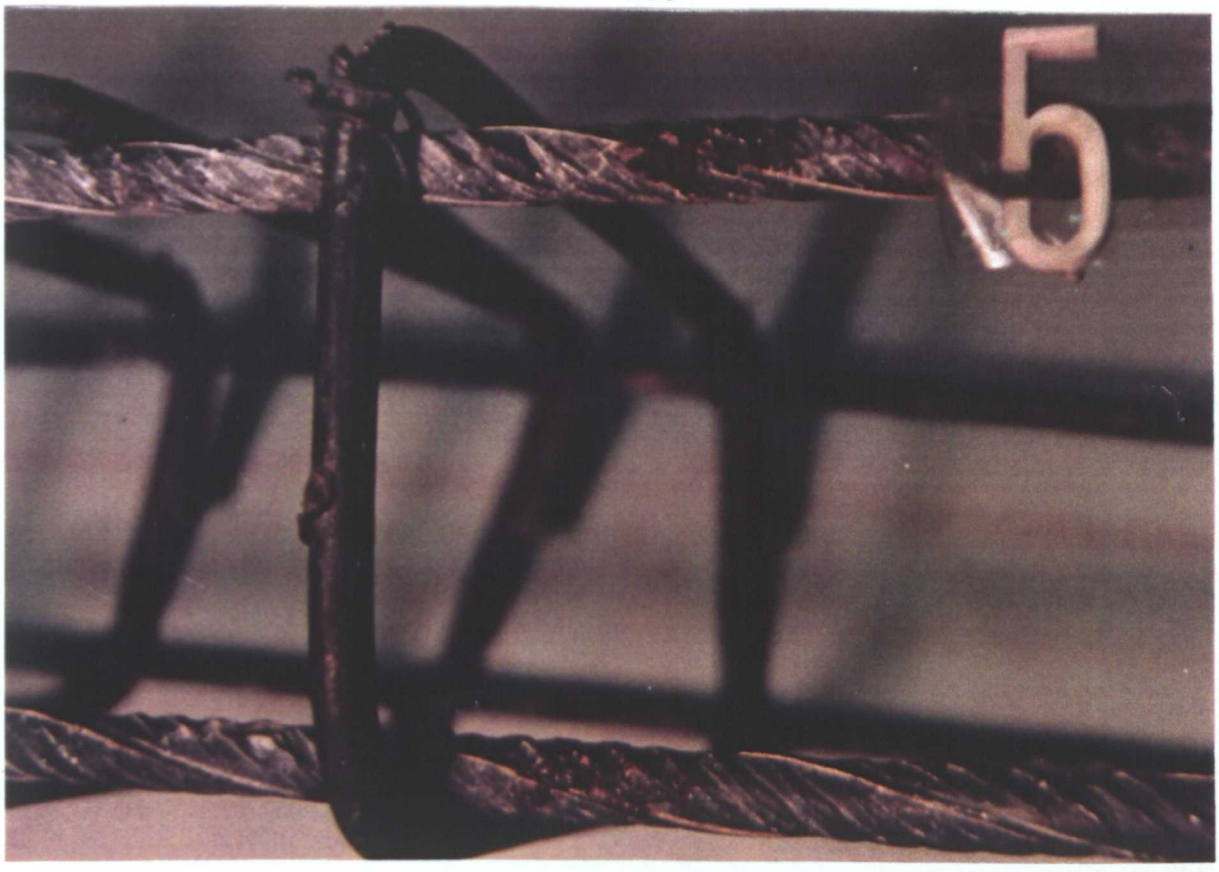

a)

b)

Figure (10-80): Localised corrosion;beam MU605W.

a)

b)

Figure (10-81): Localised corrosion;beam MU405W.

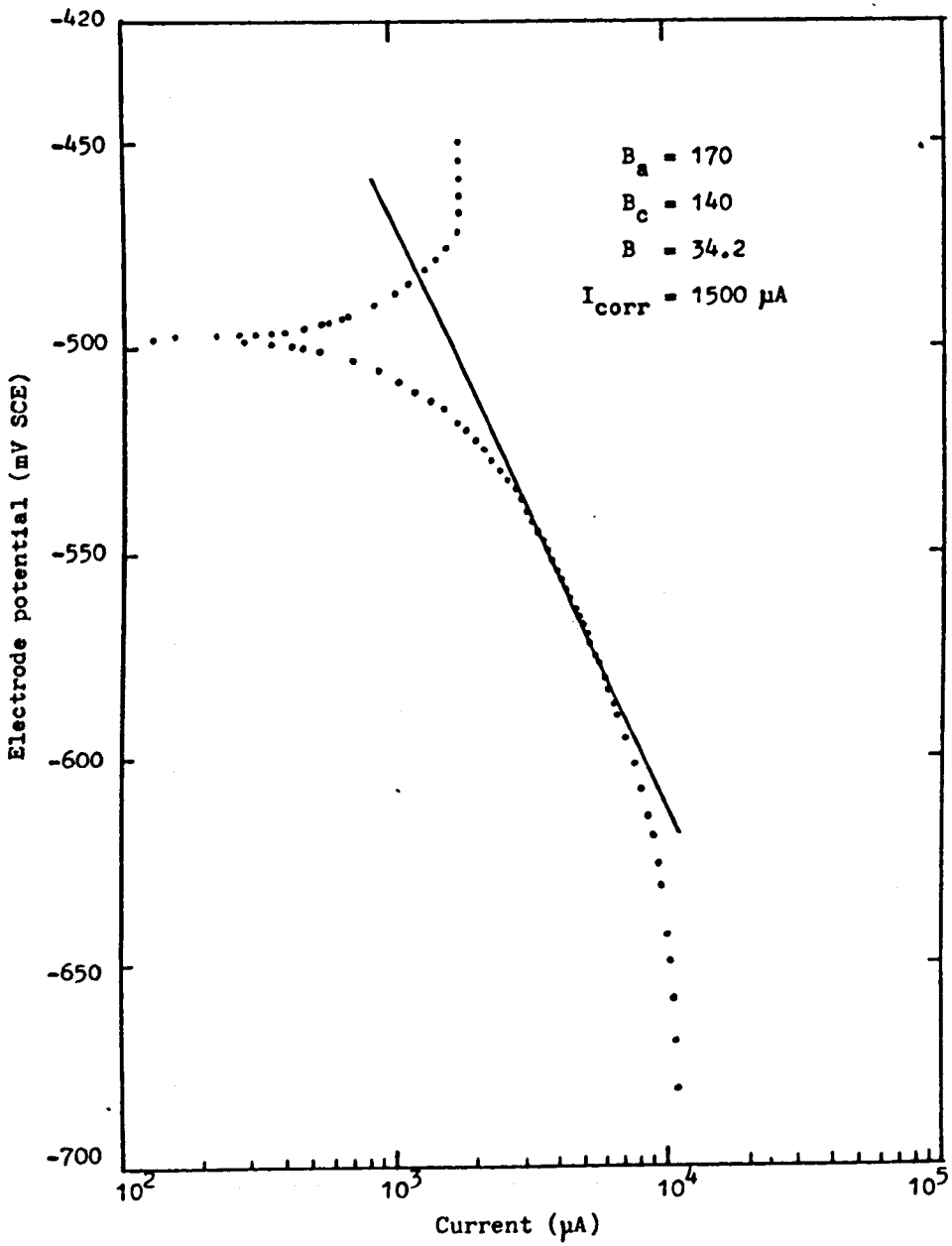

Figure (10-82): Tafel slopes;beam CF103 (long jacket, uni-directional bending).

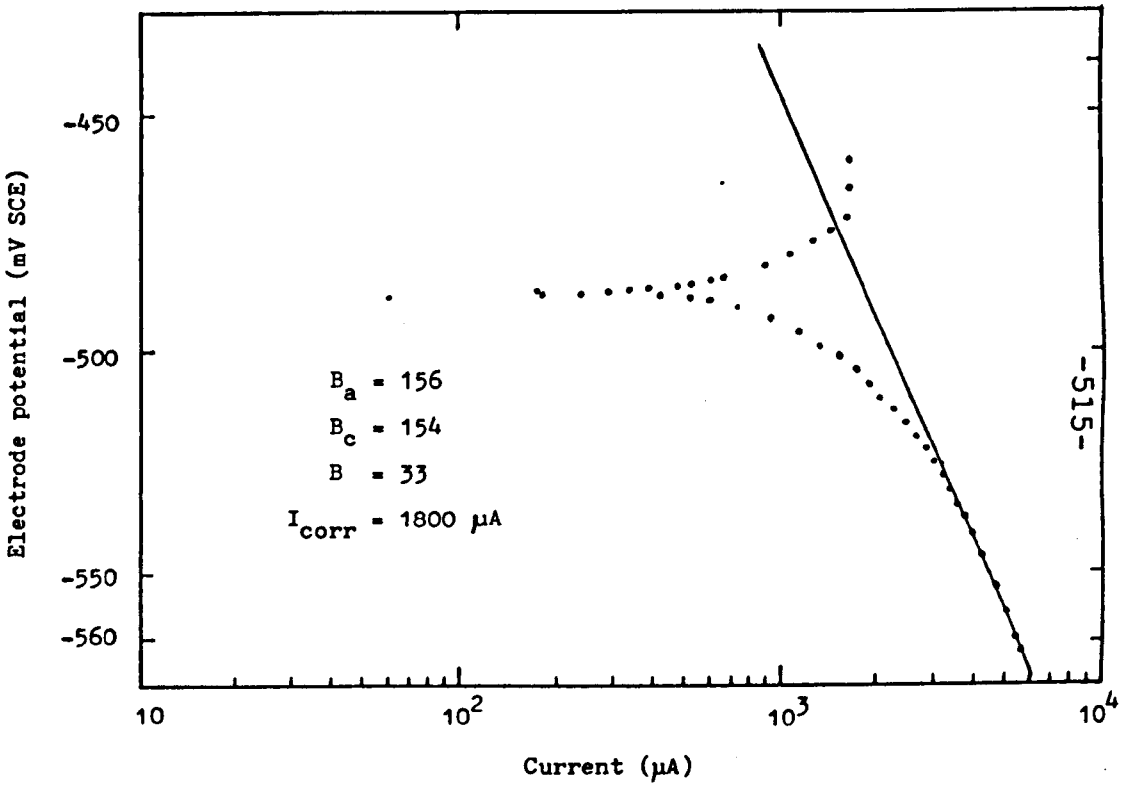

Figure (10-83): Tafel slopes;beam CF100 (long jacket, uni-directional 0.6fy).

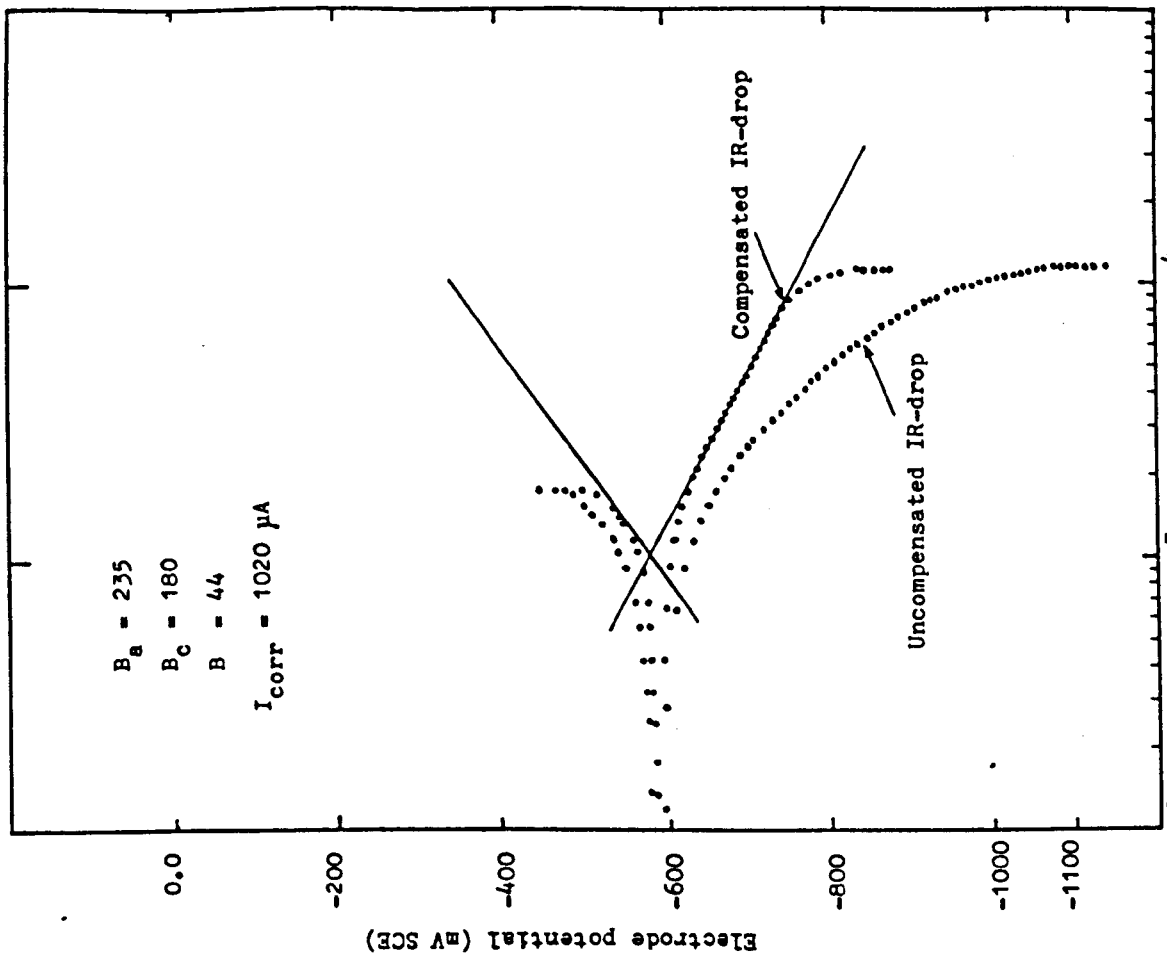

Figure (10-85): Tafel slopes;beam 1TS (totally submerged,reverse bending).

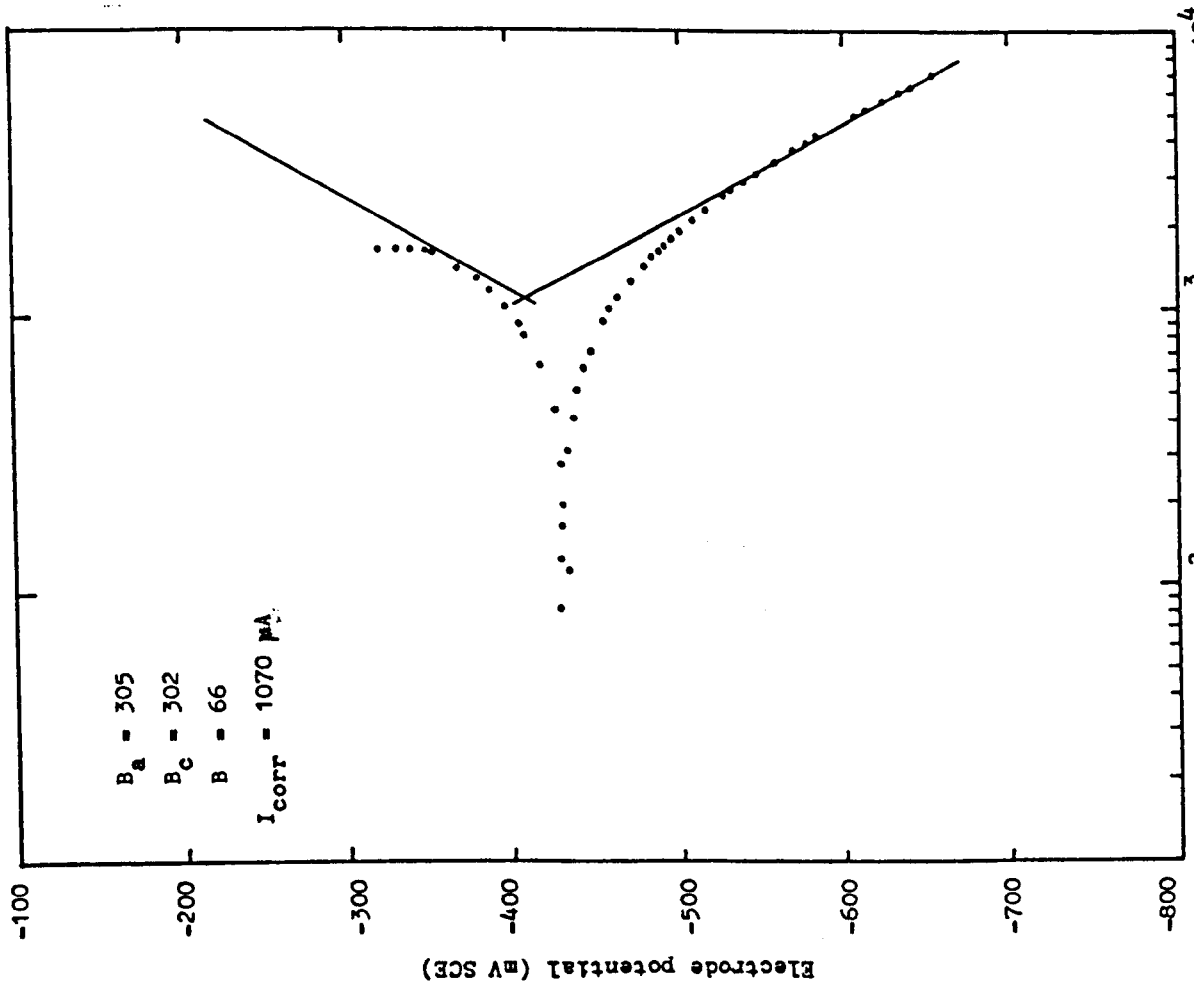

Figure (10-84): Tafel slopes;beam CF144 (long jacket, reverse bending).

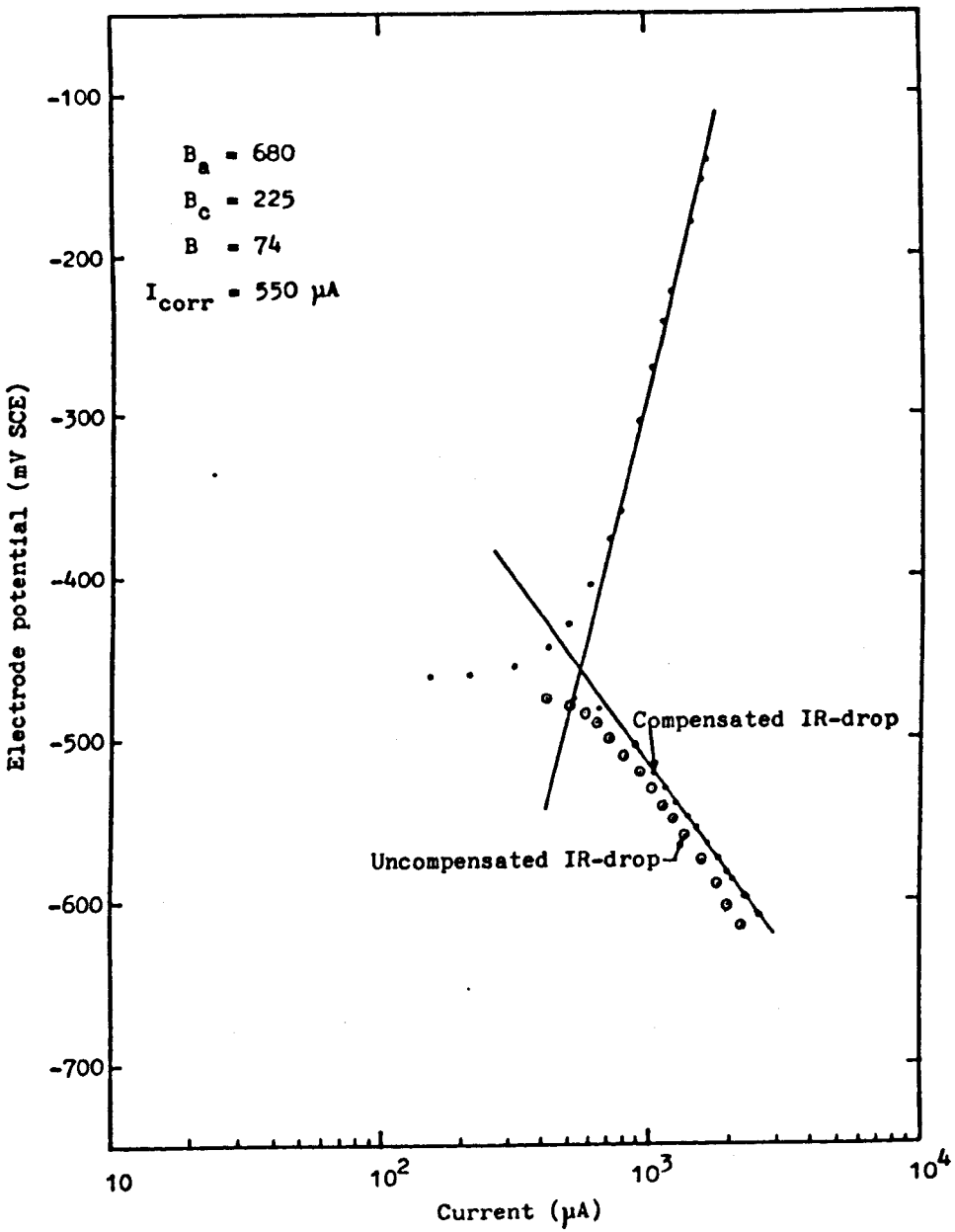

Figure (10-86): Tafel slopes;beam 2TS (totally subm erged without loading).

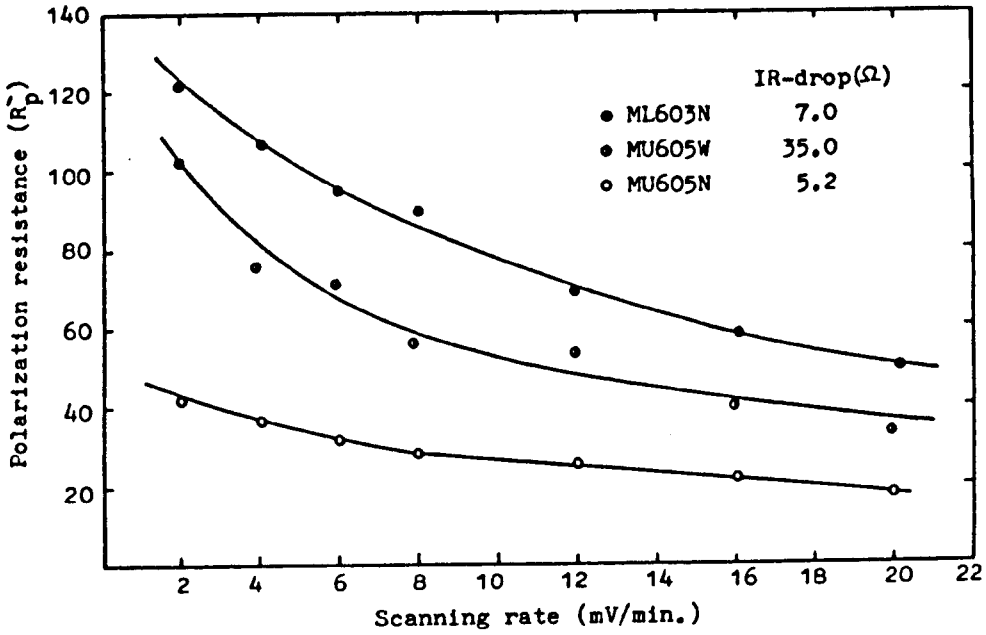

Figure (10-87): The variation of $R_p^{\sim}$ with polarization sweep rate for different test beams.

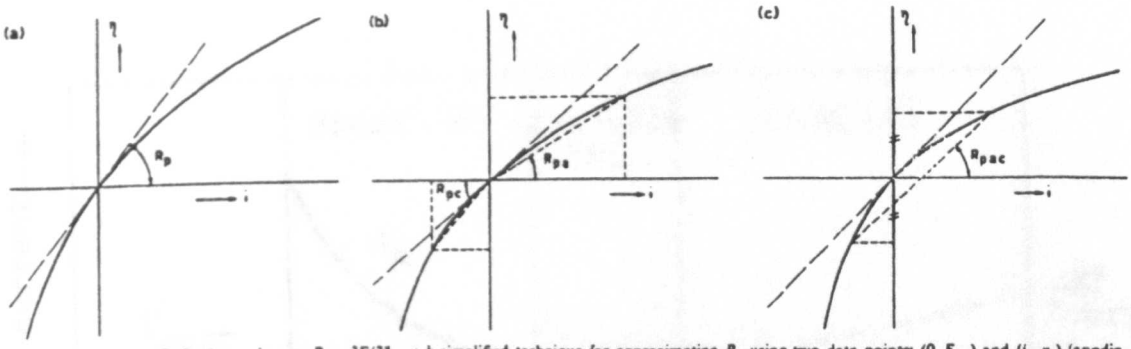

a definition of polarization resistance $R_p = \partial E/\partial i_{E_{corr}}$; *b* simplified technique for approximating R_p using two data points: $(0, E_{corr})$ and (i_a, η_a) (anodic polarization) or (i_c, η_c) (cathodic polarization); depending on shape of curve, different R_p values will be obtained for anodic and cathodic approximations, $R_{p,a}$ and $R_{p,c}$ respectively; *c* same technique as in *b*, but with measurement points arranged symmetrically about E_{corr}, giving improved approximation $R_{p,ac}$

Figure (10-88): Methods of measuring polarization resistance $\tilde{R_p}$ from over-voltage-current curves (Ref.105).

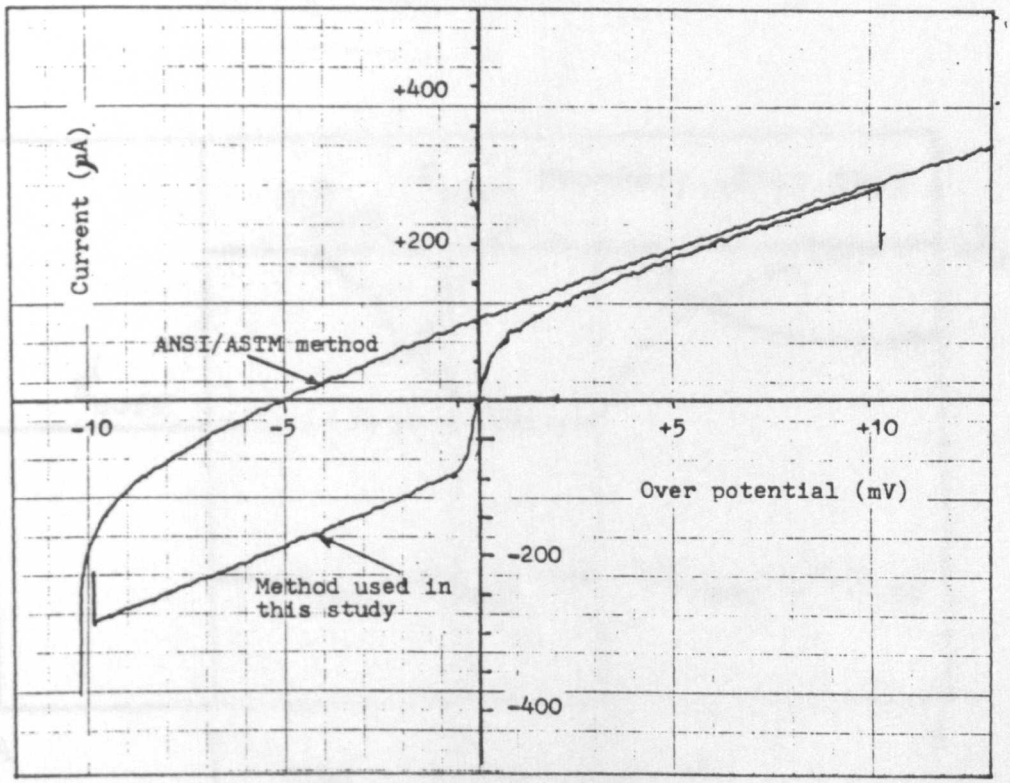

Figure (10-89): Comparison between polarization (E-I) curves obtained according to ANSI/ASTM G59-78 method and the method used in this study (measurements made on beam MU60N7D).

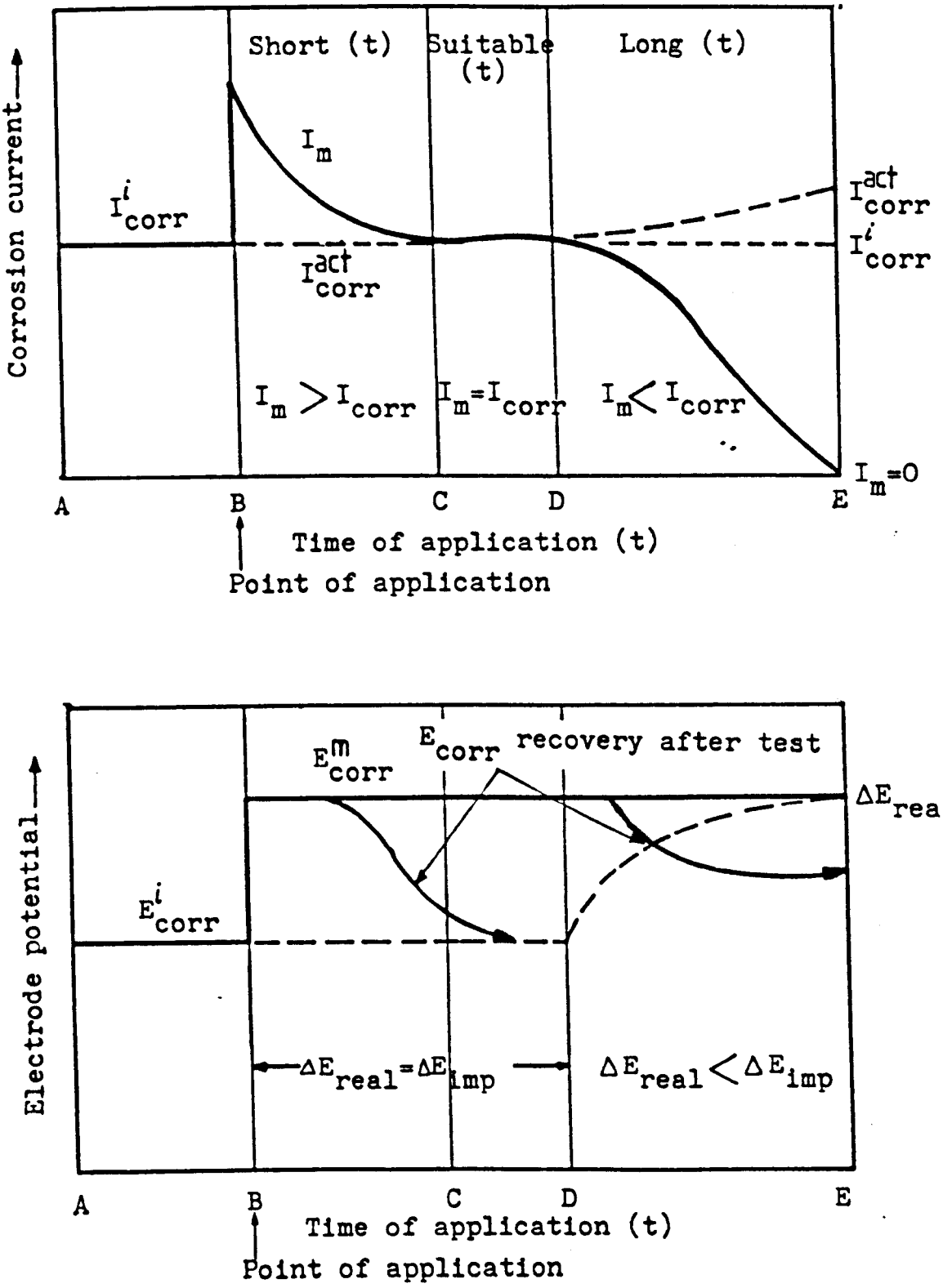

Figure (10-90): Electrochemical chages during potentiostatic measurements.

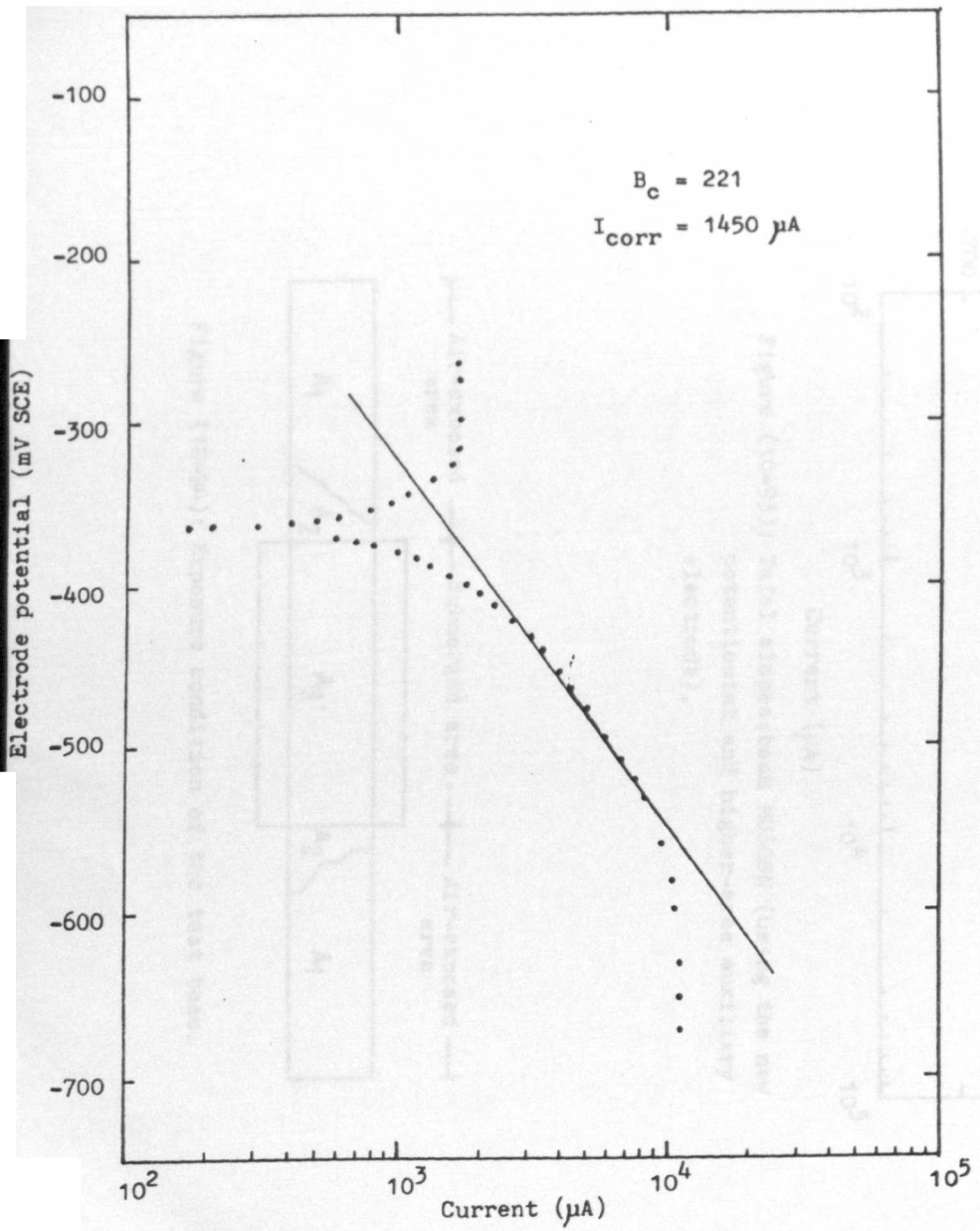

Figure (10-91): Tafel slopes;beam MU608N (using the old potentiostat and higher-area auxiliary electrode).

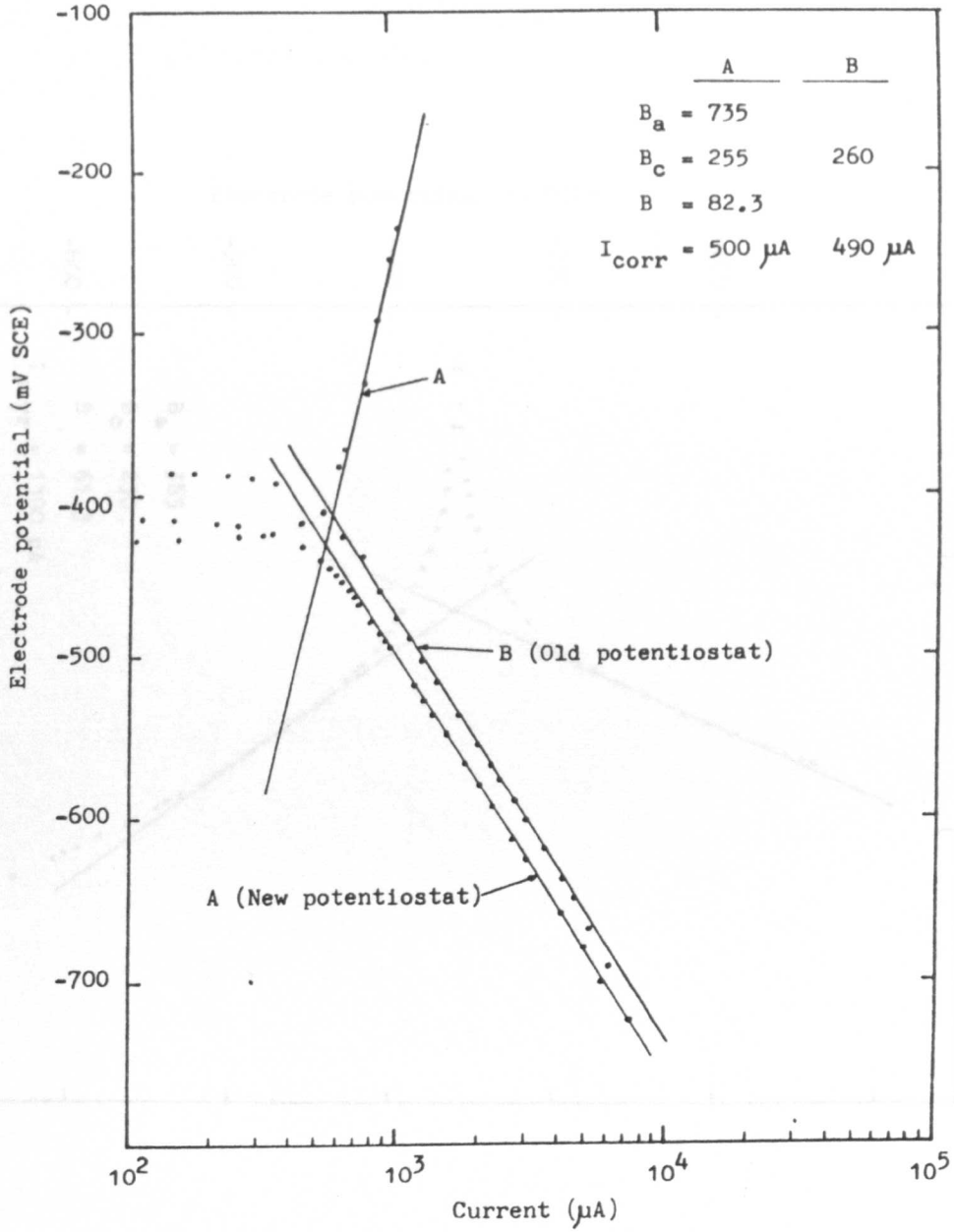

Figure (10-92): Tafel slopes;beam 2TS (obtained on the same date using the new and the old potentiostat).

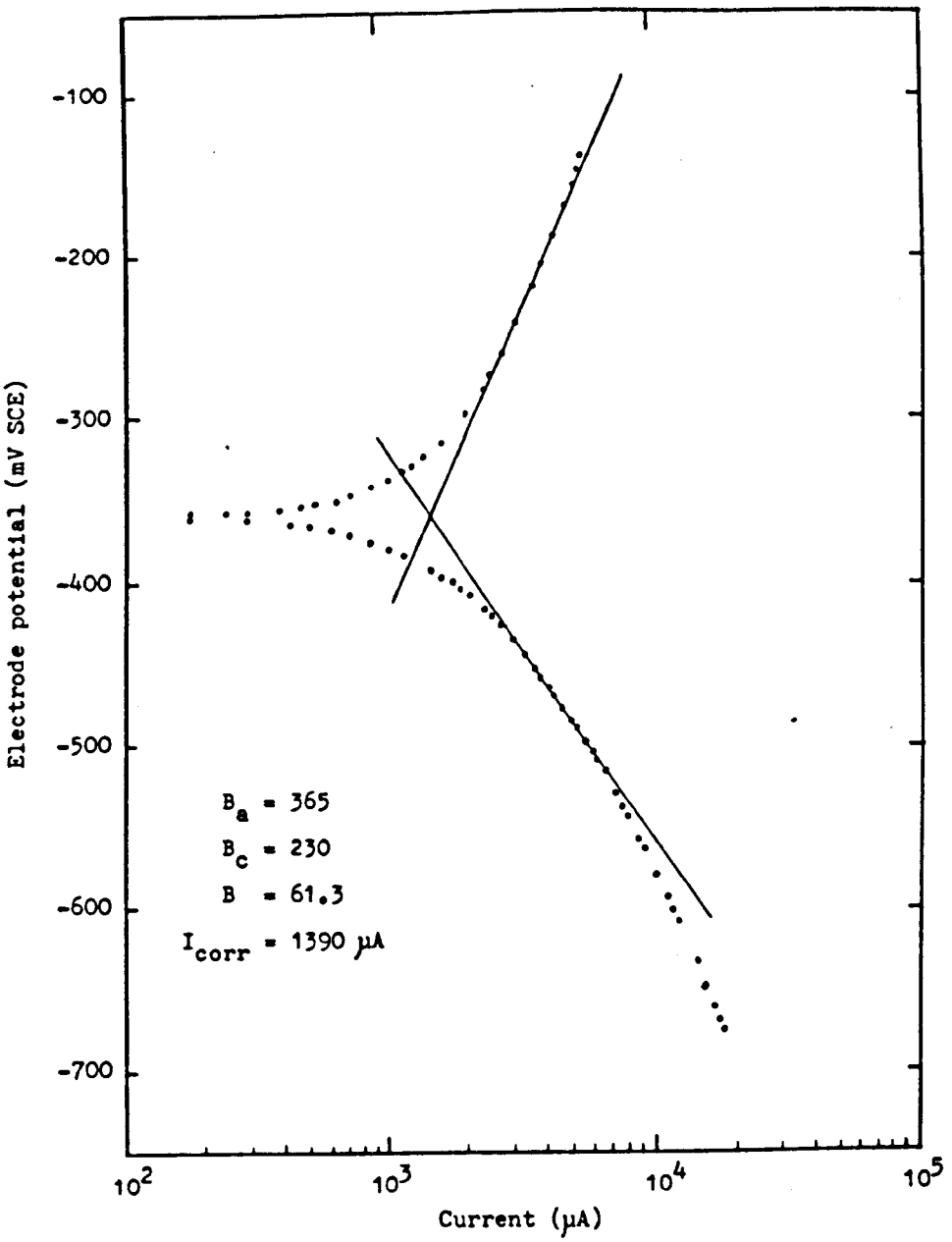

Figure (10-93): Tafel slopes;beam MU608N (using the new potentiostat and higher-area auxiliary electrode).

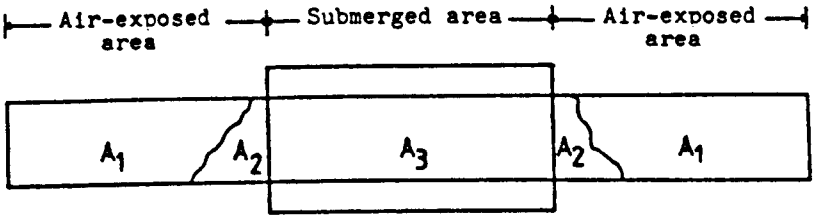

Figure (10-94): Exposure condition of the test beam.

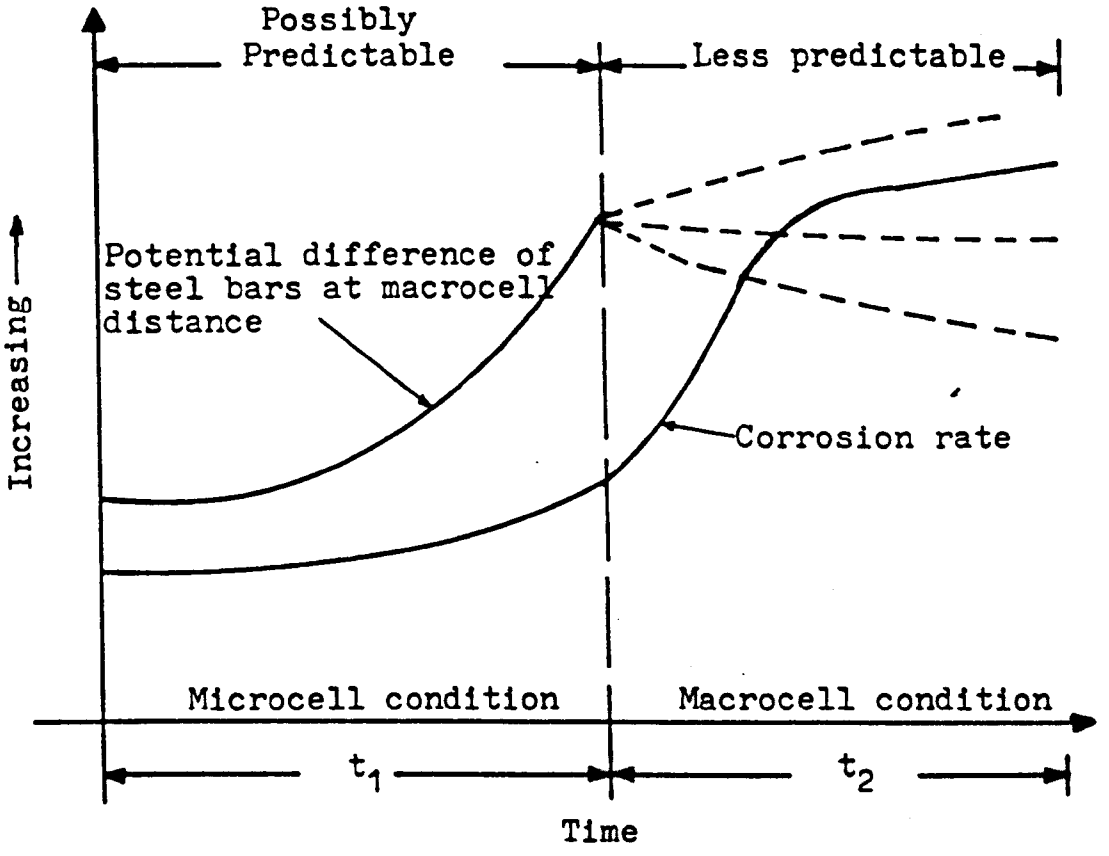

Figure (10-95): Schematic illustration of the possible interplay between the corrosion rate at crack site and the potential difference along the steel bars at macrocell distance.

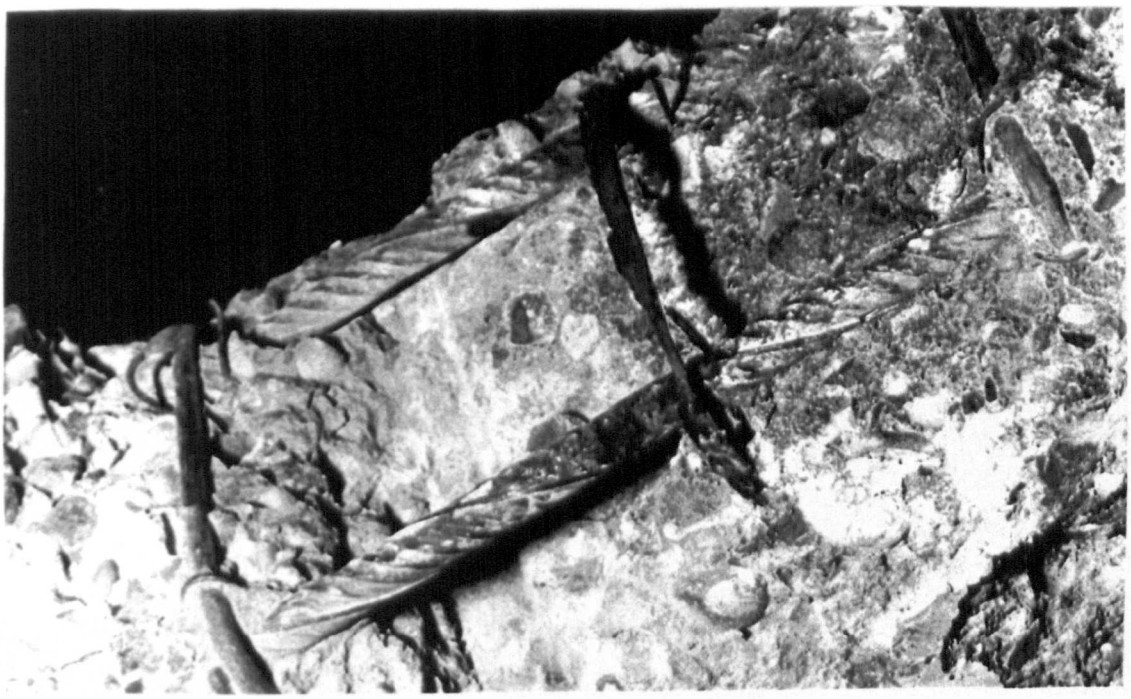

a) Considerable metal loss of shear links

b) Black residue at shear links

Figure (10-96): Beam CF100 seawater test;corrosion pattern.

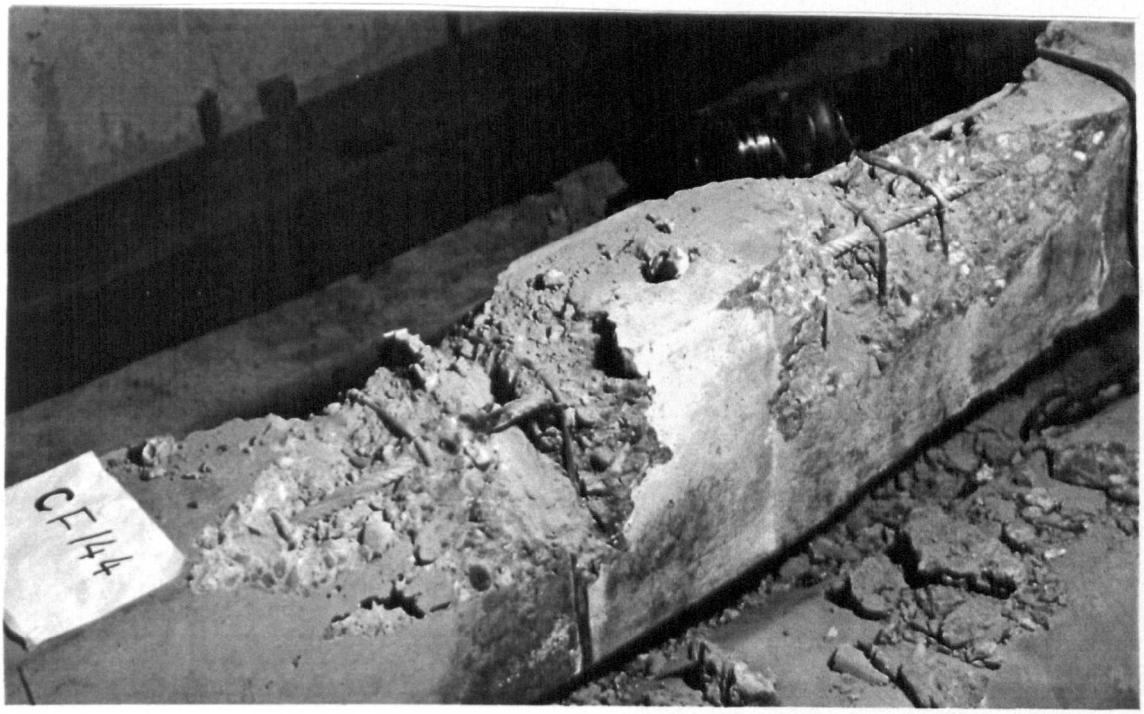

a) General view

b) Metal loss outside the jacket

Figure (10-97): Beam CF144 seawater test;corrosion pattern.

CHAPTER 11

THE PREDICTION OF CORROSION RATES OF STEEL IN CONCRETE FROM ELECTROCHEMICAL NOISE MEASUREMENTS

CHAPTER 11

THE PREDICTION OF CORROSION RATES OF STEEL IN CONCRETE FROM ELECTROCHEMICAL NOISE MEASUREMENTS

11.1 Introduction.

The technique, electrochemical noise measurement (E.C.N.), of which results are described in this chapter was looked at, at a late stage of this research as a possible extension to the main research line. At the time when the measurements actually started, the complex nature of the effect of the test conditions on the accuracy of the measuring technique had already been acknowledged, thus, considering the limited range of test conditions examined by this technique, this part of the work may be regarded as a platform for future investigations. Accordingly the aims of the present work have been:

1. To develop the hardware and a proper software necessary to operate the system for this kind of measurement.

2. To examine the limitations and the applicability of this technique for the system under research, subsequently, possible future development may be proposed.

3. To provide some preliminary indications as to the accuracy of this technique in corrosion rate prediction in complex situations like those in this work.

4. Perhaps more importantly, to establish guide lines for future work and areas requiring further investigation.

The results, however, showed some interesting indications, some of which, rather surprisingly, question some basic assumptions upon which this technique has been based. These along with other important aspects of this work will be presented in the following.

11.2 Literature Review.

Following the difficulties involved in the determination of corrosion rates using conventional polarisation measurements and potential mapping techniques (described in Section 3.3.9), attempts to introduce novel non-destructive methods for the determination of corrosion behaviour of steel embedded in reinforced concrete have resulted in some degree of success using the electrochemical noise measurement[111] technique. Results obtained by previous research workers have shown that metal-electrolyte systems exhibit spontaneous fluctuations of potential and current. These fluctuations may result from thermal agitation of charge carriers, drift from changes in environmental factors[111,232,233] and transient change in the random electrochemical process on the metal during corrosion such as the formation and repassivation of pits,[163,234] Most of the earlier studies have been concerned with noise measurements on metal/solution systems. These studies revealed that it is possible to monitor and describe the mechanism of corrosion of systems undergoing pitting and crevice corrosion by sensitive monitoring of the electrode potential.

Hladky and Dawson[232] observed bursts of noisein sensitive plots of electrode potential as a result of chloride attack and subsequent formation of visible pits, Figure 11.1a,b. Bertocci[235,236] studied the corrosion process using spectral analysis of the corrosion current and noted a relationship between the measured noise power and noise frequency for the test electrode. Using the same

technique, Hladky and Dawson[233] also observed a correlation between the nature of the corrosion attack and the low frequency fluctuation of the electrode potential. They also observed that the r.m.s. of noise amplitude is independent of the geometry and the area of the corroding electrode, in other words the r.m.s. seems to qualitatively relate to the actual penetration rate, independent of the magnitude of the area under attack.

On the other hand, a survey of literature reveals that only limited amounts of data are available on the use of this technique in the field of reinforced concrete. Research at UMIST[111] has been concerned with measurements and analysis of potential noise using spectral and statistical analysis. The work revealed the existence of a relationship between the standard deviation or r.m.s. and the rate of corrosion. The noise measurements were made either between two lengths of bar of electrodes cast into the sample or between the steel and an external reference electrode, the latter being more appropriate for larger structures. Tests on chloride contaminated and uncontaminated prisms show different type of potential fluctuation in that the contaminated concrete sustained a series of 'glitches' which were considered to be a feature of corroding electrodes undergoing pitting. Although both type of concrete exhibited similar noise spectra as shown in Figure 11.2a,b, the slope of 1/f electrochemical noise plot was different with lower slope being associated with active corrosion. Analysing electrochemical data in terms of their S.D. or r.m.s. requires less calculation and is easier for comparison purposes between different set of data, and was thus considered by the authors[111] preferable to the use of spectral density plots. Corrosion inspection on reinforced concrete walls containing water of a swimming pool showed good prediction of corrosion rate using electrochemical noise technique whereas potential mapping indicated only the potential area of corrosion risk. It was inferred therefore that, for real structures, the latter method may be restricted to use in identifying the likely regions of corrosion prior to corrosion rate determination by noise techniques.

More recently, Page and Lambert[163] carried out noise measurements on a large number of steel electrodes embedded in cement paste and concrete exposed to external source of chloride ions. Each noise measurement was followed by a measurement of corrosion rate by linear polarisation method. The results show clear linear logarithmic relationship, Figure 11.3, between corrosion rate and standard deviation of electrochemical noise of the form:

$$LOG_{10}I = 0.171 + 0.823\ LOG_{10}\ S.D. \qquad \ldots\ 11.1$$

Using this relationship it was possible to obtain predicted values of corrosion rate within a factor of 10 of the actual corrosion rate for low to moderate corrosion rates, but, for higher rate of corrosion there was a tendency for the relationship to underestimate I_{corr} and the accuracy dropped to within a factor of 100. It should be pointed out, however, that similar degree of accuracy was obtained from I_{corr}-E_{corr} plot.

The form of noise trace was found to be directly associated with corrosion rate. Distinctive trace was obtained from passive steel starting to corrode, such specimens exhibited sudden 'glitches' similar to those reported in UMIST work, they ascribed this behaviour to the formation and slow repassivation of single pits. In addition, the empirical representation (Equation 11.1) obtained earlier was employed to estimate the corrosion rate for a large reinforced concrete slab under saturated conditions in conjunction with potential mapping. The results showed sensible trends with the values of E_{corr} and together clearly identified the position of local anodic areas.

In their recent publication, Hardon, Lambert and Page[234] reported 3-part experimental research. In part 1 they examined the possible relationship between the standard deviation of noise and the corrosion current of steel reinforcement embedded in small cement paste and

concrete slabs. Part 2 investigates the relationship between S.D. and macrocell corrosion current in specimens of multiple segment designed to permit measurements of galvanic current between different regions of embedded steel having different amount of chloride concentration (Part 2). In part 3, the relationships were employed to evaluate corrosion rates of steel in a large concrete slab containing an area of chloride ions contamination. The results of part 1 and 3 were essentially similar to those reported earlier from Reference 163. In part 2, measurements on individual segments and external S.C.E. followed the same trend observed in part 1 of the investigation. However measurements on individual segments against adjacent segment of lower chloride concentration or between individual segments and all the remaining segment in an environment of low chloride concentration showed relationship dependent on the value of the galvanic current, I_{galv}. For higher values of I_{galv} where clear distinction between anodic and cathodic areas would be expected, the corrosion rate can be predicted as accurately as from measurements of noise between steel and reference electrode. At the lower values of I_{galv} where there is little difference in corrosion intensity between the two parts of the couple, the relationship is no longer clearly defined.

Attempts to obtain current noise data by measuring fluctuation in the galvanic current were unsuccessful owing to the low amplitude of these fluctuations not resolvable with the used measuring equipment. The selection of a suitable type of reference electrode is an important factor in noise measurements. Since electrodes susceptible to external interference will directly influence the shape and the amplitude of the fluctuation signals. Previous studies[111,163,232] based on experience and blank tests, have shown that saturated calomel electrode (S.C.E.) is the most suitable reference electrode as it generates less noise and drift than both copper/copper sulphate electrode and silver/silver chloride electrode and is not sensitive to photovoltaic effects.

11.3 Instrumentation.

The hardware employed for the measurement of electrochemical noise on the corrosion potential consist of a high impedance-high resolution voltmeter (Thurlby 1905a), a BBC microcomputer and an output chart recorder. The voltmeter was linked to the microcomputer by means of RS232-type interface, the chart recorder was connected in series with the voltmeter. Due to high sensitivity required for the detection of noise fluctuation, the signals were amplified before reaching the plotter by a high impedance ($10^{13}\Omega$) amplifier specially built for this purpose. The block diagram of measuring instrumentation is shown in Figure 11.4.

The microcomputer controls the rate of sampling and the length of measuring time, it also carried out the necessary statistical calculations at the required intervals and stores them on a tape recorder. The necessary software to run the system has been developed which enables 4000 readings to be taken at a required interval (multiple of 0.333 sec), calculating the S.D. at any pre-selected interval and the results to be printed out, including the potential data, in a form shown in Table 11.1a and b. A saturated calomel electrode was used through out the tests.

The procedure for obtaining ECN data consisted of monitoring the corrosion potential of the reinforcement vs. SCE for a period of 2000 sec (4000 in rare cases) with sampling intervals of 3 x 0.333 sec and analysis of the data in terms of S.D. after each 250 readings. Simultaneous E_{corr} against time plots using the chart recorder was obtained when required. The results were displayed on the microcomputer screen and printed out on completion of each measurement.

11.4 Results.

Electrochemical noise measurements have mainly been made on beam MU60N8Y. Due to the constraint of time and

in order to obtain results from apparently variable degrees of corrosion activity, the beam was fatigue tested under incrementally increased maximum load with constant minimum load. To widen the range of test conditions examined by this technique, some potential noise measurements were also made on other three beams which were concurrently under test. These beams are MU60N7D, MU60N1Y and MNS00N, apart from the last beam (with no links) all other beams were of identical overall details but different in loading history. Each noise measurement has been followed by a measurement of the corrosion rate by linear polarisation method (10 mV anodic step for 10 minutes). For beams under fatigue loading the noise measurements were determined both during cycling and with an average load being applied statically. Fluctuations in the potential were monitored at intervals of ~1 sec for a period of 2000 sec and 4000 sec in rare cases.

11.4.1 The Form of Potential Noise Traces.

The form of potential noise obtained for various conditions are shown in Figures 11.5 and 11.6. These figures also indicate the respective corrosion current at the time of measurement. The potential monitoring results presented here were made with the average load applied statically. Before the measurements, it was necessary to allow some time, typically 5 to 10 minutes, for E_{corr} to settle, otherwise it was observed that the potential trace, the initial portion in particular, exhibited linear drift of a few millivolts to more positive values (especially for the case when measurements were being taken statically after a period of cycling). The potential traces presented in these figures suggest a close relationship between the form of the trace and the corrosion state as expressed in terms of corrosion current. At low corrosion rate, Figure 11.5a,b the potential trace consists mainly of low amplitude-high frequency fluctuation, whereas moderate corrosion rate Figure 11.6 exhibited high amplitude-high frequency fluctuation with a series of "glitches" in a form of drops

of up to two-hundredth of millivolt followed by persistent recovery. The drops and recoveries were either sudden or of slow exponential form. This kind of behaviour is usually associated with pits formation[163-234] of electrodes in passive state. Beams sustaining higher corrosion rate, however, have shown waving form of high amplitude-high frequency fluctuation as shown in Figure 11.6b.

11.4.2 Cyclic vs. Static S.D. for Reinforced Concrete Beams Under Fatigue Loading.

To establish the effect of loading conditions on E.C.N. measurements, a complete noise measurement for beams under fatigue loading involves the determination of S.D. value firstly without changing the loading condition, i.e. under cyclic loading followed by a second measurements with an average load applied statically. It was observed, provided that the measurements are made at stable E_{corr}, that both measurements yielded exactly identical values of S.D. The relationship between cyclic and static S.C. for measurements obtained form MU60N8Y is diagrammed in Figure 11.7 which clearly shows a straight line of 45^{o} slope passing through all the data points with almost negligible scatter. This type of relationship was also observed in all other measurements made on beams under cyclic loading, compare for example Tables 11.1a and 11.1b for beam MU60N1Y, regardless of other test variables such as load level, time under test, beam age...etc.

This in turn, implies, from the experimental point of view, that it is possible to obtain S.D. values with equally good results without the need to modify the loading condition in line with earlier observations on polarisation measurements described in Chapter 10. Further, the results suggest that the interruption of cyclic loading by short period (~1 hr) of static loading is not likely to cause any change in the corrosion activities. In this context, experimental evidence is still required to identify more extensively the effect of rest periods including the length of such periods.

11.4.3 Effect of Period of Measurement on the Accuracy of S.D.-I_{corr} Relationship.

The values of S.D. of the potential noise were found to be changing approximately exponentially with period of measurement as illustrated in Figure 11.8. It can be seen that for a given measurement the rate of change of S.Ds were clearly decreasing at longer ECN sampling times and this is, most likely, due to the mathematical feature of standard deviation estimation. However, despite the complicating feature of S.D. sampling time variation, it is interesting to note that, for a given ECN sampling time, there appeared to be a constant relationship between S.D. of the potential noise and Icorr determined by linear polarisation method. This is shown on a coarse scale for 3 sampling periods on Figure 11.9 which clearly indicates that various periods of measurements have produced identical shaped S.D. curves. These curves were only different in their positions with respect to the y-axis which effectively means that this variable (sampling time) appears to have little or no effect on the accuracy of I_{corr}-S.D. relationship. Therefore, if the later relationship is linear, then the ECN measuring time effect would only change the constant value of the equation whereas the slope of the line remains the same.

11.4.4 The Prediction of Corrosion Rates from Electrochemical Noise Data.

Attempts to cover a wider range of corrosion activity by the incremental increase of the maximum applied load on beam MU60N8Y have not been achieved owing mainly to the reasons given in Chapter 10. Consequently, the I_{corr}-S.D. relationship given in Figure 11.10 exhibits unfilled gaps even though the figure contains results from other different beams of different loading conditions. The limited range of data has not, obviously, necessitated the presentation of data on log-log or linear-log fashion. Perhaps the only sensible conclusion which can safely be

drawn from these data is that S.D. of the potential noise increases as the I_{corr} increases. Nevertheless, despite the inconclusive nature of the global picture presented in Figure 11.10 closer inspections of individual sets of data have revealed some interesting results as to the possible correlation between different parameters as described in the following.

Continuous monitoring of I_{corr}, S.D. and E_{corr} for beam MU60N8Y are presented in Figure 11.11. The scales of the individual curves of this figure were chosen such that the small change in these parameters can more easily be observed.

It should be noted that the E_{corr} scale has been inverted so that its change with respect to the remaining parameters may be more clearly seen. The figure indicates high sensitivity to I_{corr} change in both S.D. and E_{corr} with very similar shapes suggesting a possible existence of relationships relating each one to the others. Thus individual relationships between I_{corr}-S.D. and I_{corr}-E_{corr} were examined and presented in stretched scale in Figures 11.12 and 11.13 respectively. From both figures I_{corr} can be predicted within approximately $\pm$30% of the real value (based on polarisation measurements). However, a curve relating S.D. to E_{corr}, for beam MU60N8Y, Figure 11.14, yielded particularly interesting results in that it was possible to draw a straight line connecting all the data point, line A in Figure 11.14. There was also evidence that this relationship is also valid for other different systems, although presented by small number of data point, as shown in line B of this figure which represents beam MU60N7D. The unique relationship observed between S.D. and E_{corr} indicates that exactly equal accuracy can be achieved in predicting I_{corr} by either method.

11.5 Discussion.

During the last decade, efforts to develop an electrochemical monitoring technique for on-site investigation of reinforced concrete structures have been

confronted with tremendous difficulties. These efforts were mainly concentrated on the development of laboratory-based techniques used for studies on relatively small, well isolated and quality controlled reinforced concrete specimens. Certainly, as yet, the use of corrosion potential mapping has been the most successful process in providing an insight into the electrochemical condition of the embedded reinforcement in practice and, hence, became a basis for the appraisal, rehabilitation and repair processes. It has been pointed out in Chapter 3 that although potential measurements are quick and easy, the main shortcoming has been the inability to obtain direct corrosion rate readily. However, the use of ECN technique has recently been introduced in the field of reinforced concrete. This technique is based on the possible experimental correlation between the actual penetration rate[233] and the S.D. of the noise of the electrode potentials independent of the magnitude of the area under attack. Some, although limited, successful applications in laboratory and on real structures have stimulated further research activities to explore the possible utilisation of this technique as a tool to provide quantification of the corrosion process and an indication of the pitting corrosion.

As usual with any new application, some researches[111,232,233] have, understandingly expressed their enthusiasm to the potential use of this technique in the area of reinforced concrete. Nevertheless, there is still a lot of work to be done before the technique is widely recognised as a practical and accurate one. In fact some investigations including the present one have indicated some uncertainties as to its efficiency in assessing the corrosion rate with acceptable degree of accuracy or bette accuracy than other simpler techniques i.e. potential mapping.

The following discussion highlights some important aspects of the use of this type of measurements.

11.5.1 Technical Considerations.

Due to the high sensitivity required in measuring the noise fluctuation (typically in the order of several microvolts), these measurements are highly susceptible to external interference and photovoltaic effects. To minimise these effects, some research workers[163,234] partially shielded the test specimens with a grounded metal screen, and where this measure is impractical they performed their measurements at the evening when the external effects were at a minimum. It was also observed that specimens in saturated conditions were generally less sensitive to this kind of effect since the situation helped to isolate them from the external environment.

This situation, however is less likely to be met in the on-site environment.

In the present work, although the measurements were made in submerged conditions, it was necessary to stop the fatigue rigs in the vicinity of the noise test-rig during measurement. On the other hand, the expected noise contribution of the amplifier used to obtain the noise trace via the chart recorder was also checked and found to be negligible. To eliminate the latter source of error it is preferable, however, to obtain the noise trace after the actual measurements indirectly through the mini-computer using the stored data rather than the direct manner employed in the present work.

11.5.2 A Linear Drift in Potential Trace.

Early measurements exhibited a linear drift in the potential noise trace. This kind of behaviour was also reported by other author[163,234] and believed to be due to change in the temperature and degree of saturation during the measurements. A simple linear drift[234,237] may be corrected by means of a computer program using a best fit straight line. It was observed, however, that this drift can almost completely be eliminated provided that sufficient time is allowed for Ecorr to settle before measurements. This is particularly true in the case of

low corrosion rate systems and hence no correction was required in this work.

11.5.3 Interpretation of Noise Data.

In the results section, it has been shown that, for a given beam in the corrosion system studied herein, noise measurement can predict the corrosion rate within $\pm$ 30%, Figure 11.12, of the real values as estimated by linear polarization method. This accuracy dropped to $\simeq \pm 100$ - 200% when incorporating data from other systems, Figure 11.10. It is interesting to note that this trend was also observed in data obtained from the main series which deals with the E_{corr}-I_{corr} relationship (Section 10.3 in that there existed one unique relationship valid for each individual or a group of similar test conditions. Considering a particular beam, the accuracy obtained is clearly adequate to describe the likely corrosion rate without risk or erroneous conclusion. The observed accuracy is obviously better than those obtained by Page et al[163] and Hardon et al[234], although the accuracy of the latter studies is based on data obtained from specimens under widely different corrosion states. It should be appreciated, however, that:

1. The present investigation covers a much limited range of corrosion rates than in references 163 and 234, ie. less than an order of magnitude of I_{corr}.

2. Most of the current measurements were made on relatively active conditions ie. systems under dynamic loading with considerable cracking.

According to reference 163 and 234, the active conditions examined in the present study would be expected to produce considerable scatter in I_{corr} predicted by noise measurements, that is within a factor of 100 which is appreciably less accurate than actually obtained. This may be attributed to the profound influence of specimen geometry and reinforcement configuration and perhaps

provides rather promising indications that this technique may be more applicable to real structures or full scale specimens as, is the case in the test beams of this investigation, than the small specimens used in laboratory-based investigations.

Although, as discussed in Chapter 3, drifts in E_{corr} can be associated with quite different corrosion rate trends in different corrosion systems, Figure 11.11 clearly indicates the sensitivity of both S.D. of noise and E_{corr} to changes in I_{corr} in the present system under study. Figure 11.14 expressed the relative sensitivity of these parameters by relating them graphically. The linear relationship obtained, therefore, suggests a rather important conclusion in that the S.D. of the electrochemical noise provided exactly equals predictive accuracy as obtained from E_{corr} measurements. In this context, it should be pointed out that this trend is also observed in the work of Page et al[163] and Hardon[234] particularly for high corrosion rate situation.

This observation effectively means that a simple and straight forward electrode potential measurements can produce as reliable corrosion behaviour predictions as those obtained from the more complicated and time-requiring S.D. measurements. The latter type of measurements are particularly difficult and involve complex instrumentations when required for on-site measurements.

Nevertheless, since the above stated opinion is based on a relatively limited study in the present work, it would still be useful for these relationships between S.D. of ECN, E_{corr} and corrosion current to be investigated more systematically over wider range of conditions than was possible in this work.

This observation, however, by no means undermines the potential use of this technique, as a non-perturbative technique, in providing useful insight into the corrosion state of the reinforcement as indicated by the shape of the noise trace outlined in subsection 11.4.1. Indeed, as Figures 11.5 and 11.6 show, very valuable qualitative informations may be obtained from the amplitude of

potential fluctuation in terms of whether the steel is corroding actively or not.

11.6 Summary.

The limited nature of this investigation permits the following concluding remarks to be made.

1. The S.D.'s of noise obtained under cyclic and static loading are similar for a given time of measurement and a given corroding system.

2. The period of measurement has virtually no effect on the relative accuracy of S.D. measurement.

The above two points have their direct experimental use which enables measurements to be made without changing the loading conditions and without unnecessarily long periods of test provided that the measurements are to be made after E_{corr} has been settled.

3. Initial indications from short term tests suggest that for a given test condition equal accuracy in predicting the corrosion rate can be obtained from measurements of the electrode potentials and the S.D. of the potential noise and hence future work should further investigate this relationship on a wider range of corrosion activity.

4. As the potential fluctuations reflects changes in the dynamic equilibrium of the corroded electrode, the ECN technique could provide a useful tool in describing the corrosion state by means of potential noise trace.

5. The use of this method as on-site measuring technique involves practical difficulties and inevitably requires the aid of potential mapping in order to locate areas which require closer monitoring.

6. This investigation produced further evidence as to the

requirement of establishing separate relationships for dissimilar systems. Consequently it seems unconvincing to use laboratory-deduced relationships for real structures of entirely different geometry and environmental and loading histories. This in turn imposes further restrictions on the applicability of this method for corrosion rate quantification outside the laboratory.

TABLE(7C) BEAM MU60-N1Y STATIC-AVE

a)

Time (s)	Standard Deviation	Ecorr Mean	Ecorr Min	Ecorr Max
247	3.73604E1	590.72	590.88	590.55
494	2.64107E1	590.56	590.88	590.26
742	2.15592E1	590.42	590.88	590.02
989	1.86666E1	590.29	590.88	589.75
1237	1.66923E1	590.16	590.88	589.52
1485	1.52346E1	590.03	590.88	589.27
1732	1.41016E1	589.91	590.88	589.08
1979	1.31883E1	589.80	590.88	588.88

TABLE(7B) BEAM MU60-N1Y DYNAMIC

b)

Time (s)	Standard Deviation	Ecorr Mean	Ecorr Min	Ecorr Max
247	3.75636E1	593.93	594.51	593.33
494	2.65607E1	593.92	594.51	593.31
742	2.16863E1	593.90	594.51	593.31
989	1.87807E1	593.90	594.51	593.31
1237	1.67979E1	593.90	594.51	593.30
1485	1.53342E1	593.89	594.51	593.29
1732	1.41967E1	593.89	594.51	593.29
1979	1.32796E1	593.88	594.51	593.29

Table (11-1): Typical print out of electrochemical noise data (beam MU60N1Y after 822,500 cycles)
a) measurements with average load applied statically
b) measurements during cycling.

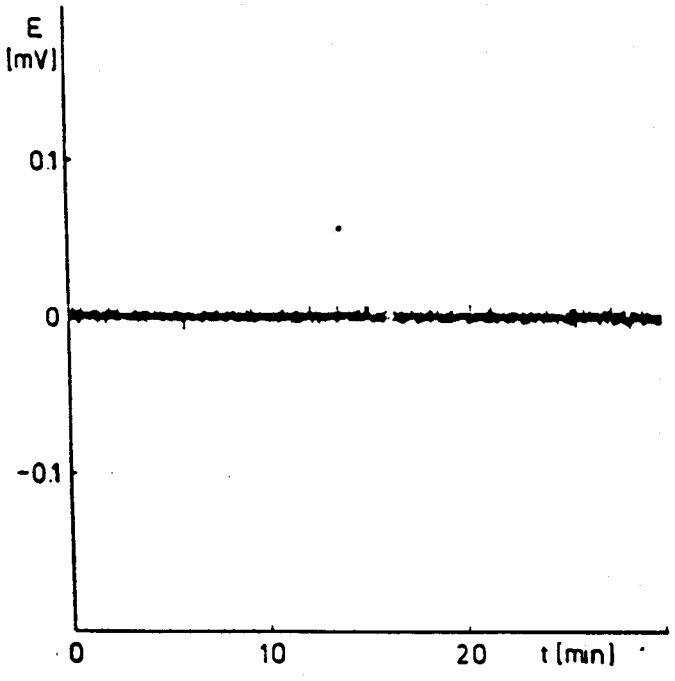

a) Electrode noise output prior to chloride ion addition.

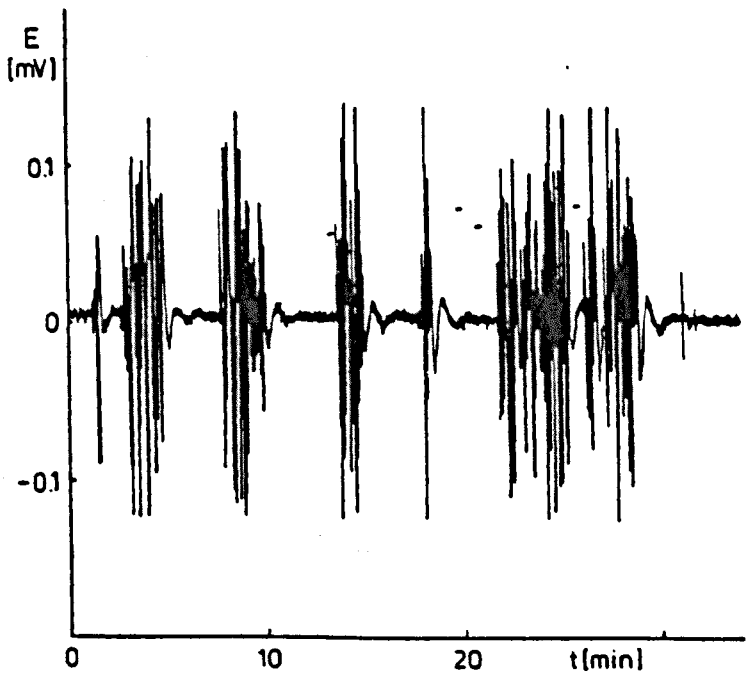

b) Electrode noise output during pit initiation period.

Figure (11-1): Pitting initiation as detected by potential noise for mild steel in a solution containing:
1000 ppm $NaNO_2$+1000 ppm NaCl
(Ref.232).

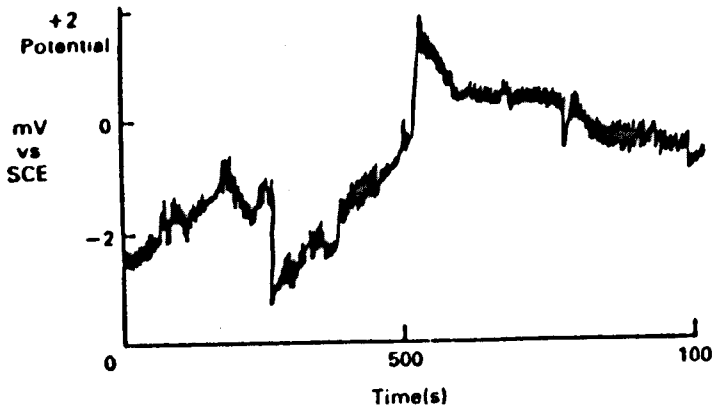

Potential/time record from uncontaminated concrete.

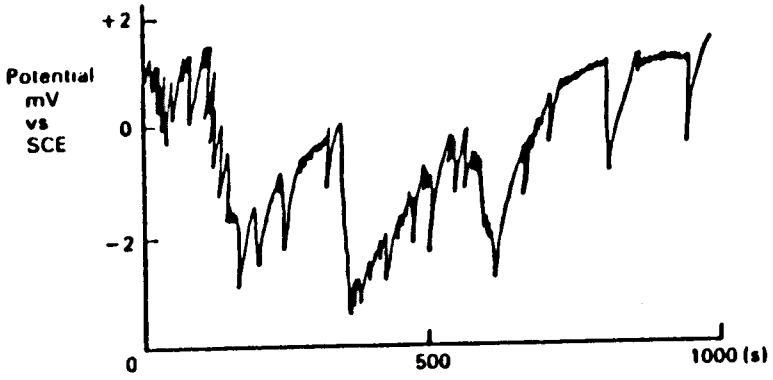

Potential/time record from chloride contaminated concrete.

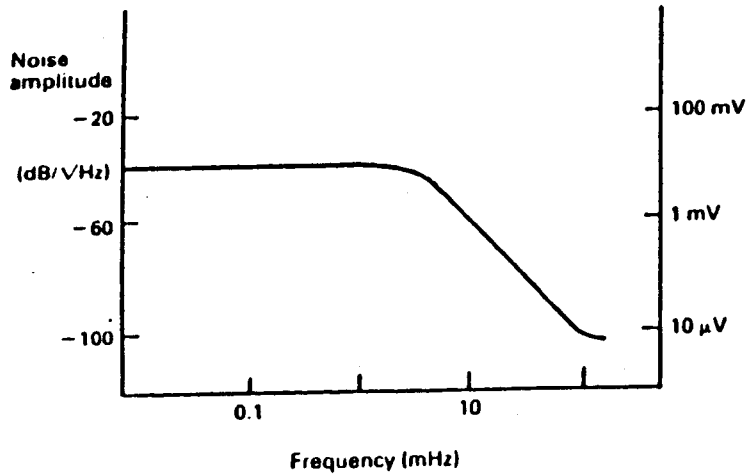

Noise spectrum from uncontaminated concrete.

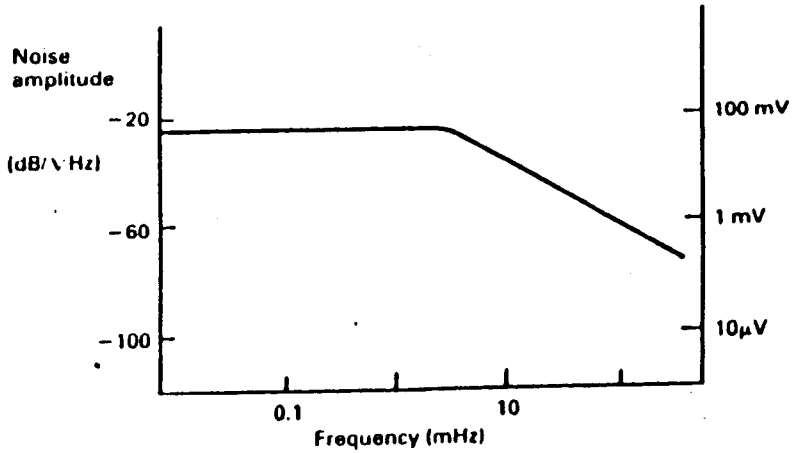

Noise spectrum from chloride contaminated concrete.

Figure (11-2): Change in potential noise trace due to chloride contamination (Ref.111).

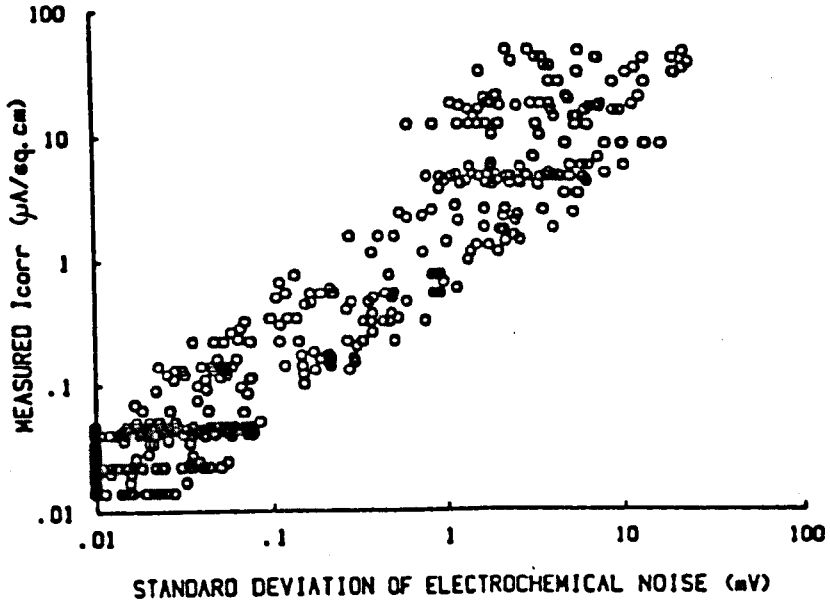

Figure (11-3): I_{corr} against standard deviation of electrochemical noise obtained by Page and Lambert from saturated cement paste and concrete small slabs (Ref.163).

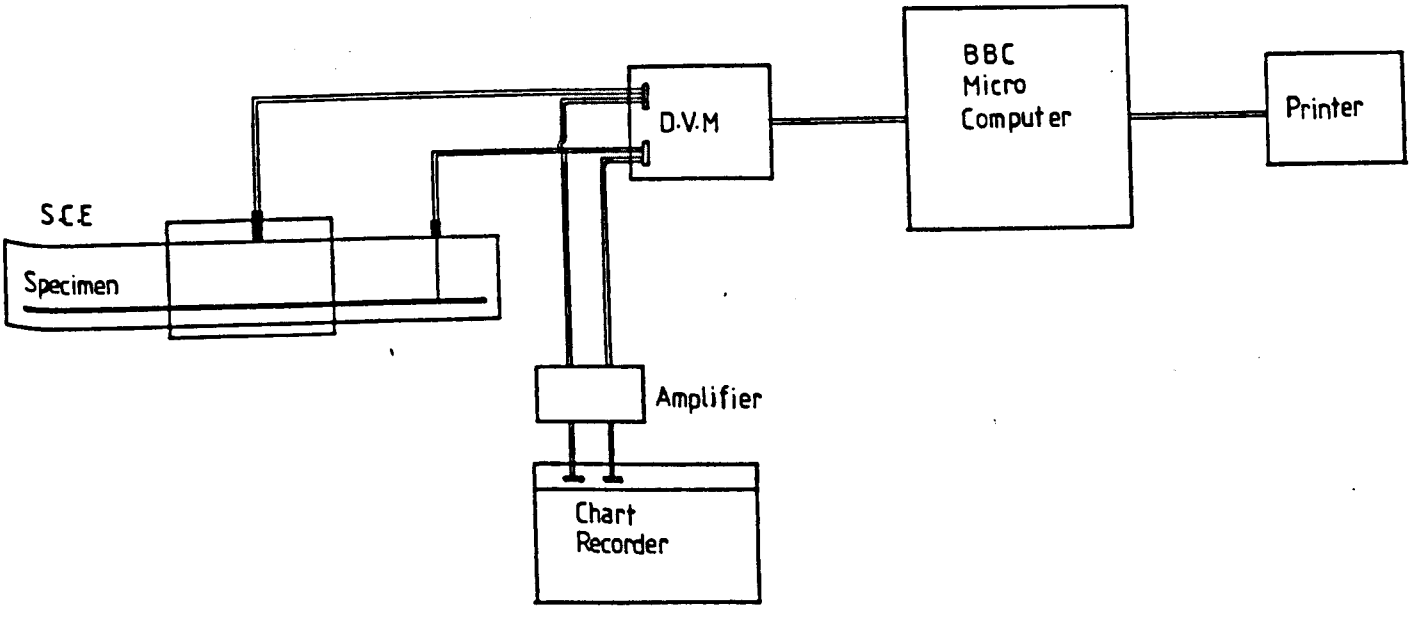

Figure (11-4): Block diagram of electrochemical noise measure instrumentation.

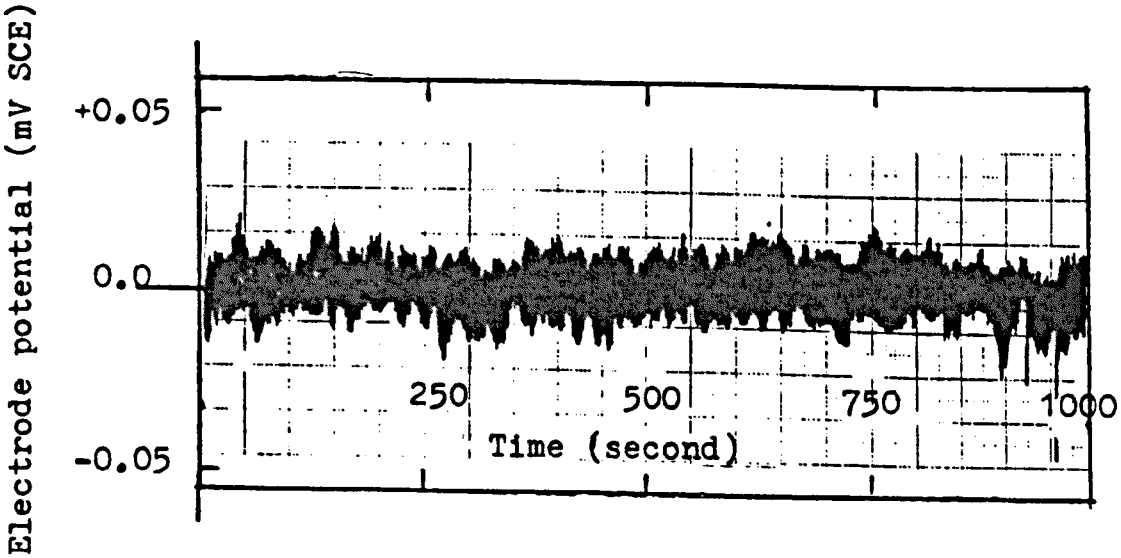

a) Beam MU60N7D;befor application of cyclic loading (the average load applied, I_{corr}= 832 μA)

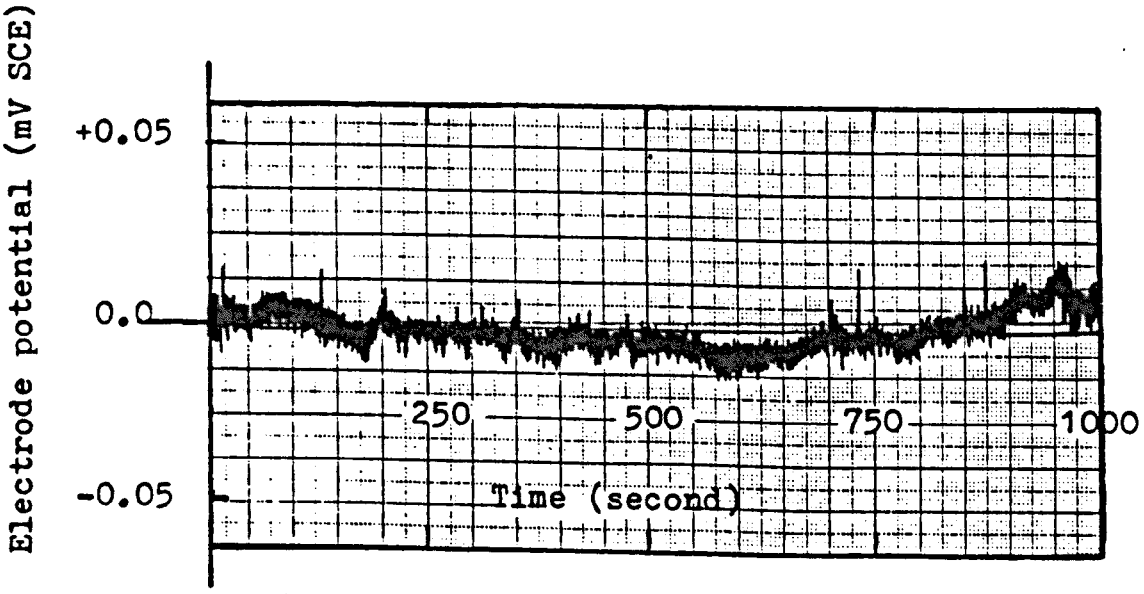

b) Beam ML403N;14days exposure with static load applied (the average load applied, I_{corr}=450 μA)

Figure (11-5): Electrochemical noise trace of low to moderate corrosion rate systems.

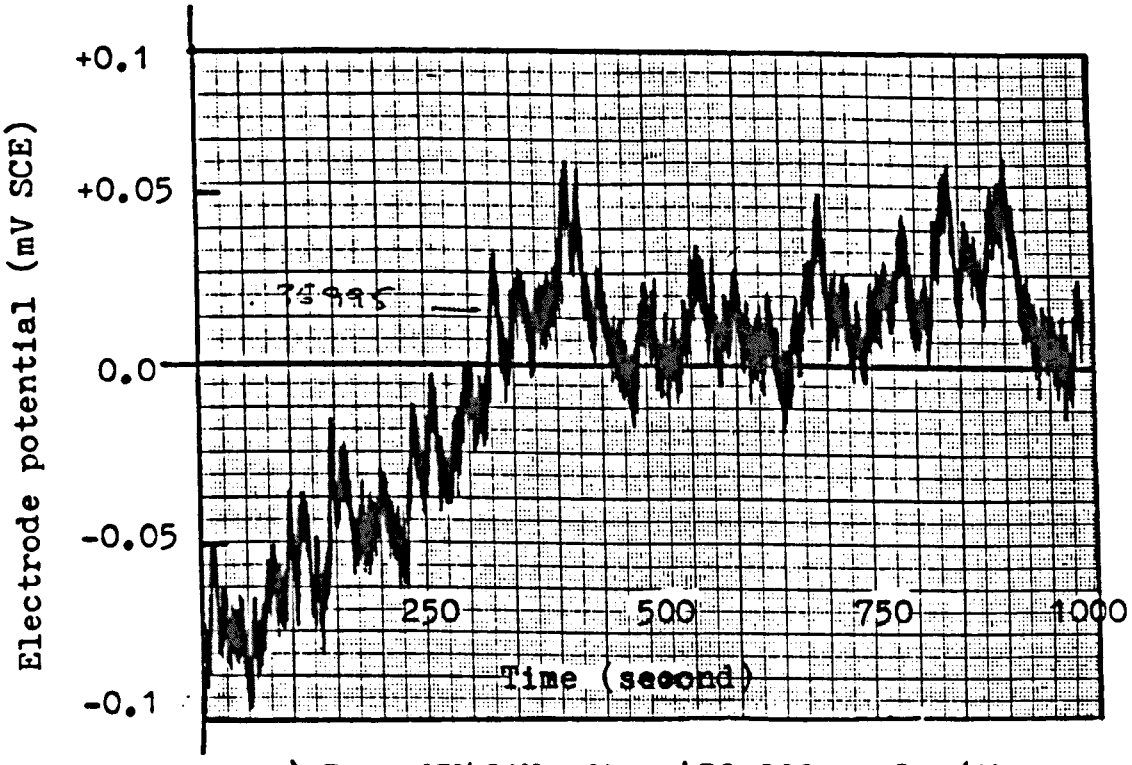

a) Beam MU401N;after 430,000 cycles(the average load applied, I_{corr}=1380 μA)

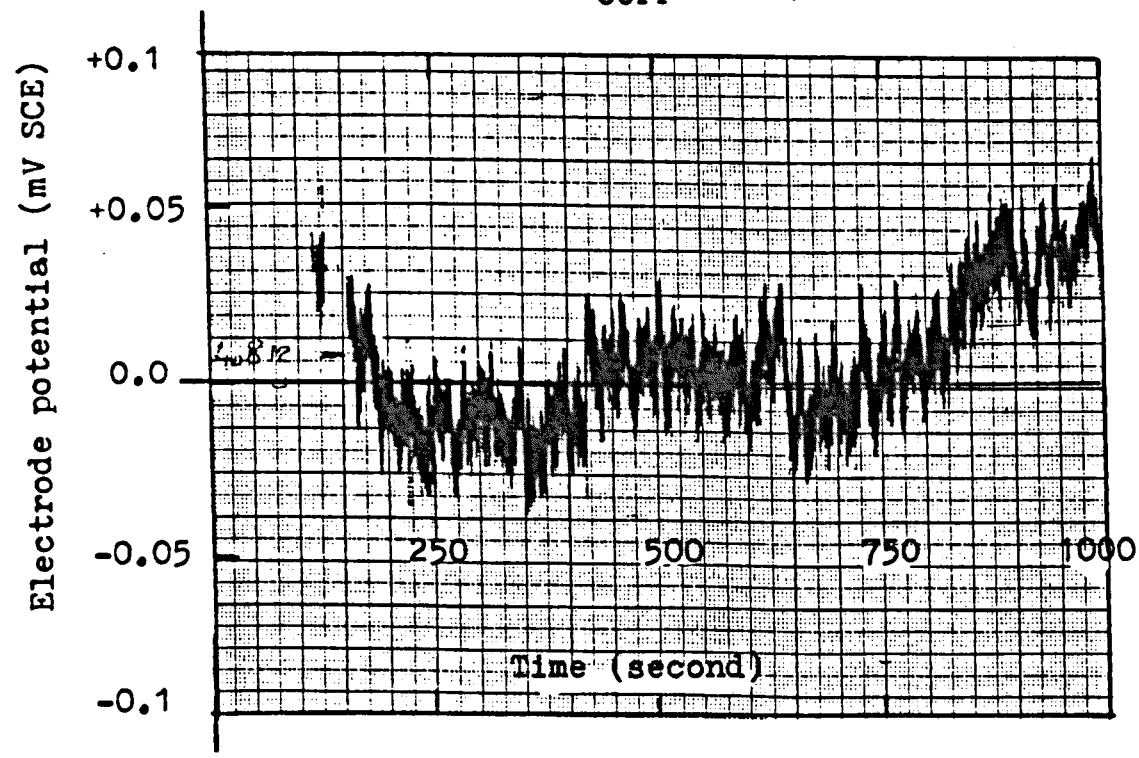

b) Beam MU603N;after 1,076,400 cycles(the average load applied, I_{corr}=1620 μA)

Figure (11-6): Electrochemical noise trace of high corrosior rate systems.

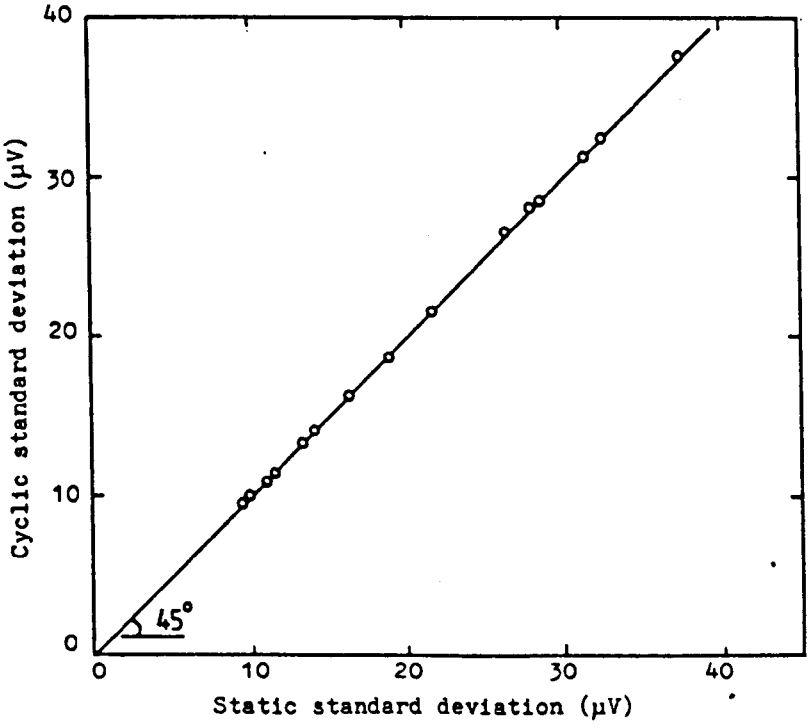

Figure (11-7): Relationship between the standard deviation obtained under cyclic loading and statically applied average load (beam MU6ON8Y)

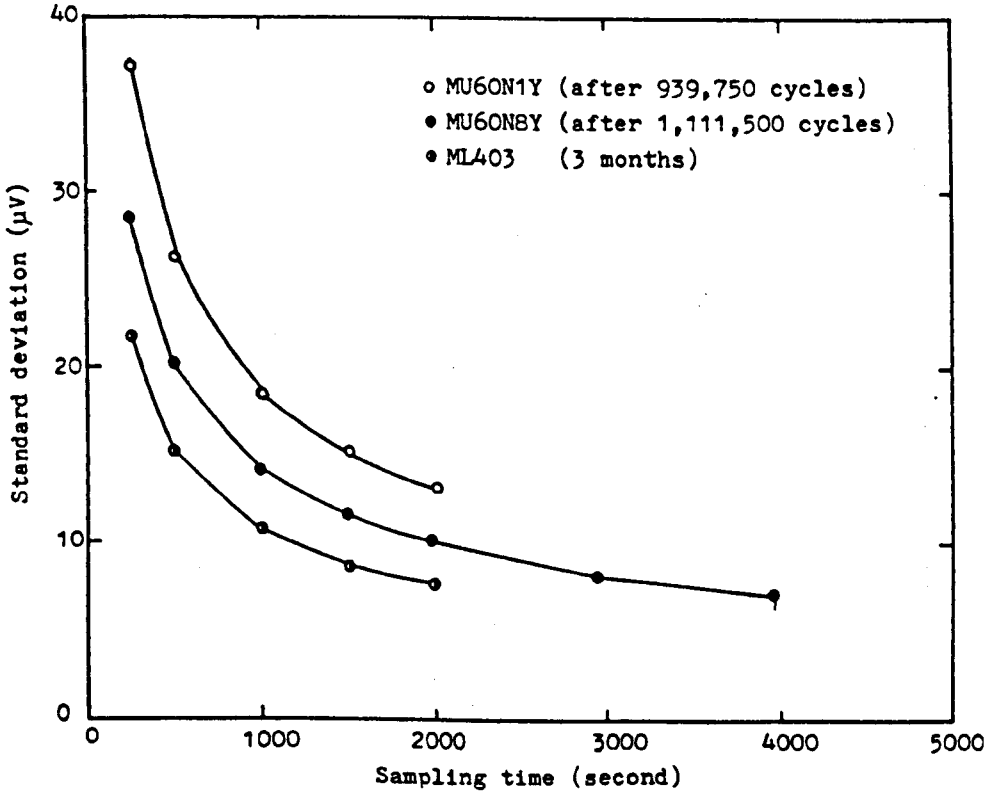

Figure (11-8): Change in S.D with sampling time.

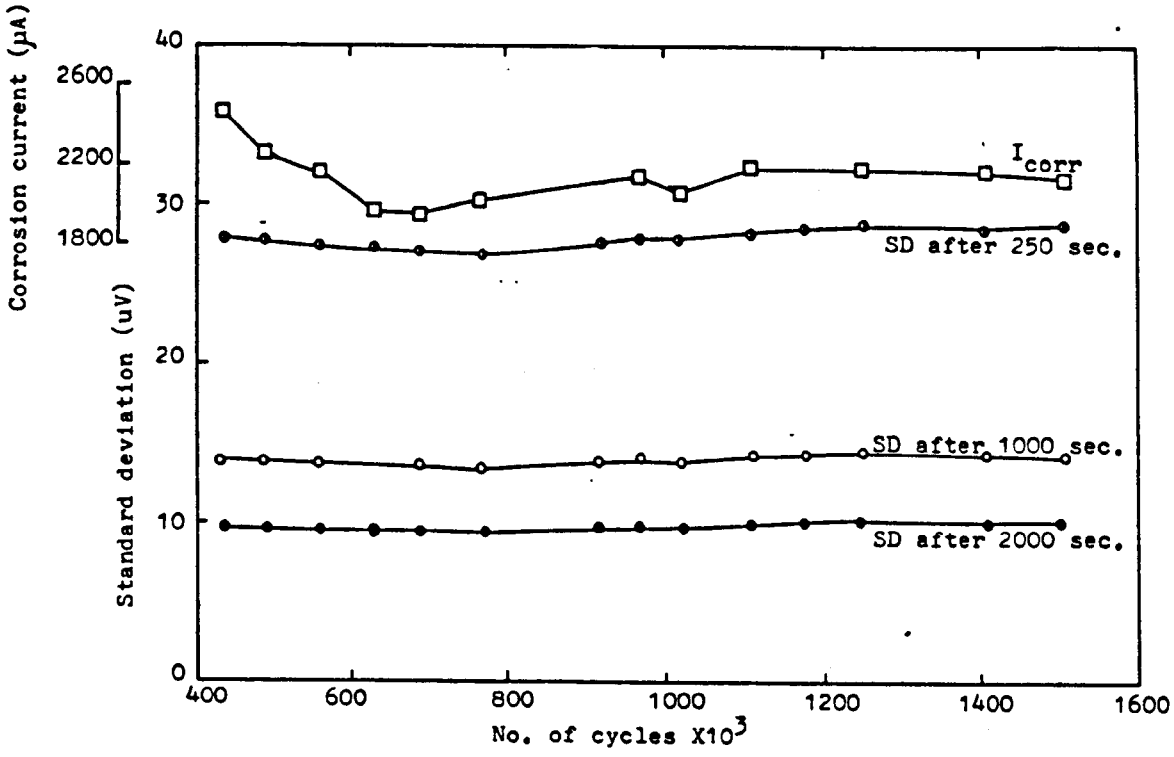

Figure (11-9): Corrosion current and standard deviation obtained after different sampling time vs. No. of cycles (beam MU60N8Y).

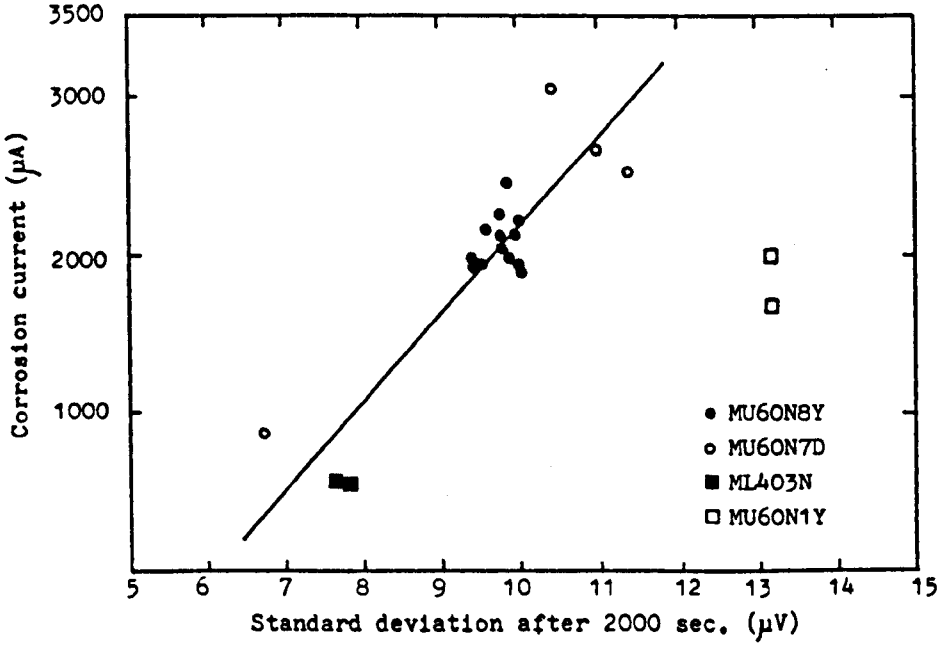

Figure (11-10): Corrosion current vs. standard deviation of electrochemical noise measured after 2000 second.

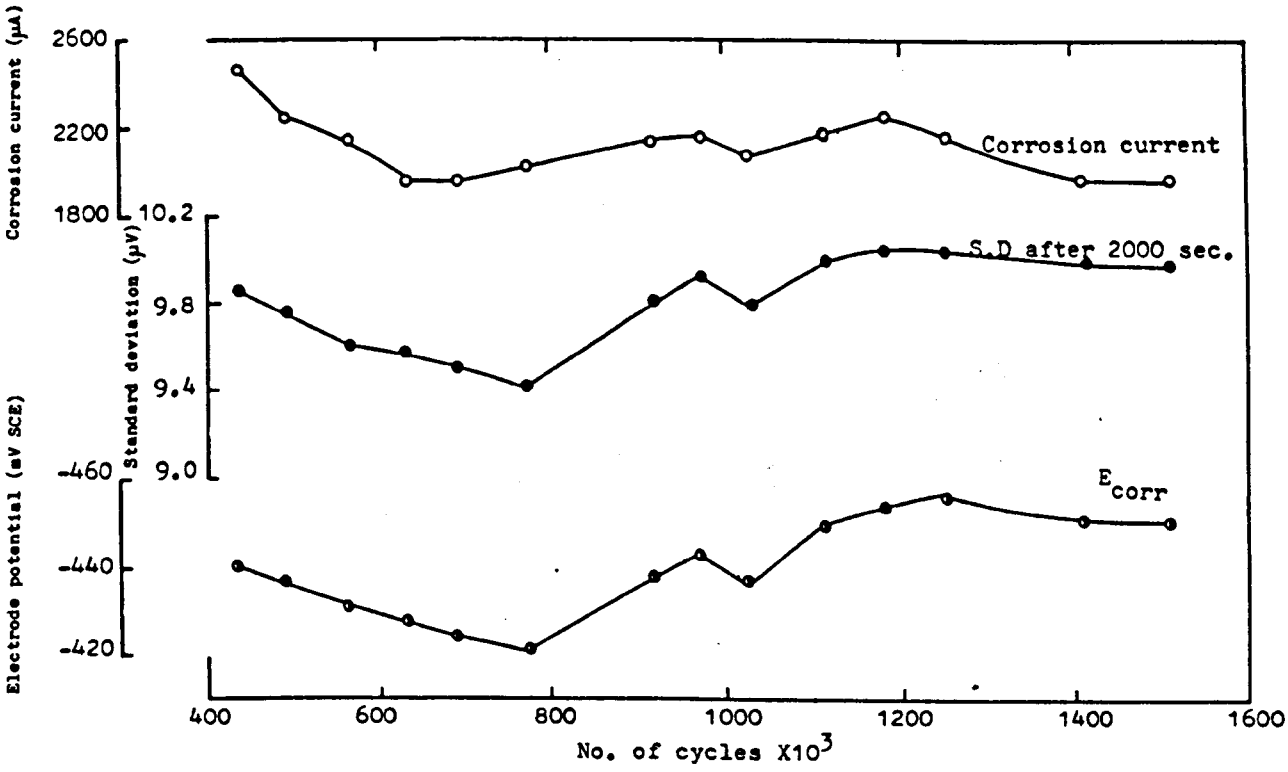

Figure (11-11): Corrosion current;standard deviation and electrode potential vs. No. of cycles (beam MU60N8Y).

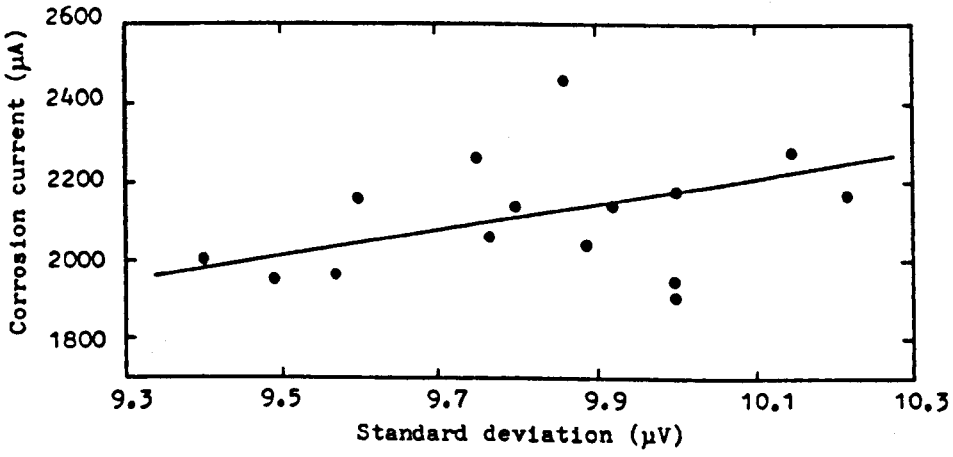

Figure (11-12): I_{corr} vs. standard deviation (after 2000 sec.) for beam MU60N8Y.

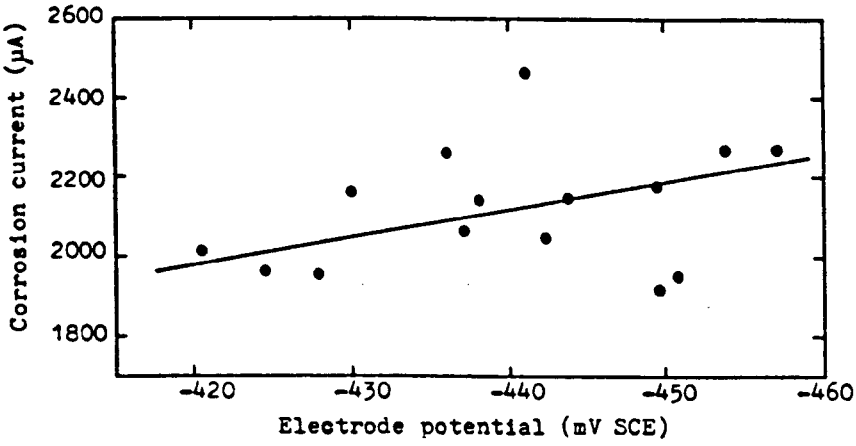

Figure (11-13): I_{corr} vs. E_{corr} for beam MU60N8Y.

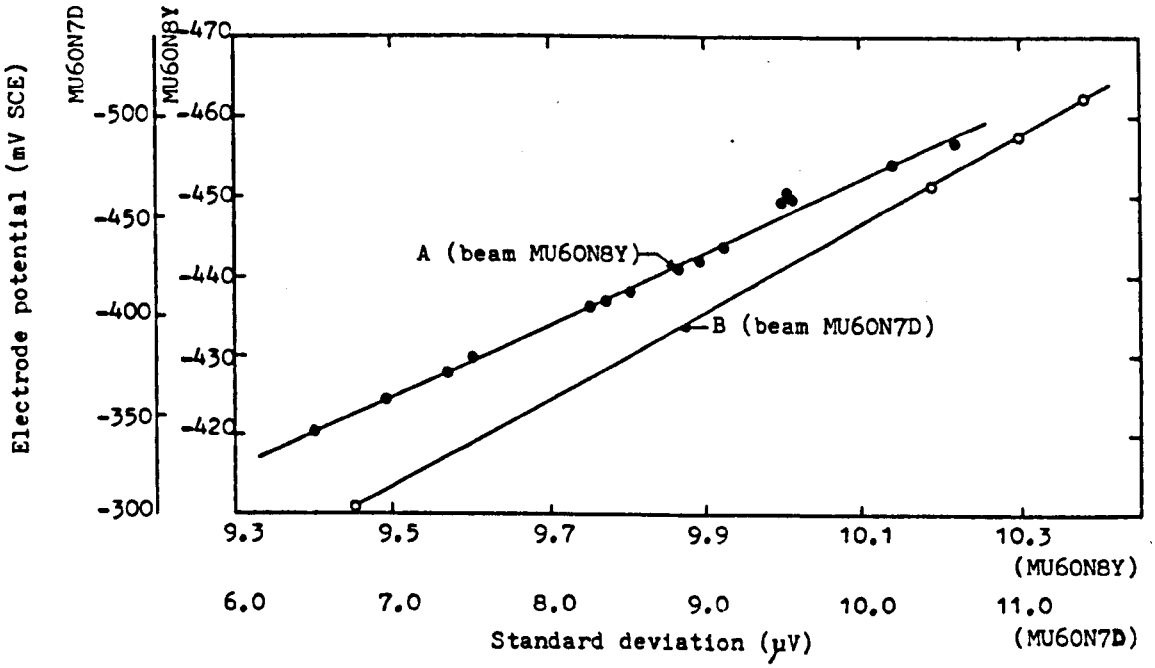

Figure (11-14): E_{corr} vs. standard deviation (after 2000 sec.) for beams MU60N8Y and MU60N7D.

CHAPTER 12

GENERAL DISCUSSION

12.1 Introduction.

12.2 The Electrochemical Effect of Crack Blocking.

12.3 The Interplay Between Stress and Corrosion Under Short Term Fatigue Loading.

12.4 The Performance of Dynamically Loaded Reinforced Concrete in Aqueous Environment.

12.5 Comment on the Experimental Approach in Dealing With Corrosion Problem.

12.6 The Design Life of Concrete Structures Sustaining Cyclic Stress in Submerged Condition.

CHAPTER 12

GENERAL DISCUSSION

12.1 Introduction.

Previous chapters have considered separately the different phenomena observed at each stage of this study. The fact that the detailed understanding of the corrosion fatigue behaviour of full-scale reinforced concrete beam is a complex task, has necessitated the adoption of the research strategy described earlier in Chapter 5. Consequently, to achieve the objectives set for this study sources of error should be carefully tackled and these include various practical and technical difficulties which had to be overcome at various stages of this work. Each of these, required separate experimental verifications and proofs. Examples of these factors are the measurements of stress variation during fatigue loading (Chapter 7), the determination of concrete resistance (Chapter 9) and the technical aspects of corrosion rate measurements (Chapter 10).

The separate parts of this study, however, may be linked to provide a clearer picture of the actual changes occurring during exposure. This is feasible for this study covers three distinctive, although closely related, conditions. These are:

1. The case where stress condition is the predominant factor, as in tests at 0.75 and 0.85 f_y load level.

2. The case where both the stress and electrochemical conditions contribute, perhaps equally, to the overall

behaviour of the test specimen, as in tests at 0.7 and 0.6 f_y load level.

3. The case where corrosion can be considered as the major contributor to the deterioration process, as in the case of dynamic tests at 0.4 f_y load level and static tests in a corrosive environment.

In this chapter, the link between the structural and the electrochemical observations will be discussed in addition to the application of these results in real life structures.

12.2 The Electrochemical Effect of Crack Blocking.

From the structural point of view, it has been demonstrated that the crack blocking effect is much more pronounced in dynamic than in static conditions. Further, under dynamic loading, there is an optimum loading level where the beneficial effect of this phenomenon is at its maximum. This was found to be at load level equivalent to 0.6 f_y (see Chapter 8). The crack blocking phenomenon, however, was coincident with changes in the electrochemical characteristics of the test beams as indicated by electrode potential and corrosion rate measurements. These changes are believed to be related to changes in the exposure condition of the embedded steel at crack sites as a result of the structural changes. The situation is simplified schematically in Figure 12.1 which may be explained as follows:-

The initial stage of loading, up to the point of structural changes due to the onset of crack blocking occur, exhibits an increase in the maximum deflection and crack width. This means that the temporarily exposed area of steel (A_1), goes on increasing. The permanently exposed area (A_2) is primarily a function of the minimum crack width, i.e. the width at minimum load and minimum deflection and this is reasonably constant at the early part of this stage and then increases at a slow rate. It should be noted that the change in both the minimum and

maximum deflections follow the pattern of change in steel stresses described earlier in Chapter 7.

Consequently, it is reasonable to assume that at this stage, the differences between the temporarily and the permanently exposed areas are increasing. The monitoring of the electrode potential during cycling has indicated an interesting behaviour which is clearly related to the above described exposure mechanism. As shown in Figure 10.18, the amplitude of fluctuation of E_{corr} on each load cycle was increasing, in line with an increase in maximum deflection, with number of cycles, (from 0.25 to 1.57 mV) up to the point where a reduction in deflection range was first recorded. This behaviour clearly confirmed that the E_{corr} value is, most probably, partly a function of steel area which is in contact with the surrounding solution and shows its sensitivity to this change even if the change in exposure is occurring over a very short time ($\simeq$3 sec) which is the time required for a half load cycle to be completed. The easy ingress of the solution into the steel caused a fall in the potentials and this is clearly load dependent. As argued in Chapter 10, during this stage, and for some considerable time afterwards, it is considered that the predominant corrosion mechanism is microcell activity at the crack sites.

At the point where blocking becomes effective, that is when both crack width range and deflection range sustained progressive reductions, the change in the temporarily exposed area is substantially reduced as the maximum deflection is virtually constant, meanwhile the permanently exposed area increases at a much faster rate in accordance with the increase in minimum deflection due to blocking. Therefore, crack blocking produces a structural change which results in a local change in the exposure condition at crack sites having the effect of:

1. Reducing the effect of load fluctuation on the corrosion activity during cycling as indicated by the reduction in the amplitude of fluctuation of E_{corr} each load cycle.

2. Increasing the local permanently exposed area as opposed to approximately constant temporarily exposed area leading to increased local probable anodic to cathodic area ratio and thus mitigates the severity of corrosion attack.

3. These two effects are dependent on load level and degree of blocking.

Accordingly, during the stable stage of E - No. of cycles curves, the amplitude of E_{corr} fluctuation during each load cycle is practically negligible indicative of little or no effect of loading on the exposure condition. The attainment of this stage, as indicated in Figures 10.24 and 10.25 is clearly load dependent, the lower the applied (initially intended) load, the earlier the steady state has been achieved. Also, it can easily be seen that the pattern of long and short-term variation in E_{corr} is exactly similar to that of polarisation measurements as indicated in Figures 10.4, 5 and 6 for measurements during cycling and by their change over the test duration given in Figures 10.44 and 10.45. However, polarisation measurement, and the potentiostatic technique in particular, indicate most clearly the fluctuation in the corrosion current during each load cycle as a result of changes in the directly exposed area. These measurements directly demonstrate decreases in the current fluctuations with exposure time as a result of crack blocking in the same way as indicated indirectly by E_{corr} fluctuations.

Moreover, when blocking has developed along the whole length of the cracks, further important alleviation effects can be produced by the development of a more effective physical barrier to the ingress of the corrodent species as well as the migration of the corrosion product which may increase the concentration polarisation effect and consequently reduce the corrosion rate. Another possible effect may be the chemical inhibiting effect as a result of a reduced rate of leaching of $Ca(OH)_2$ from the blocked cracks interior.

Nevertheless, the colour change of the deposit

indicates that mobility of the ionic species is still possible after blocking has been well established. This is also confirmed by actual Tafel plots which indicate activation polarisation control both anodically and cathodically for the majority of the tests in this work, (i.e. up to about 5 months).

For long running tests (i.e. for longer times than depicted on Figure 12.2) however, such as those presented earlier for tests in seawater, concentration polarisation effects were observed on the cathodic curves and thus suggests a possible role of blocking in restricting high corrosion process cathodically despite of stable structural behaviour. This may be attributed to increased density of the blocking material as a result of increased precipitation of corrosion product inside the deposit pores, and also to the macrocell activity which necessitates cathodic supply outside the cracks.

The above discussion suggests that crack blocking may effect the corrosion process in two ways:

a. Indirectly via the alleviation of stress condition and the subsequent local change in the anodic/cathodic area ratio and;

b. Directly via forming a physical barrier which restricts the leaching of $Ca(OH)_2$ from cracks interior, thus maintaining chemically inhibitive environment, and also restricts the movement of both the corroding species and the corrosion product. The latter effect is limited and likely to occur after longer exposure time.

12.3 Summary of the Interplay Between Stress and Corrosion Under Short Term Fatigue Loading.

Following the description of the role of crack blocking on the overall behaviour of the test beams, it becomes possible to describe the interplay between stress and corrosion for short time exposures ($\simeq$ 6 months) with respect to the major parameters monitored in this study

viz deflection, crack width, electrode potential and corrosion rate measurements. According to the discussion presented in Chapter 7 it is reasonable to consider the deflection data as an indication of the state of steel stress in the steel bars as well as the degree of cracking and thus can be reasonably linked to the exposed steel area at crack sites. The global picture of the degradation process due to fatigue loading is ideally simplified schematically in Figure 12.2 which indicates the major stages of change. It should be noted, however, that the start and end of each stage are dependent on the applied stress and the environment. Thus for a given environmental condition, the stable stage, i.e. Stage IV is attainable earlier in tests at low load level than in tests at high load levels. Referring to Figure 12.2, these stages may be described as follows.

Stage I: (From 0 to ~10^3 cycles); which marks a progressive increase in maximum deflection and the rapid development of cracks. As the minimum deflection is approximately constant during this stage, the deflection range is increasing with the solution flowing rapidly in and out the cracks. Thus the mechanism of ingress of corrodent species and ionic migration from corrosion sites is substantially different from that of exposure under static loading. The easy ingress of the solution causes depassivation of the reinforcing bars, consequently, E_{corr} moves to more negative value with increased corrosion rate (note that the corrosion rate is presented in Figure 12.2 by R'_p values and this should make no qualitative difference as the B value is approximately constant, for a given load level, in the range of exposure period examined.

Stage II: (From 10^3 to 50 x 100 x 10^3 cycles); at this stage the rate of increase in maximum deflection decreases and, due to the development of deposit at the upper regions of cracks in the concrete, the minimum deflection increases at faster rate. The deflection range starts to level off and then decreases at slow rate. Meanwhile E_{corr}

and the corrosion rate continue the trend observed in Stage I but at slower rates due to the slower rate of increase in the maximum deflection. Despite the reduced stress range, the mechanism of corrosion is essentially the same as that in Stage I. This is because, the cracks are not fully blocked and no dramatic change in the deflection range occurs which, subsequently, means small internal change in exposure condition at crack sites.

Stage III: (From 50 - 100 x 10^3 to 300 - 800 x 10^3 cycles); where the maximum deflection increases very slightly. The deflection range and stress range continue their change at substantially higher rate until the point is reached where the test is run under approximately constant condition with respect to these parameters. Blocking becomes well established and deposit covers the whole length of the cracks. The removal of the corrosion product from the bar/crack interface is restricted but still possible and probably achieved by diffusion of Fe^{2+} through the deposit. For the same reason, i.e complete blocking of cracks, leaching rate of $Ca(OH)_2$ is also reduced. The structural and geometrical change at cracks result in reduced corrosion rate and E_{corr} moves towards more positive values. Beyond this point up to the end of the exposure period ($\simeq$ 6 months) only slight change in the corroded area is expected.

Stage IV: (Beyond 300 - 800 x 10^3 cycles); at which the maximum deflection, range of deflection and steel stresses are stabilised at approximately constant values with no further increase in the amount of deposit (although small increase may occur at the early part of this stage). Consequently, the corrosion attack at the crack sites becomes stabilised due to stable exposure condition. Also, the deposit undergoes a colour change indicative of continued ionic mobility and the local oxygen supply is relatively low as indicated by the black corrosion product observed upon completion of fatigue tests. This factor, however, is not the rate determining step.

It should be mentioned, that the number of cycles

required to attain the steady state condition for each of the parameters described above is dependent on the factors which control each of them. The structural parameters, for example, are particularly sensitive to the initiation of blocking at the upper regions of the cracks. Whereas stabilisation of the electrochemical parameters depends on a complex interaction between the structural and the chemical conditions inside the cracks.

The corrosion fatigue behaviour beyond the time scale indicated on Figure 12.2 (around 5-8 months exposure) may be postulated in light of the evidences obtained from long term seawater tests as presented earlier. In this respect, long term structural behaviour may be expected to continue the trends observed in short term tests (i.e. approximately stable deflection and steel stress conditions) up to the point when the increase in corrosion rate due to the macrocell process (as described earlier) causes severe metal loss on the main bar. This would result in proportional increase in steel stresses and thereby eventually trigger final failure either by instantaneous ductile overload or by a short period of fatigue cracking initiation followed by final ductile failure.

On the other hand, metal loss on the shear links, although not necessarily cause an increase in the steel stresses of the main bars, increases the risk of fatigue failure in shear at low load level.

In any event, long term tests with continuous monitoring of the corrosion rates are necessary for more accurate assessment of the long term corrosion fatigue behaviour. In this respect, the monitoring of electrode potential can not, alone, completely, provide the required informations.

12.4 The Performance of Dynamically Loaded Reinforced Concrete in Aqueous Environment.

Previous work in corrosion fatigue of reinforced concrete has revealed an exceptionally complex behaviour that requires careful examination. One basic aspect of

this complexity concerned the nature of the deterioration occurring under these conditions. Under such cases two principal deterioration processes may occur.

1. Conventional fatigue damage in the form of fatigue cracking in reinforcing bars as well as concrete body.

2. Reduction in reinforcing steel load-carrying capacity by localised corrosion.

In circumstances more relevant to practice, i.e. low test frequency and low stress amplitude, however, an environmental factor manifested itself by the blocking of flexural cracks in the concrete by deposits. This can effectively intervene and seems to have a decisive role in the whole process that ensues its occurrence. This phenomenon has been observed in seawater and presently, as this study indicated, in 3.5% NaCl solution and tapwater. The influence of blocking is critically dependent on load level, test frequency and type of environment. With regard to these more realistic loading frequencies the available information can be summarised and described with reference to Figures 12.3 and 4 for which curve A represents components exposed to air and curve B is for components exposed to blocking - corrosion conducive aqueous environment. Four stress regions are identified and described as follows:

Region I at δ_1 and Higher.

Corresponding to stress level of $\geq$ 100% of the controlling flexural capacity of the reinforced concrete specimens. This case is equivalent to static capacity and the fatigue life is virtually zero.

Region II from δ_1 to δ_2.

In this region the observed deflection changes indicate that the stress amplitude and stiffness are increasing with time. Tests in aqueous environment

exhibit lower fatigue lives than tests in air which may be attributed to:

1. Conventional effect of a corrosive environment in accelerating fatigue failure.

2. Increasing crack width caused by the attrition effect of water flowing in and out of the cracks and the hydraulic compression on reduction of the stress from maximum value each load cycle.

3. The absence of crack blocking and its subsequent stress alleviation effect due to short life and the hydro-dynamic conditions within the cracks which inhibit the accumulation of deposit material.

Region III from δ_2, to δ_4.

Where the load level is small enough for progressive accumulation of deposit material to take place in aqueous environment, the actual stress amplitude is reduced and consequently the fatigue life increases. It is important to emphasise that the magnitude of δ_2 i.e. the stress level below which blocking phenomenon becomes effective is dependent on the type of solution. Also for a given stress level the gain in fatigue lives over those in air depends on when blocking had occurred, the earlier the formation of deposit the more the gain will be. At this stage, it is apparent that there exists two opposing environmental effect competing with each other for the dominating role of the process namely, blocking, which tends to mitigate the stress component of the fluctuating load, and corrosion, that tends to increase the same component by virtue of reducing the bar's diameter.

δ_4 is the stress level below which the differences in the environmental condition do not produce significant blocking and thus the fatigue life becomes dependent on the severity of the surrounding environment.

δ_3 falls between δ_2 and δ_4 and represents the in-air fatigue limit.

Region IV from δ_4 to δ_5.

In this region the severity of the environmental condition and the quality of concrete play the decisive role on the life of the structure. The dashed area refers to the different effect of the different environmental severity. δ_5 is the low stress level of the long life region which, can in some circumstances, of no-cracking and good quality concrete, be considered as a fatigue limit.

Figure 12.4 indicates the likely stress variation for each region during fatigue loading.

12.5 Comments on the Experimental Approach in Dealing with Corrosion Problem.

Corrosion of reinforcing bars embedded in concrete in real-life structures is a particularly time-dependent process. Even premature structural distress due to corrosion often requires several years to reach dangerous levels. It, consequently follows that the limited time scale usually available for laboratory based investigations presents a major practical problem facing attempts to translate laboratory results into design concepts for practical use. Tests such as these should be performed in natural or semi-natural environmental conditions and have a duration which is significant when compared to the life-time of an actual structure. Attempts to carry out accelerated tests may easily lead to incorrect conclusions as, as this study has indicated, the mechanism of corrosion may be substantially altered with time of exposure.

Nevertheless laboratory studies are crucial in establishing the fundamental aspects of the problem of corrosion and, therefore, if properly planned and executed, a potentially important element in solving practical corrosion problem.

Experimental investigations are often confronted with unexpected sources of error. A clear example of this kind

of difficulty has been reported earlier in this thesis, namely instrumental limitations which, as described in Chapter 10, to be identified, required a considerable deal of effort and time. Moreover, during the development of the measuring technique, further complications had to be overcome in order to obtain error-free electrochemical measurements on the embedded reinforcement. This was mainly related to the high sensitivity of such measurements to any degree of corrosion on the testing rigs in contact with the test solution. It was found that corrosion on the load points had an effect of considerably reducing (by almost an order of magnitude) the magnitude of the measured R_p value and thus results in high corrosion current. This is so despite the fact that there is no metallic contact between the testing rig and the embedded reinforcement. The reason for this behaviour is not fully understood but it is strongly recommended that corrosion of any metal, in contact with the solution, other than the reinforcing steel itself, should not be allowed otherwise the measured electrochemical parameters can note be safely considered to have been related solely to the desired system under study.

In this specific area of research, recent trends indicate three significant developments in the experimental approach to obtaining corrosion data:-

Firstly: the test specimens are increasingly made to simulate as accurately as possible the actual structural elements in terms of size, reinforcement details, environment and loading conditions. This trend has been appreciated in this study as full scale reinforced concrete beams were tested with an adjustment of the test environment (ie. pH control).

Secondly: the time-corrosion dependency is increasingly recognised which results in appreciable increases in test duration with the use of efficient monitoring techniques.

Thirdly: more attention is being paid to monitoring and inspection of structures in-service in various parts of the world when the corrosion problem of reinforced concrete has reached serious levels.

The combined effect of the above three developments has provided a greater opportunity for better understanding of the correlation between data obtained in the laboratory and that actually occurring in real service life. It thus permits further important steps to be taken towards specifying more accurately the risk of corrosion on the safety and life of reinforced concrete structures.

12.6 The design Life of Concrete Structures Sustaining Cyclic Stresses in Submerged Condition.

Corrosion of steel reinforcement is nowadays a well identified problem. The ever increasing scale of the problem worldwide has made it evident that engineers are facing rapidly growing tasks of assessing, repairing and strengthening existing structures suffering premature degradation which seriously threatens the safety of human life and the economy of society. In the U.K., the cost of the problem of corrosion is estimated[238] to be some £10 billion primarily arising from the high cost of treating corrosion damaged structures not only due to access difficulties but also to the cost of specialist material needed. However, although the economic losses may reluctantly be tolerated due to practical reasons, any loss of human life could not be allowed and this places heavy burden of responsibility on the shoulders of the engineering profession. There is, therefore, a need for structural designers and practicing engineers and even architects to acquire sufficient knowledge on corrosion and durability aspects of construction under various types of loading conditions.

In theory, it is possible to design concrete so that embedded steel should not corrode. The facts, however, as indicated by Currie[129] are:

1. If there is any chance of something being done incorrectly or inadequately, sooner or later it will be done incorrectly or inadequately.

2. It is important that engineers and the public come to

terms with the reality that all structures including reinforced concrete ones do not necessarily last for ever.

Thus, the need to assess durability more clearly has resulted in it being introduced as an additional limit state in BS8110. It is only recently, that design life of reinforced concrete structures has become a major issue. Recently, Browne[238] reported that an attempt is being made to produce a British standard to specify the life of a building in terms of the specified lives of the individual components accepting realistically their inevitable variability in relation to both performance and economic limitation.

However, the life of structures sustaining corrosion fatigue may be discussed in light of the increasingly adopted approach for the prediction of design life described earlier in Chapter 3.

This approach is based on the assumption that the time for the initiation of corrosion, t_o, should exceed the design life, t_D, by a certain safety factor and that t_o is significantly longer than the subsequent corrosion propagation stage, t_1, necessary to cause loss of serviceability.

For reinforced concrete structures subjected to appreciable cyclic and/or high static stresses sufficient to form early cracking, it is reasonable to assume that the initiation time $t_o = 0$. Consequently, the life time of the structure will be mainly dependent on the propagation rate of corrosion (ie. corrosion rate) which is in turn a function of stress/cracking situation. As discussed in Chapter 10, the almost immediate formation of cracks would cause rapid depassivation in the permanently submerged zone of the beam and the subsequent setup of the initial microcell process. For sufficiently large cracks (not clearly identified in the literature, possibly > 0.1 - 0.2 mm) under submerged condition, if the anodic dissolution of the metal, iron, remains essentially locally supported cathodically and, if macrocell conditions do not become subsequently established, then

this may be a slow process. Thus the penetration rate should not exceed 0.2 - 0.3 mm/year for more aggressive environment such as high Cl^- concentration and seawater and, possibly, at least an order of magnitude lower in Cl^- - free environment such as tapwater. However, as demonstrated herein and in previous work,[150,205] there are clear circumstances in which such relatively low corrosion rates are unlikely to prevail over long exposure periods due to macrocell activity which can thereby cause a considerable shortening of life expectancy of an affected member. Moreover, as indicated in Chapter 6, small metal loss in structures which are critically dependent on the properties and area of tension reinforcement and subjected to high intensity load, many results in rapid deterioration in the load carrying capacity and eventually rapid failure.

For less severe loading conditions, however, the effect of metal loss may become serious after variable periods depending on bar diameter and on the margin of safety provided. Considering the particular reinforcement details used in this investigation designed with a partial safety factor of 1.6, a metal loss to cause beam failure under static load equivalent to 100% of the characteristic imposed load, should imply a reduction in steel area of approximately 37.5%. This is equivalent of 2.1 mm penetration assuming that both bars at one crack site would be corroded at equal rate. This amount of metal loss may occur in as little as one to two years in circumstances particularly favouring macrocell corrosion (such as dynamic loading at high load level).

However, for beams subjected to dynamic loading at appreciably lower stress level than static strength, longer time may be required to cause failure unless accidental over-load is occurred.

The actual extent and pattern of corrosion observed for various loading conditions in this study revealed an interesting feature which is indicated in Table 10.5. This table clearly shows that, in most of the tests carried out in this study, regardless of the test conditions, larger proportion of the corroded area was found on shear links.

This important feature would imply the following possibilities.

1. Locations of shear links, where concrete cover, is clearly lower than that to the main bars, present a potential sites for crack initiation at the concrete surface.

2. Due to geometrical effect, ie. lower cover, cracks on concrete are expected to permit easier and faster corrosion on shear links than on the main bars.

3. Cracks if occurring at locations of shear links might intercept these longitudinally and thus cause possible depassivation for larger area as compared to that occurring at the main bars where cracks intercept the bars transversally.

The basis of much of the above argument is provided from the bulk of this study which is related to short term exposure at relatively low-load. However, the additional observations on of long running tests in sea water, described earlier in Chapter 10, allows more confident conclusions to be made and generalized for longer term of exposure. In particular, these long running fatigue tests demonstrated that, under low cover to links condition, high corrosion rates indicative of macrocell processes are possible in the long term, although it is believed that macrocell distance is relatively small ie. several centimeters. Thus considerable metal losses can be expected in relevant circumstances in the long term on both the main reinforcing bars and on shear links. This is so because the possible effect of low cover to shear links on the macrocell process is to cathodically support high anodic activity at crack sites as a result of higher oxygen availability than in the case of increased cover. Also the macrocell current can travel to the crack sites through the less resistive path of low cover - solution - cracks instead of internal concrete paths of higher resistivity. Conversely if cover to embedded steel is

increased then the oxygen supply to the cathodic sites would be lower with subsequent decrease in the macrocell current and the corrosion rate at cracks.

Severe metal loss on shear links is considered highly critical as it increases tremendously the probability of fatigue failure in shear. This kind of failure as indicated in Chapter 2, is already less predictable and can occur under fatigue loading in the range of 21 - 65% of the theoretical static shear strength. It is recommended therefore, for submerged structures to:

1. Reduce the effect of discontinuity in cover thickness due to shear links. This may be achieved by either increasing the concrete cover or alternatively, if possible, by reducing the use of shear links. For the latter case, the shear resistance may be provided by the tension steel.

2. The metal loss is clearly related to the occurrence of cracks at the concrete cover. The result indicates that severe long term metal loss can occur even at very low fluctuating load (0.4 f_y) which clearly exhibit small crack width. Qualitatively, therefore, cracking in the submerged condition is strongly discouraged particularly in low-cover conditions. low cover to shear links may efficiently support dangerous levels of macrocell activity promoting considerable metal loss at crack sites.

3. Particularly when high intensity fluctuating load is expected, situations should be avoided in which relatively small metal loss can present significant reduction in the total cross section area of the bar. Thus the use of bigger bar diameter is recommended as, although the penetration will be occurring at the same rate, the fluctuating component of the stress is less effective in this case as demonstrated in Chapter 6.

Finally, visual inspections have indicated that in completely submerged conditions, movement of the corrosion

product to the concrete surface is still possible even after several years of exposure. This is shown in Figure 12.5 which presents an interesting tube-form accumulation of red-corrosion product at crack sites at the soffit of the concrete beam. The continued mobility of corrosion products in submerged conditions together with the fact that black corrosion Fe_3O_4 was found at crack sites which inherently implies less expansive corrosion product would reduce the possibility of concrete spalling. Consequently visual warning of serious corrosion may not be observed in such conditions and in particular under rapidly flowing conditions. It follows that in real-life structures the situation may necessitate more elaborate inspection techniques with the possible introduction of non-destructive techniques.

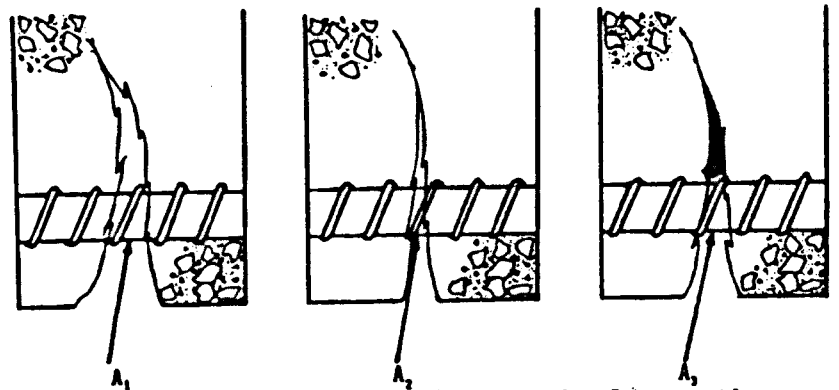

Figure (12-1): Schematic illustration of the effect of blocking materials on the permanently exposed bar area.

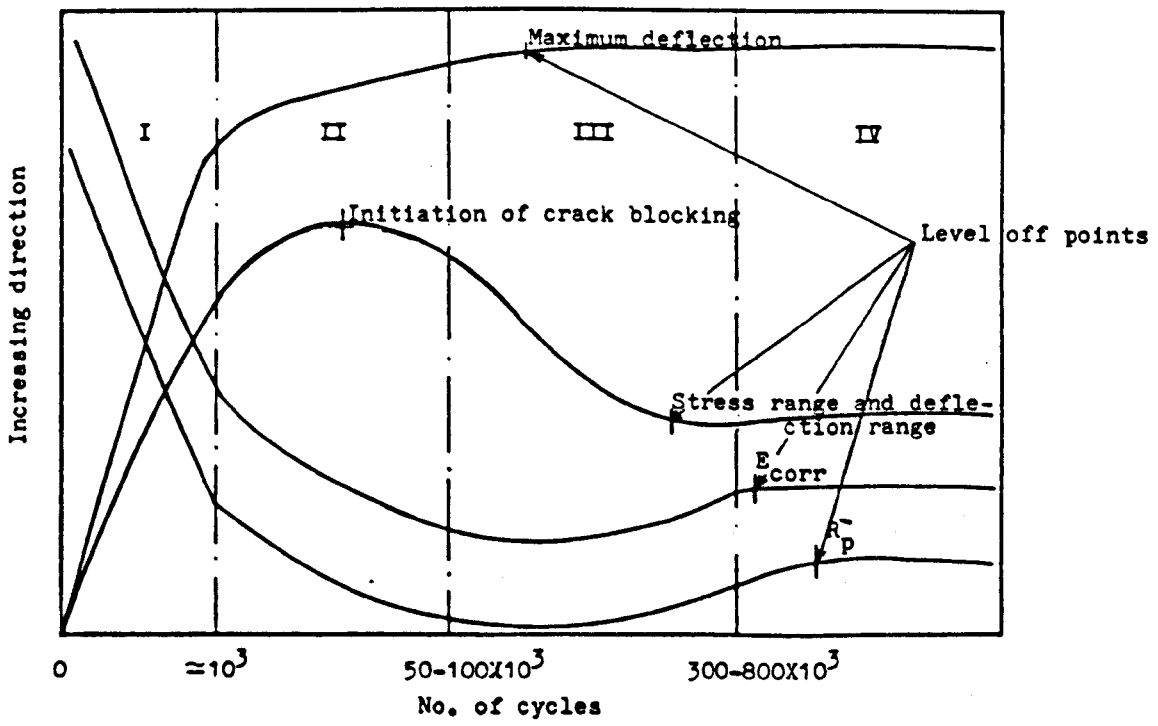

Figure (12-2): Stress-corrosion interplay for short term exposure.

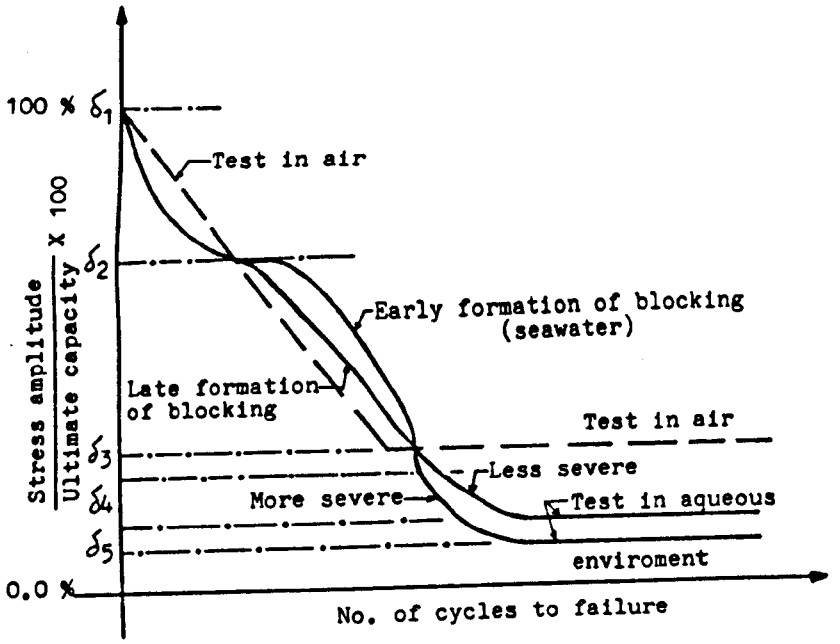

Figure (12-3): Environmental effect on the fatigue life-stress relationship at low frequency cyclic loading.

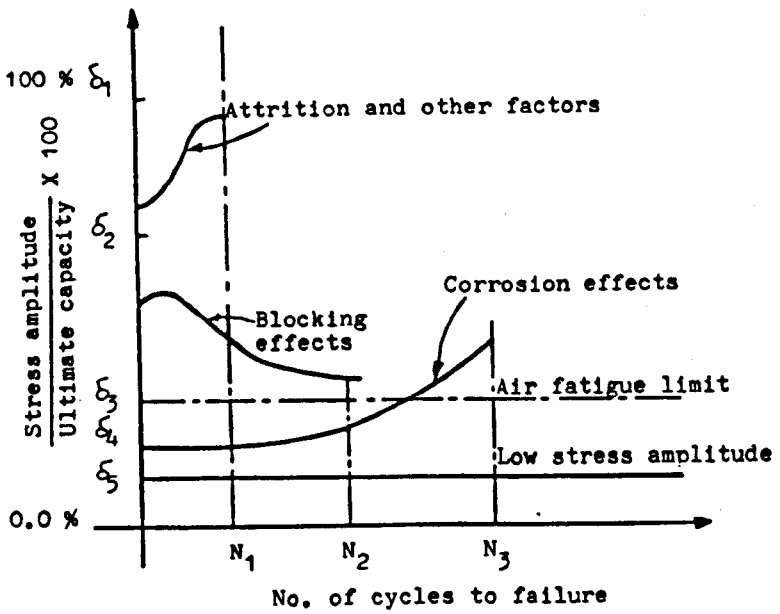

Figure (12-4): Stress variation during fatigue test in equeous environment for different stress regions.

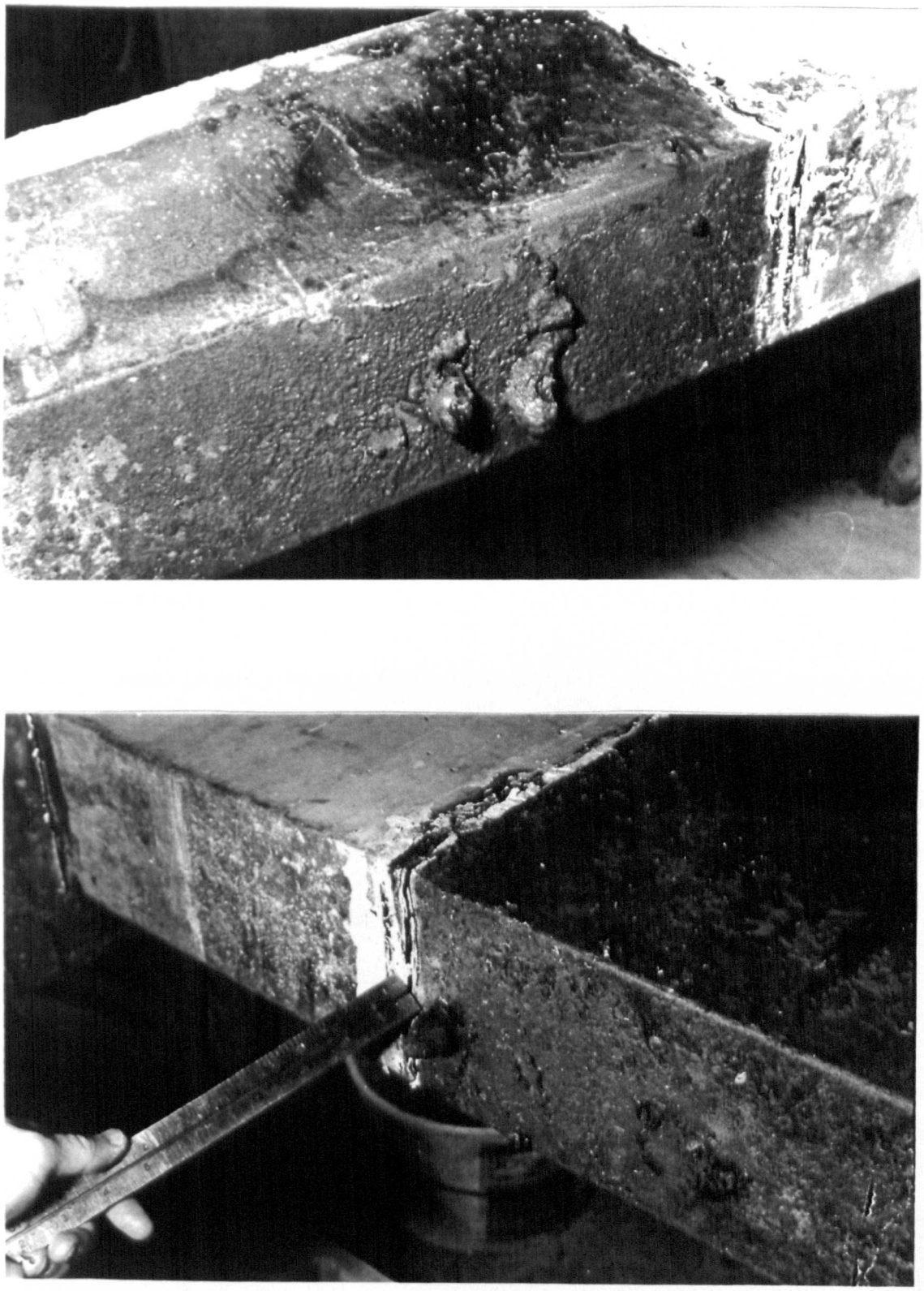

Figure (12-5): Tube-form corrosion product at the soffit of long-running test in seawater (CF100) indicative of continued ionic mobility after several years of tests.

CHAPTER 13

CONCLUSIONS AND SUGGESTIONS FOR FURTHER RESEARCH

13.1 General.

13.2 Conclusions Regarding the Structural Performance of Dynamically Loaded Reinforced Concrete.

13.3 Conclusions Regarding the Electrochemical Behaviour of Dynamically Loaded Reinforced Concrete.

13.4 Suggestions for Further Research.

CHAPTER 13

CONCLUSIONS AND RECOMMENDATIONS FOR FUTURE WORK

13.1 General.

This research has been concerned with corrosion fatigue of reinforced concrete. The research programme was planned to cover as wide a range of experimental conditions as possible, particular emphasis being focused upon dynamic loading conditions under low loads. The aims of the investigation were to provide some fundamental understanding of the phenomenon of corrosion fatigue of full scale reinforced concrete beam. The exposure conditions in tap water and sodium chloride tests were such that the most highly stressed parts of the member was totally immersed in the solution, while the remainder was surrounded by air.

The results indicated the crucial influence of the test conditions and time of exposure and dictated cautious interpretation of the experimental outputs. To provide some indications of long term exposure, a limited comparison study with other concurrently available long running tests from another research programme in seawater.

Electrochemical techniques were extensively employed particularly in Stage II of the research to provide various electrochemical data. For proper utilisation of these data, formidable difficulties had to be overcome which necessitated careful measuring practice and preliminary tests. These techniques, however, proved highly reliable in describing different types of electrochemical behaviour and were found to be compatible with the actual metal loss observed upon completion of

tests.

In general, the study indicates that the corrosion behaviour of embedded steel in concrete elements which are subjected to cyclic loading sufficient to form cracks is very complex. It also introduces the idea of change in the corrosion mechanism with exposure time from predominantly microcell to predominantly macrocell activity. This seems to describe successfully the considerable variation in the rate of metal loss observed between short and long term exposure. Consequently, unlike most other characteristics of reinforced concrete, the results suggest that the extrapolation of long term corrosion behaviour using short term indications is an extremely doubtful approach.

Both the structural and the electrochemical behaviour of dynamically loaded reinforced concrete beams are load dependent. Low level loads permit longer exposure time before fatigue failure and also introduce other stress mitigation effects due to the development of crack blocking and, therefore, tend to facilitate circumstances in which performance may be primarily determined by corrosion effects.

As a result of this investigation the following conclusions may be drawn.

13.2 Conclusions Regarding the Structural Performance of Dynamically Loaded Reinforced Concrete.

1. Test results showed the profound effect of load level on the structural behaviour of the test beams and the degree of intervention of other environmental effects (i.e. corrosion and blocking). When fatigue tested in tapwater and chloride solution, reinforced concrete beams exhibited the phenomenon of cyclic stiffening similar to, but less effective than, that observed in seawater. This was due to the formation of white deposit of $CaCO_3$ at cracks. Dynamic loading stimulates blocking more than static loading. Progressive blocking changes the loading condition from constant amplitude to multiple stage

variable amplitude.

2. In evaluating the effect of blocking, the relationship between changes in deflection and stress ranges, as proposed by Paterson,[59] may be used. The use of the area under the curve method, however, estimates more realistically the actual variation in stresses than the average stress method.

3. The effect of type of environment is greatly diminished at high load level. Fatigue fracture of reinforcement always occurred at points corresponding with cracks in the concrete. The initiation stage of failure cracks in the steel occupies a large proportion of the fatigue life. Cracks propagation by striation mechanism is very limited due to high load intensity, instead cracks propagate by ductile fracture mechanism.

4. For beams subjected to fatigue loading with more than one bar, fatigue crack are likely to initiate and grow at different rates for different bars leading to unbalanced increase of stresses in the bars. Therefore, it is recommended that, for high intensity fluctuating load in particular, situations should be avoided, in which relatively small cracks or metal loss due to corrosion can result in significant reduction in the total cross section area of the used bar. This may be achieved by using bigger bar diameters of equivalent area.

5. There is a tendency for various design curves to predict higher endurance for high load reverse bending tests than actually obtained in this study.

13.3 Conclusions Regarding the Electrochemical Behaviour of Dynamically Loaded Reinforced Concrete.

Concrete Resistance.

1. The instrumental (positive feed-back) elimination of the IR-drop was found to be extremely difficult for

complex reinforcement configurations. The current interruption technique was developed, examined and established as a powerful and simple tool in determining the IR-drop for complex multiple path system.

2. The evaluation of different techniques for the measurement of reinforced concrete resistance may be based on their influence on the electrochemical condition of the system and the degree of error resulting from polarisation effects.

The Electrochemical Measurements.

3. The appropriate choice of the technical variables for Rp determination (i.e. sweep rate and waiting time for potentiodynamic and potentiostatic techniques respectively) depends critically on the test conditions. These variables should be initially determined for every unknown system or when the test conditions substantially change during the test. Polarisation measurements, however, are troublesome for low conductivity systems such as reinforced concrete in tapwater.

4. The shape of the polarisation Tafel plots of steel embedded in concrete provide vital information on the reaction rate determining step in addition to other kinetic parameters. This kind of measurement, however, can cause electrode perturbation particularly in low corrosion rate conditions.

5. Electrochemical measurements on embedded steel are sensitive to any degree of corrosion of other metal components in contact with the test solution and this should be prevented to obtain error-free results. Also, the instrumental limitations of the measuring equipment should be carefully examined at early stage of the research.

Corrosion Process.

6. Corrosion initiates at sufficiently wide cracks and proceeds by slow microcell activity which is sensitive to local environmental changes at cracks. Under favourable conditions such as:

- aggressive environment
- high potential difference between cracked and uncracked area
- efficient cathodic supply and low cover

The microcell may change to more dangerous macrocell process causing considerable metal loss. Therefore, unless very small, cracks are strongly discouraged in submerged reinforced concrete elements. This phenomenon, i.e. change in corrosion mechanism makes the life prediction of a reinforced concrete structure extremely complex and unreliable. Wrong conclusions may be reached if the behaviour assessment is based on short term exposure.

7. Low concrete cover to links may provide an efficient cathodic current supply to fuel active anodic dissolution at cracks through a macrocell process provided that other provisions for this process are met.

8. During microcell process, analogous displacement of E_{corr} and I_{corr} and thus good correlation may be obtained between these parameters for each individual corrosion system. During macrocell activity, however, this kind of relationship is greatly diminished.

9. A foreknowledge of the electrochemical history of reinforced concrete structure is necessary for more reliable interpretation of potential data.

10. Concrete cover discontinuity at links sites are potential locations for crack initiation on the concrete surface. Therefore, greater amount of corrosion was

observed on links (longitudinally intercept the concrete cracks) which increases the risk of fatigue failure in shear. This may be avoided either by increasing the concrete cover or, if possible, by reducing the use of links. Research on this area is required.

11. Despite well established crack blocking. Corrosion product is still mobile from crack areas and thus spalling of concrete is less likely under submerged conditions than partially moist or dry conditions.

12. Any study on the corrosion properties of reinforced concrete should take into account the fact that the test results are very likely to be affected by the experimental details and thus generalisation of results on other systems of substantially different details is a very delicate task. In this respect, it is strongly recommended that such tests be performed on full scale concrete elements with reinforcing details similar to those used in practice.

Electrochemical Noise Measurements (ECN).

13. The shape of the ECN trace could provide important indications as to the corrosion activity of the system under measurements. However, indications suggest that in qualitative terms, this technique may yield similar accuracy for corrosion rate estimation to that obtained from much easier and less time consuming potential measurements.

13.4 Suggestions for Further Research.

Based on previous research and the present study, the following areas of research may be recommended for further research.

1. More extensive and detailed investigation on the actual changes in steel stresses during dynamic loading for different regime in air and in aqueous environment.

The influence of complex loading spectra including variable rest periods and the effect of stirrups on crack locations may also be investigated.

2. Research is required on the effects of the important factor of cover to links on both the anodic and the cathodic behaviour of cracked and uncracked reinforced concrete element using constant cracked to uncracked steel area ratio, (one possible way of achieving this would be to place the links inside the main bars so as to leave the cover to the latter unchanged). Continuous electrochemical monitoring and Tafel plots in particular may provide a clearer picture of the development of corrosion process with time.

3. More devoted research would be useful to examine in detail the hypothesis of the change in the corrosion process mechanism from microcell to macrocell predominance. In this respect, information on the potential distribution and change with time of the cracked and uncracked areas are of great importance.

4. The effect of different environmental exposure and the splash zone in particular on the microcell and macrocell activity. (A condition may be investigated in which water is splashed on the air parts of the beams used in this study).

5. Study, in more detail and for wider range of test conditions including real structures, of the electrochemical noise technique (ECN) on reinforced concrete structures. Emphasis may be focussed on the shape of the ECN traces and its correlation with the corrosion activity.

REFERENCES

1. Figg, J.W., Concrete, No. 5, 1980, p.34.
2. Page, C.L., Treadaway, K.W., Nature, Vol.297, No. 13, May 1982, p. 109.
3. Building Research Establishment, Digest 263, July 1982.
4. Gjorv, D.E., ACI publication , SP-49, Detroit, 1975, p. 1.
5. Somerville, G., The Structural Engineer, Vol. 64A, No. 2, 1986, p.60.
6. Hoff, G.C., Concrete International, Vol. 7, No. 8, 1985, p. 12.
7. Naesje, K., Proc. Conf. on Concrete in the Marine Environment, London, Sept. 1986, p. 405.
8. Sharp, J.V., As Reference 7, p. 1.
9. Mehta, P.K., "Durability of Concrete in Marine Environment - A Review", ACI publication, SP-65, Detroit, p.1, 1980.
10. Scheffey, C., Civil Engineering - ASCE, July 1971, p. 41.
11. Westerberg, B, Proceeding BOSS Conference, 1976.
12. Taylor, H.P. and Sharp, J.V., The Structural Engineer, No. 3, Vol, 56A, March 1978, p. 69.
13. Tilly, G.P., Fatigue of Engineering Materials and Structures, Vol, 2, 1979, p. 251.
14. Tilly, G.P., Materiaux et Constructions, Vol. 17, No. 97, 1984, p. 43.
15. Gerwick, B. Jr., Concrete International, Vol. 7, No. 8, 1985, p. 34.
16. Weibull, W., "Fatigue Testing and Analysis of Results", Pergamon Press, London, 1961, p. 65.
17. Mann, J.Y., "Fatigue of Materials", Melbourne University Press, Melbourne, 1967, p. 5.
18. Nordby, G.M., J. ACI, Vol. 55, August 1958, p. 191.
19. Arthur, P.D., et al, Concrete, No. 5, 1979, p. 26.
20. Katwan, M.J., et al, Proceeding International Conference on Structural Faults and Repair, London, 1987, p. 191.
21. Browne, R.D. and Damome, P.L., Proc. Conf. on

Underwater Construction Technology, Univ. College, Cardiff, 1975.

22. Bannister, J.L., The Structural Engineer, No. 3, Vol. 56A, March 1978, p. 82.
23. Lacroix, R., Paper Presented at the International Conference on Underwater Construction Technology, University College, Cardiff, 1975.
24. Venables, R.K., et al, Proc. Conf. on Concrete in the Marine Environment, London, Sept., 1986, p. 25.
25. Kiyomiya, O. et al, as Reference 7, p. 13.
26. Ruiz, W.M. and Winter, G., J. of the Structural Division, Proc. ASCE, Vol. 95, No. ST6, June 1968.
27. Waagaard, K., Proc. 9th Offshore Technology Conference, Houston, 1977, Paper No. 3009.
28. Salah el Din, A.S. and Lovegrove, J.M., Fatigue of Engineering Materials and Structures, Vol. 3, No. 4, 1980, p. 315.
29. Moncrieff, M.L., Concrete, January, 1972, p. 26.
30. Sinha, B.P., et al, J. ACI, vol. 61, No. 8, August 1964.
31. Hawkins, N.M., ACI publication, SP-41, Detroit, 1974, p. 203.
32. Fidjestol, B. and Nilsen, N. ACI publication SP-65, Detroit, 1980, p. 205.
33. Aziz, M.A., Corrosion of Reinforcement in Concrete Construction, Society of Chemical Industry, London, 1983, p. 91.
34. Stratfull, R.F., Highway Research Record 433, 1973, p. 1.
35. Hartt, W.H., Design of Fatigue and Fracture Resistant Structures, ASTM STP-761, 1982, p.91.
36. ACI committee 215, "Consideration for Design of Concrete Structures Subjected to Fatigue Loading", J. ACI, March 1974.
37. Forrest, P.G., "Fatigue of Metals", Pergamon Press, London, 1962.
38. Waagaard, K., Fatigue of Concrete Structures, ACI publication SP-75, Detroit, 1982, p. 373.
39. Findley, W.N., "Test Procedure and Technique", Manual of Fatigue Testing, ASTM SPT-91, 1949.

40. Holmen, J.O., as Reference 38, p. 71.
41. Siemes, A.J., as Reference 38, p. 343.
42. Taira, S., et al, ASTM STP-675, 1979, p. 135.
43. Kitagawa, H. and Takahashi, S., as Reference 42, p. 420.
44. Hetherington, G.B., "Fatigue of Reinforced Concrete in Air, Chloride Solution and Seawater", MSc Thesis, University of Sydney, March 1981.
45. Miner, M.A., Transactions, ASME, Vol. 67, 1945.
46. Hilsdorf, H. and Kesler, C., J. ACI, Vol. 63, No. 10, October 1966.
47. British Steel Corporation, Swinden Laboratories, Contract Report, RSC/2459/1/84, 1984.
48. Snowdon, L.C., Building Research Station, CP 7/71, 1971.
49. Taylor, H., et al, The Structural Engineer, No. 3, Vol. 56A, March 1978.
50. Moss, D., "Bending Fatigue of High-Yield Reinforcing Bars in Concrete", TRRL Report 748, 1982.
51. MacGregor, J., et al, J. ACI, Vol. 68, No. 3, 1971.
52. Weck, T., Nordic Concrete Research, Oslo, No. 1, Dec. 1982.
53. Soretz, S., as Reference 31, p. 35.
54. Burton, K. and Hognestad, E., J. ACI, Vol. 64, May 1967.
55. Jhamb, I. and MacGregor, J., as Reference 31, p. 139.
56. Bannister, J., Concrete, Vol. 3, No. 10, October 1969, p. 405.
57. Katagiri, K., Awatani, J. and Omura, A., "Dislocation Structures Around the Crack Tips in the Early Stage in Fatigue of Iron", ASTM, STP-675, 1979, p. 106.
58. Manfred, A. and Fisher, J., Highway Research Record, No. 400, 1972.
59. Paterson, W., Dill, M., Newby, R., Concrete in the Oceans Report P6, CIRIA, London, April 1981.
60. Lynch, S., as Reference 57, p. 174.
61. Paris, P., Proc. 10th Sagamore Army Material Research Conference, Syracuse University Press, 1964.
62. Naaman, A., as Reference 38, p. 25.
63. Abeles, P., et al, as Reference 31, p. 237.

64. Kormeling, H., et al, J. ACI, vol. 77, No. 1, January-February 1980.
65. Jagdish, L., "Dynamic Response of Reinforced Concrete Flexural Members", MSc Thesis, The Ohio State University, 1970.
66. Bishara, A., as Reference 38, p. 235.
67. Bennett, E., as Reference 38, p. 177.
68. Sparks, P., Menzies, J., The Structural Engineer, No. 11, Vol. 51, 1973, p. 413.
69. Lovegrove, J. and Salah, E., as Reference 38, p. 133.
70. Aas-Jakobsen, K. and Lenschow, R., J. ACI, Vol. 70, No. 3, 1973.
71. Bertero, V. and McClure, G., J. ACI, Vol. 61, No. 10, 1964.
72. Balaguru, P. and Shah, S., as Reference 38, p. 153.
73. Whaley, C. and Neville, A., Magazine of Concrete Research, Vol. 25, No. 84, September 1973, p. 145.
74. Chang, T. and Kesler, C., J. ACI, Vol. 54, No. 12, 1958, p. 1033.
75. Chang, T. and Kesler, C., J. ACI, Vol. 55, No. 2, 1958, p. 245.
76. Raithby, K. and Galloway, J., as Reference 31, p. 15.
77. Kesler, C., Proc. Highway Research Record 33, 1953, p. 251.
78. Hockenhull, B., Report P6/11. Concrete in the Oceans Project, CIRIA, London.
79. Arthur, P., et al, as Reference 38, p. 1.
80. Bjuggren, U., J. ACI, Vol. 64, No. 10, 1967, p. 625.
81. LeCamns, B., Laboratories du Batiment et des Travaux Publics, Paris, 1946.
82. Lambotte, H. and Baus, R., "Experimental Study of the Effect of Fatigue on the Behaviour of Reinforced Concrete Beams", Revue C, No. 3, 1963.
83. Verna, J. and Stelson, T., J. ACI, Vol. 60, No. 6, 1963.
84. Barnoff, R., Paper presented at ACI Committee 408 Meeting, New York, April 1970.
85. Higai, T., Paper presented at 14th Meeting of Japan Congress of Materials Research, Kyoto, September 1970.

86. Stelson, T. and Cernica, J., "Fatigue Properties of Concrete Beams", J. ACI, Vol. 55, No. 2, 1958, p. 255.
87. West, J., "Basic Corrosion and Oxidation", Ellis Horwood, Chichester, second addition, 1986.
88. Chandler, K., "Marine and Offshore Corrosion", Butterworth, London, 1985.
89. Stern, M., Geary, A., " J. Electrochem., Soc., Vol. 104, No. 1, 1957, p. 56.
90. Gonzalez, J. and Andrade, M., Corrosion 85, Paper 257, Boston, USA, 1985.
91. Bandy, R., Corr. Sci., Vol. 20, 1980, p. 1017.
92. Feitler, H., Material Protection and Performance, October, 1970.
93. Stern, M., Weisert, E., Proc. ASTM, Vol. 59, 1959, p. 1280.
94. Wagner, C. and Traud, W., Z. Electrochem., Vol. 44, 1938, p. 391.
95. Simmons, E., Corrosion, Vol. 11, 1955, p. 255.
96. Skold, R. and Larson, T., Corrosion, Vol. 14, 1957, p. 139t.
97. Stern, M., Corrosion, Vol. 14, p. 440t, 1958, p. 440t.
98. Mansfield, F., Corr. Sci., Vol. II, 1971, p. 787.
99. Leory, R., Corrosion, Vol. 29, No. 7, 18973, p. 272.
100. Callow, L., et al, Br. Corr. J., Vol II, No. 3, 1976, p. 132.
101. Barnartt, S., Corr. Sci., Vol 9, p. 145, 1969, p. 145.
102. Oldham, K. and Mansfeld, F., Corrosion, Vol. 27, No. 10, 1971, p. 434.
103. Mansfled, F., Corrosion, Vol. 32, No. 4, 1976, p. 143.
104. Gonzalez, J., et al, Corr. Sci, Vol. 25, No. 10, 1985, p. 917.
105. Ijesseling, F,. Br. Corr. J., Vol. 21, No. 2, 1986, p. 95.
106. Oldham, K. and Mansfeld, F., Corr. Sci., Vol. 13, 1973, p. 813.
107. Mansfeld, F., Corr., Vol. 29, No. 10, 1973, p. 397.

108. Callow, L., et al, Br. Corr. J., Vol. II, No. 3, 1976, p. 123.
109. Hodgkiess, T,. "Corrosion", Notes for Master Degree in Building Services Engineering, University of Glasgow.
110. Hope, B., et al, Cem. Conc. Res., Vol. 16, 1986, p. 771.
111. Dawson, J., As Reference 33, p. 175.
112. Gonzalez, J., et al, Corr. Sci., Vol. 25, No. 7, 1985, p. 519.
113. John, D., et al, Br. Corr. J., Vol. 16, No. 2, 1981, p. 519.
114. Boyd, W. and Tripler, A., Materials Protection, No. 10, 1968, p. 40.
115. Cornet, I., et al, Materials Protection, No. 3, 1968, p. 44.
116. Hausmann, D., Materials Protection, No. 11, 1967, p. 19.
117. Hansson, C., Cem. Conc. Res., Vol. 14, 1984, p. 574.
118. Wilkins, N. and Lawrence, P., As Reference 33, p. 119.
119. Pourbaix, M., Corr. Sci., Vol. 14, Jan. 1974, p. 25.
120. ACI Committee 222, J. ACI, Vol. 82, No.1, 1985, p. 3.
121. Treadaway, K., As Reference 33, p. 101.
122. Cavalier, P. and Vassie, P., Proc. Instn. Civ. Engrs. Part 1, Vol. 70, Aug. 1981, p. 481.
123. Rasheeduzzafar, et al, Conc. Inter., Vol. 7, No. 9, 1985, p. 48.
124. Rasheeduzzafar, et al, J. ACI, vol. 81, No. 1, 1984, p. 13.
125. Seki, H., Conc. Inter., Vol. 3, No. 3, 1981, p. 57.
126. Darwin, D., et al, Conc. Inter., Vol. 7, No. 5, 1985, p. 20.
127. Perkins, P., Conc. Inter., Vol. 3, No. 4, 1981, p. 75.
128. Atimtay, E. and Ferguson, P., Materials Protection, No. 12, 1974, P. 18.
129. Currie, R,. As Reference 33, P. 11.
130. Erlin, B. and Verbeck, G., As Reference 4, p. 39.
131. Mehta, P. and Gerwick, B., Conc. Inter., Vol. 4, No.

10, 1982, p. 45.
132. Gonzalez, J., et al, As Reference 33, P. 159.
133. Wood, R. and Wyatt, B., As Reference 20, P. 263.
134. Fattuhi, N., As Reference 20, p. 255.
135. Cox, T., Concrete, Dec. 1986, p. 9.
136. Cook, H. and McCoy, W., As Reference 3, P. 20.
137. Kawadkar, K. and Krishnamoorthy, S., Cem. Conc. Res,. Vol II, 1981, p. 103.
138. Arya, C. and Buenfeld, N., As Reference 20 , p. 137.
139. Building Research Establishment Digest, 264, August 1982.
140. Gjorv, O., Cem. Conc. Res., Vol. 9, 1979, p. 229.
141. Page, C. and El Tarras, A., Cem. Conc. Res., Vol II, 1981, p. 395.
142. Holden, W., et al, As Reference 33, p. 143.
143. Erlin, B. and Verbeck, J., As Reference 9, p. 34.
144. Arup, H,. As Reference 33, p. 151.
145. Beeby, A., Concrete in the Oceans, Report No. 1, CIRIA, London, 1978.
146. Grimes, W., et al, Corrosion, Vol. 35, No. 7, 1979, p. 309.
147. Tuutti, K., The Swedish Cement and Concrete Research Institute, Report 6:78, Stockholm.
148. Tremper, B., J. ACI, Vol. 18, No. 10, 1947, p. 1137.
149. Beeby, A., Conc. Inter., Vol. 5, No. 2, 1983, p. 35.
150. Hodgkiess, T., et al, Materials Performance, Vol. 23, No. 7, 1984, p. 27.
151. Hope, B., et al, Cem. Conc. Res., Vol. 15, 1985, p. 525.
152. Gonzalez, J. and Andrade, C., Br. Corr. J., Vol. 17, No. 1, 1982, p. 21.
153. Browne, R., Durability of Building Materials, Vol. 1, 1982, p. 113.
154. Clear, K., Report No. FHWA/RD-82/028, Federal Highway Administration, Washington, D.C., 1982.
155. Bazant, Z., Proc. ASCE, Vol. 105, No. ST6, 1979, p. 1137.
156. Bazant, Z., Proc. ASCE, Vol. 105, No. ST6, 1979, p. 1155.
157. Gronvold, F., 2nd Int. Seminar on Electrochemistry

and Corrosion of Steel in Concrete, Copenhagen, 1982.
158. Page, C., Mag. Conc. Res., No. 137, Dec. 1986, p. 174.
159. Browne, R., Durability of Building Material, No. 1, 1982, p. 113.
160. Tuuti, K., As Reference 33, p. 193.
161. Browne, R., As Reference 33, p. 193.
162. Berke, N. and Stark, P., Conc. Inter., Vol. 7, No. 9, p. 42,1985.
163. Page, C. and Lambert, P., Final Report to TRRL, Crowthorne, 1986.
164. Weyers, R., Cady, P., J. ACI, Vol. 81, No. 11, 1984, p. 618.
165. Stratfull, R., Materials Performance, Vol. 13, No. 4, 1974, p. 24.
166. Stratfull, R., As Reference 33, p. 287.
167. Venables, R., et al, As Reference 7, p. 25.
168. Slater, J., Material Performance, Vol. 18, No. 6, 1979, p. 34.
169. Flick, L. and Lloyd, P., Corrosion of Reinforcing Steel in Concrete, ASTM, STP-713, 1980, p. 93.
170. Browne, R., et al, As Reference 7, p. 321.
171. Coote, A., et al, As Reference 7, p. 333.
172. Stratfull, R., highway Research Record 433, 1973, p. 12.
173. ASTM C876-80, Annual Book of ASTM Standards, Part 10.
174. Wood, J., et al, As Reference 20, Vol. 2, p. 407.
175. Hansson, I. and Hansson, C., Cem. Conc. Res., Vol. 13, 1983, p. 675.
176. Cherry, B. and Kashmirian, A., Br. Corr. J., Vol. 18, No. 4, 1983, p. 194.
177. Whittington, H., et al, Mag. Conc. Res., Vol. 33, No. 114, Mar. 1981, p. 48.
178. Calleja, J., J. ACI, Vol. 48, Mar. 1952, p. 525.
179. Calleja, J., J. ACI, Vol. 50, Nov. 1953, p. 249.
180. Taylor, M. and Arulanandan, K., Cem. Conc. Res., Vol. 4, 1974, p. 881.
181. McCarter, W. and Curran, P., Mag. Conc. Res., Vol. 36, No. 126, Mar. 1984, p. 42.
182. Morelli, R. and Forde, M., As Reference 20, Vol. 2,

p. 411.

183. Wilkins, N., Material Development Division, AERE Harwell, Jan., 1982.
184. Langford, P. and Broomfield, J., Construction Repair, Vol. 1, No. 2, May 1987, p. 32.
185. Monfore, G., J. PCA Res. Dev. Lab., Vol. 10, May 1968, p. 35,
186. Hammond, E. and Robson, T., The Engineer, Vol. 199, Jan. 1955, p. 78.
187. Hammond, E. and Robson, T., The Engineer, Vol. 199, Jan. 1955, p. 114.
188. Woelfl, G. and Lauer, K., Cem. Conc. Agg., Vol. 1, No. 2, 1979, p. 64.
189. Spencer, R., J. ACI, Vol. 34, Sept. 1937, p. 45.
190. Hausmann, D., J. ACI, Vol. 61, Feb. 1964, p. 171.
191. Hughes, B., et al, Mag. Conc. Res., Vol. 37, No. 133, Dec. 1985, p. 243.
192. Calleja, J., J. ACI, Vol. 49, Dec. 1952, p. 329.
193. Boast, W., J. ACI, Vol. 33, Nov. 1936, p. 131.
194. McCarter, W., et al, Proc. Instn. Civ. Engrs., Part 2, Vol. 71, Mar. 1981, p. 167.
195. Martin, B., Material Performance, Vol. 20, Jan. 1981, p. 52.
196. Stratfull, R., Material Protection, Mar. 1968, p. 29.
197. Jones, G. and Christian, S., J. Ame. Chem. Soc., Vol. 57, Feb. 1935, p. 272.
198. Silverman, D., Corrosion, Vol. 36, No.8, 1982, p.453.
199. Gerwick, B., J. PCI, Sept. 1981, p. 82.
200. Okamura, H. and Hisamatsu, Y., Materials Performance, Vol. 15, July 1976, p. 43.
201. Paterson, W., As Reference 9, p. 419.
202. Roper, H. and Hetherington, G., As Reference 38, p. 307.
203. Paterson, W. and Dill, M., Concrete in the Oceans, Projects 5b, 5e and A4 Final Report, Nov. 1984.
204. Banerjee, H., et al, Proc. Boss, Delft, July 1985.
205. Nilsen, N. and Espelid, B., Corrosion 85, Boston, Massachusetts, March 1985, Paper 261.
206. Hodgkiess, T. and Arthur, P., Concrete in the Oceans, Project 5C, Final Report, 1986.

207. Espelid, B., et al, As Reference 7, p. 393.
208. Abrams, D,. Proc. ASTM, Vol. 13, 1913, p. 884.
209. Abrams, D., University of Illinois, Engineering Experimental Station, Bull. No. 71, 1913.
210. Gilkey, H., Proc. ASTM, Vol. 26, 1929, p. 470.
211. Gilkey, H., Proc. ASTM, Vol. 26, 1929, p. 593.
212. Bogue, R., Discussion Paper, Proc. ASTM, Vol. 29, 1929, p. 608.
213. Turner, L., Concrete and Constructional Engineering, Vol. 32, Feb. 1937, p. 141.
214. Whitlam, E., The Structural Engineer, Vol. 32, Sept. 1954, p. 235.
215. Dhir, R., J. ACI, Vol. 70, No. 3, Mar. 1973, p. 231.
216. Munday, J., et al, Proc. 1st Australian Conference on Engineering Material, The University of New South Wales, 1974, p. 231.
217. Trinh, J. and Peyronnet, J., Annales de Institute Technique du Batiment et des Travaux Publics, No. 360, April 1978, p. 42.
218. British Standards Institution, BS 8110, BSI London, 1985.
219. British Standards Institution, BS 5400, BSI London, 1978.
220. ACI Committee 357, ACI J., Vol. 75, No. 12, 1978, p. 684.
221. Det Norske Veritas, "Rules for the Design, Construction and Inspection of Offshore Structures", Appendix D., Concrete Structure, DNV, Norway, 1980.
222. FIP Commission on Concrete Sea Structures, "Recommendation for the Design and Construction of Concrete Sea Structures", Appendix D, Concrete Structure, DNV, Norway, 1980.
223. NPD, "Regulation for the Structural Design of Fixed Structures on the Norwegian Continental Shelf", Norwegian Petroleum Directorate, 1977.
224. Booth, E., et al, As Reference 7, p. 187.
225. Butler, J., "Carbon Dioxide Equilibria and their Applications", Addison-Wesley Publishing Company, California, 1986, p. 185.
226. Neville, A., "Properties of Concrete", Pitman

Publishers, London, 2nd Edition, 1973, p. 12.

227. Fontana, M., "Corrosion Engineering", McGraw-Hill, London, 1986, p. 198.
228. Grimaldi, G., et al, Br. Corr. J., Vol. 21, No. 1, 1986, p. 55.
229. Wilkins, N., et al, Concrete in the Oceans Phase II, P1a Final Report, Cement and Concrete Association, 1985.
230. Okada, K. and Miyagawa, T., As Reference 9, p. 237.
231. Hodgkiess, T., et al, Desalination, 66, 1987, p. 147 .
232. Hladky, K. and Dawson, J., Corr. Sci., Vol. 21, No. 4, 1981, p. 317.
233. Hladky, K. and Dawson, J., Corr. Sci., Vol. 22, No. 3, 1982, p. 217.
234. Hardon, R., et al, "Paper Presented at the 28th Corrosion Science Symposium, Sept. 1987.
235. Bertocci, U., J. Electroch. Soc., 127, 1980, p. 1931.
236. Bertocci, U., J. Electroch. Soc., 128, 1981, p. 520.
237. Lambert, P., Private Communication, Sept., 1987.
238. Browne, D., Paper Presented at a Seminar Organised by the Institution of Structural Engineers in Association with the Corrosion Control Engineering Joint Venture, London, July 1988, p.
239. Hodgkiess, T., Private Communication, 1988.

APPENDICES

Appendix A: Working Stress and Deflection Calculations.

Appendix B: Equilibria in the CO_2/Water System.

APPENDIX A

Working Stress and Deflection Calculations

This appendix presents the calculations used to relate the applied flexural load and the stress in the tensile reinforcement.

Calculations were made on the assumptions that:

1. Lacing bars are assumed to carry very small load in compression zone.
2. In moment calculation, the dead load is assumed to be zero (high applied load/dead load ratio).

Working Stress Calculation

$F = 0$ leads to

steel tension + concrete tension = concrete compression

$$A_s.f_s + \frac{b.}{2} f'_c (250 - x) = f_c.x.\frac{b}{2} \quad \ldots 1$$

substitute values of:

$$f_c = f_s.\frac{x}{220 - x} \cdot \frac{E_c}{E_s} \quad \ldots 2$$

$$f'_c = f''_c \frac{250 - x}{220 - x} \quad \ldots 3$$

where $f''_c = 1\ N/mm^2$

$$A_s f_s + \frac{b}{2}\frac{(250 - x)^2}{(220 - x)} = \frac{f_s . x^2 . b}{2(220 - x)} \cdot \frac{E_c}{E_s} \quad \ldots 4$$

To find the moment M, take moment of force about the neutral axis, NA:

$$M = A_s f_s (220 - x) + \frac{b}{3}.\frac{(250 - x)^3}{(220 - x)} = \frac{f_s x^3 b}{3(220 - x)} . \frac{E_c}{E_s}$$

$$\ldots 5$$

Taking trial values of x in Equations 4 and 5 the corresponding values of f_s and M can be obtained as shown in Table A.1 and the graph shown in Figure A.2 can be constructed.

x (mm)	f_s (N/mm^2)	M (KNm)
50	787	25.72
51	571	18.80
57	199	6.93
60	144	5.20

Table A.1: Trial values of x and the corresponding f_s and M values.

From Figure A.2 the applied moment for a given steel stress can be obtained. From Figure A.3, relating the applied load p to maximum bending moment gives:

$$p = 2M \qquad \ldots 6$$

Therefore the procedure to obtain the load magnitude necessary to produce the required stress in the tension steel, can be summarised as follows.

1. Obtain x from a given f_s using curve (f_s) in Figure A.2.

2. Extrapolate M for the resulted x from curve (M) in Figure A.2.

3. Obtain p using Equation 6.

Deflection Calculation.

Figure A.2 was also used to calculate the deflection, hence from x f_s and the corresponding x the curvature $1/r_b$ can be determined using the equation:

$$\frac{1}{r_b} = \frac{f_s}{(d - x)E_s} \qquad \ldots 7$$

and the short term deflection "a" equals:

$$a = K L^2 \frac{1}{r_b} \qquad \ldots 8$$

where L = is the effective span of the member
K = is a constant that depends on the slope of the bending moment diagram.

For the particular loading arrangements employed in this research:

$$K = 0.125 - \frac{a^2}{6}$$

where $a = \frac{1}{L} = 0.357.$

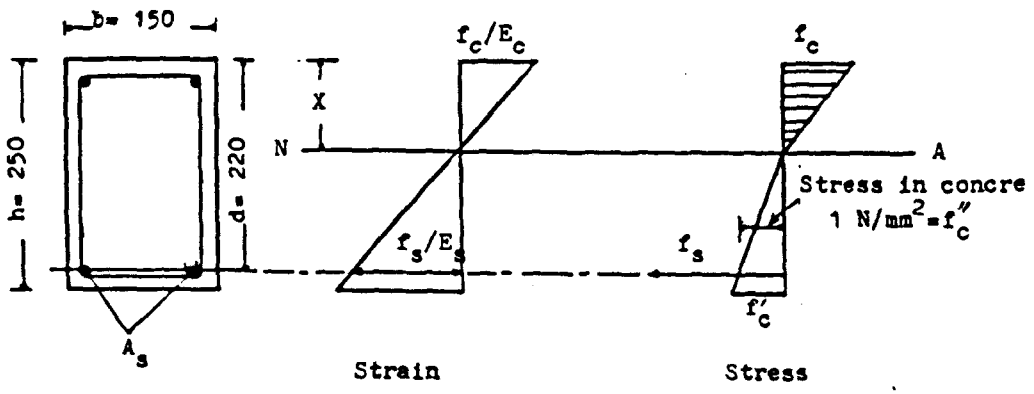

Figure (A-1): Details of beam cross section and assumption made in calculation.

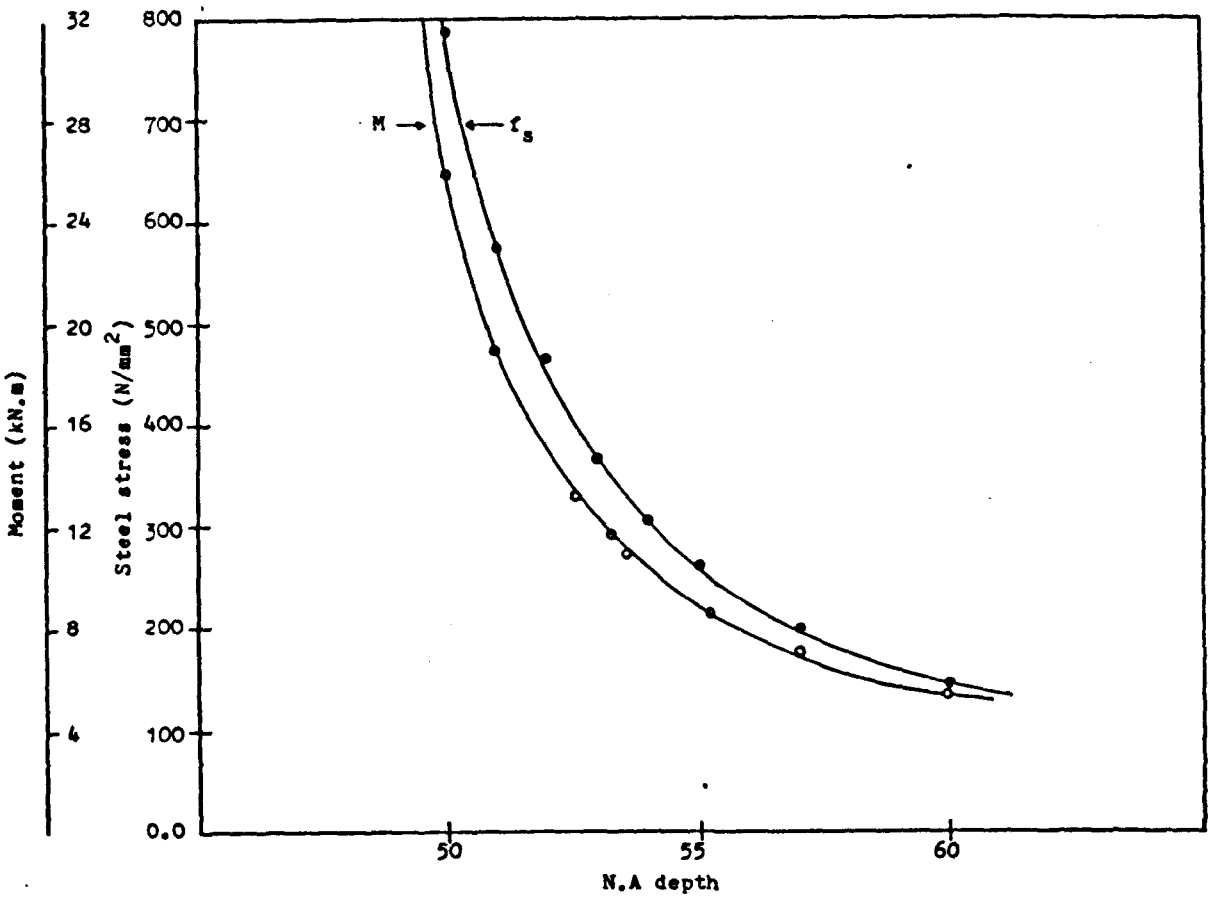

Figure (A-2): Moment,steel stress relationship with N.A depth.

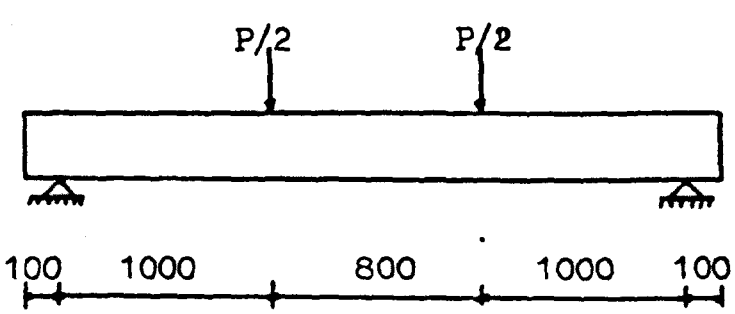

Figure (A-3): Test beams loading configuration.

APPENDIX B

Equilibria in the CO_2/Water System

The dissolution of CO_2 in water obeys the equilibrium:

$$CO_{2(g)} = CO_{2(aq)} \qquad K_H = 10^{-1.5} \qquad ...1.B$$

where the subscripts (g) and (aq) represented CO_2 in the gaseous atmosphere and dissolved in water respectively.

K_H is the thermodynamic equilibrium constant for the dissolution process at 25°C [note: all equilibrium constants quoted in the following analysis refer to 25°C].

Some $CO_{2(aq)}$ hydrolyses:

$$CO_{2(aq)} + H_2O = H_2CO_3 , \qquad K_2 = 10^{-2.8} \qquad ...2.B$$

The H_2CO_3 dissociates according to the equilibrium:

$$H_2CO_3 = H^+ + (HCO_3)^- \qquad K_3 = 10^{-3.5} \qquad ...3.B$$

and $(HCO_3)^-$ can yield $(CO_3)^{2-}$

$$(HCO_3)^- = H^+ + (CO_3)^{2-} \qquad K_4 = 10^{-10.3} \qquad ...4.B$$

Because very little $CO_{2(aq)}$ in fact hydrates to H_2CO_3, it is convenient to consider a hypothetical species:

$$H_2CO_3^* = CO_{2(aq)} + H_2CO_3 \quad \text{ie. } C_{H_2CO_3^*} \simeq C_{CO_{2(aq)}}$$

in which case the formation of $(HCO_3)^-$ can be expressed:

$$H_2CO_3^* = H^+ + (HCO_3)^- \qquad K_5 = 10^{-6.3} \qquad ...5.B$$

The equilibrium expression for reaction 5.B is:

$$\frac{a_{(HCO_3)^-} \times a_{H^+}}{a_{H_2CO_3^*}} = K_5 = 10^{-6.3}$$

Where a_{H^+}... etc refers to the activity of the species. Rearranging the above equation,

$$a_{(HCO_3)^-} = 10^{-6.3} \times \frac{a_{(H_2CO_3^*)}}{a_{H^+}}$$

A value for $a_{H_2CO_3^*}$ can be obtained from a consideration of the CO_2 dissolution equilibria from Reaction 1.B:

$$\frac{a_{CO_{2(aq)}}}{a_{CO_{2(g)}}} = 10^{-1.5}$$

Assuming ideal behaviour in the gaseous atmosphere, $a_{CO_{2(g)}}$ can be replaced by the partial pressure of CO_2 in the normal atmosphere ($10^{-3.5}$ atm),

hence, $a_{CO_2(aq)} = 10^{-1.5} \times 10^{-3.5} = 10^{-5}$

$\simeq a_{H_2CO_3^*}$ (as reasoned earlier)

and $$a_{HCO_3^-} = \frac{10^{-6.3} \times 10^{-5}}{a_{H^+}} = \frac{10^{-11.3}}{a_{H^+}}$$

or

$$-\log_{10} [a_{HCO_3^-}] = 11.3 - pH \qquad ...6.B$$

from Equation B4:

$$a_{CO_3^{2-}} = \frac{10^{-10.3} \times a_{HCO_3^-}}{a_{H^+}}$$

$$= \frac{10^{-10.3}}{a_{H^+}} \times \frac{10^{-11.3}}{a_{H^+}}$$

or

$$-\log_{10} (a_{CO_3^{2-}}) = 21.6 - 2\,pH \qquad ...7.B$$

Dissolution of $Ca(OH)_2$

When the water comes into contact with the concrete beam, dissolution of $Ca(OH)_2$ will occur:

$$Ca(OH)_2(solid) = Ca^{2+} + 2(OH)^- \qquad ...8.B$$

Let us assume, initially, that dissolution occurs up to the point at which the water becomes saturated with $Ca(OH)_2$ i.e. to solubility equilibrium according to:

$$\frac{a_{Ca^{2+}} \times (a_{(OH)^-})^2}{a_{Ca(OH)_2}} = K = 5.01 \times 10^{-6} \quad \ldots 9.B$$

Assuming that pure $Ca(OH)_2$ is dissolving $a_{Ca(OH)_2}$ can be taken as unity. The dissolution reaction (8.B) yields $2(OH)^-$ for every Ca^{2+} ion.

$$\text{hence,} \quad C_{(OH)^-} = 2\, C_{Ca^{2+}} + C_{(OH^-)_0} \quad \ldots 10.B$$

where $C_{(OH)^-_o}$ is the concentration of $(OH)^-$ in the test solution before coming into contact with concrete. For tapwater, the pH is 8 (and for NaCl it is lower than this). Since at 25°C, $a_{H^+} \times a_{OH^-} = 1 \times 10^{-14}$, this means $a_{(OH^-)_o}$ is around 10^{-6}. Since the activity coefficient, f_{OH^-}, is near to unity (see later) $C_{OH^-_o} < 10^{-5}$ (since a = cf) which is much less than the concentration of $(OH)^-$ ions introduced into the solution by subsequent dissolution of $Ca(OH)_2$. Thus $C_{(OH)^-_o}$ can be ignored and from 9.B and 10.B above, we can write:

$$[C_{Ca^{2+}}\ f_{Ca^{2+}}] \times [2C_{Ca^{2+}}\ f_{OH^-}]^2 = 5.01 \times 10^{-6} \quad \ldots 11.B$$

Estimates of the activity coefficient, $f_{Ca^{2+}}$ and $f_{(OH)^-}$, obtained from expressions available in the literature have been provided[239]:

For 3.5% NaCl/saturated $Ca(OH)_2$,

$$f_{Ca^{2+}} = 0.31, \quad f_{(OH)^-} = 0.75$$

For tapwater/saturated $Ca(OH)_2$,

$$f_{Ca^{2+}} = 0.33, \quad f_{(OH)^-} = 0.76$$

(Note: These similar activity coefficients in solution of widely-different ionic strength arise due to the tendency at higher ionic strength for the relationship between these 2 parameters to reverse).

Because of the close values of activity coefficient in NaCl and tapwater, it is only necessary to do the calculations for one of them, say NaCl.

Using Equation 11.B:

$$C_{Ca^{2+}} = \sqrt[3]{\frac{5.01 \times 10^{-6}}{0.31 \times 4 \times 0.75^2}} = 1.93 \times 10^{-2}$$

and from Equation 9.B

$$a_{(OH)^-} = \sqrt[3]{\frac{5.01 \times 10^{-6}}{1.93 \times 10^{-2} \times 0.31}} = 2.89 \times 10^{-2}$$

hence, $$a_{H^+} = \frac{10^{-14}}{2.89 \times 10^{-2}} = 34.6 \times 10^{-4}$$

and pH = 12.46

This calculated pH for saturated Ca(OH) is fairly close to our values (up to 11.5) measured in the experiments and thereby gives some support to the

assumption that $Ca(OH)_2$ initially being dissolved from the concrete up to the point of saturation.

Estimate of Precipitation of $CaCO_3$.

For this purpose, the value $C_{Ca}2+ = 1.93 \times 10^{-2}$ may be used (as calculated earlier), and note that for the extended duration of the tests, the test solution pH was held at about 8.5.

Using Equation 7.B:

$$-\log_{10} a_{(CO_3)}2- = 21.6 - 2\ pH = 21.6 - 17 = 4.6$$

hence, $a_{(CO_3)}2- = 2.51 \times 10^{-5}$

Consequently ion activity product in the water,

$$[a_{Ca}2+ \times a_{(CO_3)}2-] = 1.93 \times 10^{-2} \times 2.51 \times 10^{-5}$$

$$= 4.84 \times 10^{-7}$$

and this value is well in excess of the solubility product, K_{sp}, for $CaCO_3$ which is 4.6×10^{-9}, thus predicting that the water is super saturated with $CaCO_3$.